

DEVELOPMENT OF COPPER COMPLEXES CONTAINING QUINOLINE DERIVATIVES AS
PHOTOREDOX CATALYSTS FOR ATRA REACTIONS



A Dissertation Submitted in Partial Fulfillment of the Requirements
for the Degree of Doctor of Philosophy in Chemistry

Department of Chemistry

FACULTY OF SCIENCE

Chulalongkorn University

Academic Year 2021

Copyright of Chulalongkorn University

การพัฒนาสารประกอบเชิงซ้อนทองแดงที่มีอนุพันธ์ควิโนลีนเพื่อเป็นตัวเร่งปฏิกิริยารีดอกซ์เชิงแสง
สำหรับปฏิกิริยาเอทีอาร์เอ



วิทยานิพนธ์นี้เป็นส่วนหนึ่งของการศึกษาตามหลักสูตรปริญญาวิทยาศาสตรดุษฎีบัณฑิต
สาขาวิชาเคมี ภาควิชาเคมี
คณะวิทยาศาสตร์ จุฬาลงกรณ์มหาวิทยาลัย
ปีการศึกษา 2564
ลิขสิทธิ์ของจุฬาลงกรณ์มหาวิทยาลัย

ปวีตรา ไชยบุตร : การพัฒนาสารประกอบเชิงซ้อนทองแดงที่มีอนุพันธ์ควิโนลีนเพื่อเป็นตัวเร่ง
 ปฏิกิริยารีดอกซ์เชิงแสงสำหรับปฏิกิริยาเอทีอาร์เอ. (DEVELOPMENT OF COPPER COMPLEXES
 CONTAINING QUINOLINE DERIVATIVES AS PHOTOREDOX CATALYSTS FOR ATRA
 REACTIONS) อ.ที่ปรึกษาหลัก : ศ. ดร.มงคล สุขวัฒนาสินธุ์, อ.ที่ปรึกษาร่วม : ศ. ดร.สัมฤทธิ์
 วัชรสินธุ์, Prof. Oliver Reiser

ปฏิกิริยาการเติมผ่านการส่งต่อแรดิคัล (ATRA) โดยใช้ตัวเร่งปฏิกิริยาเชิงแสงได้รับความสนใจเป็น
 อย่างมากสำหรับการสร้างพันธะ C-C หรือ C-S ในการสังเคราะห์สารตามหลักการเคมีสีเขียว ส่วนแรกของ
 วิทยานิพนธ์เกี่ยวข้องกับการสังเคราะห์และพิสูจน์ทราบโครงสร้างสารที่มีอนุพันธ์ควิโนลีนและเมทิลพริดีน (1Q,
 2Q และ 3Q) สำหรับใช้เป็นลิแกนด์ในการเตรียมสารประกอบเชิงซ้อนกับไอออนทองแดงเพื่อใช้เป็นตัวเร่ง
 ปฏิกิริยาเชิงแสงในปฏิกิริยาการเติมแอลคิลเฮไลด์บนแอลคีนโดยเปรียบเทียบกับสารประกอบเชิงซ้อน
 Cu(II)-TPMA พบว่าสารประกอบเชิงซ้อนไอออนทองแดงกับลิแกนด์ที่มีอนุพันธ์ควิโนลีนหนึ่งหน่วยและเมทิลพริ
 ดีนสองหน่วย Cu(II)-1Q สามารถเร่งปฏิกิริยาได้ดีที่สุด ซึ่งแอลคีนมากกว่า 20 ตัวอย่าง ให้ผลิตภัณฑ์ที่เกิดจาก
 ปฏิกิริยาการเติมลงบนพันธะคู่อย่างจำเพาะทั้งตำแหน่งและสเตอริโอเคมี การศึกษากลไกการเกิดปฏิกิริยา
 สอดคล้องกับการแตกตัวของพันธะ Cu(II)-X ด้วยแสง ได้สารประกอบเชิงซ้อน Cu(I) ที่รีดิวซ์สารประกอบฮาโล
 เจนผ่านการถ่ายทอดอิเล็กตรอนเดียวเกิดเป็นแรดิคัลที่จับอยู่กับสารประกอบเชิงซ้อน Cu(II) ซึ่งการเติมเบสหรือ
 AIBN ที่เป็นตัวตั้งฮาโลเจนช่วยให้ปฏิกิริยาของการเติมฮาโลฟอร์มเกิดได้ดีขึ้น โดยการป้องกันการเสื่อมสภาพ
 ของตัวเร่งปฏิกิริยาจากกรด ส่วนที่สองเกี่ยวข้องกับการสังเคราะห์และพิสูจน์ทราบโครงสร้างสารที่มีหมู่แทนที่ใน
 ตำแหน่ง C5 ของลิแกนด์ 1Q ด้วยอะตอมหนัก (1Q-I) หมู่ดึงอิเล็กตรอน (1Q-CN) และหมู่ให้อิเล็กตรอน (1Q-
 OMe) และเปรียบเทียบสมบัติการเป็นตัวเร่งปฏิกิริยาเคมีเชิงแสงกับ Cu(II)-1Q ในปฏิกิริยาการเติมซัลโฟนิลคลอ
 ไรด์ลงบนแอลคีน ซึ่งพบว่าหมู่แทนที่บน 1Q มีผลเพียงเล็กน้อยต่อร้อยละของผลผลิตจึงเลือกใช้ Cu(II)-1Q ใน
 การศึกษาต่อ พบว่าปฏิกิริยาการเติมซัลโฟนิลคลอไรด์บนโอเลฟิน (40 ตัวอย่าง) ทั้งที่มีเบสหรือไม่มีเบสภายใต้
 แสงสีฟ้า (LED) หรือแสงขาวสามารถเกิดปฏิกิริยาอย่างมีประสิทธิภาพ และการเติมซัลโฟนิลคลอไรด์ลงบนแอล
 ไคนให้ผลิตภัณฑ์ที่มีสเตอริโอไอโซเมอร์เป็น E เท่านั้น ซึ่งถือเป็นครั้งแรกที่พบในปฏิกิริยาที่เร่งด้วยสารประกอบ
 เชิงซ้อนของไอออนทองแดงที่มีลิแกนด์ชนิดเดียว เพื่อปรับสมบัติเชิงแสง ได้ทำการสังเคราะห์ลิแกนด์ที่ขยาย
 ระบบคอนจูเกตบนตำแหน่ง C5 ของลิแกนด์ 1Q ได้เป็นลิแกนด์ 1Q-Ph และ 1Q-DMAP ซึ่งผลการศึกษา
 เบื้องต้นพบว่า Cu(II)-1Q-Ph และ Cu(II)-1Q-DMAP มีประสิทธิภาพการเป็นตัวเร่งปฏิกิริยาเชิงแสงที่ดีขึ้นเมื่อ
 เปรียบเทียบกับ Cu(II)-1Q

สาขาวิชา เคมี

ปีการศึกษา 2564

ลายมือชื่อนิสิต

ลายมือชื่อ อ.ที่ปรึกษาหลัก

ลายมือชื่อ อ.ที่ปรึกษาร่วม

ลายมือชื่อ อ.ที่ปรึกษาร่วม

5872819723 : MAJOR CHEMISTRY

KEYWORD: ATRA reaction, Addition reactions of olefins, Chlorosulfonylation, Copper-quinoline complex, Haloalkylation, Photocatalyst

Pawittra Chaibuth : DEVELOPMENT OF COPPER COMPLEXES CONTAINING QUINOLINE DERIVATIVES AS PHOTOREDOX CATALYSTS FOR ATRA REACTIONS. Advisor: Prof. MONGKOL SUKWATTANASINITT Co-advisor: Prof. SUMRIT WACHARASINDHU, Prof. Oliver Reiser

The photocatalytic for C-C and C-S bond formations by ATRA reaction is an attractive topic in green organic synthesis. In the first part of this dissertation, a series of aminoquinoline-methylpyridine conjugates (1Q, 2Q, and 3Q) was synthesized, characterized, and used as a ligand for complexing Cu(II) ion. The ligand containing one aminoquinoline unit and two methylpyridine (1Q), gave the complex with the highest catalytic activity for haloalkylation of alkenes. The reaction proceeds well with high chemo- regio- and stereoselectivity for over 20 examples of alkenes. The mechanistic study is consistent with the visible-light-induced homolysis (VLH) of Cu(II)-X bond to Cu(I) complexes which subsequently reduces the alkyl halide via a single electron transfer (SET) to form the Cu(II) bound radical. A base additive or AIBN which acts as a halogen atom transfer (XAT) reagent promotes the ATRA product yields of haloform substrate by preventing acid poisoning of the catalyst. In the second part, the Cu(II) complexes of C5 substituted-1Q derivatives, including a heavy atom (1Q-I), electron-withdrawing group (1Q-CN), and electron-donating group (1Q-OMe) were prepared and studied for photocatalytic chlorosulfonylation of olefins (C-S bond formation). The substituents showed little effect to the product yields thus the more readily synthesized ligand 1Q was further optimized. The reactions effectively provided a broad scope of olefin substrates (40 examples) in the absence or presence of base under blue LED or white light. The reactions on alkynes also gave only *E*-selective products. This is the first time for observation of exclusive formation of *E*-isomer in the reaction catalyzed by a homoleptic copper complex. To tune photophysical properties, the extended conjugation at the C5 position of the quinoline ring, ligands 1Q-Ph and 1Q-DMAP were prepared. The preliminary study of these ligands showed an improvement in the catalytic activity in comparison with Cu(II)-1Q complex.

Field of Study: Chemistry

Academic Year: 2021

Student's Signature

Advisor's Signature

Co-advisor's Signature

Co-advisor's Signature

ACKNOWLEDGEMENTS

I would like to express my sincere gratitude to my advisor, Professor Dr. Mongkol Sukwattanasinitt, my co-advisors, Professor Dr. Sumrit Wacharasindhu and Professor Dr. Oliver Reiser, for excellent instructions, valuable guidance and kind encouragement throughout the course of this research.

I would like to gratefully acknowledge the committees, namely Professor Dr. Vudhichai Parasuk, Assistant Professor Pannee Leeladee, Assistant Professor Tanatorn Khotavivatana, and Assistant Professor Kittipong Chainok and the external committee, Assistant Professor Filip Kielar, for their precious suggestions and recommendations and generous supports for the experimental equipment and knowledge.

My sincere thanks also go to Assistant Professor Dr. Anawat Ajavakom, Professor Dr. Paitoon Rashatasakhon, and Dr. Sakulsuk Unarunotai for their constructive discussions and suggestions during my research group meeting.

Moreover, I would like to specially thank Dr. Jutawat Hojitsiriyant, Dr. Kanokthorn Boonkitpatarakul, Dr. Nattawut Yotapan, and Dr. Warothorn Paisuwan, for their kind training and assistance. I would like to gratitude to my coworkers, Nontakarn Chuaytanee, Apiwat Promchat, Jadetapong Klahan, Yuttana Senpradit and MAPS group members for their inspirations, motivations, and collaborations.

Sincere thanks are also extended to Dr. Sebastian Engl, Dr. Nicolai Wurzer, Alexander Reichle, Jinwei Shi and Reiser's group members for their willingful help and knowledge sharing during my working at the University of Regensburg.

Thanks also go to all technicians and collaborative workers. This research would not be accomplished without their help and supports.

I wish to thank my financial support from the Science Achievement Scholarship of Thailand, SAST for my Ph.D. study.

Finally, I would like to express my thankfulness to my loving and caring family and friends for their best encouragement through this research period.

Pawittra Chaibuth

TABLE OF CONTENTS

	Page
.....	iii
ABSTRACT (THAI).....	iii
.....	iv
ABSTRACT (ENGLISH).....	iv
ACKNOWLEDGEMENTS.....	v
TABLE OF CONTENTS.....	vi
LIST OF TABLES.....	xii
LIST OF FIGURES.....	xiii
LIST OF ABBREVIATIONS.....	18
CHAPTER I INTRODUCTION.....	20
1.1 Visible light photoredox catalysis.....	20
1.2 Atom transfer radical addition (ATRA).....	22
1.3 Copper catalyzed ATRA for C-C bond formation.....	24
1.4 Copper catalyzed ATRA for C-S bond formation.....	29
CHAPTER II EXPERIMENT.....	35
2.1 Reagents and materials.....	35
2.2 Analytical instruments.....	36
2.3 Synthetic procedures for quinoline derivatives.....	37
2.3.1 Synthesis of 1Q.....	37
2.3.2 Synthesis of 2Q.....	38
2.3.2.1 Synthesis of I-Q.....	38

2.3.2.2	Synthesis of QP	39
2.3.2.3	Synthesis of 2Q	40
2.3.3	Synthesis of 3Q.....	41
2.3.4	Synthesis of 1Q-I.....	42
2.3.5	Synthesis of 1Q-OMe.....	43
2.3.6	Synthesis of 1Q-CN.....	44
2.3.7	Synthesis of 1Q-Ph.....	45
2.3.8	Synthesis of 1Q-DMAP.....	46
2.4	Synthetic procedure for some isolated copper complexes.....	47
2.4.1	Synthesis of $[\text{Cu}^{\text{II}}(1\text{Q})\text{Cl}]^+$	47
2.4.2	Synthesis of $[\text{Cu}^{\text{II}}(2\text{Q})\text{Cl}]^+$	47
2.4.3	Synthesis of $[\text{Cu}^{\text{II}}(3\text{Q})\text{Cl}]^+$	47
2.5	Photophysical study	48
2.5.1	UV-Visible spectroscopy	48
2.5.2	Molar absorption coefficient (ϵ).....	48
2.6	Electrochemical study.....	48
2.7	Excited state calculation.....	49
2.8	X-ray crystallography	49
2.8.1	Crystallography structures of copper complexes.....	49
2.8.2	Crystallography structures of chlorosulfonylation products	49
2.9	General experimental procedure for ATRA	50
2.9.1	Reaction using AIBN.....	50
2.9.2	Reaction without AIBN	50
2.9.3	The large-scale synthesis	51

2.9.4	The relative emission spectra of light source	51
2.9.5	Determination of percent NMR yield of the addition product.	52
2.9.6	Spectroscopic data of ATRA products	55
2.10	General procedure for chlorosulfonylation under blue light.....	64
2.10.1	General procedure for chlorosulfonylation under white light	64
2.10.2	The large-scale synthesis of compound 3ja	65
2.10.3	Spectroscopic data of chlorosulfonylation products	66
CHAPTER III RESULTS AND DISCUSSION FOR COPPER CATALYZED HALOALKYLATION (C-C FORMATION).....		
3.1	Synthesis and characterization of Cu(II) complexes	87
3.1.1	Synthesis and characterization of quinoline ligands	87
3.1.2	Synthesis and characterization of Cu(II) complexes	90
3.2	Photophysical and electrochemical properties	92
3.2.1	UV-vis absorption and emission	92
3.2.2	Cyclic voltammetry and reduction potentials	94
3.3	Study of catalytic properties for haloalkylation (C-C formation)	96
3.3.1	Screening of catalyst.....	96
3.3.3	Addition of various alkyl halides to terminal alkenes.....	102
3.3.4	Addition of various alkyl halides to internal alkenes	110
3.3.5	Addition of inactive alkyl halide to styrene.....	116
3.3.6	Addition of various alkyl halides to alkenes in the absence of catalyst	117
3.3.7	Cyclization reaction of diene	118
3.4	Proposed mechanism.....	119
3.4.1	Kinetic study.....	120

3.4.2	Evidences for Cu(I) generation from Cu(II) via VIHC.....	122
3.4.3	Evidences for Cu(I) generation via XAT using AIBN as reducing agent	123
CHAPTER IV RESULTS AND DISCUSSION FOR COPPER CATALYZED		
CHLOROSULFONYLATION (C-S FORMATION).....		
4.1	Synthesis and characterization of ligands.....	127
4.2	Photophysical and electrochemical properties	129
4.2.1	UV-vis absorption spectroscopy.....	130
4.2.2	Cyclic voltammetry and reduction potentials	132
4.3	Study of catalytic properties for chlorosulfonylation (C-S formation).....	134
4.3.1	Optimization.....	134
4.3.2	Chlorosulfonylation of various alkenes	136
4.3.3	Chlorosulfonylation of various alkenes and alkynes in the presence of Na ₂ CO ₃ additive.	140
4.3.4	Chlorosulfonylation of various sulfonyl chlorides	143
4.3.5	Chlorosulfonylation of various olefins under white light.	144
4.3.6	Proposed mechanism	146
4.4	Study of other ligands.....	146
4.4.1	Synthesis and characterization	147
4.4.2	Photophysical and electrochemical properties.....	148
4.4.2.1	UV-vis absorption spectroscopy.....	149
4.4.2.2	Cyclic voltammetry and reduction potentials	151
4.4.3	Preliminary study of catalytic properties for chlorosulfonylation (C-S formation).....	153
CHAPTER V CONCLUSIONS		
154		

APPENDIX A The Atom transfer radical addition (ATRA) for haloalkylation (C-C formation).....	156
A.1 Synthesis and characterization of Cu(II) complexes.....	156
A.1.1 X-ray crystallography.....	156
A.1.2 ^1H NMR and ^{13}C spectra.....	160
A.1.3 IR spectra	174
A.1.4 Mass spectrum.....	176
A.1.5 Elemental analysis.....	184
A.1.6 UV-Visible spectroscopy.....	185
A.2 Study of catalytic properties for haloalkylation (C-C formation).....	187
A.2.1 ^1H NMR and ^{13}C spectra of Products.....	189
APPENDIX B The atom transfer radical addition (ATRA) for halosulfonylation (C-S formation).....	221
B.1 Ligands and Cu(II) complexes.....	221
B.1.1 ^1H NMR and ^{13}C spectra.....	221
B.1.2 IR spectra	241
B.1.3 Mass spectrum.....	243
B.1.4 UV-Visible spectroscopy.....	248
B.2 Study of catalytic properties for chlorosulfonylation (C-S formation).....	251
B.2.1 Reversibility study of complexation and decomplexation	251
B.2.2 ^1H NMR and ^{13}C spectra.....	253
B.2.3 X-ray Crystallography of Products.....	296
REFERENCES	297
VITA.....	307



จุฬาลงกรณ์มหาวิทยาลัย
CHULALONGKORN UNIVERSITY

LIST OF TABLES

	Page
Table 3.1 Selected bond lengths (Å) and bond angles (°) for Cu(II) complexes.....	91
Table 3.2 Summary of absorption of ligands and Cu(II) complexes in CH ₃ CN.....	93
Table 3.3 Summary of electrochemical data for Cu-ligand complexes.....	94
Table 3.4 The excited-state potential of copper complexes in CH ₃ CN.	96
Table 3.5 Condition optimization for ATRA of CHCl ₃ on styrene.....	101
Table 3.6 Comparison of alkyl chloride with alkyl bromide in the addition reaction to alkenes in the absence of photocatalyst under white light.	117
Table 3.7 Optimization for ATRC reaction.....	118
Table 3.8 ATRA of CHCl ₃ on styrene in various solvents in the absence of reducing agent.....	123
Table 4.1 Summary of absorption of ligands and Cu(II) complexes in CH ₃ CN.....	132
Table 4.2 The electrochemical data of Cu(II) complexes generated <i>in situ</i> from CuCl ₂ and various ligands in CH ₃ CN.....	133
Table 4.3 Catalytic activity screening of Cu(II) complexes with various ligands.....	136
Table 4.4 Reaction optimization for base additives.....	143
Table 4.5 Summary of absorption of ligands and Cu(II) complexes in CH ₃ CN.....	151
Table 4.6 The electrochemical data of Cu(II) complexes generated <i>in situ</i> from CuCl ₂ and various ligands in CH ₃ CN.....	152

LIST OF FIGURES

	Page
Figure 1.1 Quenching mode of photo catalysis.....	20
Figure 1.2 The classical metal complexes as photocatalysts.....	21
Figure 1.3 Transition metal complexes used as catalysts in ATRA reaction.....	23
Figure 1.4 Proposed mechanism for copper catalyzed ATRA.....	24
Figure 1.5 Copper catalyzed intramolecular ATRC reaction.....	25
Figure 1.6 Common nitrogen-based ligands used in Cu-mediated ATRA and ATRC. ...	25
Figure 1.7 ATRC of α -chloro- β -keto esters by using of CuCl and bpy as a catalyst... 26	26
Figure 1.8 ATRA reaction catalyzed by $\text{Tp}^x\text{Cu}(\text{NCMe})$	26
Figure 1.9 ATRA reaction catalyzed by $[\text{Cu}(\text{dap})_2\text{Cl}]$	27
Figure 1.10 Proposed mechanism for ATRA reaction catalyzed by $[\text{Cu}(\text{dap})_2\text{Cl}]$	27
Figure 1.11 Photo-mediated ATRA reaction using mixed ligand copper complexes....	28
Figure 1.12 Photo-mediated ATRA reaction using $[\text{Cu}(\text{TPMA})\text{Cl}]\text{Cl}$ as a catalyst.....	28
Figure 1.13 Photo-mediated ATRC of dienes using $[\text{Cu}(\text{TPMA})\text{Cl}]\text{Cl}$ as a catalyst.	29
Figure 1.14 Proposed mechanism for photo-mediated copper-catalyzed ATRA in the presence of reducing agent.	29
Figure 1.15 Photo-mediated chloride trifluoromethylation of electron deficient alkenes.....	30
Figure 1.16 Photo-mediated trifluoromethylsulfonylation of the unactivated alkenes.30	30
Figure 1.17 Simplified mechanism for Cu(II) catalyzed chlorosulfonylation via initial visible-light-induced homolysis (VLIH) of Cu-Cl bond.....	31
Figure 1.18 Photo-mediated copper-catalyzed chlorosulfonylation using $[\text{Cu}(\text{dap})_2]\text{Cl}$ and $[\text{Cu}(\text{dap})\text{Cl}_2]$ as photocatalysts.....	32

Figure 1.19 Photo-mediated chlorosulfonylation using $[\text{Cu}(\text{dmp})_2\text{Cl}]\text{Cl}$ as a photocatalyst.....	32
Figure 1.20 Photo-mediated copper-catalyzed chlorosulfonylation.....	33
Figure 1.21 Design principle of ligands 1Q-3Q.	34
Figure 1.22 Structure of quinoline derivatives used in this study.....	34
Figure 2.1 In-house made photoreactor equipped with a) white LEDs b) White CFL..	51
Figure 2.2 Normalized emission spectra of white CFL (black), white LEDs (grey), blue LEDs (Blue), green LEDs (green) and red LEDs (red) lines.	52
Figure 2.3 ^1H NMR spectra of crude product, after flash column chromatography, from the reaction between styrene and CCl_4 in CD_3OD , in the presence of toluene internal standard.	53
Figure 2.4 ^1H NMR spectra of crude product, after flash column chromatography, from the reaction between styrene and CHCl_3 in CD_3OD , in the presence of toluene internal standard.	54
Figure 2.5 Reaction set up for chlorosulfonylation.	65
Figure 3.1 Synthesis of ligand 1Q, 2Q and 3Q.	88
Figure 3.2 ^1H NMR spectra of 8-aminoquinoline, 1Q, 2Q and 3Q in $\text{DMSO}-d_6$	89
Figure 3.3 The coordination environment around the $\text{Cu}(\text{II})$ atom and coordination geometry of ligands a) $\text{Cu}(\text{II})\cdot\text{TPMA}$, b) $\text{Cu}(\text{II})\cdot\text{1Q}$, c) $\text{Cu}(\text{II})\cdot\text{2Q}$, and d) $\text{Cu}(\text{II})\cdot\text{3Q}$	91
Figure 3.4 Normalized absorption (solid lines) and emission (dot lines) spectra excited at absorption λ_{max} (See Table 3.2) of a) ligands and b) $\text{Cu}(\text{II})\cdot\text{ligand}$ complexes in CH_3CN at ambient temperature.	93
Figure 3.5 Cyclic voltammogram of $\text{Cu}(\text{II})$ complexes at 1.0 mM in CH_3CN	94
Figure 3.6 ^1H NMR yields of addition product from ATRA reactions between styrene and CCl_4 in the presence of $\text{Cu}(\text{II})$ and various ligands using toluene as internal standard (see Figure 2.3 for ^1H NMR spectra).	97

Figure 3.7 Time dependence study for reaction of styrene with CCl_4 catalyzed by Cu(II) complexes of various ligands. Yields were determined by ^1H NMR with toluene as internal standard.	98
Figure 3.8 ^1H NMR yields of screening reaction between styrene and various alkyl halides catalyzed by a Cu(II) complex of 1Q using toluene as internal standard.	98
Figure 3.9 Copper catalyzed ATRAs of various alkyl halides to terminal alkenes. Yields are determined from ^1H NMR integrations of all alkene protons and aliphatic protons of product, respectively, against methyl protons of toluene internal standard (Figure 2.3 and 2.4).	103
Figure 3.10 ^1H NMR spectra of crude product, after flash column chromatography, from reaction between acrylonitrile and CBrCl_3 in CD_3OD , in the presence of toluene internal standard.	104
Figure 3.11 ^1H NMR spectra of crude product, after flash column chromatography, from reaction between methyl acrylate and CBrCl_3 in CD_3OD , in the presence of toluene internal standard.	105
Figure 3.12 ^1H NMR spectra of crude product, after flash column chromatography, from reaction between methyl methacrylate and CBrCl_3 in CD_3OD , in the presence of toluene internal standard.	106
Figure 3.13 ^1H Proposed mechanism for reaction of terminal alkene with CBrCl_3 catalyzed by Cu(II) complex.	108
Figure 3.14 ^1H NMR spectra of crude product, after flash column chromatography, from reaction between methyl methacrylate and CBrCl_3 with 0 – 3.0 mol% of $\text{CuCl}_2 \cdot 1\text{Q}$ loading in CD_3OD , in the presence of toluene internal standard.	109
Figure 3.15 Copper catalyzed ATRAs of various alkyl halides to internal alkenes.	110
Figure 3.16 Substitution reaction test of halide product in methanol.	111
Figure 3.17 NOESY-NMR spectra of 5e.	112
Figure 3.18 NOESY-NMR spectra of 5'e.	113

Figure 3.19 ^1H NMR spectra of crude product, after flash column chromatography, from reaction between 1,2-dihydronaphthalene and CCl_4 in the presence of toluene internal standard.	114
Figure 3.20 ^1H NMR spectra of crude product, after flash column chromatography, from reaction between 1,2-dihydronaphthalene and CBr_4 in the presence of toluene internal standard.	115
Figure 3.21 Copper catalyzed ATRAs of inactive alkyl halide (1.50 mmol, 3.00 equiv) to styrene (500 μmol , 1.00 equiv).	116
Figure 3.22 Proposed mechanism.....	119
Figure 3.23 Kinetic plots for ATRA of styrene and CCl_4 catalyzed by a) $\text{CuCl}/1\text{Q}$ b) $\text{CuCl}_2\cdot 1\text{Q}$ with $[\text{Styrene}]:[\text{CCl}_4]:[\text{Cu}] = [1.00]:[1.50]:[0.01]$ under light, heat, or light/dark condition standard.	121
Figure 3.24 Absorption spectra of copper complex solutions before and after being placed under white light a) 1.0 mM $\text{CuCl}_2\cdot 1\text{Q}$ in methanol (blue lines) compared with 0.1 mM $\text{CuCl}/1\text{Q}$ in methanol (red line).	122
Figure 3.25 Absorption spectra of copper complex solutions before and after being placed under white light a) 2mM $\text{CuCl}_2\cdot 1\text{Q}$ in CH_3CN in the presence of 15 eq. AIBN b) 2mM $\text{CuCl}_2\cdot 1\text{Q}$ in CH_3CN in the absence of AIBN.	124
Figure 3.26 The ^1H NMR spectra for Cu(I) complex generation from Cu(II) complex.	125
Figure 3.27 The EPR spectra for Cu(I) complex generation from Cu(II) complex.....	126
Figure 4.1 Synthesis of ligand, 1Q-I, 1Q-CN and 1Q-OMe.....	128
Figure 4.2 ^1H NMR spectra of 1Q, 1Q-I, 1Q-CN and 1Q-OMe in $\text{DMSO}-d_6$	129
Figure 4.3 Absorption spectra of a) 0.1 mM 1Q, 1Q-I, 1Q-CN and 1Q-OMe b) $\text{CuCl}_2\cdot 1\text{Q}$, $\text{CuCl}_2\cdot 1\text{Q-I}$, $\text{CuCl}_2\cdot 1\text{Q-CN}$ and $\text{CuCl}_2\cdot 1\text{Q-OMe}$ in CH_3CN	131
Figure 4.4 Cyclic voltammogram of Cu(II)•ligand complexes at 1.0 mM in CH_3CN	133
Figure 4.5 Isolated yields of products from chlorosulfonylation of various alkenes.	139

Figure 4.6 Isolated yields of products from chlorosulfonylation of various alkenes in the presence of Na_2CO_3 additive.	142
Figure 4.7 Isolated yields of products from chlorosulfonylation using various sulfonyl chlorides. ^a Determined by ^1H NMR yield using 1,3,5-trimethoxybenzene as an internal standard.....	144
Figure 4.8 Isolated yields of products from chlorosulfonylation of various olefins under white light.	145
Figure 4.9 Simplified mechanism for Cu(II) catalyzed chlorosulfonylation via initial visible-light-induced homolysis (VLIH) of Cu-Cl bond.....	146
Figure 4.10 Synthesis of ligand 1Q-Ph and 1Q-DMAP.	147
Figure 4.11 ^1H NMR spectra of 1Q, 1Q-Ph and 1Q-DMAP in $\text{DMSO}-d_6$	148
Figure 4.12 Absorption spectra of a) 0.1 mM 1Q, 1Q-Ph and 1Q-DMAP b) 0.1 mM $\text{CuCl}_2 \bullet 1\text{Q}$, and $\text{CuCl}_2 \bullet 1\text{Q-Ph}$ and $\text{CuCl}_2 \bullet 1\text{Q-DMAP}$ in CH_3CN	150
Figure 4.13 Cyclic voltammogram of Cu(II)•ligand complexes at 1.0 mM in CH_3CN	151
Figure 4.14 Photocatalytic activity study of Cu(II) complexes with 1Q, 1Q-Ph and 1Q-DMAP in chlorosulfonylation of styrene.	153

LIST OF ABBREVIATIONS

ATRA	atom transfer radical addition
AIBN	azobisisobutyronitrile
calcd	calculated
CDCl ₃	deuterated chloroform
CFL	compact fluorescent lamp
dap	2,9-bis(p-anisyl)-1,10-phenanthroline)
dmp	2,9-dimethyl-1,10-phenanthroline
DMF	<i>N,N</i> -dimethylformamide
DMSO	dimethylsulfoxide
ddd	doublet of doublet of doublet (NMR)
dt	doublet of triplet (NMR)
d	doublet (NMR)
dd	doublet of doublet (NMR)
equiv	equivalent (s)
ESI	electrospray ionization
g	gram (s)
Hz	Hertz
h	hour (s)
IR	infrared
<i>J</i>	coupling constant
LED	light-emitting diode
min	minute (s)
mg	milligram (s)
mL	milliliter (s)
mmol	millimole (s)
m/z	mass per charge
m	multiplet (NMR)
M	molar
MHz	megahertz

NMR	nuclear magnetic resonance
ppm	part (s) per million
rt	room temperature
s	singlet (NMR)
SET	single electron transfer
TLC	thin layer chromatography
TON	turn over number
TPMA	Tris(2-pyridylmethyl)amine
UV	ultraviolet light
μL	microliter (s)
δ	chemical shift
$^{\circ}\text{C}$	degree Celsius
$E_{1/2}$	half wave potential
λ	wavelength
λ_{em}	maximum emission wavelength
$\lambda_{\text{max}}, \lambda_{\text{abs}}$	maximum absorption wavelength
τ	excited state lifetime
% yield	percentage yield

CHAPTER I INTRODUCTION

1.1 Visible light photoredox catalysis

A 'photocatalysis' reaction refers to the reaction that is promoted by the synergistic of light and photocatalysts to engage in the electron transfer process with substrates upon the photoexcitation. It becomes one of the most attractive reactions for the development of 'Green' processes, with an emphasis that a given transformation is achievable by green energy sources, utilization of catalytic protocols with safe and ecologically benign reagents and solvents under mild conditions. The photocatalytic quenching of an excited state photocatalyst via single electron transfer (SET) or energy transfer process is generally divided into two modes depending on the nature and reduction potentials of quenchers and photocatalyst (Figure 1.1). In the oxidative quenching cycle, after irradiation excited-photocatalyst or PC^* donates the electron to the oxidative quencher before receiving an electron from the electron donor. If the excited-photocatalyst accepts the electron from the reductive quencher and then donates the electron to the electron acceptor this pathway is called a reductive quenching cycle.

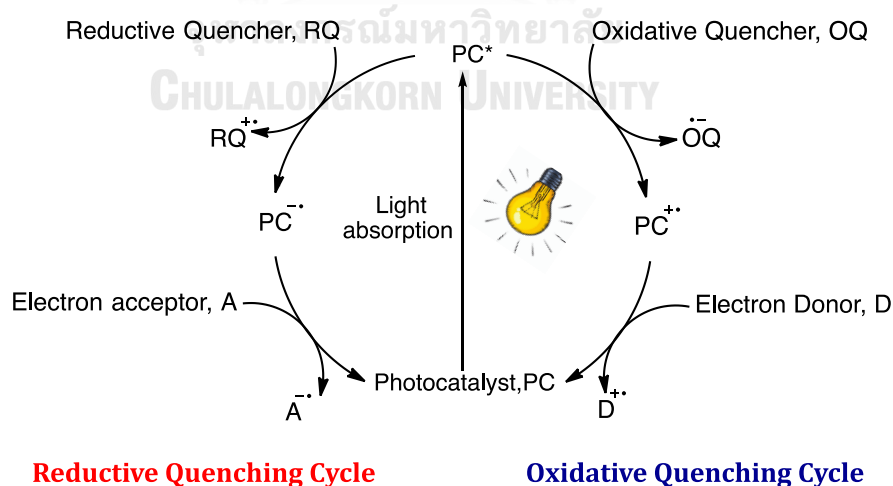
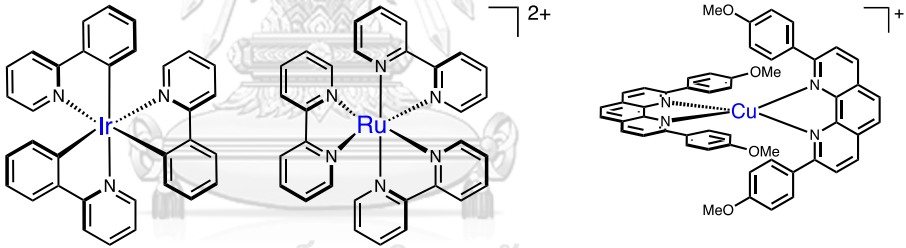


Figure 1.1 Quenching mode of photo catalysis.

Up to date, a variety of organic dyes sensitizers and transition metal complexes have been studied and developed. Even though the organic dye photocatalyst beneficially provides a low-cost and metal-free reaction as a ‘Green’ catalyst of choice, the lower photostability, and redox property feasibly limit the scope of the reaction. The arguably best-known metal photocatalysts are based on iridium and ruthenium complexes due to their long-excited state lifetimes combined with their ability for a SET process to other compounds under irradiation with light (Figure 1.2) [1-5]. Nevertheless, the high cost and toxicity of these metals constrain the scalability for photocatalytic applications. With a low cost and toxicity, the copper complex was introduced as an alternative photocatalyst. The most effective and well-known copper catalyst is $[\text{Cu}(\text{dap})_2]^+$ [6] also known as Sauvage catalyst [7]. The flexibility of ligand combining with copper, to tune the redox potential and its photoexcitation properties, is an advantage for the drastic development of this metal photocatalyst for widespread reaction over the last decade [8-11].



	$\text{fac-Ir}(\text{ppy})_3$	$[\text{Ru}(\text{bpy})_3]^{2+}$	$[\text{Cu}(\text{dap})_2]^+$
λ_{abs}	375 nm	452 nm	437 nm
λ_{em}	494 nm	615 nm	670 nm
$E_{1/2} (\text{M}^+/\text{M})$	+1.29 V	-0.81 V	+0.66 V
$E_{1/2} (\text{M}^+/\text{M}^*)$	+0.77 V	-1.73 V	-1.43 V
τ	1900 ns	1100 ns	270 ns

Figure 1.2 The classical metal complexes as photocatalysts.

ppy = 2-phenylpyridine, **bpy** = 2,2'-bipyridine, **dap** = 2,9-bis(p-anisyl)-1,10-phenanthroline, λ_{abs} = maximum absorption wavelength, λ_{em} = maximum emission wavelength, $E_{1/2}$ = half wave potential, and τ = excited state lifetime.

1.2 Atom transfer radical addition (ATRA)

Atom transfer radical addition (ATRA) has proven to be a powerful tool for the functionalization of alkenes [12-14]. Being atom economic and versatile, this type of reaction provides a variety of functionalized compounds that can be used for further synthesis of chemical feedstocks, advanced materials, and pharmaceuticals [15-17].

The history of ATRA

Not long after the discovery of anti-Markovnikov in the addition reaction of hydrogen bromide to unsymmetrical alkenes by peroxide initiators through the radical process in the early 1940s, the additions of alkyl halides to olefins in the presence of radical initiators or light were reported and later known as Kharasch reaction. Although the reactions proceeded well under the presence of peroxide or light, they need a highly active and excess of the alkyl halide to provide respectable yields [18, 19]. In 1956, Kochi suggested the termination process of radical intermediate in the presence of metal halides (CuCl_2 or FeCl_2) through the inner sphere electron transfer mechanism which implied a possible role of metal ions in the addition reaction [20]. The proposed involvement of metal ions is consistent with the discovery by Minisci's group that iron leached into the reaction can increase the chain transfer reaction rate. They explained that iron was oxidized by chlorine radical to give iron(III) chloride as a byproduct. A year later, Minisci and Vofsi, and Asscher reported a transition metal-catalyzed atom transfer radical addition or TMC-ATRA [21, 22]. The transition metal-catalyzed atom transfer radical addition is currently achieved with various complexes of several metals such as iron [23, 24], ruthenium [25-27], iridium [28], copper [29, 30], niobium [31], and nickel [32] under either thermal or photo conditions (Figure 1.3).

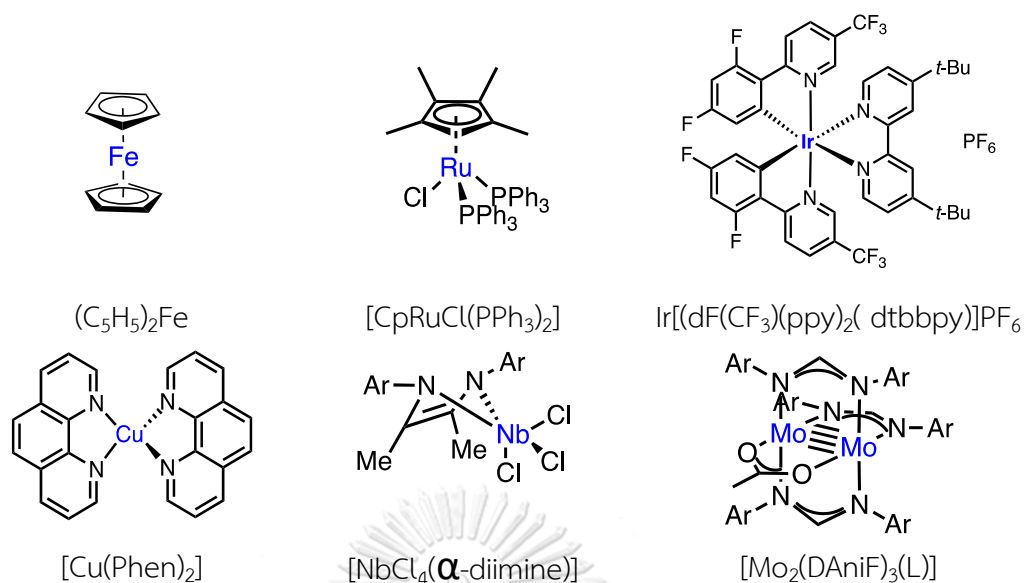


Figure 1.3 Transition metal complexes used as catalysts in ATRA reaction.

The commonly accepted mechanism proposed for metal-catalyzed ATRA is shown in Figure 1.4 [33]. The initial step is metal-induced homolytic cleavage of the carbon-halogen bond. This step generates a metal-halide and alkyl radical. The generated alkyl radical then adds to a double bond to afford another alkyl radical intermediate which rapidly abstracts halogen atom from the metal-halide to regenerate the active metal species for the next reaction cycle [34]. The desired addition product is continuously formed. However, the combination or the polymerization of the alkyl radicals can lead to competitive products and disturb the catalytic cycles.

To achieve a selective ATRA reaction, Matyjaszewski has suggested 3 factors for concerns in this reaction. First, the overall radical concentration in the reaction must be low (k_{d1} and $k_{d2} \gg k_{a1}$ and k_{a2}) to avoid the radical-radical combination. Second, the catalyst reactivation must be slower than the starting material activation ($k_{a1} \gg k_{a2}$) to prevent further activation of the addition product. Third, the oxidation must be faster than the propagation ($k_{d2} \gg k_p$) to avoid any polymerization [35]. These criteria implied that the active species of the metal catalyst must be always present at low concentrations but unceasingly regenerated in the reaction.

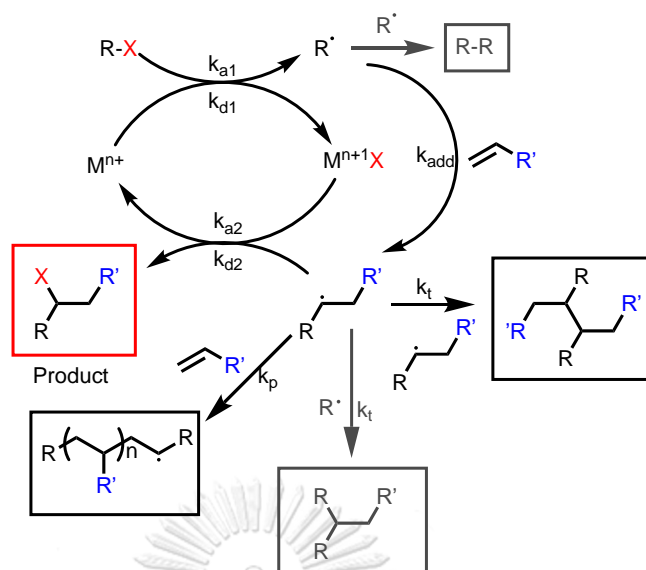


Figure 1.4 Proposed mechanism for copper catalyzed ATRA.

1.3 Copper catalyzed ATRA for C-C bond formation

Copper is one of the most attractive choices for the metal center of ATRA catalysts owing to its natural abundance and low toxicity. Copper-mediated atom transfers radical cyclization or ATRC of a molecule containing both active alkyl halide and alkene groups can also provide carbon-carbon cyclization which is useful in synthesizing natural products and pharmaceuticals. The pioneering work was found in the synthesis of bicyclic γ -lactams and γ -lactones by Nagashima and co-workers (Figure 1.5) [36, 37]. Cu(I) chloride was used to produce bicyclic compounds with chloromethyl substituent. Nevertheless, the drawbacks of these reactions are the requirements for a large amount of copper salt and relatively high temperatures. The high temperature used is inappropriate for intermolecular addition of readily polymerizable alkenes such as methyl methacrylate (MMA), methyl acrylate (MA), styrene, vinyl acetate (VA), and acrylonitrile (AN) due to the competitive polymerization.

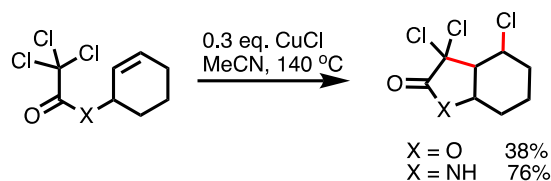


Figure 1.5 Copper catalyzed intramolecular ATRC reaction.

Several ligands have been developed for the improvement of both activity and selectivity of copper catalysts (Figure 1.6). These ligands are nitrogen-based ligands such as phenanthroline [38], pyridine [39, 40], tris(2-pyridylmethyl)amine [41-46], and tris(pyrazolyl)borate [47-50] which can stabilize the generated Cu(I) intermediates. Several copper complexes typically used as low as 0.01 equivalent. Moreover, the reaction time and temperature have been significantly decreased.

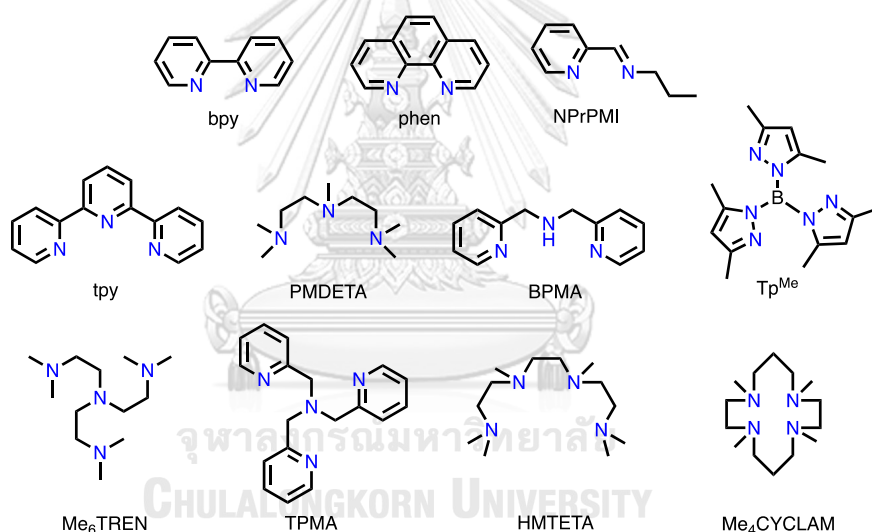


Figure 1.6 Common nitrogen-based ligands used in Cu-mediated ATRA and ATRC.

Copper complexes with bipyridine (**bpy**) are one of the primary active catalysts used in ATRA and ATRC reactions. This catalyst showed high activity for catalyzing the addition of chloromethyl ketones to olefins. In 2006, Yang and co-workers investigated the ATRC reaction of unsaturated α -chloro- β -keto esters to obtain various cyclic compounds in moderate to high yield (Figure 1.7) [39]. Furthermore, a recent study by Hu and co-workers suggested the addition of α,α,α -trichloromethyl ketones to styrene derivatives under low temperatures and benign conditions in high

yield. Nevertheless, in both studies, a large amount of copper complex is still needed [40].

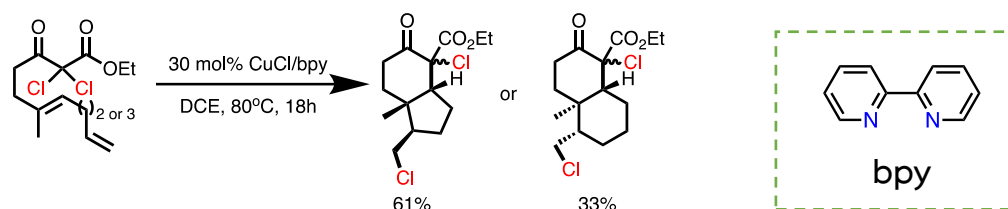


Figure 1.7 ATRC of α -chloro- β -keto esters by using of CuCl and **bpy** as a catalyst.

Tris(pyrazolyl)borate derivatives (Tpx) were first studied by Perez and co-workers for the transfer of carbene, nitrene, and oxo groups to hydrocarbons. Afterward, they turned their attention to constructing this ligand family for ATRA reaction. They reported active copper complexes with these ligands, TpxCu(NCMe) for the addition of CCl₄ and CHCl₃ to olefins under mild conditions (Figure 1.8). A few years later, they successfully extended the substrate scope to polychlorinated esters and sulfonyl chlorides. They noted that steric and electron-donating substituents on the pyrazole rings enhance the efficiency of the complexes [47, 48, 50]. The mechanistic and computational studies revealed that the CH₃CN additive affected the rate of styrene addition by controlling the radical concentration in reaction via the complexation of generated copper with the additive [49].

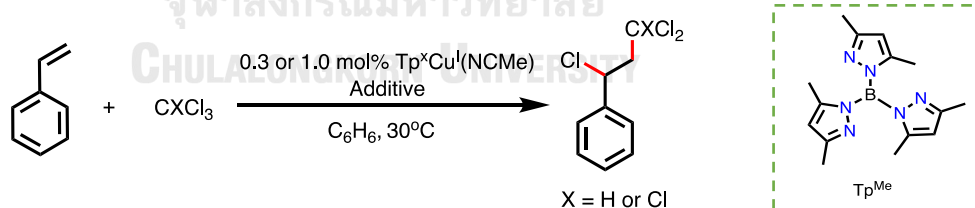


Figure 1.8 ATRA reaction catalyzed by TpxCu(NCMe).

Up to date, phenanthroline derivatives are recognized as the most active ligands for photo-mediated ATRA reactions due to their ability to harvest energy from UV-visible light and stabilize the excited state of the generated Cu(I) complexes. These allowed the activation of less active alkyl halides and expanded the scopes of the alkene substrates. The pioneering work by Reiser and co-workers demonstrate

the ATRA reaction of alkyl bromide to an olefin using $[\text{Cu}(\text{dap})_2\text{Cl}]$ under green light (530 nm) as shown in Figure 1.9 [6].

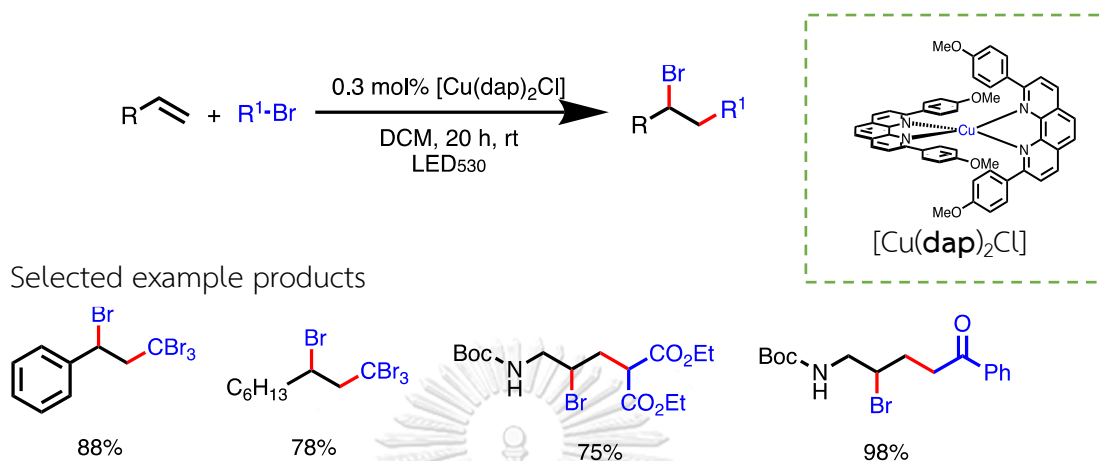


Figure 1.9 ATRA reaction catalyzed by $[\text{Cu}(\text{dap})_2\text{Cl}]$.

The mechanism was proposed through singlet electron transfer from the excited state, $[\text{Cu}(\text{dap})_2]^*$ to organohalide to generate a radical intermediate which adds to an alkene. Then generated addition radical accept an electron from generated $\text{Cu}(\text{II})$ and regenerate active $\text{Cu}(\text{I})$ for the next catalytic cycle as shown in Figure 1.10.

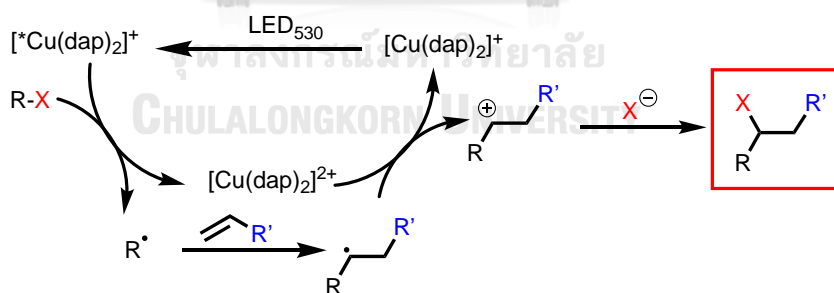


Figure 1.10 Proposed mechanism for ATRA reaction catalyzed by $[\text{Cu}(\text{dap})_2\text{Cl}]$.

A few years later, the same group reported mixed ligand $\text{Cu}(\text{I})$ complexes of phenanthroline and bis-isonitrile ligand. The result suggested the incorporation of these wide-bite-angle ligands improved both the photophysical properties of the complexes and catalytic activity between the alkyl halides and alkenes (Figure 1.11) [38].

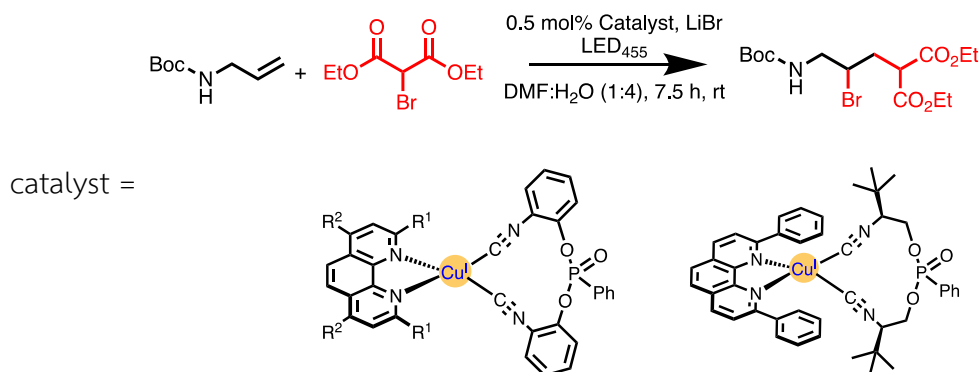


Figure 1.11 Photo-mediated ATRA reaction using mixed ligand copper complexes.

Another, simple but also an effective catalyst for ATRA reaction is copper complex with tris(2-pyridylmethyl)amine or TPMA ligand (Figure 1.12). In 2007, Pintauer group reported ATRA reaction of CCl_4 and CHCl_3 with alkenes by using complexes of CuCl and CuCl_2 with TPMA as a catalyst in the presence of AIBN as an activator for regenerating active catalyst, ICAR under heating at $60\text{ }^\circ\text{C}$ [41]. This complex was successfully used in both thermal and photocatalytic conditions for the additions of various alkyl halides to active alkenes. Later on, the same group also expanded the scopes of alkyl halide [42], ligands [51, 52], and reducing agents [43, 53] for the ATRA reactions.

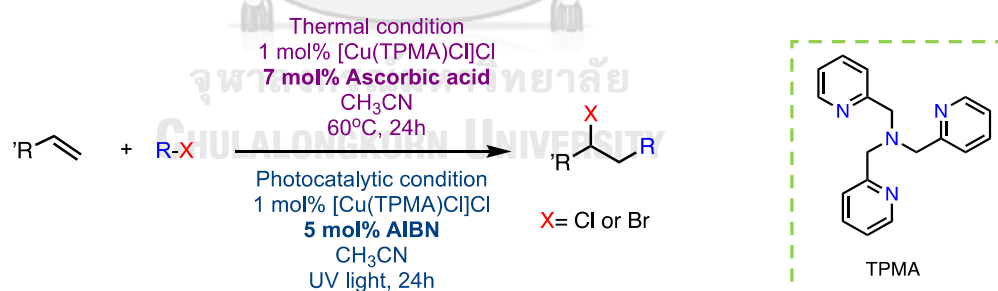


Figure 1.12 Photo-mediated ATRA reaction using $[\text{Cu}(\text{TPMA})\text{Cl}]\text{Cl}$ as a catalyst.

In 2011, they successfully performed this reaction under UV light at ambient temperature. The reactions gave various addition products of active alkenes with high yield and conversion. The cyclization reactions of 1,6-dienes with CCl_4 were also achieved (Figure 1.13) [46].

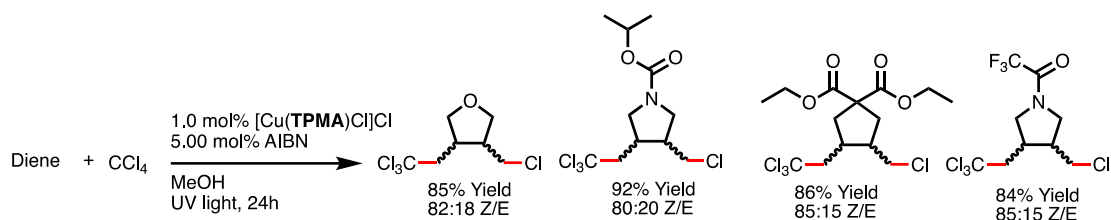


Figure 1.13 Photo-mediated ATRC of dienes using $[\text{Cu}(\text{TPMA})\text{Cl}]\text{Cl}$ as a catalyst.

The mechanism starts with the activation of the initiator radical under thermal or light conditions to generate an active Cu(I) complex in the catalytic cycle (Figure 1.14). As the catalyst continuously regenerates in the reaction it benefits to set up the reaction from the easy handle Cu(II) complexes in low catalyst loading. However, the major role of light in those studies was attributed to the photodecomposition of AIBN to form isobutyronitrile radical which in turn serves as the reducing agent [38]. The role of light in the direct excitation of copper complexes has not been mentioned.

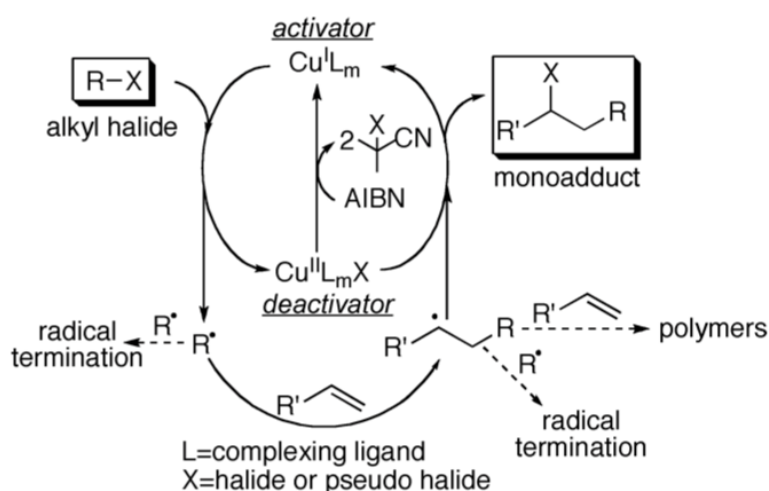


Figure 1.14 Proposed mechanism for photo-mediated copper-catalyzed ATRA in the presence of reducing agent.

1.4 Copper catalyzed ATRA for C-S bond formation

Chlorosulfonylation is a recent advancement for copper-catalyzed reactions under either thermal or photo conditions [54-56]. This reaction is attractive as a facile step in the synthesis of sulfone derivatives, [57-67] which are an important class of

natural products, pharmaceuticals, and bioactive molecules [68-75]. In 2015, Dolber group studied the photo-mediated ATRA reaction of a fluoroalkylsulfonyl chloride to an electron-deficient alkene in the presence of $[\text{Cu}(\text{dap})_2]\text{Cl}$ as a photocatalyst. Under the optimized condition, only the chlorofluoroalkylation products that are from SO_2 extrusion were observed (Figure 1.15) [76].

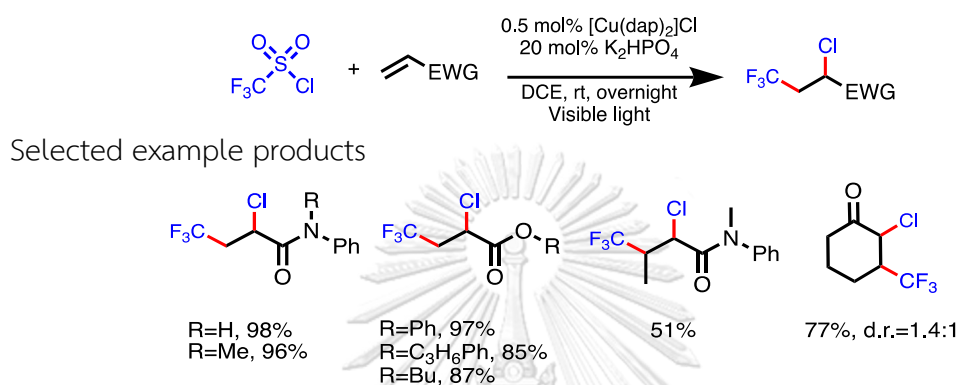


Figure 1.15 Photo-mediated chloride trifluoromethylation of electron deficient alkenes.

In the same year, Reiser group successfully developed the unprecedented photo-mediated trifluoromethylchlorosulfonylation of the unactivated alkenes without extrusion of SO_2 (Figure 1.16). A variety of β -trifluoromethylethanesulfonyl chloride products were achieved in respectable to good yields. The study suggested the dual role of copper catalyst as an electron transfer agent and coordinating reactant with SO_2Cl through the inner sphere catalytic process [77].

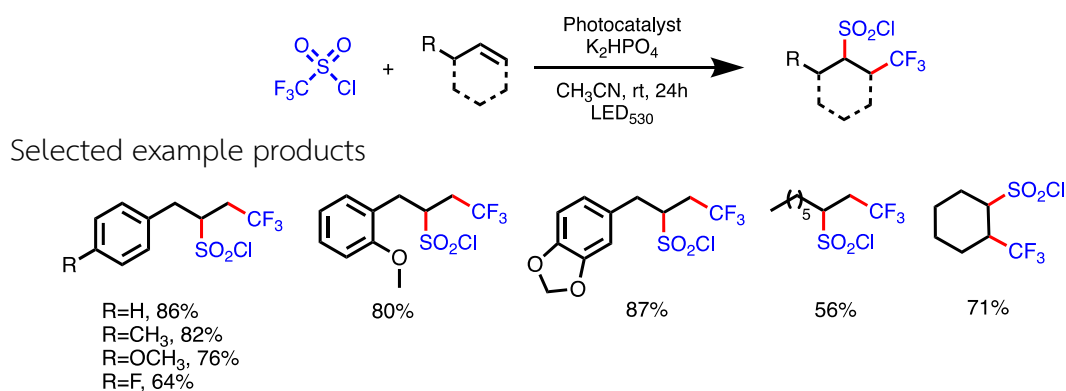


Figure 1.16 Photo-mediated trifluoromethylsulfonylation of the unactivated alkenes.

Recently, air-stable Cu(II) complexes with phenanthroline ligands have also been demonstrated to be robust and effective photocatalyst precursors for various ATRA processes based on the facile visible-light-induced homolysis (VLIH) that Cu(II)-halide complexes undergo upon irradiation to form the active Cu(I) species (Figure 1.17) [78, 79].

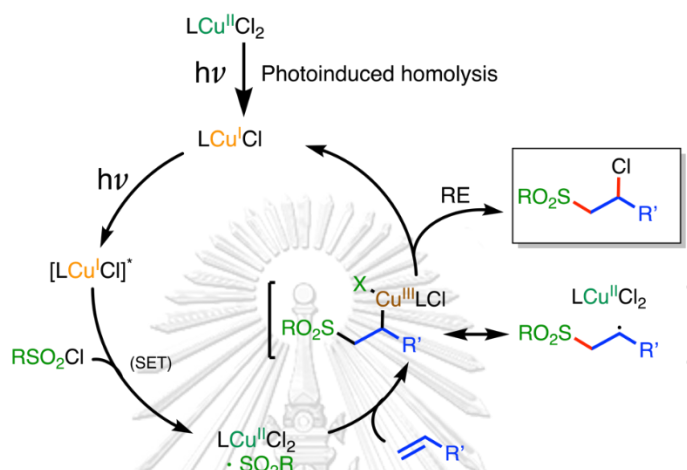
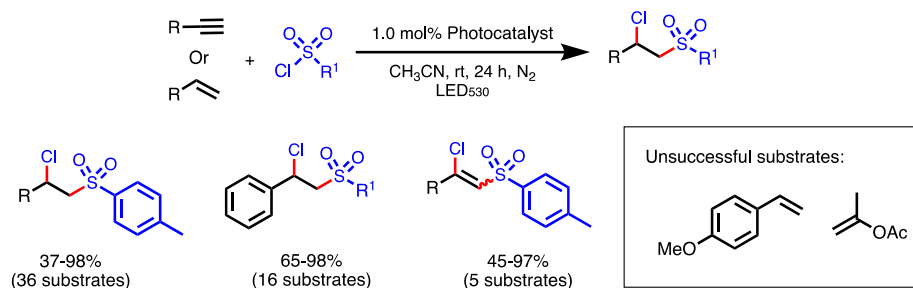


Figure 1.17 Simplified mechanism for Cu(II) catalyzed chlorosulfonylation via initial visible-light-induced homolysis (VLIH) of Cu-Cl bond.

In 2018, $[Cu(\mathbf{dap})_2]Cl$ along with an air-stable $[Cu(\mathbf{dap})Cl_2]$ was first introduced as robust and effective photocatalyst precursors, which most likely act as precursors for catalytically active Cu(I) species for chlorosulfonylation of activated and unactivated olefins (Figure 1.18) [78]. The addition smoothly occurs without extrusion of SO_2 . Nevertheless, these complexes tend to suffer from degradation, especially in the presence of trace acids, which is most likely caused by ligand exchange followed by protonation.



Photocatalyst =

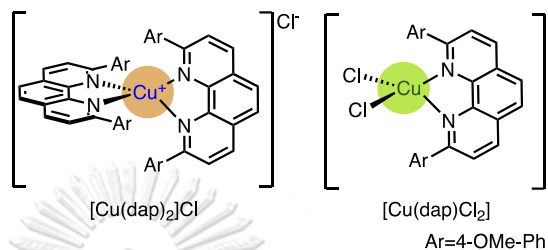
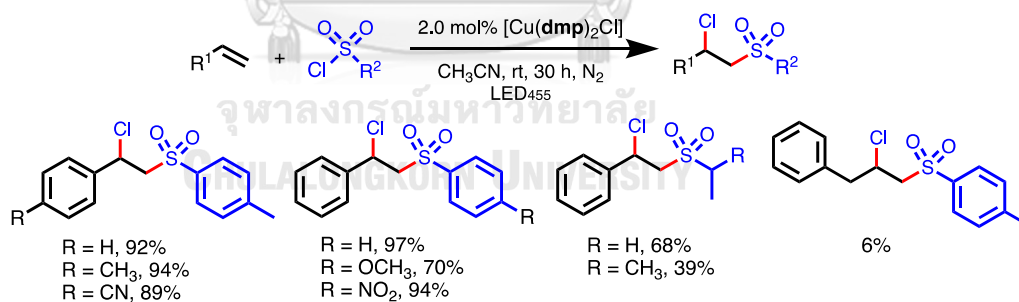


Figure 1.18 Photo-mediated copper-catalyzed chlorosulfonylation using [Cu(dap)₂]Cl and [Cu(dap)Cl₂] as photocatalysts.

Later on, copper complexes with 2,9-dimethyl-1,10-phenanthroline (**dmp**), [Cu(dmp)₂]Cl, and [Cu(dmp)₂Cl]Cl, were also reported as robust and economic alternative ligands for ATRA reactions to provide a various of 1,2-difunctionalized alkenes (Figure 1.19) [79].



Photocatalyst =

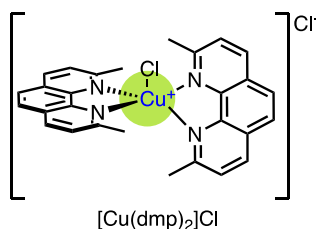


Figure 1.19 Photo-mediated chlorosulfonylation using [Cu(dmp)₂Cl]Cl as a photocatalyst.

During the same period, Hu and co-workers also suggested that the heteroleptic Cu(I) complex efficiently catalyzed this reaction with the high diastereoselective addition of alkyne substrates (Figure 1.20). Even though the reaction efficiently proceeds with a broad substrate scope with good functional group tolerance for substituted styrene, many highly photoactive compounds were reported as unsuccessful olefins as mostly resulted from competitive polymerization. As same as the deactivated alkenes, the incorporated electron-withdrawing group, and internal olefins were found less effective under the optimized condition [80].

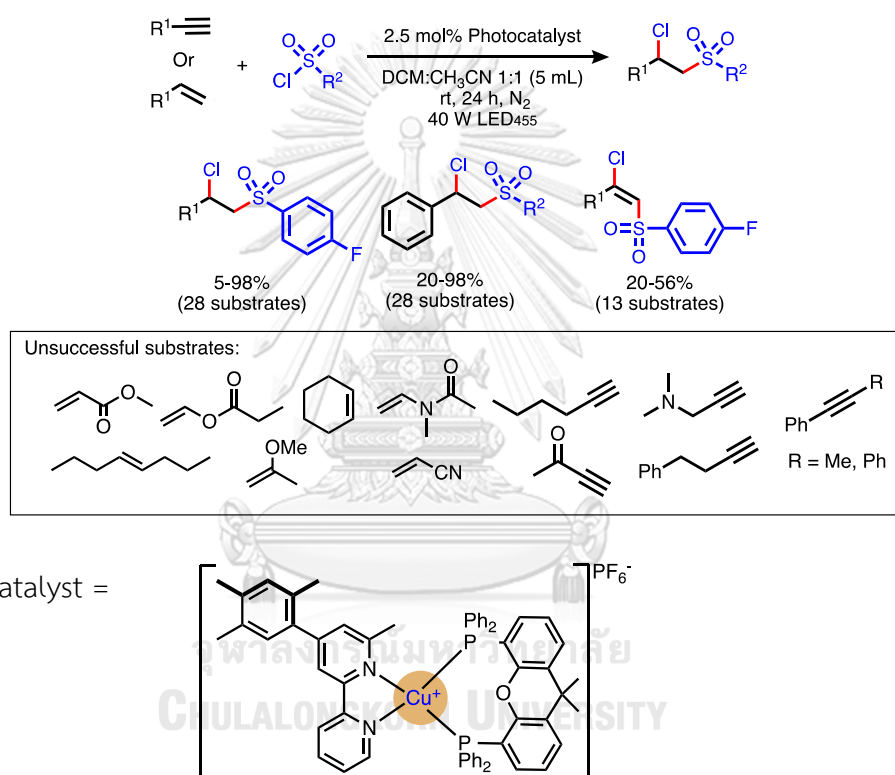


Figure 1.20 Photo-mediated copper-catalyzed chlorosulfonylation.

Besides the bidentate ligands, tri- and tetradentate ligands have found less attention as constituents of metal photocatalysts, although multidentate coordination should rigidify the complex and this way extend excited-state lifetimes being essential for efficient intramolecular SET processes. Intrigued by the excellent results of Pintauer et al, who showed that a Cu(II) complex of tris(2-pyridylmethyl)amine (TPMA) in the presence of AIBN or ascorbic acid as a reducing agent is effective in the thermal or UV-mediated coupling of perhaloalkanes and

alkenes [41, 43, 46, 53, 81, 82], the development of tripyridyl methylamine core further aiming at photocatalysts that can operate under visible light conditions are set out (Figure 1.21). Replacing some of the pyridinylmethyl groups in **TPMA** with quinoline rings, which have higher absorptivity at a longer wavelength and electron-accepting ability, may be used to form copper complexes capable of photo catalyzed ATRA reaction.

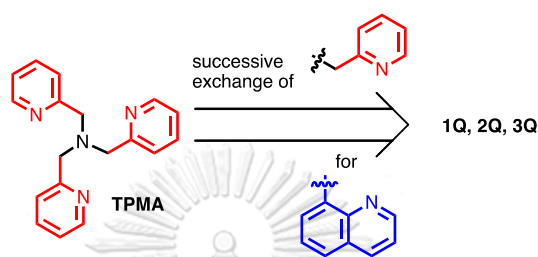


Figure 1.21 Design principle of ligands 1Q-3Q.

1.6 Objectives and scopes

This research work aims to develop a new photocatalyst for ATRA reactions from Cu(II) complexes of quinoline derivatives. The structures of quinoline derivatives investigated in this work are presented in Figure 1.22. The ATRA reactions being investigated are haloalkylation and chlorosulfonylation of olefins for C-C bond and C-S bond formation, respectively.

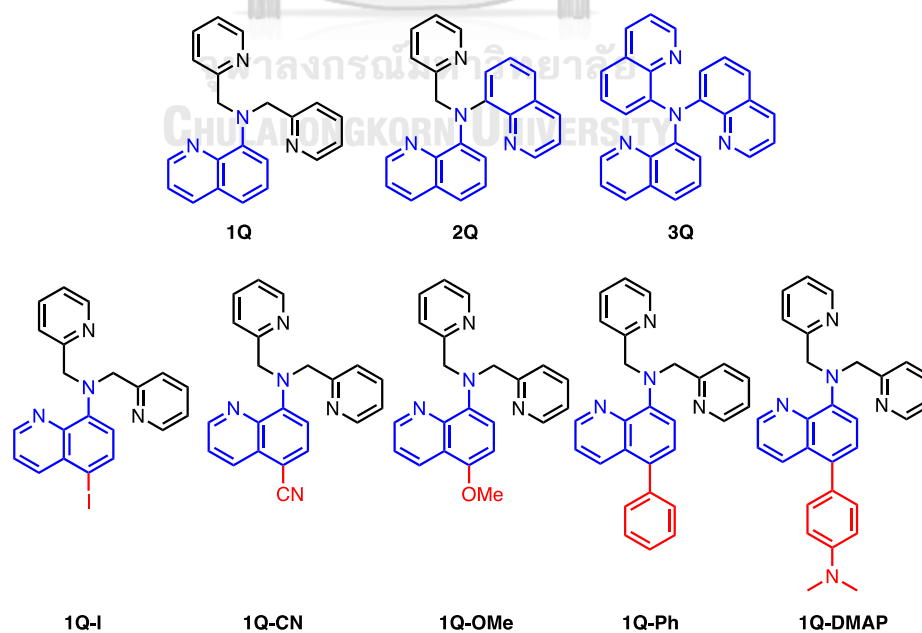


Figure 1.22 Structure of quinoline derivatives used in this study.

CHAPTER II EXPERIMENT

2.1 Reagents and materials

All commercial chemical materials were used without further purification and weight was calculated based on the purity mentioned in the container. The weight of compounds was calculated based on the purity mentioned on the container. 8-Aminoquinoline, 2-(chloromethyl)pyridine hydrochloride and alkyl halides were purchased from TCI Tokyo Chemical Industry (Japan). Cu(II) chloride, Cu(II) bromide, and Cu(I) Chloride were purchased from Merck (Germany). Tris(2-pyridylmethyl) amine (TPMA) was purchased from Sigma-Aldrich and TCI Tokyo Chemical Industry (Japan). Alkenes were purchased from Sigma Aldrich, Merck (Germany), Acros, or TCI Tokyo Chemical Industry (Japan). Alkyl halides were purchased from TCI Tokyo Chemical Industry (Japan). Chlorosulfonylating agents were purchased from Sigma-Aldrich. AIBN was purchased from Chemieleva Pharmaceutical (China). Potassium iodide, potassium carbonate, and other reducing agents. All deuterated solvents for NMR Yield calculations were purchased from Cambridge Isotope Laboratories (USA). Other solvents for the synthesized reaction are analytical grades from TCI Tokyo Chemical Industry (Japan). The reactions were monitored by TLC and visualized by a dual short (254 nm) / long (366 nm) wavelength UV lamp. Column chromatography was run on Merck silica oxide 60 (70–230 mesh) (for the column chromatography of addition products) or Merck aluminium oxide 90 active neutral (for the column chromatography of ligands). Solvents used for extraction and chromatography such as dichloromethane, hexane, and ethyl acetate were commercial grade and distilled before use. DI water was used in all aqueous experiments. Quinoline derivatives were synthesized according to a modified literature procedure. Cu(II) complexes were synthesized according to previously published literature.

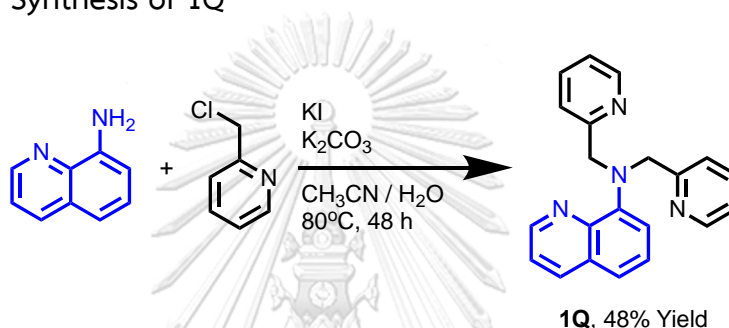
2.2 Analytical instruments

^1H NMR, ^{19}F NMR, ^{13}C NMR, and 2D-NMR spectra were obtained using a Bruker advance 300 MHz, 400 MHz, and 600 MHz spectrometer, Varian 400 MHz spectrometer, or Jeol 500 MHz with chemical shifts given in (ppm) relative to residual solvent peak (CH_3CN at 1.96 ppm, CH_3OH at 3.31 ppm, $(\text{CH}_3)_2\text{SO}$ at 2.50 ppm, CHCl_3 at 7.26 ppm for ^1H NMR, and 77.2 ppm for ^{13}C NMR. MestReNova and topspin software were used to investigate NMR spectra. Coupling constants (J) were given in Hertz (Hz). Elemental analyses for C, H, and N were recorded at Department of Chemistry, Faculty of Science, Mahidol University on Perkin-Elmer 2400 Series CHNS/O Elemental Analyzer. Electrospray mass spectra (ESI) were recorded at Department of Chemistry, Faculty of Science, Chulalongkorn University on micrOTOF-Q II™ ESI-Qq-TOF mass spectrometer and the Central Analytical Laboratory at the Department of Chemistry of the University of Regensburg on Agilent Technologies 6540 UHD Accurate-Mass Q-TOF LC/MS. UV-vis spectra were obtained using HP 8453 UV-visible spectrometer in 1.00 cm path-length quartz cuvettes at room temperature. The molar absorption coefficient (ϵ) of ligands and complexes were determined from the solutions with at least 5 different concentrations diluted from stock solutions. Cyclic voltammetry experiments were conducted on uAutolab III potentiostat using a standard three-electrode system: glassy carbon working electrode, Ag/AgCl reference electrode, and Pt-wire auxiliary electrode. The EPR spectra were recorded by Scientific and technological Research Equipment Centre, STREC, Chulalongkorn University using EMXmicro -Bruker spectrometer operating at X band (9.84 GHz). Crystallography structures of copper complexes; X-ray diffraction data were performed by Materials and Textiles Technology, Faculty of Science and Technology, Thammasat University using a Bruker D8 VENTURE CMOS PHOTON II with graphite monochromated $\text{Cu-K}\alpha$ ($\lambda = 1.54178 \text{ \AA}$) radiation at 100 K or a Bruker D8 QUEST CMOS PHOTON II with graphite monochromated $\text{Mo-K}\alpha$ ($\lambda = 0.71073 \text{ \AA}$) radiation at 296 K. Crystallography structures of chlorosulfonylation products, X-ray crystallographic analysis was performed by the Central Analytic Department of the University of Regensburg using an Agilent Technologies SuperNova, an Agilent

Technologies Gemini R Ultra, an Agilent GV 50 or a Rigaku GV 50 diffractometer. The irradiation for ATRA was done using an in-house made photoreactor equipped with white LEDs or Philips Helix 32 W white CFL, E27 6500K cool daylight, 2080 lumen 70 lm/W. The irradiation for chlorosulfonylation was done using blue light-emitting diodes CREE XP or Oslon SSL (2.5 W electric power @700 mA, $\lambda_{\max} = 530$ nm) or Philips Helix 32 W white CFL, E27 6500K cool daylight, 2080 lumen 70 lm/W.

2.3 Synthetic procedures for quinoline derivatives

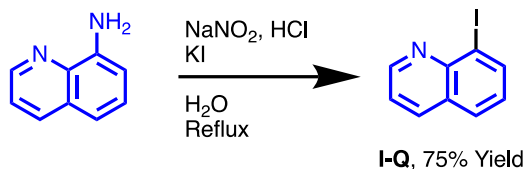
2.3.1 Synthesis of 1Q



A *N,N*-bis(pyridin-2-ylmethyl)quinolin-8-amine, **1Q** was synthesized applying from the reported procedure [83]. A mixture of 8-aminoquinoline (1.44 g, 10.0 mmol), 2-(chloromethyl)pyridine hydrochloride (6.56 g, 40.0 mmol), K_2CO_3 (3.46 g, 25.0 mmol), and KI (330 mg, 2.00 mmol) in acetonitrile and distilled water (4:1, 50.0 mL) was refluxed for 48 hours. A brown crude was extracted with dichloromethane and brine 3 times. The product was purified by column chromatography on alumina gel (hexane:EtOAc = 8:2, $R_f = 0.26$). The product was obtained as a clear crystal after recrystallization (1.56 g, 48% Yield). 1H -NMR (400 MHz, $DMSO-d_6$): δ 8.84 (dd, 1H), 8.47 (d, $J = 4.7$ Hz, 2H), 8.28 (dd, $J = 8.2, 2.0$ Hz, 1H), 7.70-7.62 (m, 2H), 7.51 (d, $J = 7.6$ Hz, 2H), 7.51 (dd, $J = 8.2, 4.0$ Hz, 1H), 7.40 (d, $J = 8.1$ Hz, 1H), 7.30 (dd, $J = 8.1, 7.6$ Hz, 1H), 7.24-7.16 (m, 2H), 7.04 (d, $J = 7.6$ Hz, 1H) 4.89 (s, 4H) ppm. ^{13}C NMR (101 MHz, $DMSO-d_6$, 298K): δ 158.86, 148.80, 148.01, 147.30, 142.59, 140.03, 137.19, 136.47, 130.23, 123.04, 122.01, 121.88, 118.51, 87.00, 58.73. HRMS (ESI-TOF) m/z : $[M+H]^+$ Calc. for $C_{21}H_{19}N_4$ 327.1604; Found 327.1608. Anal. Calc. for $C_{21}H_{18}N_4$: C, 77.28; H, 5.56; N, 17.17; Found C, 77.02; H, 5.18; N, 17.30.

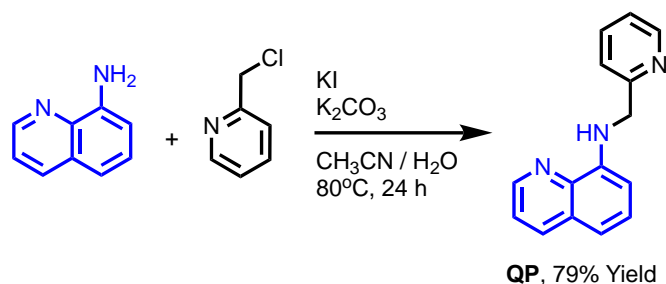
2.3.2 Synthesis of 2Q

2.3.2.1 Synthesis of I-Q



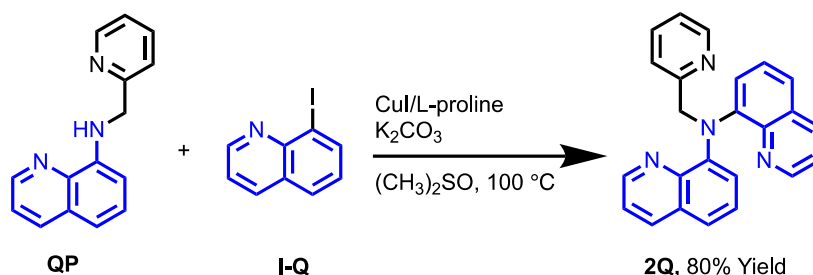
An 8-iodoquinoline, **I-Q** was synthesized according to the reported procedure. A mixture of 8-aminoquinoline (500 mg, 3.50 mmol) and water (2.50 mL) was heated and stirred until all starting material dissolved. The mixture was cooled in an ice bath and added concentrated hydrochloric (2.50 mL) to form a red solution. An ice-cool solution of sodium nitrite (390 mg, 5.70 mmol) in water (2.50 mL) was slowly dropped into the solution and the solution changed to a reddish transparent solution. The solution of potassium iodide (965 mg, 5.80 mmol) in water (1.50 mL) was added. The solution turns dark brown with black precipitate. Then the solution was heated at 80 °C for 10 minutes and left at room temperature for 1 hour. The golden-brown portion was obtained. The solution was neutralized by adding of sodium hydroxide solution obtained a black precipitate. The solution was filtered, and the solution part was extracted with dichloromethane and water. The product was purified by column chromatography on alumina gel (hexane:EtOAc = 9.5:0.5, R_f = 0.71). The product was obtained as a yellow to a brown oil (664.0 mg, 75% Yield). $^1\text{H-NMR}$ (400 MHz, $\text{DMSO-}d_6$): δ 8.97 (d, J = 7.7 Hz, 1H), 8.36 (m, 2H), 8.00 (d, J = 7.8 Hz, 1H), 7.59 (dd, J = 7.7, 3.8 Hz, 1H), 7.36 (dd, J = 7.3, 7.8 Hz, 1H) ppm. $^{13}\text{C NMR}$ (101 MHz, $\text{DMSO-}d_6$, 298K): δ 151.73, 146.25, 139.86, 136.97, 129.12, 128.58, 128.03, 122.39, 103.66. HRMS (ESI-TOF) m/z : $[\text{M}+\text{H}]^+$ Calc. for $\text{C}_9\text{H}_7\text{IN}$ 255.9618; Found 255.9676.

2.3.2.2 Synthesis of QP



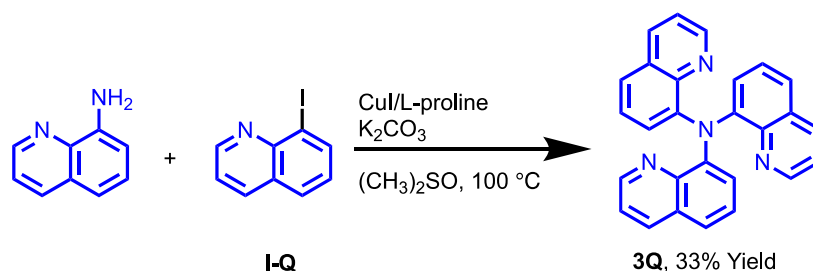
A *N*-(pyridin-2-ylmethyl)quinolin-8-amine, **QP** was synthesized applying from the reported procedure [83]. A mixture of 8-aminoquinoline (1.44 g, 10.0 mmol), 2-(chloromethyl)pyridine hydrochloride (1.64 g, 10.0 mmol), K_2CO_3 (6.91 g, 50.0 mmol) and KI (0.17 g, 1.00 mmol) in 50.0 mL in acetonitrile and distilled water was heat at 80.0 °C for 24 hours. A brown crude was evaporated and extracted with dichloromethane and water 3 times. The organic phase was dried over magnesium sulphate, filtrate, and evaporated to dryness by rotary evaporator. The product was purified by column chromatography on alumina gel (hexane:EtOAc = 9.5:0.5, R_f = 0.46). The product was obtained as a yellow oil (1.86 g, 7.91 mmol, 79% Yield). 1H NMR (400 MHz, CD_3CN) δ 8.78 (dd, J = 4.2, 1.6 Hz, 1H), 8.61 (dd, J = 4.6, 1.6 Hz, 1H), 8.15 (dd, J = 8.3, 1.7 Hz, 1H), 7.69 (td, J = 7.6, 1.8 Hz, 1H), 7.46 (dd, J = 8.3, 4.2 Hz, 1H), 7.40 – 7.33 (m, 2H), 7.24 (dd, J = 7.5, 4.9 Hz, 1H), 7.10 (d, J = 8.2 Hz, 1H), 6.66 (d, J = 7.7 Hz, 1H), 4.65 (s, 2H). ^{13}C NMR (101 MHz, CD_3CN) δ 158.61, 149.09, 147.22, 144.49, 136.62, 135.91, 128.68, 127.73, 122.13, 121.67, 121.45, 117.28, 114.02, 105.03, 48.19. HRMS (ESI-TOF) m/z : $[M+H]^+$ Calc. for $C_{15}H_{14}N_3$ 236.1182; Found 236.1293

2.3.2.3 Synthesis of 2Q



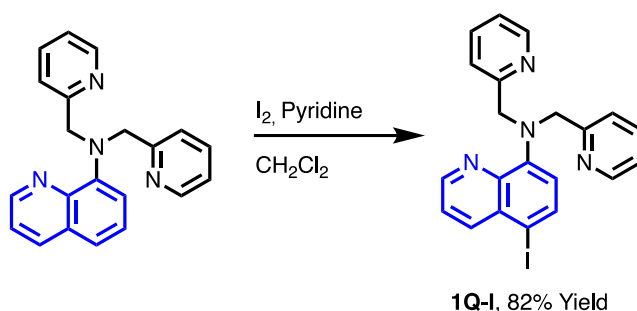
A *N*-(pyridin-2-ylmethyl)-*N*-(quinolin-8-yl)quinolin-8-amine, **2Q** was synthesized according to Ullman-type aryl-amination [84]. A mixture of *N*-(pyridin-2-ylmethyl)quinolin-8-amine (1.18 g, 5.00 mmol), 8-iodoquinoline (1.40 g, 5.50 mmol), K_2CO_3 (1.38 g, 10.0 mmol), CuI (1.00 mg, 5.00 μmol) and L-proline (1.00 mg, 10.0 μmol) in dimethyl sulfoxide was stirred at 100 $^\circ\text{C}$ for 24 hours. The dark brown crude was extracted with ethyl acetate and water for a few times. The organic phase was dried over magnesium sulphate, filtrate, and evaporated to dryness by rotary evaporator. The product was purified by column chromatography on alumina (hexane:EtOAc = 7:3, R_f = 0.64). The bright yellow solid was obtained after recrystallization (1.45 g, 80% Yield). ^1H NMR (400 MHz, $(\text{CH}_3)_2\text{SO}$, 298K): δ 8.54 (d, J = 3.4 Hz, 2H), 8.46 (d, J = 4.4 Hz, 1H), 8.26 (d, J = 7.8 Hz, 2H), 7.94 (d, J = 7.8 Hz, 1H), 7.58 (t, J = 7.8 Hz, 1H), 7.53 (d, J = 7.9 Hz, 2H), 7.39 (dd, J = 7.8, 3.4 Hz, 2H), 7.34 (t, J = 7.9 Hz, 2H), 7.21 (d, J = 7.9 Hz, 2H), 7.17 – 7.11 (m, 1H), 5.60 (s, 2H). ^{13}C NMR (101 MHz, $(\text{CH}_3)_2\text{SO}$, 298K): δ 160.00, 148.37, 148.01, 146.94, 142.40, 136.25, 136.17, 129.38, 126.47, 122.09, 121.95, 121.76, 121.32, 120.99, 59.67. HRMS (ESI-TOF) m/z : $[\text{M}+\text{H}]^+$ Calc. for $\text{C}_{24}\text{H}_{19}\text{N}_4$ 363.1604; Found 363.1614. Anal. Calc. for $\text{C}_{24}\text{H}_{18}\text{N}_4$: C, 79.54; H, 5.01; N, 15.46; Found C, 78.22; H, 4.39; N, 15.84.

2.3.3 Synthesis of 3Q



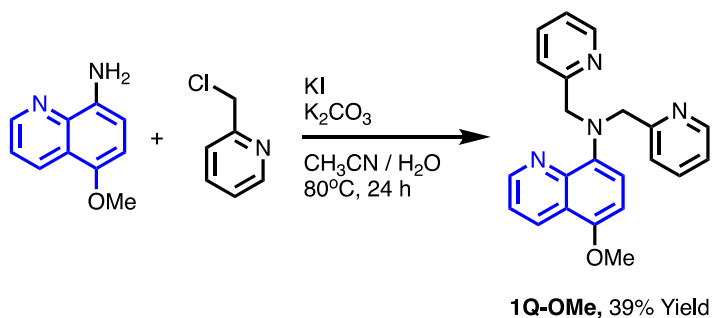
A tri(quinolin-8-yl)amine, **3Q** was synthesized according to reported Ullman-type aryl-amination [84]. A mixture of 8-aminoquinoline (144 mg, 1.00 mmol), 8-iodoquinoline (510 mg, 2.00 mmol), CuI (38.1 mg, 200 μmol), L-proline (46.2 mg, 400 μmol) and K_2CO_3 (553 mg, 4.00 mmol) in dimethyl sulfoxide was stirred at 100 $^\circ\text{C}$ overnight. The dark brown crude was extracted with ethyl acetate and water for several times and dried with magnesium sulphate. The product was purified by column chromatography on alumina (hexane:EtOAc = 1:1, R_f = 0.54). The product was recrystallized in methanol to produce a yellow solid (132 mg, 33% Yield). ^1H NMR (400 MHz, $(\text{CH}_3)_2\text{SO}$, 298K): δ 8.37 (d, J = 3.9 Hz, 3H), 8.27 (d, J = 8.2 Hz, 3H), 7.61 (d, J = 8.1 Hz, 3H), 7.38 – 7.29 (m, 6H), 7.00 (d, J = 7.5 Hz, 3H). ^{13}C NMR (101 MHz, $(\text{CH}_3)_2\text{SO}$, 298K): δ 148.19, 147.74, 142.74, 135.96, 129.32, 126.51, 124.28, 122.77, 120.88. HRMS (ESI-TOF) m/z : $[\text{M}+\text{H}]^+$ Calc. for $\text{C}_{27}\text{H}_{19}\text{N}_4$ 399.1604; Found 399.1680. Anal. Calc. for $\text{C}_{24}\text{H}_{18}\text{N}_4$: C, 81.39; H, 4.55; N, 14.06; Found: C, 81.15; H, 4.20; N, 14.56.

2.3.4 Synthesis of 1Q-I



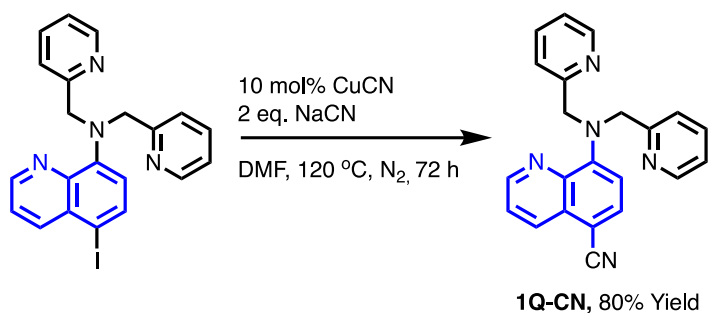
A 5-iodo-*N,N*-bis(pyridin-2-ylmethyl)quinolin-8-amine, **1Q-I** was synthesized via iodination of **1Q**. The **1Q** (233 mg, 700 μmol) was dissolved in pyridine (5.00 mL) and dichloromethane (5.00 mL) and cool the solution to 0 °C. Iodine (630 mg, 2.50 mmol) was added to the solution. The solution turns to a dark brown color. The solution was removed from ice bath after 1 hour and added a supplementary portion of iodine (270 mg, 1.10 mmol). Then the solution was stirred at room temperature for 1 hour. A saturated solution of sodium thiosulfate was gradually added to the solution until the brown color disappears. Crude was extracted with dichloromethane and water 3 times. The product was purified by column chromatography on alumina gel (hexane:EtOAc = 7:3, R_f = 0.66). The product was recrystallized in dichloromethane and hexane receiving a light-yellow solid (260.0 mg, 82% yield). $^1\text{H-NMR}$ (400 MHz, $\text{DMSO-}d_6$): δ 8.80 (dd, J = 4.1, 1.2 Hz, 1H), 8.47 (d, J = 4.5 Hz, 2H), 8.27 (dd, J = 8.5, 1.2 Hz, 1H), 7.86 (d, J = 8.3 Hz, 1H), 7.67 (td, J = 7.7, 1.4 Hz, 2H), 7.61 (dd, J = 8.5, 4.1 Hz, 1H), 7.50 (d, J = 7.7 Hz, 2H), 7.26 – 7.14 (m, 2H), 6.84 (d, J = 8.3 Hz, 1H), 4.91 (s, 4H) ppm. $^{13}\text{C NMR}$ (101 MHz, $\text{DMSO-}d_6$, 298K): δ 158.86, 148.80, 148.01, 147.30, 142.59, 140.03, 137.19, 136.47, 130.23, 123.04, 122.01, 121.88, 118.51, 87.00, 58.73. HRMS (ESI-TOF) m/z : $[\text{M}+\text{H}]^+$ Calc. for $\text{C}_{21}\text{H}_{18}\text{IN}_4$ 453.0571; Found 453.0578.

2.3.5 Synthesis of 1Q-OMe



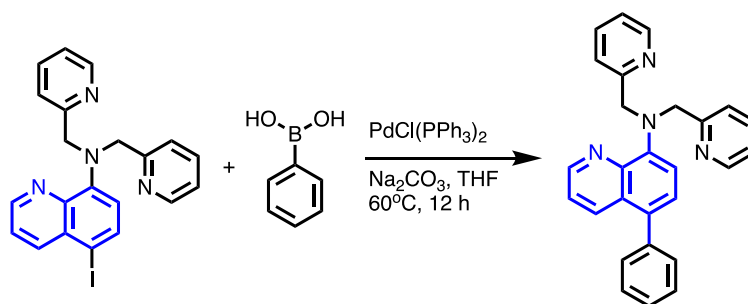
A 5-methoxy-*N,N*-bis(pyridin-2-ylmethyl)quinolin-8-amine, **1Q-OMe** was synthesized applying from the reported procedure [83]. A mixture of 5-methoxy-8-aminoquinoline (432 mg, 2.50 mmol), 2-(chloromethyl) pyridine hydrochloride (1.55 g, 9.50 mmol), KI (41.0 mg, 2.00 mmol) and K_2CO_3 (498 mg, 3.60 mmol) in 50.0 mL acetonitrile was refluxed for 48 hours. A brown crude was extracted with ethyl acetate and brine for 3 times. The product was purified by column chromatography on alumina gel (hexane:EtOAc = 8:2, R_f = 0.26) Yellow solid was obtained as a product (345.0 mg, 39% Yield). 1H -NMR (400 MHz, $DMSO-d_6$) δ 8.94 (dd, J = 4.0, 1.6 Hz, 1H), 8.49 (dd, J = 8.4, 1.6 Hz, 1H), 8.45 (d, J = 4.7 Hz, 2H), 7.65 (td, J = 7.7, 1.5 Hz, 2H), 7.57 – 7.51 (m, 3H), 7.20 – 7.16 (m, 2H), 7.01 (d, J = 8.5 Hz, 1H), 6.78 (d, J = 8.5 Hz, 1H), 4.71 (s, 4H), 3.86 (s, 3H) ppm. ^{13}C NMR (101 MHz, $DMSO-d_6$) δ 159.42, 149.37, 148.63, 148.59, 143.10, 139.27, 136.32, 130.54, 122.10, 121.91, 121.09, 120.47, 118.85, 104.42, 59.04, 55.65. HRMS (ESI-TOF) m/z : $[M+H]^+$ Calc. for $C_{22}H_{21}N_4O$ 357.1710; Found 357.1717.

2.3.6 Synthesis of 1Q-CN



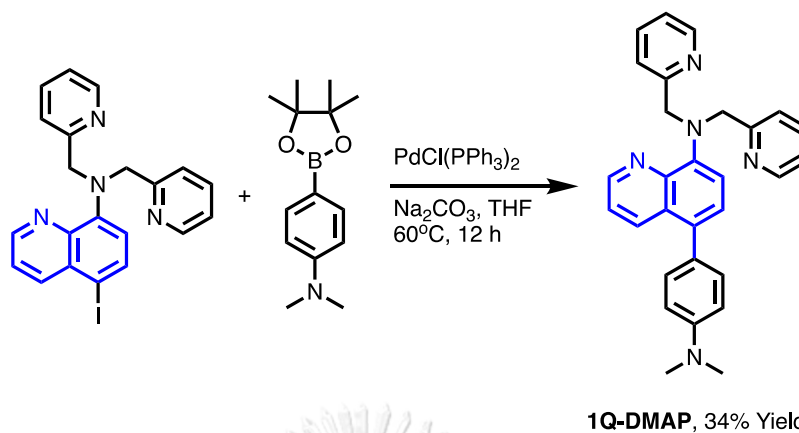
A 8-(bis(pyridin-2-ylmethyl))quinoline-5-carbonitrile amine, **1Q-CN** was synthesized via the Rosenmund-Von Braun reaction. The **1Q-I** (678 mg, 1.4 mmol), CuCN (13.0 mg 140 μ mol) NaCN (141 mg, 2.90 mmol) were dissolved in dried dimethylformamide, DMF. The reaction was refluxed under nitrogen atmosphere for 72 hours. The reaction was diluted with ammonium chloride solution and extracted with ethyl acetate. The product was purified by column chromatography on alumina gel (hexane:EtOAc = 7:3, R_f = 0.31) A product was obtained as a yellow solid (404 mg, 80% yield). ^1H NMR (400 MHz, DMSO- d_6) δ 8.76 (d, J = 1.4 Hz, 1H), 8.50 (d, J = 4.7 Hz, 2H), 8.38 (d, J = 8.4 Hz, 1H), 7.88 (d, J = 8.5 Hz, 1H), 7.78 – 7.63 (m, 3H), 7.45 (d, J = 7.8 Hz, 2H), 7.24 (t, J = 4.7 Hz, 2H), 6.98 (d, J = 8.5 Hz, 1H), 5.20 (s, 4H) ppm. ^{13}C NMR (101 MHz, DMSO- d_6) δ 158.74, 151.22, 149.52, 147.90, 140.11, 137.14, 134.59, 133.56, 129.71, 123.87, 122.63, 122.16, 118.44, 113.68, 96.93, 59.36. HRMS (ESI-TOF) m/z : $[\text{M}+\text{H}]^+$ Calc. for $\text{C}_{22}\text{H}_{18}\text{N}_5$ 352.1567; Found 352.1557.

2.3.7 Synthesis of 1Q-Ph

**1Q-Ph**, 37% Yield

A 5-phenyl-*N,N*-bis(pyridin-2-ylmethyl)quinolin-8-amine, **1Q-Ph** was synthesized via the Suzuki-Miyaura reaction. The 5-iodo-*N,N*-bis(pyridin-2-ylmethyl)quinolin-8-amine, **1Q-I** (680 mg, 1.50 mmol) and phenylboronic acid (220 mg, 1.80 mmol) were dissolved in the mixture of H₂O and THF. The reaction was bubbled with N₂ gas for 15 minutes. [PdCl₂(PPh₃)₂] (53.0 mg, 75.0 μmol) and Na₂CO₃ (239 mg, 2.30 mmol) were added to the reaction mixture. The reaction was stirred as 60 °C for 12 h. The reaction was diluted with ammonium chloride solution and extracted with dichloromethane. Organic phase was dried with sodium sulfate and purified by column chromatography on alumina gel (hexane:EtOAc = 7:3, R_f = 0.58). The off-yellow solid was obtained after recrystallization (224 mg, 37% Yield). ¹H NMR (400 MHz, DMSO-*d*₆) δ 8.84 (dd, *J* = 4.0, 1.7 Hz, 1H), 8.48 (ddd, *J* = 4.9, 1.8, 0.9 Hz, 2H), 8.16 (dd, *J* = 8.6, 1.8 Hz, 1H), 7.70 (td, *J* = 7.6, 1.8 Hz, 2H), 7.59 (dt, *J* = 7.9, 1.2 Hz, 2H), 7.51 – 7.45 (m, 3H), 7.43 – 7.36 (m, 3H), 7.27 (d, *J* = 7.9 Hz, 1H), 7.21 (ddd, *J* = 7.5, 4.8, 1.2 Hz, 2H), 7.12 (d, *J* = 8.0 Hz, 1H), 4.91 (s, 4H). ¹³C NMR (101 MHz, DMSO-*d*₆) δ 159.75, 149.27, 147.85, 146.23, 142.37, 139.51, 137.02, 134.55, 132.11, 130.33, 129.02, 127.68, 127.65, 127.60, 122.53, 122.43, 121.84, 116.94, 59.23. HRMS (ESI-TOF) *m/z*: [M+H]⁺ Calc. for C₂₇H₂₃N₄ 403.1917; Found 403.1919.

2.3.8 Synthesis of 1Q-DMAP



A 5-(4-(dimethylamino)phenyl)-*N,N*-bis(pyridin-2-ylmethyl)quinolin-8-amine, **1Q-DMAP** was synthesized via the Suzuki-Miyaura reaction. The 5-iodo-*N,N*-bis(pyridin-2-ylmethyl)quinolin-8-amine, **1Q-I** (800 mg, 1.80 mmol) and 4-(*N,N*-dimethylamino)phenyl boronic acid, pinacol ester (525 g, 2.10 mmol) were dissolved in the mixture of H₂O and THF. The reaction was bubbled with N₂ gas for 15 minutes. [PdCl₂(PPh₃)₂] (62.0 mg, 0.10 mmol) and Na₂CO₃ (281 mg, 2.70 mmol) were added to the reaction mixture. The reaction was stirred as 60 °C for 12 hours. The reaction was diluted with ammonium chloride solution and extracted with dichloromethane. Organic phase was dried with sodium sulfate, filtrate, and evaporate to dryness. The crude was purified by column chromatography on alumina gel (hexane:EtOAc = 7:3, R_f = 0.48). The yellow solid was obtained after recrystallization (269.0 mg, 34% yield). ¹H NMR (400 MHz, DMSO-*d*₆) δ 8.86 (d, *J* = 2.4 Hz, 1H), 8.49 (d, *J* = 4.4 Hz, 2H), 8.26 (d, *J* = 8.6 Hz, 1H), 7.72 (t, *J* = 7.5 Hz, 2H), 7.62 (d, *J* = 7.7 Hz, 2H), 7.49 (dd, *J* = 8.5, 4.0 Hz, 1H), 7.23 (dd, *J* = 7.9, 3.6 Hz, 5H), 7.12 (d, *J* = 8.0 Hz, 1H), 6.84 (d, *J* = 8.6 Hz, 2H), 4.89 (s, 4H), 2.96 (s, 6H) ppm. ¹³C NMR (101 MHz, DMSO-*d*₆, 298K): δ 159.88, 150.04, 149.23, 147.75, 145.43, 136.95, 134.88, 132.86, 130.87, 127.95, 127.00, 122.46, 121.46, 117.45, 112.85, 59.28, 55.36, 40.69, 40.59, 40.49, 40.28, 40.07, 39.86, 39.65, 39.44. HRMS (ESI-TOF) *m/z*: [M+H]⁺ Calc. for C₂₉H₂₈N₅ 446.2339; Found 446.2399.

2.4 Synthetic procedure for some isolated copper complexes

2.4.1 Synthesis of $[\text{Cu}^{\text{II}}(\mathbf{1Q})\text{Cl}]^+$

The copper complex with ligand **1Q** was synthesized using a modification of the procedure reported by Tomislav group [41]. A round-bottom flask (25.0 mL) equipped with a magnetic stirring bar was charged with **1Q** (326 mg, 1.00 mmol, 1.00 equiv) and dissolved with chloroform (5.00 mL). A dissolved copper(II) chloride (134 mg, 1.00 mmol, 1.00 equiv) in chloroform (5.00 mL) was slowly added and the mixture was stirred at room temperature for 10 minutes. The complex was precipitated upon the addition of hexane (50.0 mL). The complex was collected by vacuum filtration using a Buchner funnel. The complex was washed twice with cold hexane and dried under a vacuum. HRMS (ESI-TOF) m/z : $[\text{M}]^+$ Calc. for $[\text{Cu}^{\text{II}}(\mathbf{1Q})\text{Cl}]^+$ 424.0511; Found 424.0637. $E_{1/2 \text{ SCE}} = -0.29$, $\lambda_{\text{max}} = 291$ and ϵ [m^2/mol] = 5457.

2.4.2 Synthesis of $[\text{Cu}^{\text{II}}(\mathbf{2Q})\text{Cl}]^+$

A round-bottom flask (25.0 mL) equipped with a magnetic stirring bar was charge with **2Q** (362 mg, 1.00 mmol, 1.00 equiv) and dissolved with chloroform (5.00 mL). A dissolved copper(II) chloride (134 mg, 1.00 mmol, 1.00 equiv) in chloroform (5.00 mL) was slowly added and the mixture was stirred at room temperature for 10 minutes. The complex was precipitated upon the addition of hexane (50.0 mL). The complex was collected by vacuum filtration using a Buchner funnel. The green solid was washed twice with cold hexane and dried under vacuum. The complex was washed twice with cold hexane and dried under a vacuum. HRMS (ESI-TOF) m/z : $[\text{M}]^+$ Calc. for $[\text{Cu}^{\text{II}}(\mathbf{2Q})\text{Cl}]^+$ 460.0511; Found 460.0519. $E_{1/2 \text{ SCE}} = -0.17$, $\lambda_{\text{max}} = 292$ and ϵ [m^2/mol] = 6704.

2.4.3 Synthesis of $[\text{Cu}^{\text{II}}(\mathbf{3Q})\text{Cl}]^+$

A round-bottom flask (25.0 mL) equipped with a magnetic stirring bar was charge with **3Q** (398 mg, 1.00 mmol, 1.00 equiv) and dissolved with chloroform (5.00 mL). A dissolved copper(II) chloride (134 mg, 1.00 mmol, 1.00 equiv) in chloroform (5.00 mL) was slowly added and the mixture was stirred at room temperature for 10 minutes. The complex was precipitated upon the addition of hexane (50.0 mL). The complex was collected by vacuum filtration using a Buchner funnel. The green solid

was washed twice with cold hexane and dried under a vacuum. The complex was washed twice with cold hexane and dried under vacuum. HRMS (ESI-TOF) m/z : $[M]^+$ Calc. for $[Cu^{II}(3Q)Cl]^+$ 496.0511; Found 496.0553. $E_{1/2\text{ SCE}} = -0.03$, $\lambda_{\text{max}} = 294$ and ϵ $[m^2/mol] = 7321$.

2.5 Photophysical study

2.5.1 UV-Visible spectroscopy

The stock solutions of 1.00 mM ligands and copper complexes in acetonitrile were prepared. The absorption spectra of all ligands and copper complexes were recorded from acetonitrile solutions (100 μM) in the wavelength range of 200-900 nm at ambient temperature.

2.5.2 Molar absorption coefficient (ϵ)

Molar absorption coefficients (ϵ) of ligands and copper complexes in acetonitrile were estimated from UV-vis absorption spectra in the concentrations range of 20.0 - 100 μM . The intensities at maximum absorption wavelength (λ_{max}) of each compound were plotted against the concentration (M). The best fit lines were set through the origin. Molar Absorptivity Coefficients (ϵ) were obtained from the slopes of these plots according to the following equation:

$$A = \epsilon bC$$

Where A is the absorbance,
 ϵ is the Molar absorption coefficient ($\text{M}^{-1}\text{cm}^{-1}$),
 b is the cell path length (cm), and
 C is the concentration (M)

2.6 Electrochemical study

Complex solutions (2.00 mM) were prepared by dissolving CuCl_2 and corresponding ligands in dry acetonitrile containing 100 mM tetra-*n*-butylammonium hexafluorophosphate (NH_4PF_6) as supporting electrolyte. The cyclic voltammetry experiments were conducted using a standard three-electrode system: Glassy carbon working electrode, Ag/AgCl reference electrode, and Pt-wire auxiliary electrode with measurements carried out under N_2 atmosphere at a scanning rate (V) of 50.0 mV s^{-1} .

Potentials were measured relative to a ferrocenium/ferrocene couple ($E_{Fc^+/Fc}^0 = 0.08255$ V versus Ag/AgCl in CH_3CN) which was used as an external standard.

2.7 Excited state calculation

The excited copper complex, $E_{1/2}^*$ was calculated according to the equation:

$$E_{1/2}^* = E_{gap} - E_{1/2}$$

Where the redox potentials, $E_{1/2}$ were measured relative to ferrocene and reported in reference to the SCE electrode. The energy gaps (E_{gap}) were determined by using the onset of the longest wavelength absorption ($\lambda_{on\ set}$) following equation:

$$E_{gap} = \frac{1240}{\lambda_{on\ set}}$$

2.8 X-ray crystallography

2.8.1 Crystallography structures of copper complexes

Crystals of the complexes suitable for X-ray analysis were obtained via crystallization of copper(II) chloride with the corresponding ligands in methanol or acetonitrile at room temperature. The good-quality single crystals were mounted to hollow glass fiber. The data were recorded using graphite monochromated Cu-K α ($\lambda = 1.54178$ Å) radiation at 100 K or graphite monochromated Mo-K α ($\lambda = 0.71073$ Å) radiation at 296 K. Data reduction was performed using SAINT and SADABS was used for absorption correction [85]. The structure was solved with the ShelXT structure solution program using combined Patterson and dual-space recycling methods [86]. The structure was refined by least squares using ShelXL [87]. All non-H atoms were refined anisotropically. The hydrogen atoms attached to carbon atoms were positioned geometrically with C–H = 0.93–0.97 Å and refined using a riding-model approximation with fixed displacement parameters $U_{iso}(H) = 1.2U_{eq}(C)$. The O–H hydrogen atoms were placed in geometrically idealized positions and refined by using a riding model.

2.8.2 Crystallography structures of chlorosulfonylation products

The suitable crystals of the products for X-ray analysis were obtained via crystallization of products in ethyl acetate and hexane at room temperature. The

suitable crystals of addition products were mounted on a Lindemann tube oil and kept at a steady temperature of $T = 293$ K during data collection. The structures were solved with the ShelXT (Scheldrick 2015) structure solution program using the Intrinsic Phasing solution method and by using Olex2 as the graphical interface. The model was refined with ShelXL using Least Squares minimization.

2.9 General experimental procedure for ATRA

2.9.1 Reaction using AIBN

Alkene (500 μmol , 1.00 equiv), alkyl halide (750 μmol , 1.50 equiv), reducing agent (25.0 μmol , 5.00 mol%), copper(II) chloride (5.00 μmol , 1.00 mol%), ligand (5.00 μmol , 1.00 mol%), and toluene (internal standard) (500 μmol , 1.00 equiv) were added to an NMR tube. Deuterated acetonitrile or methanol was added to the mixture until a total volume of 500 μL was obtained. The reaction mixture was purged by a stream of nitrogen gas for a minute. The NMR tube was sealed with a standard polyethylene cap and wrapped with Teflon tape to ensure a tight seal. The reaction tube was placed under a white light source (LED or CFL) with an electric cooling fan to maintain a reaction temperature of 35 $^{\circ}\text{C}$ for the entire reaction period (Figure 2.1). Alkene conversions and yields were obtained via ^1H NMR spectroscopy.

2.9.2 Reaction without AIBN

All starting materials except AIBN were mixed in an NMR tube. Deuterated methanol was added to the mixture until the total volume of 500 μL was obtained. The reaction also bubbles a nitrogen gas, seals with a standard polyethylene cap, and wraps with Teflon tape. The reaction tube was placed under a white CFL with an electric fan to maintain the reaction temperature of 35 $^{\circ}\text{C}$ for 24 hours (Figure 2.1b). The isolated products were obtained from flash column chromatography and their structures were confirmed via ^1H NMR and ^{13}C NMR.

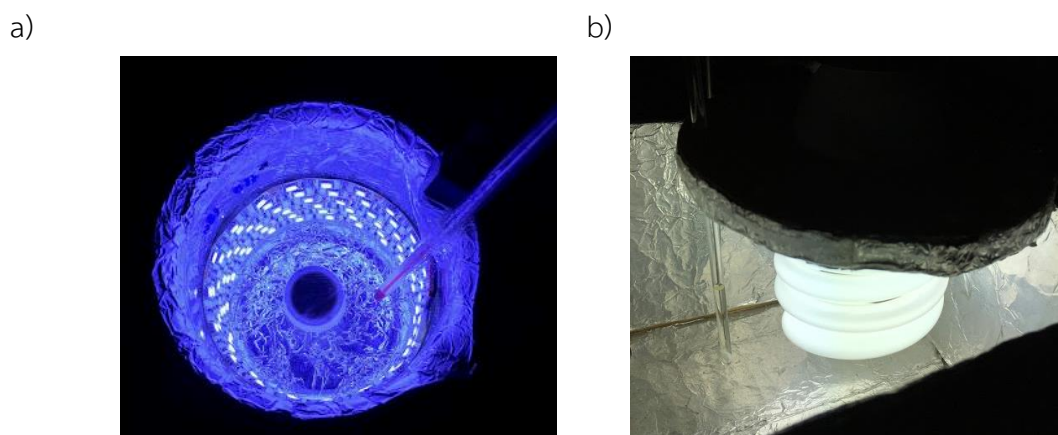


Figure 2.1 In-house made photoreactor equipped with a) white LEDs b) White CFL.

2.9.3 The large-scale synthesis

The Large-scale syntheses were carried out according to the procedure described above by using alkene (5.00 mmol, 1.00 equiv), alkyl halide (7.50 mmol, 1.50 equiv), copper(II) chloride (50.0 μmol , 1.00 mol%), and ligand (50.0 μmol , 1.00 mol%) were dissolved in dried MeOH or *i*-PrOH. The reaction bottle was placed under a white CFL with an electric fan to maintain the reaction temperature of 35 °C for a given time (Figure 2.1b). Alkene conversions and yields were obtained via ^1H NMR spectroscopy.

2.9.4 The relative emission spectra of light source

The relative emission spectra of light sources in this study were recorded using ocean optics USB2000 fiber optic spectrometer. The emission spectra of specified blue, green, and red LEDs showed narrow emission bands around 400 - 500 nm, 500 - 600 nm, and 600 - 700 nm, respectively (Figure 2.2). The emission spectrum of white LEDs showed a broad emission in the white light region from 400 - 700 nm while the emission spectrum of white compact fluorescent lamp, CFL showed mixed emission of slim peaks ($\sim 10 - 30$ nm) including small emission peak in UV region.

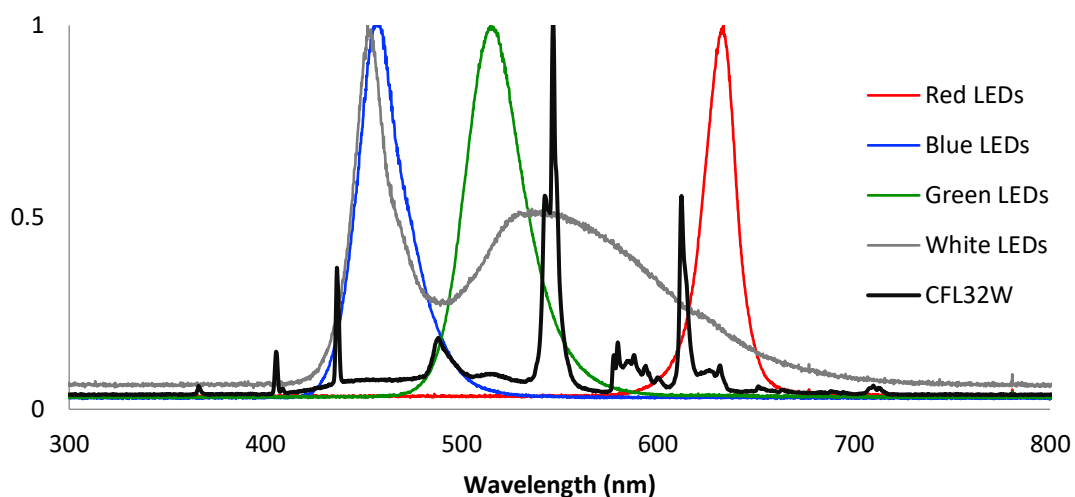
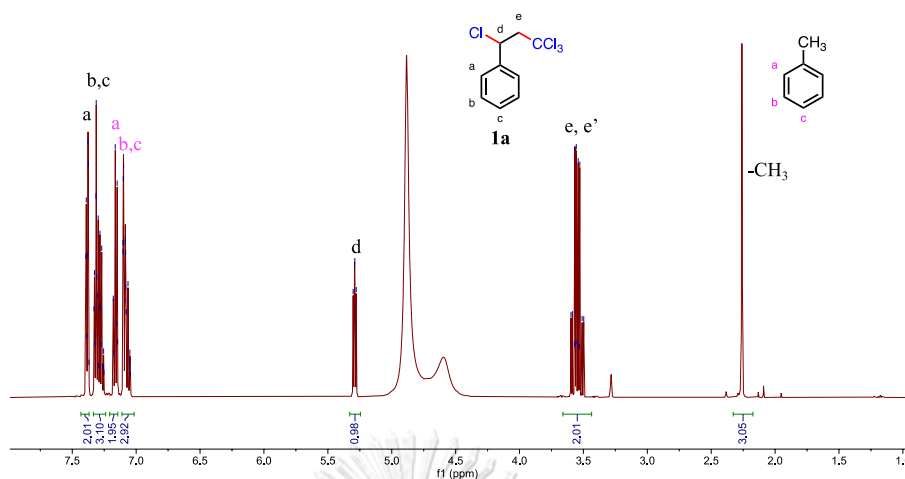


Figure 2.2 Normalized emission spectra of white CFL (black), white LEDs (grey), blue LEDs (Blue), green LEDs (green) and red LEDs (red) lines.

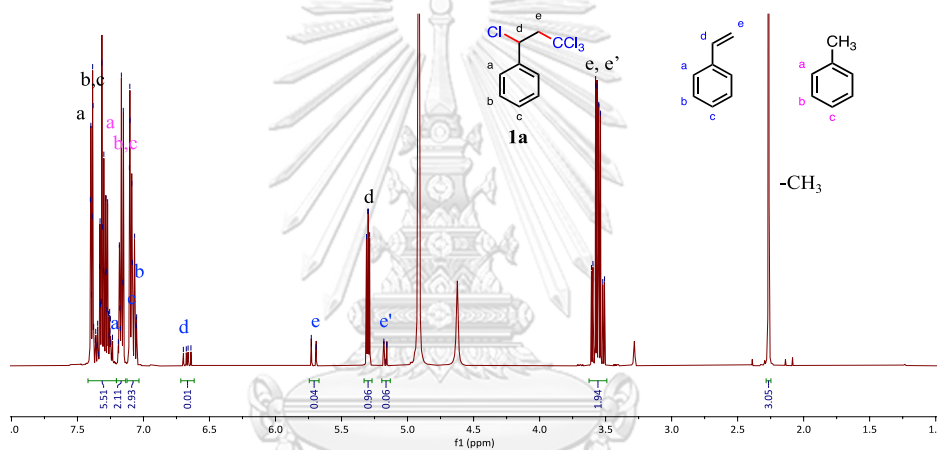
2.9.5 Determination of percent NMR yield of the addition product.

The percent NMR yield is determined from integrations of aliphatic protons of product, against methyl protons of toluene internal standard as shown in Figures 2.3-2.4.

Spectrum for 100% conversion and 100% Yield



Spectrum for 95% conversion and 96% Yield



Spectrum of styrene (substrate) and toluene (internal standard) mixture

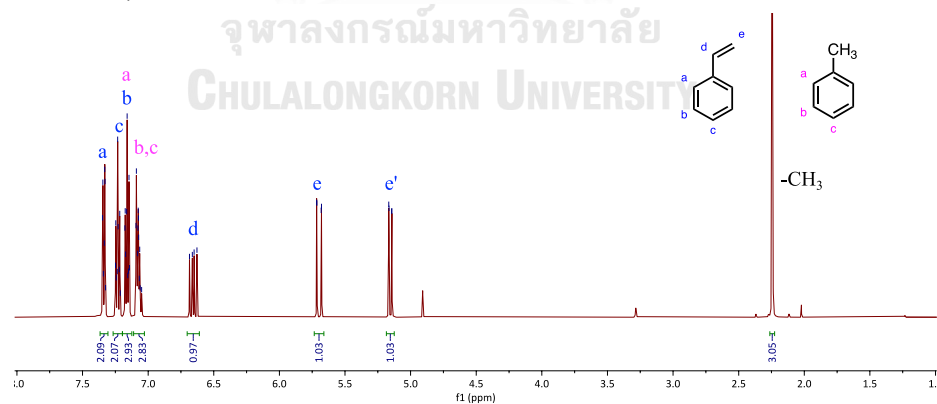
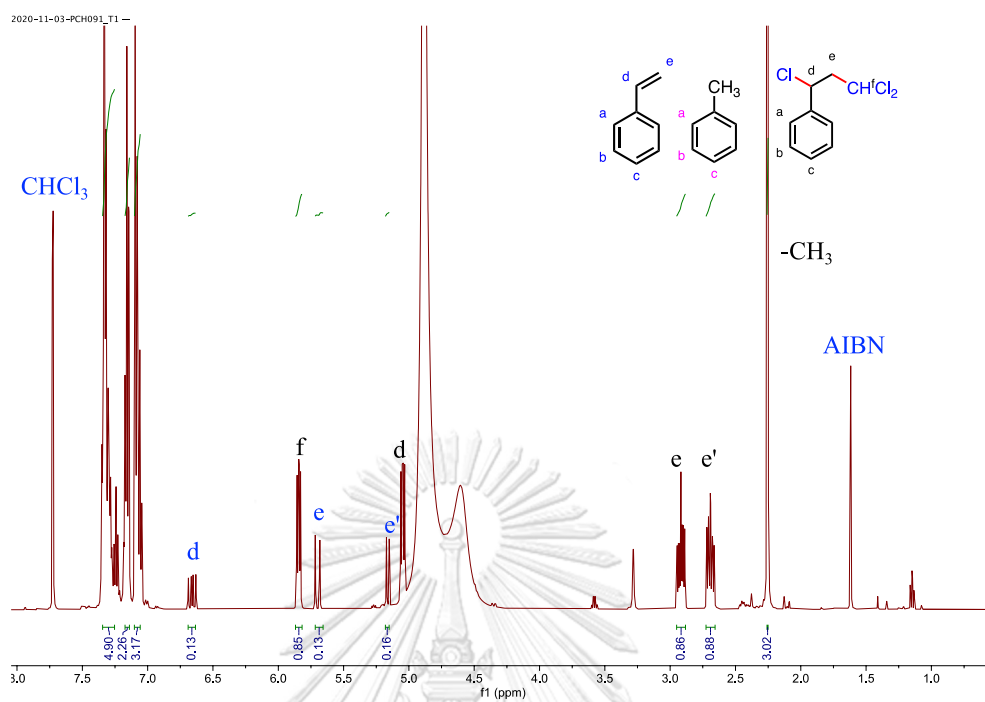


Figure 2.3 ¹H NMR spectra of crude product, after flash column chromatography, from the reaction between styrene and CCl₄ in CD₃OD, in the presence of toluene internal standard.

Spectrum for 87% conversion and 86% Yield



Spectrum for 40% conversion and 40% Yield

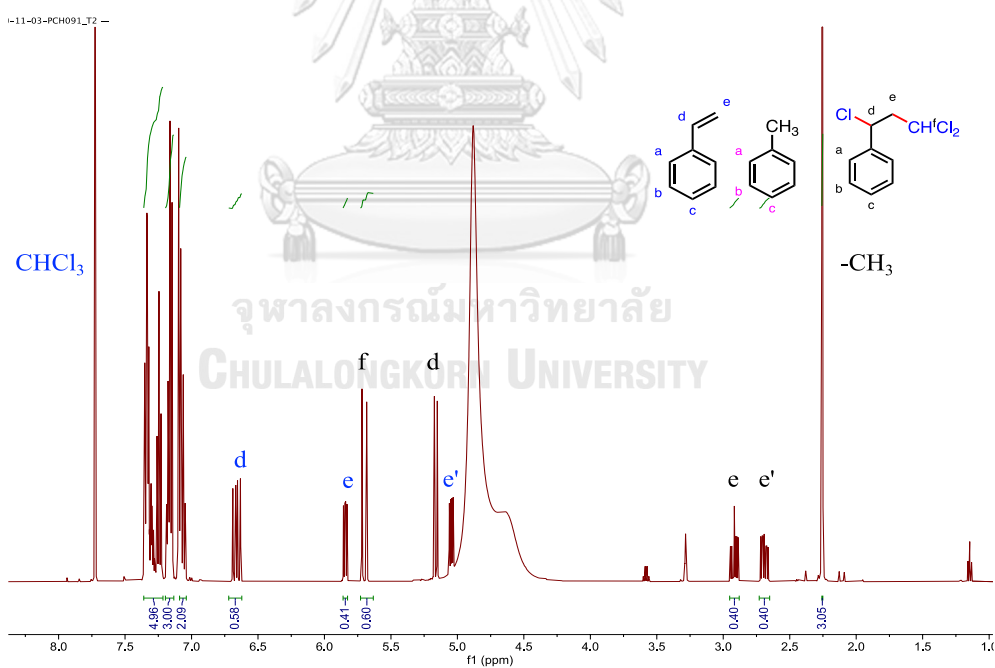
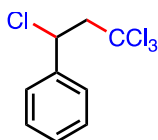


Figure 2.4 ¹H NMR spectra of crude product, after flash column chromatography, from the reaction between styrene and CHCl₃ in CD₃OD, in the presence of toluene internal standard.

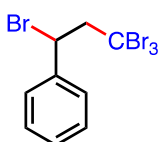
2.9.6 Spectroscopic data of ATRA products

The spectroscopic data of ATRA products were characterized in comparison with previous reports [88, 89].



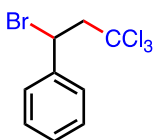
(1,3,3,3-tetrachloropropyl)benzene, 1a

^1H NMR (500 MHz, CDCl_3) δ 7.46 – 7.41 (m, 2H), 7.41 – 7.35 (m, 2H), 7.38 – 7.30 (m, 1H), 5.30 (dd, $J = 6.4, 5.4$ Hz, 1H), 3.62 (dd, $J = 15.4, 5.4$ Hz, 1H), 3.54 (dd, $J = 15.3, 6.5$ Hz, 1H). ^{13}C NMR (126 MHz, CDCl_3) δ 140.50, 129.03, 127.48, 96.30, 62.78, 58.38. ^{13}C NMR (101 MHz, acetone- d_6) δ 140.67, 128.86, 128.82, 127.60, 96.47, 61.89, 58.40.



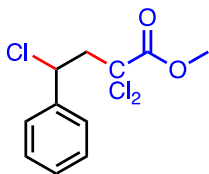
(1,3,3,3-tetrabromopropyl)benzene, 1b

^1H NMR (400 MHz, $\text{DMSO}-d_6$) δ 7.64 (d, $J = 7.5$ Hz, 2H), 7.44 – 7.32 (m, 3H), 5.45 (dd, $J = 7.7, 3.9$ Hz, 1H), 4.24 (dd, $J = 15.8, 7.7$ Hz, 1H), 4.08 (dd, $J = 15.8, 3.9$ Hz, 1H). ^{13}C NMR (101 MHz, $\text{DMSO}-d_6$) δ 141.45, 129.28, 129.19, 128.73, 65.28, 51.45, 36.52.



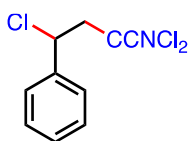
(1-bromo-3,3,3-trichloropropyl)benzene, 1c

^1H NMR (400 MHz, $\text{DMSO}-d_6$) δ 7.62 (d, $J = 7.3$ Hz, 2H), 7.42 – 7.31 (m, 3H), 5.58 (dd, $J = 8.0, 4.6$ Hz, 1H), 4.00 (dd, $J = 15.5, 8.0$ Hz, 1H), 3.82 (dd, $J = 15.5, 4.6$ Hz, 1H). ^{13}C NMR (101 MHz, $\text{DMSO}-d_6$) δ 141.24, 129.28, 129.15, 128.47, 97.40, 61.35, 48.79.



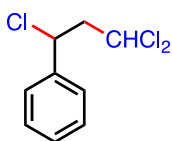
Methyl-2,2,4-trichloro-4-phenylbutanoate, 1d

^1H NMR (400 MHz, $\text{DMSO-}d_6$) δ 7.54 – 7.47 (m, 2H), 7.39 (qd, $J = 8.0, 7.1, 4.0$ Hz, 3H), 5.38 (dd, $J = 7.5, 6.0$ Hz, 1H), 3.69 (d, $J = 1.1$ Hz, 3H), 3.48 (ddd, $J = 15.1, 7.6, 1.0$ Hz, 1H), 3.36 – 3.27 (m, 2H). ^{13}C NMR (101 MHz, $\text{DMSO-}d_6$) δ 165.44, 140.05, 129.38, 129.15, 128.05, 82.98, 59.10, 55.09, 52.91.



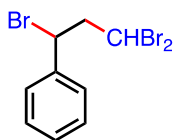
2,2,4-trichloro-4-phenylbutanenitrile, 1e

^1H NMR (500 MHz, CDCl_3) δ 7.55 – 7.36 (m, 1H), 5.22 (t, $J = 6.7$ Hz, 0H), 3.37 (dd, $J = 15.1, 7.1$ Hz, 0H), 3.22 (dd, $J = 15.1, 6.4$ Hz, 0H). ^{13}C NMR (126 MHz, CDCl_3) δ 138.74, 129.74, 129.30, 127.62, 114.55, 66.15, 57.58, 55.97.



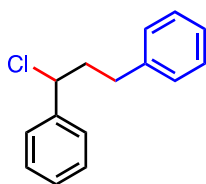
(1,3,3-trichloropropyl)benzene, 1f

^1H NMR (400 MHz, $\text{DMSO-}d_6$) δ 7.54 (d, $J = 6.8$ Hz, 2H), 7.41 (m, 3H), 6.20 (dd, $J = 8.5, 4.6$ Hz, 1H), 5.24 (dd, $J = 9.6, 4.7$ Hz, 1H), 3.17-3.09 (m, 1H), 2.92 – 2.85 (m, 1H). ^{13}C NMR (101 MHz, $\text{DMSO-}d_6$) δ 139.94, 129.41, 129.30, 127.83, 71.95, 60.13, 51.34.



(1,3,3-tribromopropyl)benzene, 1g

^1H NMR (500 MHz, CDCl_3) δ 7.42 – 7.32 (m, 5H), 5.63 (dd, J = 8.1, 5.8 Hz, 1H), 5.11 (dd, J = 8.9, 5.7 Hz, 1H), 3.28 (ddd, J = 14.8, 9.0, 5.7 Hz, 1H), 3.07 (ddd, J = 15.2, 8.0, 5.7 Hz, 1H). ^{13}C NMR (126 MHz, CDCl_3) δ 139.61, 129.22, 129.20, 127.55, 53.94, 51.58, 42.42.



1-chloro-1,3-diphenylpropane, 1h

^1H NMR (500 MHz, CDCl_3) δ 7.43 – 7.38 (m, 4H), 7.36 – 7.32 (m, 3H), 7.26 – 7.22 (m, 3H), 4.86 (dd, J = 8.6, 5.8 Hz, 1H), 2.85 (ddd, J = 14.4, 9.0, 5.7 Hz, 1H), 2.76 (ddd, J = 13.9, 8.7, 6.7 Hz, 1H), 2.50 (dtd, J = 14.4, 8.7, 5.7 Hz, 1H), 2.37 (dddd, J = 14.4, 8.9, 6.8, 5.8 Hz, 1H). ^{13}C NMR (126 MHz, CDCl_3) δ 141.76, 140.79, 128.85, 128.69, 128.50, 127.16, 126.34, 62.99, 41.53, 33.28.



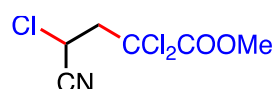
2,4,4,4-tetrachlorobutanenitrile, 2a

^1H NMR (500 MHz, CDCl_3) δ 4.86 (dd, J = 8.6, 4.0 Hz, 1H), 3.60 (dd, J = 15.2, 8.6 Hz, 1H), 3.35 (dd, J = 15.2, 4.1 Hz, 1H). ^{13}C NMR (126 MHz, CDCl_3) δ 115.87, 93.82, 77.44, 77.38, 77.18, 76.93, 59.17, 37.96.



2,4,4,4-tetrabromobutanenitrile, 2b

^1H NMR (500 MHz, CDCl_3) δ 4.65 (ddd, $J = 9.3, 3.1, 0.6$ Hz, 1H), 3.97 (ddd, $J = 15.5, 9.2, 0.6$ Hz, 1H), 3.75 (ddd, $J = 15.5, 3.1, 0.6$ Hz, 1H). ^{13}C NMR (126 MHz, CDCl_3) δ 116.40, 63.18, 31.84, 22.98.



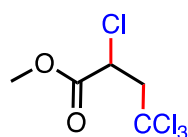
Methyl 2,2,4-trichloro-4-cyanobutanoate, 2c

^1H NMR (500 MHz, CDCl_3) δ 4.83 (dd, $J = 8.0, 5.5$ Hz, 1H), 3.94 (s, 3H), 3.35 (dd, $J = 15.1, 8.0$ Hz, 1H), 3.19 (dd, $J = 15.1, 5.5$ Hz, 1H). ^{13}C NMR (126 MHz, CDCl_3) δ 165.00, 115.87, 79.36, 55.13, 50.16, 37.96.



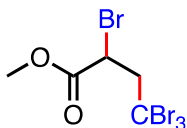
2-bromo-4,4,4-trichlorobutanenitrile, 2da

^1H NMR (500 MHz, CDCl_3) δ 4.68 (ddd, $J = 9.7, 3.5, 0.6$ Hz, 1H), 3.64 (ddd, $J = 15.0, 9.7, 0.6$ Hz, 1H), 3.41 (ddd, $J = 15.0, 3.5, 0.6$ Hz, 1H). ^{13}C NMR (126 MHz, CDCl_3) δ 116.24, 94.65, 59.41, 20.23.



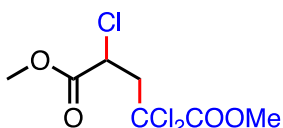
Methyl-2,4,4,4-tetrachlorobutanoate, 3a

^1H NMR (500 MHz, CDCl_3) δ 4.60 (dd, $J = 8.0, 3.7$ Hz, 1H), 3.81 (s, 3H), 3.75 (dd, $J = 15.2, 8.0$ Hz, 1H), 3.21 (dd, $J = 15.2, 3.7$ Hz, 1H). ^{13}C NMR (126 MHz, CDCl_3) δ 168.85, 95.45, 58.32, 53.63, 51.52.



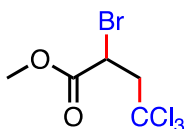
Methyl-2,4,4,4-tetrabromobutanoate, 3b

^1H NMR (500 MHz, CDCl_3) δ 4.48 (dd, $J = 9.1, 2.3$ Hz, 1H), 4.20 (dd, $J = 15.5, 9.1$ Hz, 1H), 3.80 (s, 3H), 3.63 (dd, $J = 15.6, 2.3$ Hz, 1H). ^{13}C NMR (126 MHz, CDCl_3) δ 169.36, 62.47, 53.71, 40.09, 34.53.



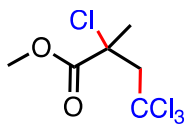
Dimethyl-2,2,4-trichloropentanedioate, 3c

^1H NMR (500 MHz, CDCl_3) δ 4.64 – 4.57 (m, 1H), 3.88 (d, $J = 0.5$ Hz, 3H), 3.80 (d, $J = 0.5$ Hz, 3H), 3.37 (dd, $J = 15.3, 6.8$ Hz, 1H), 3.10 (dd, $J = 15.3, 5.8$ Hz, 1H). ^{13}C NMR (126 MHz, CDCl_3) δ 168.96, 165.66, 81.02, 54.85, 53.58, 52.01, 49.06.



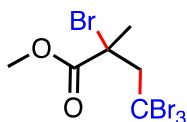
Methyl-2-bromo-4,4,4-trichlorobutanoate, 3da

^1H NMR (500 MHz, CDCl_3) δ 4.55 (ddd, $J = 9.4, 2.7, 0.6$ Hz, 1H), 3.85 (dd, $J = 15.2, 9.4$ Hz, 0H), 3.79 (s, 2H), 3.28 (dd, $J = 15.2, 2.7$ Hz, 1H). ^{13}C NMR (126 MHz, CDCl_3) δ 169.37, 96.10, 58.54, 53.61, 37.75.



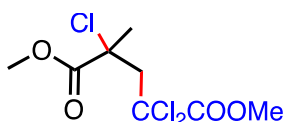
Methyl-2,4,4,4-tetrachloro-2-methylbutanoate, 4a

^1H NMR (500 MHz, CDCl_3) δ 3.98 (d, $J = 15.3$ Hz, 1H), 3.81 (d, $J = 0.7$ Hz, 3H), 3.45 (dd, $J = 15.3, 0.6$ Hz, 1H), 2.00 (s, 3H). ^{13}C NMR (126 MHz, CDCl_3) δ 170.22, 94.66, 64.67, 62.30, 53.64, 26.41.



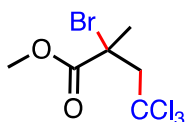
Methyl-2,4,4,4-tetrabromo-2-methylbutanoate, 4b

^1H NMR (500 MHz, CDCl_3) δ 4.64 (d, $J = 15.5$ Hz, 1H), 3.88 (d, $J = 15.5$ Hz, 1H), 3.80 (d, $J = 0.7$ Hz, 3H), 2.23 (s, 3H). ^{13}C NMR (126 MHz, CDCl_3) δ 170.55, 65.91, 57.59, 53.65, 31.46, 26.26.



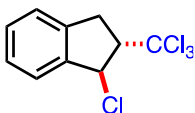
Dimethyl-2,2,4-trichloro-4-methylpentanedioate, 4c

^1H NMR (500 MHz, CDCl_3) δ 3.87 (s, 3H), 3.78 (s, 3H), 3.53 (d, $J = 15.2$ Hz, 1H), 3.42 (dd, $J = 15.1, 0.6$ Hz, 1H), 1.79 (s, 3H). ^{13}C NMR (126 MHz, CDCl_3) δ 170.72, 166.02, 80.76, 65.39, 54.84, 53.69, 28.20.



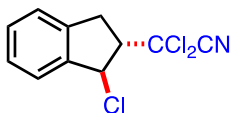
Methyl-2-bromo-4,4,4-trichloro-2-methylbutanoate, 4da

^1H NMR (500 MHz, CDCl_3) δ 4.20 (d, $J = 15.3$ Hz, 1H), 3.79 (s, 3H), 3.54 (d, $J = 15.3$ Hz, 1H), 2.18 (s, 3H). ^{13}C NMR (126 MHz, CDCl_3) δ 170.67, 95.14, 62.76, 55.39, 53.60, 26.63.



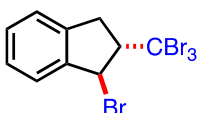
***anti*-1-chloro-2-(trichloromethyl)-2,3-dihydro-1H-indene, 5a**

^1H NMR (500 MHz, CDCl_3) δ 7.50 – 7.38 (m, 1H), 7.33 (td, $J = 4.0, 1.1$ Hz, 2H), 5.64 (dd, $J = 4.3, 1.0$ Hz, 1H), 3.94 (dddd, $J = 9.9, 5.3, 4.3, 0.8$ Hz, 1H), 3.59 (ddd, $J = 17.2, 9.2, 1.0$ Hz, 1H), 3.34 (ddd, $J = 17.3, 5.6, 1.0$ Hz, 1H). ^{13}C NMR (126 MHz, CDCl_3) δ 141.23, 140.09, 129.65, 128.02, 125.75, 124.60, 101.43, 69.45, 64.07, 36.19.



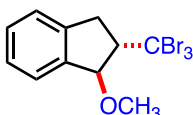
***anti*-2,2-dichloro-2-(1-chloro-2,3-dihydro-1*H*-inden-2-yl)acetonitrile, 5b**

^1H NMR (500 MHz, CDCl_3) δ 7.48 – 7.41 (m, 1H), 7.34 (dq, J = 5.2, 1.7 Hz, 2H), 7.30 – 7.25 (m, 1H), 5.58 (dd, J = 5.0, 1.7 Hz, 1H), 3.77 – 3.63 (m, 1H), 3.58 (dd, J = 16.8, 9.1 Hz, 1H), 3.27 (dd, J = 16.9, 6.2 Hz, 1H). ^{13}C NMR (126 MHz, CDCl_3) δ 140.69, 138.95, 129.94, 128.38, 125.65, 124.69, 114.67, 70.65, 63.25, 62.27, 34.90.



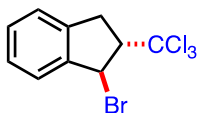
***anti*-1-bromo-2-(tribromomethyl)-2,3-dihydro-1*H*-indene, 5c**

^1H NMR (500 MHz, CDCl_3) δ 7.46 – 7.40 (m, 1H), 7.31 – 7.27 (m, 2H), 7.25 – 7.20 (m, 1H), 5.64 (dd, J = 3.0, 0.8 Hz, 1H), 4.20 (ddd, J = 9.1, 3.9, 3.0 Hz, 1H), 3.59 (ddt, J = 17.6, 9.1, 0.7 Hz, 1H), 3.32 – 3.18 (m, 1H). ^{13}C NMR (126 MHz, CDCl_3) δ 141.30, 141.01, 129.31, 127.34, 125.43, 124.84, 88.62, 67.99, 46.96, 38.35.



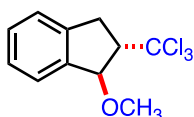
anti*-1-methoxy-2-(tribromomethyl)-2,3-dihydro-1*H*-indene, 5'*c

^1H NMR (500 MHz, CDCl_3) δ 7.42 (d, J = 7.4 Hz, 1H), 7.37 – 7.20 (m, 4H), 5.00 (d, J = 3.4 Hz, 1H), 3.74 (ddd, J = 8.9, 5.0, 3.5 Hz, 1H), 3.54 (s, 3H), 3.45 (ddd, J = 17.3, 8.8, 1.0 Hz, 1H), 3.09 (dd, J = 17.4, 5.0 Hz, 1H). ^{13}C NMR (126 MHz, CDCl_3) δ 141.31, 140.97, 129.31, 127.33, 125.43, 124.83, 88.70, 67.95, 56.51, 46.92, 38.33.



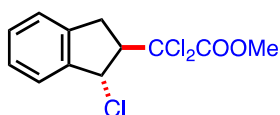
***anti*-1-bromo-2-(trichloromethyl)-2,3-dihydro-1*H*-indene, 5d**

^1H NMR (500 MHz, CDCl_3) δ 7.50 – 7.39 (m, 1H), 7.36 – 7.27 (m, 3H), 7.25 – 7.17 (m, 2H), 5.79 (d, $J = 3.4$ Hz, 2H), 4.07 (ddd, $J = 9.3, 4.4, 3.4$ Hz, 1H), 3.63 (dd, $J = 17.4, 9.3$ Hz, 2H), 3.38 (dd, $J = 17.5, 4.4$ Hz, 2H). ^{13}C NMR (126 MHz, CDCl_3) δ 141.99, 140.47, 129.60, 128.05, 126.11, 124.59, 101.67, 69.53, 53.15, 36.03.



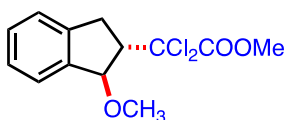
***anti*-1-methoxy-2-(trichloromethyl)-2,3-dihydro-1*H*-indene, 5'd**

^1H NMR (500 MHz, CDCl_3) δ 7.45 – 7.40 (m, 1H), 7.36 – 7.24 (m, 3H), 5.14 (t, $J = 3.7$ Hz, 1H), 3.60 (dtd, $J = 8.6, 5.0, 3.4$ Hz, 1H), 3.57 – 3.52 (m, 3H), 3.52 – 3.45 (m, 1H), 3.23 (dt, $J = 17.4, 4.2$ Hz, 1H). ^{13}C NMR (126 MHz, CDCl_3) δ 141.26, 140.98, 129.31, 127.34, 125.36, 124.80, 87.39, 65.34, 56.68, 35.76.



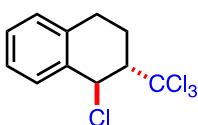
***anti*-methyl-2,2-dichloro-2-1-chloro-2,3-dihydro-1*H*-inden-2-yl)acetate, 5e**

^1H NMR (500 MHz, CDCl_3) δ 7.42 – 7.39 (m, 1H), 7.31 – 7.28 (m, 2H), 7.23 – 7.19 (m, 1H), 5.55 (d, $J = 5.0$ Hz, 1H), 3.92 (d, $J = 0.6$ Hz, 3H), 3.83 (dddd, $J = 9.0, 6.1, 5.0, 0.6$ Hz, 1H), 3.49 (ddd, $J = 16.8, 9.2, 0.8$ Hz, 1H), 3.16 (dd, $J = 16.8, 6.2$ Hz, 1H). ^{13}C NMR (126 MHz, CDCl_3) δ 165.84, 141.37, 140.01, 129.45, 127.88, 125.49, 124.57, 86.47, 63.15, 61.18, 54.77, 35.00.



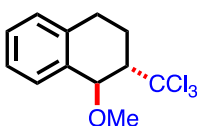
***anti*-methyl-2,2-dichloro-2-(1-methoxy-2,3-dihydro-1*H*-inden-2-yl)acetate, 5e,**

^1H NMR (500 MHz, CDCl_3) δ 7.38 (ddd, $J = 7.3, 1.4, 0.8$ Hz, 1H), 7.37 – 7.17 (m, 4H), 5.08 (d, $J = 4.7$ Hz, 1H), 3.88 (s, 3H), 3.52 (ddd, $J = 8.9, 6.0, 4.6$ Hz, 1H), 3.46 (s, 3H), 3.41 – 3.32 (m, 1H), 3.01 (dd, $J = 16.7, 6.0$ Hz, 1H). ^{13}C NMR (126 MHz, CDCl_3) δ 166.42, 141.17, 141.02, 129.05, 127.23, 124.97, 124.89, 87.06, 86.26, 56.74, 56.42, 54.60, 34.11.



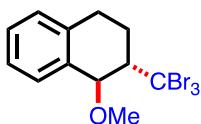
***anti*-1-chloro-2-(trichloromethyl)-1,2,3,4-tetrahydronaphthalene, 6a**

^1H NMR (500 MHz, CDCl_3) δ 7.34 (dd, $J = 7.2, 1.9$ Hz, 1H), 7.25 (td, $J = 7.3, 1.7$ Hz, 2H), 7.18 (dd, $J = 6.8, 1.8$ Hz, 1H), 5.52 (d, $J = 1.9$ Hz, 1H), 3.68 (ddd, $J = 9.2, 7.0, 1.9$ Hz, 1H), 3.03 (ddd, $J = 15.7, 11.8, 4.2$ Hz, 1H), 2.87 (dt, $J = 15.4, 4.7$ Hz, 1H), 2.66 (ddt, $J = 13.7, 7.0, 4.6$ Hz, 1H), 1.91 – 1.81 (m, 1H). ^{13}C NMR (126 MHz, CDCl_3) δ 138.79, 136.04, 129.48, 128.95, 128.13, 127.20, 102.55, 64.33, 57.65, 26.86, 26.75.



***anti*-1-methoxy-2-(trichloromethyl)-1,2,3,4-tetrahydronaphthalene, 6'a**

^1H NMR (500 MHz, CDCl_3) δ 7.29 – 7.25 (m, 2H), 7.23 – 7.18 (m, 2H), 4.59 (d, $J = 1.8$ Hz, 1H), 3.31 (ddd, $J = 10.2, 7.1, 1.9$ Hz, 1H), 3.20 (s, 3H), 2.89 (dddd, $J = 12.8, 11.8, 4.2, 2.4$ Hz, 1H), 2.71 (dt, $J = 14.8, 4.0$ Hz, 1H), 2.54 (ddt, $J = 13.2, 7.5, 3.9$ Hz, 1H), 1.68 (tdd, $J = 13.1, 10.2, 4.0$ Hz, 1H). ^{13}C NMR (126 MHz, CDCl_3) δ 140.14, 134.67, 130.23, 128.54, 127.82, 126.13, 103.38, 79.94, 62.02, 55.56, 27.59, 27.34.



***anti*-1-methoxy-2-(tribromomethyl)-1,2,3,4-tetrahydronaphthalene, 6'b**

^1H NMR (500 MHz, CDCl_3) δ 7.29 – 7.25 (m, 2H), 7.21 (t, $J = 6.7$ Hz, 2H), 4.53 – 4.45 (m, 1H), 3.48 – 3.39 (m, 1H), 3.20 (d, $J = 0.9$ Hz, 3H), 2.98 – 2.90 (m, 1H), 2.75 – 2.64 (m, 2H). ^{13}C NMR (126 MHz, CDCl_3) δ 140.41, 134.78, 130.54, 128.62, 127.70, 126.07, 81.68, 64.96, 55.53, 49.32, 30.17, 27.49.

2.10 General procedure for chlorosulfonylation under blue light

A flame dried Schlenk tube (10.0 mL) was equipped with a magnetic stirring bar. The CuCl_2 (1.34 mg, 10.0 μmol) and 1Q (3.26 mg, 10.0 μmol) were dissolved in anhydrous dichloromethane (2.00 mL) in a prepared Schlenk tube. Then sulfonyl chloride (500 μmol , 1.00 equiv) was added to the reaction for activated alkene. Besides, sulfonyl chloride (500 μmol , 1.00 equiv) and Na_2CO_3 (500 μmol , 1.00 equiv) were added to the reaction for inactivated alkene. The reaction was sealed with a screwcap and subsequently degassed by three consecutive freeze-pump-thaw cycles. After that, the alkene (0.500 - 1.00 mmol, 1.00 - 2.00 equiv) was added to the reaction under nitrogen atmosphere and sealed with Teflon sealed inlet for a glass rod. The reaction was stirred under light irradiation at 455 nm in a cool water bath for a given time as shown in Fig. S1a. The reaction was monitored by TLC. Afterward, the reaction mixture was concentrated in vacuo and the residue was purified by flash column chromatography on silica gel (hexane/EtOAc).

2.10.1 General procedure for chlorosulfonylation under white light

A test tube with a screwcap (10.0 mL) equipped with a magnetic stirring bar. The CuCl_2 (1.34 mg, 10.0 μmol) and 1Q (3.26 mg, 10.0 μmol) were dissolved in anhydrous dichloromethane (2.00 mL) in a prepared tube. Then sulfonyl chloride (500 μmol , 1.00 equiv), Na_2CO_3 (500 μmol , 1.00 equiv), and alkene (500 μmol , 1.00 equiv) was added to the reaction. The solution was bubbled under nitrogen gas for a minute and sealed with a screwcap and wrapped with Teflon tape to ensure a tight seal. The reaction tube was placed under a white light source with an electric cooling fan to maintain a reaction temperature of 35 $^\circ\text{C}$ for the entire reaction period.

as shown in Fig. S1c. The reaction was monitored by TLC. Afterward, the reaction mixture was concentrated in vacuo and the residue was purified by flash column chromatography on silica gel (eluent hexane/EtOAc).

2.10.2 The large-scale synthesis of compound 3ja

A flame dried Schlenk tube (40.0 mL) was equipped with a magnetic stirring bar. The CuCl_2 (13.4 mg, 100 μmol) and **1Q** (32.6 mg, 100 μmol) were dissolved in anhydrous dichloromethane (20.0 mL) in a prepared Schlenk tube. Then benzenesulfonyl chloride (883 mg, 5.00 mmol, 1.00 equiv) was added to the reaction. The reaction was sealed with a screwcap and subsequently degassed by three consecutive freeze-pump-thaw cycles. After that allyl methacrylate (757 mg, 6.00 mmol, 1.20 equiv) was added to the reaction under nitrogen atmosphere and sealed with Teflon sealed inlet for a glass rod. The reaction was stirred with 4 times irradiation at 455 nm for 16 hours in a cool water bath for a given time as shown in Figure 2.5b. The reaction was monitored by TLC. Afterward, the reaction mixture was concentrated in vacuo and the residue was purified by column chromatography on silica gel (hexane:EtOAc = 9:1, R_f = 0.34) to afford 3ja as a clear oil (1.30 g, 86% yield).

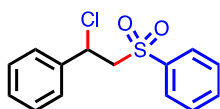
a)

b)



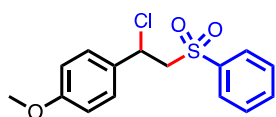
Figure 2.5 Reaction set up for chlorosulfonylation.

2.10.3 Spectroscopic data of chlorosulfonylation products



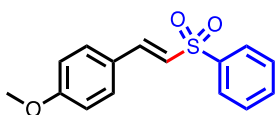
(1-chloro-2-(phenylsulfonyl)ethyl)benzene, **3aa**

Following the general procedure, **3aa** was prepared from benzenesulfonyl chloride (88.3 mg, 500 μmol , 1.00 equiv) and styrene (52.1 mg, 500 μmol , 1.00 equiv). The crude product was purified by flash column chromatography (hexane:EtOAc = 4:1, R_f = 0.40) to afford **3aa** as a white solid (92.7 mg, 66% yield). ^1H NMR (400 MHz, CDCl_3) δ 7.74 (dd, J = 8.4, 1.3 Hz, 2H), 7.61 – 7.55 (m, 1H), 7.44 (t, J = 7.8 Hz, 2H), 7.26 (m, 5H), 5.35 (t, J = 6.9 Hz, 1H), 3.97 (dd, J = 14.8, 6.9 Hz, 1H), 3.87 (dd, J = 14.8, 7.0 Hz, 1H). ^{13}C NMR (101 MHz, CDCl_3) δ 139.24, 138.47, 133.84, 129.23, 129.19, 128.95, 128.15, 127.18, 64.10, 55.09. HRMS (ESI-TOF) m/z : $[\text{M}+\text{Na}]^+$ Calc. for $\text{C}_{14}\text{H}_{13}\text{ClO}_2\text{SNa}$ 303.0217 Found 303.0219.



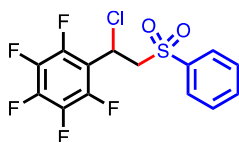
1-(1-chloro-2-(phenylsulfonyl)ethyl)-4-methoxybenzene, **3ba**

Following the general procedure, **3ba** was prepared from benzenesulfonyl chloride (88.3 mg, 500 μmol , 1.00 equiv) and 4-methoxystyrene (67.1 mg, 500 μmol , 1.00 equiv). The crude product was purified by flash column chromatography (hexane:EtOAc = 9:1, R_f = 0.30) to afford **3ba** as a clear oil (111.6 mg, 85% yield). ^1H NMR (400 MHz, CDCl_3) δ 7.72 (dd, J = 8.4, 1.3 Hz, 2H), 7.58 (ddt, J = 8.7, 7.1, 1.2 Hz, 1H), 7.49 – 7.40 (m, 2H), 7.18 (d, J = 8.8 Hz, 2H), 6.76 (d, J = 8.8 Hz, 2H), 5.33 (dd, J = 7.6, 6.5 Hz, 1H), 3.96 (dd, J = 14.8, 6.5 Hz, 1H), 3.88 (dd, J = 14.8, 7.6 Hz, 1H), 3.78 (s, 3H) ppm. ^{13}C NMR (101 MHz, CDCl_3) δ 160.14, 139.29, 133.70, 130.40, 129.10, 128.55, 128.14, 114.23, 64.13, 55.36, 55.04.



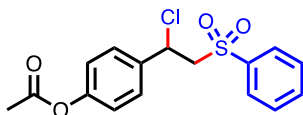
(*E*)-1-methoxy-4-(2-(phenylsulfonyl)vinyl)benzene, (*E*)-4ba

Following the general procedure, **4ba** was prepared from benzenesulfonyl chloride (88.3 mg, 500 μmol , 1.00 equiv) and 4-methoxystyrene (67.1 mg, 500 μmol , 1.00 equiv). The crude product was purified by flash column chromatography (hexane:EtOAc = 9:1, R_f = 0.23) to afford **4ba** as a brown solid (20.6 mg, 15% yield). ^1H NMR (300 MHz, CDCl_3) δ 8.00 – 7.88 (m, 2H), 7.69 – 7.49 (m, 4H), 7.47 – 7.36 (m, 2H), 6.95 – 6.82 (m, 2H), 6.71 (d, J = 15.3 Hz, 1H), 3.83 (s, 3H) ppm. ^{13}C NMR (75 MHz, CDCl_3) δ 162.11, 142.33, 141.17, 133.21, 130.43, 129.31, 127.55, 124.99, 124.44, 114.55, 55.48. HRMS (ESI-TOF) m/z : $[\text{M}+\text{Na}]^+$ Calc. for $\text{C}_{15}\text{H}_{14}\text{O}_3\text{SNa}$ 297.0561 Found 297.0556.



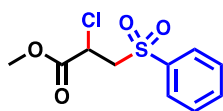
1-(1-chloro-2-(phenylsulfonyl)ethyl)-2,3,4,5,6-pentafluorobenzene, **3ca**

Following the general procedure, **3ca** was prepared from benzenesulfonyl chloride (88.3 mg, 500 μmol , 1.00 equiv) and 2,3,4,5,6-pentafluorobenzene (97.1 mg, 500 μmol , 1.00 equiv). The crude product was purified by flash column chromatography (hexane:EtOAc = 9:1, R_f = 0.40) to afford **3ca** as a white solid (98.5 mg, 53% yield). ^1H NMR (400 MHz, CDCl_3) δ 7.84 – 7.77 (m, 2H), 7.71 – 7.63 (m, 1H), 7.55 (t, J = 7.8 Hz, 2H), 5.62 (dd, J = 10.3, 4.9 Hz, 1H), 4.19 (dd, J = 14.6, 10.3 Hz, 1H), 3.91 (dd, J = 14.6, 4.9 Hz, 1H) ppm. ^{13}C NMR (101 MHz, CDCl_3) δ 146.08, 143.58, 140.70, 138.88, 138.39, 136.40, 134.43, 129.78, 127.92, 112.18, 60.46, 42.68. ^{19}F NMR (376 MHz, CDCl_3) δ -140.76 (s, 2F), -151.69 (tt, J = 21.0, 3.2 Hz, 1F), -161.01 (td, J = 21.8, 8.1 Hz, 2F). ^{19}F NMR is reported in comparison with previous report [90]. HRMS (ESI-TOF) m/z : $[\text{M}+\text{H}]^+$ Calc. for $\text{C}_{14}\text{H}_9\text{ClF}_5\text{O}_2\text{S}$ 370.9926 Found 370.9931.



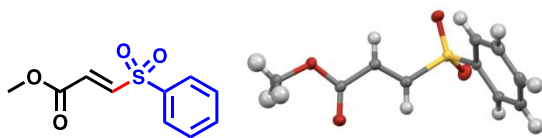
4-(1-chloro-2-(phenylsulfonyl)ethyl)phenyl acetate, **3da**

2-chloro-1-(phenylsulfonyl)propan-2-yl Following the general procedure, **3da** was prepared from benzenesulfonyl chloride (88.3 mg, 500 μ mol, 1.00 equiv) and 4-methoxystyrene (67.1 mg, 500 μ mol, 1.00 equiv). The crude product was purified by flash column chromatography (hexane:EtOAc = 4:1, R_f = 0.40) to afford **3da** as a white solid (64.9 mg, 38% yield). ^1H NMR (400 MHz, CDCl_3) δ 7.76 – 7.68 (m, 2H), 7.63 – 7.54 (m, 1H), 7.46 (ddd, J = 8.1, 6.9, 1.1 Hz, 2H), 7.27 (d, J = 8.6 Hz, 2H), 6.98 (d, J = 8.6 Hz, 2H), 5.35 (t, J = 7.0 Hz, 1H), 3.96 (dd, J = 14.8, 6.8 Hz, 1H), 3.85 (dd, J = 14.8, 7.2 Hz, 1H), 2.29 (s, 3H) ppm. ^{13}C NMR (101 MHz, CDCl_3) δ 169.00, 151.09, 139.10, 135.88, 133.92, 129.26, 128.38, 128.07, 122.11, 64.14, 54.41, 21.12. HRMS (ESI-TOF) m/z : $[\text{M}+\text{Na}]^+$ Calc. for $\text{C}_{16}\text{H}_{15}\text{ClNaO}_4\text{S}$ 361.0272 Found 361.0271.



methyl 2-chloro-3-(phenylsulfonyl)propanoate, **3ea**

Following the general procedure, **3ea** was prepared from benzenesulfonyl chloride (88.3 mg, 500 μ mol, 1.00 equiv) and methyl acrylate (86.1 mg, 1.00 mmol, 2.00 equiv). The crude product was purified by flash column chromatography (hexane:EtOAc = 9:1, R_f = 0.14) to afford **3ea** as a clear oil (67.0 mg, 51% yield). ^1H NMR (400 MHz, CDCl_3) δ 7.88 – 7.81 (m, 2H), 7.67 – 7.58 (m, 1H), 7.57 – 7.46 (m, 2H), 4.56 (dd, J = 8.4, 5.1 Hz, 1H), 3.94 (dd, J = 14.5, 8.4 Hz, 1H), 3.67 (s, 3H), 3.54 (dd, J = 14.5, 5.1 Hz, 1H) ppm. ^{13}C NMR (101 MHz, CDCl_3) δ 167.62, 138.69, 134.46, 129.54, 128.31, 59.66, 53.64, 48.66. HRMS (ESI-TOF) m/z : $[\text{M}+\text{H}]^+$ Calc. for $\text{C}_{10}\text{H}_{12}\text{ClO}_4\text{S}$ 263.0139 Found 263.0146.



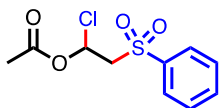
Methyl-(*E*)-3-(phenylsulfonyl)acrylate, (*E*)-4ea

Following the general procedure, **4ea** was prepared from benzenesulfonyl chloride (88.3 mg, 500 μ mol, 1.00 equiv) and methyl acrylate (86.1 mg, 1.00 mmol, 2.00 equiv). The crude product was purified by flash column chromatography (hexane:EtOAc = 9:1, R_f = 0.10) to afford **4ea** as a white solid (48.7 mg, 43% yield). ^1H NMR (400 MHz, CDCl_3) δ 7.86 (d, J = 7.3 Hz, 2H), 7.63 (t, J = 7.6 Hz, 1H), 7.53 (t, J = 7.7 Hz, 2H), 7.28 (d, J = 15.2 Hz, 1H), 6.78 (d, J = 15.2 Hz, 1H), 3.74 (s, 3H) ppm. ^{13}C NMR (101 MHz, CDCl_3) δ 163.91, 143.46, 138.45, 134.42, 130.52, 129.66, 128.35, 52.81. HRMS (ESI-TOF) m/z : $[\text{M}+\text{H}]^+$ Calc. for $\text{C}_{10}\text{H}_{11}\text{O}_4\text{S}$ 227.0373 Found 227.0374 263.0146.



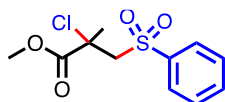
(*E*)-3-(phenylsulfonyl)acrylonitrile, (*E*)-4fa

Following the general procedure, (*E*)-**4fa** was prepared from benzenesulfonyl chloride (88.3 mg, 500 μ mol, 1.00 equiv) and acrylonitrile (53.1 mg, 1.00 mmol, 2.00 equiv). The crude product was purified by flash column chromatography (hexane:EtOAc = 4:1, R_f = *E* 0.37, *Z* 0.13) to afford (*E*)-**4fa** as a white solid (55.1 mg, 78%). ^1H NMR (400 MHz, CDCl_3) δ 8.00 – 7.93 (m, 2H), 7.84 – 7.75 (m, 1H), 7.73 – 7.64 (m, 2H), 7.28 (d, J = 15.7 Hz, 1H), 6.61 (d, J = 15.7 Hz, 1H) ppm. ^{13}C NMR (101 MHz, CDCl_3) δ 149.06, 137.30, 135.08, 129.97, 128.55, 113.31, 110.70. HRMS (ESI-TOF) m/z : $[\text{M}+\text{H}]^+$ Calc. for $\text{C}_9\text{H}_8\text{NO}_2\text{S}$ 194.0270 Found 194.0269.



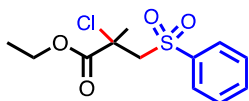
1-chloro-2-(phenylsulfonyl)ethyl acetate, **3ga**

Following the general procedure, **3ga** was prepared from benzenesulfonyl chloride (88.3 mg, 500 μ mol, 1.00 equiv) and (86.1 mg, 1.00 mmol, 2.00 equiv). The crude product was purified by flash column chromatography (hexane:EtOAc = 9:1, R_f = 0.18) to afford **3ga** as a white solid (111 mg, 85% yield). ^1H NMR (400 MHz, CDCl_3) δ 7.89 (dt, J = 7.2, 1.4 Hz, 2H), 7.75 – 7.66 (m, 1H), 7.60 (dd, J = 8.5, 7.2 Hz, 2H), 6.76 (dd, J = 9.3, 2.6 Hz, 1H), 3.95 (dd, J = 14.8, 9.3 Hz, 1H), 3.72 (dd, J = 14.8, 2.6 Hz, 1H), 1.89 (s, 3H) ppm. ^{13}C NMR (101 MHz, CDCl_3) δ 167.46, 139.03, 134.37, 129.56, 128.18, 76.39, 62.31, 20.39. HRMS (ESI-TOF) m/z : $[\text{M}+\text{Na}]^+$ Calc. for $\text{C}_{10}\text{H}_{11}\text{ClO}_4\text{SNa}$ 284.9959 Found 284.9958.



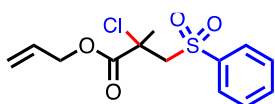
Methyl-2-chloro-2-methyl-3-(phenylsulfonyl)propanoate, **3ha**

Following the general procedure, **3ha** was prepared from benzenesulfonyl chloride (88.3 mg, 500 μ mol, 1.00 equiv) and methyl methacrylate (50.1 mg, 500 μ mol, 1.00 equiv). The crude product was purified by flash column chromatography (hexane:EtOAc = 9:1, R_f = 0.34) to afford **3ha** as a white solid (129 mg, 98% yield). ^1H NMR (300 MHz, CDCl_3) δ 7.99 – 7.87 (m, 2H), 7.74 – 7.62 (m, 1H), 7.59 (ddt, J = 8.3, 6.7, 1.3 Hz, 2H), 4.16 (d, J = 14.1 Hz, 1H), 3.83 (s, 3H), 3.76 (d, J = 14.1 Hz, 1H), 2.03 (s, 3H) ppm. ^{13}C NMR (75 MHz, CDCl_3) δ 169.19, 140.27, 134.19, 129.46, 128.03, 65.46, 62.24, 53.78, 26.82. HRMS (ESI-TOF) m/z : $[\text{M}+\text{H}]^+$ Calc. for $\text{C}_{11}\text{H}_{14}\text{ClO}_4\text{S}$ 277.0296 Found 277.0297.



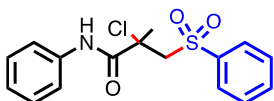
Ethyl-2-chloro-2-methyl-3-(phenylsulfonyl)propanoate, **3ia**

Following the general procedure, **3ia** was prepared from benzenesulfonyl chloride (88.3 mg, 500 μmol , 1.00 equiv) and ethyl methacrylate (57.1 mg, 500 μmol , 1.00 equiv). The crude product was purified by flash column chromatography (hexane:EtOAc = 9:1, R_f = 0.34) to afford **3ia** as a yellow oil (142 mg, 97% yield). ^1H -NMR (300 MHz, CDCl_3): δ 7.88 - 7.91 (m, 2H), 7.68 - 7.63 (m, 1H), 7.59 - 7.54 (m, 2H), 4.29 - 4.21 (m, 1H), 4.14 (d, J = 14.1 Hz, 1H), 3.74 (d, J = 14.1 Hz, 1H), 2.01 (s, 2H) ppm. ^{13}C NMR (75 MHz, CDCl_3) δ 168.59, 140.36, 134.17, 129.44, 127.96, 65.33, 63.00, 62.39, 26.70, 13.87. HRMS (ESI-TOF) m/z : $[\text{M}+\text{H}]^+$ Calc. for $\text{C}_{12}\text{H}_{16}\text{ClO}_4\text{S}$ 291.0452 Found 291.0456.



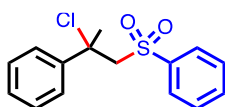
Allyl 2-chloro-2-methyl-3-(phenylsulfonyl)propanoate, **3ja**

Following the general procedure, **3ja** was prepared from benzenesulfonyl chloride (88.3 mg, 500 μmol , 1.00 equiv) and allyl methacrylate (63.1 mg, 500 μmol , 1.00 equiv). The crude product was purified by flash column chromatography (hexane:EtOAc = 9:1, R_f = 0.34) to afford **3ja** as a clear oil (149 mg, 99% yield). ^1H -NMR (300 MHz, CDCl_3) δ 7.94 - 7.85 (m, 2H), 7.66 (ddt, J = 8.4, 6.6, 1.3 Hz, 1H), 7.62 - 7.50 (m, 2H), 5.95 (ddt, J = 17.2, 10.4, 5.4 Hz, 1H), 5.45 - 5.24 (m, 2H), 4.69 (ddt, J = 5.4, 3.8, 1.4 Hz, 2H), 4.16 (d, J = 14.1 Hz, 1H), 3.76 (d, J = 14.1 Hz, 1H), 2.03 (s, 3H). ^{13}C NMR (75 MHz, CDCl_3) δ 168.31, 140.28, 134.21, 131.17, 129.46, 128.00, 119.20, 67.34, 65.34, 62.33, 26.72. HRMS (ESI-TOF) m/z : $[\text{M}+\text{H}]^+$ Calc. for $\text{C}_{13}\text{H}_{16}\text{ClO}_4\text{S}$ 303.0452 Found 303.0452.



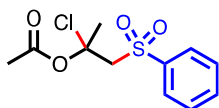
2-chloro-2-methyl-N-phenyl-3-(phenylsulfonyl)propenamide, **3ka**

Following the general procedure, **3ka** was prepared from benzenesulfonyl chloride (88.3 mg, 500 μmol , 1.00 equiv) and N-phenyl methacrylamide (82.2 mg, 500 μmol , 1.00 equiv). The crude product was purified by flash column chromatography (hexane:EtOAc = 7:3, R_f = 0.36) to afford **3ka** as a brown solid (169 mg, 100% yield). ^1H NMR (400 MHz, CDCl_3) δ 8.58 (s, 1H), 7.97 – 7.90 (m, 2H), 7.65 – 7.54 (m, 1H), 7.51 (m, 4H), 7.35 (dd, J = 8.5, 7.4 Hz, 2H), 7.22 – 7.13 (m, 1H), 4.24 (d, J = 14.6 Hz, 1H), 3.76 (d, J = 14.6 Hz, 1H), 1.94 (s, 3H) ppm. ^{13}C NMR (101 MHz, CDCl_3) δ 167.15, 140.57, 136.81, 133.95, 129.29, 129.08, 128.11, 125.40, 120.68, 66.30, 65.32, 30.98. HRMS (ESI-TOF) m/z : $[\text{M}+\text{H}]^+$ Calc. for $\text{C}_{16}\text{H}_{17}\text{ClNO}_3\text{S}$ 338.0612 Found 338.0617.



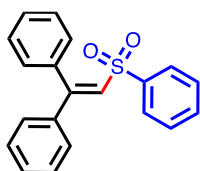
(2-chloro-1-(phenylsulfonyl)propan-2-yl)benzene, **3la**

Following the general procedure, **3m** was prepared from benzenesulfonyl chloride (88.3 mg, 500 μmol , 1.00 equiv) and alpha methyl styrene (59.1 mg, 500 μmol , 1.00 equiv). The crude product was purified by flash column chromatography (hexane:EtOAc = 9:1, R_f = 0.24) to afford **3la** as a pale-orange solid (105 mg, 71% yield). ^1H NMR (300 MHz, CDCl_3) δ 7.57 – 7.45 (m, 3H), 7.44 – 7.28 (m, 4H), 7.24 – 7.11 (m, 3H), 4.19 (d, J = 14.7 Hz, 1H), 4.01 (d, J = 14.7 Hz, 1H), 2.39 (s, 3H) ppm. ^{13}C NMR (75 MHz, CDCl_3) δ 141.03, 140.01, 133.35, 129.04, 128.51, 128.26, 127.76, 126.55, 69.64, 67.59, 29.75. HRMS (ESI-TOF) m/z : $[\text{M}+\text{Na}]^+$ Calc. for $\text{C}_{15}\text{H}_{15}\text{ClO}_2\text{SNa}$ 317.0373 Found 317.0373.



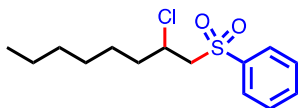
2-chloro-1-(phenylsulfonyl)propan-2-yl acetate, **3ma**

Following the general procedure, **3ma** was prepared from benzenesulfonyl chloride (88.3 mg, 500 μ mol, 1.00 equiv) and isopropenyl acetate (100 mg, 1.00 mmol, 2.00 equiv). The crude product was purified by flash column chromatography (hexane:EtOAc = 9:1, R_f = 0.20) to afford **3ma** as a brown solid (82.6 mg, 60% yield). ^1H NMR (300 MHz, CDCl_3) δ 7.96 – 7.86 (m, 2H), 7.74 – 7.62 (m, 1H), 7.59 (ddt, J = 8.4, 6.6, 1.4 Hz, 2H), 4.80 (d, J = 14.5, Hz, 1H), 3.65 (d, J = 14.5 Hz, 1H), 2.26 (s, 3H), 1.96 (s, 3H) ppm. ^{13}C NMR (75 MHz, CDCl_3) δ 168.46, 139.91, 134.21, 129.48, 128.19, 93.27, 63.57, 31.77, 21.78. HRMS (ESI-TOF) m/z : $[\text{M}+\text{Na}]^+$ Calc. for $\text{C}_{11}\text{H}_{12}\text{ClO}_4\text{SNa}$ 299.0115 Found 299.0117.



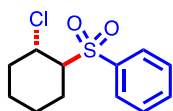
(2-(phenylsulfonyl)ethene-1,1-diyl) benzene, **4na**

Following the general procedure, **4na** was prepared from benzenesulfonyl chloride (88.3 mg, 500 μ mol, 1.00 equiv) and 1,1-diphenylethylene (90.1 mg, 500 μ mol, 1.00 equiv). The crude product was purified by flash column chromatography (hexane:EtOAc = 9:1, R_f = 0.24) to afford **4na** as a white solid (26.2 mg, 16% yield). ^1H NMR (400 MHz, CDCl_3) δ 7.57 – 7.50 (m, 2H), 7.44 (t, J = 7.4 Hz, 1H), 7.36 – 7.20 (m, 8H), 7.20 – 7.11 (m, 2H), 7.07 – 7.00 (m, 2H), 6.98 (s, 1H). ^{13}C NMR (101 MHz, CDCl_3) δ 155.23, 141.50, 139.12, 135.48, 132.85, 130.35, 129.79, 128.90, 128.79, 128.69, 128.62, 128.24, 127.88, 127.66. HRMS (ESI-TOF) m/z : $[\text{M}+\text{H}]^+$ Calc. for $\text{C}_{20}\text{H}_{17}\text{O}_2\text{S}$ 321.0944 Found 321.0946.



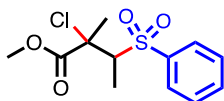
((2-chlorooctyl)sulfonyl)benzene, 3oa

Following the general procedure, **3oa** was prepared from benzenesulfonyl chloride (88.3 mg, 500 μ mol, 1.00 equiv) and 1-octene (112 mg, 1.00 mmol, 2.00 equiv). The crude product was purified by flash column chromatography (hexane:EtOAc = 9:1, R_f = 0.43) to afford **3oa** as a clear yellow oil (128 mg, 89% yield). ^1H NMR (300 MHz, CDCl_3) δ 7.97 – 7.87 (m, 2H), 7.72 – 7.60 (m, 1H), 7.56 (td, J = 8.0, 2.3 Hz, 2H), 4.30 (dt, J = 8.4, 6.4 Hz, 1H), 3.57 (dd, J = 14.7, 6.4 Hz, 1H), 3.46 (ddd, J = 14.7, 6.4 Hz, 1H), 1.95 (m, 1H), 1.83 – 1.64 (m, 1H), 1.52 – 1.34 (m, 2H), 1.26 (m, 6H), 0.86 (td, J = 6.8, 2.5 Hz, 3H) ppm. ^{13}C NMR (75 MHz, CDCl_3) δ 139.48, 134.12, 129.42, 128.18, 63.45, 54.52, 37.95, 31.56, 28.43, 25.73, 22.53, 14.06. HRMS (ESI-TOF) m/z : $[\text{M}+\text{H}]^+$ Calc. for $\text{C}_{14}\text{H}_{22}\text{ClO}_2\text{S}$ 289.1024 Found 289.1030.



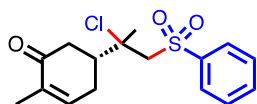
((2-chlorocyclohexyl)sulfonyl)benzene, *anti*-3pa

Following the general procedure, *anti*-**3pa** was prepared from benzenesulfonyl chloride (88.3 mg, 0.50 mmol, 1.00 equiv) and cyclohexene (82.1 mg, 1.00 mmol, 2.00 equiv). The crude product was purified by flash column chromatography (hexane:EtOAc = 9:1, R_f = 0.43) to afford *anti*-**3pa** as a white solid (87.7 mg, 68% yield). ^1H NMR (300 MHz, CDCl_3) δ 7.99 – 7.87 (m, 2H), 7.72 – 7.60 (m, 1H), 7.63 – 7.50 (m, 2H), 4.36 (m, 1H), 3.32 (m, 1H), 2.40 – 2.15 (m, 2H), 2.03 – 1.84 (m, 1H), 1.85 – 1.66 (m, 3H), 1.53 – 1.31 (m, 2H) ppm. ^{13}C NMR (75 MHz, CDCl_3) δ 138.99, 133.85, 129.18, 128.76, 77.28, 67.63, 55.64, 34.52, 23.76, 22.62. HRMS (ESI-TOF) m/z : $[\text{M}+\text{H}]^+$ Calc. for $\text{C}_{12}\text{H}_{16}\text{ClO}_2\text{S}$ 259.0554 Found 259.0554.



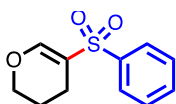
Methyl-2-chloro-2-methyl-3-(phenylsulfonyl)butanoate, **3qa**

Following the general procedure, **3qa** was prepared from benzenesulfonyl chloride (88.3 mg, 0.50 mmol, 1.00 equiv) and methyl (*E*)-2-methylbut-2-enoate (114 mg, 1.00 mmol, 2.00 equiv). The crude product was purified by flash column chromatography (hexane:EtOAc = 9:1, R_f = 0.20) to afford **3qa** as a white solid (117 mg, 80% yield). ^1H NMR (300 MHz, CDCl_3) δ 7.93 – 7.83 (m, 2H), 7.73 – 7.61 (m, 1H), 7.64 – 7.51 (m, 2H), 4.20 (q, J = 7.1 Hz, 1H), 3.92 (s, 3H), 1.99 (s, 3H), 1.50 (d, J = 7.1 Hz, 3H) ppm. ^{13}C NMR (75 MHz, CDCl_3) δ 170.29, 139.00, 134.17, 129.39, 128.52, 67.06, 65.59, 53.70, 21.92, 10.78. HRMS (ESI-TOF) m/z : $[\text{M}+\text{H}]^+$ Calc. for $\text{C}_{12}\text{H}_{16}\text{ClO}_4\text{S}$ 291.0452 Found 291.0455.



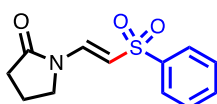
5-(2-chloro-1-(phenylsulfonyl)propan-2-yl)-2-methylcyclohex-2-en-1-one, **3ra**

Following the general procedure, **3ra** was prepared from benzenesulfonyl chloride (88.3 mg, 500 μmol , 1.00 equiv) and (*R*)-carvone (150 mg, 1.00 mmol, 2.00 equiv). The crude product was purified by flash column chromatography (hexane:EtOAc = 9:1, R_f = 0.21) to afford **3ra** as a clear oil (159 mg, 98% yield). ^1H NMR (300 MHz, CDCl_3) δ 7.90 – 7.78 (m, 2H), 7.62 (m, 1H), 7.52 (tdd, J = 7.2, 3.3, 1.6 Hz, 2H), 6.74 – 6.64 (m, 1H), 3.69 (dd, J = 17.9, 14.3 Hz, 1H), 3.52 (dd, J = 14.3, 10.6 Hz, 1H), 2.94 (qt, J = 10.0, 4.1 Hz, 1H), 2.73 – 2.29 (m, 4H), 1.93 – 1.81 (d, J = 16.8, 3H), 1.72 (dt, J = 2.6, 1.3 Hz, 3H) ppm. **Isomer 3ra-1** ^{13}C NMR (75 MHz, CDCl_3) δ 198.37, 143.86, 140.36, 135.11, 134.26, 129.60, 127.72, 72.40, 65.21, 43.65, 39.24, 28.96, 27.76, 15.57. **Isomer 3ra-2** ^{13}C NMR (75 MHz, CDCl_3) δ 197.93, 143.68, 140.32, 135.25, 134.23, 129.57, 127.76, 72.37, 65.02, 43.41, 39.75, 28.88, 27.08, 15.60. HRMS (ESI-TOF) m/z : $[\text{M}+\text{H}]^+$ Calc. for $\text{C}_{16}\text{H}_{20}\text{ClO}_3\text{S}$ 327.0816 Found 327.0823.



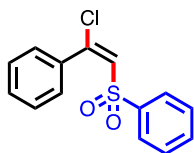
5-(phenylsulfonyl)-3,4-dihydro-2H-pyran, **4sa**

Following the general procedure, **4sa** was prepared from benzenesulfonyl chloride (88.3 mg, 500 μmol , 1.00 equiv) and 3,4-dihydro-2H-pyran (84.1 mg, 1.00 mmol, 2.00 equiv). The crude product was purified by flash column chromatography (hexane:EtOAc = 9:1, R_f = 0.14) to afford **4sa** as a white solid (56.3 mg, 43% yield). ^1H NMR (400 MHz, CDCl_3) δ 7.93 – 7.77 (m, 2H), 7.62 (s, 1H), 7.63 – 7.54 (m, 2H), 7.56 – 7.47 (m, 2H), 4.06 – 3.99 (m, 2H), 2.17 (td, J = 6.3, 1.4 Hz, 2H), 1.92 – 1.80 (m, 2H) ppm. ^{13}C NMR (75 MHz, CDCl_3) δ 153.82, 140.58, 132.88, 129.11, 127.47, 115.09, 66.62, 20.79, 18.89. HRMS (ESI-TOF) m/z : $[\text{M}+\text{H}]^+$ Calc. for $\text{C}_{11}\text{H}_{13}\text{O}_3\text{S}$ 225.0580 Found 225.0580.



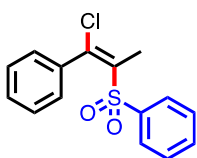
(*E*)-1-(2-(phenylsulfonyl)vinyl)pyrrolidin-2-one, (*E*)-**4ta**

Following the general procedure, (*E*)-**4ta** was prepared from benzenesulfonyl chloride (88.3 mg, 500 μmol , 1.00 equiv) and 1-vinyl-2-pyrrolidone (111 mg, 1.00 mmol, 2.00 equiv). The crude product was purified by flash column chromatography (hexane:EtOAc = 4:1, R_f = 0.34) to afford (*E*)-**4ta** as a white solid (62.5 mg, 43% yield). ^1H NMR (400 MHz, CDCl_3) δ 8.09 (d, J = 13.7 Hz, 1H), 7.93 – 7.86 (m, 2H), 7.63 – 7.54 (m, 1H), 7.52 (dd, J = 8.3, 6.6 Hz, 2H), 5.73 (d, J = 13.7 Hz, 1H), 3.50 (t, J = 7.2 Hz, 2H), 2.55 (t, J = 8.2 Hz, 2H), 2.22 – 2.10 (m, 2H) ppm. ^{13}C NMR (101 MHz, CDCl_3) δ 174.22, 142.03, 136.16, 132.99, 129.24, 127.23, 110.30, 45.14, 30.69, 17.44. HRMS (ESI-TOF) m/z : $[\text{M}+\text{H}]^+$ Calc. for $\text{C}_{12}\text{H}_{14}\text{NO}_3\text{S}$ 252.0689 Found 252.0693.



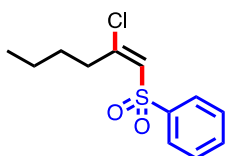
(E)-1-chloro-2-(phenylsulfonyl)vinylbenzene, (E)-6aa

Following the general procedure, **(E)-6aa** was prepared from benzenesulfonyl chloride (88.3 mg, 500 μmol , 1.00 equiv) and phenylacetylene (102 mg, 1.00 mmol, 2.00 equiv). The crude product was purified by flash column chromatography (hexane:EtOAc = 5:1, R_f = 0.54) to afford **(E)-6aa** as a white solid (134 mg, 96% yield). ^1H NMR (400 MHz, CDCl_3) δ 7.52 (dd, J = 8.4, 1.3 Hz, 2H), 7.53 – 7.40 (m, 1H), 7.37 – 7.20 (m, 7H), 6.85 (s, 1H) ppm. ^{13}C NMR (101 MHz, CDCl_3) δ 148.50, 140.51, 134.29, 133.55, 130.87, 130.75, 129.02, 128.85, 128.08, 127.74. HRMS (ESI-TOF) m/z : $[\text{M}+\text{H}]^+$ Calc. for $\text{C}_{14}\text{H}_{12}\text{ClO}_2\text{S}$ 279.0241 Found 279.0245.



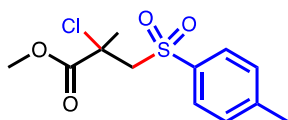
((1-chloro-1-phenylprop-1-en-2-yl)sulfonyl)benzene, (E)-6ba

Following the general procedure, **(E)-6ba** was prepared from benzenesulfonyl chloride (88.3 mg, 500 μmol , 1.00 equiv) and 1-phenyl-1-propene (116 mg, 1.00 mmol, 2.00 equiv). The crude product was purified by flash column chromatography (hexane:EtOAc = 9:1, R_f = 0.40) to afford **(E)-6ba** as a clear oil (129 mg, 88% yield). ^1H NMR (400 MHz, CDCl_3) δ 7.56 – 7.46 (m, 3H), 7.41 – 7.30 (m, 3H), 7.33 – 7.23 (m, 2H), 7.24 – 7.16 (m, 2H), 2.38 (s, 3H) ppm. ^{13}C NMR (101 MHz, CDCl_3) δ 144.43, 140.32, 137.84, 136.84, 133.20, 129.51, 128.87, 128.85, 127.94, 127.75, 18.02. HRMS (ESI-TOF) m/z : $[\text{M}+\text{H}]^+$ Calc. for $\text{C}_{15}\text{H}_{14}\text{ClO}_2\text{S}$ 293.0398 Found 293.0404.



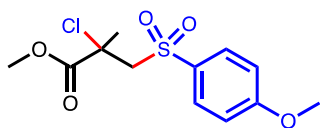
((2-chlorohex-1-en-1-yl)sulfonyl)benzene, (*E*)-6ca

Following the general procedure, (*E*)-6ca was prepared from benzenesulfonyl chloride (88.3 mg, 500 μmol , 1.00 equiv) and 1-hexyne (82.1 mg, 1.00 mmol, 2.00 equiv). The crude product was purified by flash column chromatography (hexane:EtOAc = 9:1, R_f = 0.54) to afford (*E*)-6ca as a clear oil (86.9 mg, 67% yield). ^1H NMR (400 MHz, CDCl_3) δ 7.95 – 7.87 (m, 2H), 7.70 – 7.61 (m, 1H), 7.62 – 7.52 (m, 2H), 6.53 (s, 1H), 2.99 – 2.91 (m, 2H), 1.64 – 1.52 (m, 2H), 1.44 – 1.31 (m, 2H), 0.93 (t, J = 7.3 Hz, 3H) ppm. ^{13}C NMR (101 MHz, CDCl_3) δ 155.03, 141.37, 133.72, 129.45, 128.59, 127.38, 34.79, 29.69, 22.04, 13.81. HRMS (ESI-TOF) m/z : $[\text{M}+\text{H}]^+$ Calc. for $\text{C}_{12}\text{H}_{15}\text{ClO}_2\text{S}$ 259.0554 Found 259.0557.



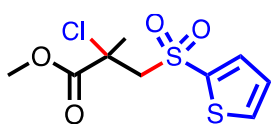
Methyl-2-chloro-2-methyl-3-tosylpropanoate, 3ib

Following the general procedure, 3ib was prepared from 4-toluenesulfonyl chloride (95.3 mg, 500 μmol , 1.00 equiv) and methyl methacrylate (50.1 mg, 500 μmol , 1.00 equiv). The crude product was purified by flash column chromatography (hexane:EtOAc = 9:1, R_f = 0.31) to afford 3ib as a white solid (125 mg, 86% yield). ^1H NMR (300 MHz, CDCl_3) δ 7.84 – 7.73 (m, 2H), 7.42 – 7.32 (m, 2H), 4.14 (d, J = 14.1 Hz, 1H), 3.83 (s, 3H), 3.73 (d, J = 14.1 Hz, 1H), 2.46 (s, 3H), 2.02 (s, 3H) ppm. ^{13}C NMR (75 MHz, CDCl_3) δ 169.22, 145.31, 137.37, 130.04, 128.06, 65.54, 62.29, 53.75, 26.78, 21.72 ppm. HRMS (ESI-TOF) m/z : $[\text{M}+\text{H}]^+$ Calc. for $\text{C}_{12}\text{H}_{16}\text{ClO}_4\text{S}$ 291.0452 Found 291.0456.



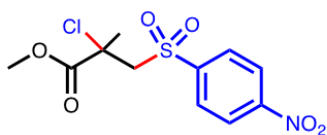
Methyl 2-chloro-3-((4-methoxyphenyl)sulfonyl)-2-methylpropanoate, **3ic**

Following the general procedure, **3ic** was prepared from 4-methoxybenzenesulfonyl chloride (103.3 mg, 500 μmol , 1.00 equiv) and methyl methacrylate (50.1 mg, 500 μmol , 1.00 equiv). The crude product was purified by flash column chromatography (hexane:EtOAc = 9:1, R_f = 0.14) to afford **3ic** as a clear oil (141 mg, 92% yield). ^1H NMR (300 MHz, CDCl_3) δ 7.74 (d, J = 8.9 Hz, 1H), 6.95 (d, J = 8.9 Hz, 1H), 4.04 (d, J = 14.1 Hz, 1H), 3.81 (s, 3H), 3.75 (s, 3H), 3.66 (d, J = 14.1 Hz, 1H), 1.93 (s, 3H) ppm. ^{13}C NMR (75 MHz, CDCl_3) δ 169.26, 164.10, 131.77, 130.33, 114.58, 65.73, 62.36, 55.80, 53.76, 26.79. HRMS (ESI-TOF) m/z : $[\text{M}+\text{H}]^+$ Calc. for $\text{C}_{12}\text{H}_{16}\text{ClO}_5\text{S}$ 307.0401 Found 307.0407.



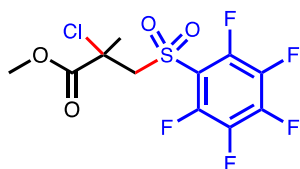
Methyl 2-chloro-2-methyl-3-(thiophen-2-ylsulfonyl)propanoate, **3id**

Following the general procedure, **3id** was prepared from 2-thiophenesulfonyl chloride (88.3 mg, 500 μmol , 1.00 equiv) and methyl methacrylate (50.1 mg, 500 μmol , 1.00 equiv). The crude product was purified by flash column chromatography (hexane:EtOAc = 4:1, R_f = 0.37) to afford **3id** as a white solid (159 mg, 98% yield). ^1H NMR (300 MHz, CDCl_3) δ 7.80 – 7.68 (m, 2H), 7.16 (dd, J = 5.0, 3.8 Hz, 1H), 4.27 (d, J = 14.1 Hz, 1H), 3.88 (d, J = 14.1 Hz, 1H), 3.83 (s, 3H), 2.03 (s, 3H) ppm. ^{13}C NMR (75 MHz, CDCl_3) δ 169.04, 141.23, 134.84, 134.78, 128.08, 66.79, 62.17, 53.83, 26.74. HRMS (ESI-TOF) m/z : $[\text{M}+\text{H}]^+$ Calc. for $\text{C}_{12}\text{H}_{16}\text{ClO}_5\text{S}$ 282.9860 Found 282.9861.



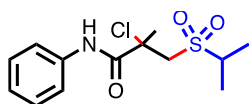
Methyl 2-chloro-2-methyl-3-((4-nitrophenyl)sulfonyl)propanoate, **3ie**

Following the general procedure, **3ie** was prepared from 4-nitrobenzenesulfonyl chloride (111 mg, 500 μmol , 1.00 equiv) and methyl methacrylate (50.1 mg, 500 μmol , 1.00 equiv). The crude product was purified by flash column chromatography (hexane:EtOAc = 9:1, R_f = 0.16). ^1H NMR (300 MHz, CDCl_3) δ 8.37 (d, J = 8.9 Hz, 2H), 8.09 (d, J = 8.9 Hz, 2H), 4.10 (d, J = 14.4 Hz, 1H), 3.86 (d, J = 14.4 Hz, 1H), 3.82 (s, 3H), 1.96 (s, 3H). ^{13}C NMR (75 MHz, CDCl_3) δ 169.12, 145.81, 129.69, 129.16, 124.60, 65.58, 62.22, 54.05, 27.24. ^{13}C NMR (75 MHz, CDCl_3) δ 169.12, 145.81, 129.69, 129.16, 124.60, 65.58, 62.22, 54.05, 27.24. HRMS (ESI-TOF) m/z : $[\text{M}+\text{H}]^+$ Calc. for $\text{C}_{11}\text{H}_{13}\text{ClNO}_6\text{S}$ 322.0147 Found 322.0148.



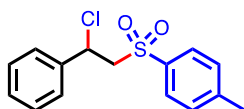
Methyl 2-chloro-2-methyl-3-((perfluorophenyl)sulfonyl)propanoate, **3if**

Following the general procedure, **3if** was prepared from pentafluorobenzenesulfonyl chloride (136 mg, 500 μmol , 1.00 equiv) and methyl methacrylate (50.1 mg, 500 μmol , 1.00 equiv). The crude product was purified by flash column chromatography (hexane:EtOAc = 9:1, R_f = 0.16). ^1H NMR (300 MHz, CDCl_3) δ 4.23 (d, J = 14.8 Hz, 1H), 4.05 (d, J = 14.8 Hz, 1H), 3.86 (s, 3H), 2.02 (s, 3H). ^{13}C NMR (75 MHz, CDCl_3) δ 168.80, 146.99, 143.40, 139.77, 136.45, 66.84, 62.29, 54.07, 27.54. ^{19}F NMR (376 MHz, CDCl_3) δ -135.86 – -136.13 (m, 2F), -142.81 (tt, J = 21.0, 7.8 Hz, 1F), -157.95 – -158.30 (m, 2F). ^{19}F NMR is reported in comparison with previous report [90]. HRMS (ESI-TOF) m/z : $[\text{M}+\text{H}]^+$ Calc. for $\text{C}_{11}\text{H}_9\text{ClF}_5\text{O}_4\text{S}$ 366.9825 Found 366.9829.



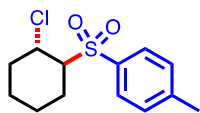
2-chloro-3-(isopropylsulfonyl)-2-methyl-N-phenylpropanamide, **3ug**

Following the general procedure, **3ug** was prepared from 4-isopropylbenzenesulfonyl chloride (71.3 mg, 0.50 mmol, 1.00 equiv) and N-phenylmethacrylamide (82.2 mg, 500 μ mol, 1.00 equiv). The crude product was purified by flash column chromatography (Hexanes:EtOAc = 4:1, R_f = 0.14) to afford **3ug** as an off-white solid (130 mg, 86% yield). ^1H NMR (400 MHz, CDCl_3) δ 8.47 (s, 1H), 7.47 – 7.40 (m, 2H), 7.31 – 7.22 (m, 2H), 7.08 (td, J = 7.2, 1.2 Hz, 1H), 3.99 (d, J = 14.4 Hz, 1H), 3.48 (d, J = 14.4 Hz, 1H), 3.13 (hept, J = 6.9 Hz, 1H), 1.90 (s, 3H), 1.29 (dd, J = 6.9, 2.6 Hz, 6H). ^{13}C NMR (101 MHz, CDCl_3) δ 167.47, 136.80, 129.10, 125.40, 120.76, 66.26, 58.74, 55.80, 31.13, 15.26, 15.10. HRMS (ESI-TOF) m/z : $[\text{M}+\text{H}]^+$ Calc. for $\text{C}_{13}\text{H}_{19}\text{ClNO}_3\text{S}$ 304.0769 Found 304.0775.



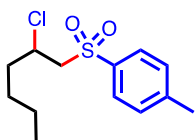
1-((2-chloro-2-phenylethyl)sulfonyl)-4-methylbenzene, **3ab**

Following the general procedure, **3ab** was prepared from 4-methylbenzenesulfonyl chloride (95.4 mg, 500 μ mol, 1.00 equiv) and styrene (52.1 mg, 500 μ mol, 1.00 equiv). The crude product was purified by flash column chromatography (hexane:EtOAc = 9:1, R_f = 0.20) to afford **3ab** as a white solid (146 mg, 99% yield). ^1H NMR (500 MHz, CDCl_3) δ 7.62 (d, J = 8.1 Hz, 2H), 7.26 (s, 5H), 7.23 (d, J = 8.1 Hz, 2H), 5.32 (t, J = 6.9 Hz, 1H), 3.93 (dd, J = 14.9, 6.9 Hz, 1H), 3.83 (dd, J = 14.9, 6.9 Hz, 1H), 2.40 (s, 3H). ^{13}C NMR (101 MHz, CDCl_3) δ 144.88, 138.67, 136.32, 129.77, 129.05, 128.89, 128.19, 127.14, 64.22, 55.13, 21.59.



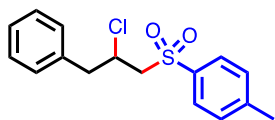
1-((2-chlorocyclohexyl)sulfonyl)-4-methylbenzene, *anti*-3pb

Following the general procedure, ***anti*-3pb** was prepared from 4-methylbenzenesulfonyl chloride (95.4 mg, 500 μmol , 1.00 equiv) and 1-cyclohexene (82.1 mg, 1.00 mmol, 2.00 equiv) The crude product was purified by flash column chromatography (hexane:EtOAc = 9:1, R_f = 0.30) to afford ***anti*-3pb** as a clear oil (114 mg, 82% yield). ^1H NMR (500 MHz, CDCl_3) δ 7.81 – 7.74 (m, 2H), 7.36 – 7.31 (m, 2H), 4.34 (td, J = 7.0, 4.0 Hz, 1H), 3.28 (ddd, J = 7.8, 6.5, 4.8 Hz, 1H), 2.43 (s, 3H), 2.38 – 2.29 (m, 1H), 2.25 – 2.16 (m, 1H), 1.89 (dddd, J = 16.8, 8.3, 4.9, 2.1 Hz, 1H), 1.78 – 1.70 (m, 3H), 1.46 – 1.36 (m, 2H). ^{13}C NMR (101 MHz, CDCl_3) δ 144.83, 135.93, 129.78, 128.75, 67.59, 55.65, 34.34, 23.69, 22.50, 22.46, 21.62.



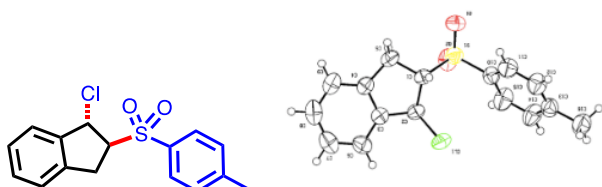
1-((2-chlorohexyl)sulfonyl)-4-methylbenzene, **3vb**

Following the general procedure, **3vb** was prepared from 4-methylbenzenesulfonyl chloride (95.4 mg, 500 μmol , 1.00 equiv) and 1-hexene (84.2 mg, 1.00 mmol, 2.00 equiv) The crude product was purified by flash column chromatography (hexane:EtOAc = 9:1, R_f = 0.30) to afford **3vb** as a clear oil (129 mg, 93% yield). ^1H NMR (500 MHz, CDCl_3) δ 7.80 – 7.74 (m, 2H), 7.34 (d, J = 8.2 Hz, 2H), 4.27 (dt, J = 6.3, 3.9 Hz, 1H), 3.54 (dd, J = 14.6, 6.3 Hz, 1H), 3.44 (dd, J = 14.6, 6.3 Hz, 1H), 2.42 (s, 3H), 1.94 (m, 1H), 1.77 – 1.67 (m, 1H), 1.47 – 1.24 (m, 4H), 0.86 (t, J = 7.2 Hz, 3H). ^{13}C NMR (101 MHz, CDCl_3) δ 145.11, 136.62, 129.98, 128.13, 63.51, 54.58, 37.58, 27.84, 21.86, 21.60, 13.79.



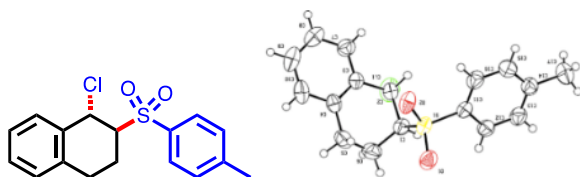
1-chloro-2-tosyl-2,3-dihydro-1H-indene, **3wb**

Following the general procedure, **3wb** was prepared from 4-methylbenzenesulfonyl chloride (95.4 mg, 500 μmol , 1.00 equiv) and 3-phenyl-1-propene (59.1 mg, 500 μmol , 1.00 equiv) The crude product was purified by flash column chromatography (hexane:EtOAc = 9:1, R_f = 0.20) to afford **3wb** as a clear oil (129 mg, 83% yield). ^1H NMR (500 MHz, CDCl_3) δ 7.82 – 7.77 (m, 2H), 7.37 – 7.27 (m, 5H), 7.24 – 7.19 (m, 2H), 4.50 (dq, J = 7.7, 6.2 Hz, 1H), 3.52 (d, J = 6.2 Hz, 2H), 3.29 (dd, J = 14.3, 5.5 Hz, 1H), 3.10 (dd, J = 14.3, 7.7 Hz, 1H), 2.45 (s, 3H). ^{13}C NMR (126 MHz, CDCl_3) δ 145.35, 136.46, 136.01, 130.15, 129.74, 128.71, 128.30, 127.44, 62.43, 54.58, 43.96, 21.79.



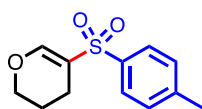
1-chloro-2-tosyl-2,3-dihydro-1H-indene, *anti*-**3xb**

Following the general procedure, *anti*-**3xb** was prepared from 4-methylbenzenesulfonyl chloride (95.4 mg, 500 μmol , 1.00 equiv) and 1H-indene (58.1 mg, 500 μmol , 1.00 equiv) The crude product was purified by flash column chromatography (hexane:EtOAc = 9:1, R_f = 0.3) to afford *anti*-**3xb** as a white solid (154 mg, 100% yield). ^1H NMR (500 MHz, CDCl_3) δ 7.83 – 7.80 (m, 2H), 7.38 – 7.32 (m, 3H), 7.27 – 7.24 (m, 2H), 7.21 – 7.15 (m, 1H), 5.69 (d, J = 4.9 Hz, 1H), 4.15 (ddd, J = 9.0, 6.2, 4.9 Hz, 1H), 3.53 (dd, J = 17.0, 6.2 Hz, 1H), 3.44 (dd, J = 17.0, 9.0 Hz, 1H), 2.45 (s, 3H). ^{13}C NMR (101 MHz, CDCl_3) δ 145.33, 140.32, 138.91, 134.87, 130.03, 129.62, 128.80, 128.02, 125.24, 124.55, 72.69, 60.63, 31.91, 21.68.



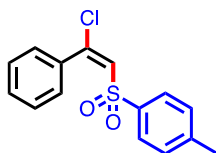
1-chloro-2-tosyl-2,3-dihydro-1H-indene, *anti*-3yb

Following the general procedure, ***anti*-3yb** was prepared from 4-methylbenzenesulfonyl chloride (95.4 mg, 500 μmol , 1.00 equiv) and 1,2-dihydronaphthalene (65.1 mg, 500 μmol , 1.00 equiv). The crude product was purified by flash column chromatography (hexane:EtOAc = 9:1, R_f = 0.30) to afford ***anti*-3yb** as an eggshell color-solid (154 mg, 100% yield). ^1H NMR (500 MHz, CDCl_3) δ 7.80 – 7.74 (m, 2H), 7.35 (m, 3H), 7.24 – 7.20 (m, 2H), 7.07 (m, 1H), 5.57 (d, J = 3.5 Hz, 1H), 3.84 (ddd, J = 6.2, 5.1, 3.5 Hz, 1H), 3.07 (ddd, J = 16.9, 8.9, 5.1 Hz, 1H), 2.89 (dt, J = 16.9, 6.2 Hz, 1H), 2.56 (ddt, J = 14.6, 8.9, 5.6 Hz, 1H), 2.46 (s, 3H), 2.24 (dq, J = 14.6, 6.2 Hz, 1H). ^{13}C NMR (101 MHz, CDCl_3) δ 145.22, 135.96, 135.08, 133.60, 130.10, 129.98, 129.44, 128.82, 128.78, 126.81, 67.37, 54.05, 25.51, 21.66, 19.90.



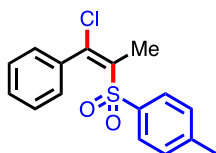
5-(4-methylbenzene)-3,4-dihydro-2H-pyran, 4sb

Following the general procedure, **4sb** was prepared from 4-methylbenzenesulfonyl chloride (95.4 mg, 500 μmol , 1.00 equiv) and 3,4-dihydro-2H-pyran (210.3 mg, 2.50 mmol, 5.00 equiv). The crude product was purified by flash column chromatography (hexane:EtOAc = 9:1, R_f = 0.10) to afford **4sb** as white solid (78.8 mg, 64% yield). ^1H NMR (500 MHz, CDCl_3) δ 7.73 – 7.70 (m, 2H), 7.58 (s, 1H), 7.29 (d, J = 8.0 Hz, 2H), 4.02 – 3.99 (m, 2H), 2.41 (s, 3H), 2.15 (td, J = 6.3, 1.4 Hz, 2H), 1.86 – 1.81 (m, 2H). ^{13}C NMR (126 MHz, CDCl_3) δ 153.47, 143.78, 137.70, 129.79, 127.59, 115.47, 66.62, 21.63, 20.87, 18.94.



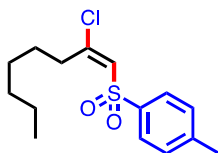
1-((2-chloro-2-phenylvinyl)sulfonyl)-4-methylbenzene, (*E*)-6ab

Following the general procedure, (*E*)-6ab was prepared from 4-methylbenzenesulfonyl chloride (95.4 mg, 500 μmol , 1.00 equiv) and ethynylbenzene (51.1 mg, 500 μmol , 1.00 equiv). The crude product was purified by flash column chromatography (hexane:EtOAc = 9:1, R_f = 0.10) to afford (*E*)-6ab as white solid (145 mg, 99% yield). ^1H NMR (500 MHz, CDCl_3) δ 7.52 – 7.48 (m, 2H), 7.45 – 7.40 (m, 1H), 7.40 – 7.33 (m, 4H), 7.23 – 7.19 (m, 2H), 6.92 (s, 1H), 2.40 (s, 3H). ^{13}C NMR (101 MHz, CDCl_3) δ 147.93, 144.58, 137.71, 134.39, 131.04, 130.63, 129.63, 128.85, 127.99, 127.78, 21.57.



1-((1-chloro-1-phenylprop-1-en-2-yl)sulfonyl)-4-methylbenzene, (*E*)-6bb

Following the general procedure, (*E*)-6bb was prepared from 4-methylbenzenesulfonyl chloride (95.4 mg, 500 μmol , 1.00 equiv) and prop-1-yn-1-ylbenzene (58.1 mg, 500 μmol , 1.00 equiv). The crude product was purified by flash column chromatography (hexane:EtOAc = 9:1, R_f = 0.10) to afford (*E*)-6bb as eggshell color- solid (134 mg, 87% yield). ^1H NMR (500 MHz, CDCl_3) δ 7.42 – 7.38 (m, 2H), 7.37 – 7.32 (m, 1H), 7.31 – 7.26 (m, 2H), 7.22 – 7.19 (m, 2H), 7.18 – 7.14 (m, 2H), 2.38 (s, 3H), 2.33 (s, 3H). ^{13}C NMR (126 MHz, CDCl_3) δ 144.31, 144.09, 137.90, 137.37, 137.08, 129.56, 129.52, 128.87, 127.95, 21.69, 18.13. ^1H NMR (500 MHz, acetone- d_6) δ 7.46 – 7.43 (m, 2H), 7.38 – 7.34 (m, 1H), 7.33 – 7.27 (m, 4H), 7.23 – 7.19 (m, 2H), 2.38 (s, 3H), 2.28 (s, 3H). ^{13}C NMR (126 MHz, acetone- d_6) δ 144.56, 143.45, 138.18, 137.71, 137.33, 129.71, 129.37, 128.80, 127.90, 127.83, 20.67, 17.38.



1-((2-chloro-1-octeny)sulfonyl)-4-methylbenzene, (*E*)-6db

Following the general procedure, (*E*)-6db was prepared from 4-methylbenzenesulfonyl chloride (95.4 mg, 500 μmol , 1.00 equiv) and 1-octyne (110 mg, 1.00 mmol, 2.00 equiv). The crude product was purified by flash column chromatography (hexane:EtOAc = 20:1, R_f = 0.36) to afford (*E*)-6db as white solid (148 mg, 96% yield). ^1H NMR (500 MHz, CDCl_3) δ 7.77 (d, J = 8.3 Hz, 2H), 7.36 – 7.33 (m, 2H), 6.51 (s, 1H), 2.95 – 2.89 (m, 2H), 2.44 (s, 3H), 1.60 – 1.53 (m, 2H), 1.31 – 1.23 (m, 6H), 0.90 – 0.87 (m, 3H). ^{13}C NMR (101 MHz, CDCl_3) δ 154.42, 144.74, 138.53, 130.01, 128.94, 127.40, 34.90, 31.44, 28.46, 27.51, 22.43, 21.59, 13.97.

CHAPTER III
RESULTS AND DISCUSSION
FOR COPPER CATALYZED HALOALKYLATION (C-C FORMATION)

The results of the development of Cu(II) complexes containing quinoline derivatives as photoredox catalysts in atom transfer radical addition (ATRA) for haloalkylation (C-C formation) are discussed in 4 sections according to the following order: synthesis and characterization of Cu(II) complexes, photophysical and electrochemical properties, study of catalytic properties for haloalkylation (C-C formation), and proposed mechanism.

3.1 Synthesis and characterization of Cu(II) complexes

This section is divided into 2 parts i.e., synthesis and characterization of quinoline ligands (**1Q**, **2Q** and **3Q**) and synthesis and characterization of Cu(II) complexes. The numeric characterization data for ^1H NMR, ^{13}C NMR, HRMS, and elemental analysis are presented in the experimental section. The X-ray data, elemental results, NMR, IR and HRMS spectra along with the signal assignments are provided in appendix A.

3.1.1 Synthesis and characterization of quinoline ligands

The synthesis of ligand **1Q**, **2Q**, and **3Q** are shown in Figure 3.1. The **1Q** was obtained via nucleophilic substitution of commercially available 8-aminoquinoline to 4.00 equivalent of 2-(chloromethyl)pyridine in the presence of base and KI catalyst for 48 hours. The **1Q** was isolated by column chromatography in 48% yield along with **QP** as a minor product. The **QP** was synthesized in the same reaction using 1.00 equivalent of 2-(chloromethyl)pyridine for 24 hours. The **QP** was obtained in 79% yield. **QP** was used for further synthesis of ligand **2Q** via Ullmann type coupling reaction with 8-iodoquinoline using CuI and L-proline as a catalyst in the presence of base. The **2Q** was obtained in 80% yield. The same reaction was applied for preparing of ligand **3Q** from the coupling between 8-aminoquinoline and 8-iodoquinoline. The **3Q** was obtained in 33% yield.

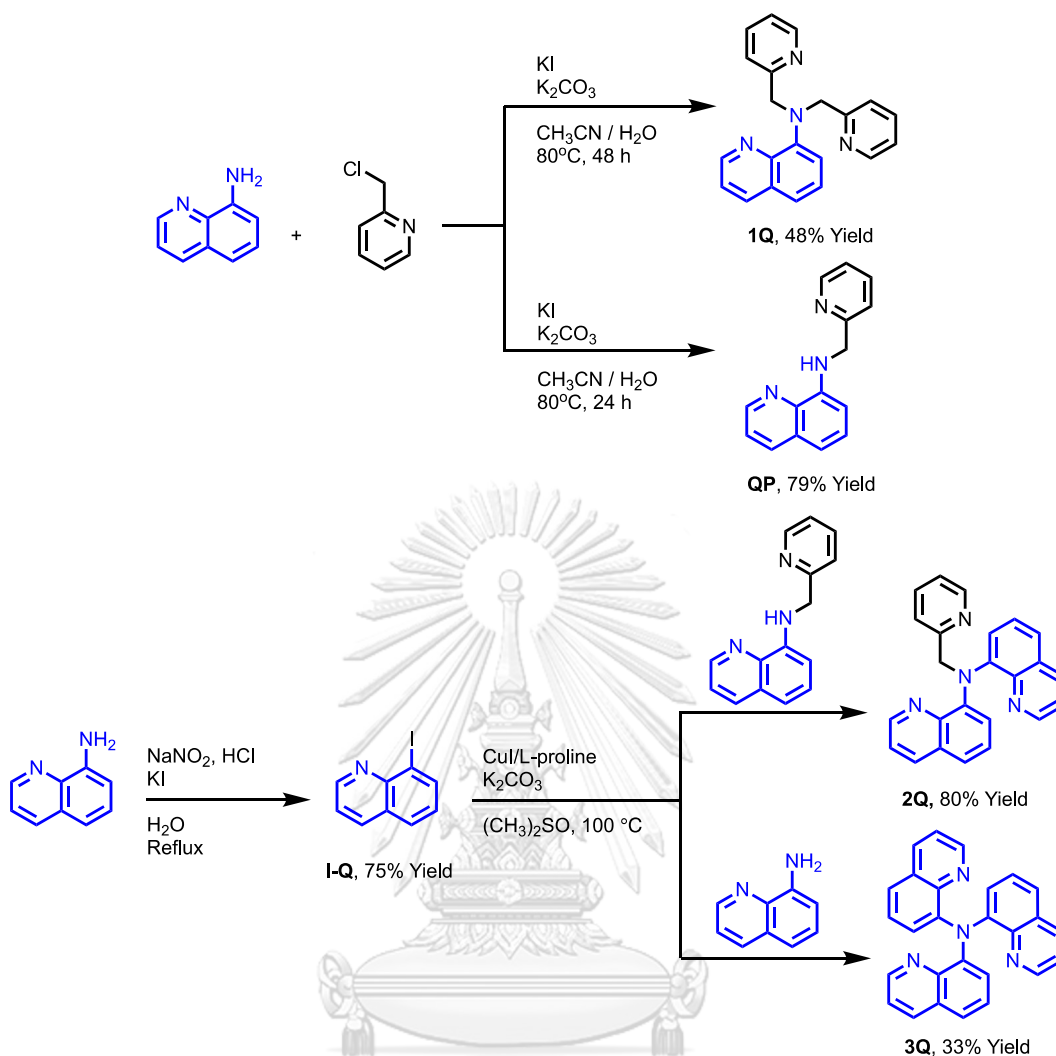


Figure 3.1 Synthesis of ligand **1Q**, **2Q** and **3Q**.

The ^1H NMR spectra of 8-aminoquinoline, **1Q**, **2Q** and **3Q** are shown in Figure 3.2. The signals and integrations were assigned to all protons in the corresponding ligand structures. The absence of primary amine in 8-aminoquinoline (H^g) confirmed the formation of tertiary amine in all ligands. The singlet signals of methylene proton (H^k) with corresponding to number of protons in ligand **1Q** and **2Q** appeared at 4.89 and 5.60 ppm, respectively. The aromatic protons (H^a - H^j) were assigned according to number of remained protons which suggested the ratio of 2:1 and 1:2 of picolyl and quinoline moieties in ligand **1Q** and **2Q**, respectively. For the ligand **3Q**, the aromatic protons were downfield as the increasing of amino quinoline number which results from shielding effect of adjacent quinoline moieties of this rigid structure. The

assigned protons were confirmed by the correlation of ^1H NMR and ^{13}C NMR from 2D NMR experiments (Figure A.2-A.20). The IR and HRMS spectra of synthesized ligands are provided in Figure A21-A23 and Figure A27-A31, respectively.

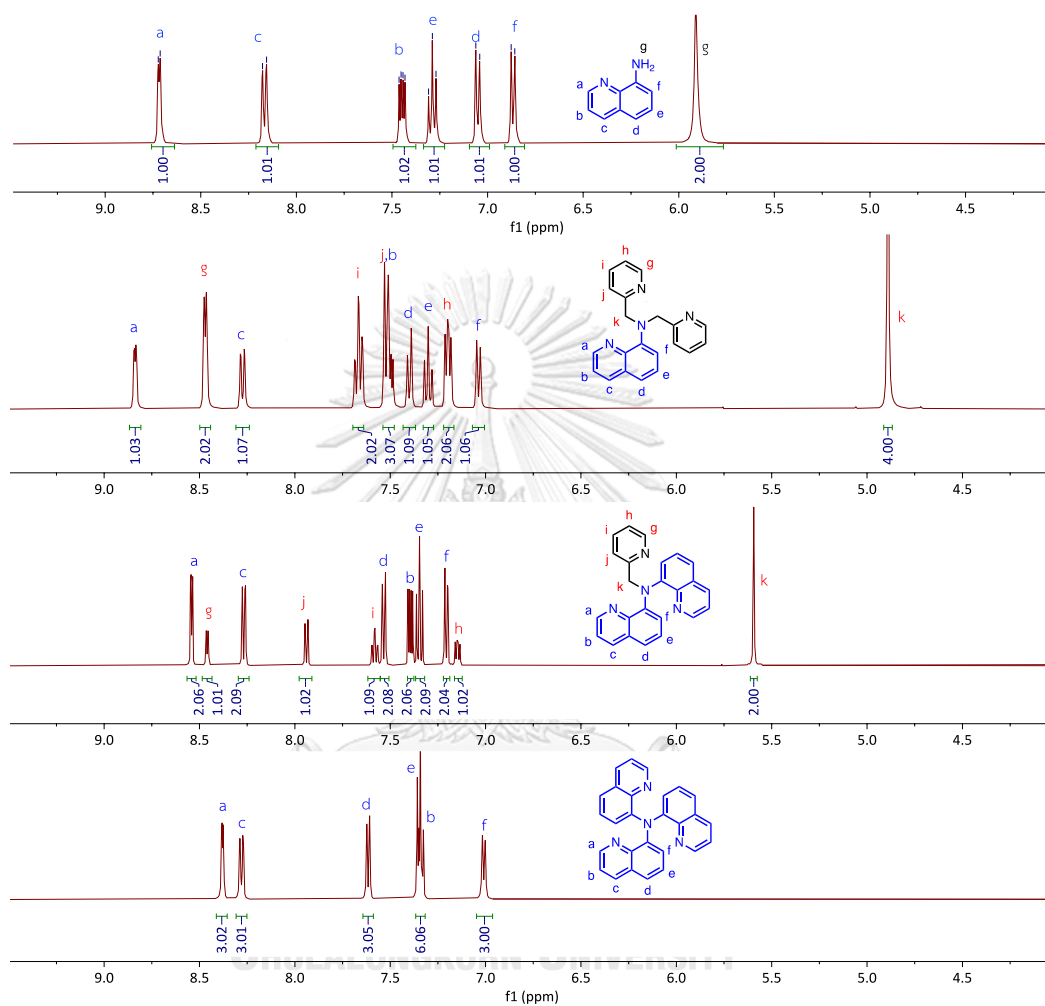


Figure 3.2 ^1H NMR spectra of 8-aminoquinoline, **1Q**, **2Q** and **3Q** in DMSO- d_6 .

3.1.2 Synthesis and characterization of Cu(II) complexes

The Cu(II) complexes with the ligand **1Q-3Q** were synthesized, for catalytic comparison with *in situ* catalyst, using a modification of the procedure reported by Tomislav group [41]. Generally, the complex was obtained simply by stirring a mixture solution of an equimolar of CuCl₂ and the ligand in chloroform followed by precipitation in hexane. The obtained complexes were characterized by X-ray crystallography, IR, and HRMS spectroscopy. The IR and HRMS spectra are provided in Figure A.24-26 and Figure A.32-34, respectively, and the X-ray crystallography results are discussed here.

The crystallography was achieved to establish the stoichiometry and coordination mode of the ligand in the complex. Single crystals of the complexes CuCl₂•**1Q**, CuCl₂•**2Q**, and CuCl₂•**3Q**, suitable for X-ray analysis were obtained through slow evaporation of acetonitrile or methanol solutions of copper(II) chloride with the corresponding ligands at room temperature. The single crystal structures are shown in Figure 3.3 and the selected bond lengths (Å) and bond angles (°) were summarized in Table 3.1 in comparison with CuCl₂•**TPMA** complex [41]. The X-ray results revealed the structures of CuCl₂•**1Q**, CuCl₂•**2Q** consist of discrete cationic complex [Cu^{II}(ligand)Cl]⁺ and non-coordinating chloride anions, while for the CuCl₂•**3Q** complex, the non-coordinating tetrachlorocuprate anionic counterion was observed. In all the complexes, the Cu(II) centers of the cationic species are pentacoordinate CuN₄Cl coordination spheres and adopt distorted square pyramidal coordination geometry with the N1, N2, N3, and Cl1 in the basal plane and atom N4 in the apical position (Figure 3.3 and Figure A.1). The Cu–Cl bond lengths of these complexes are similar to those reported for Cu(II)•**TPMA** complex [41], however, the Cu–N bond lengths with the *N*-quinoline are slightly longer than the Cu–N bond lengths with the *N*-pyridine and *N*-amino moiety (Table 3.1 and A.2) that may differentiate the catalytic properties of these quinoline complexes from that of Cu(II)•**TPMA** complex.

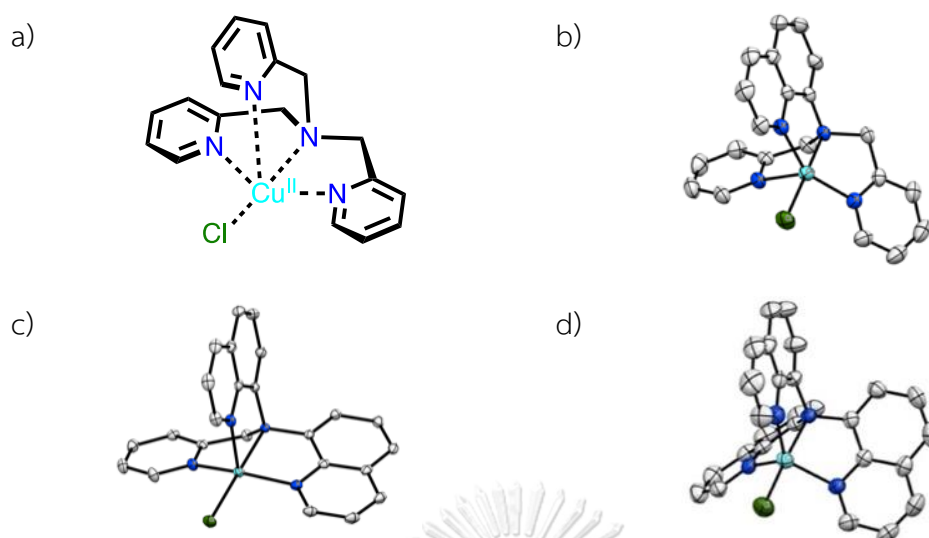


Figure 3.3 The coordination environment around the Cu(II) atom and coordination geometry of ligands a) Cu(II)•TPMA, b) Cu(II)•1Q, c) Cu(II)•2Q, and d) Cu(II)•3Q.

Table 3.1 Selected bond lengths (Å) and bond angles (°) for Cu(II) complexes.

Complex	Cu ^{II} •TPMA[41]	Cu ^{II} •1Q	Cu ^{II} •2Q	Cu ^{II} •3Q
Cu–N1	2.0481	1.9986	2.0016	2.0960
Cu–N2	2.0759	2.0676	2.1034	2.1092
Cu–N3 ^a	2.0759	1.9954	1.9981	2.0160
Cu–N4 ^a	2.0759	2.2738	2.1361	2.0750
Cu–Cl	2.2369	2.2540	2.2573	2.2154
N1–Cu–N2	80.71	81.30	81.02	82.00
N1–Cu–N3 ^a	80.71	150.36	152.77	79.40
N1–Cu–N4 ^a	80.71	94.17	101.16	81.80
N2–Cu–N3 ^a	117.45	83.77	83.62	103.8
N3 ^a –Cu–N4 ^a	117.45	107.66	98.70	130.6
N4 ^a –Cu–N2	117.45	78.55	81.71	118.10
Cl–Cu–N1	180.00	97.68	97.43	98.24
Cl–Cu–N2	99.29	175.12	177.36	176.65
Cl–Cu–N3 ^a	99.29	99.19	96.97	98.25
Cl–Cu–N4 ^a	99.29	97.31	100.73	100.91

^a N3 and N4 in Table 1 are N2ⁱ and N2ⁱⁱ for TPMA complex in Figure 3.3.

3.2 Photophysical and electrochemical properties

The photophysical properties and electrochemical properties of ligands and their Cu(II) complexes including UV-vis absorption, emission, molar absorption coefficients (ϵ), electrochemical data and excited state potential are discussed in this section.

3.2.1 UV-vis absorption and emission

The UV-vis absorption and emission spectra of all ligands and CuCl₂•ligand were recorded in acetonitrile (Figure 3.4) and molar absorption coefficients (ϵ) were summarized in Table 3.2. The spectrum of **TPMA** showed a single absorption band with λ_{\max} at 257 nm, corresponding to the π - π^* transition in the pyridine rings (Figure 3.4a). The absorption bands of **1Q-3Q** are around 350-400 nm, corresponding to the π - π^* transition in quinoline rings, being shifted considerably to longer wavelengths compared to **TPMA**. The increase of the number of quinoline moieties in ligand **2Q** and **3Q** slightly shifted the λ_{\max} to the longer wavelengths (365 and 374 nm, respectively) likely due to the increase of probability for the lone pair electron delocalization from the amino group to the quinoline rings.

The spectrum of CuCl₂•**TPMA** showed hypsochromic shift of π - π^* transition in pyridine rings to around 250 nm and shoulder at ~300 nm (Figure 3.4b). The result indicated the coordinated of pyridine moieties with copper ions which decrease the electron delocalization in pyridine molecule. The similar phenomena found in Cu(II)•**1Q-3Q** which the absorption of coordinated quinoline moieties blue shift to ~300 nm, along with a new weak absorption band around 600-900 nm corresponding to d - d transition in Cu(II) complexes. The emission spectra show complete quenching of the fluorescence around 460-500 nm of **1Q-3Q** in the corresponding Cu(II) complexes. However, only partial fluorescence quenching was observed for Cu(II)•**TPMA**. These results suggest that Cu(II)•**1Q-3Q** are more effective than Cu(II)•**TPMA** for ligand to metal charge transfer (LMCT) processes at higher wavelengths.

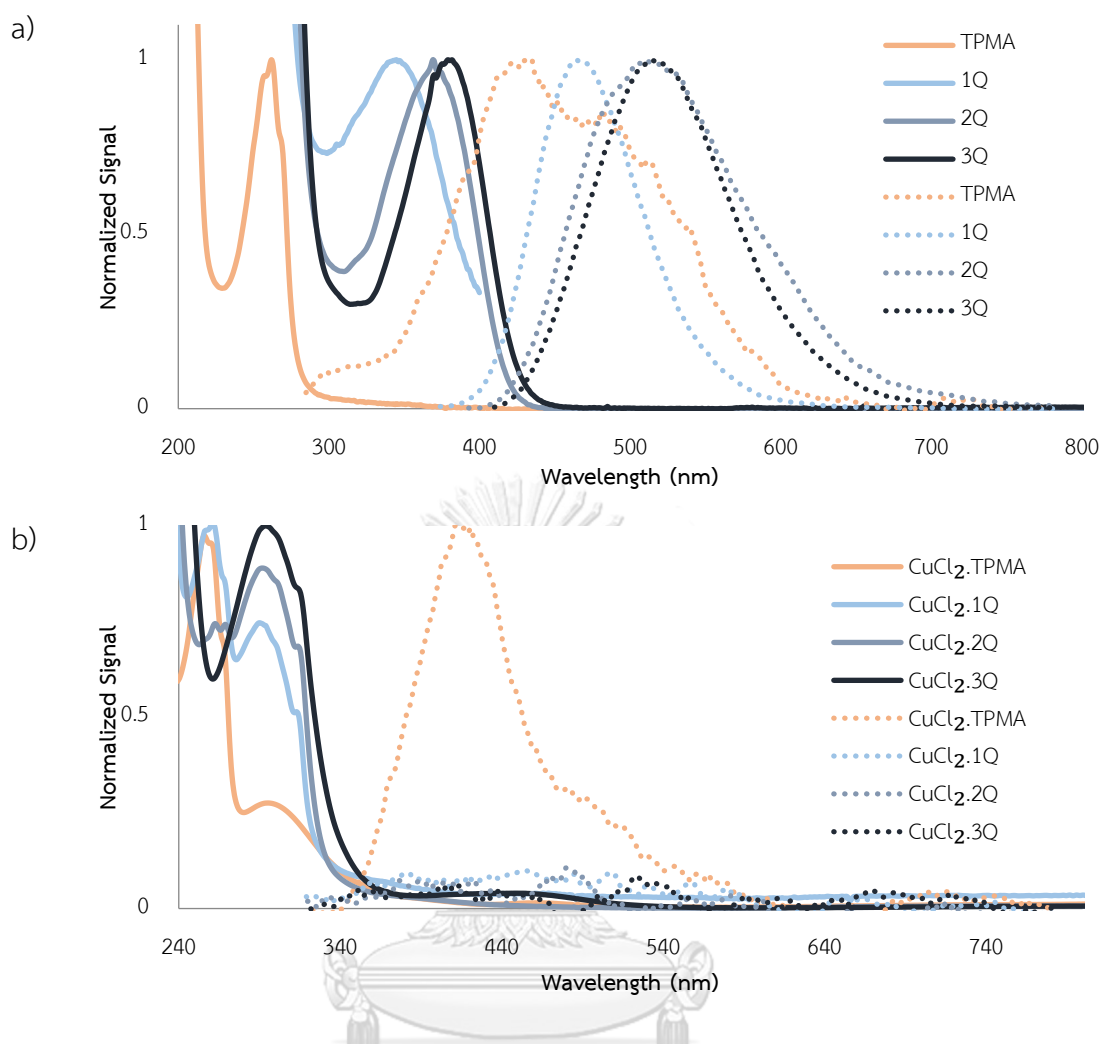


Figure 3.4 Normalized absorption (solid lines) and emission (dot lines) spectra excited at absorption λ_{\max} (See Table 3.2) of a) ligands and b) Cu(II)•ligand complexes in CH₃CN at ambient temperature.

Table 3.2 Summary of absorption of ligands and Cu(II) complexes in CH₃CN.

	Ligand		Cu(II) Complex	
	λ_{\max} (nm)	ϵ (M ⁻¹ cm ⁻¹)	λ_{\max} (nm)	ϵ (M ⁻¹ cm ⁻¹)
TPMA	257	8611	295	2858
1Q	346	3703	291	5457
2Q	365	6151	292	6704
3Q	382	8878	294	7321

3.2.2 Cyclic voltammetry and reduction potentials

The electrochemical data were obtained from the cyclic voltammetry experiments of Cu(II) complexes in comparison with $\text{CuCl}_2 \cdot \text{TPMA}$ and preformed $[\text{Cu}(\text{II})\mathbf{1QCl}]\text{Cl}$ in acetonitrile using ferrocene as an external standard as shown in Figure 3.5 and summarized in Table 3.3. The normalized currents show excellent reversibility in all complexes. The cyclic voltammograms obtained from the preformed and *in situ* generated Cu(II) complexes of **1Q** are essentially identical. The results indicated efficient complexation between the Cu(II) ion with **1Q**. From Table 3.3, the reduction potential ($E_{1/2 \text{ re}}$) of $\text{CuCl}_2 \cdot \text{TPMA}$ is -0.74 V while the $\text{CuCl}_2 \cdot \mathbf{1Q}$, $\text{CuCl}_2 \cdot \mathbf{2Q}$, and $\text{CuCl}_2 \cdot \mathbf{3Q}$ sequentially decrease the reduction potential to -0.67 V, -0.55 V and -0.41 V, respectively. This result indicates that the increase of quinoline moieties decrease the reduction potential of the Cu(II) complexes.

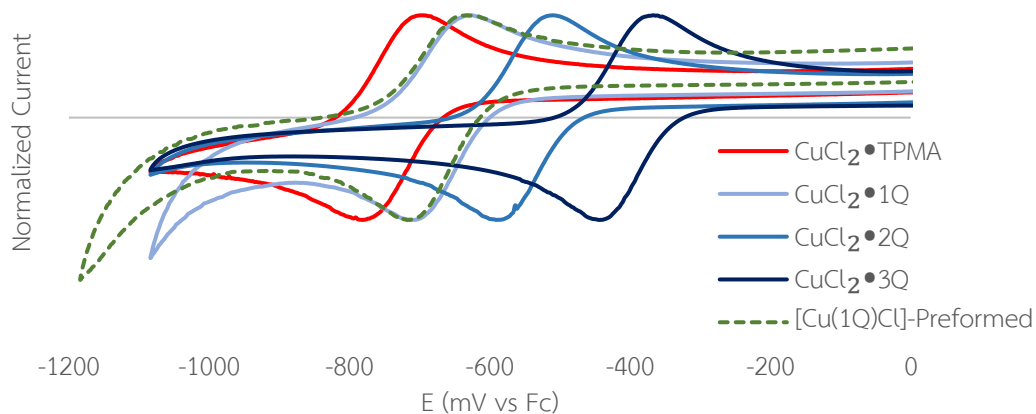


Figure 3.5 Cyclic voltammogram of Cu(II) complexes at 1.0 mM in CH_3CN .

Table 3.3 Summary of electrochemical data for Cu-ligand complexes.

Complex	ΔE_p [mV]	i_{pa}/i_{pc}	$E_{1/2 \text{ re}}$ (Fc) (V)
$\text{CuCl}_2/\text{TPMA}$	73	0.99	-0.74
$\text{CuCl}_2/\mathbf{1Q}$	71	0.94	-0.67
$\text{CuCl}_2/\mathbf{2Q}$	88	0.90	-0.55
$\text{CuCl}_2/\mathbf{3Q}$	76	1.00	-0.41

The standard reduction potentials (Vs SCE) of the Cu(II) and Cu(I) complexes at the ground state and excited state were estimated from the cyclic voltammetry and absorption spectroscopy (Table 3.4). The reduction potentials in reference to the SCE electrode, $E_{1/2\text{ re}}(\text{SCE})$, were calculated from equation (1). The energy gaps (E_{gap}) were estimated from onset absorption wavelength ($\lambda_{\text{on set}}$) of the Cu(II) complexes using equation (2). The excited state of Cu(II) and Cu(I) complexes were estimated from reduction potentials and onset absorption wavelength ($\lambda_{\text{on set}}$) in equation (3) and (4), respectively.

$$E_{1/2\text{ re}}(\text{SCE}) = E_{1/2\text{ re}}(\text{Fc}) + 0.38\text{ V} \quad (1)$$

$$E_{\text{gap}} = 1240/\lambda_{\text{on set}} \quad (2)$$

$$E_{1/2}(\text{Cu}^{2+}\text{L})^* = E_{1/2} + E_{\text{gap}} \quad (3)$$

$$E_{1/2}(\text{Cu}^+\text{L})^{*c} = E_{1/2} - E_{\text{gap}} \quad (4)$$

The redox potentials at the ground state of all Cu(II) complexes are negative indicating the complexes are more stable than the corresponding Cu(I) complexes. However, according to their highly positive potentials, these Cu(II) complexes should be readily reduced to Cu(I) complexes in the excited state. Furthermore, the replacement of one or two pyridine ring in **TPMA** with quinoline rings increases the excited state redox potential of the Cu(II)•**1Q** and Cu(II)•**2Q** complexes. The redox potentials at the excited state of all Cu(I) complexes are more negative than the reduction potentials of alkyl polyhalides (E_{Re}° of CCl_4 , CBr_4 , and CHCl_3 are -0.64, -0.48 and -0.90 V, respectively) [91] that should ensure effective photo-electron transfer from the copper catalyst to these alkyl halide substrates.

Table 3.4 The excited-state potential of copper complexes in CH₃CN.

Ligand	Cu(II)•Ligand				Cu(I)•Ligand		
	$E_{1/2\text{ re}}$ (V vs SCE)	$\lambda_{\text{on set}}$	E_{gap}	$E_{1/2\text{ re}}^*$ (V vs SCE)	$\lambda_{\text{on set}}$	E_{gap}	$E_{1/2\text{ re}}^*$ (V vs SCE)
TPMA	-0.36	510	2.43	2.07	578	2.15	-1.79
1Q	-0.29	520	2.38	2.10	603	2.06	-1.77
2Q	-0.17	545	2.28	2.10	640	1.94	-1.77
3Q	-0.03	600	2.07	2.04	756	1.64	-1.61

3.3 Study of catalytic properties for haloalkylation (C-C formation)

3.3.1 Screening of catalyst

The synthesized quinoline derivatives were studied in comparison with **TPMA** as ligands in copper-catalyzed atom transfer radical addition (ATRA) reactions using styrene and CCl₄ as the model substrates under white LED irradiation (Figure 3.6). The screening condition was established following the reported protocol by Pintauer and co-workers [35, 46, 53] which calls for the combination of Cu(II)•**TPMA** and AIBN. The operation involved an *in situ* generation of each copper complex from CuCl₂ and the ligand (1.00 mol%) in the presence of 5.0 mol% AIBN in acetonitrile. The new Cu(II) complexes with ligand **1Q**, **2Q** and **3Q** cleanly gave the ATRA product **1a** with ¹H-NMR yields above 90% within 24 hours. These yields are two times higher than that obtained from the reaction with the Cu(II)•**TPMA** complex. In addition, the using a preformed Cu(II)•**1Q** complex was equally effective to *in situ* generated complex. Thus, the *in situ* generation of the complex will be used for next study to avoid complication associated with the preparation and isolation of the preformed complex.

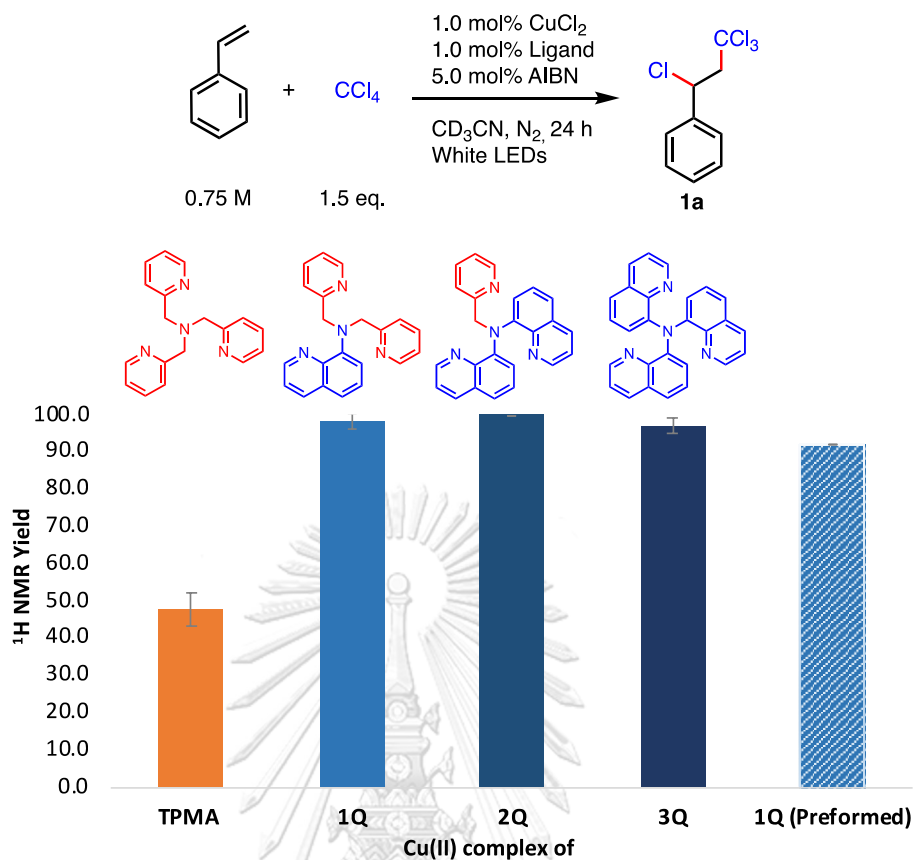


Figure 3.6 ^1H NMR yields of addition product from ATRA reactions between styrene and CCl_4 in the presence of Cu(II) and various ligands using toluene as internal standard (see Figure 2.3 for ^1H NMR spectra).

In line with these findings, the time dependence study displayed the faster reaction rate of these quinoline complexes than that of TPMA ligand which almost complete after 16 hours (Figure 3.7). From all results, the ligand **1Q** showed slightly faster reaction rate. Therefore, the ligand **1Q** will be employed for further study of the ATRA reaction.

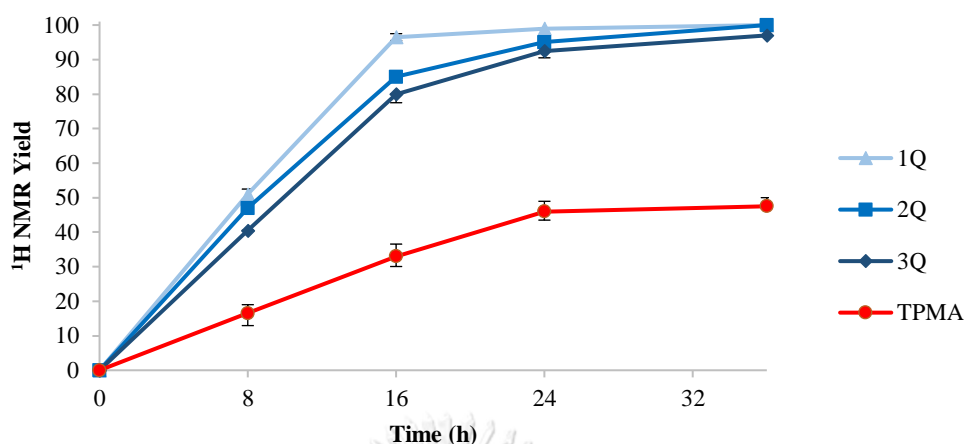


Figure 3.7 Time dependence study for reaction of styrene with CCl₄ catalyzed by Cu(II) complexes of various ligands. Yields were determined by ¹H NMR with toluene as internal standard.

3.3.2 Optimization

Having identified **1Q** as the most suitable ligand, in terms of catalytic activity and ease of synthesis, a set of perhaloalkanes (CCl₄, CBr₄, CHCl₃, and CHBr₃) was briefly evaluated for the ATRA reaction with styrene (Figure 3.8). From the results, high yields (≥ 90%) were obtained with CCl₄ and CBr₄, while lower but still appreciable yields were found with CHCl₃ and CHBr₃.

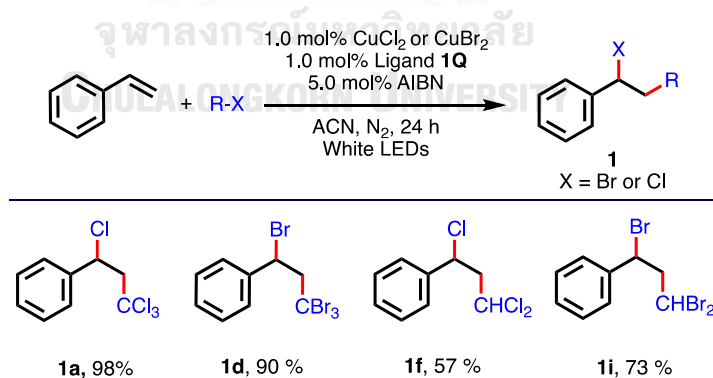


Figure 3.8 ¹H NMR yields of screening reaction between styrene and various alkyl halides catalyzed by a Cu(II) complex of **1Q** using toluene as internal standard.

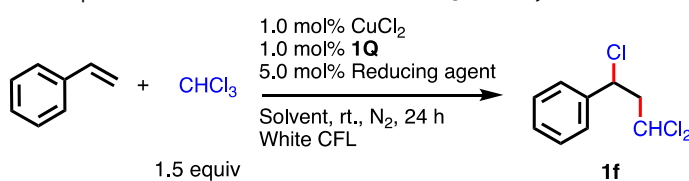
CuCl₂ was used for CCl₄ and CHCl₃ and CuBr₂ was used for CBr₄ and CHBr₃.

To study in detail the effects of the reaction conditions, the ATRA reaction of styrene and CHCl_3 , a less reactive alkyl halide, was used as a model reaction (Table 3.5). Changing the light source from white LEDs to a white CFL source (Figure 2.1, for emission spectra of the light sources see Figure 2.2) under otherwise unchanged conditions result in an increase of the yield from 53 to 64% (Entry 1). Screening of solvents (Entry 2-5) indicated that methanol, being an ecologically benign solvent, gave the highest yield, which may be attributed to the higher solubility of CuCl_2 in this solvent. Notably, the use of methanol as the solvent gave even higher yield than in chloroform, which also is the substrate for the reaction. The reaction in the absence of both CuCl_2 and **1Q** gave no addition product along with the formation of a transparent gel that suggested polymerization of styrene (Entry 6). These results revealed that the $\text{Cu(II)}\cdot\mathbf{1Q}$ complex was essential for promoting the ATRA and inhibiting the radical polymerization reaction. Increasing the reaction time to 48 hours (Entry 7) or employing 3 equivalents of CHCl_3 (Entry 8) resulted in a virtually quantitative yield of the addition product **1f**.

Nevertheless, the role of AIBN for these reactions remains puzzling: According to previous studies, AIBN is assumed to be a reducing agent to convert the Cu(II) to Cu(I) complexes [46, 82]. The reducing agents such as hydrazine, glucose, ascorbic acid, and sodium ascorbate for the $\text{Cu(II)}\cdot\mathbf{1Q}$ (Entry 9-12) were screened. Unfortunately, the other reducing agents were less efficient than AIBN. **1f** was also formed in the absence of any reducing agent, however, in significantly lower yield (Entry 13). Given the success of $\text{Cu(II)}\cdot\mathbf{phen}$ as catalysts for ATRA reactions, [78, 79] for which is shown that the corresponding Cu(I) complexes are readily formed by a visible-light-induced homolysis (VLH), [92] i.e. $\text{LCu(II)Cl}_2 \rightarrow \text{LCu(I)Cl} + \text{Cl}\cdot$, [93] the necessity for a reducing agent for $[\text{Cu(II)Cl}\cdot\mathbf{1Q}]\text{Cl}$ is not obvious (see mechanistic discussion). When CuCl was used in place of CuCl_2 , the yield for **1f** indeed is increased (Entry 16), suggesting that Cu(I) is the catalytically active species. Moreover,

the ATRA reaction did not proceed in the absence of either ligand **1Q** or copper (Entry 14-15) confirming that a free radical process initiated by AIBN is not operating and ligand **1Q** is an important component for our copper catalyzed ATRA reaction under white light. As the final controls, little or no reaction takes place in the dark (Entry 18, 19) or under white light with CuCl alone (Entry 17). This result differed from the study by the Mitani group who showed the feasibility of some ATRA reactions being promoted by CuCl and UV irradiation [94]. The results also confirm the involvement of both a photo-reduction of Cu(II) to Cu(I) complex and photo-activation of Cu(I) complex in the addition reaction catalysis.



Table 3.5 Condition optimization for ATRA of CHCl_3 on styrene.

Entry	Solvent	Reducing agent	Other variation	Conv. [%] ^a	Yield [%] ^a
1	CD_3CN	AIBN	-	65	64
2	$(\text{CD}_3)_2\text{SO}$	AIBN	-	43	43
3	$(\text{CD}_3)_2\text{CO}$	AIBN	-	46	46
4	CDCl_3	AIBN	-	73	72
5	CD_3OD	AIBN	-	87	86 (82) ^b
6	CD_3OD	AIBN	No $\text{CuCl}_2 \cdot \mathbf{1Q}$	25	0
7	CD_3OD	AIBN	48 h	99	98
8	CD_3OD	AIBN	3 equiv CHCl_3	100	100
9	CD_3OD	Hydrazine	-	74	73
10	CD_3OD	D-glucose	-	67	67
11	CD_3OD	L-ascorbic acid	-	61	60
12	CD_3OD	Sodium-ascorbate	-	57	55
13	CD_3OD	-	-	40	40
14	CD_3OD	-	No 1Q	0	0
15	CD_3OD	-	No CuCl_2	0	0
16	CD_3OD	-	CuCl instead of CuCl_2	73	71
17	CD_3OD	-	CuCl instead of CuCl_2 /No 1Q	0	0
18	CD_3OD	-	CuCl instead of CuCl_2 /Dark	11	5
19	CD_3OD	-	Dark	0	0

^a Conversion and yield are determined from ^1H NMR integrations of all alkene protons of styrene and aliphatic protons of product, respectively, against methyl protons of toluene internal standard (Figure 2.4). ^b Isolated yield.

3.3.3 Addition of various alkyl halides to terminal alkenes

To shed further light on the role of AIBN for the title reaction, several ATRA reactions promoted by Cu(II)X_2 /**1Q** in the absence of AIBN were evaluated (Figure 3.9). Notably, halides such as CX_4 or CX_3EWG (EWG = electron-withdrawing group) that are particularly facile to be reduced by Cu(I) gave excellent yields in the addition with styrene (**1a-1e**). Obviously, the active Cu(I)-complex is efficiently formed, presumably via light-induced homolysis, upon which facile electron transfer to the halide initiates the ATRA reaction. These results suggest that AIBN is not necessary for the reduction of Cu(II)•1Q . The substrate scope of this ATRA reaction to electron deficient alkenes, i.e., acrylonitrile, methyl acrylate and methyl methacrylate have extended. The addition of CCl_4 and CBr_4 to each alkene substrate gives a single regioselective product in excellent yield (**2a-4a** and **2b-4b**). The yields of the addition products are virtually the same as the conversions of the substrates in all reactions (Table A.3 and A.4) indicating no competitive polymerization occurred which confirms the effective suppression of polymerization by the copper catalyst. The addition of CCl_3COOMe to methyl methacrylate gave an excellent yield of **4c** but the addition to the other two alkenes gave only low yields of **2c** and **3c**. Apparently, the success of this ATRA reaction depends largely on both the activity of alkyl halide reagents and the stability of the carbon radical generated from the alkene substrates.

Interestingly, the addition of the mixed halide reagent, CBrCl_3 , to each of these alkenes gave a mixture of products containing CCl_3/Br groups and CBrCl_2/Cl groups as well as their 2 crossover products in excellent total yield (Figure 3.10-Figure 3.12). These results indicated the competition between C-Cl and C-Br bond dissociation.

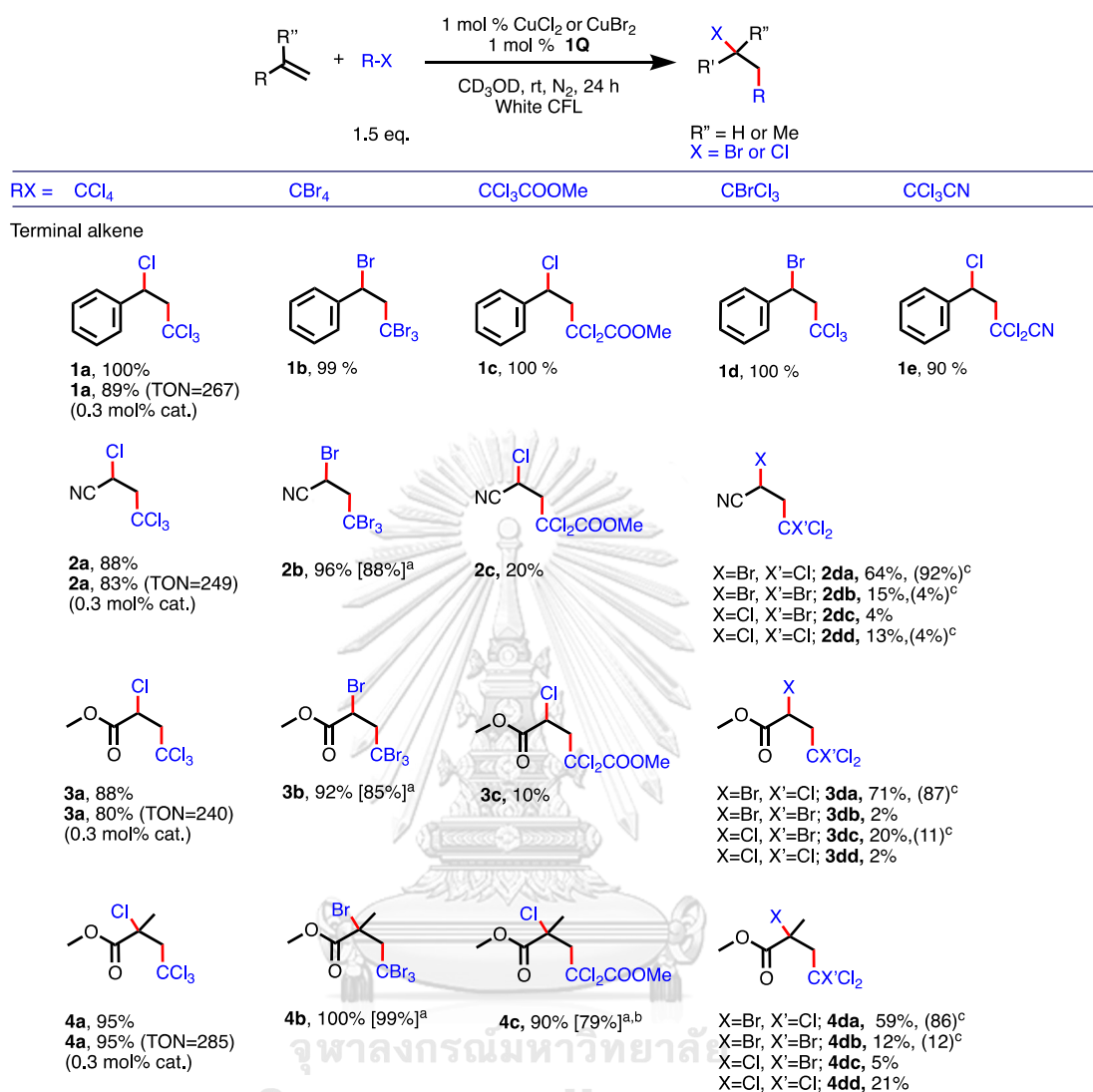
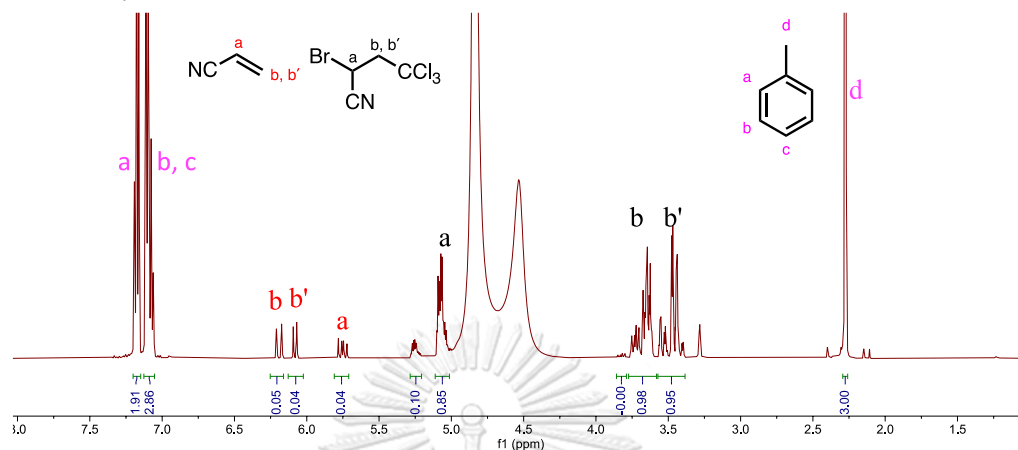


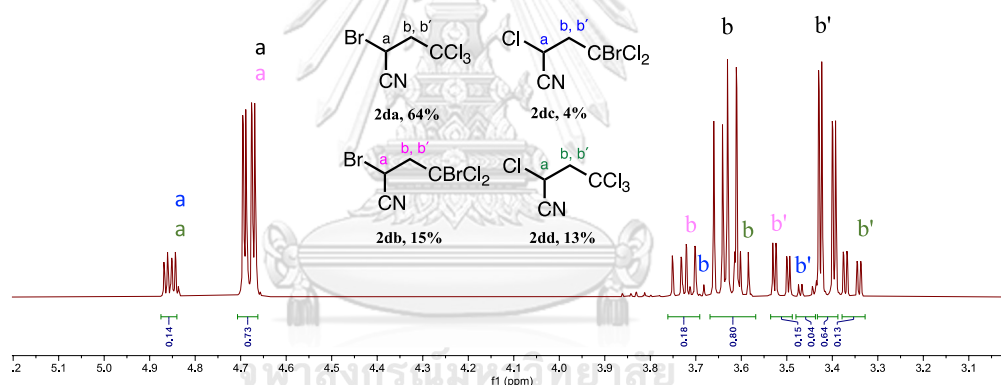
Figure 3.9 Copper catalyzed ATRAs of various alkyl halides to terminal alkenes. Yields are determined from ¹H NMR integrations of all alkene protons and aliphatic protons of product, respectively, against methyl protons of toluene internal standard (Figure 2.3 and 2.4).

^aIsolated yield. ^b1.1136 g of product was isolated from 5 mmol scale reaction in CH₃OH after 24 h. ^c0.3 mol% of catalyst was used to prevent the formation of CBrCl₂/Cl addition products, 48h.

Spectrum for 96% conversion and 94% yield, calculated from ^1H NMR integrations of all alkene protons (red), aliphatic protons of product (black) and methylene protons of toluene (pink).



Spectrum for product ratio determination based on 94% yield, calculated from ^1H NMR integrations of aliphatic protons of each addition product.



Purified **2a** from the reaction between acrylonitrile and CCl_4

*product **2dd** = **2a**

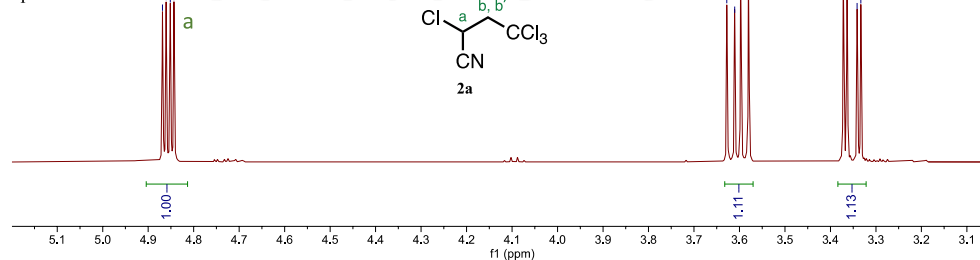
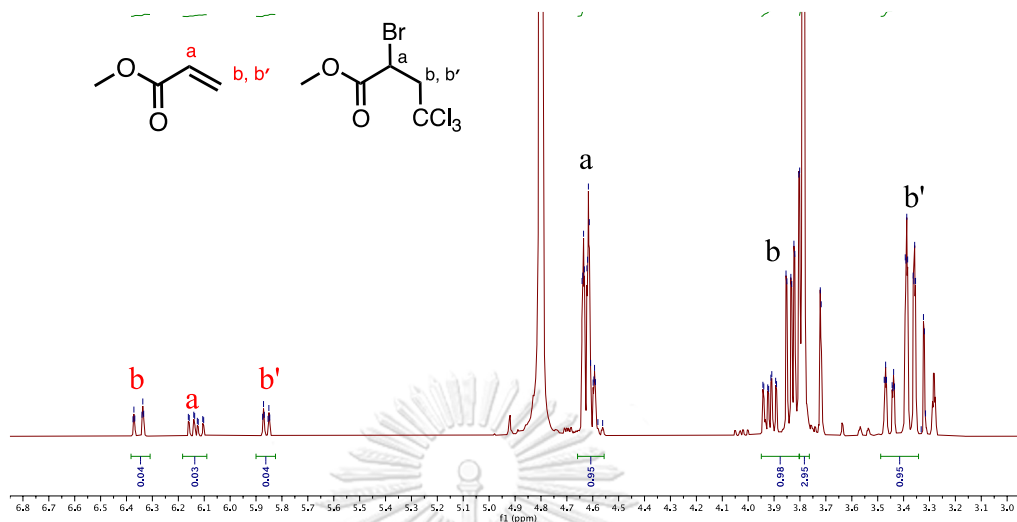


Figure 3.10 ^1H NMR spectra of crude product, after flash column chromatography, from reaction between acrylonitrile and CBrCl_3 in CD_3OD , in the presence of toluene internal standard.

Spectrum for 96% conversion and 95% yield, calculated from ^1H NMR integrations of all alkene protons (red) and aliphatic protons of product (black).



Spectrum for product ratio determination based on 95% yield, calculated from ^1H NMR integrations of aliphatic protons of each addition product.

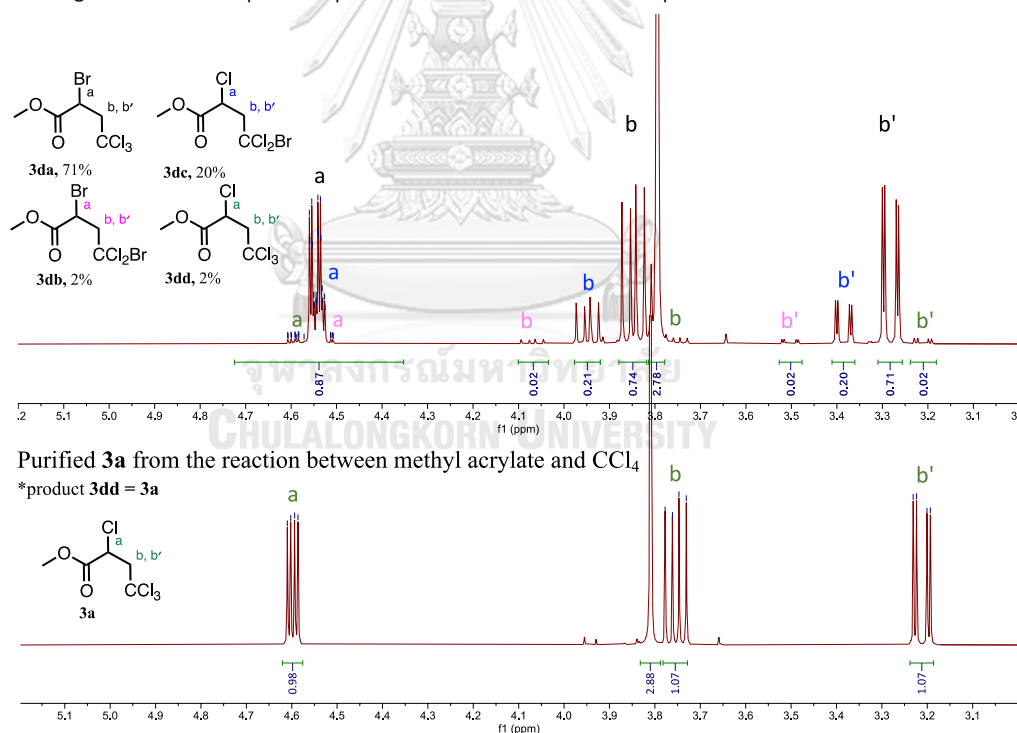
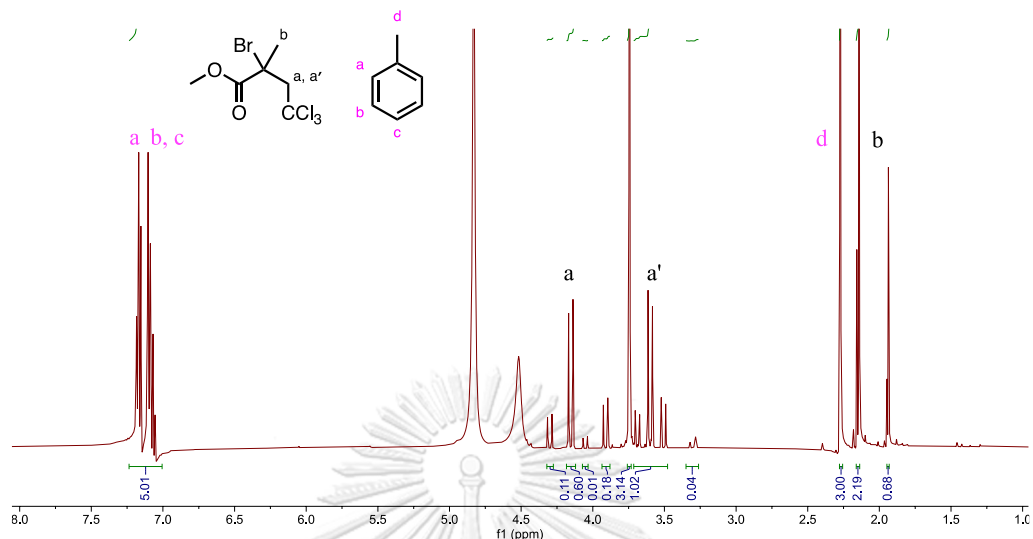
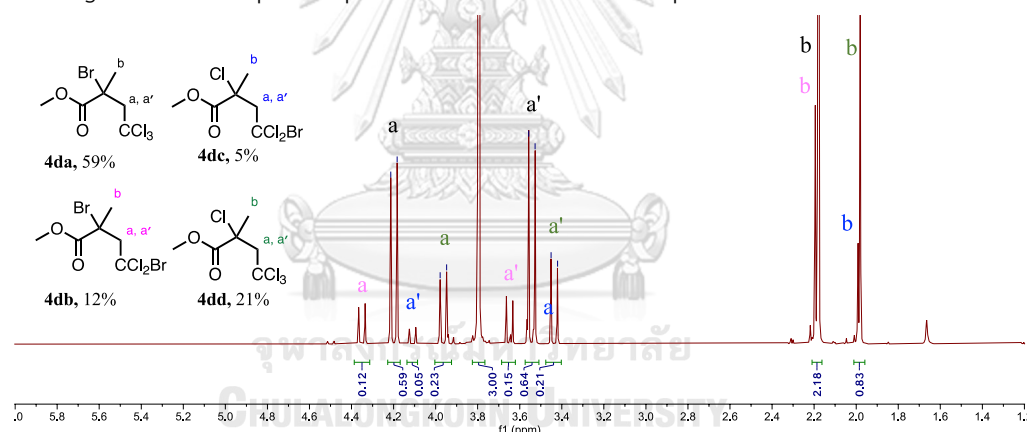


Figure 3.11 ^1H NMR spectra of crude product, after flash column chromatography, from reaction between methyl acrylate and CBrCl_3 in CD_3OD , in the presence of toluene internal standard.

Spectrum for 100% conversion and 97% yield, calculated from ^1H NMR integrations of aliphatic protons of product (black) and methylene protons of toluene (pink).



Spectrum for product ratio determination based on 97% yield, calculated from ^1H NMR integrations of aliphatic protons of each addition product.



Purified **4a** from the reaction between methyl methacrylate and CCl_4

*product **4dd** = **4a**

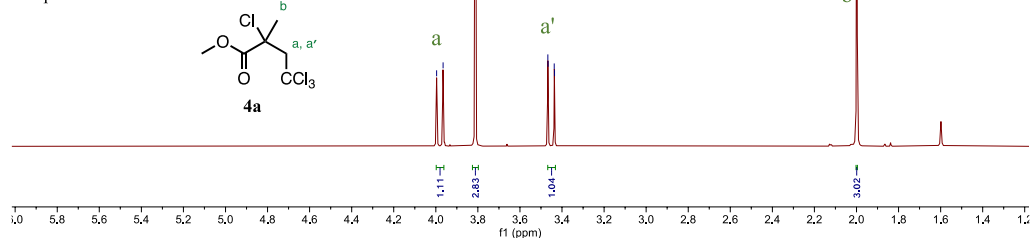


Figure 3.12 ^1H NMR spectra of crude product, after flash column chromatography, from reaction between methyl methacrylate and CBrCl_3 in CD_3OD , in the presence of toluene internal standard.

As previously mentioned, the addition of CBrCl_3 to styrene gave only a single product resulted from only the C-Br bond dissociation and Br abstraction but the mixture of products was obtained from the addition to these electron deficient alkenes. Since the addition of the alkyl radical to the electron deficient alkene generates a less stable radical intermediate, this step may be the rate determining step in the reactions of electron deficient alkenes. This in turn allows the previous steps to establish the equilibrium between the copper catalyzed C-Br and C-Cl bond dissociations. Furthermore, the C-Cl bond formation from the RE process of the copper bound radical of the electron deficient alkene becomes more competitive in comparison with the Br abstraction pathway. The mechanism explains the formations of all products was proposed Figure 3.13.

The incorporation of CCl_3 group into the product can occur either via the direct photolysis or copper activated routes and the incorporation of Br group can occur either via the reductive elimination or Br abstraction routes. The formation of the major product is in good agreement with these many possible pathways. On the other hand, the incorporation of CCl_2Br group into the product can occur via the copper activated route and the incorporation of Cl group can occur via the reductive elimination route. These limited pathways lead to the other products.

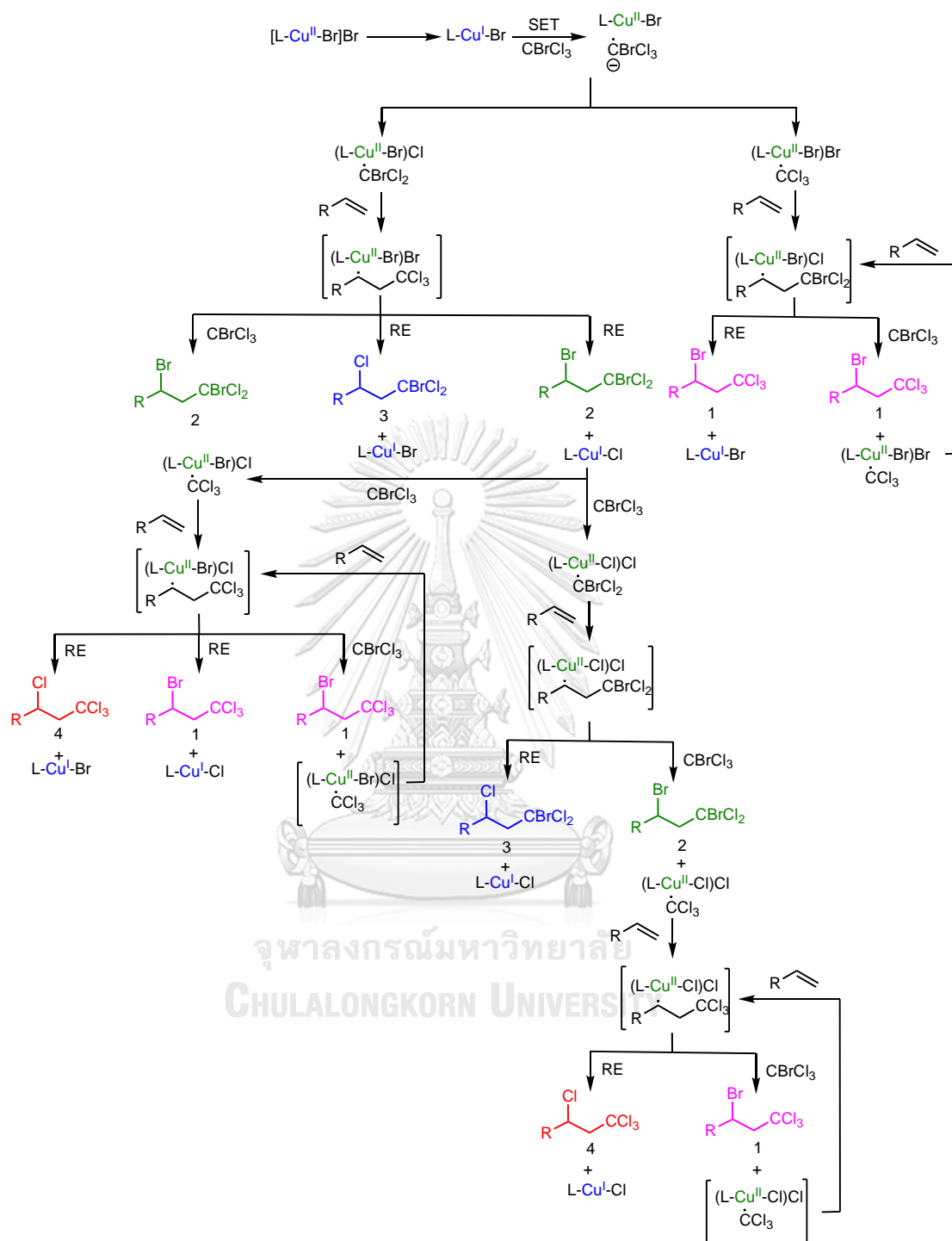


Figure 3.13 ^1H Proposed mechanism for reaction of terminal alkene with CBrCl_3 catalyzed by Cu(II) complex.

Since the addition reaction of CBrCl_3 to electron deficient alkene, methyl methacrylate is not occurred without copper catalyst (Figure 3.14). This result indicated the necessity of copper bound with radical intermediate throughout addition process and prevent the polymerization. To avoid the addition of the CCl_2Br group from copper activated route, the catalyst amount was reduced from 1 to 0.3 mol%. The regioselectivity of the reaction was vastly improved that only **2d-4d** resulting from CCl_3/Br addition were obtained in excellent yields. These results supported our hypothesis and proposed mechanism in Figure 3.13.

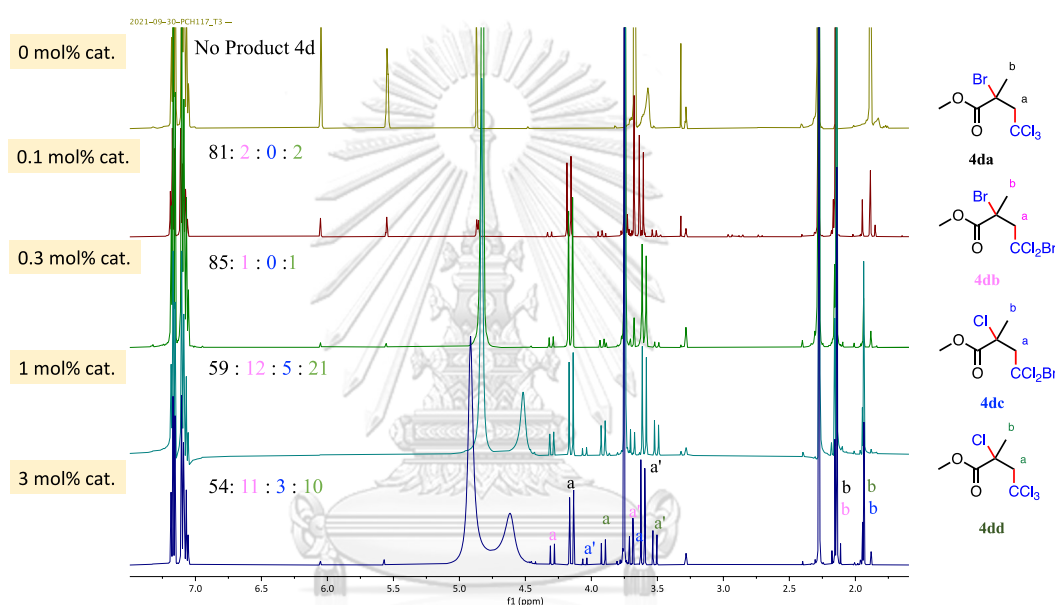


Figure 3.14 ^1H NMR spectra of crude product, after flash column chromatography, from reaction between methyl methacrylate and CBrCl_3 with 0 – 3.0 mol% of $\text{CuCl}_2 \cdot 1\text{Q}$ loading in CD_3OD , in the presence of toluene internal standard.

3.3.4 Addition of various alkyl halides to internal alkenes

Next, the additions between a various alkyl halides and cyclic alkenes (1*H*-indene and 1,2-dihydronaphthalene) were investigated (Figure 3.15). The reactions of 1*H*-indene with CCl₄ or CCl₃CN gave a single regioselective addition product, **5a** or **5b**, respectively. Surprisingly, the reaction with CCl₃COOMe, CBrCl₃ and CBr₄ in methanol gave not only the expected alkyl halide addition products but also the methoxy ether products (**5'c** – **5'e**). These methoxy products were higher with the alkyl bromide, in comparison with the alkyl chloride, suggesting that the original addition products reacted with methanol solvent via a nucleophilic substitution.

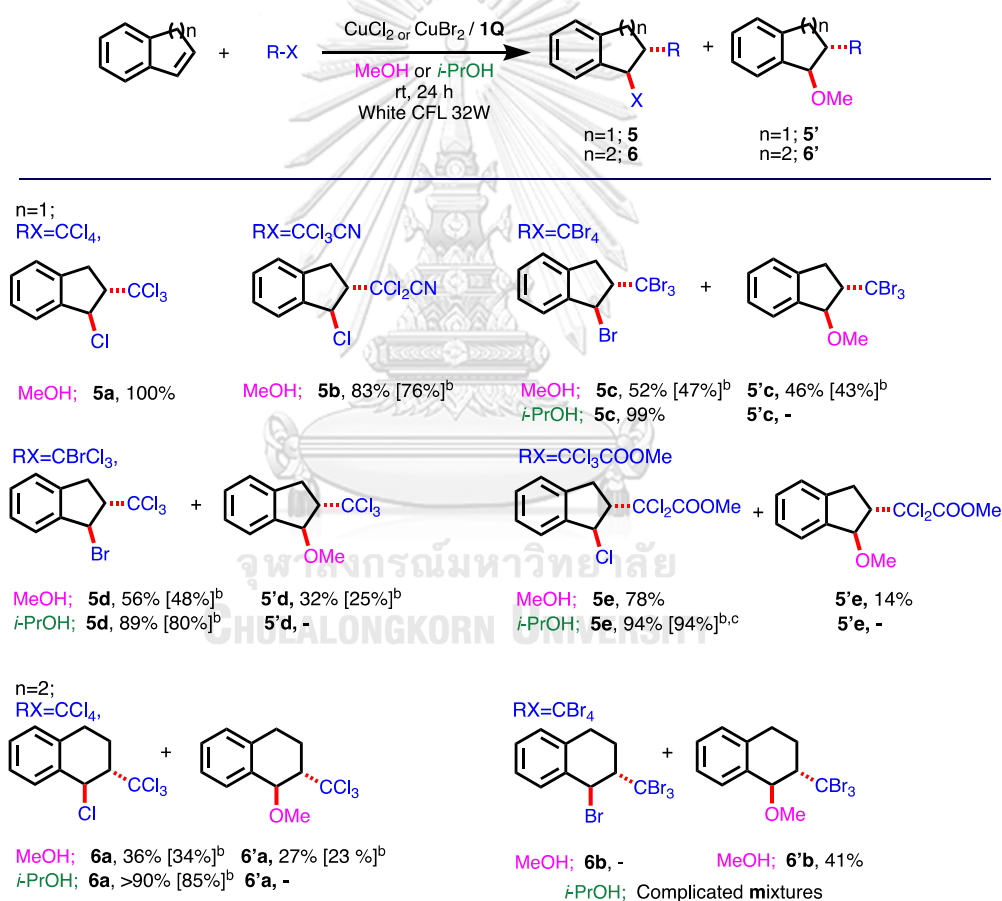


Figure 3.15 Copper catalyzed ATRAs of various alkyl halides to internal alkenes.

^a Yields were determined from ¹H NMR integrations of aliphatic protons of product, against methyl protons of toluene internal standard. ^b Isolated yield. ^c 1.4014 g of product was isolated after 48h of a reaction at 5 mmol scale.

To confirm this hypothesis, the isolated **5e** was stirred in methanol for 24 hours. A substantial amount of the methoxy product was formed, especially at elevated temperatures (Figure 3.16).

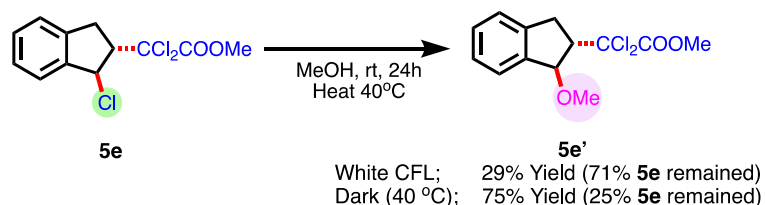


Figure 3.16 Substitution reaction test of halide product in methanol

To mitigate the nucleophilic substitution reaction, a less nucleophilic alcohol, isopropanol was used. The reactions efficiently gave only alkyl halide addition products (**5c-5e**) in excellent NMR yields and some products were isolated with similar yields to demonstrate the usefulness of this reaction in synthesis. It is important to note that the methoxy substituted product was not observed for the reactions of all alkyl halides with acyclic alkenes. The substitution reactions may thus be facilitated by the precipitation of the neighboring group presumably located at the *anti*-position to the halide leaving group on the cyclopentane ring. Therefore, the original addition product was likely the *anti*-diastereomer and this copper catalyzed ATRA reaction is diastereoselective. The stereoisomers of the addition products were confirmed by NOESY NMR spectra in Figure 3.17. The retention products observed for the methoxy substituted products by NOESY NMR spectra in Figure 3.18.

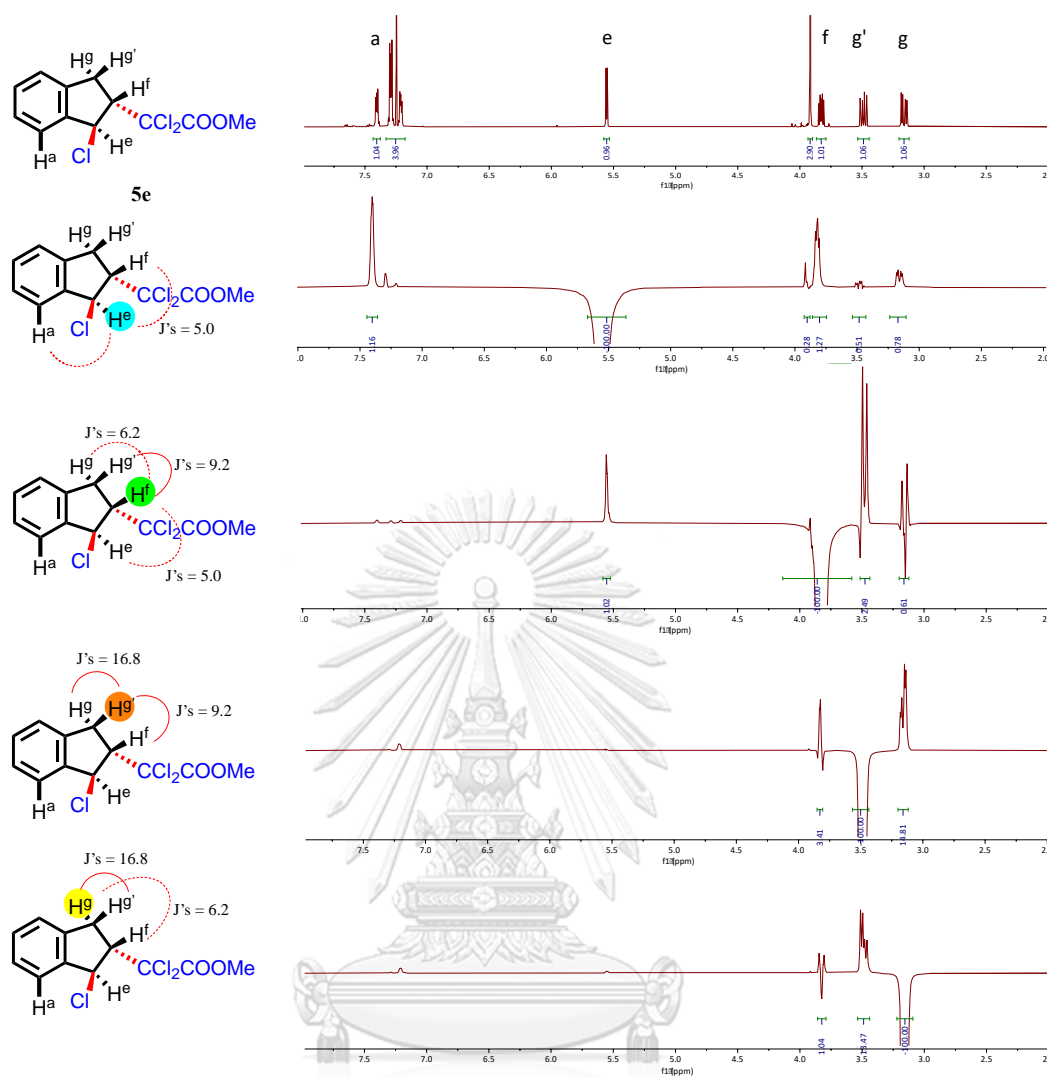


Figure 3.17 NOESY-NMR spectra of **5e**.

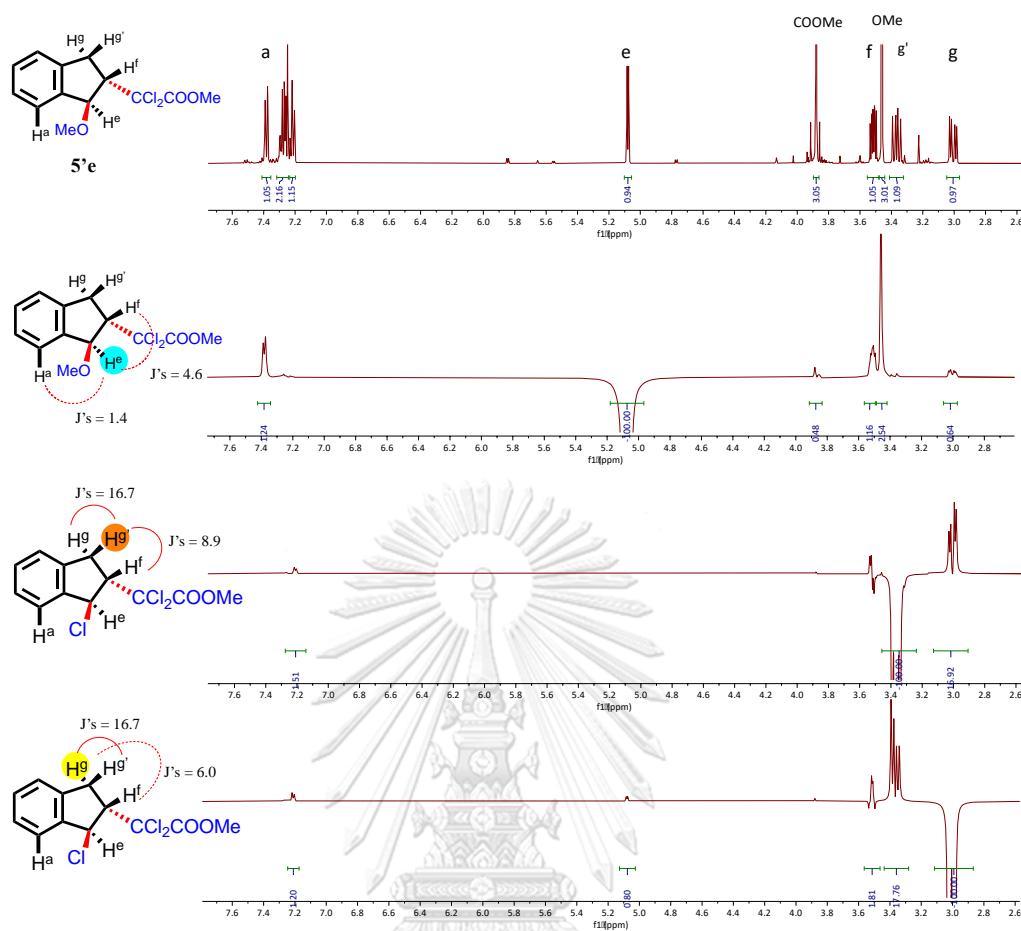
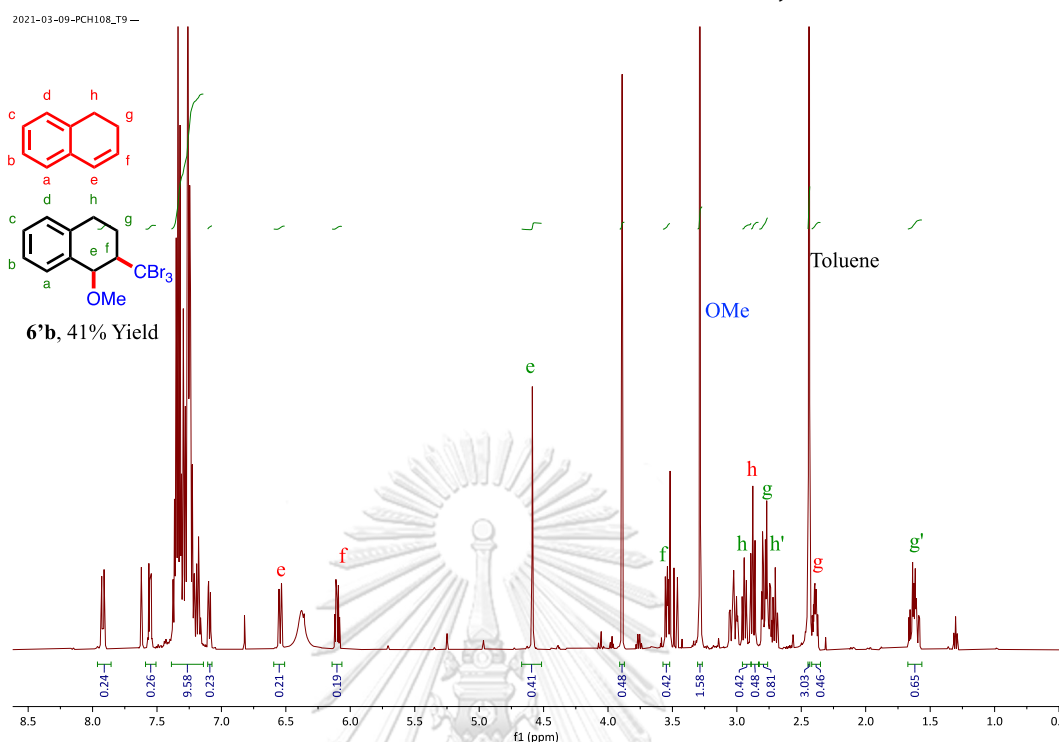


Figure 3.18 NOESY-NMR spectra of **5'e**.

The additions on less rigid cyclic alkene, 1,2-dihydronaphthalene, in methanol showed more tendency to form the methoxy substituted products (**6'a** and **6'b**) for both CCl_4 and CBr_4 . These results may be attributed to that 1,2-dihydronaphthalene can easily adapt the *anti*-periplanar positions of the leaving group (Cl or Br) and the neighboring group (CCl_3 or CBr_3). Again, these substitution reactions could be efficiently suppressed by using isopropanol instead of methanol. Therefore, the addition product from CCl_4 was selectively obtained in excellent yield in isopropanol (Figure 3.19). Unfortunately, the addition of CBr_4 to 1,2-dihydronaphthalene in *i*-PrOH gave a mixture of a few *i*-propoxy substituted products along with other by-products (Figure 3.20).

Spectrum for reaction in methanol, 80% conversion and 41% yield of **6'b**



Spectrum for reaction in *i*-PrOH

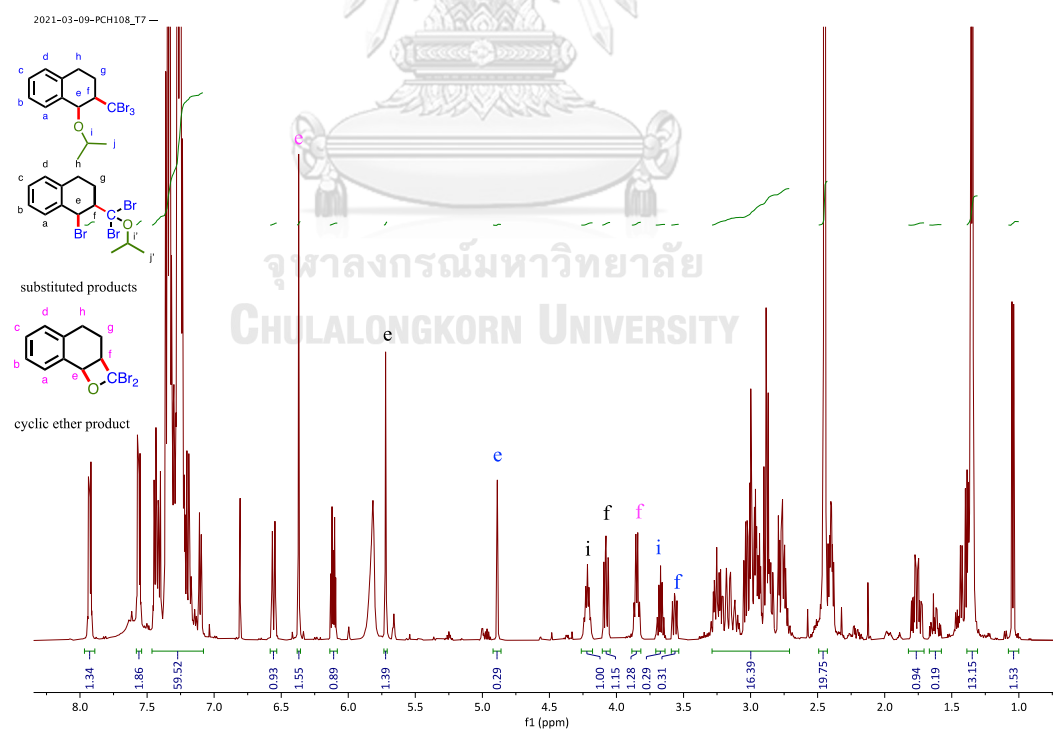


Figure 3.20 ^1H NMR spectra of crude product, after flash column chromatography, from reaction between 1,2-dihydronaphthalene and CBr_4 in the presence of toluene internal standard.

3.3.5 Addition of inactive alkyl halide to styrene

Even though the reaction of active alkyl halide to various alkenes in the absence of AIBN obtained the addition product in good to excellent yields. An inactive halide such as CHCl_3 , CHBr_3 , $\text{CBrF}_2\text{COOEt}$ and benzyl chloride, however, give significantly lower yields under the same reaction conditions when AIBN is omitted (Figure 3.21). However, performing these reactions in the presence of Na_2CO_3 (0.2 equiv) greatly increased the yield (**1f**, **1g** and **1i**) to very high levels. The role of base additive in ATRA reaction has been attributed to scavenging HX arising via hydrogen atom transfer (HAT) from initially formed X^\bullet that causes protonation of the nitrogen ligand and thus deterioration of the copper complexes [78].

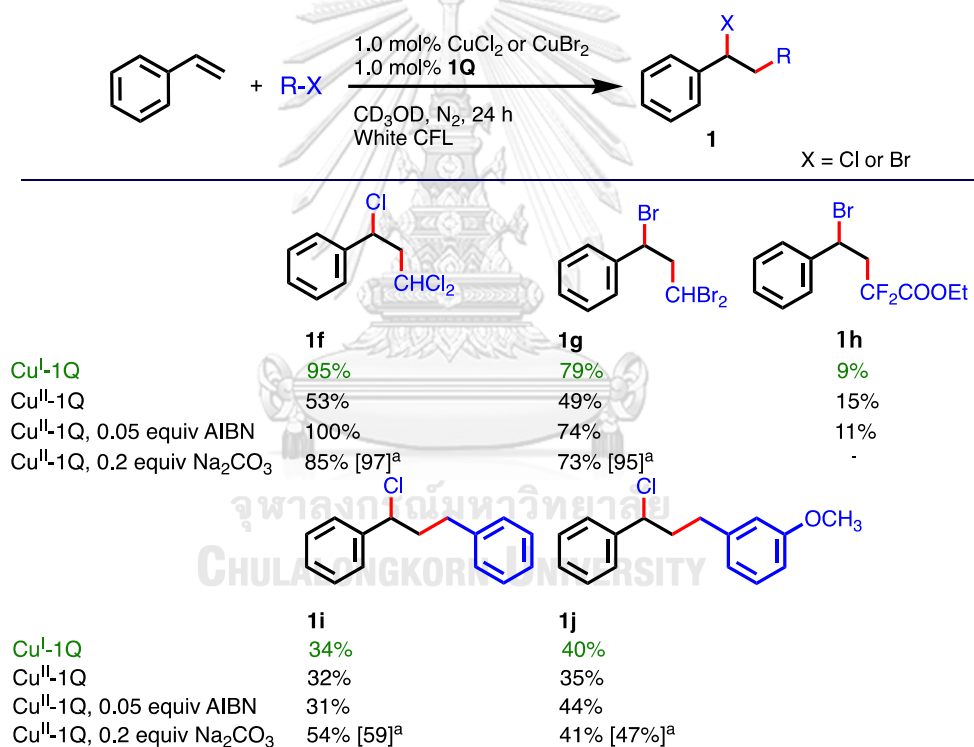


Figure 3.21 Copper catalyzed ATRAs of inactive alkyl halide (1.50 mmol, 3.00 equiv) to styrene (500 μmol , 1.00 equiv).

Yields were determined from ^1H NMR integrations of all alkene protons and aliphatic protons of product, respectively, against methyl protons of toluene internal standard. ^a72h reaction.

3.3.6 Addition of various alkyl halides to alkenes in the absence of catalyst

The additions of active alkyl bromides (CBr_4) to styrene and indene in the absence of copper catalyst or radical initiator under this photoreaction condition still efficiently gave the addition products in high yields (Table 3.6, Entry 1 and 2), while the active alkyl chlorides (CCl_4 , CCl_3CN , and CCl_3COOMe) did not react without the copper catalyst (Entry 4-7). These results suggest that the active alkyl bromides (C-Br dissociation energy = 285 kJ/mol, $\lambda = 420$ nm) can also undergo a direct photolysis to initiate the free radical chain addition reaction [34]. However, the C-Cl bond (327 kJ/mol, $\lambda = 366$ nm) was too strong to be directly dissociated by white light. These results in agreement with previous observation by Zeitler group [95].

Table 3.6 Comparison of alkyl chloride with alkyl bromide in the addition reaction to alkenes in the absence of photocatalyst under white light.



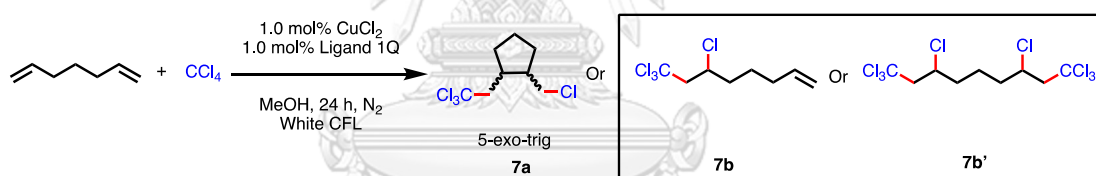
Entry	Alkene	R-X	Solvent	%Con	%Yield
1	Styrene	CBr_4	CD_3OD	68	58
2	1 <i>H</i> -Indene	CBr_4	<i>i</i> -PrOH	100	90
3	Methyl methacrylate	CBr_4	CD_3OD	70	0
4	Styrene	CCl_4	CD_3OD		N.R.
5	1 <i>H</i> -Indene	CCl_4	CH_3OH		N.R.
6	1 <i>H</i> -Indene	CCl_3COOMe	CH_3OH		N.R.
7	1 <i>H</i> -Indene	CCl_3CN	CH_3OH		N.R.

^aThe reactions were performed under white CFL at ambient temperature for 24h.

3.3.7 Cyclization reaction of diene

For the cyclization reaction, the reaction between 1,6-heptadiene and CCl_4 were used as model reactants. The preliminary screening results are shown in Table 3.7. The reaction gave a mixture of the cyclization product **7a** along with the addition products **7b** and **7b'** (Entry 1). When the reaction concentration and equivalent of CCl_4 were decreased, the reaction selectivity toward cyclization was improved (Entry 2-4). However, the reaction conversion and yield dramatically dropped at the lowest concentration tested (Entry 4) probably due to insufficient amount of the catalyst. By increasing the catalyst loading from 1.00 mol% to 2.50 mol%, the conversion and yields of the reaction improved (Entry 5 and 6). However, the high catalyst loading decrease the cyclization selectivity. For further optimization, increasing the reaction time for entry 4 may improve the reaction conversion and yields. Changing the reaction solvent may also affect the reaction selectivity.

Table 3.7 Optimization for ATRC reaction.



Entry	[M]	CCl_4 (eq.)	Cat. (mol%)	% Con ^a	%Yield ^b	
					7a	7b
1	1.00	1.5	1.0	92	39	40
2	0.50	1.2	1.0	86	48	22
3	0.25	1.1	1.0	91	60	15
4	0.10	1.1	1.0	29	24	2
5	0.10	1.1	2.5	80	59	7
6	0.10	1.1	5.0	92	54	29

^a%Conversion was calculated from ^1H NMR signals of remaining alkene. ^b%Yield were estimated from CHCl and CH_2CCl_3 ^1H NMR signals of the products. Toluene was used as an internal standard.

3.4 Proposed mechanism

From the catalytic reaction study, a mechanism is proposed for the copper-catalyzed photo-addition of an alkyl halide to an alkene as shown in Figure 3.22. First, Cu(I) complex was generated from Cu(II) complexes via visible-light-induced homolysis (VLIH) or halogen atom transfer (XAT) process. For VIHC, the base additive was used to scavenging HX arising via hydrogen atom transfer (HAT). For the reaction using AIBN as the additive, AIBN acts as a halogen atom transfer (XAT) reagent, rather than forming Cu(I)X by the homolytic cleavage of Cu(II)X₂ complex. By this way, the active Cu(I) complex is generated without the build-up of HX in the course of the reaction. Next, the generated Cu(I) complex is subsequently photo-activated to enter the photoredox catalytic cycle. The photo activated Cu(I) complex then reduces the alkyl halide via a single electron transfer (SET), followed by the R-X bond dissociation to form the Cu(II) bound radical to be consistent with the observation of the polymerization of styrene in the absence but not in the presence of the copper catalyst.

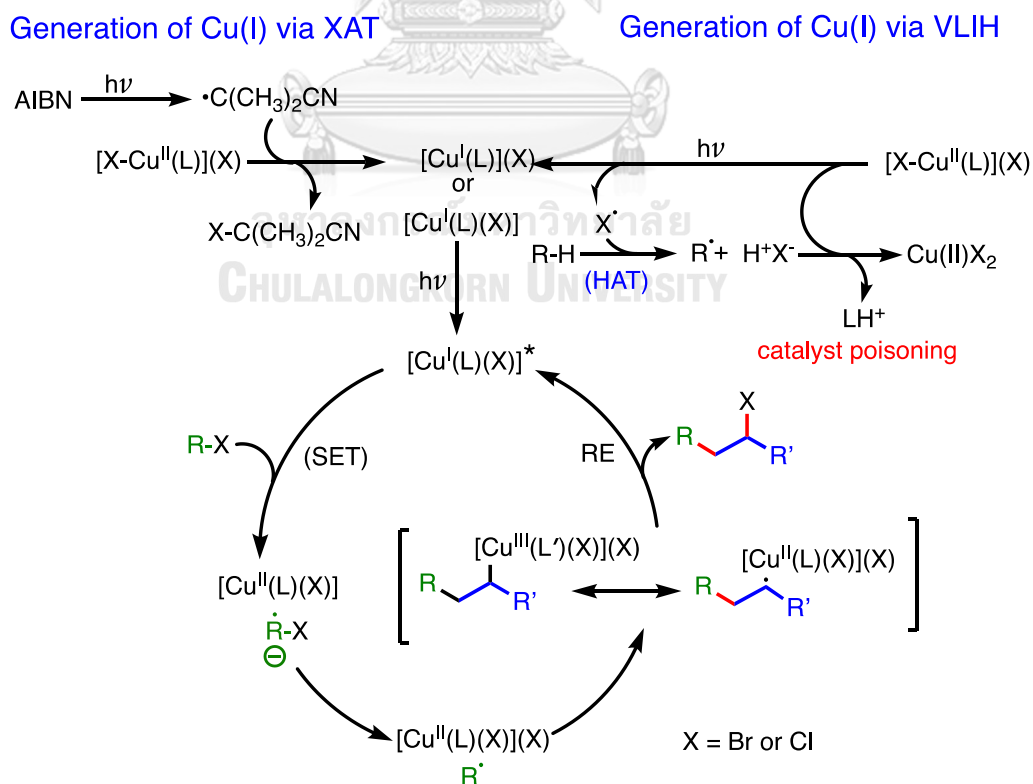


Figure 3.22 Proposed mechanism.

To support the proposed mechanism, a kinetic study and spectroscopy study (UV-Vis, NMR and EPR) were performed. The results gave strong evidences for Cu(I) generation from Cu(II) via VIHC and Cu(I) generation from Cu(II) via XAT using AIBN as a reducing agent, which are presented and discussed in the following sections.

3.4.1 Kinetic study

The kinetic study between styrene and CCl_4 using $\text{CuCl}/\mathbf{1Q}$ in methanol without AIBN under CFL light revealed the high efficiency of Cu(I) complex that photocatalyzed the reaction to be completed within 9 hours (Figure 3.23a). Switching the light on and off every 3 hours showed that the reaction proceeded much faster in the presence of light. In addition, the reaction in the dark at 40°C showed slower reaction and lower final yield (50%). These results suggest that the activation of the Cu(I) complex for SET is a photo process. The similar results, with slightly slower reaction rate, were observed with the experiments using $\text{CuCl}_2/\mathbf{1Q}$ (Figure 3.23b) consistent with the requirement of Cu(II) to Cu(I) conversion in the reaction mechanism. The very low final yield (<10%) obtained from the reaction using $\text{CuCl}_2/\mathbf{1Q}$ conducted in the dark also confirmed that the generation Cu(I) complex is also a photo process.

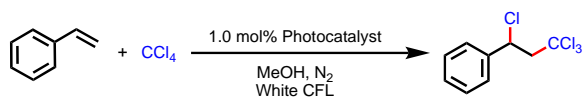
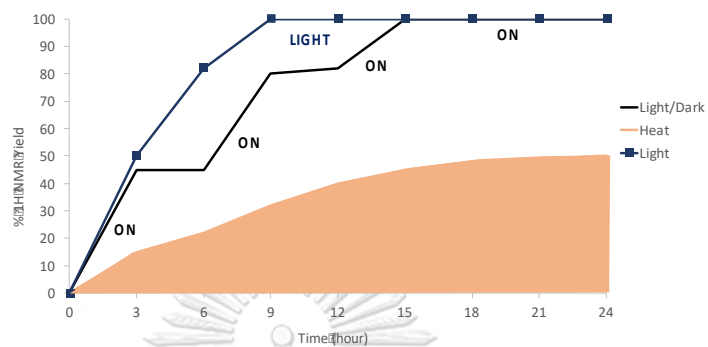
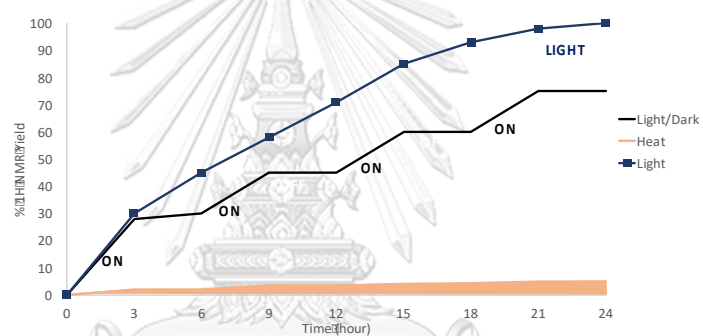
a) Photocatalyst = $\text{CuCl}/\mathbf{1Q}$ b) Photocatalyst = $\text{CuCl}_2/\mathbf{1Q}$ 

Figure 3.23 Kinetic plots for ATRA of styrene and CCl_4 catalyzed by a) $\text{CuCl}/\mathbf{1Q}$ b) $\text{CuCl}_2/\mathbf{1Q}$ with $[\text{Styrene}]:[\text{CCl}_4]:[\text{Cu}] = [1.00]:[1.50]:[0.01]$ under light, heat, or light/dark condition standard.

3.4.2 Evidences for Cu(I) generation from Cu(II) via VIHC

The UV absorption experiment was set up to establish the generation of active Cu(I) from Cu(II) under this condition (Figure 3.24). From the beginning, absorption spectrum of CuCl/1Q and CuCl₂•1Q in methanol are shown in red line and blue line, respectively. The absorption spectrum of CuCl/1Q showed an absorption peak around 460 nm. The irradiation of the solution of CuCl₂•1Q in methanol with CFL light resulted in an increase of an absorption peak at the same position observed in the spectrum of CuCl/1Q solution. These results confirmed the generation of active under this condition. These results strongly support our hypothesis that the VLH of Cu(II) to Cu(I) complex can effectively proceed in methanol.

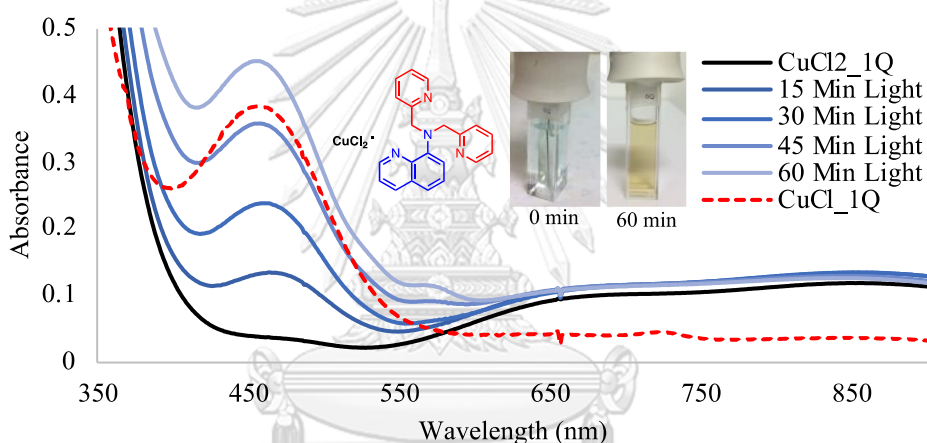
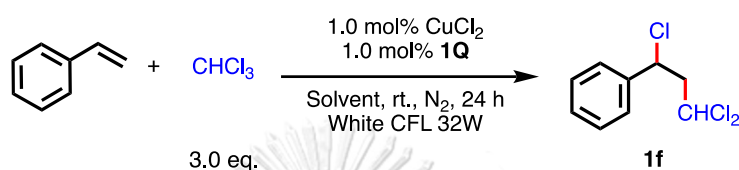


Figure 3.24 Absorption spectra of copper complex solutions before and after being placed under white light a) 1.0 mM CuCl₂•1Q in methanol (blue lines) compared with 0.1 mM CuCl/1Q in methanol (red line).

For more evidence, the ATRA reaction between CHCl₃ and styrene in various solvents were studied in Table 3.8. The addition products were observed in various polar solvents such as dichloromethane or dimethyl sulfoxide. The highest yield was found when using chloroform, reagent as a solvent. For the low polarity solvent, acetone and benzene showed no conversion which due to the low solubility of catalyst. The addition yield in methanol and *tert*-Butanol gave a similar yield indicate that the methanol is not reducing agent for this reaction. These results strongly support the photo-generation of Cu(I) complex via visible-light-induced homolysis

(VLIH). Lastly, the addition in acetonitrile was drop from 64% yield in the presence of AIBN (Table 3.5, Entry 1) to 2% yield in the absence of AIBN (Table 3.8, Entry 2). This result somehow suggested the disruption of acetonitrile to catalyst and prevent the photo cleavage process.

Table 3.8 ATRA of CHCl_3 on styrene in various solvents in the absence of reducing agent.



Entry	Solvent	%Con.	%Yield
1	Methanol	56	53
2	Acetonitrile	4	2
3	Dimethyl sulfoxide	38	24
4	Acetone	0	0
5	Chloroform	68	63
6	Benzene	0	0
7	Dichloromethane	-	47
8	<i>tert</i> -Butyl alcohol	-	52

3.4.3 Evidences for Cu(I) generation via XAT using AIBN as reducing agent

The UV absorption experiment in acetonitrile solution supported this observation. The absorption peak around 460 nm was only observed when the solution of $\text{CuCl}_2 \cdot \mathbf{1Q}$ was irradiated in the presence of AIBN (Figure 3.25a) while very small peak was observed in the absence of AIBN (Figure 3.25b).

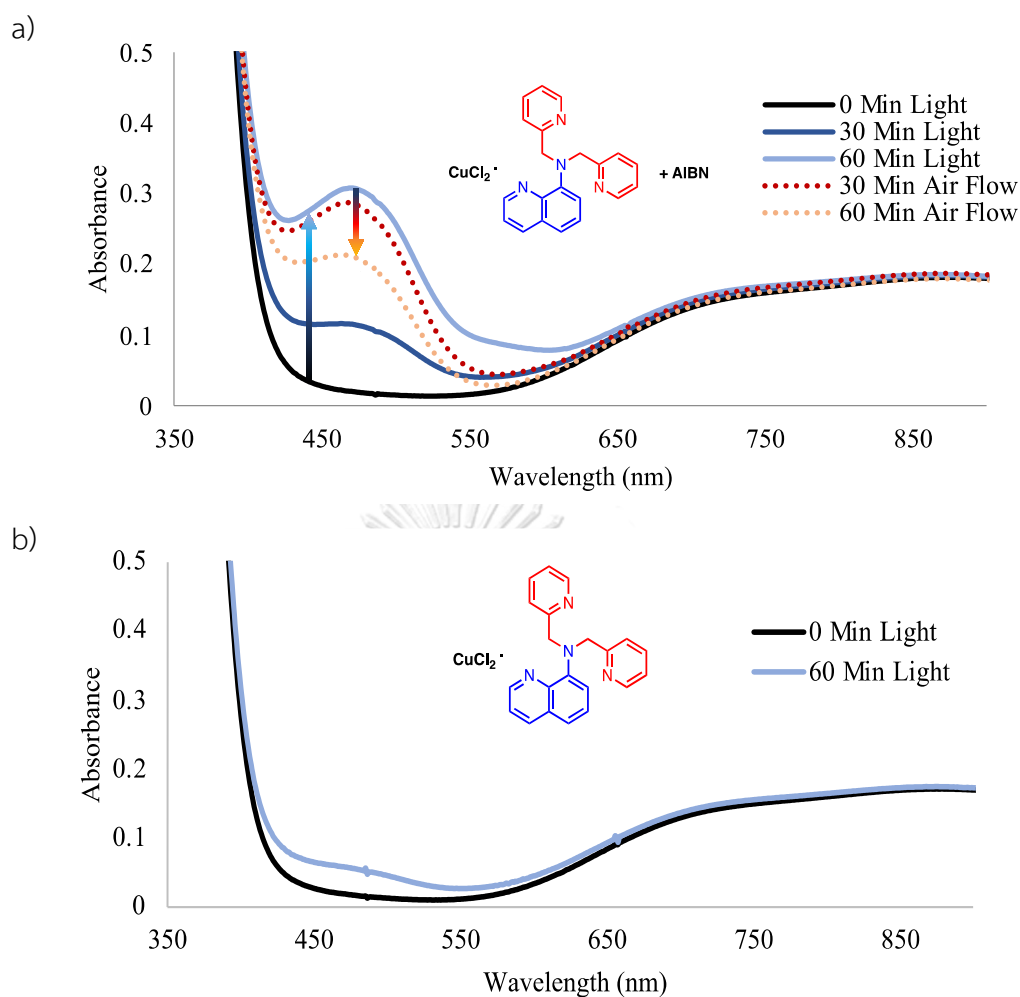


Figure 3.25 Absorption spectra of copper complex solutions before and after being placed under white light a) 2mM $\text{CuCl}_2 \cdot \mathbf{1Q}$ in CH_3CN in the presence of 15 eq. AIBN b) 2mM $\text{CuCl}_2 \cdot \mathbf{1Q}$ in CH_3CN in the absence of AIBN.

The *in situ* generated complexes of $\text{CuCl}_2 \cdot \mathbf{1Q}$ in the presence and absence of AIBN in CD_2Cl_2 showed no observable signals corresponding to the complex (Figure 3.26) mainly due to its paramagnetic nature. In the absence of AIBN, the ^1H NMR spectrum after 7 hours of white light irradiation showed similar pattern of the Cu(I) complex but not at the same chemical shifts implying that another form of Cu(I) complex was generated. In the presence of AIBN, the irradiation gave a ^1H NMR signals at the same position with those of *in-situ* generated Cu(I) complex. It is also interesting to note that stronger and cleaner signals of the Cu(I) complex was obtained in the presence of AIBN confirming that AIBN facilitated the generation of

Cu(I) complex from Cu(II) complex. Furthermore, the ^1H NMR signals in the aliphatic region corresponding to AIBN showed a new signal at 1.90 ppm corresponding to $\text{CCl}(\text{CH}_3)_2\text{CN}$ [96] that can confirm the role of AIBN in the halogen abstractor process.

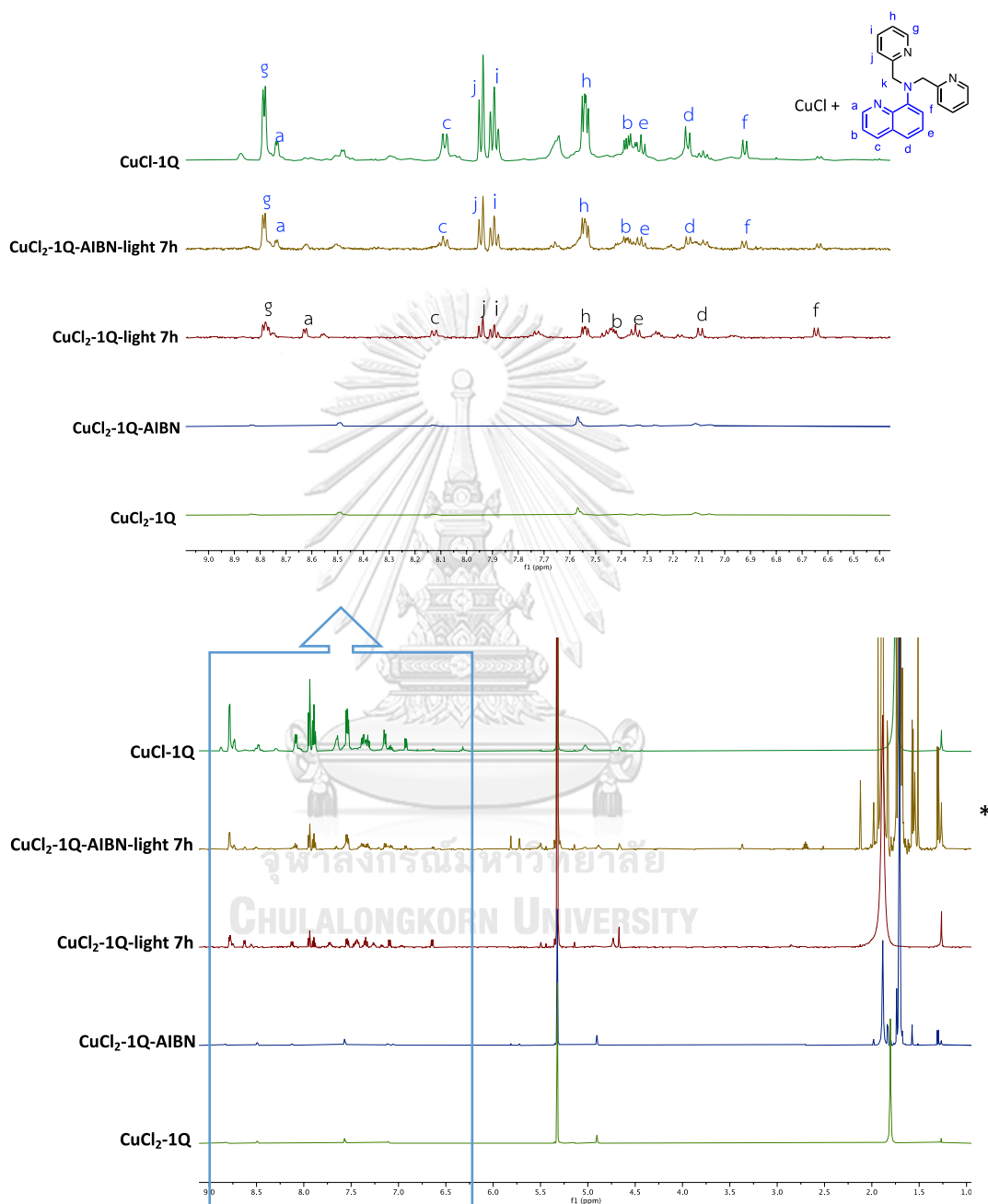


Figure 3.26 The ^1H NMR spectra for Cu(I) complex generation from Cu(II) complex.

The EPR spectrum of *in situ* generated $\text{CuCl}_2 \cdot 1\text{Q}$ complexes in the presence and absence of AIBN in dried CH_3CN were investigated in comparison with $\text{CuCl} \cdot 1\text{Q}$ (Figure 3.27). In the presence of AIBN, the decrease of Cu(II) complex signal after irradiation confirmed the generation of Cu(I) complex. In the absence of AIBN, the Cu(II) complex spectrum shows less change of the signal. The EPR results thus agree well with the ^1H NMR results.

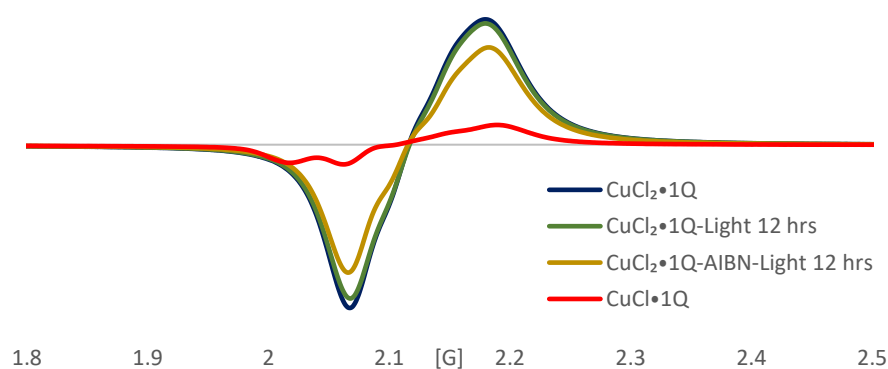


Figure 3.27 The EPR spectra for Cu(I) complex generation from Cu(II) complex.

CHAPTER IV
RESULTS AND DISCUSSION
FOR COPPER CATALYZED CHLOROSULFONYLATION (C-S FORMATION)

The results of the development of copper complexes containing quinoline derivatives as photoredox catalysts in atom transfer radical addition (ATRA) for chlorosulfonylation (C-S formation) are discussed in 4 sections according to the following order: synthesis and characterization of ligands, photophysical and electrochemical properties, study of catalytic properties for chlorosulfonylation (C-S formation), and study of other ligands.s

4.1 Synthesis and characterization of ligands

The synthesis and characterization of C5-substituted **1Q** derivatives (**1Q-I**, **1Q-CN** and **1Q-OMe**) are discussed here. The numeric characterization data for ^1H NMR, ^{13}C NMR, and HRMS of the are presented in the experimental section. The ^1H NMR, ^{13}C NMR, COSY, HSQC, HMBC, IR and HRMS spectra along with the signal assignments are provided in the appendix B.

The synthesis of **1Q** derivatives with different substituent on quinoline ring at C5, ligand **1Q-I**, **1Q-CN** and **1Q-OMe** are shown in Figure 4.1. The **1Q-I** was obtained from iodination in the presence of Lewis base under the low temperature. The product **1Q-I** was isolated in good yield and used for further synthesis of **1Q-CN**. The ligand **1Q-CN** could be prepared from the Rosenmund-Von Braun reaction with sodium cyanide in the presence of Cu(I) as a catalyst. The quantitative yield was obtained. The **1Q-OMe** was synthesized via a nucleophilic substitution of commercially available 5-methoxy-8-aminoquinoline and 2-(chloromethyl)pyridine in the presence of base and KI catalyst in 39% yield.

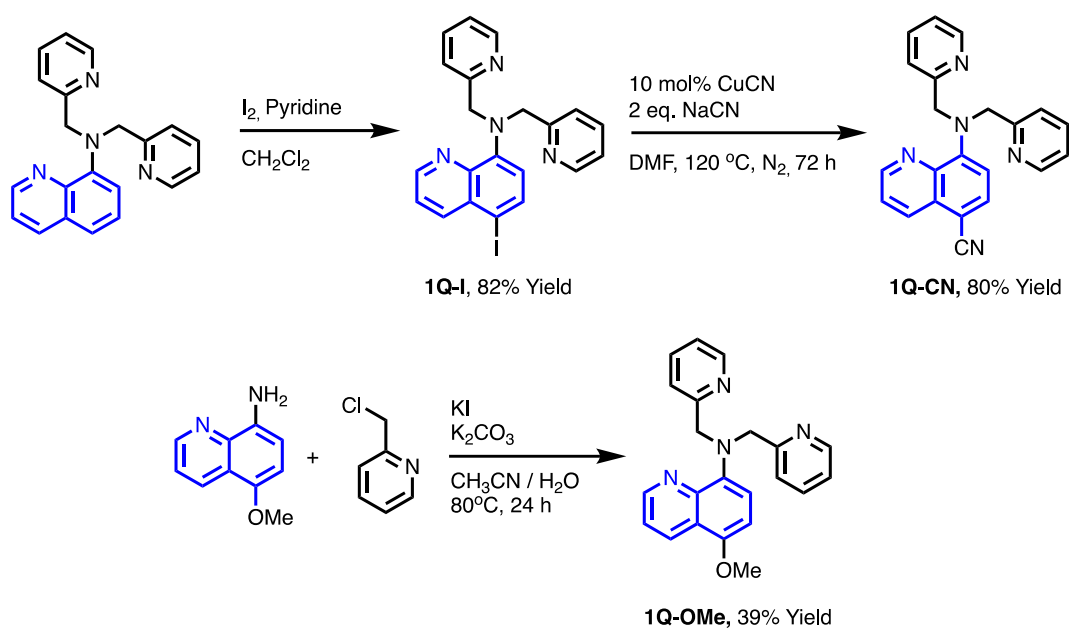


Figure 4.1 Synthesis of ligand, **1Q-I**, **1Q-CN** and **1Q-OMe**.

The 1H NMR spectra of **1Q-I**, **1Q-CN** and **1Q-OMe** are shown in Figure 4.2 in comparison with ligand **1Q**. The integrations of all aliphatic and aromatic signal were corresponded to number of assigned protons with absence of doublet signal of H^d proton at C5 position in all ligands. The changing of coupling signal of proton H^e from triplet to doublet in all spectra confirmed the substituent at C5 position. For **1Q-OMe**, the new signal of H^l proton appeared at 3.86 ppm. The assigned protons were confirmed by the correlation of 1H NMR and ^{13}C NMR from 2D NMR experiments (Figure B2-B15).

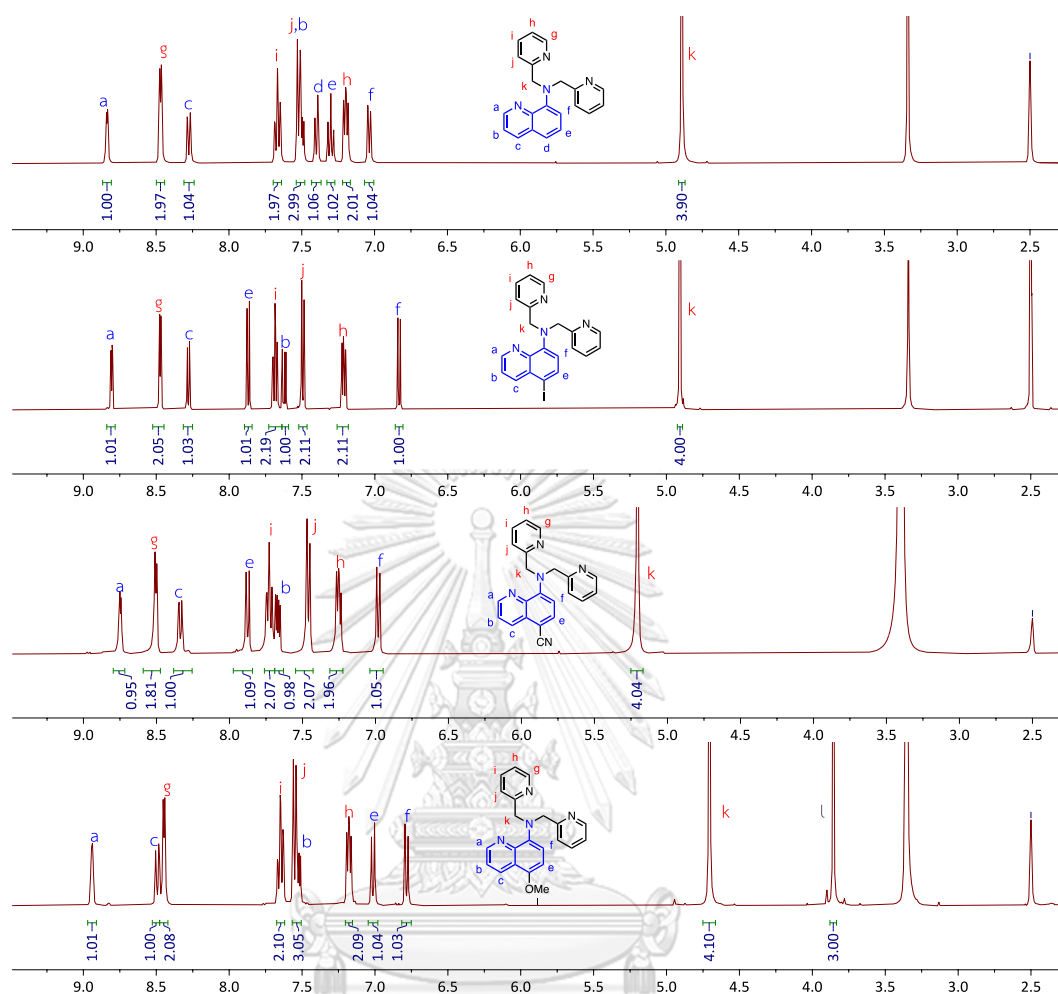


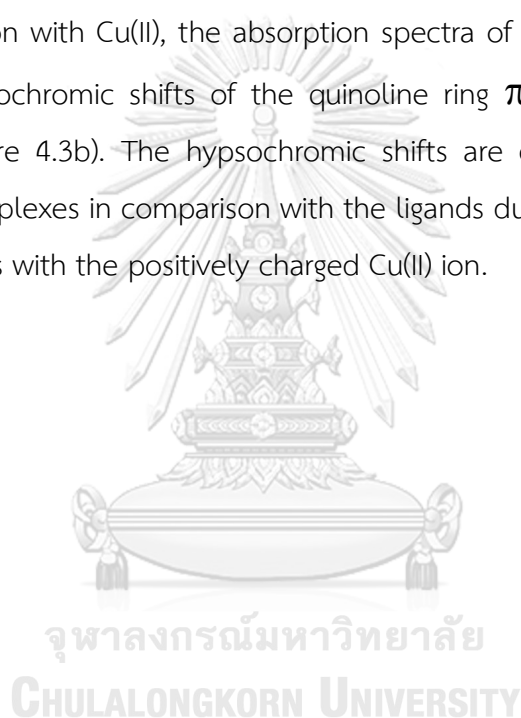
Figure 4.2 ^1H NMR spectra of **1Q**, **1Q-I**, **1Q-CN** and **1Q-OMe** in $\text{DMSO-}d_6$.

4.2 Photophysical and electrochemical properties

The photophysical and electrochemical properties of ligands and their Cu(II) complexes including UV-vis absorption, molar absorption coefficients (ϵ), electrochemical data and excited state potential are discussed in this section.

4.2.1 UV-vis absorption spectroscopy

The UV-vis absorption spectra of ligands were recorded in acetonitrile (Figure 4.3a) and molar absorption coefficients (ϵ) were summarized in Table 4.1. With the substitution on **C5** of the quinoline ring, the absorption spectra of **1Q-I**, **1Q-CN** and **1Q-OMe** showed red shift of quinoline absorption band with the λ_{max} around 350-380 nm. The Ligand **1Q-CN** showed longest wavelength from longer conjugation of nitrile group. The results indicate that the heavy atom, electron withdrawing group, electron donating group slightly lower the band gap of the aminoquinoline moiety. Upon complexation with Cu(II), the absorption spectra of **1Q-I**, **1Q-CN** and **1Q-OMe** showed the hypsochromic shifts of the quinoline ring π - π^* transitions to around 310-320 nm (Figure 4.3b). The hypsochromic shifts are consistent with the lower HOMO of the complexes in comparison with the ligands due to the coordination of N lone pair electrons with the positively charged Cu(II) ion.



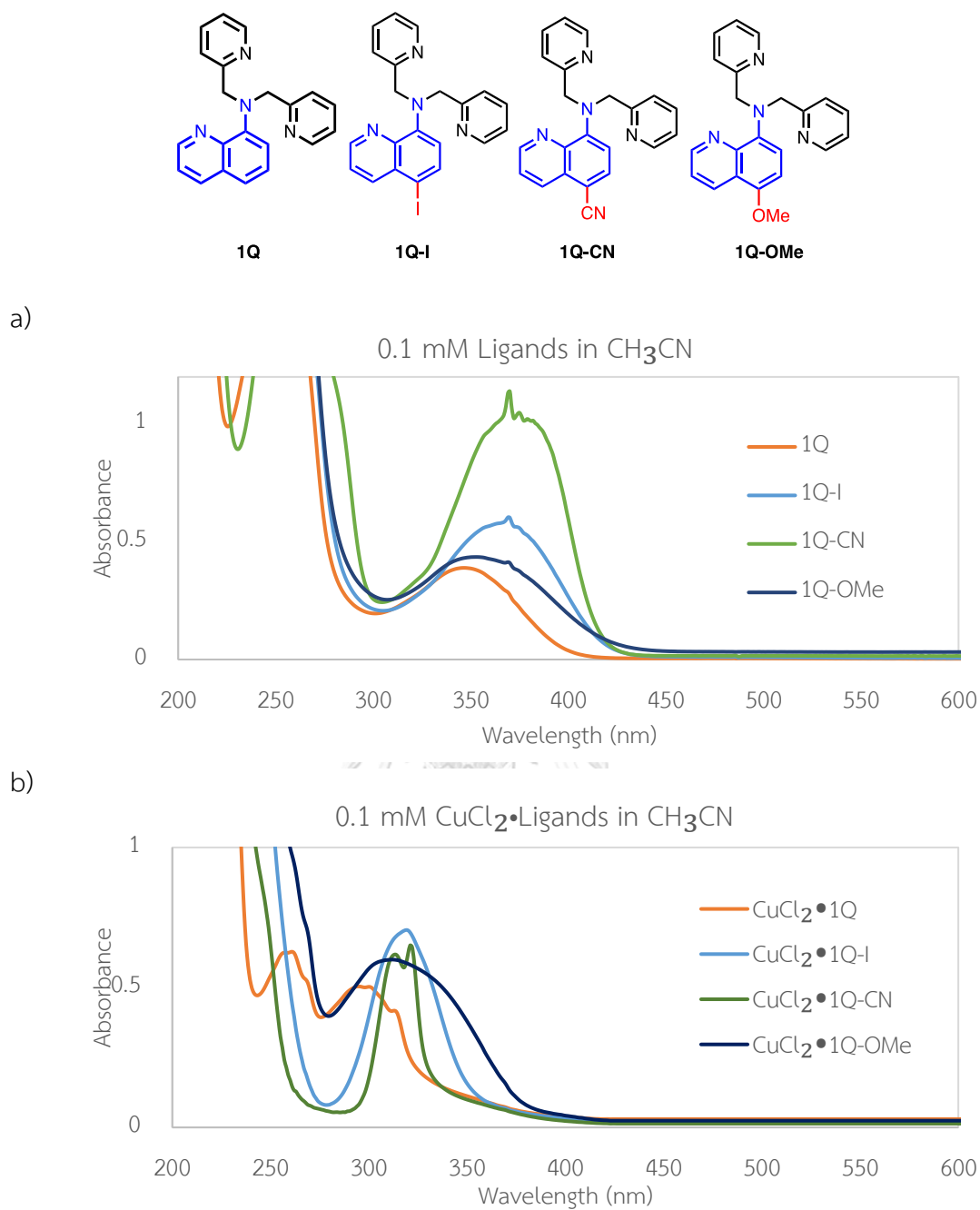


Figure 4.3 Absorption spectra of a) 0.1 mM **1Q**, **1Q-I**, **1Q-CN** and **1Q-OMe** b) **CuCl₂•1Q**, **CuCl₂•1Q-I**, **CuCl₂•1Q-CN** and **CuCl₂•1Q-OMe** in CH₃CN.

Table 4.1 Summary of absorption of ligands and Cu(II) complexes in CH₃CN.

	Ligand		Cu(II) Complex	
	λ_{\max} (nm)	ϵ (M ⁻¹ cm ⁻¹)	λ_{\max} (nm)	ϵ (M ⁻¹ cm ⁻¹)
1Q	342	3336	294	5891
1Q-I	369	5050	319	7016
1Q-CN	378	9591	321	6334
1Q-OMe	351	4209	312	6002

4.2.2 Cyclic voltammetry and reduction potentials

The electrochemical data were obtained from the cyclic voltammetry experiments. The voltammogram of Cu(II) complexes in comparison with CuCl₂•**1Q** using ferrocene as an external standard are shown in Figure 4.4. The normalized currents show excellent reversibility in all complexes. The reduction potentials, $E_{1/2, re}$ (Vs Fc), were determined from the cyclic voltammogram and summarized in Table 4.2. The standard reduction potentials (Vs SCE) of the Cu(II) and Cu(I) complexes at the ground state and excited state were estimated from the cyclic voltammetry and absorption spectroscopy. The reduction potentials (Vs SCE) of CuCl₂•**1Q-I**, CuCl₂•**1Q-CN** and CuCl₂•**1Q-OMe** are -0.24, -0.14 and -0.32 V, respectively. The results showed that the reduction potentials of Cu(II) complexes with electron deficient ligands became less negative with the ligand having an electron withdrawing group (CuCl₂•**1Q-CN**) but more negative with the ligand having an electron donating group (CuCl₂•**1Q-OMe**). The excited state potential ($E_{1/2}^*$) of Cu(II) complexes were calculated from energy gaps and redox potentials. The results showed that the reduction potentials of Cu(II) complexes with electron deficient ligands became more positive with the ligand having an electron withdrawing group (CuCl₂•**1Q-CN**) but less positive with the ligand having an electron donating group (CuCl₂•**1Q-OMe**). These results suggested the greater reducing abilities of Cu(II) complex with less electron density ligand. Lastly, the excited potential ($E_{1/2}^*$) of Cu(I) complexes were estimated. The results showed that the excited potentials of Cu(I) complexes more negative with the ligand having an electron donating group (CuCl₂•**1Q-OMe**, -1.79 V) and less

negative with the ligand having an electron withdrawing group ($\text{CuCl}_2 \cdot \mathbf{1Q-CN}$, -1.75 V).

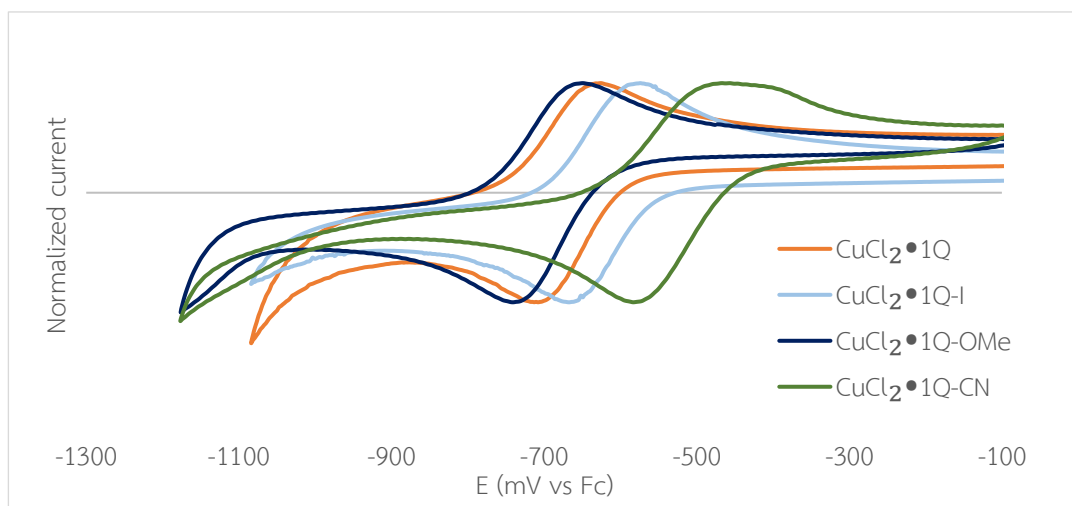


Figure 4.4 Cyclic voltammogram of $\text{Cu(II)} \cdot \text{ligand}$ complexes at 1.0 mM in CH_3CN .

Table 4.2 The electrochemical data of Cu(II) complexes generated *in situ* from CuCl_2 and various ligands in CH_3CN .

Ligand	Cu(II)•Ligand					Cu(I)•Ligand		
	$E_{1/2 \text{ re}}$ (V vs Fc)	$E_{1/2 \text{ re}}^b$ (V vs SCE)	$\lambda_{\text{on set}}$	E_{gap}^a (V)	$E_{1/2 \text{ re}}^{*c}$ (V vs SCE)	$\lambda_{\text{on set}}$	E_{gap}^a (V)	$E_{1/2 \text{ re}}^{*c}$ (V vs SCE)
1Q	-0.67	-0.29	520	2.38	2.10	603	2.06	-1.77
1Q-I	-0.62	-0.24	556	2.23	1.99	635	1.95	-1.63
1Q-CN	-0.52	-0.14	521	2.38	2.24	600	2.07	-1.75
1Q-OMe	-0.70	-0.32	520	2.38	2.07	643	1.93	-1.79

^a $E_{\text{gap}} = 1240/\lambda_{\text{on set}}$. ^b $E_{1/2 \text{ re}}(\text{SCE}) = E_{1/2 \text{ re}}(\text{Fc}) - 0.38 \text{ V}$. ^c $E^* = E_{\text{gap}} - E_{1/2}$

4.3 Study of catalytic properties for chlorosulfonylation (C-S formation)

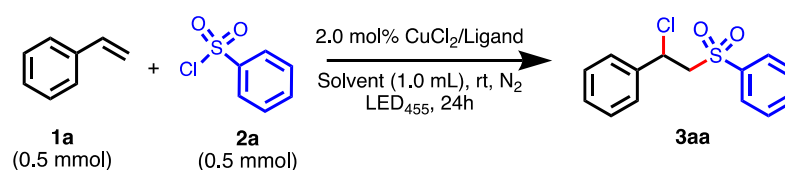
4.3.1 Optimization

To expand the scope of photo-mediated ATRA reaction, photo-mediated chlorosulfonylation was studied. Following our previously reported method successfully used in the copper-catalyzed haloalkylation [97], the addition of benzenesulfonyl chloride (**2a**) to styrene (**1a**) using 2.0 mol% of CuCl₂ and the tested ligand in acetonitrile under blue LED (455 nm, 2.5w) irradiation at room temperature for 24 hours was used as an initial model reaction condition (Table 4.3). Simple 1,10-phenanthroline (**phen**) and tris(2-pyridylmethyl)amine (**TPMA**) ligands were used for comparison with our quinoline based ligands. The reaction using either **phen** or **TPMA** provided the addition product **3aa** at very low yields (< 10%) (Entry 1 and 2) while those using our quinoline ligands gave significantly higher yields (Entry 3-8). The results clearly demonstrated that these tetradentate quinoline based ligands provided more catalytically favorable electronic and steric environment for the copper-metal center than the simple bidentate **phen** ligand. Furthermore, the presence of quinoline moiety increases the light absorption in the visible range in comparison with **TPMA** that enhances the VLIH conversion of the Cu(II) complex to Cu(I) complex. However, the reaction using ligand containing three units of quinoline (**3Q**) gave significantly lower yield (Entry 5) probably due to the steric hindrance around the copper center that prevent an efficient catalytic cycle. The substituent on C5 of the quinoline ring, including heavy atom, electron withdrawing group and electron donating group, (**1Q-I**, **1Q-CN** and **1Q-OMe**) showed little effect to the reaction yield (Entry 6-8) thus the more readily synthesized ligand **1Q** was further optimized. When the reaction was performed by using **1Q**, no product was observed for the LED 530 nm (Entry 9) and comparable yield (56%) was obtained for the LED 367 nm (Entry 10). The results are consistent with the electronic absorption band of Cu-**1Q** which appears at the energy higher than the green light (Figure B.41a).

Our previous study showed that the VLIH conversion of Cu(II) to active Cu(I) complex was more effective in CH₃OH in comparison with CH₃CN [97]. This catalytic reaction was thus tested in CH₃OH. However, no addition product was observed

due to rapid methanolysis of benzenesulfonyl chloride to form methyl benzenesulfonate (Entry 11). Nevertheless, when the reaction was conducted in CH_2Cl_2 , a reliably improved yield was obtained (Entry 12). The reaction yields appreciably increased with the increase of the catalyst amount or the alkene equivalent (Entry 13-14). Moreover, the extension of the reaction time to 48 hours improved the product yield up to 91% (Entry 15). This result indicates robustness of the catalytic activities of the $\text{Cu(II)}\cdot\mathbf{1Q}$ under prolong irradiation. In the absence of copper or the ligand (Entry 16-17), no product was observed that clearly confirmed the essential role of the copper complex for this reaction. In addition, the reaction did not proceed under the dark condition (Entry 18-19) consistent with the mechanism in which both generation and activation of the Cu(I) complex are photo processes.



Table 4.3 Catalytic activity screening of Cu(II) complexes with various ligands.

Entry	Ligand	Solvent	Condition variation	Yield [%] ^a
1	Phen	CH ₃ CN	-	4
2	TPMA	CH ₃ CN	-	7
3	1Q	CH ₃ CN	-	53
4	2Q	CH ₃ CN	-	57
5	3Q	CH ₃ CN	-	16
6	1Q-I	CH ₃ CN	-	35
7	1Q-CN	CH ₃ CN	-	45
8	1Q-OMe	CH ₃ CN	-	44
9	1Q	CH ₃ CN	LED 530 nm	ND
10	1Q	CH ₃ CN	LED 367 nm	56
11	1Q	CH ₃ OH	-	ND ^b
12	1Q	CH ₂ Cl ₂	-	60
13	1Q	CH ₂ Cl ₂	4.0 mol% CuCl ₂ • 1Q	73
14	1Q	CH ₂ Cl ₂	3.0 equiv 1a	80
15	1Q	CH ₂ Cl ₂	48 h	91
16	1Q	CH ₂ Cl ₂	No CuCl ₂	ND
17	1Q	CH ₂ Cl ₂	No 1Q	ND
18	1Q	CH ₂ Cl ₂	dark	ND
19	1Q	CH ₂ Cl ₂	CuCl• 1Q , dark	ND

^aYield determined by ¹H NMR using 1,3,5-trimethoxybenzene as the standard added after product purification. ^bND = not detected.

4.3.2 Chlorosulfonylation of various alkenes

Next, the reactions between benzenesulfonyl chloride and various alkenes were investigated using 2.0 mol% of CuCl₂•**1Q** in CH₂Cl₂ under blue LED light (Figure 4.5). The monosubstituted ethylenes (**1a-1g**) were used as the first set of alkene substrates. As described previously, the chlorosulfonylation of styrene gave 60% and 91% of the addition product (**3aa**) with the reaction time of 24 and 48 hours, respectively. The reaction of 4-methoxy styrene proceeded faster to give a quantitative combined yield of addition and

substitution products (**3ba** and **4ba**) within 24 hours. The substitution product **4ba** is a result of dehydrohalogenation of the initially formed addition product **3ba** during the reaction work up [80]. It is important to note that **1b** was previously reported as an unsuccessful substrate using another catalytic system due to the competitive polymerization of this highly active alkene [59, 78]. The successful addition using this Cu-**1Q** complex may be attributed to the stronger interaction between the alkyl radical intermediate with the copper metal center that prevent the polymerization. The reactions of relatively electron deficient styrene derivatives were more sluggish giving moderate to low yields of the addition products **3ea-3fa**. These results are likely due to the electrophilic nature of the radical intermediate [76]. Under this reaction condition, the alkene having heteroatom directly attached to the double bond (**3g**) did not give any addition product (**3ga**). This result is initially quite surprising as the addition radical intermediate is expected to gain resonance stabilizing effect from an unshared electron on the heteroatom [98]. The absence of addition product observed in the case of this alkene may thus be attributed to the catalyst poisoning by HCl which formed via Cl• abstracting α -hydrogen atom from the addition product [97].

For 1,1-disubstituted ethylenes **1h-1m**, the reaction proceeded smoothly to produce good to excellent yields of **3ha-3ma**. These disubstituted alkenes lack of α -hydrogen that effectively preclude the formation of HCl. In addition, the methyl substituent also provides stabilizing effect to the radical intermediate. This methyl stabilizing effect was confirmed by the high chemoselectivity observed in the chlorosulfonylation of the diene **1j** to produce **3ja** exclusively. The gram scale reaction of this alkene also gave **3ja** in excellent isolated yield. The catalytic activity also shows amide functional group tolerance that quantitative yield of **3ka** was obtained from **1k** without *N*-sulfonylation. Interestingly, the beneficial effect of the extra methyl substituent on styrene was lower than that the reaction of α -methylstyrene (**1l**) gave slightly higher yield of **3la** in than that of styrene. Furthermore, the methyl substituent

also has little beneficial effect on the reaction of methyl substituted vinyl acetate which still gave poor yield of **3ma**. This result can again be attributed to the catalyst poisoning by the acid formed by the H abstraction from the acetyl group. The reaction of 1,1-diphenyl substituted ethylene was rather ineffective giving low yield of the addition-elimination product **4na**. Two phenyl substituents may provide stabilizing effect to the radical intermediate, but their bulkiness probably prevent effective coordination between the radical intermediate with the copper metal center. The isolated substitution product **4na** is the result of dehydrochlorination of the initially formed addition product **3na** (unobserved).



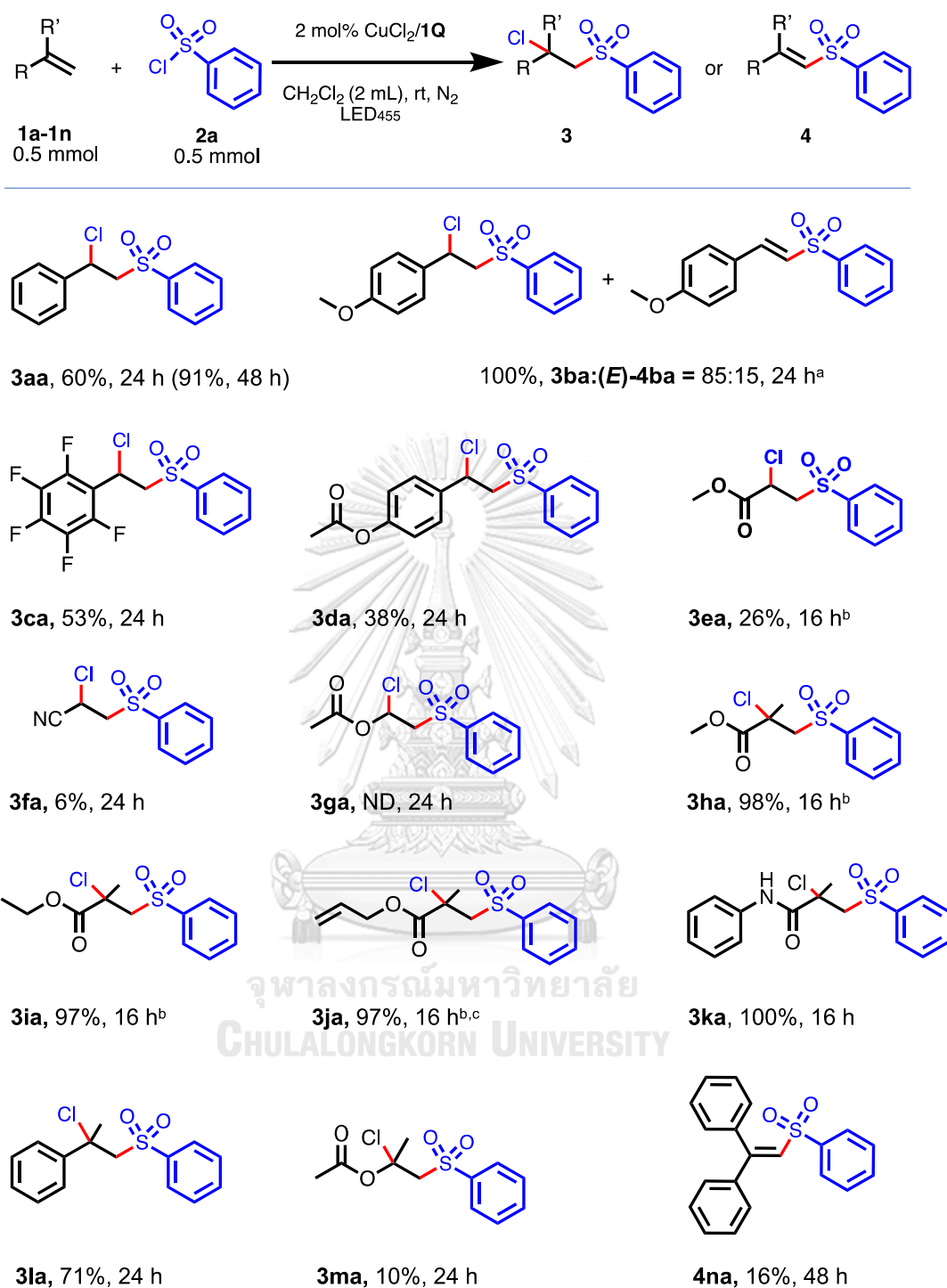


Figure 4.5 Isolated yields of products from chlorosulfonylation of various alkenes.

^aDetermined by ¹H NMR yield using toluene as an internal standard. ^b1.2 equivalent of alkene was used. ^cBenzenesulfonyl chloride (5.00 mmol) and alkene (6.00 mmol) were used for gram scale synthesis, 1.30 g of isolated **3ja** was obtained.

4.3.3 Chlorosulfonylation of various alkenes and alkynes in the presence of Na₂CO₃ additive.

In order to prevent catalyst poisoning by acid, the reactions in the presence of Na₂CO₃ base additive which has been reported to promote the catalytic efficiency for ruthenium [1] and copper catalyzed ATRA reactions by alleviating catalyst poisoning via acid scavenging effect were investigated [78, 97]. Satisfyingly, the reactions of all previously unsuccessful alkene substrates **1e-1g** and **1m** were dramatically improved to give significantly higher yields of the addition products **3ea-3ga** and **3ma** (Figure 4.6). Unfortunately, the base additive has no effect on the reaction of highly steric 1,1-diphenyl substituted ethylene (**1n** in Figure 4.5). Under this basic condition, the yields of addition-elimination products i.e., **4ea** and **4fa** became more pronounced for certain electron deficient alkenes. The formation of single *E*-stereoisomer of **4ea** (confirmed by X-ray structure) suggests an E2 process for the dehydrohalogenation. The elimination process could be avoided or promoted by using different bases (Table 4.4) and the reversibility of the complexation and decomplexation between Cu(I) and **1Q** under basic and acidic conditions observed by UV-Vis spectroscopy also confirmed the role of base (Figure B.41).

The basic reaction condition was also used for testing the chlorosulfonylation of other challenging alkenes (**1o-1t**) and alkynes (**5a-5c**). The addition of 1-octene, a simple unactivated terminal aliphatic alkene, gave good yield of **3oa**. Remarkably, the reaction of internal alkenes such as cyclohexene and 2-methyl-2-butenoate ester, previously unsuccessful or unreported substrates, [78, 80] gave respectable yields of diastereoselective *anti*-**3pa** and **3qa**. The results demonstrated superior catalytic activity of Cu-**1Q**, in comparison with Cu(**dap**)Cl₂ and Cu(**dmp**)₂Cl catalysts for the addition of internal olefins (see Table B.1 for more results), presumably due to less clouded **1Q** ligand allowing greater accessibility to the copper metal center. For the substrate containing both terminal and internal alkene (**1r**), the addition gave excellent yield of **3ra** indicating high selectivity toward terminal over internal double bond. In addition, the double bond with etherate-O and

amido-N substituents (**1s** and **1t**), also previously unsuccessful or unreported substrates, gave significant yields of the addition-elimination product **4sa** and (*E*)-**4ta**. These results are promising for further optimization and expanding the substrate scope for this catalytic system.

The substrate scope of the reaction using Cu-**1Q** catalyst was extended to various alkynes. Beside the generally high yield of products **6aa-6ca**, two more beneficial effects on the chlorosulfonylation of alkynes were observed. First, the previously reported inactive aliphatic alkyne, [62, 80] 1-hexyne, gave a satisfactory yield of **6ca**. Second, only *E*-alkene was obtained from the addition of all alkynes using this catalytic system.



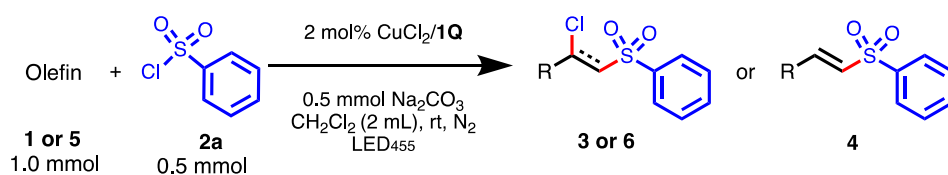
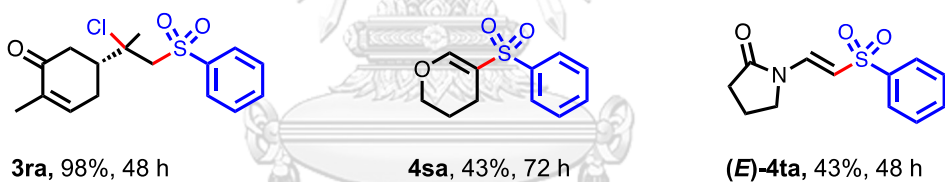
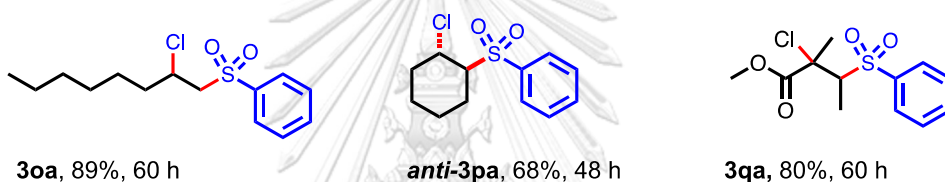
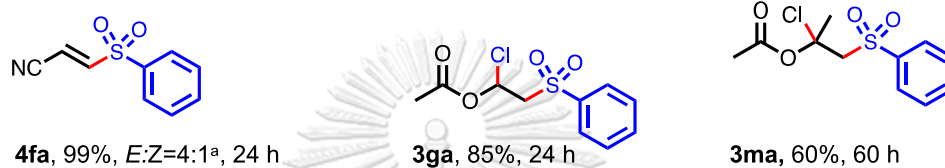
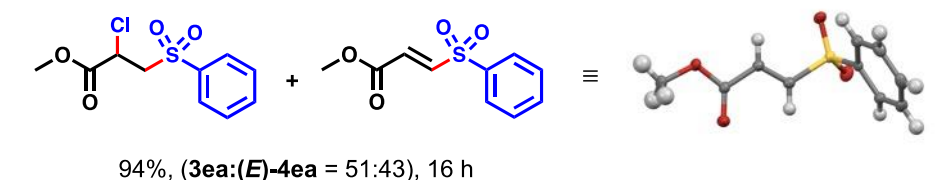
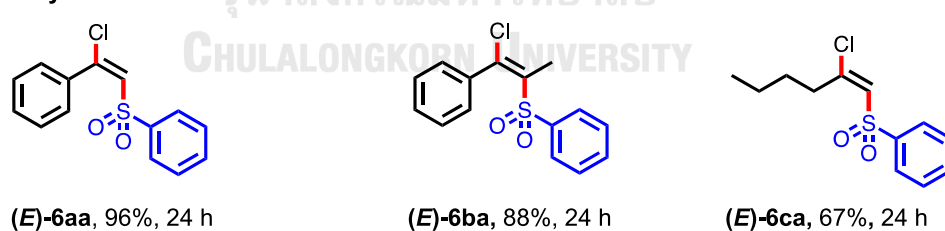
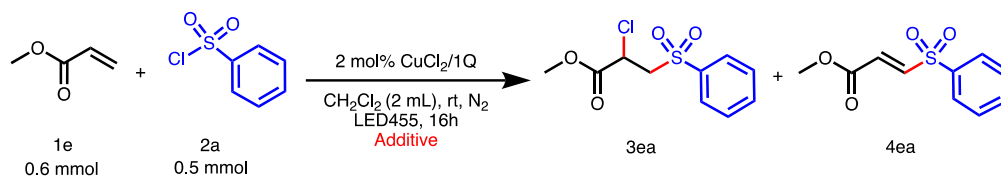
**Alkene****Alkyne**

Figure 4.6 Isolated yields of products from chlorosulfonylation of various alkenes in the presence of Na_2CO_3 additive.

^a*E* and *Z* isomers were identified by ^1H NMR in comparison with the previous literature reports [3a, 5f] and toluene was used as an internal standard for determining *E*:*Z* ratio.

Table 4.4 Reaction optimization for base additives.

Entry	Additive (equiv)	Yield (%) ^a	
		3ea	4ea
1	no	26	-
2	Na ₂ CO ₃ (1)	51	43
3	NaHCO ₃ (1)	94	6
4	NaHCO ₃ (0.2)	92 ^b	-
5	NaOAc (1)	18	70
6	NaOAc (2)	-	80 ^b

^aDetermined by ¹H NMR yield using toluene as an internal standard. ^bisolated yield.

4.3.4 Chlorosulfonylation of various sulfonyl chlorides

The scope of sulfonyl chloride for this new photocatalytic system using methyl methacrylate (**1i**) as the alkene substrate are investigated (Figure 4.7). The chlorosulfonylation of all sulfonyl chlorides (**2b-2f**) gave respectable yields of the addition products (**3ib-3if**) within 16 hours. Some of the addition products **3ie** and **3if** were prone to elimination that also gave substitution products **4ie** and **4if** after purification. The aliphatic sulfonyl chloride **2g** also efficiently added to an alkene (**1u**) affording the expected addition product **3ug**. These results demonstrated a wide scope of sulfonyl chloride.

structures included in Figure 4.8) that is consistent with the inner sphere mechanism previously proposed for other copper catalysts [80, 99]. The mechanism is involved the insertion of alkene to generate the carbon coordinated copper intermediate, followed by the reductive elimination. Under this white light condition, the yield of addition-elimination product **4sb** could be improved by using higher equivalents of dihydropyran **1s** (cf. **4sa** in Figure 4.6). For addition of both terminal and internal alkyne also gave high yields of diastereoselective (*E*)-products (**6ab**, **6bb** and **6db**). Notably, the reactions of inactive aliphatic alkynes gave similar yields with the active aromatic alkynes.

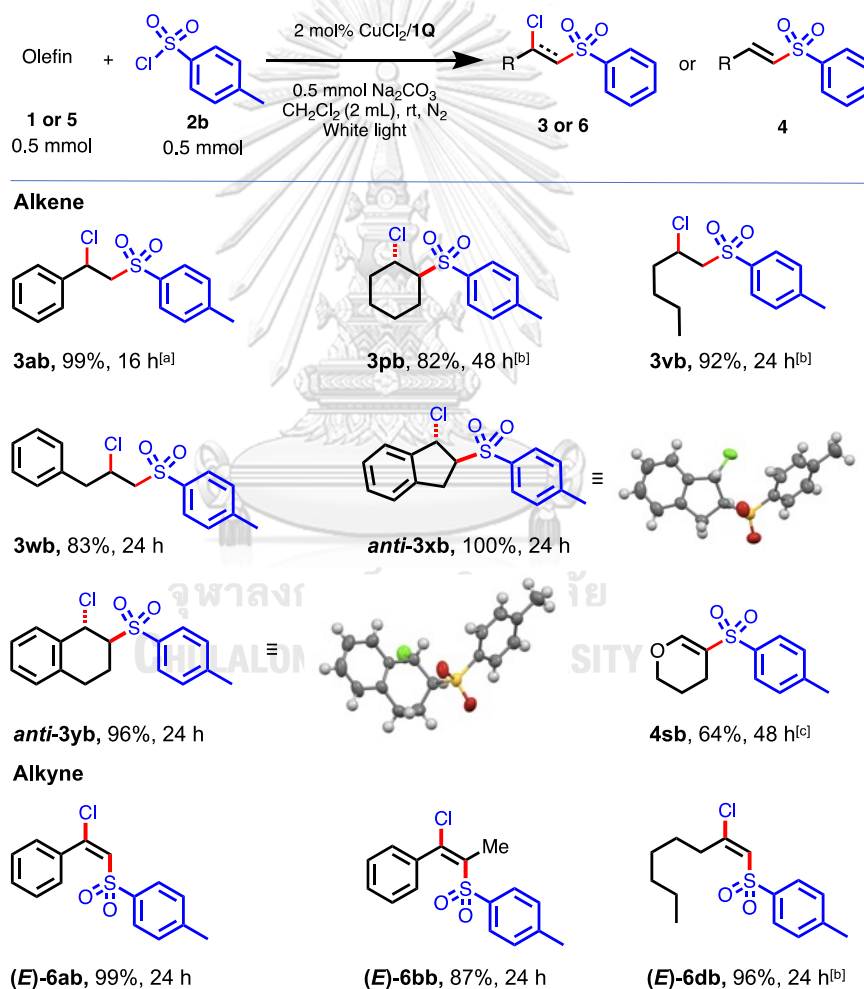


Figure 4.8 Isolated yields of products from chlorosulfonylation of various olefins under white light.

^a0.2 equivalent NaHCO₃ was used. ^b2.00 equivalent of olefin was used. ^c5.0 equivalent of olefin was used.

4.3.6 Proposed mechanism

A mechanism has been proposed to involve a visible-light-induced homolysis (VLIH) of Cu(II) to Cu(I) without any external reducing agent (Figure 4.9). These Cu(II) complexes are described to be more stable and conveniently prepared under less rigorous condition in comparison with the Cu(I) complexes.

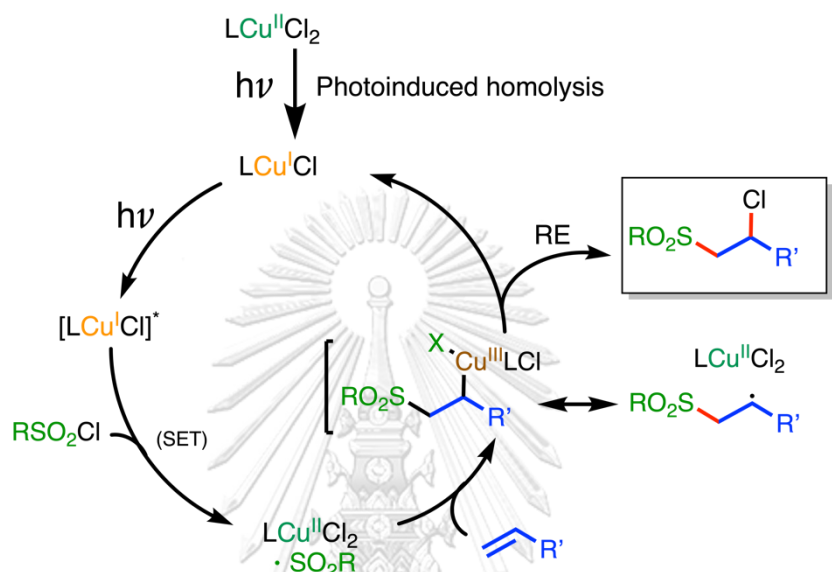


Figure 4.9 Simplified mechanism for Cu(II) catalyzed chlorosulfonylation via initial visible-light-induced homolysis (VLIH) of Cu-Cl bond.

4.4 Study of other ligands

To tuning of photophysical properties of ligand **1Q**, the extended conjugation at C5 position, ligands **1Q-Ph** and **1Q-DMAP** were prepared. This section is divided into 3 parts which are synthesis and characterization of **1Q-Ph** and **1Q-DMAP**, photophysical and electrochemical properties and preliminary study of catalytic properties for chlorosulfonylation (C-S formation).

4.4.1 Synthesis and characterization

The synthesis of **1Q** derivatives with different substituent on quinoline ring at C5, ligand **1Q-Ph** and **1Q-DMAP** are shown in Figure 4.10. The **1Q-Ph** and **1Q-DMAP** were synthesized via Suzuki-Miyaura reaction by coupling of **1Q-I** to phenylboronic acid and 4-(*N,N*-dimethylamino)phenyl boronic acid, pinacol ester, respectively. The **1Q-Ph** and **1Q-DMAP** were obtained after recrystallization in 37% and 34% yield, respectively. The numeric characterization data for ^1H NMR, ^{13}C NMR, and HRMS of the are presented in the experimental section. The ^1H NMR, ^{13}C NMR, COSY, HSQC, HMBC, IR and HRMS spectra along with the signal assignments are provided in the appendix B.

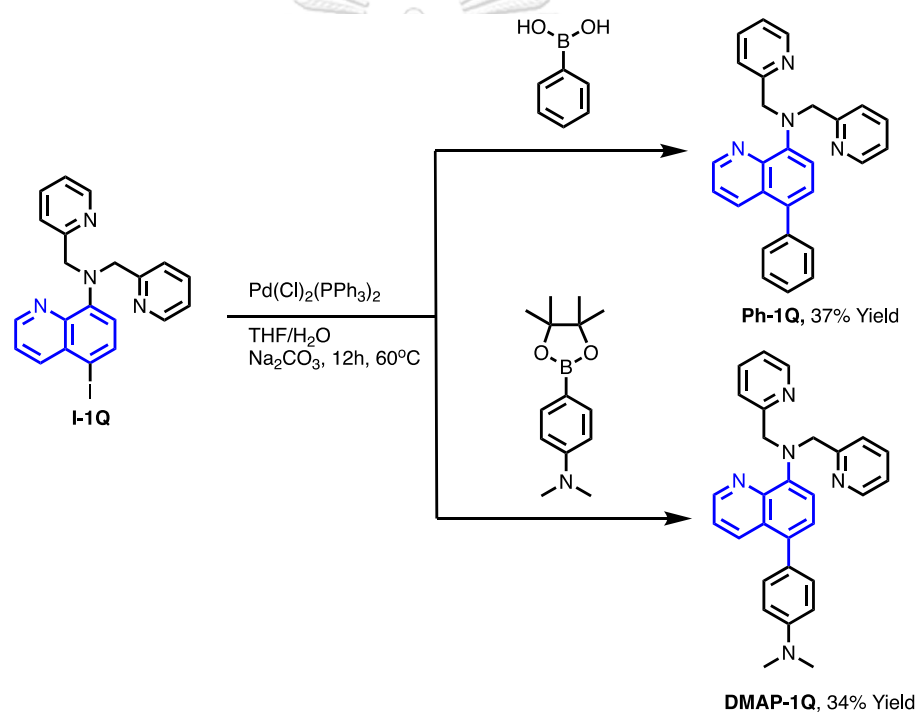


Figure 4.10 Synthesis of ligand **1Q-Ph** and **1Q-DMAP**.

The ^1H NMR spectra of **1Q-Ph** and **1Q-DMAP** are shown in Figure 4.11 in comparison with ligand **1Q**. The integrations of all aliphatic and aromatic signal were corresponded to number of assigned protons with absence of doublet signal of H^d proton at C5 position in all ligands. The changing of coupling signal of proton H^e from triplet to doublet in all spectra confirmed the substituent at C5 position. For ligand **1Q-Ph**, the extra signals of extended phenyl proton H^l and H^n appeared at 7.36–7.43

ppm and H^m at 7.45–7.51 ppm. In ¹H NMR spectrum of ligand **1Q-DMAP**, the extended dimethylaminophenyl group showed a singlet signal of methyl protons (Hⁿ) at 2.96 ppm and doublet signals of H^l and H^m at 7.23 ppm and 6.84 ppm, respectively. The assigned protons were confirmed by the correlation of ¹H NMR and ¹³C NMR from 2D NMR experiments (Figure B16–B25).

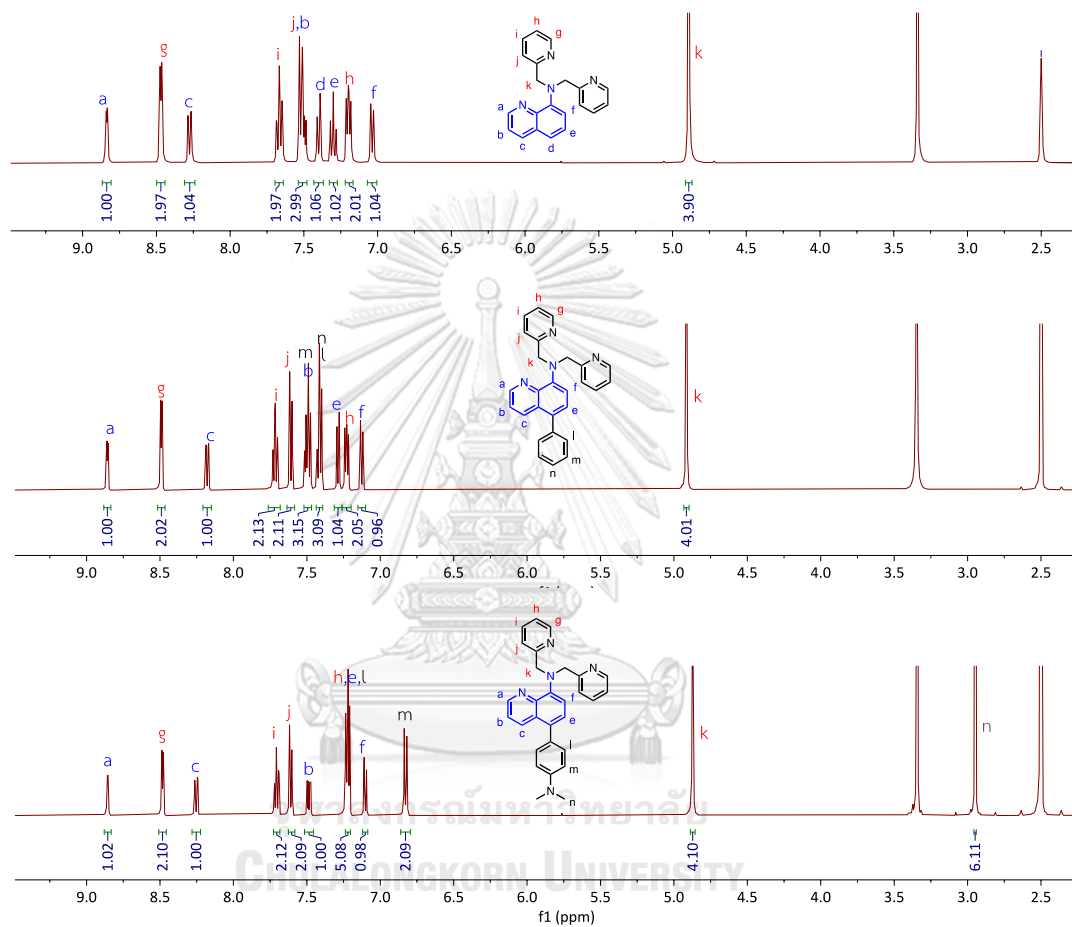


Figure 4.11 ¹H NMR spectra of **1Q**, **1Q-Ph** and **1Q-DMAP** in DMSO-*d*₆.

4.4.2 Photophysical and electrochemical properties

The photophysical properties and electrochemical properties of ligands and their Cu(II) complexes including UV-vis absorption, molar absorption coefficients (ϵ), electrochemical data and excited state potential are discussed in this section.

4.4.2.1 UV-vis absorption spectroscopy

The UV-vis absorption spectra of ligands **1Q-Ph** and **1Q-DMAP** were recorded in acetonitrile in comparison with ligand **1Q** (Figure 4.12a) and the molar absorption coefficients (ϵ) were summarized in Table 4.5. With the extend conjugation on **C5** of the quinoline ring, **1Q-Ph** and **1Q-DMAP** showed red shift of absorption band with the λ_{\max} around 340-375 nm. The results indicate the π -conjugation extension can lower the band gap of the aminoquinoline moiety by the resonance effect.

The spectrum of Cu(II) complexes with extended conjugate in $\text{CuCl}_2 \bullet \mathbf{1Q-Ph}$ and $\text{CuCl}_2 \bullet \mathbf{1Q-DMAP}$ showed the hypsochromic shift of π - π^* transition of quinoline rings to around 310-317 nm (Figure 4.12b). For $\text{CuCl}_2 \bullet \mathbf{1Q-DMAP}$, new broad peak in visible range around 400nm was observed.



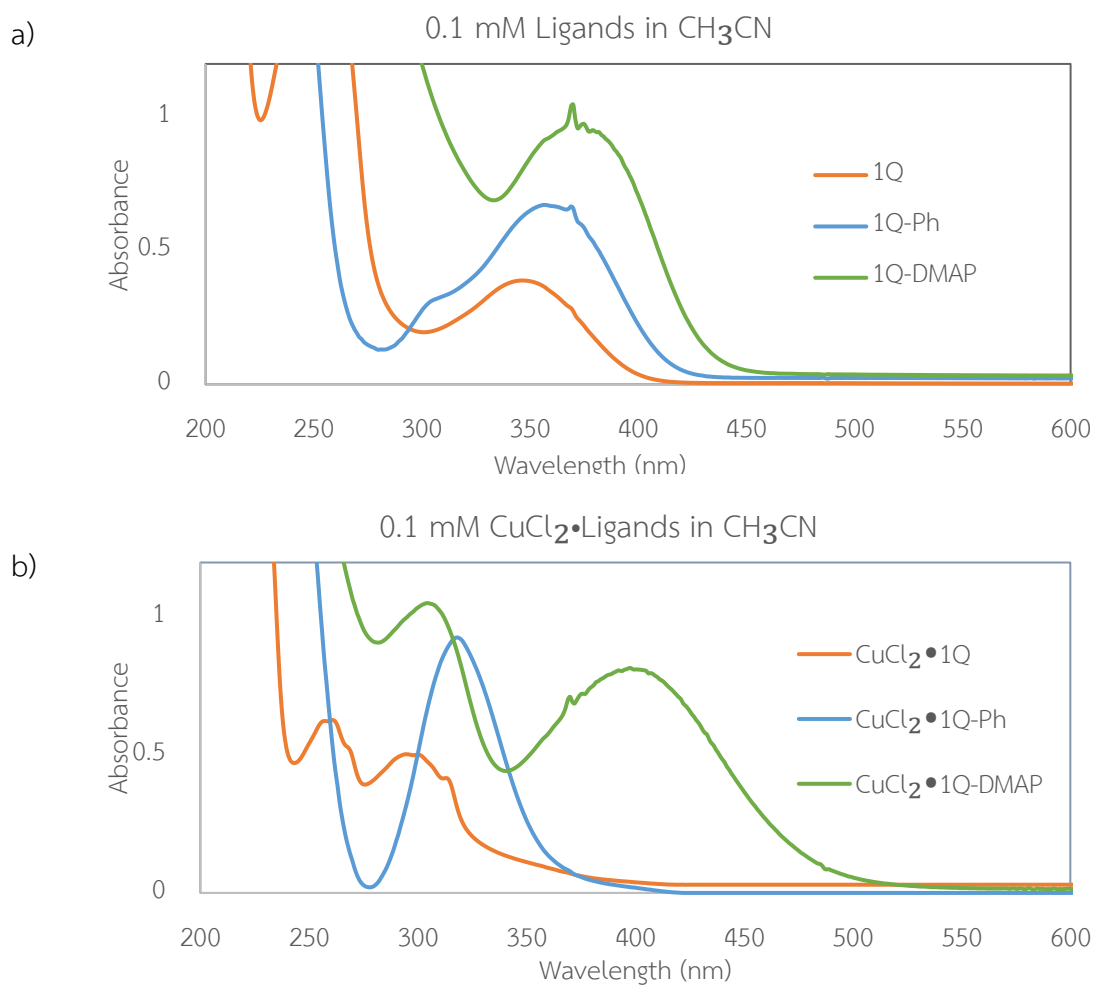
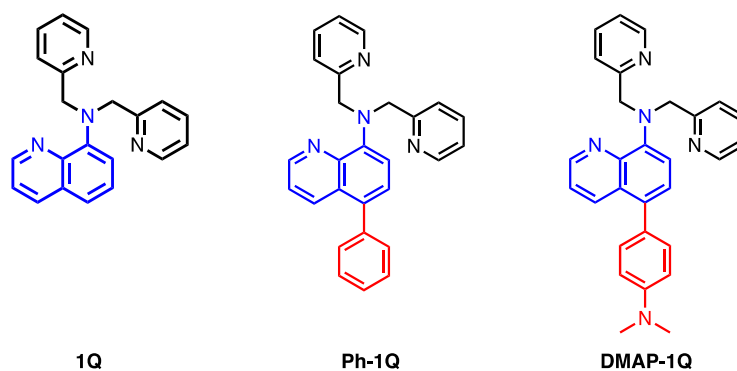


Figure 4.12 Absorption spectra of a) 0.1 mM **1Q**, **1Q-Ph** and **1Q-DMAP** b) 0.1 mM **CuCl₂•1Q**, and **CuCl₂•1Q-Ph** and **CuCl₂•1Q-DMAP** in CH₃CN.

Table 4.5 Summary of absorption of ligands and Cu(II) complexes in CH₃CN.

	Ligand		Cu(II) Complex	
	λ_{\max} (nm)	ϵ (M ⁻¹ cm ⁻¹)	λ_{\max} (nm)	ϵ (M ⁻¹ cm ⁻¹)
1Q	346	3703	291	5457
1Q-Ph	358	6642	317	10358
1Q-DMAP	378	8662	398	7600

4.4.2.2 Cyclic voltammetry and reduction potentials

The electrochemical data of CuCl₂•1Q-Ph and CuCl₂•1Q-DMAP were obtained from the cyclic voltammetry experiments ferrocene as an external standard as shown in Figure 4.13. The normalized currents show excellent reversibility in all complexes. The reduction potentials, the energy gaps and the excited state potential ($E_{1/2}^*$) were summarized in Table 4.6. The CuCl₂•1Q-Ph and CuCl₂•1Q-DMAP showed negative reduction potential similar to CuCl₂•1Q. At the excited state, the reduction potential ($E_{1/2}^*$) of CuCl₂•1Q-Ph and CuCl₂•1Q-DMAP are slightly less positive than that of CuCl₂•1Q. The reduction potential of the excited state ($E_{1/2}^*$) of CuCl•1Q-Ph and CuCl•1Q-DMAP are slightly less negative than that of CuCl•1Q.

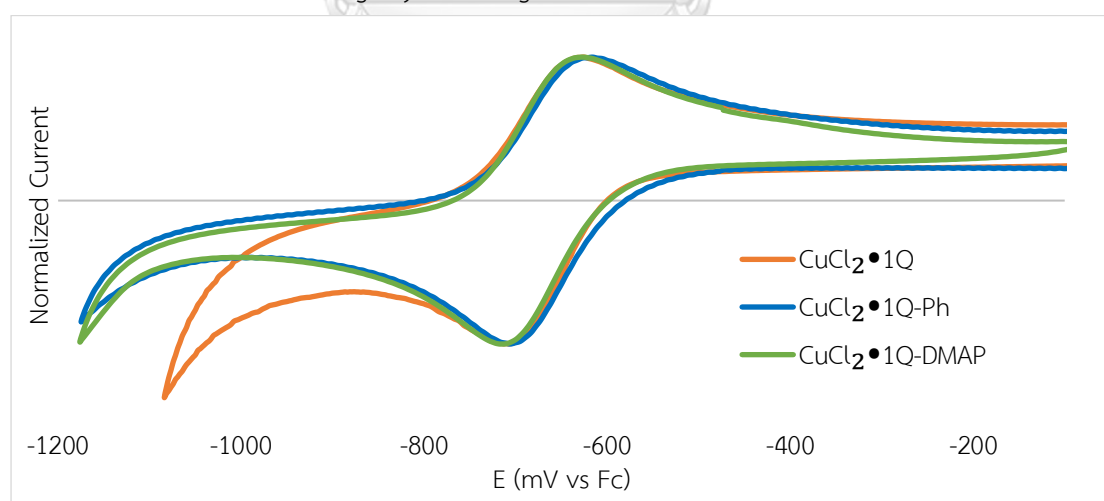
**Figure 4.13** Cyclic voltammogram of Cu(II)•ligand complexes at 1.0 mM in CH₃CN.

Table 4.6 The electrochemical data of Cu(II) complexes generated *in situ* from CuCl₂ and various ligands in CH₃CN.

Ligand	Cu(II)•Ligand					Cu(I)•Ligand		
	$E_{1/2\text{ re}}$ (V vs Fc)	$E_{1/2\text{ re}}^b$ (V vs SCE)	λ_{onset}	E_{gap}^a (V)	$E_{1/2\text{ re}}^{*c}$ (V vs SCE)	λ_{onset}	E_{gap}^a (V)	$E_{1/2\text{ re}}^{*c}$ (V vs SCE)
1Q	-0.67	-0.29	520	2.38	2.10	603	2.06	-1.77
1Q-Ph	-0.66	-0.28	511	2.43	2.06	611	2.07	-1.75
1Q-DMAP	-0.67	-0.29	567	2.19	1.90	620	2.00	-1.71

^a $E_{\text{gap}} = 1240/\lambda_{\text{onset}}$. ^b $E_{1/2\text{ re}}(\text{SCE}) = E_{1/2\text{ re}}(\text{Fc}) - 0.38\text{ V}$. ^c $E^* = E_{\text{gap}} - E_{1/2}$



4.4.3 Preliminary study of catalytic properties for chlorosulfonylation (C-S formation)

The Cu(II) complexes with ligands **Ph-1Q** and **Ph-DMAP** were studied for the photo-mediated chlorosulfonylation of styrene in comparison with Cu(II)•**1Q** (Figure 4.14). Interestingly, the addition yields were improved to 68% and 89% when using Cu(II)•**1Q-Ph** and Cu(II)•**1Q-DMAP**, respectively. The extension of π -conjugation increases the absorptivity of the ligands in the visible range (Figure 4.12). Therefore, these π -conjugated extended ligands are promising for copper catalyzed photo ATRA reactions.

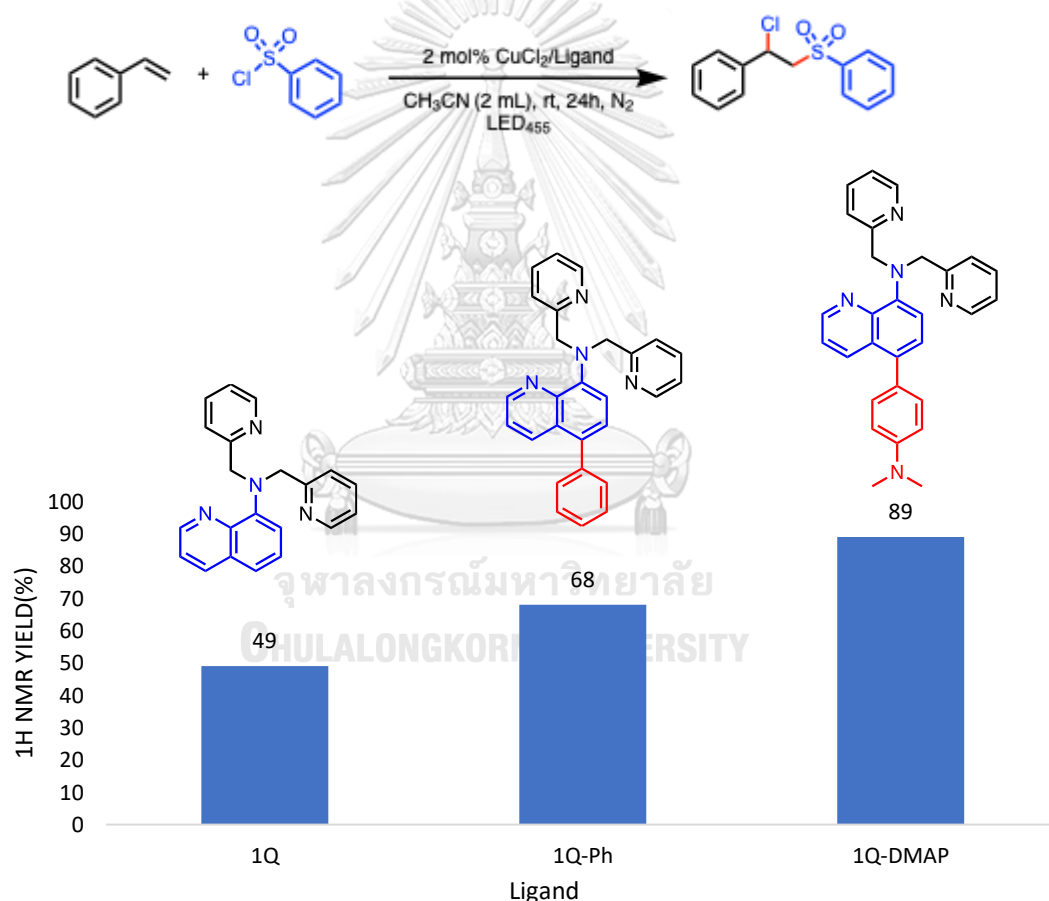


Figure 4.14 Photocatalytic activity study of Cu(II) complexes with **1Q**, **1Q-Ph** and **1Q-DMAP** in chlorosulfonylation of styrene.

CHAPTER V

CONCLUSIONS

In the first part of this dissertation, a series of aminoquinoline-methylpyridine conjugates containing one (**1Q**), two (**2Q**), and three quinoline rings (**3Q**) were successfully synthesized and used as ligands for preparation of Cu(II) complex photocatalysts in atom transfer radical addition (ATRA) reaction. The Cu(II)•**1Q** complex was found to have the highest catalytic activity for haloalkylation of alkenes (> 20 examples) giving good to excellent yields of the addition products via C-C bond formation. The reaction proceeds with high chemo- regio- and stereoselectivity without observable polymerizations of alkenes. The mechanistic study are consistent with the visible-light-induced homolysis (VLH) of Cu(II)•X bond to Cu(I) complex which subsequently reduces the alkyl halide via a single electron transfer (SET) to form the Cu(II) bound radical. The role of commonly employed additives AIBN and Na₂CO₃ is evaluated, suggesting that these additives alleviate catalyst poisoning by preventing the build-up of HX in the course of the reactions. This quinoline based ligand thus offers a robust environment for Cu(II) to effectively promote photo-mediated ATRA reactions for haloalkylation of alkenes.

In the second part, the Cu(II) complexes of C5 substituted-**1Q** derivatives, including a heavy atom (**1Q-I**), electron withdrawing group (**1Q-CN**) and electron donating group (**1Q-OMe**), were prepared, and studied for C-S bond formation via photocatalytic chlorosulfonylation of olefins. The simple quinoline based ligand **1Q** was proven to be suitable ligand for Cu(II) in generating a robust and highly active photocatalyst for chlorosulfonylations of various olefins. The Cu(II)•**1Q** complex can catalyzed the chlorosulfonylation of activated and unactivated olefins which have been previously reported as unsuccessful substrates. The addition of base additive can prevent acid poisoning of the catalyst. This Cu(II)-**1Q** was also the first copper homoleptic complex that gave diastereoselective additions of alkyne substrates to give only the *E* alkene products. The extended conjugation at C5 position of **1Q** ligands, namely **1Q-Ph** and **1Q-DMAP**, showed potential improvement of the

catalytic activity in comparison with Cu(II)•1Q complex probably due to higher absorptivity in the visible range.

All in all, This study has demonstrated that Cu(II) complexes with tetradentate quinoline ligands are effective and robust catalysts for photo-mediated haloalkylation and chlorosulfonylation of olefins. In the future, evaluation of these ligand series for other ATRA reactions will be interesting.



APPENDIX A

The Atom transfer radical addition (ATRA) for haloalkylation (C-C formation)

A.1 Synthesis and characterization of Cu(II) complexes

A.1.1 X-ray crystallography

Table A.1 Crystal data and structure refinement for all the complexes.

Identification code	[Cu ^{II} (1Q)Cl]Cl	[Cu ^{II} (2Q)Cl]Cl	[Cu ^{II} (3Q)Cl][CuCl ₄]
Empirical formula	C ₂₁ H ₂₀ Cl ₂ CuN ₄ O	C ₄₈ H ₄₀ Cl ₄ Cu ₂ N ₈ O ₂	C ₅₄ H ₃₆ Cl ₆ Cu ₃ N ₈
Formula weight	478.85	1029.76	1200.23
Temperature/K	296	100	296
Crystal system	monoclinic	monoclinic	triclinic
Space group	<i>P</i> 2 ₁ / <i>c</i>	<i>P</i> 2 ₁ / <i>n</i>	<i>P</i> -1
<i>a</i> /Å	16.6661(8)	13.3798(14)	13.9396(18)
<i>b</i> /Å	9.3649(5)	24.690(3)	15.824(2)
<i>c</i> /Å	14.0474(8)	14.1358(14)	16.096(2)
α /°	90	90	111.357(4)
β /°	109.943(2)	108.542(2)	98.835(4)
γ /°	90	90	115.205(4)
Volume/Å ³	2060.99(19)	4427.3(8)	2783.9(6)
<i>Z</i>	4	4	2
ρ_{calc} /g/cm ³	1.543	1.545	1.432
μ /mm ⁻¹	1.339	3.816	1.466
<i>F</i> (000)	980.0	2104.0	1210.0
Crystal size/mm ³	0.38 × 0.34 × 0.3	0.26 × 0.26 × 0.21	0.34 × 0.32 × 0.19
Radiation	MoK α (λ = 0.71073 Å)	CuK α (λ = 1.54178 Å)	MoK α (λ = 0.71073 Å)
2 θ range for data collection/°	6.378 to 56.656	7.506 to 144.96	5.842 to 57.642
Reflections collected	40421	52938	76310
Independent reflections	5132	8704	14494
<i>R</i> _{int} , <i>R</i> _{sigma}	0.0556, 0.0309	0.0308, 0.0209	0.0475, 0.0353
Data/restraints/parameters	5132/0/265	8704/0/583	14494/92/686
Goodness-of-fit on <i>F</i> ²	1.035	1.036	1.028
<i>R</i> ₁ , <i>wR</i> ₂ [<i>I</i> ≥ 2 σ (<i>I</i>)]	0.0317, 0.0725	0.0248, 0.0659	0.0420, 0.1124
<i>R</i> ₁ , <i>wR</i> ₂ [all data]	0.0441, 0.0776	0.0257, 0.0666	0.0631, 0.1251
Largest diff. peak/hole / e Å ⁻³	0.31/-0.39	0.37/-0.49	0.66/-0.63

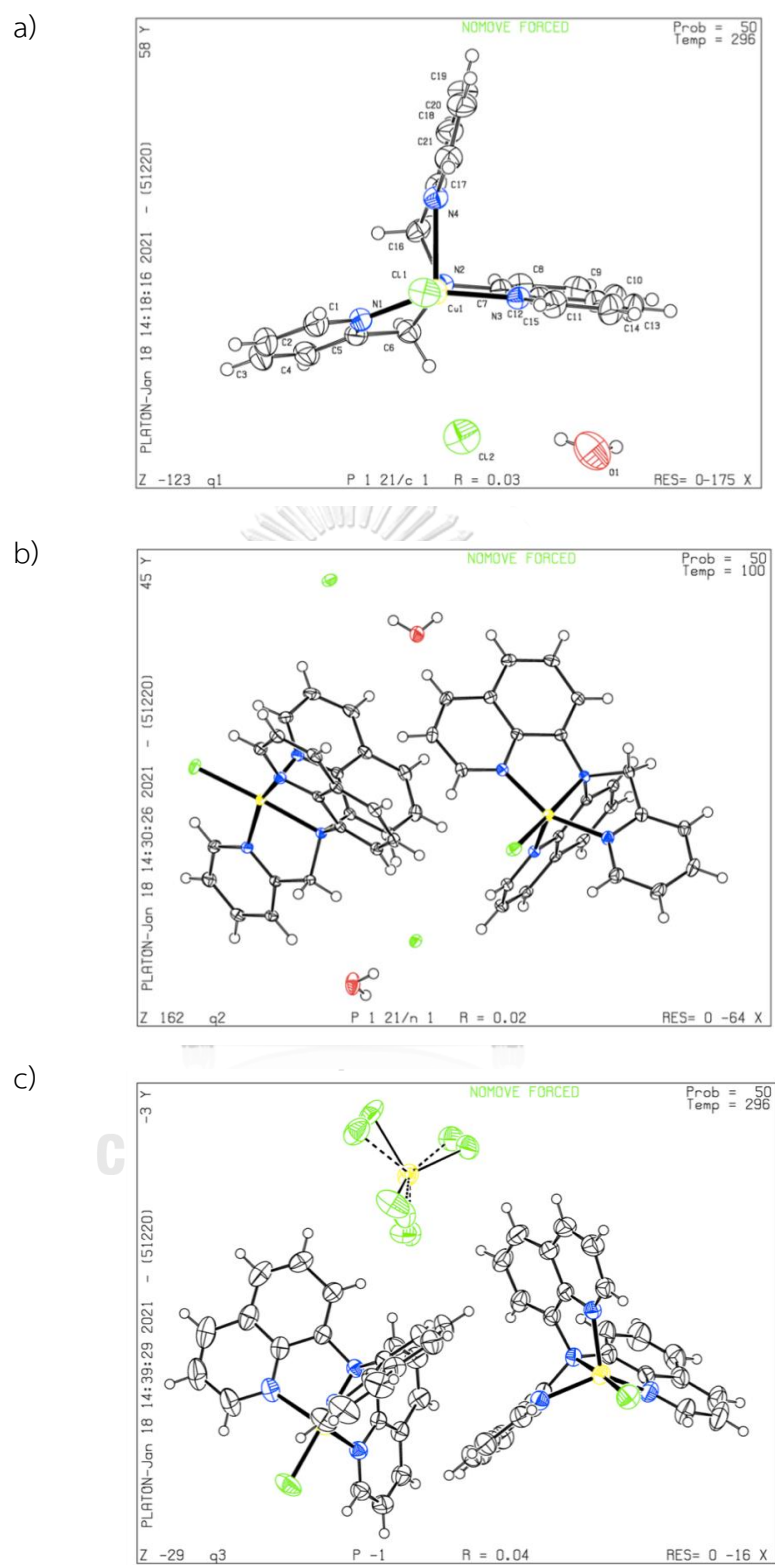


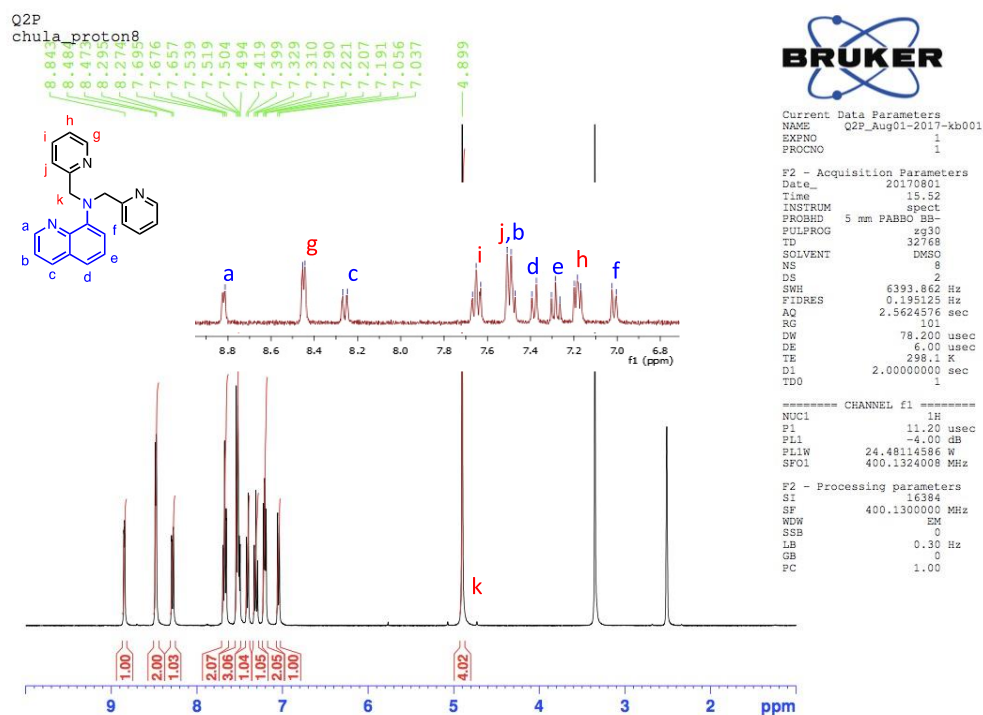
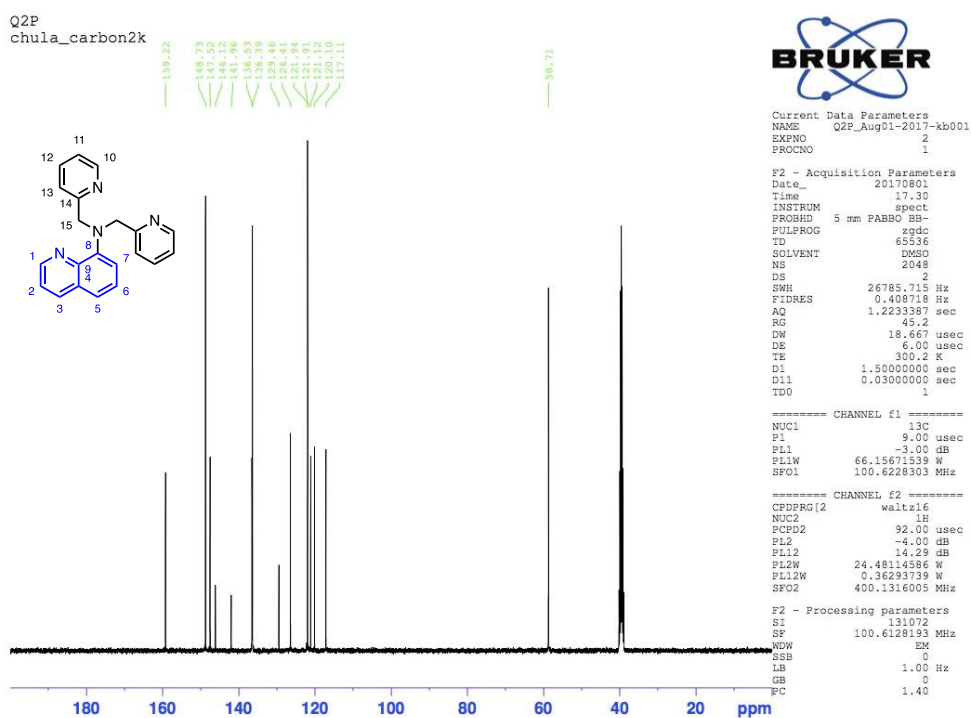
Figure A.1 Ellipsoid plots of a) $[\text{Cu}^{\text{II}}(\mathbf{1Q})\text{Cl}]\text{Cl}$, b) $[\text{Cu}^{\text{II}}(\mathbf{2Q})\text{Cl}]\text{Cl}$ and c) $[\text{Cu}^{\text{II}}(\mathbf{3Q})\text{Cl}][\text{CuCl}_4]$ complexes.

Table A.1 Selected bond lengths (Å) and bond angles (°) for all the complexes.

[Cu^{II}(1Q)Cl]Cl			
Cu1–Cl1	2.2540 (5)	Cu1–N3	1.9954 (15)
Cu1–N1	1.9986 (15)	Cu1–N4	2.2738 (15)
Cu1–N2	2.0676 (13)		
Cl1–Cu1–N4	97.31 (4)	N2–Cu1–N4	78.55 (5)
N1–Cu1–Cl1	97.68 (5)	N3–Cu1–Cl1	99.19 (4)
N1–Cu1–N2	81.30 (6)	N3–Cu1–N1	150.36 (6)
N1–Cu1–N4	107.66 (6)	N3–Cu1–N2	83.77 (6)
N2–Cu1–Cl1	175.12 (4)	N3–Cu1–N4	94.17 (6)
[Cu^{II}(2Q)Cl]Cl			
Cu1–Cl1	2.2573 (4)	Cu2–Cl2	2.2385 (4)
Cu1–N1	2.0016 (12)	Cu2–N5	1.9947 (13)
Cu1–N2	2.1034 (12)	Cu2–N6	2.1222 (12)
Cu1–N3	1.9981 (13)	Cu2–N7	1.9944 (12)
Cu1–N4	2.1361 (13)	Cu2–N8	2.1445 (12)
N1–Cu1–Cl1	97.43 (4)	N5–Cu2–Cl2	96.16 (4)
N1–Cu1–N2	81.02 (5)	N5–Cu2–N6	81.19 (5)
N1–Cu1–N4	101.16 (5)	N5–Cu2–N8	100.17 (5)
N2–Cu1–Cl1	177.36 (3)	N6–Cu2–Cl2	171.05 (3)
N2–Cu1–N4	81.71 (5)	N6–Cu2–N8	81.32 (5)
N3–Cu1–Cl1	96.97 (4)	N7–Cu2–Cl2	96.75 (4)
N3–Cu1–N1	152.77 (5)	N7–Cu2–N5	156.39 (5)
N3–Cu1–N2	83.62 (5)	N7–Cu2–N6	83.01 (5)
N3–Cu1–N4	98.70 (5)	N7–Cu2–N8	94.65 (5)
N4–Cu1–Cl1	100.73 (4)	N8–Cu2–Cl2	107.59 (4)
[Cu^{II}(3Q)Cl][CuCl₄]			
Cu1–Cl1	2.2154 (8)	Cu2–N8	2.077 (2)
Cu1–N1	2.096 (2)	Cu3–Cl3	2.2371 (18)
Cu1–N2	2.1092 (19)	Cu3–Cl4	2.271 (2)
Cu1–N3	2.016 (2)	Cu3–Cl5	2.2720 (18)
Cu1–N4	2.075 (2)	Cu3–Cl6	2.2383 (17)
Cu2–Cl2	2.2267 (8)	Cu3A–Cl3A	2.248 (11)
Cu2–N5	1.997 (2)	Cu3A–Cl4A	2.398 (13)
Cu2–N6	2.1279 (19)	Cu3A–Cl5A	2.144 (8)
Cu2–N7	2.034 (2)	Cu3A–Cl6A	2.138 (9)
N1–Cu1–Cl1	98.24 (6)	N7–Cu2–N6	81.14 (8)
N1–Cu1–N2	79.36 (8)	N7–Cu2–N8	108.40 (10)
N2–Cu1–Cl1	176.65 (6)	N8–Cu2–Cl2	99.07 (7)

N3-Cu1-Cl1	98.25 (7)	N8-Cu2-N6	81.69 (8)
N3-Cu1-N1	130.61 (9)	Cl3-Cu3-Cl4	100.96 (10)
N3-Cu1-N2	81.71 (8)	Cl3-Cu3-Cl5	99.01 (8)
N3-Cu1-N4	118.15 (9)	Cl3-Cu3-Cl6	133.06 (9)
N4-Cu1-Cl1	100.91 (6)	Cl4-Cu3-Cl5	134.81 (11)
N4-Cu1-N1	103.76 (8)	Cl6-Cu3-Cl4	97.80 (10)
N4-Cu1-N2	81.99 (8)	Cl6-Cu3-Cl5	97.37 (8)
N5-Cu2-Cl2	97.15 (6)	Cl3A-Cu3A-Cl4A	93.6 (6)
N5-Cu2-N6	82.69 (8)	Cl5A-Cu3A-Cl3A	99.7 (4)
N5-Cu2-N7	130.76 (9)	Cl5A-Cu3A-Cl4A	126.3 (7)
N5-Cu2-N8	114.77 (9)	Cl6A-Cu3A-Cl3A	145.4 (5)
N6-Cu2-Cl2	179.21 (6)	Cl6A-Cu3A-Cl4A	91.3 (6)
N7-Cu2-Cl2	98.41 (6)	Cl6A-Cu3A-Cl5A	104.8 (4)



A.1.2 ^1H NMR and ^{13}C spectraFigure A.2 ^1H NMR spectrum of ligand 1Q.Figure A.3 ^{13}C NMR spectrum of ligand 1Q.

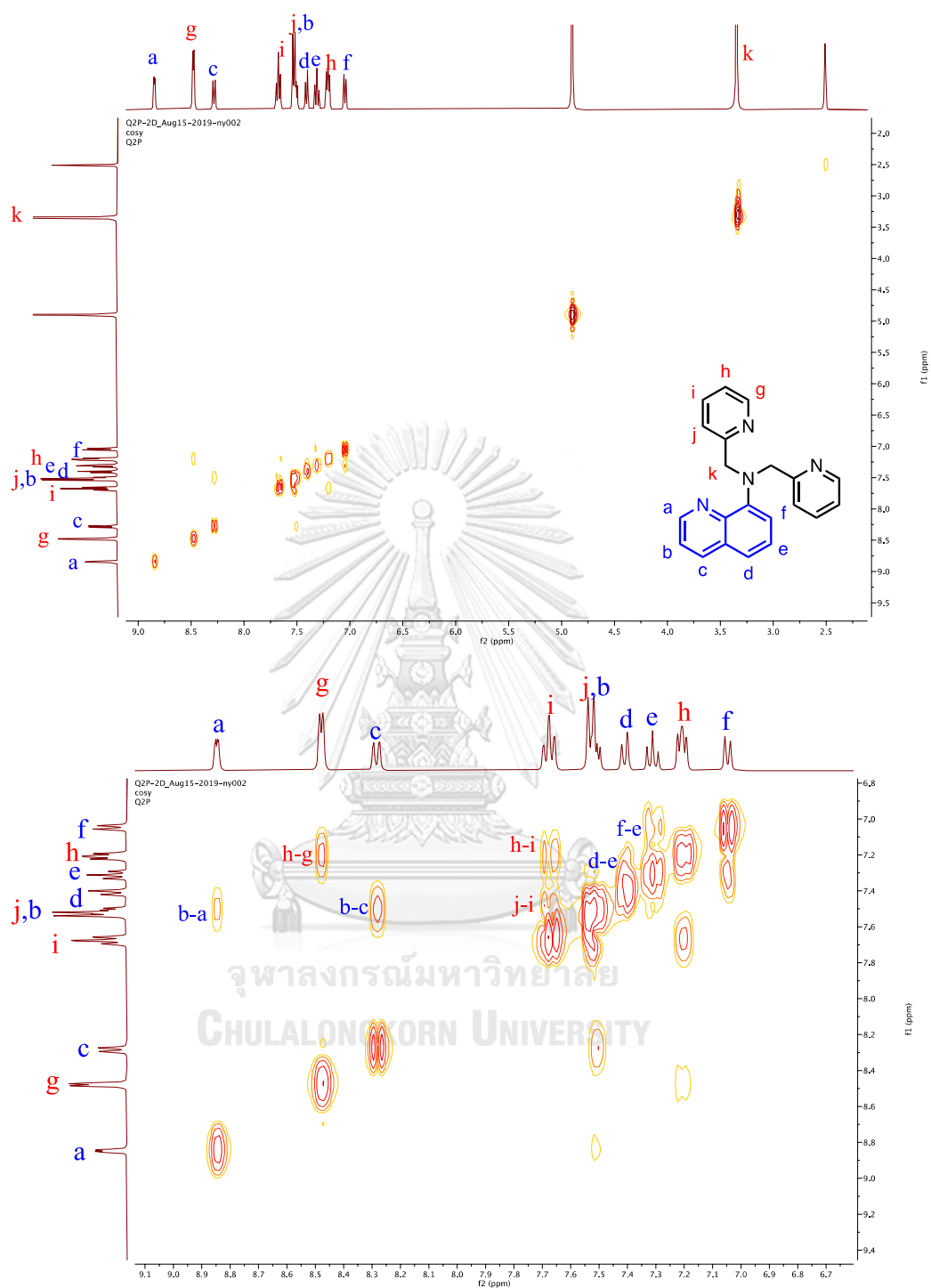


Figure A.4 COSY spectrum of ligand 1Q.

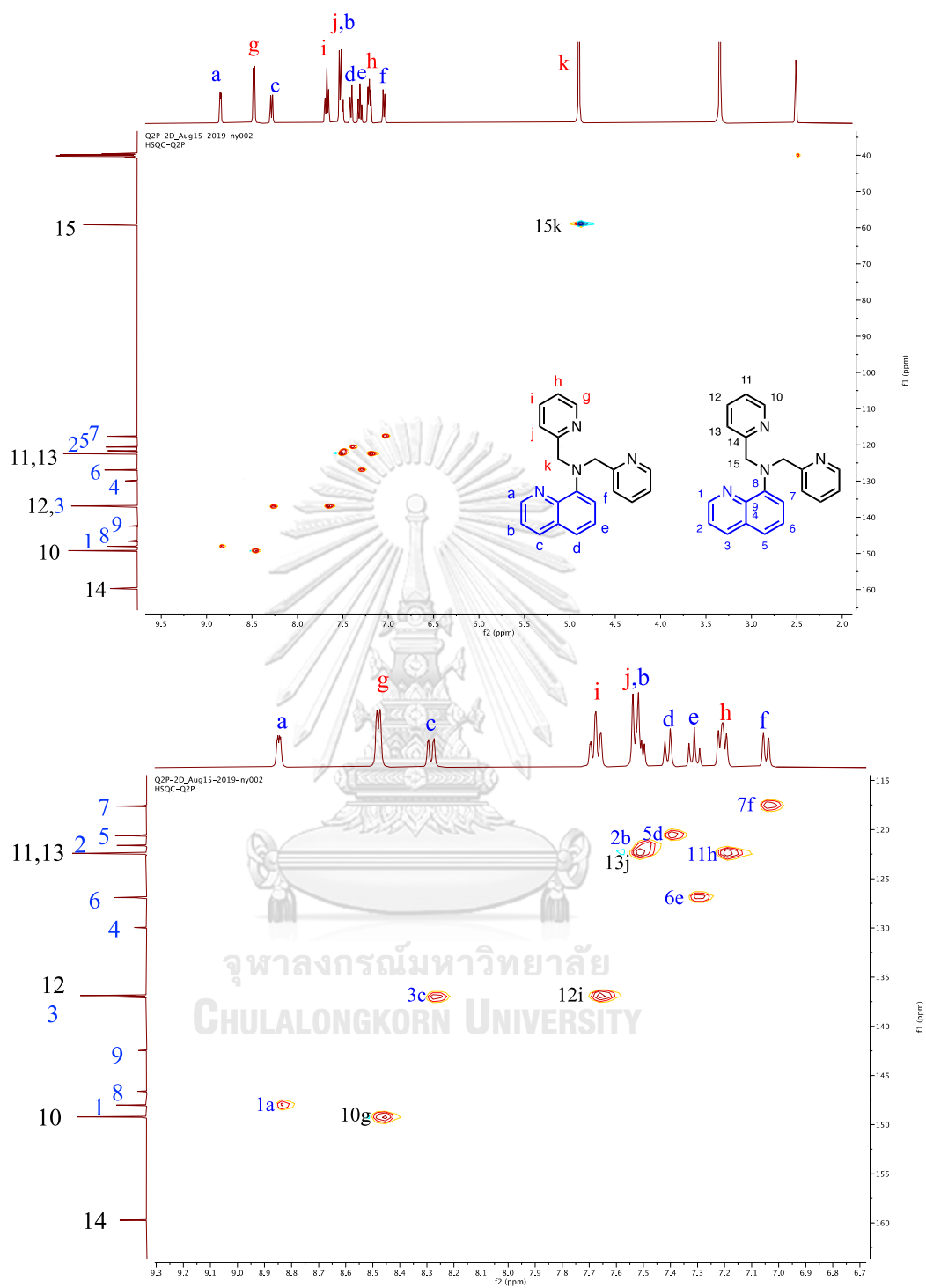


Figure A.5 HSQC spectrum of ligand 1Q.

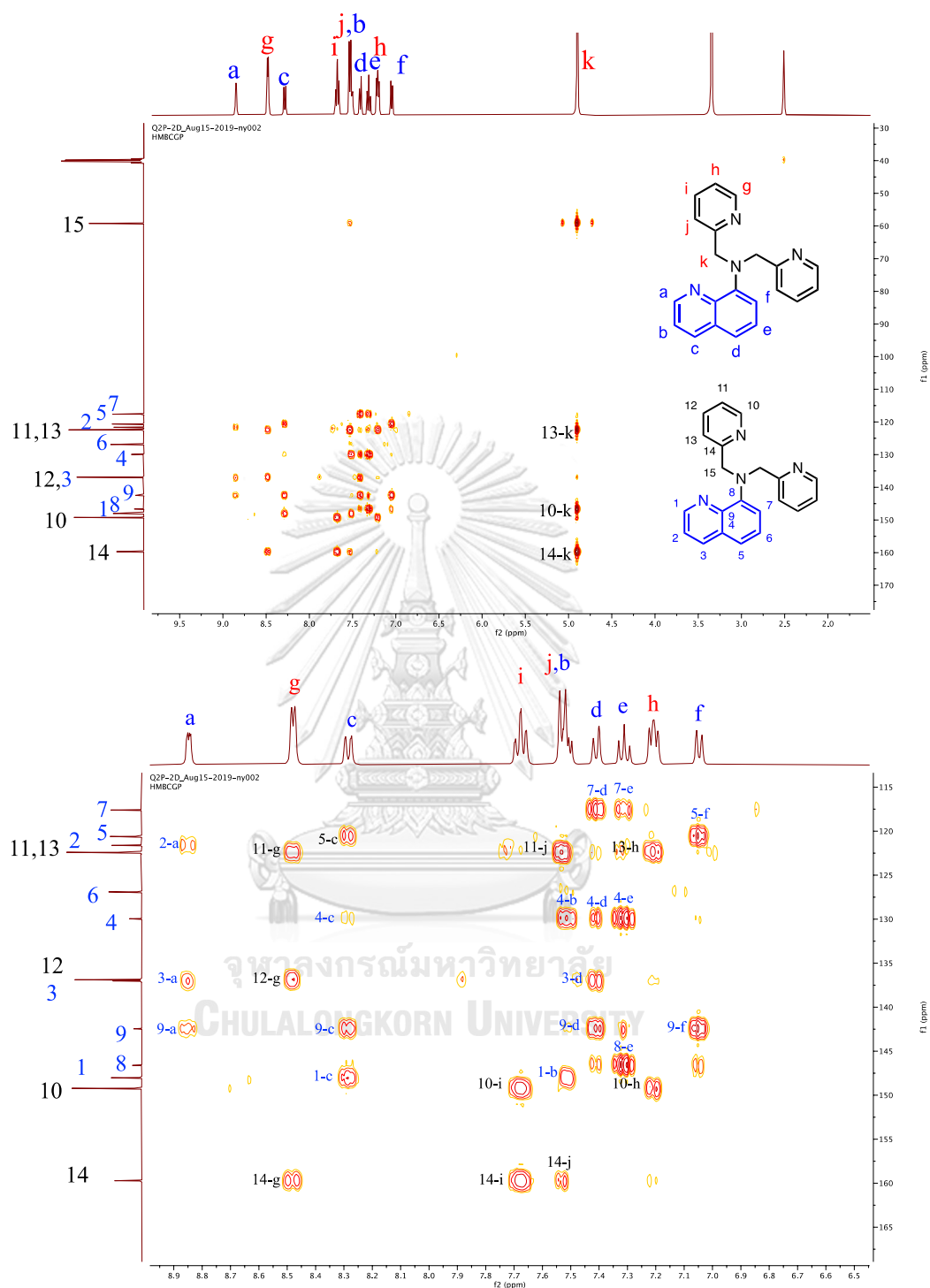
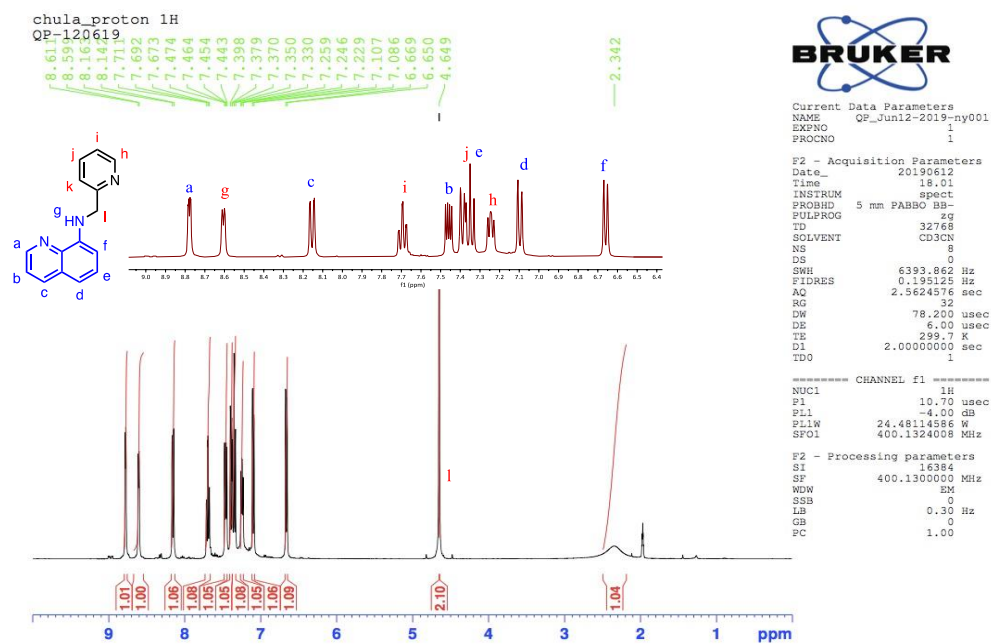
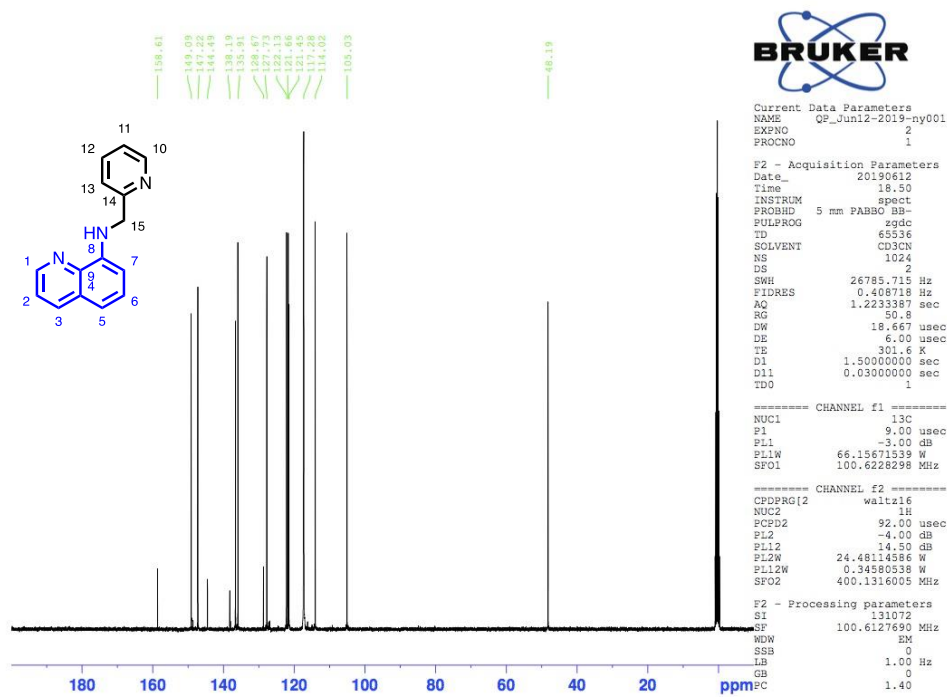
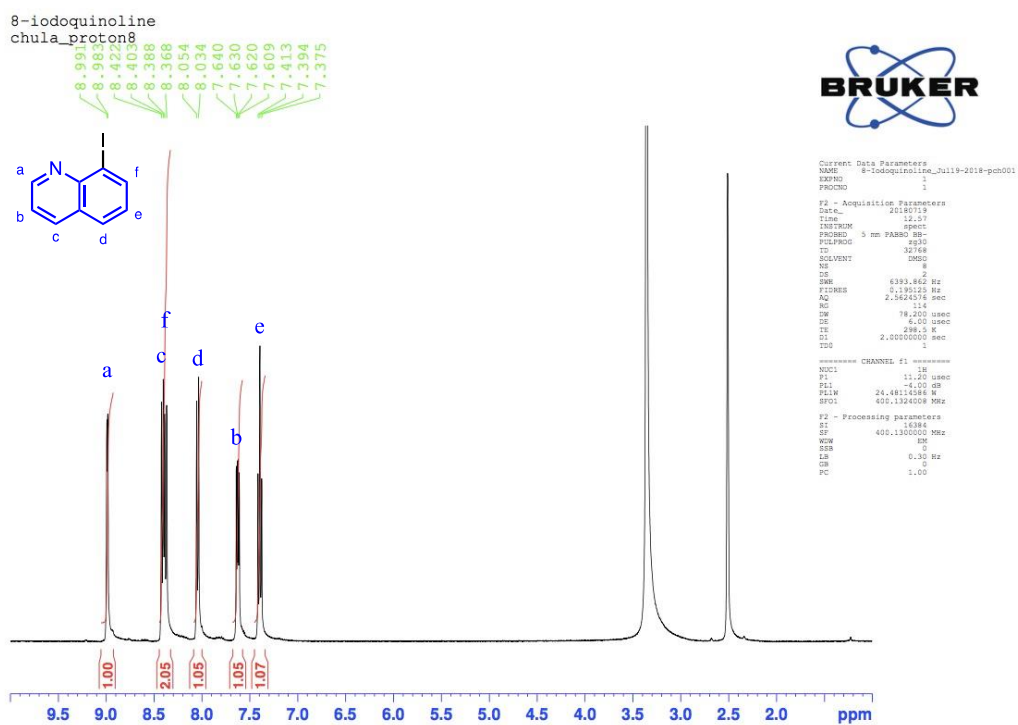
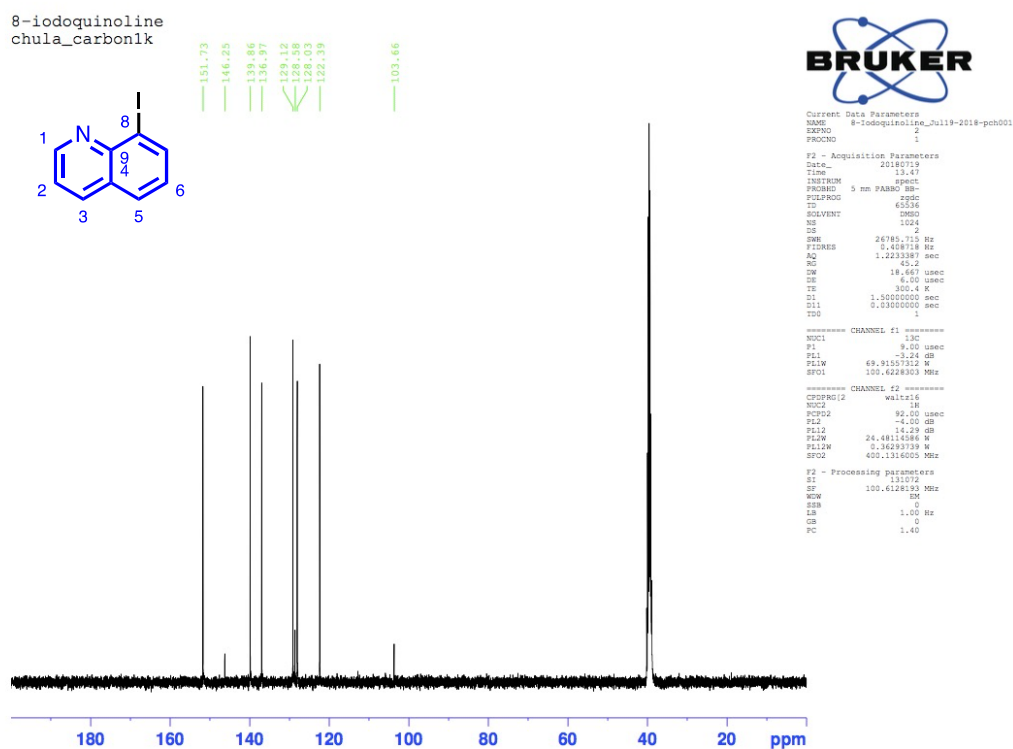
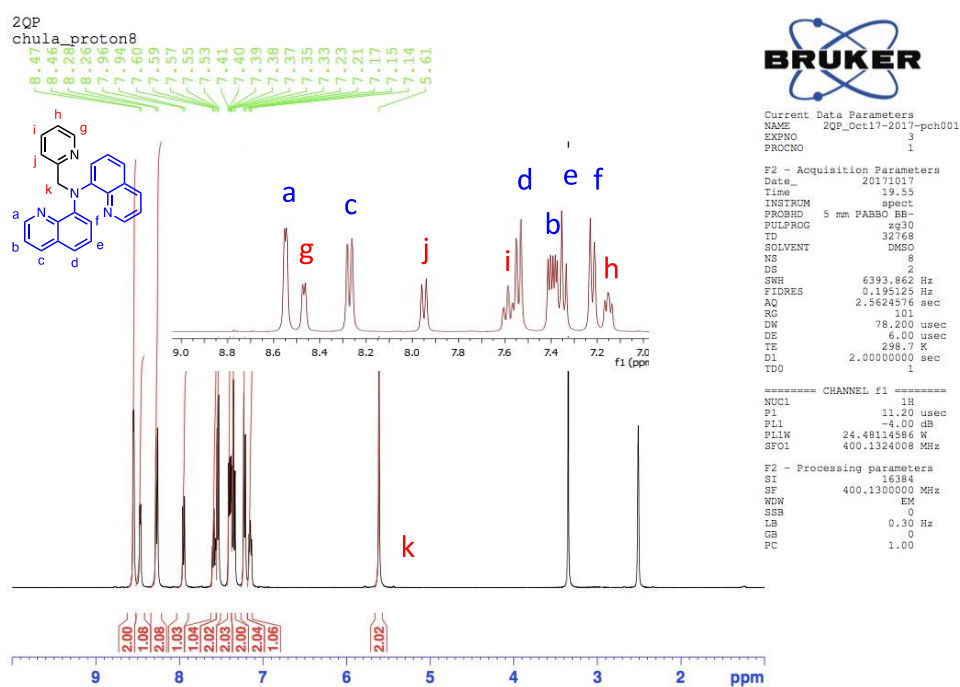
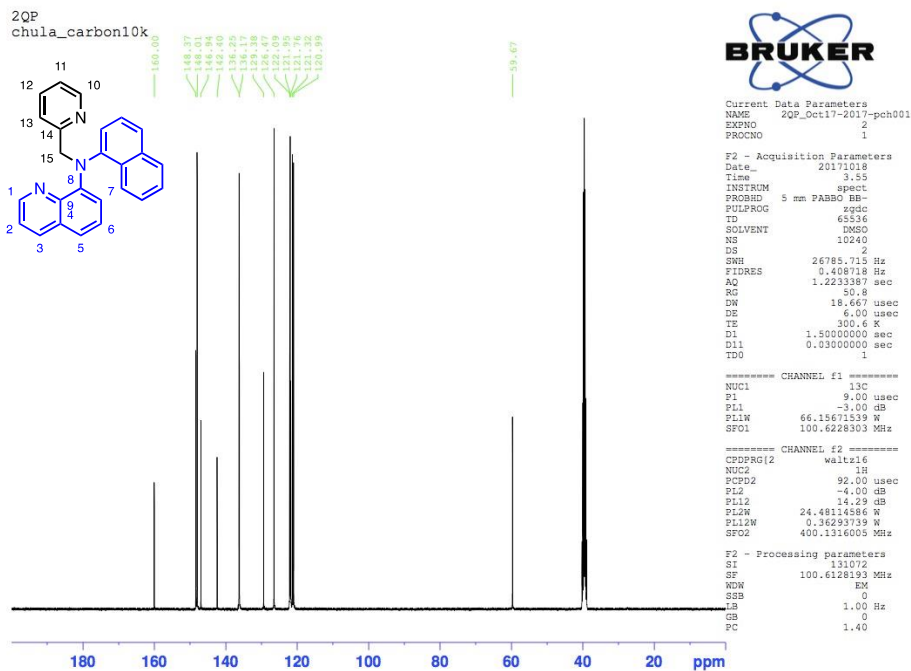


Figure A.6 HMBC spectrum of ligand 1Q.

Figure A.7 ^1H NMR spectrum of ligand QP.Figure A.8 ^{13}C NMR spectrum of ligand QP.

Figure A.9 ^1H NMR spectrum of ligand I-Q.Figure A.10 ^{13}C NMR spectrum of ligand, I-Q.

Figure A.11 ^1H NMR spectrum of ligand 2Q.Figure A.12 ^{13}C NMR spectrum of ligand 2Q.

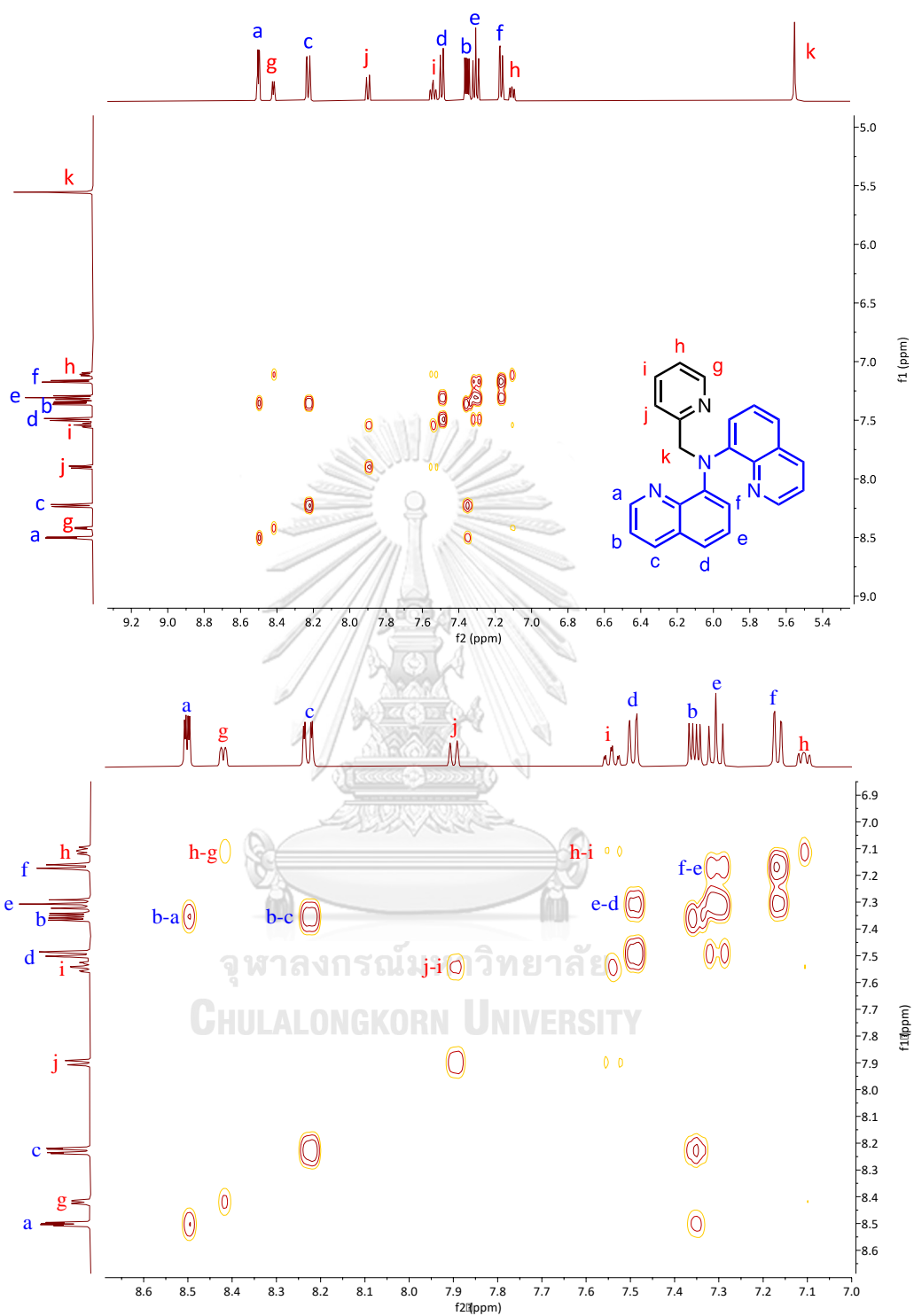


Figure A.13 COSY spectrum of ligand 2Q.

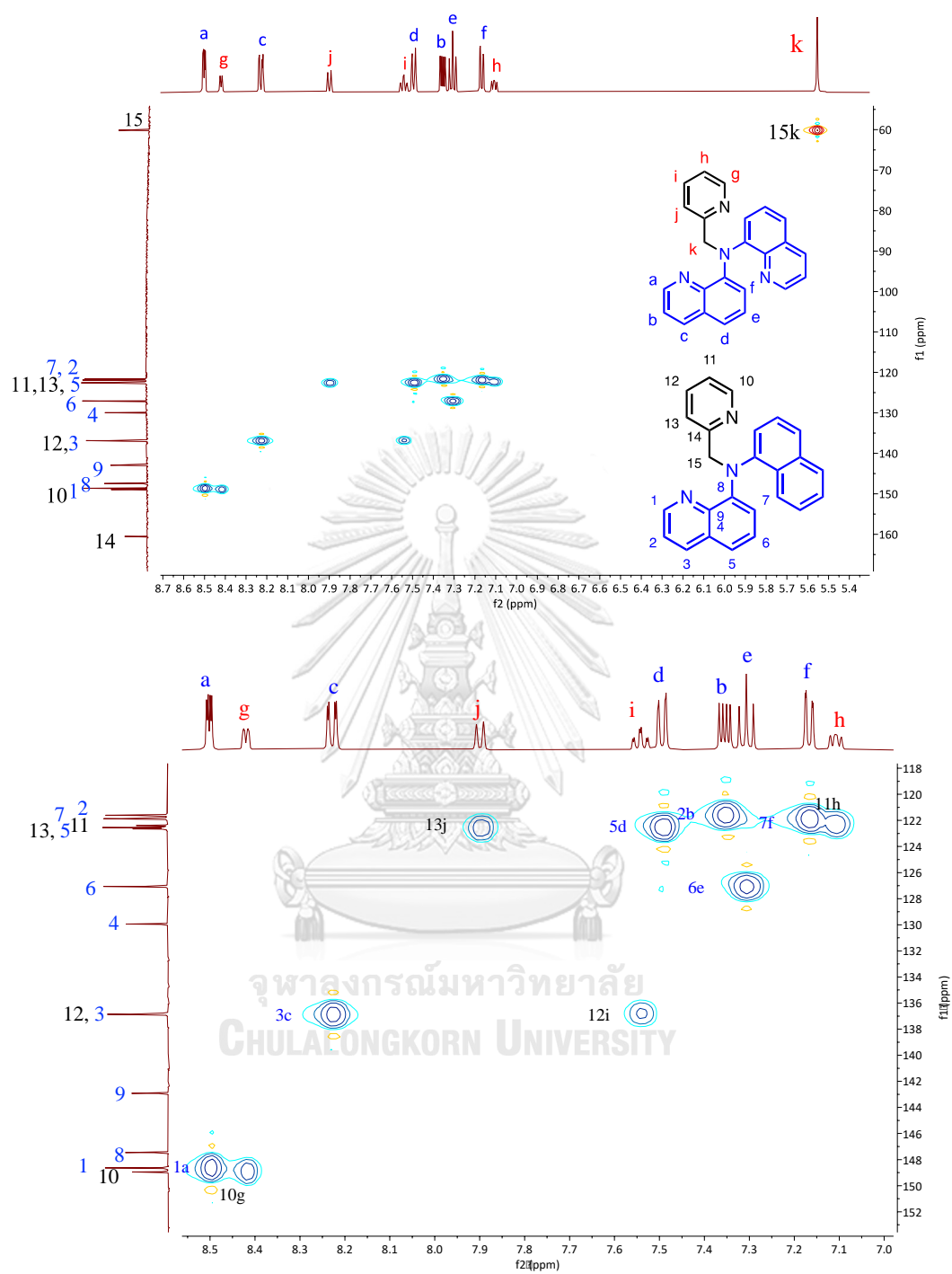


Figure A.14 HSQC spectrum of ligand 2Q.

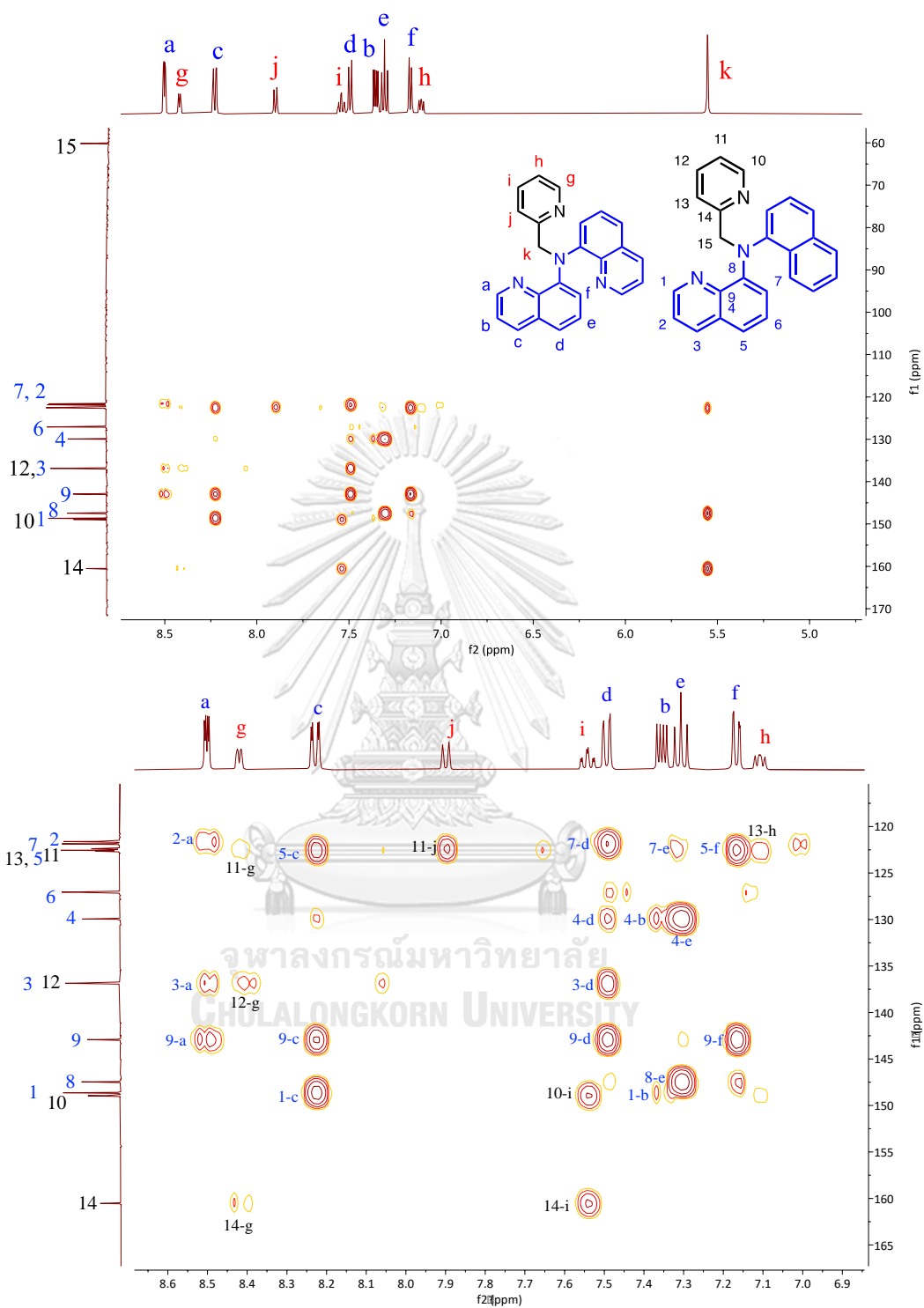
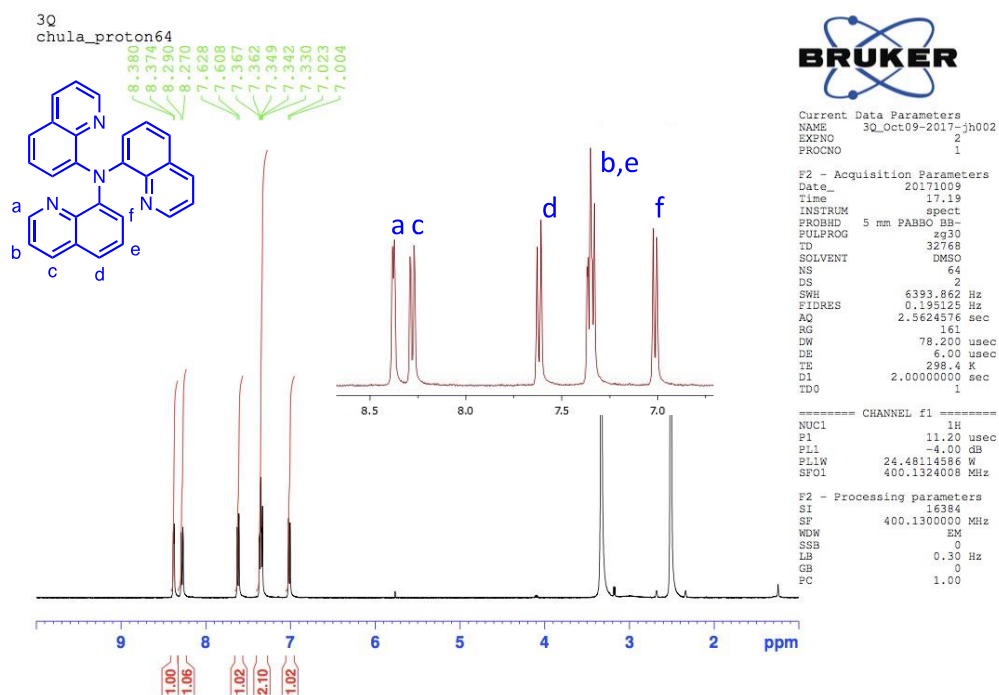
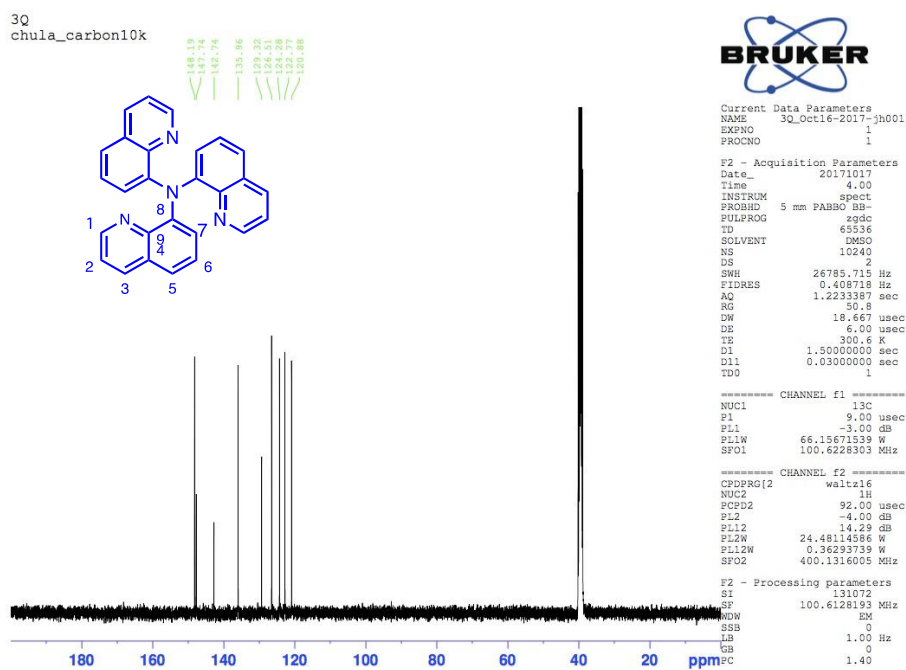


Figure A.15 HMBC spectrum of ligand 2Q.

Figure A.16 ^1H NMR spectrum of ligand 3Q.Figure A.17 ^{13}C NMR spectrum of ligand 3Q.

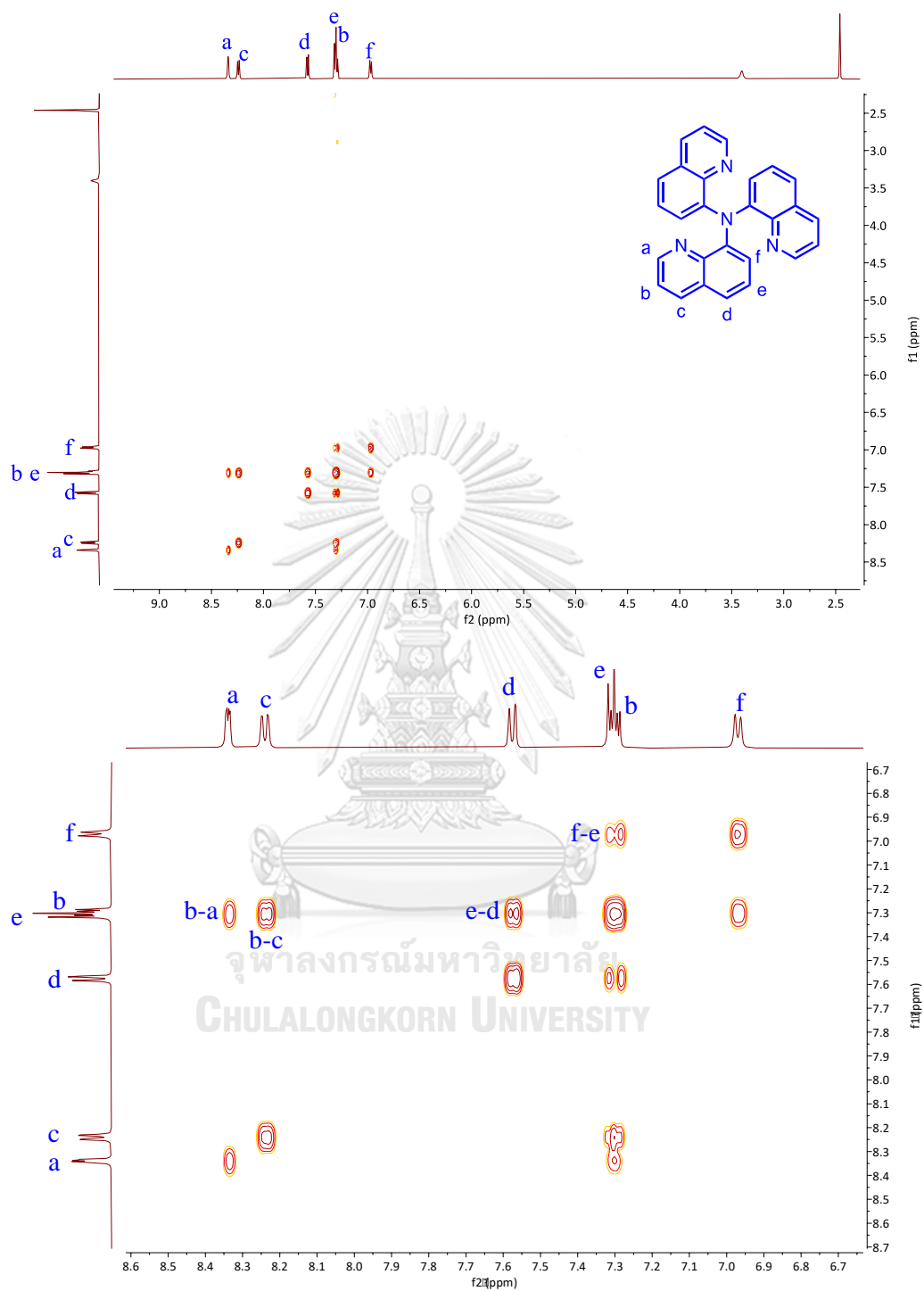


Figure A.18 COSY spectrum of ligand 3Q.

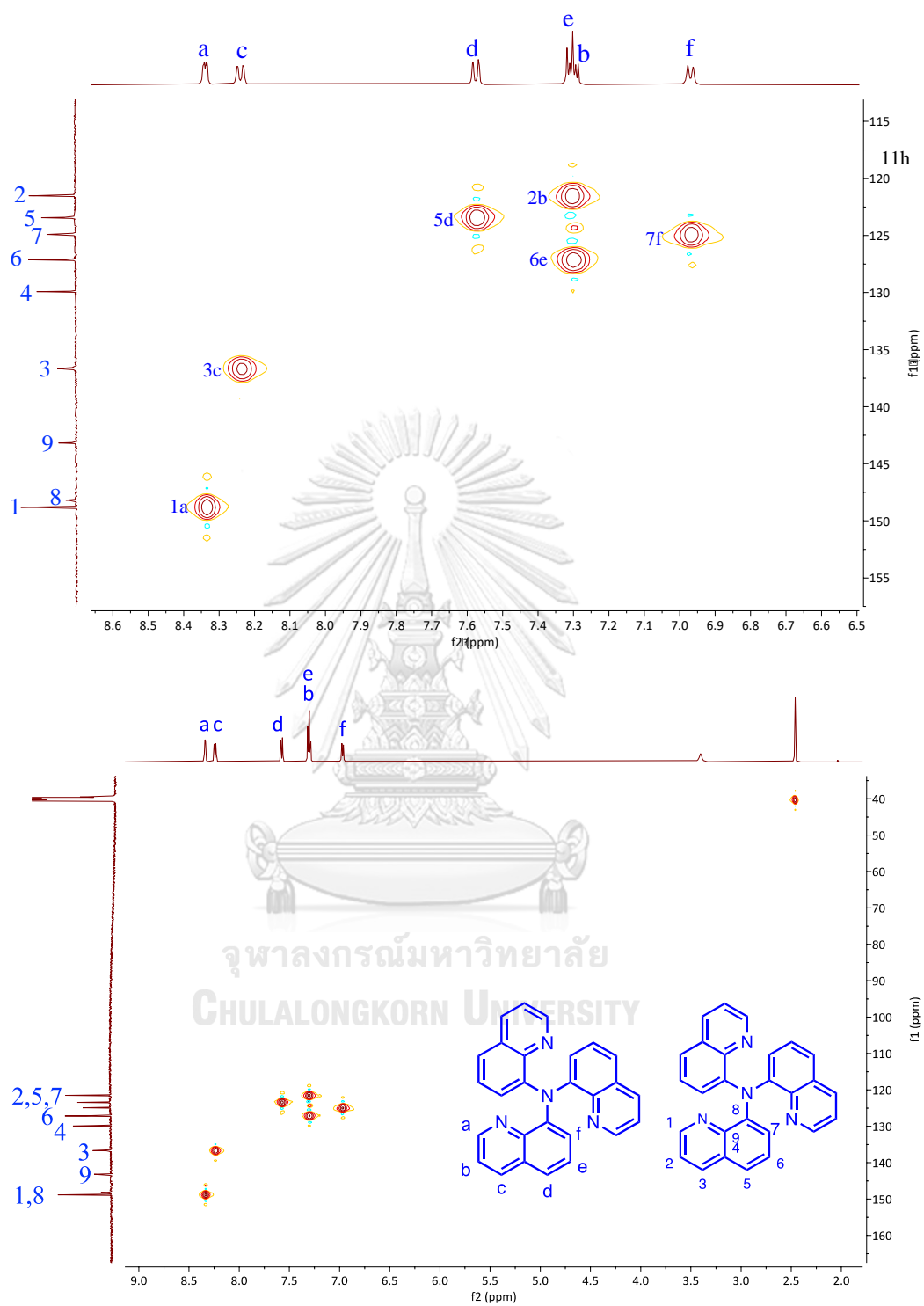


Figure A.19 HSQC spectrum of ligand 3Q.

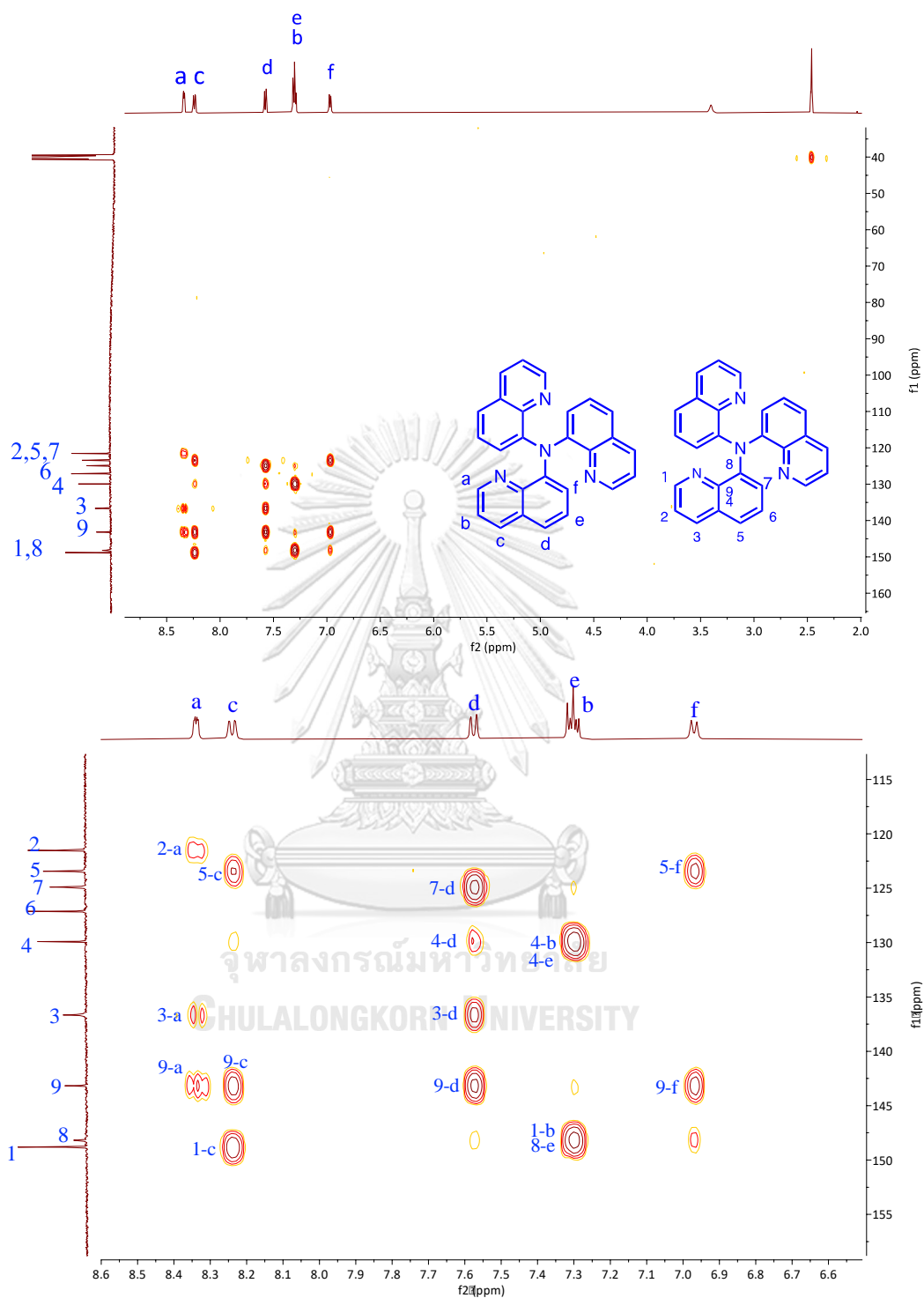


Figure A.20 HMBC spectrum of ligand 3Q.

A.1.3 IR spectra

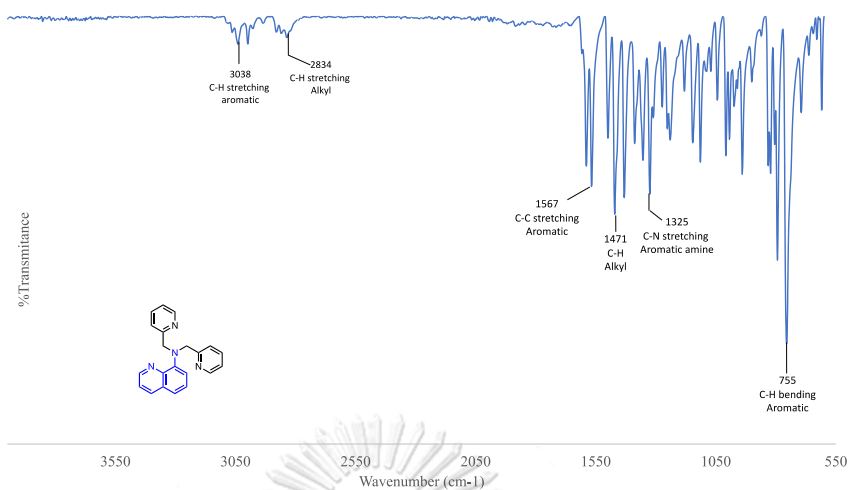


Figure A.21 IR spectrum of ligand 1Q.

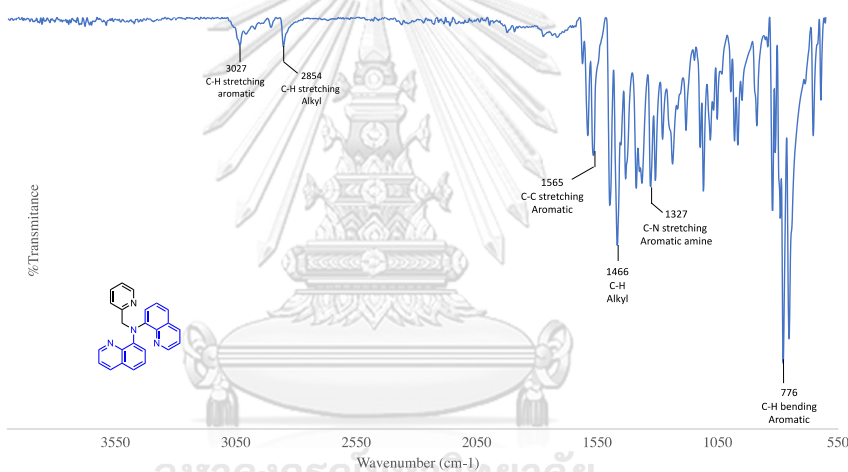


Figure A.22 IR spectrum of ligand 2Q.

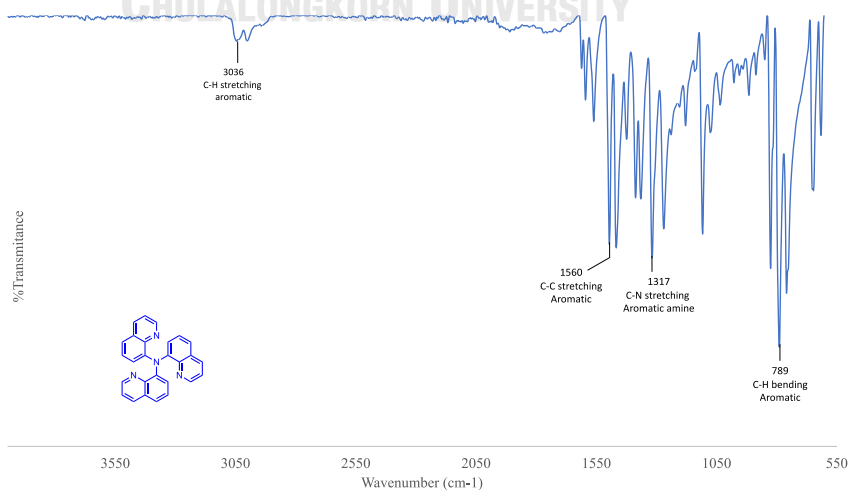
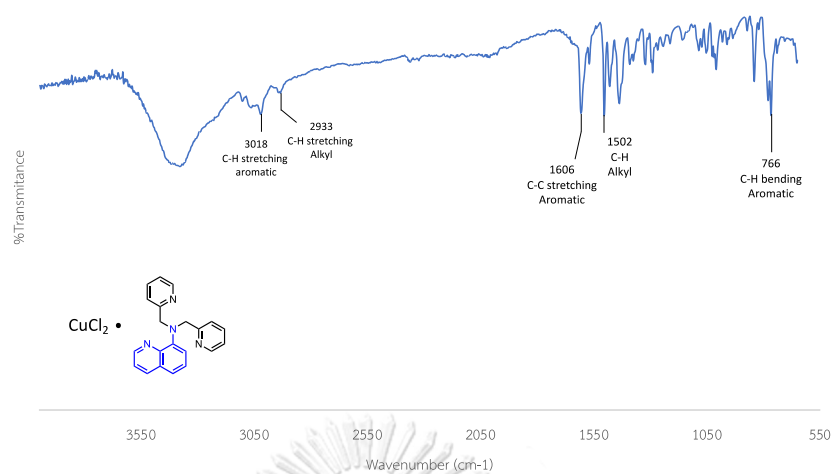
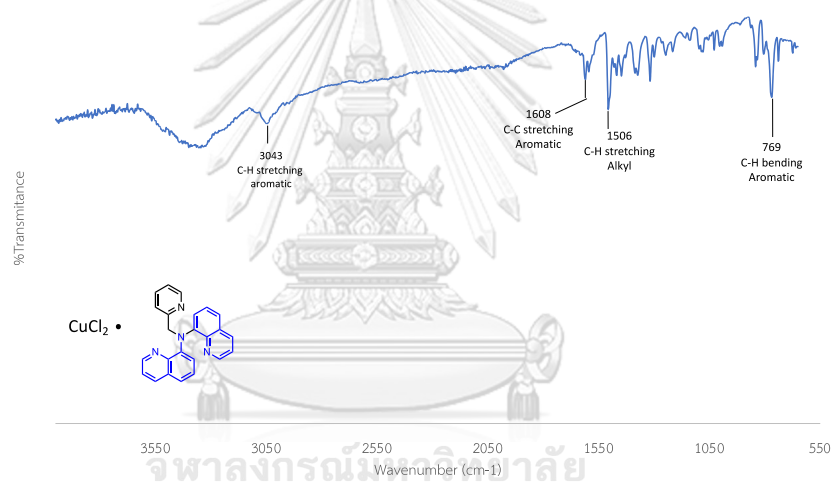
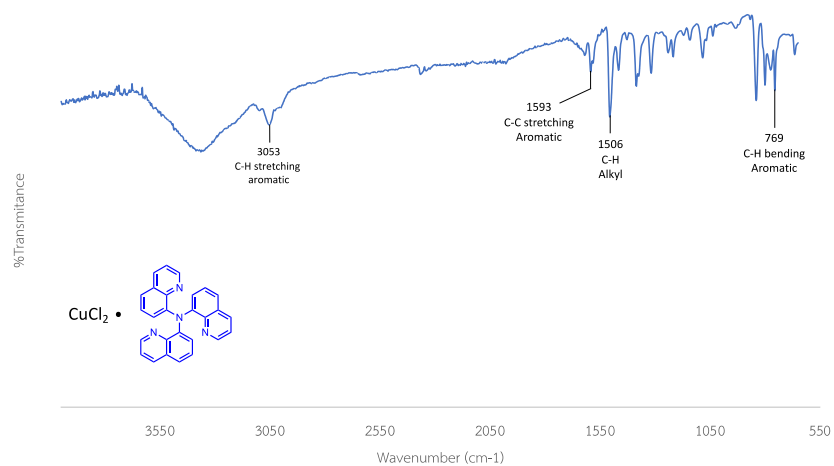


Figure A.23 IR spectrum of ligand 3Q.

Figure A.24 IR spectrum of ligand $\text{CuCl}_2 \cdot 1\text{Q}$.Figure A.25 IR spectrum of ligand $\text{CuCl}_2 \cdot 2\text{Q}$.Figure A.26 IR spectrum of ligand $\text{CuCl}_2 \cdot 3\text{Q}$.

A.1.4 Mass spectrum

Mass Spectrum List Report

Analysis Info		Acquisition Date	8/15/2017 4:31:18 PM
Analysis Name	D:\Data\Data Service\170815_pos_Q2P_white crys-5.d	Operator	Chem CU.
Method	NV_pos_0.3min_profile_1segment_lowNubulizerDrygas.m	Instrument / Ser#	micrOTOF-Q II 10335
Sample Name	170815_pos_Q2P_white crys-5		
Comment			

Acquisition Parameter					
Source Type	ESI	Ion Polarity	Positive	Set Nebulizer	0.4 Bar
Focus	Not active	Set Capillary	4000 V	Set Dry Heater	200 °C
Scan Begin	50 m/z	Set End Plate Offset	-500 V	Set Dry Gas	4.0 l/min
Scan End	1500 m/z	Set Collision Cell RF	150.0 Vpp	Set Divert Valve	Waste

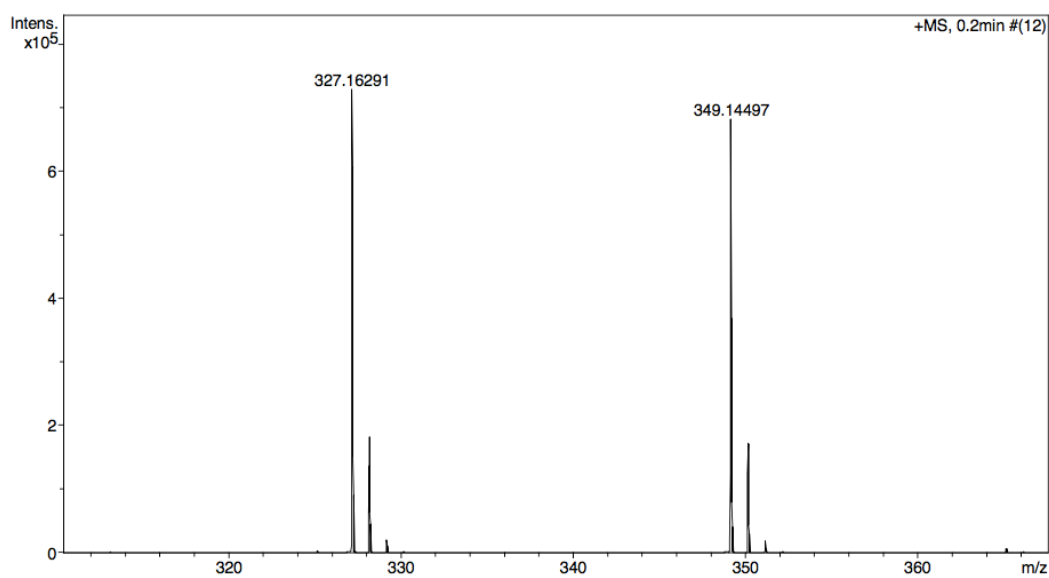
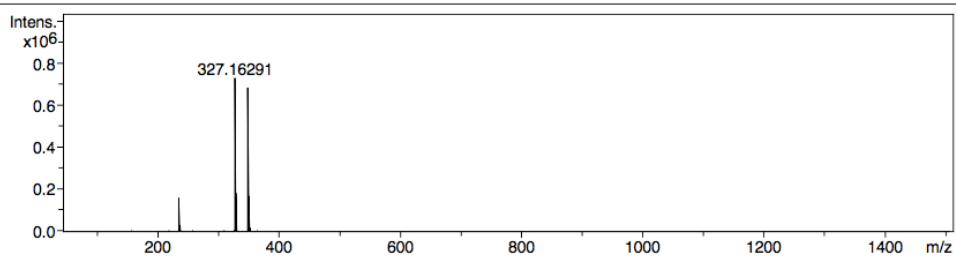


Figure A.27 Mass spectrum of ligand 1Q.

Mass Spectrum List Report

Analysis Info

Analysis Name D:\Data\Data Service\20160930_POS_AC13.d
Method tune_low_forrest_pos_Naformate.m
Sample Name 20160930_POS_AC13
Comment

Acquisition Date 9/30/2016 4:10:12 PM

Operator Chem CU.
Instrument / Ser# micrOTOF-Q II 10335

Acquisition Parameter

Source Type	ESI	Ion Polarity	Positive	Set Nebulizer	0.4 Bar
Focus	Not active	Set Capillary	4500 V	Set Dry Heater	180 °C
Scan Begin	50 m/z	Set End Plate Offset	-500 V	Set Dry Gas	4.0 l/min
Scan End	1500 m/z	Set Collision Cell RF	150.0 Vpp	Set Divert Valve	Waste

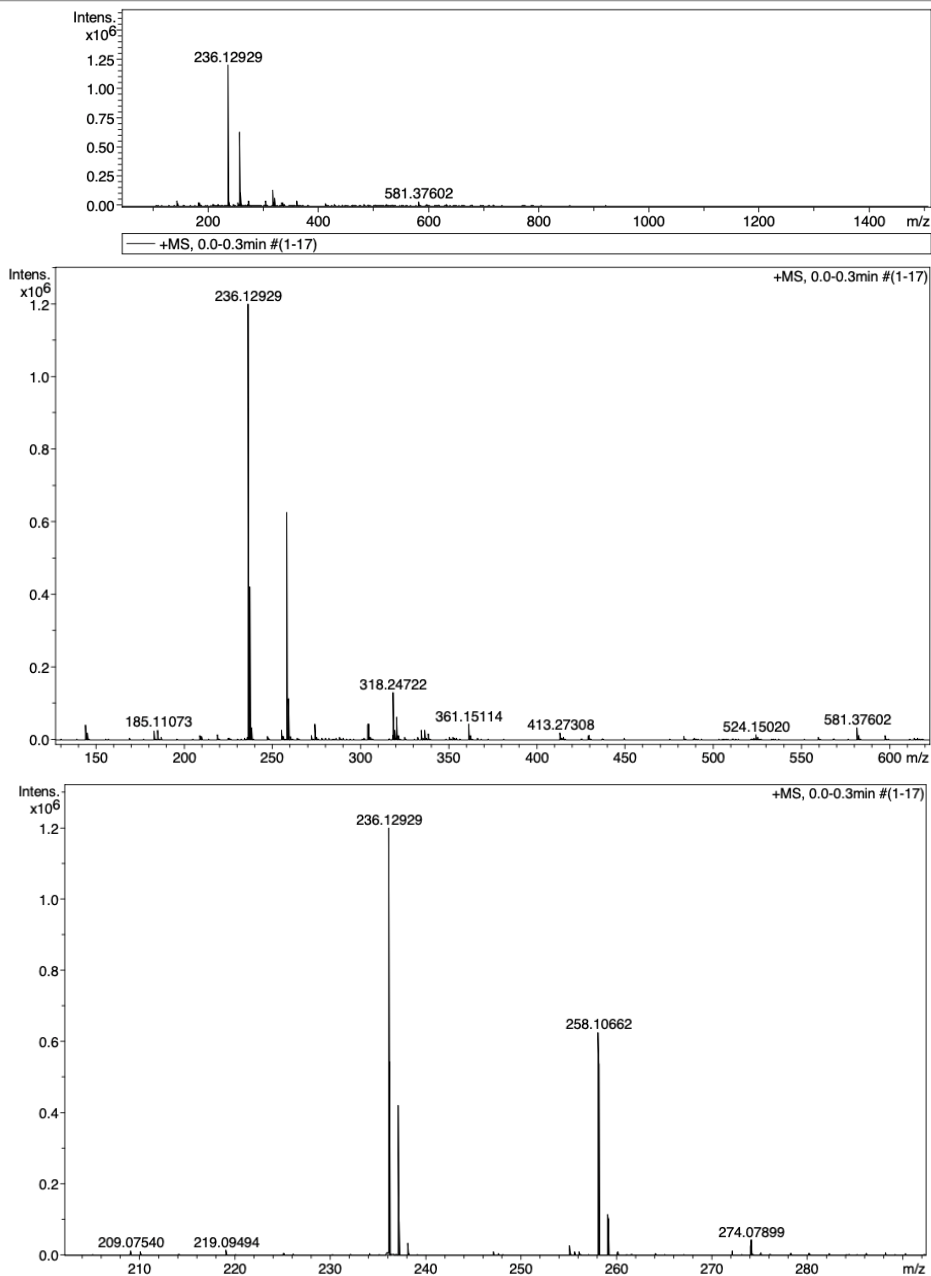


Figure A.28 Mass spectrum of ligand QP.

Mass Spectrum List Report

Analysis Info
Analysis Name D:\Data\Data Service\170908_pos_8-I-quinoline-2.d Acquisition Date 9/8/2017 10:12:04 AM
Method NV_pos_0.3min_profile_1segment_lowNubulizerDrygas.m Operator Chem CU.
Sample Name 170908_pos_8-I-quinoline-2 Instrument / Ser# micrOTOF-Q II 10335
Comment

Acquisition Parameter

Source Type	ESI	Ion Polarity	Positive	Set Nebulizer	0.4 Bar
Focus	Not active	Set Capillary	4000 V	Set Dry Heater	200 °C
Scan Begin	50 m/z	Set End Plate Offset	-500 V	Set Dry Gas	4.0 l/min
Scan End	1500 m/z	Set Collision Cell RF	150.0 Vpp	Set Divert Valve	Waste

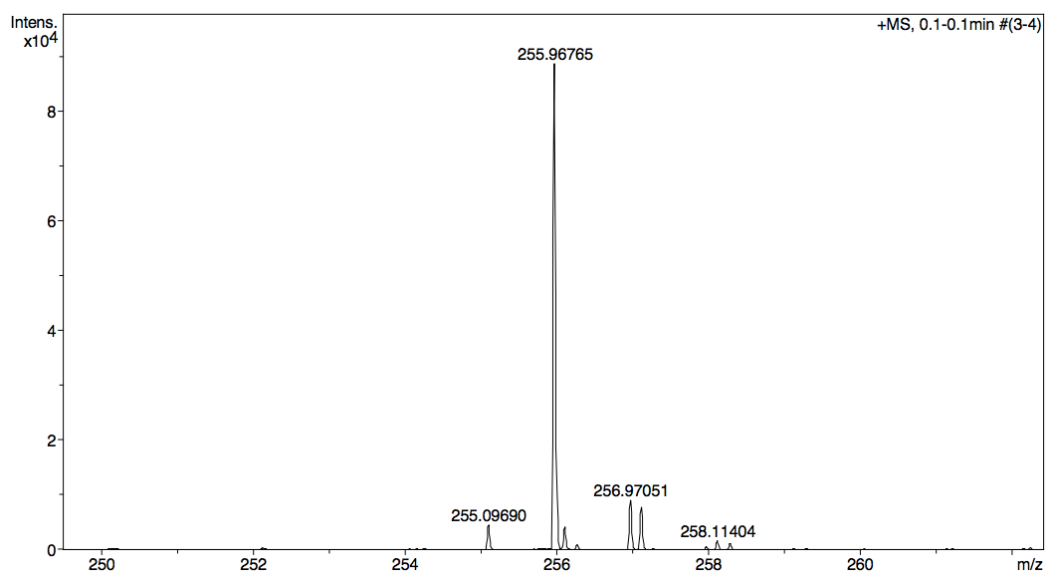
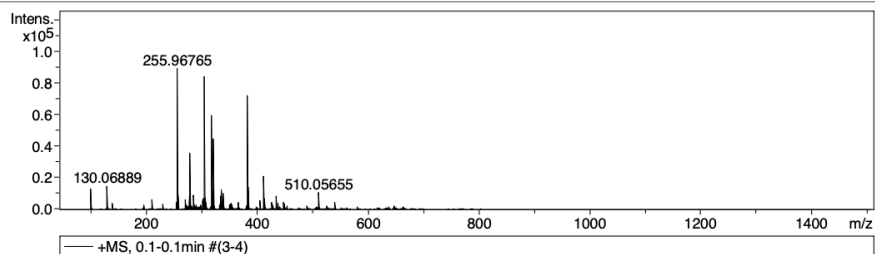


Figure A.29 Mass spectrum of ligand I-Q.

Mass Spectrum List Report

Analysis Info
Analysis Name: D:\Data\Data Service\171103_pos_2QP.d
Method: NV_pos_0.3min_profile_1segment_lowNubulizerDrygas.m
Sample Name: 171103_pos_2QP
Comment:
Acquisition Date: 11/3/2017 11:19:46 AM
Operator: CU.
Instrument / Ser#: microTOF-Q II 10335

Acquisition Parameter

Source Type	ESI	Ion Polarity	Positive	Set Nebulizer	0.4 Bar
Focus	Not active	Set Capillary	4000 V	Set Dry Heater	200 °C
Scan Begin	50 m/z	Set End Plate Offset	-500 V	Set Dry Gas	4.0 l/min
Scan End	1500 m/z	Set Collision Cell RF	150.0 Vpp	Set Divert Valve	Waste

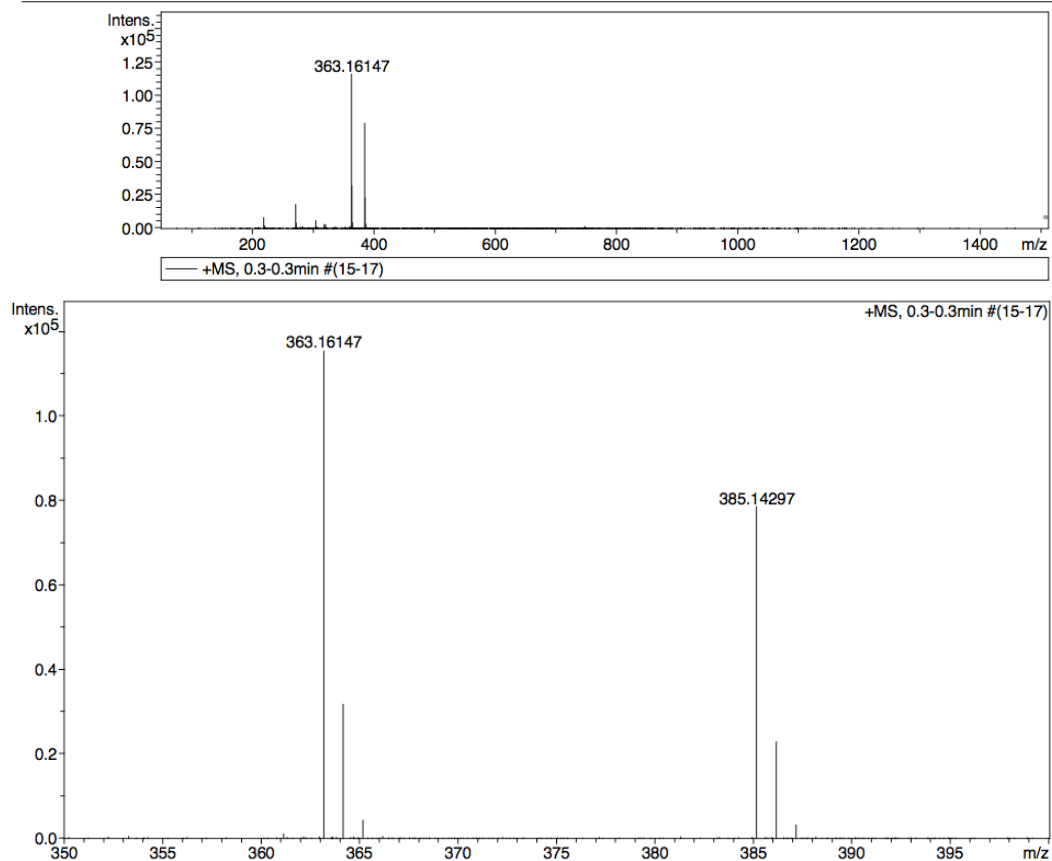


Figure A.30 Mass spectrum of ligand 2Q.

Mass Spectrum List Report

Analysis Info
Analysis Name D:\Data\Data Service\170908_pos_NC3_3Q.d Acquisition Date 9/8/2017 10:42:40 AM
Method NV_pos_0.3min_profile_1segment_lowNubulizerDrygas.m Operator Chem CU.
Sample Name 170908_pos_NC3_3Q Instrument / Ser# micrOTOF-Q II 10335
Comment

Acquisition Parameter

Source Type	ESI	Ion Polarity	Positive	Set Nebulizer	0.4 Bar
Focus	Not active	Set Capillary	4000 V	Set Dry Heater	200 °C
Scan Begin	50 m/z	Set End Plate Offset	-500 V	Set Dry Gas	4.0 l/min
Scan End	1500 m/z	Set Collision Cell RF	150.0 Vpp	Set Divert Valve	Waste

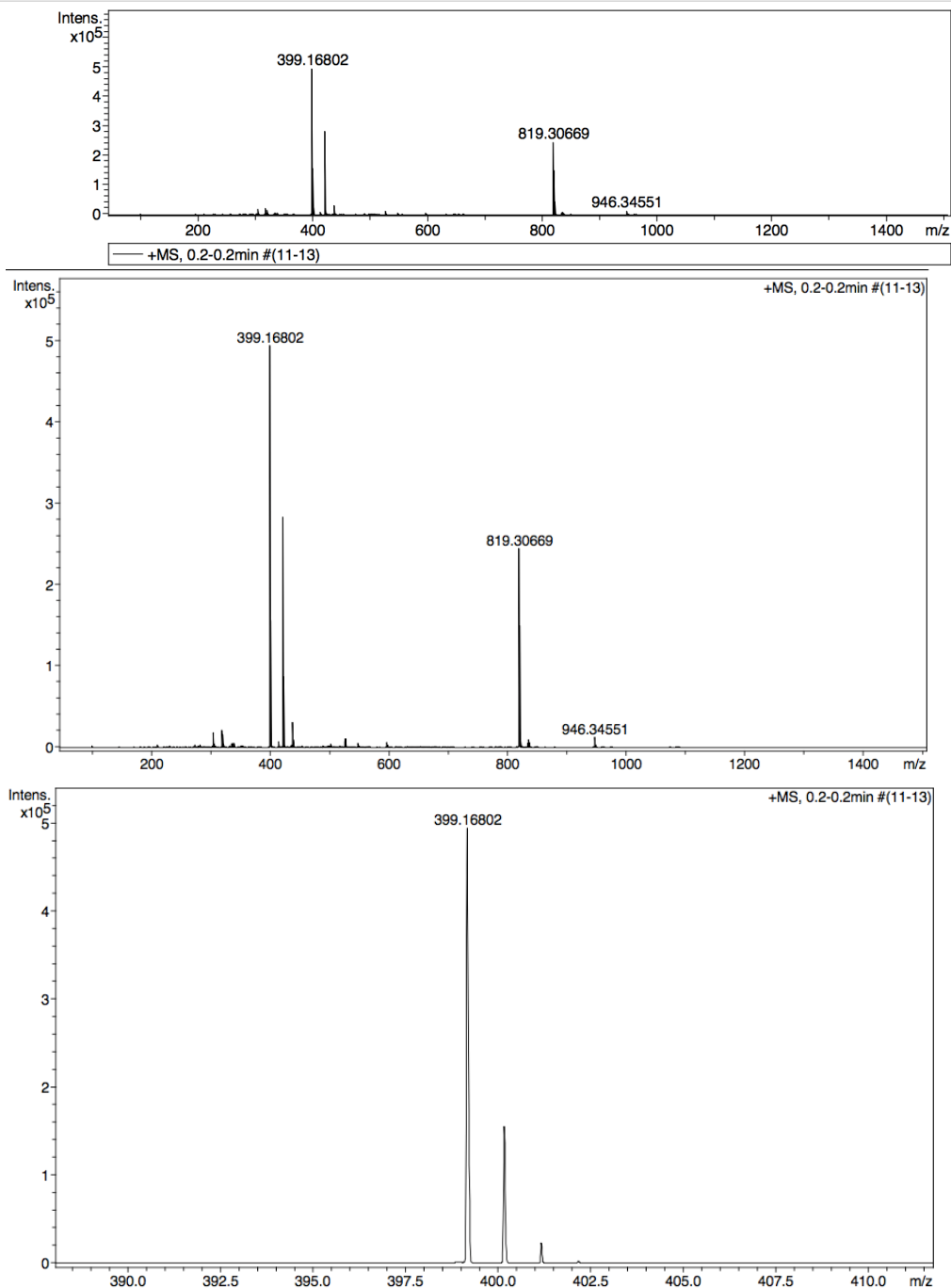


Figure A.31 Mass spectrum of ligand 3Q.

Mass Spectrum List Report

Analysis Info
Analysis Name D:\Data\Data Service\20161129_pos_CP6(Q2P).d Acquisition Date 11/29/2016 3:21:55 PM
Method NV_pos_0.3min_profile_1segment.m Operator Chem CU.
Sample Name 20161129_pos_CP6(Q2P) Instrument / Ser# micrOTOF-Q II 10335
Comment

Acquisition Parameter

Source Type	ESI	Ion Polarity	Positive	Set Nebulizer	3.0 Bar
Focus	Not active	Set Capillary	4000 V	Set Dry Heater	200 °C
Scan Begin	50 m/z	Set End Plate Offset	-500 V	Set Dry Gas	8.0 l/min
Scan End	1500 m/z	Set Collision Cell RF	150.0 Vpp	Set Divert Valve	Waste

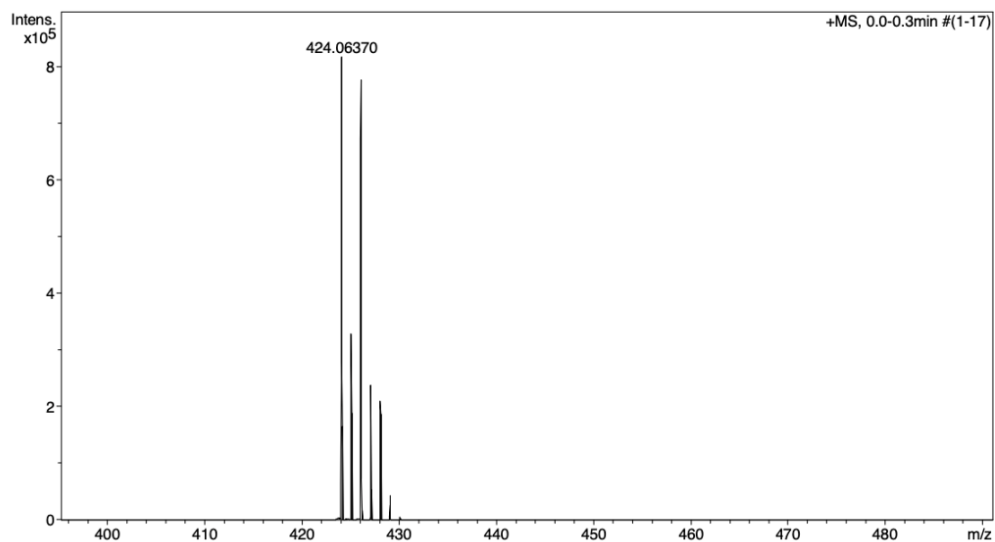
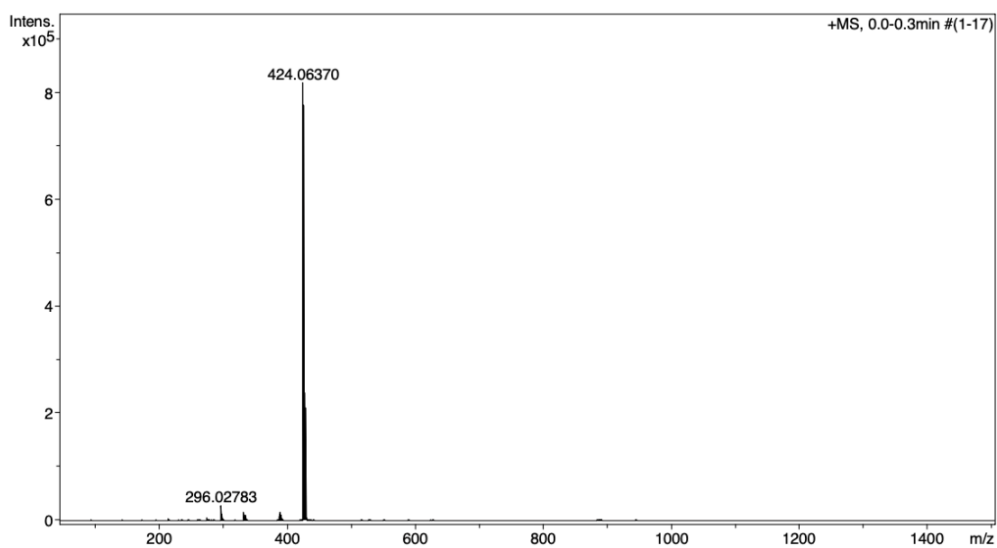
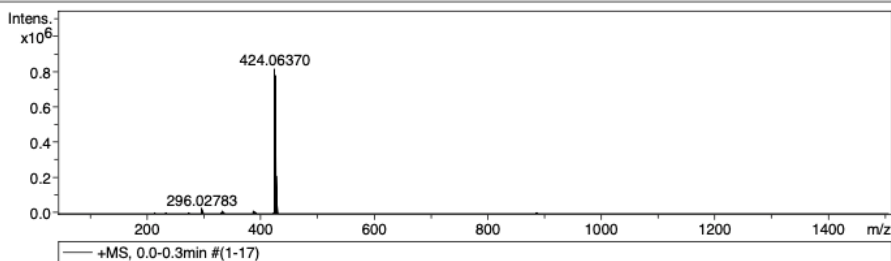


Figure A.32 Mass spectrum of $[\text{Cu}^{\text{I}}(1\text{Q})\text{Cl}]^+$.

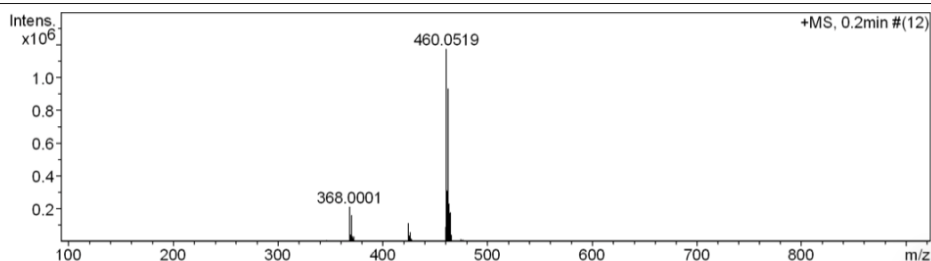
Mass Spectrum List Report

Analysis Info

Analysis Name	OSCUPC27082019001_1.d	Acquisition Date	8/27/2019 7:43:30 AM
Method	Tune_wide_POS_Tawatchai_05Feb2016.m	Operator	Administrator
Sample Name	CuCl ₂ .2Q	Instrument	micrOTOF 72
	CuCl ₂ .2Q		

Acquisition Parameter

Source Type	ESI	Ion Polarity	Positive	Set Corrector Fill	50 V
Scan Range	n/a	Capillary Exit	150.0 V	Set Pulsar Pull	337 V
Scan Begin	50 m/z	Hexapole RF	400.0 V	Set Pulsar Push	337 V
Scan End	3000 m/z	Skimmer 1	70.0 V	Set Reflector	1300 V
		Hexapole 1	25.0 V	Set Flight Tube	9000 V
				Set Detector TOF	2295 V



#	m/z	I	I%	S/N	Res.
1	296.9008	5476	0.5	10.3	23151
2	333.0319	5884	0.5	11.4	5075
3	346.0384	9990	0.9	19.9	5098
4	368.0001	211546	18.0	438.6	4986
5	369.0031	41795	3.6	86.4	5229
6	369.9983	161308	13.7	334.9	5014
7	371.0005	31159	2.7	64.4	5093
8	371.9967	30408	2.6	62.9	4985
9	372.9977	5955	0.5	12.0	4906
10	374.1757	5625	0.5	11.3	21871
11	424.0745	113782	9.7	248.2	4989
12	425.0770	35889	3.1	78.0	5013
13	426.0729	56355	4.8	122.9	5214
14	427.0758	15653	1.3	33.8	5043
15	459.7671	7892	0.7	17.4	2043
16	460.0519	1173304	100.0	2653.6	4914
17	460.6254	7272	0.6	16.0	1205
18	461.0550	310534	26.5	702.6	4981
19	461.6411	5428	0.5	11.8	1782
20	462.0499	931582	79.4	2110.9	4951
21	463.0528	230935	19.7	523.4	5080
22	464.0476	179830	15.3	407.9	5280
23	465.0491	41714	3.6	94.3	5434
24	466.0531	5649	0.5	12.4	4695
25	474.0656	14261	1.2	32.2	4990
26	476.0640	12179	1.0	27.5	5149
27	957.0695	9725	0.8	20.6	5745
28	959.0666	7176	0.6	15.0	5179
29	1443.1434	5513	0.5	11.2	51376
30	2339.4275	5642	0.5	12.2	67064

Figure A.33 Mass spectrum of ligand [Cu^{II}(2Q)Cl]⁺.

Mass Spectrum List Report

Analysis Info		Acquisition Date	4/20/2018 9:11:21 AM
Analysis Name	D:\Data\Data Service\180419_pos_CuCl2(3Q)-2.d	Operator	CU
Method	NV_pos_0.3min_profile_1segment_lowNubulizerDrygas.m	Instrument / Ser#	micrOTOF-Q II 10335
Sample Name	180419_pos_CuCl2(3Q)-2		
Comment			

Acquisition Parameter

Source Type	ESI	Ion Polarity	Positive	Set Nebulizer	0.4 Bar
Focus	Not active	Set Capillary	4000 V	Set Dry Heater	200 °C
Scan Begin	50 m/z	Set End Plate Offset	-500 V	Set Dry Gas	4.0 l/min
Scan End	1500 m/z	Set Collision Cell RF	800.0 Vpp	Set Divert Valve	Waste

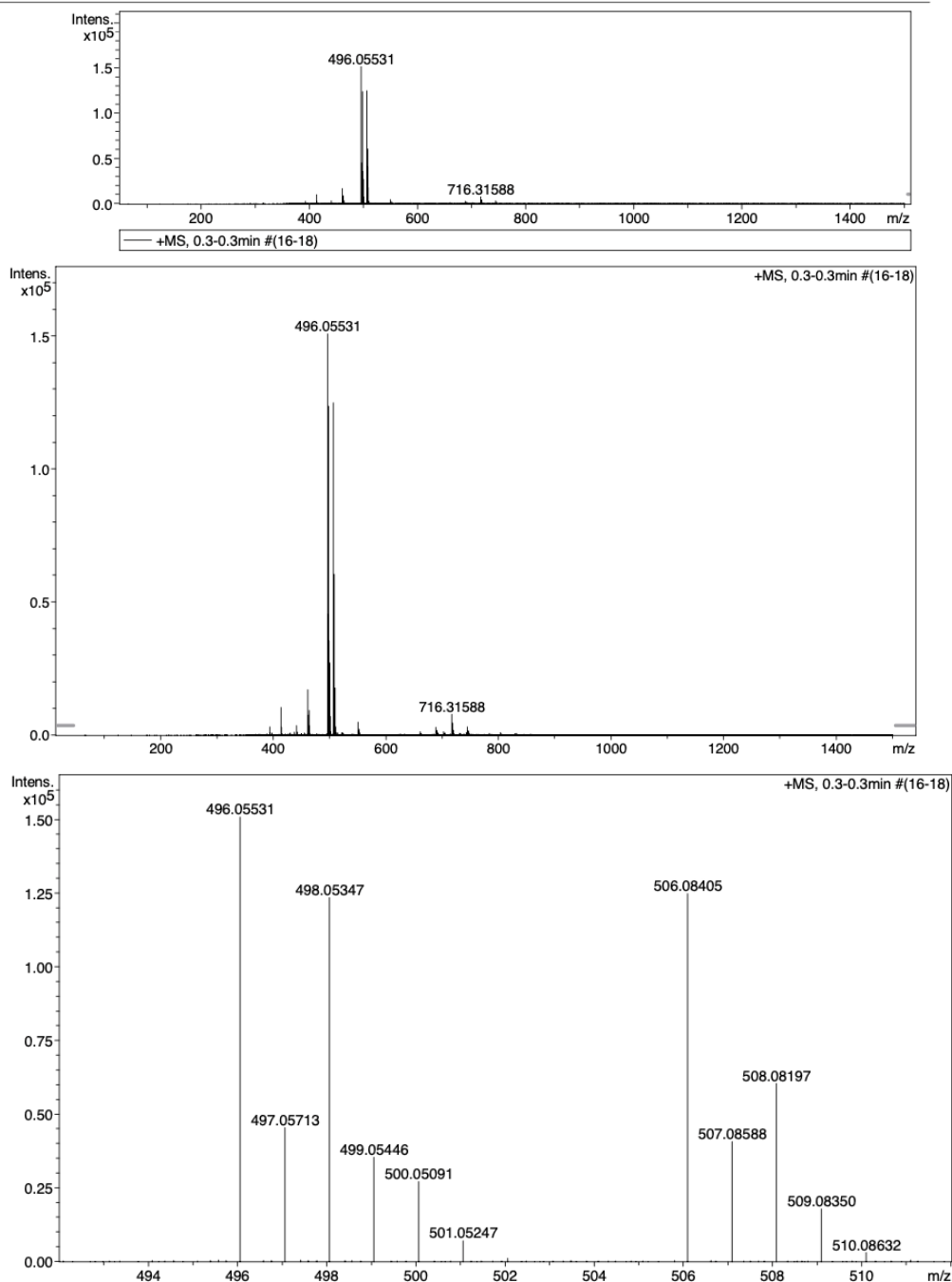


Figure A.34 Mass spectrum of ligand $[\text{Cu}^{\text{II}}(3\text{Q})\text{Cl}]^+$.

A.1.5 Elemental analysis

The sample code **Q2P**, **2QP** and **3Q** are ligand **1Q**, **2Q** and **3Q**, respectively.

RESULT FROM CHN ELEMENTAL ANALYSIS

Sender Ch.pawittra

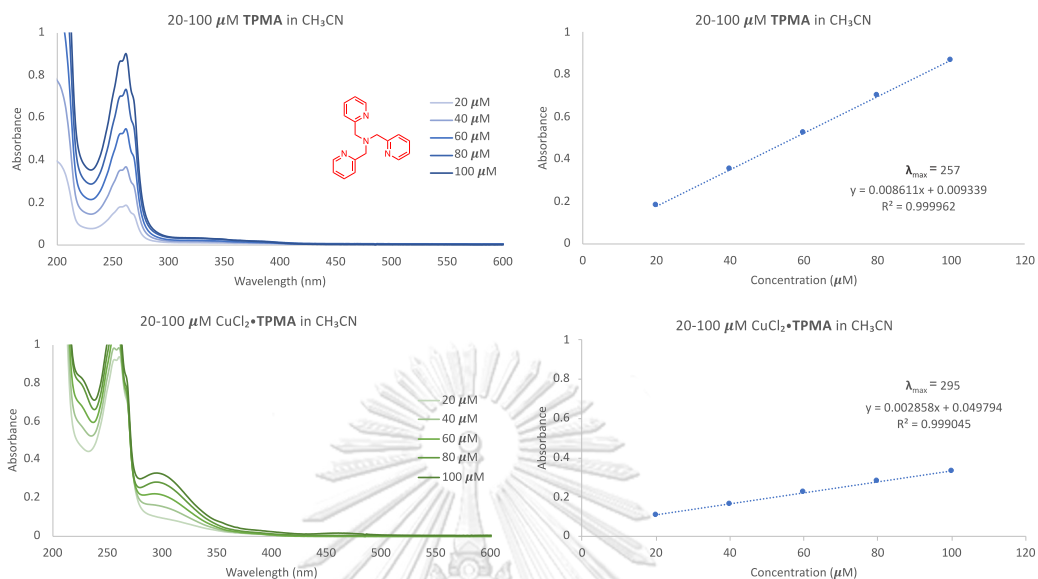
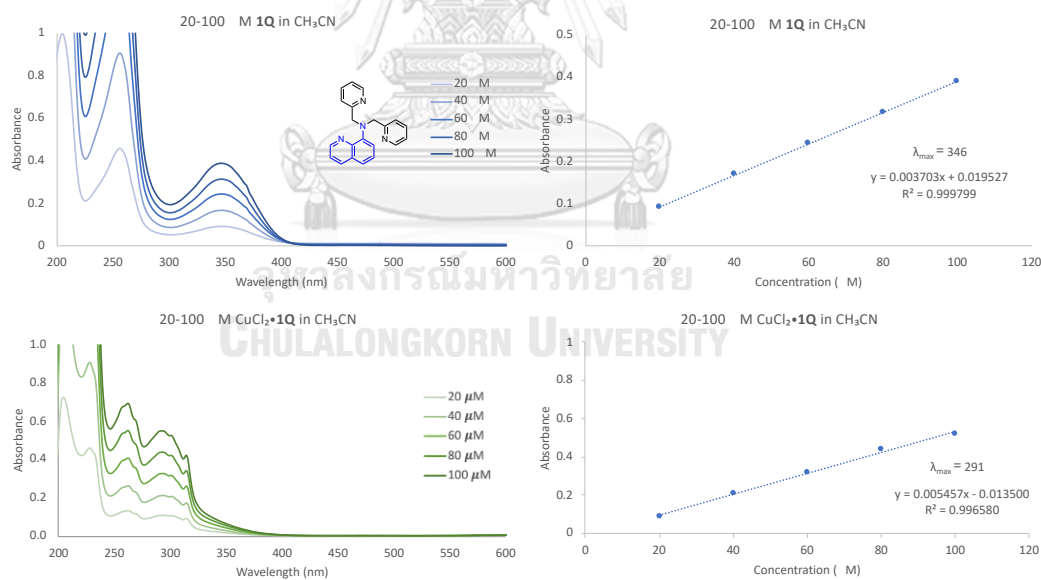
Date 17-07-2018

NO.	Sample code	Analysis required			Remark
		%C	%H	%N	
1	Q2P	77.02	5.18	17.30	
2	2QP	78.22	4.39	15.84	
3	3Q	81.15	4.20	14.56	

OPERATER ID: NATTHAPAT

Perkin-Elmer 2400 Series CHNS/O Analyser

A.1.6 UV-Visible spectroscopy

Figure A.35 Absorption spectrum of TPMA and $\text{CuCl}_2 \cdot \text{TPMA}$.Figure A.36 Absorption spectrum of 1Q and $\text{CuCl}_2 \cdot 1\text{Q}$.

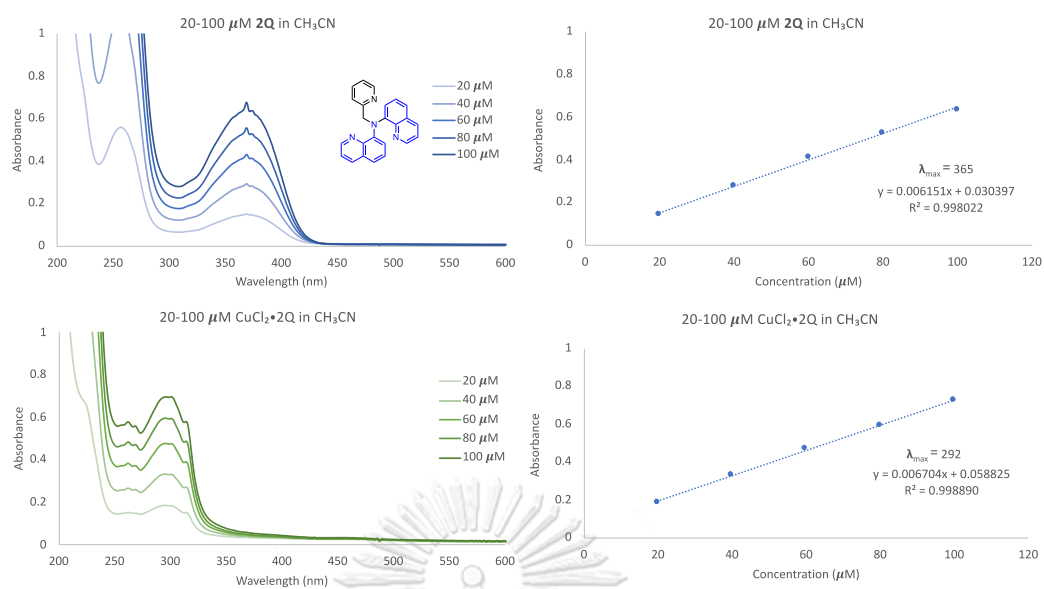


Figure A.37 Absorption spectrum of 2Q and $\text{CuCl}_2 \cdot 2\text{Q}$.

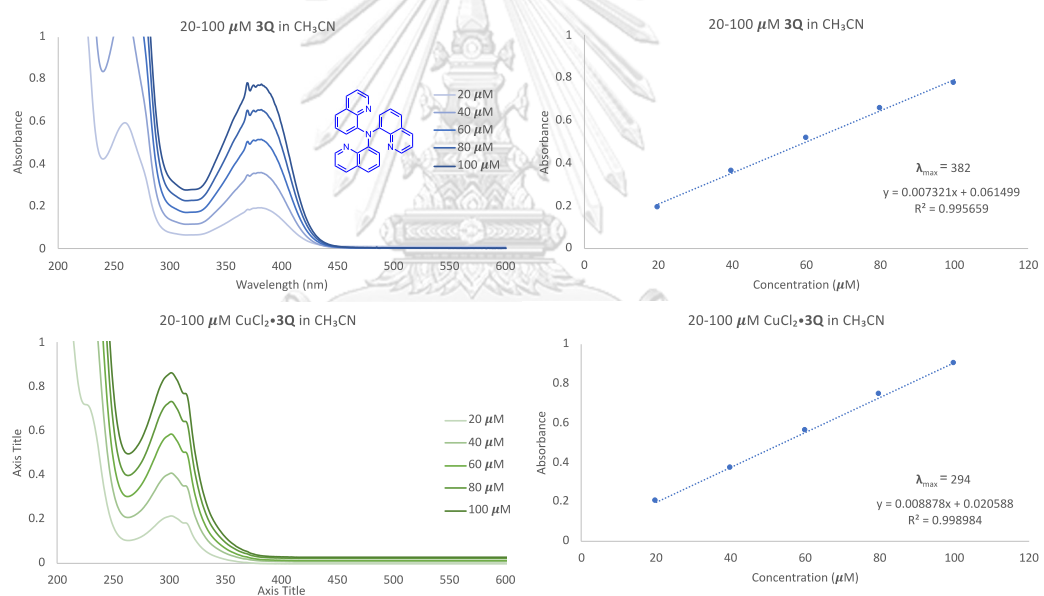
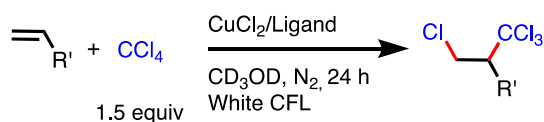


Figure A.38 Absorption spectrum of 3Q and $\text{CuCl}_2 \cdot 3\text{Q}$.

A.2 Study of catalytic properties for haloalkylation (C-C formation)

Table A.2 Conversions, yields and turn over numbers obtained from addition reaction of CCl_4 to various alkenes catalyzed by Cu(II) complexes of various ligands



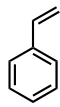
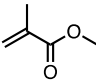
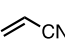
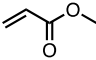
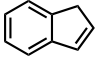
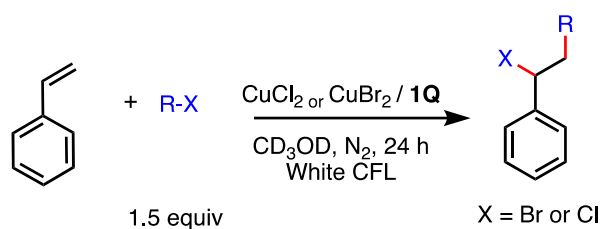
Alkene	[M]	Mol% cat.	1Q		2Q		3Q		TPMA	
			%Con.	%Yield (TON)	%Con.	%Yield	%Con.	%Yield	%Con.	%Yield (TON)
	1.0	1.0	100	100 (100)	100	100	65	65	71	71 (100)
	3.0	0.3	94	89 (267)					19	13 (39)
	3.0	0.1	27	17 (170)						
	4.8	0.1	37	16 (160)					7	4 (40)
	1.0	1.0	95	95	99	99	54	53	73	73
	3.0	0.3	99	95 (285)						
	1.0	1.0	89	88	71	66	17	14	66	64
	3.0	0.3	86	83 (249)						
	1.0	1.0	90	88	68	64	0	0	64	63
	3.0	0.3	90	80 (240)						
	1.0	1.0	96	91					98	96

Table A.3 Substrate conversions and product yields for reactions of styrene with various alkyl halides in methanol with and without AIBN.

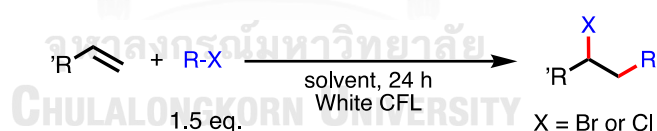


Alkyl halide (equiv)	With AIBN (5 mol %)		Without AIBN	
	%Con	% Yield	%Con	% Yield
CBr ₄	100	98	100	99
CBrCl ₃	100	100	100	100
CCL ₃ COOMe	100	100	100	100
CCL ₃ CN	100	94	100	90
CHCl ₃ ^a	100	100	54	53
CHBr ₃ ^a	75	74	51	49

^aThe reactions were performed under white CFL at ambient temperature for 24h.

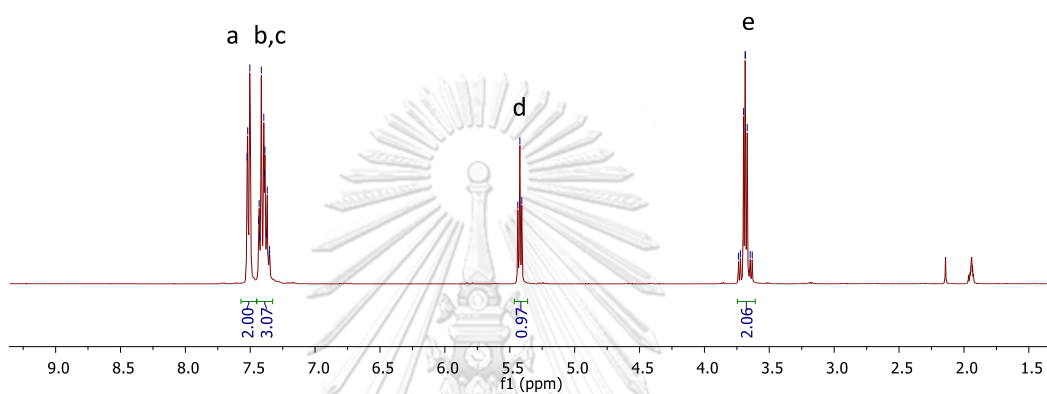
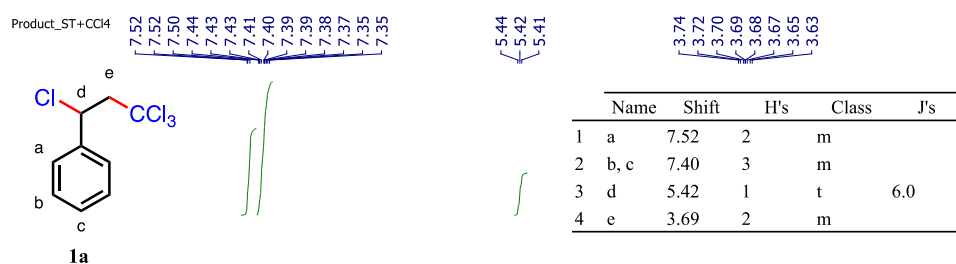
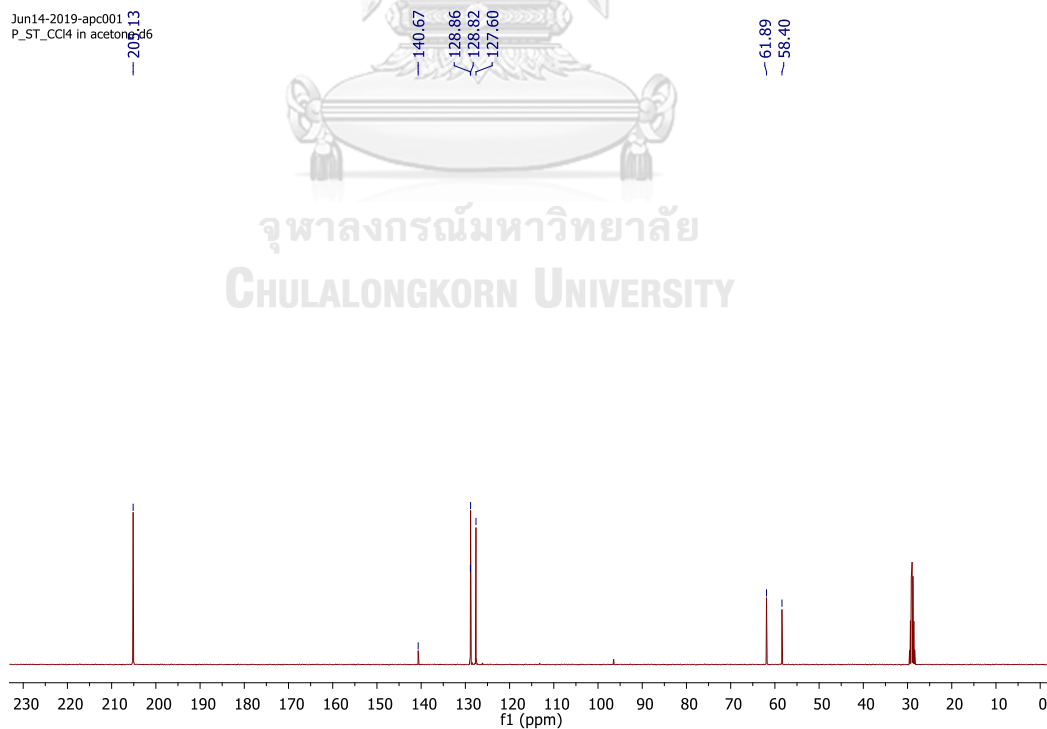
^a3.0 equivalent of alkyl halide was used.

Table A.4 Comparison of alkyl chloride with alkyl bromide in the addition reaction to alkenes in the absence of photocatalyst under white light.



Entry	Alkene	R-X	Solvent	%Con	%Yield
1	Styrene	CBr ₄	CD ₃ OD	68	58
2	1 <i>H</i> -Indene	CBr ₄	<i>i</i> -PrOH	100	90
3	Methyl methacrylate	CBr ₄	CD ₃ OD	70	0
4	Styrene	CCL ₄	CD ₃ OD		N.R.
5	1 <i>H</i> -Indene	CCL ₄	CH ₃ OH		N.R.
6	1 <i>H</i> -Indene	CCL ₃ COOMe	CH ₃ OH		N.R.
7	1 <i>H</i> -Indene	CCL ₃ CN	CH ₃ OH		N.R.

^aThe reactions were performed under white CFL at ambient temperature for 24h.

A.2.1 ^1H NMR and ^{13}C spectra of ProductsFigure A.39 ^1H NMR spectrum of (1,3,3,3-tetrachloropropyl)benzene, **1a**.Figure A.40 ^{13}C NMR spectrum of (1,3,3,3-tetrachloropropyl)benzene, **1a**.

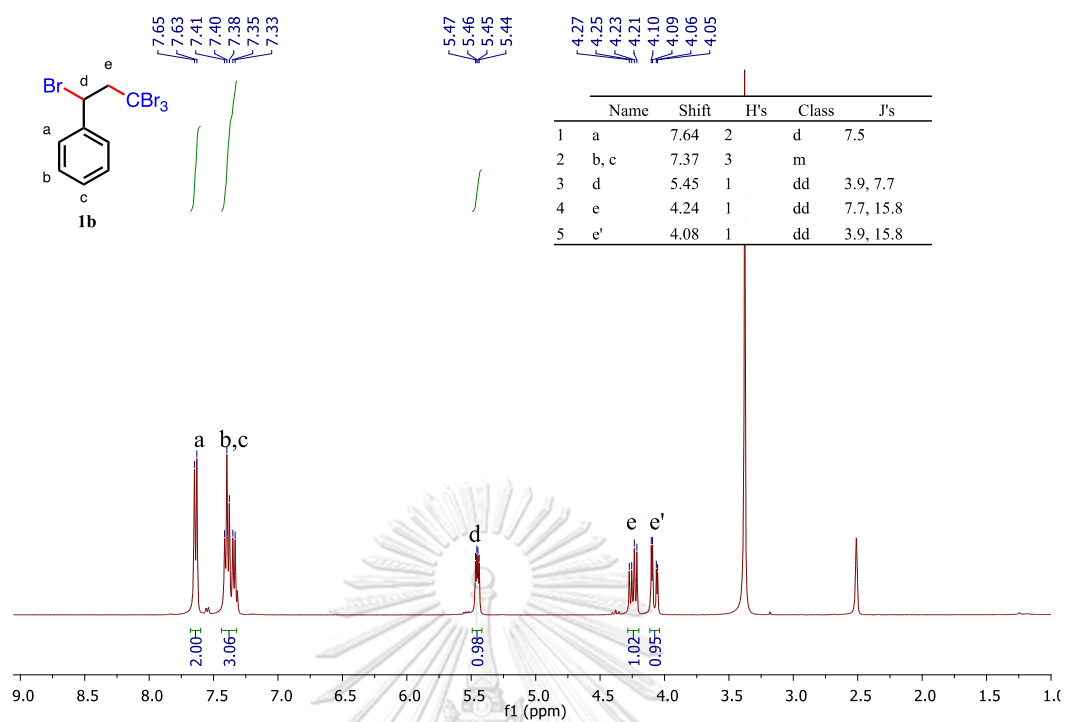


Figure A.41 ^1H NMR spectrum of (1,3,3,3-tetrabromopropyl)benzene, **1b**.

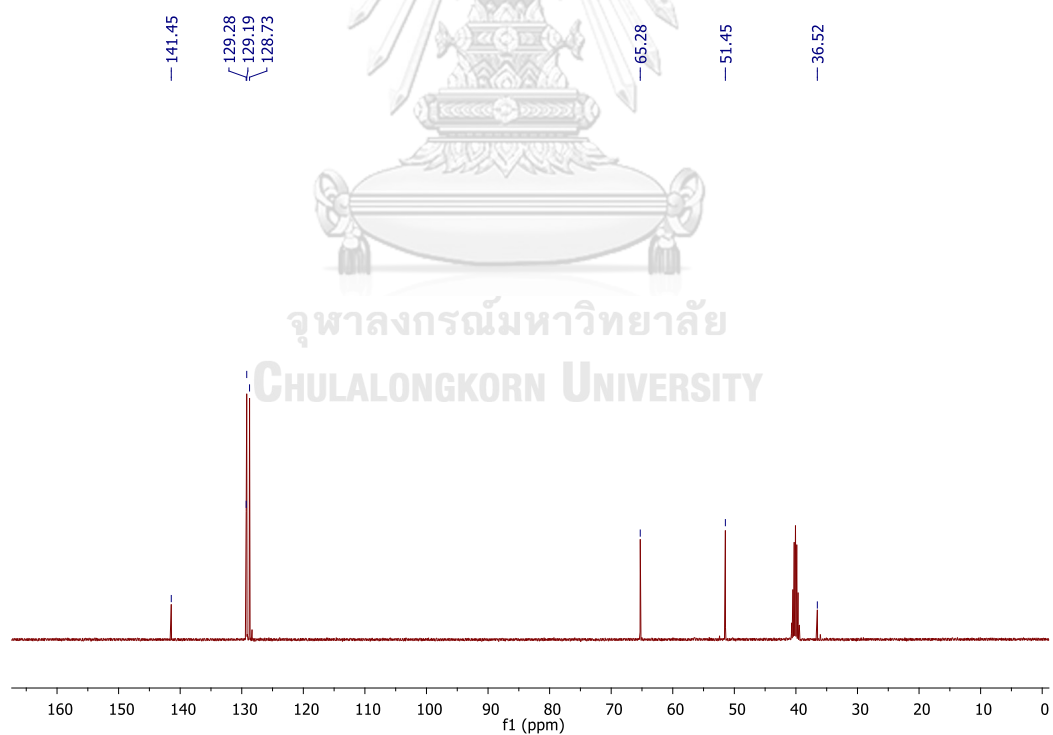


Figure A.42 ^{13}C NMR spectrum of (1,3,3,3-tetrabromopropyl)benzene, **1b**.

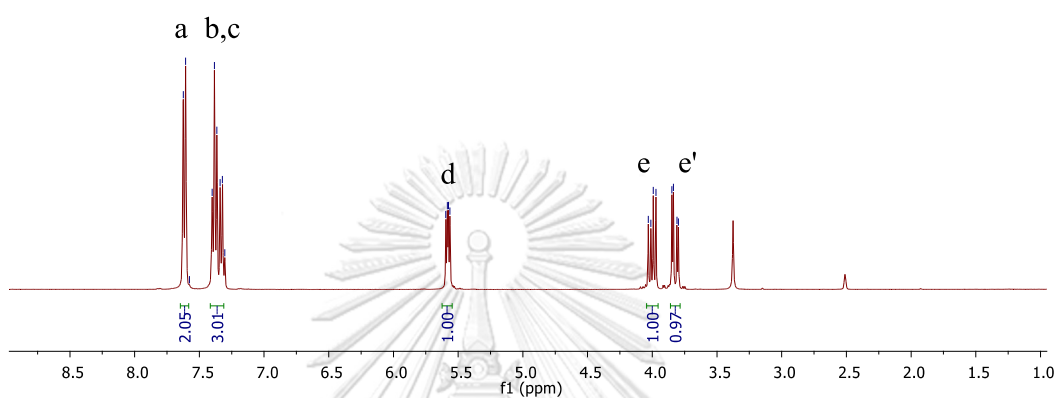
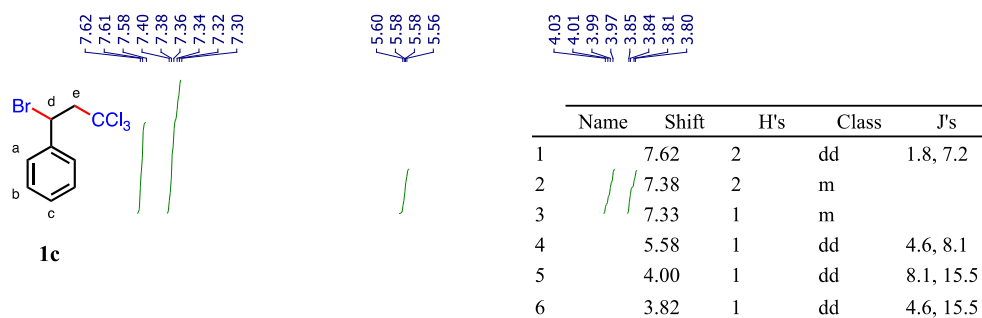


Figure A.43 ^1H NMR spectrum of (1-bromo-3,3,3-trichloropropyl)benzene, **1c**.

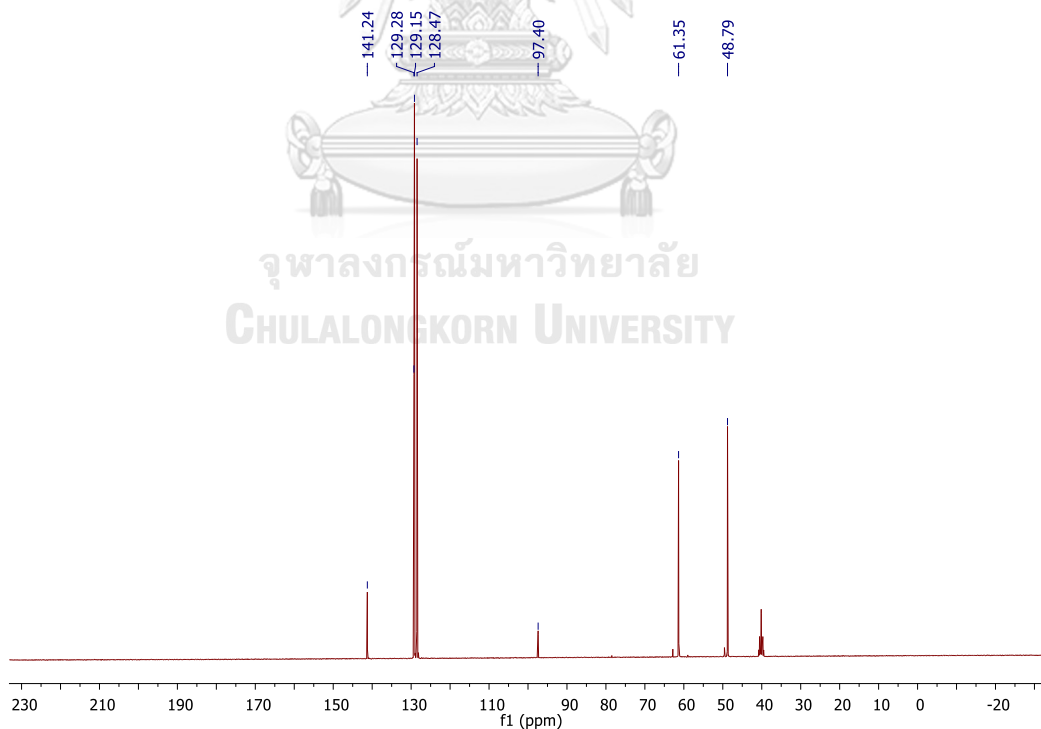


Figure A.44 ^{13}C NMR spectrum of (1-bromo-3,3,3-trichloropropyl)benzene, **1c**.

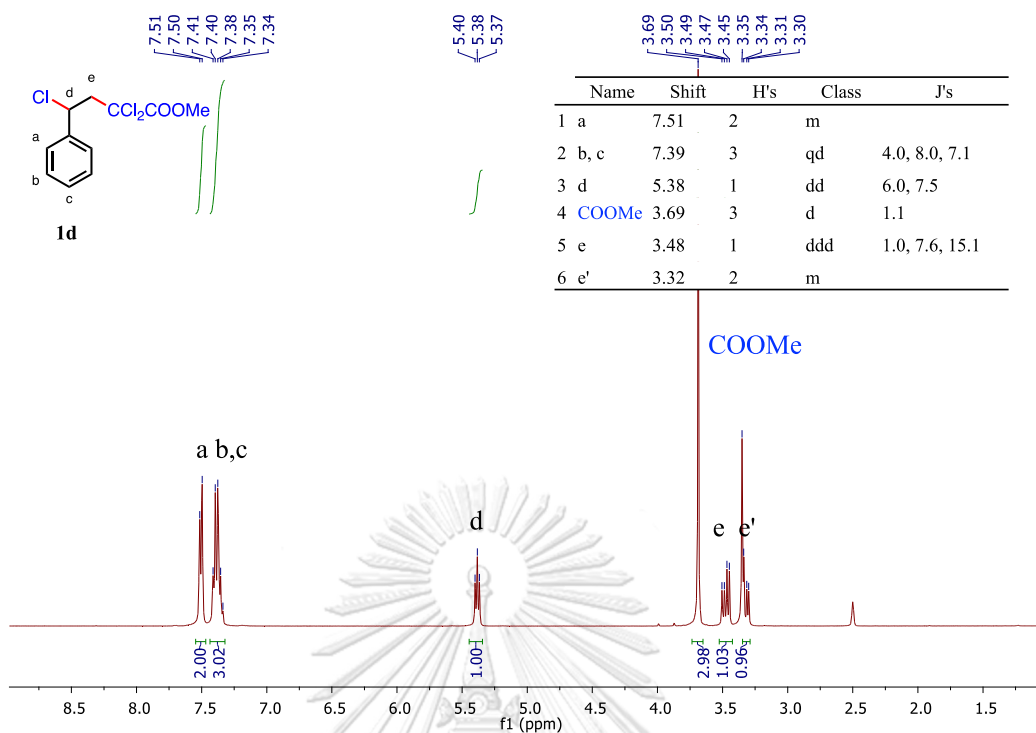


Figure A.45 ^1H NMR spectrum of methyl 2,2,4-trichloro-4-phenylbutanoate, **1d**.

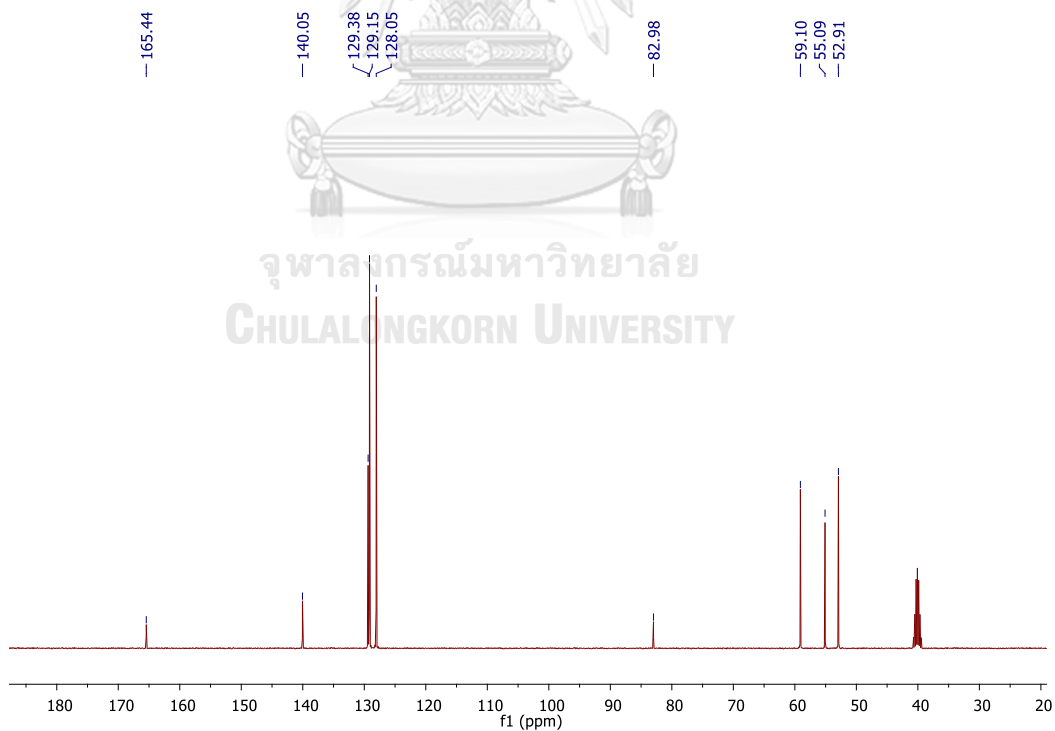


Figure A.46 ^{13}C NMR spectrum of methyl 2,2,4-trichloro-4-phenylbutanoate, **1d**.

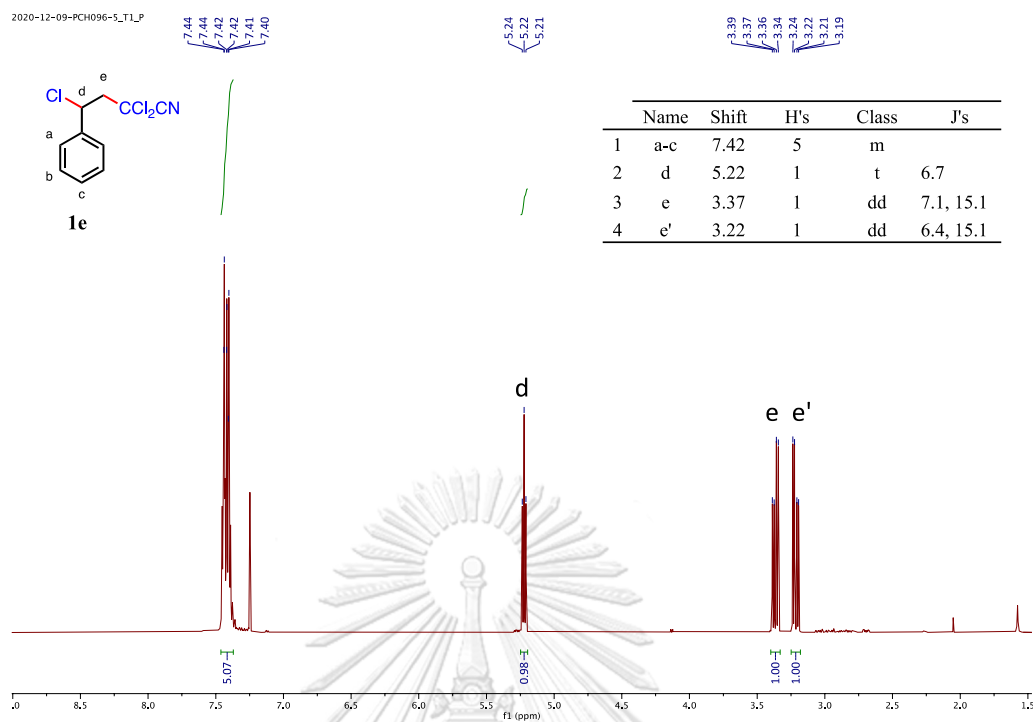


Figure A.47 ^1H NMR spectrum of 2,2-dichloro-2-(1-chloro-2,3-dihydro-1H-inden-2-yl)acetonitrile, **1e**.

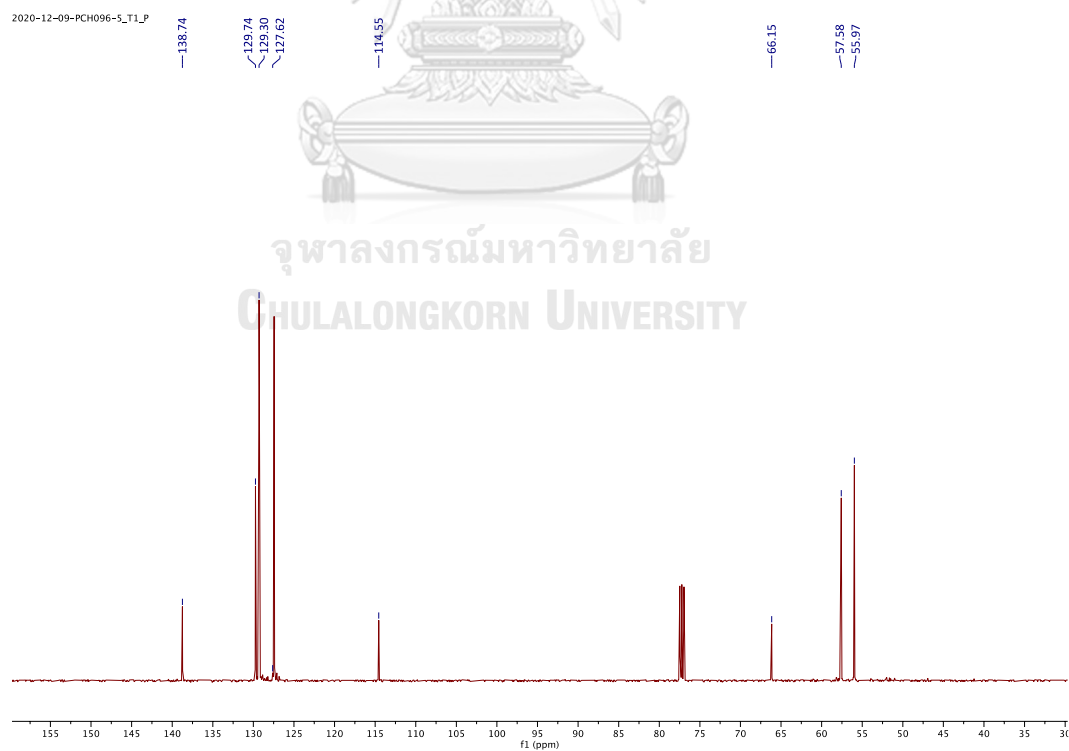


Figure A.48 ^{13}C NMR spectrum of 2,2-dichloro-2-(1-chloro-2,3-dihydro-1H-inden-2-yl)acetonitrile, **1e**.

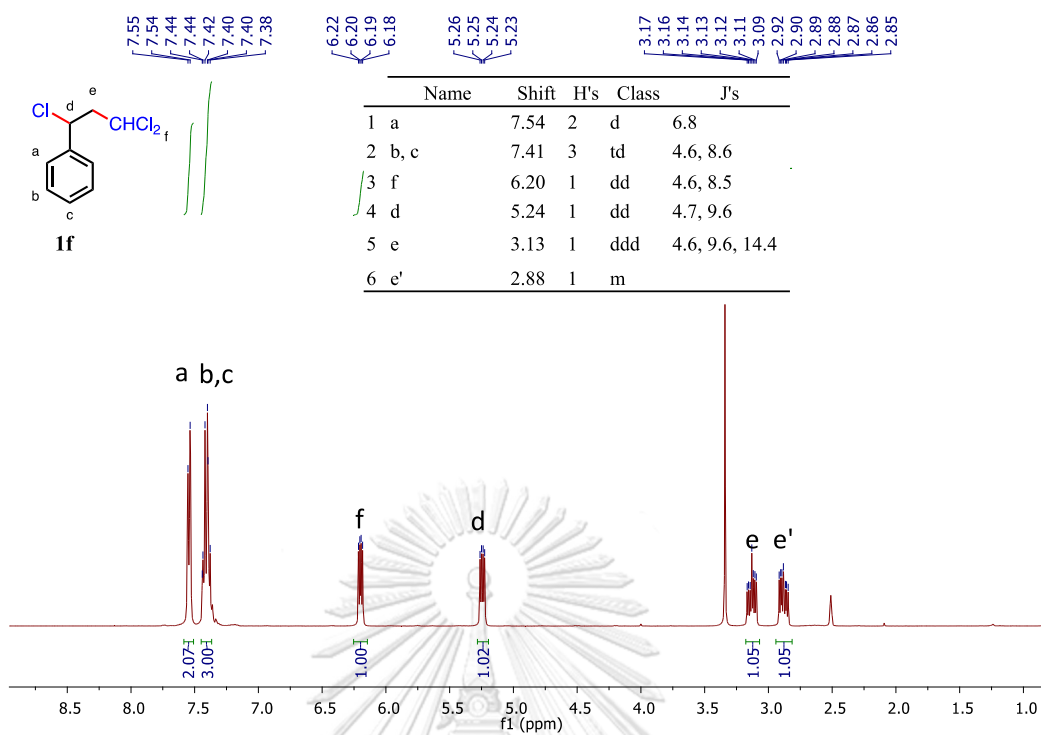


Figure A.49 ^1H NMR spectrum of (1,3,3-trichloropropyl)benzene, **1f**.

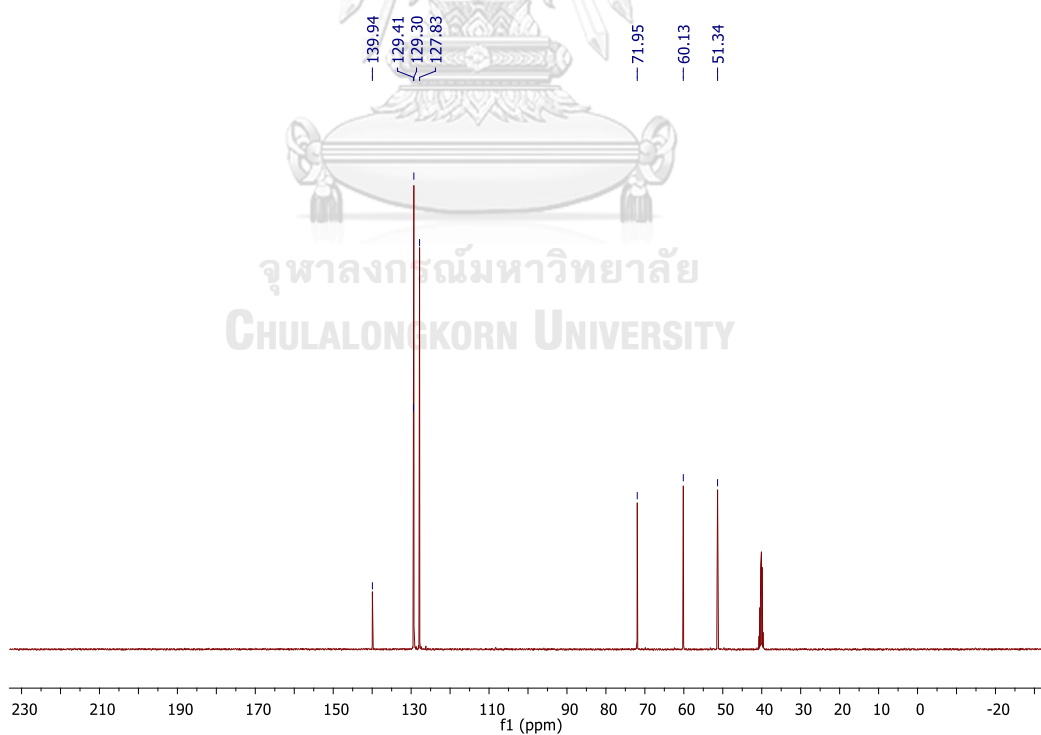


Figure A.50 ^{13}C NMR spectrum of (1,3,3-trichloropropyl)benzene, **1f**.

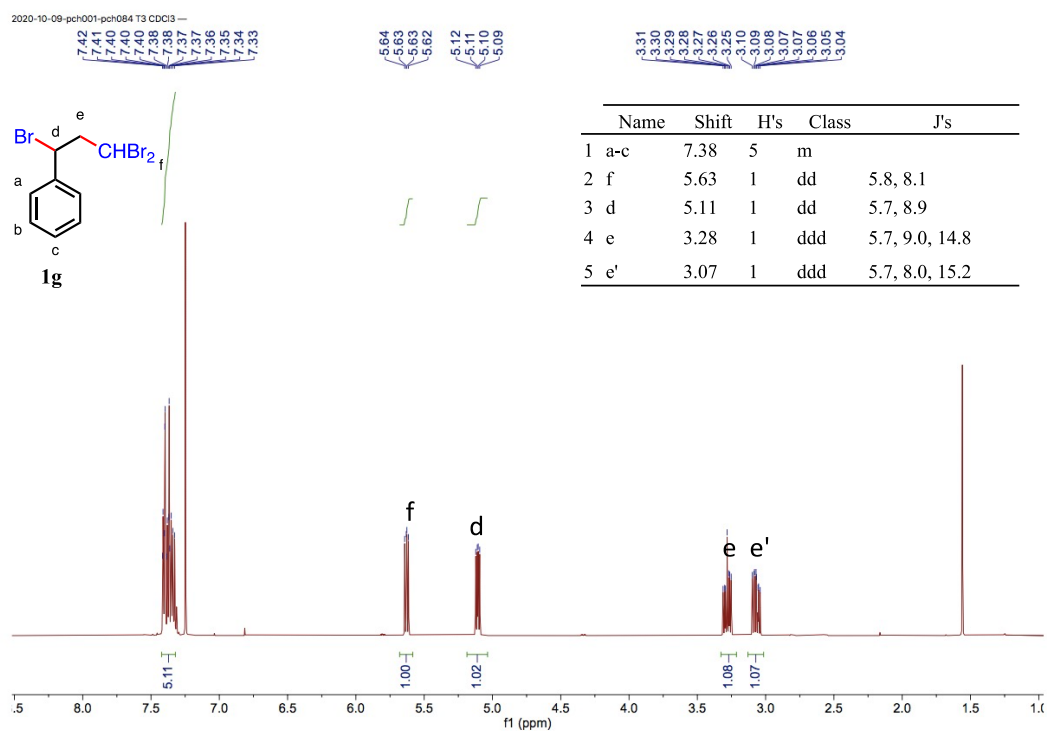


Figure A.51 ^1H NMR spectrum of (1,3,3-tribromopropyl)benzene, **1g**.

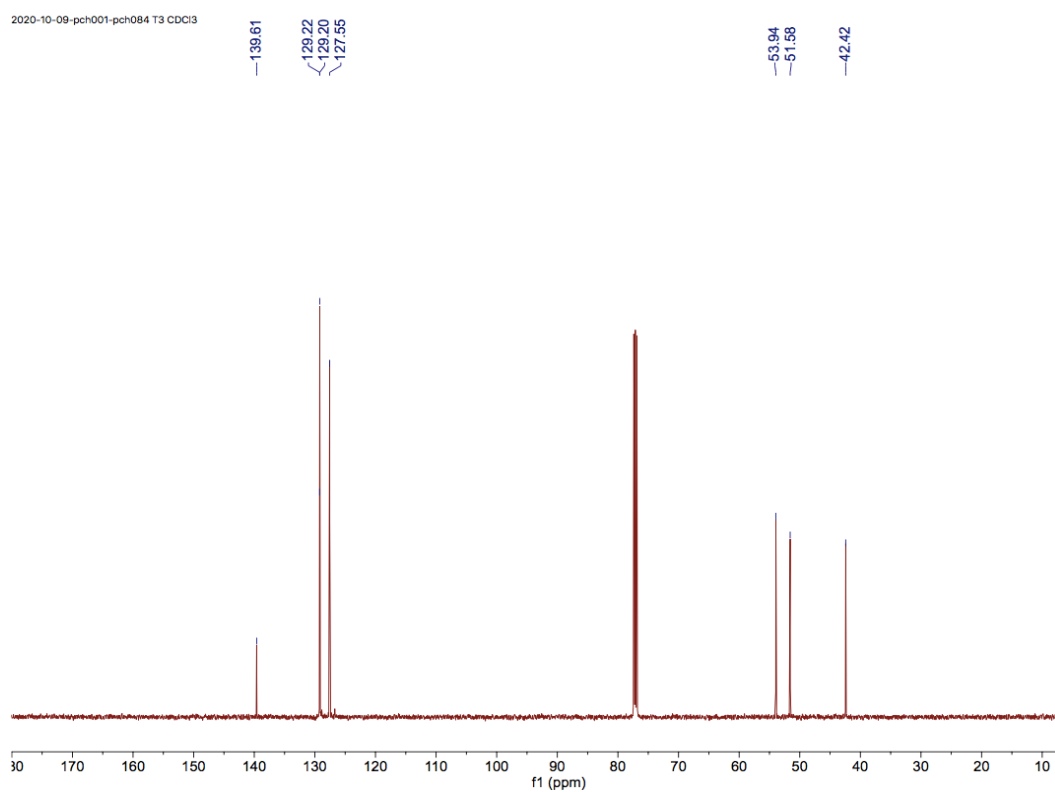


Figure A.52 ^{13}C NMR spectrum of (1,3,3-tribromopropyl)benzene, **1g**.

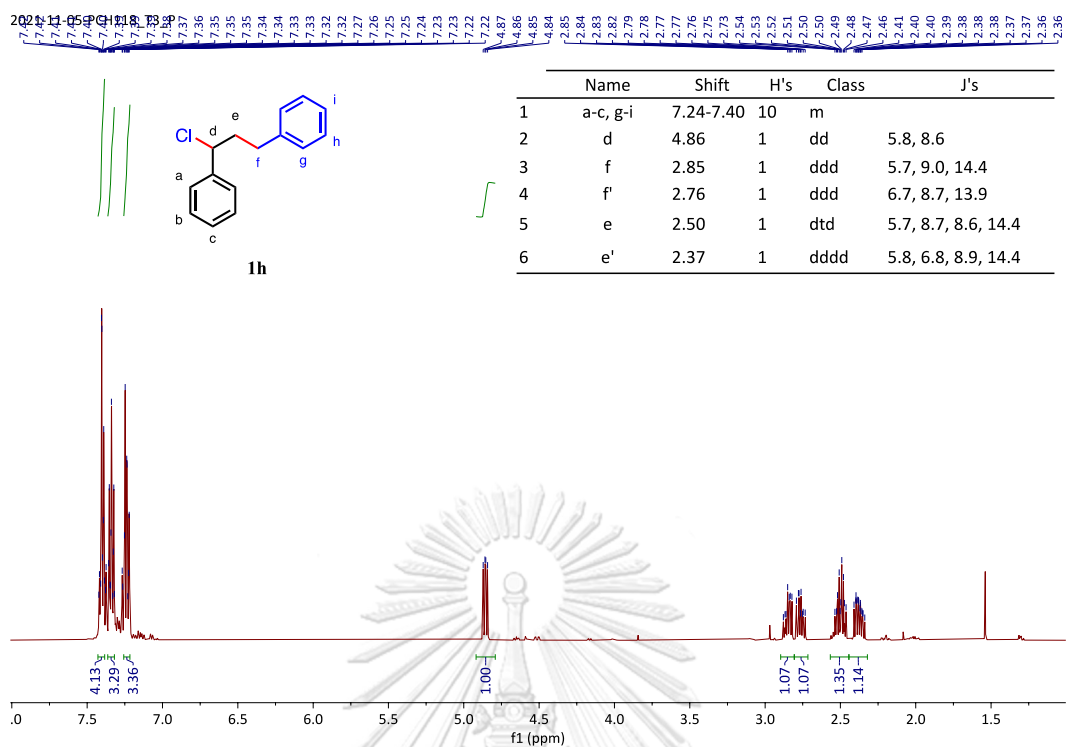


Figure A.53 ^1H NMR spectrum of 1-Chloro-1,3-diphenylpropane, **1h**.

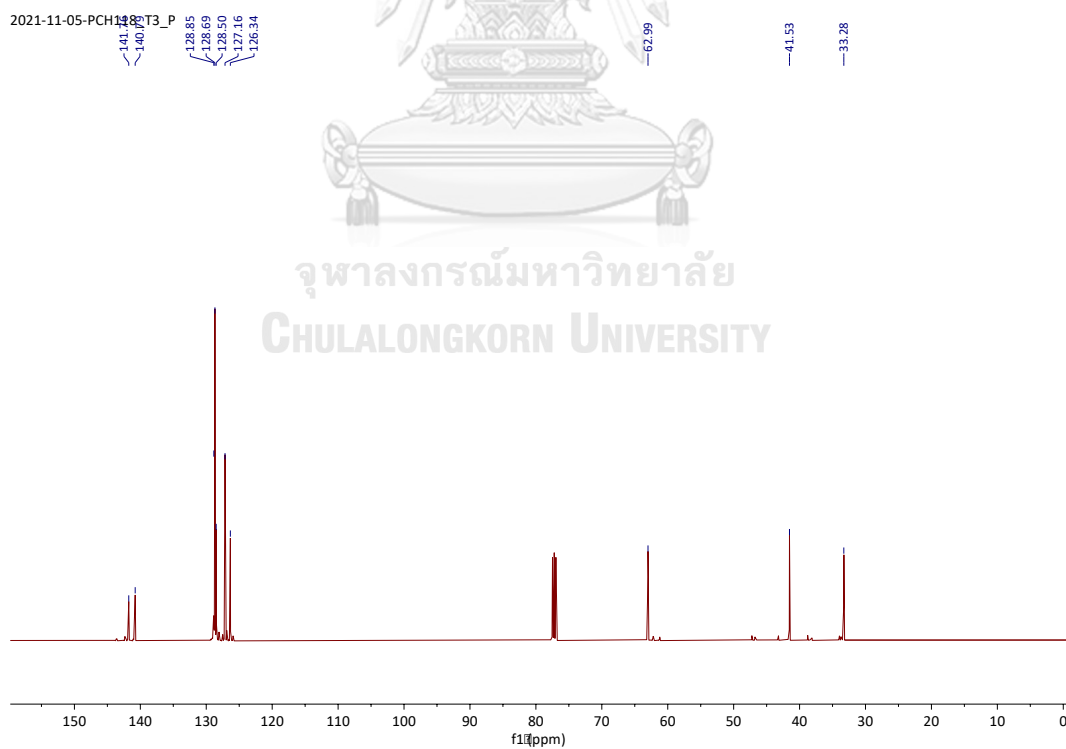
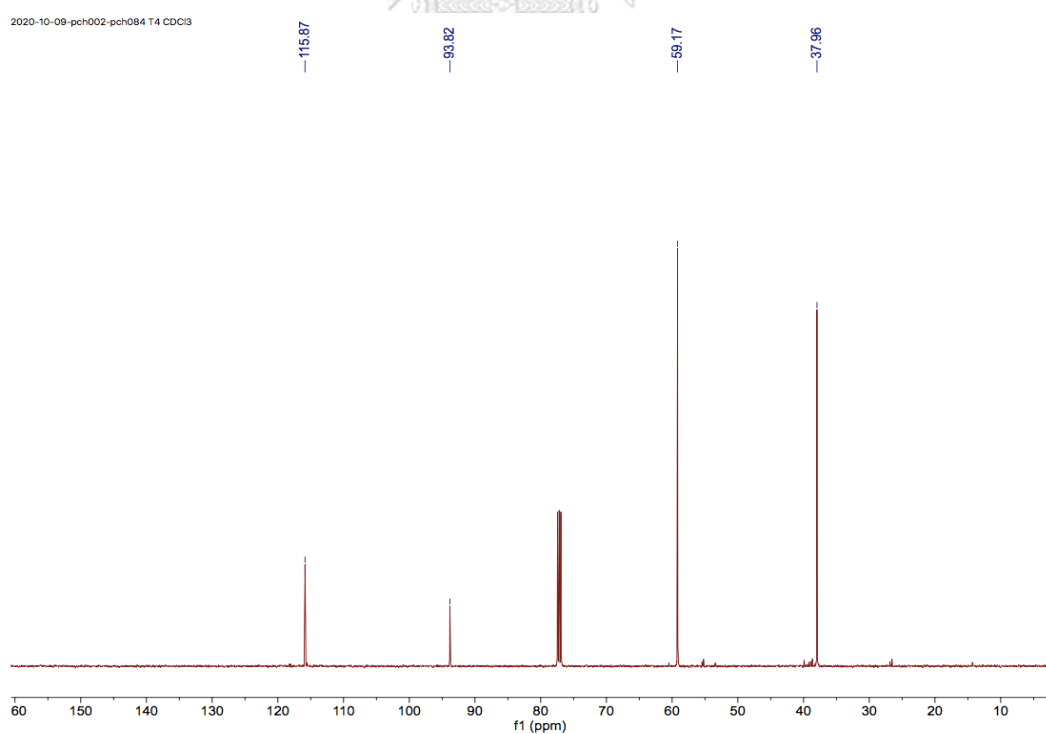
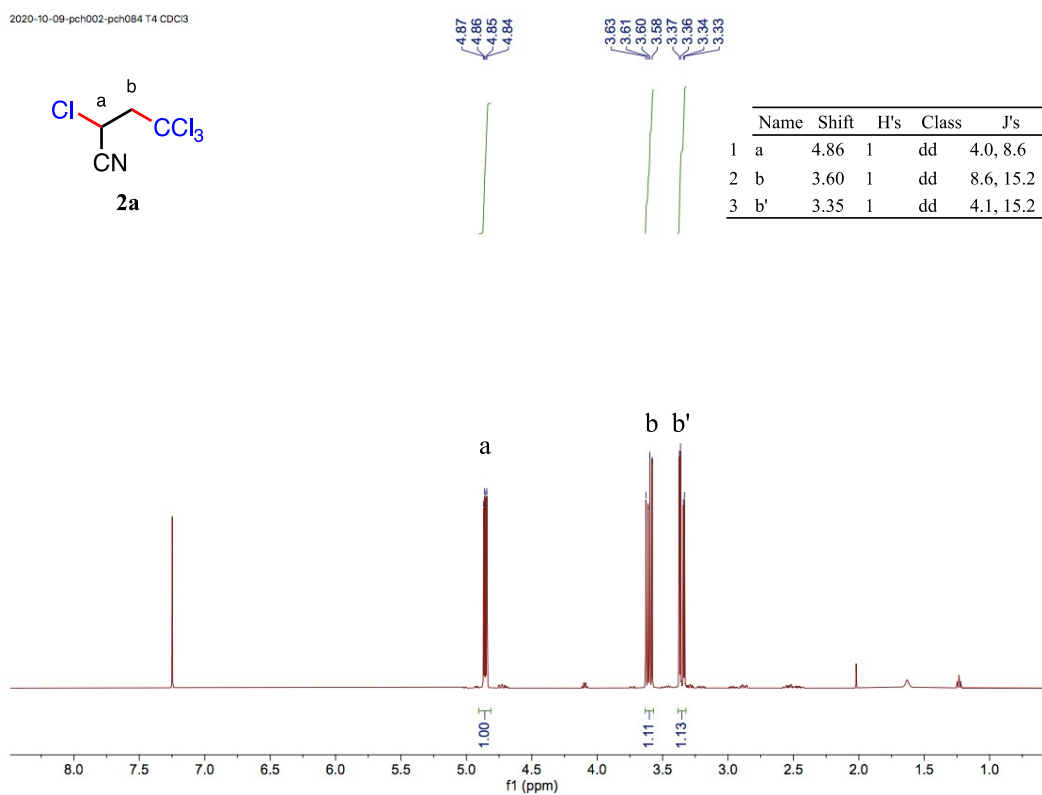
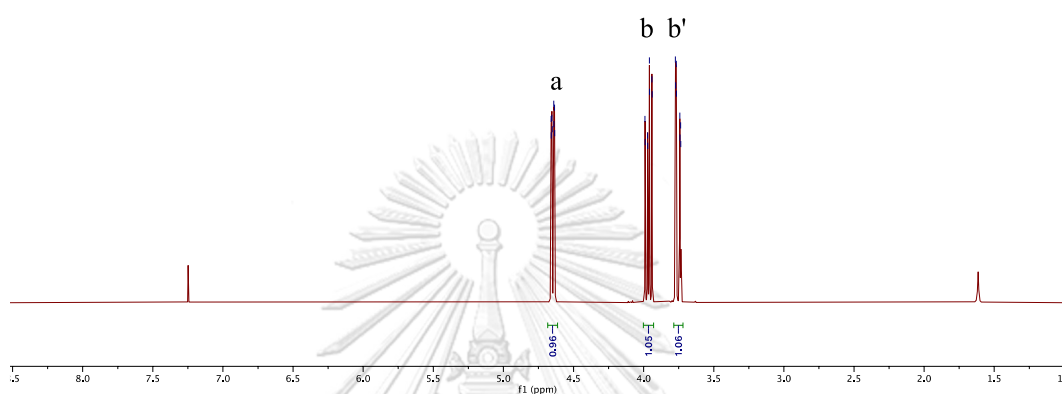
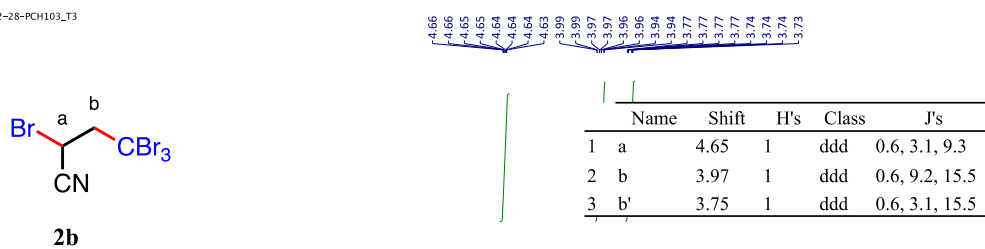


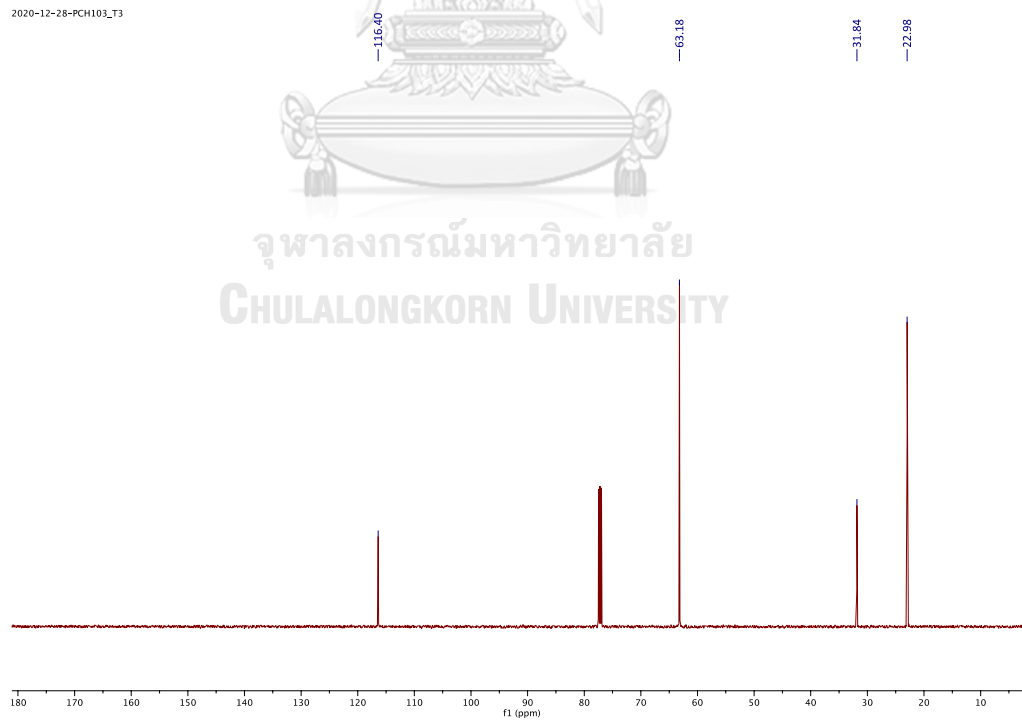
Figure A.54 ^{13}C NMR spectrum of 1-Chloro-1,3-diphenylpropane, **1h**.



2020-12-28-PCH103_T3

Figure A.57 ^1H NMR spectrum of 2,4,4,4-tetrabromobutanenitrile, **2b**.

2020-12-28-PCH103_T3

Figure A.58 ^{13}C NMR spectrum of 2,4,4,4-tetrabromobutanenitrile, **2b**.

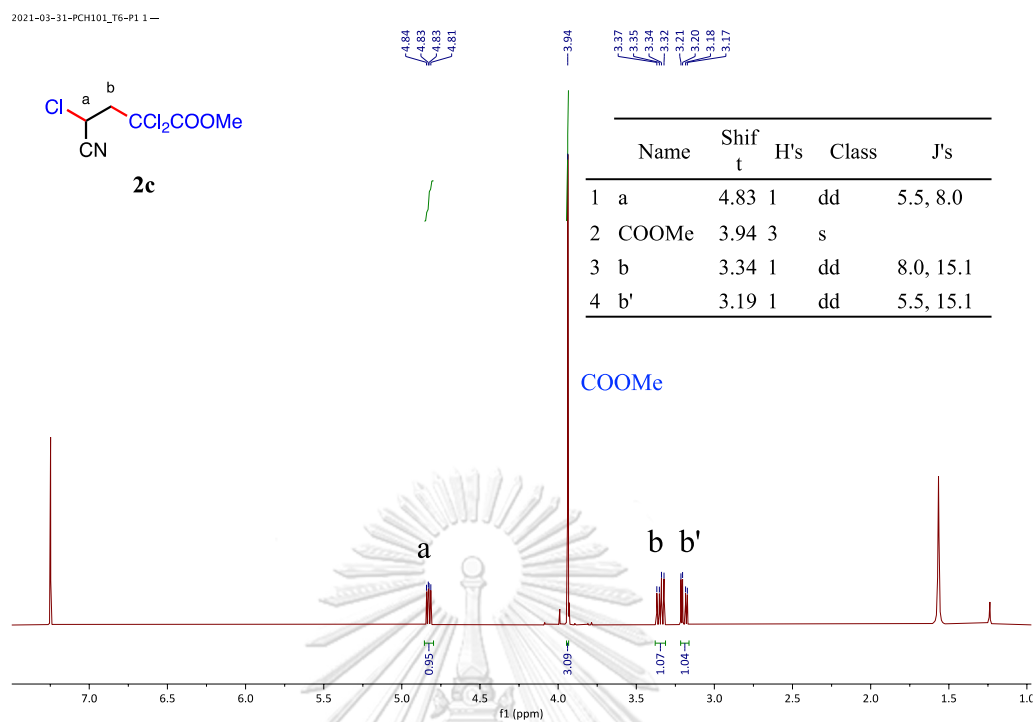


Figure A.59 ^1H NMR spectrum of methyl 2,2,4-trichloro-4-cyanobutanoate, **2c**.

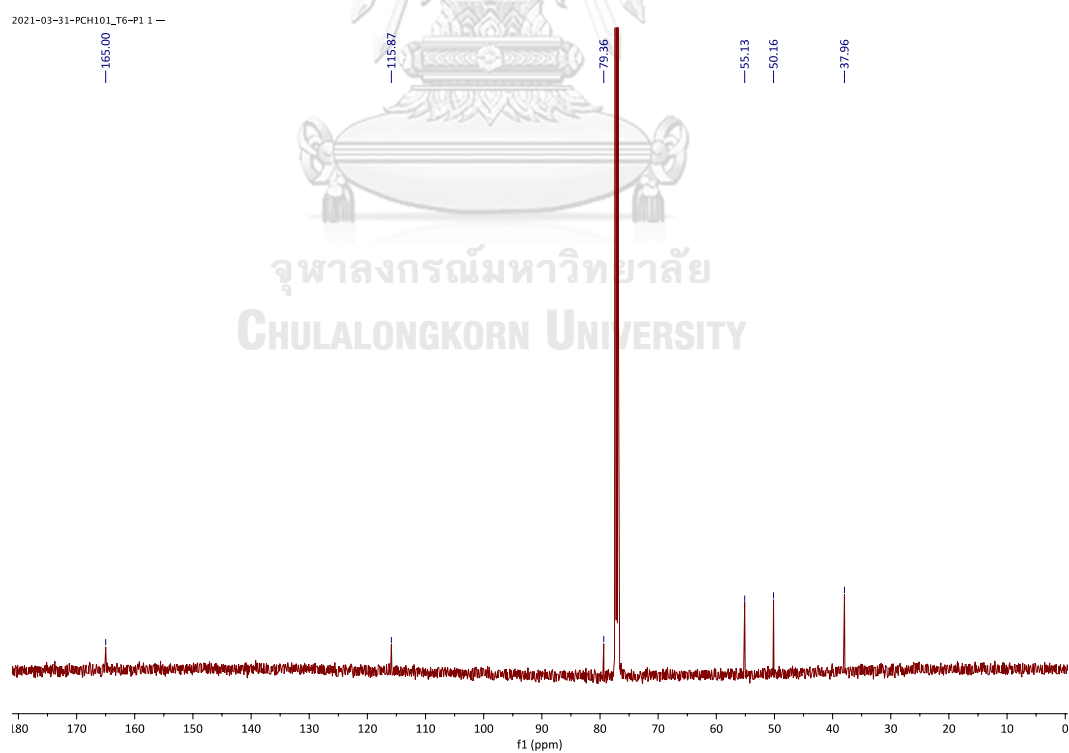
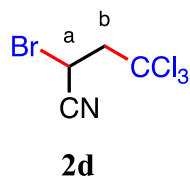
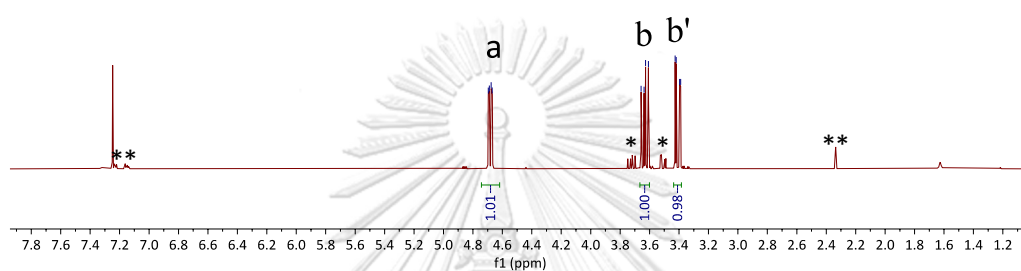


Figure A.60 ^{13}C NMR spectrum of methyl 2,2,4,4-tetrachlorobutanoate, **2c**.

2021-11-05_PCH123_T6_P



Name	Shift	H's	Integral	Class	J's
1	a	4.68	1	1.01	dd 3.5, 9.7
2	b	3.63	1	1.00	dd 9.7, 15.2
3	b'	3.41	1	0.98	dd 3.5, 15.2



*By-product see Figure 3.10. **Toluene was used as an internal standard.

Figure A.61 ^1H NMR spectrum of 2-bromo-4,4,4-trichlorobutanenitrile, **2da**.

2021-11-05_PCH123_T6_P

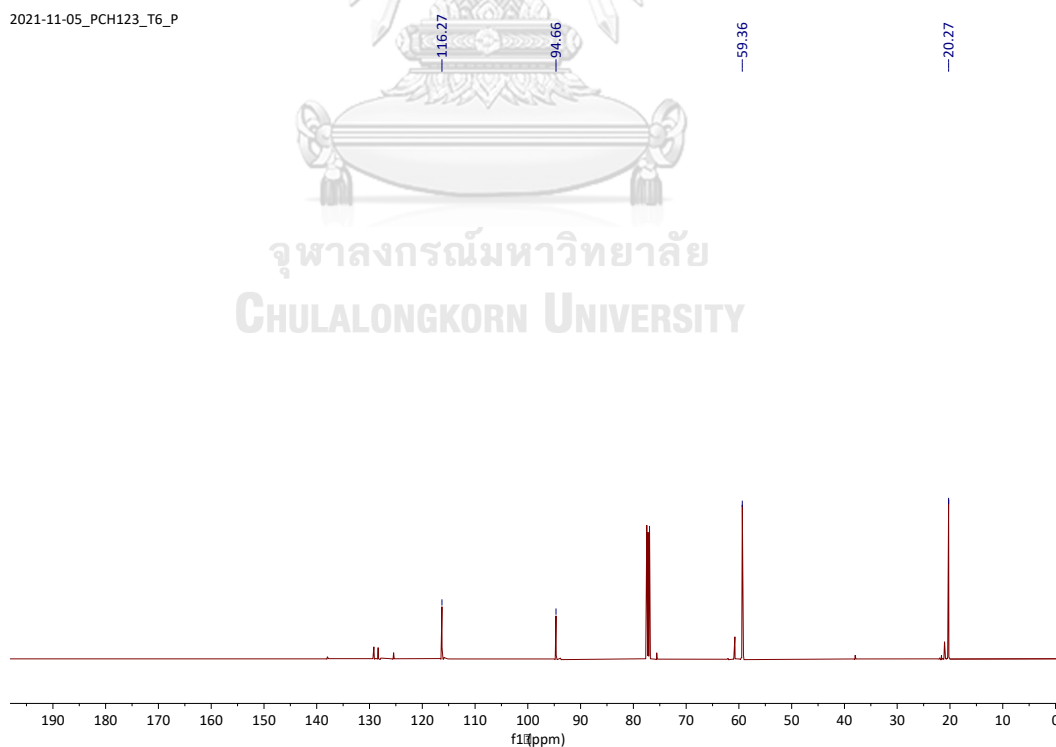


Figure A.62 ^{13}C NMR spectrum of 2-bromo-4,4,4-trichlorobutanenitrile, **2da**.

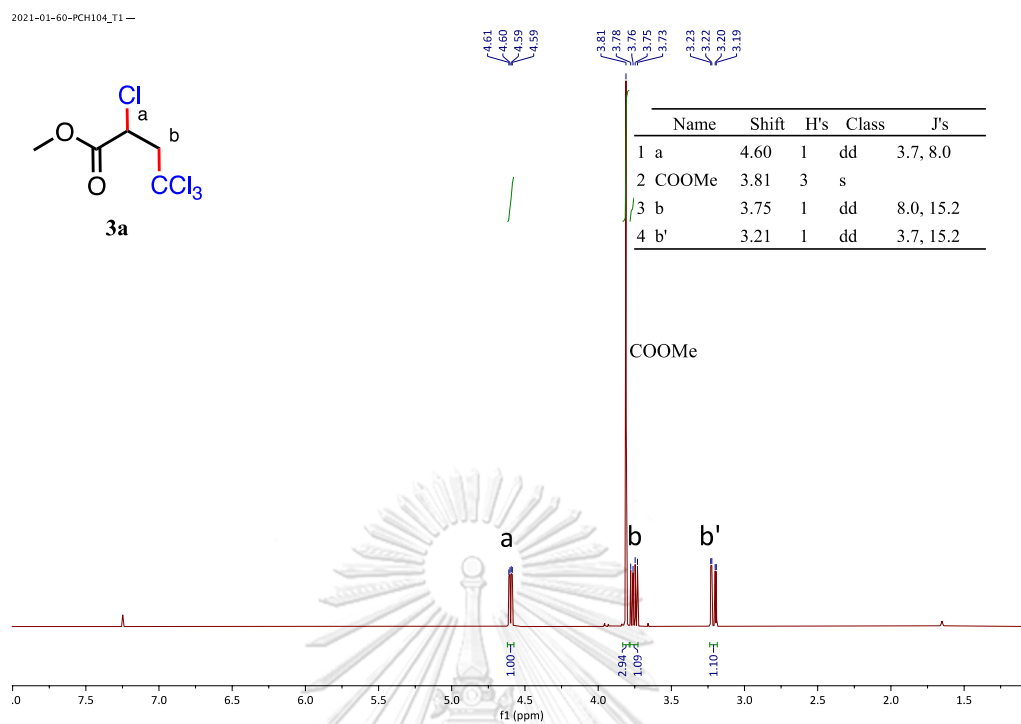


Figure A.63 ^1H NMR spectrum of methyl 2,4,4,4-tetrachlorobutanoate, **3a**.

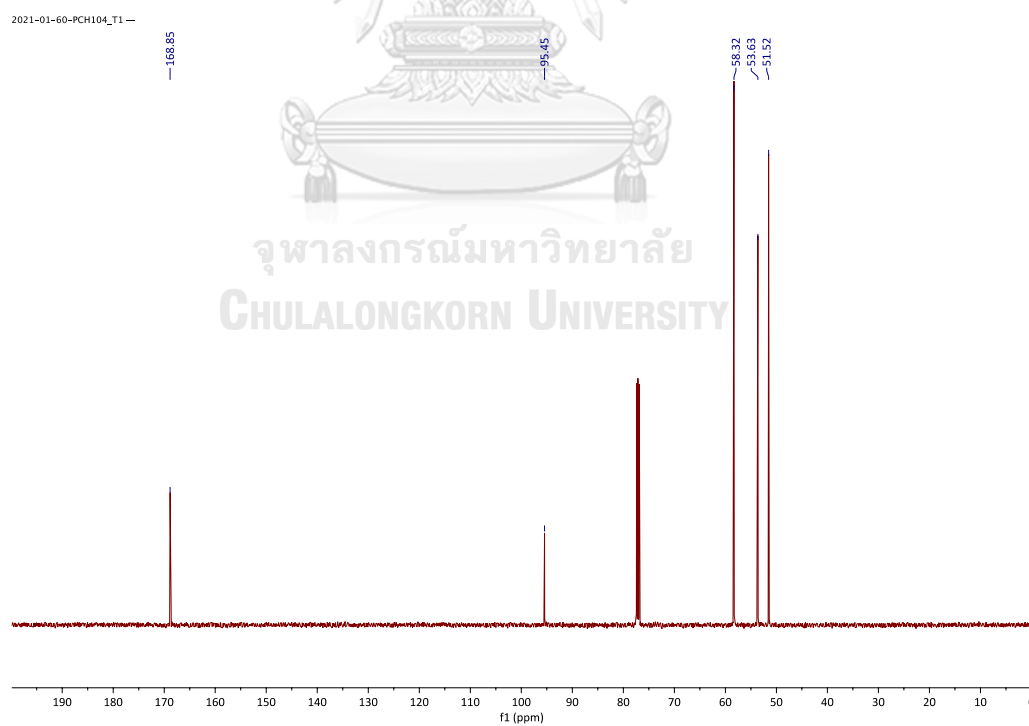


Figure A.64 ^{13}C NMR spectrum of methyl 2,4,4,4-tetrachlorobutanoate, **3a**.

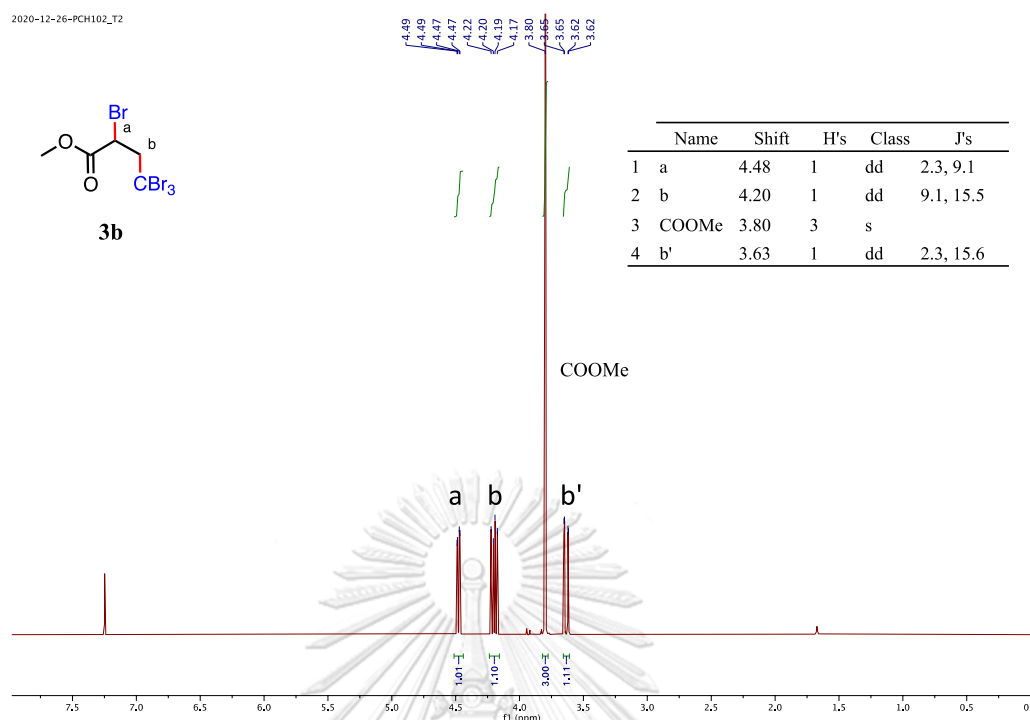


Figure A.65 ^1H NMR spectrum of methyl 2,4,4,4-tetrabromobutanoate, **3b**.

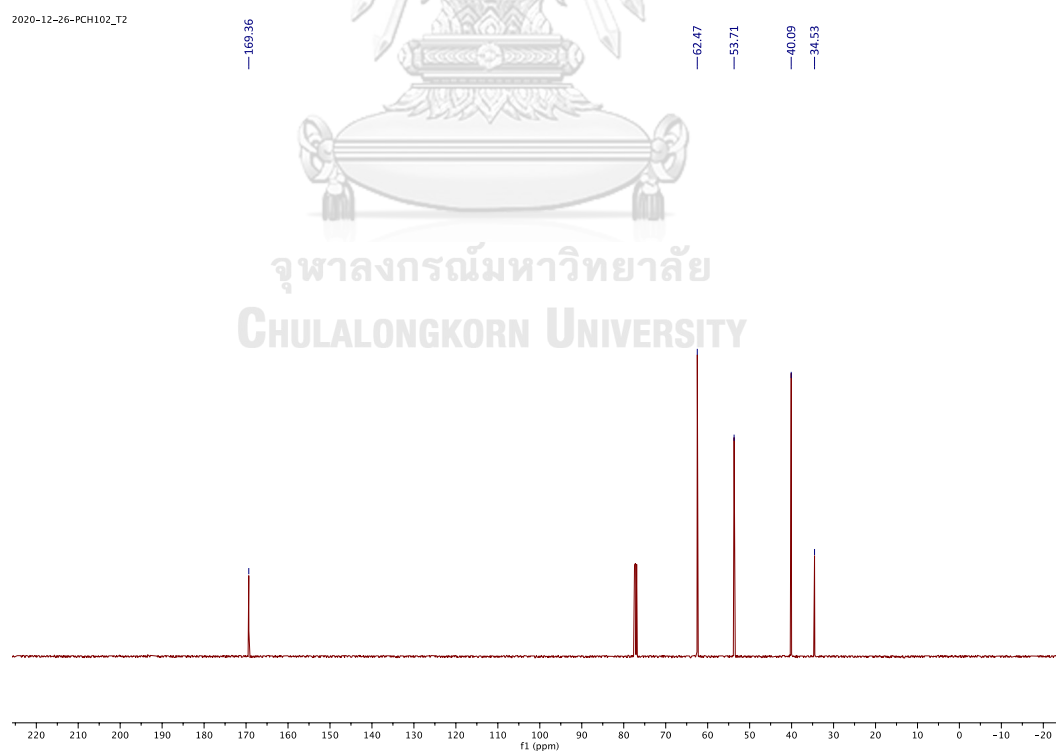


Figure A.66 ^{13}C NMR spectrum of methyl 2,4,4,4-tetrabromobutanoate, **3b**.

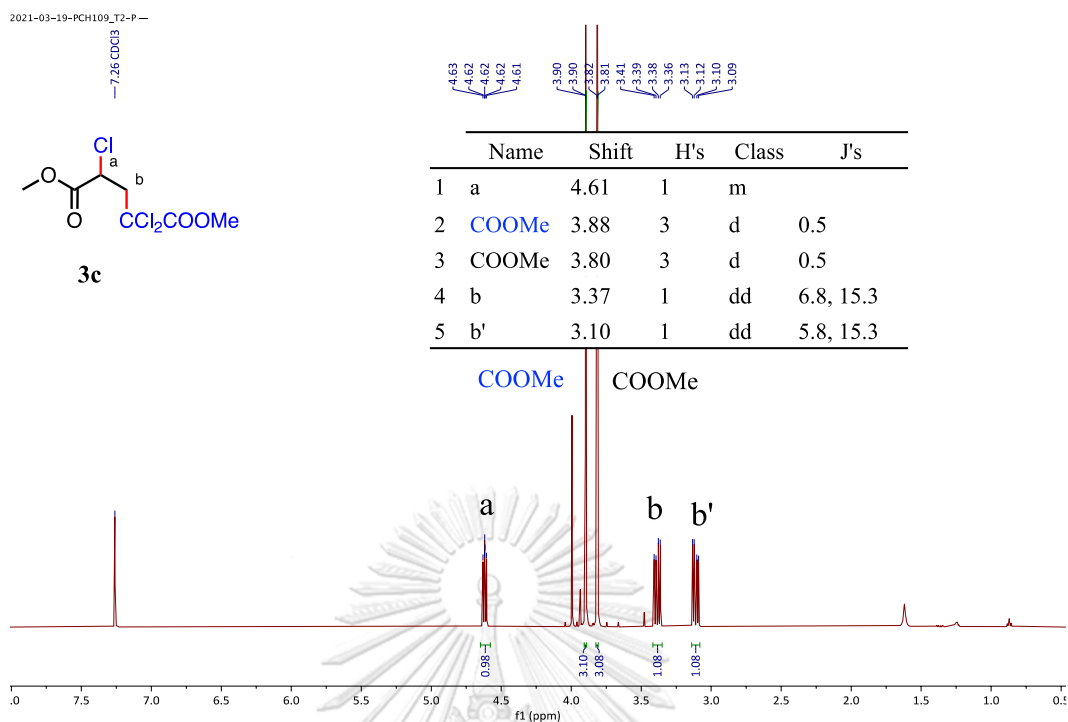


Figure A.67 ¹H NMR spectrum of dimethyl 2,2,4-trichloropentanedioate, **3c**.

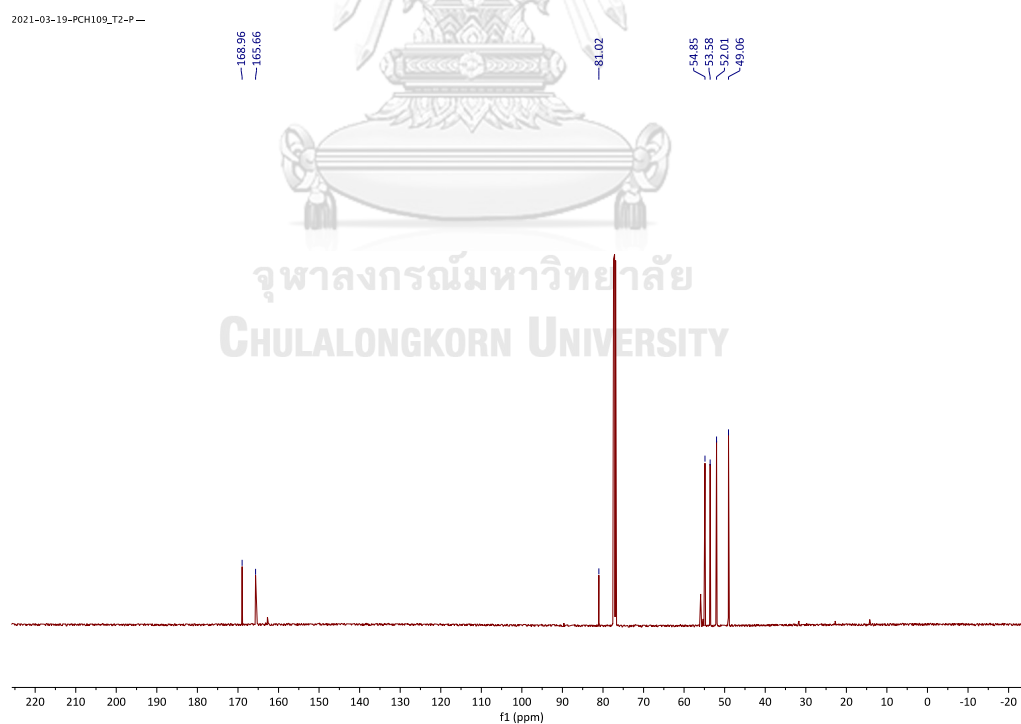
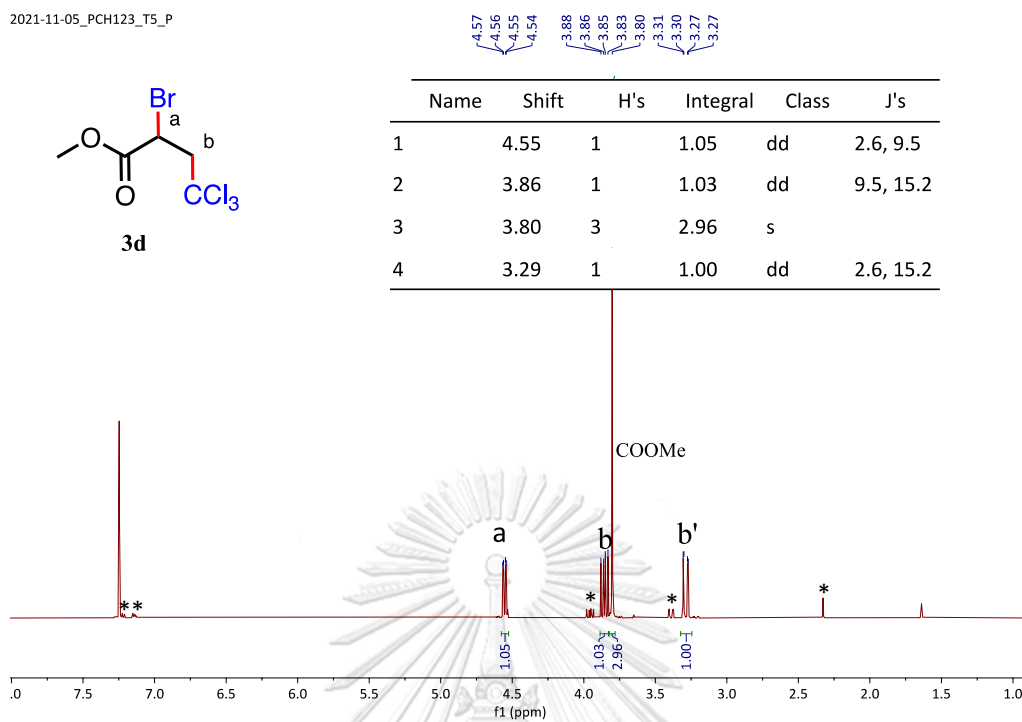


Figure A.68 ¹³C NMR spectrum of dimethyl 2,2,4-trichloropentanedioate, **3c**.

2021-11-05_PCH123_T5_P



* by-product see Figure 3.11, **toluene was used as an internal standard

Figure A.69 ^1H NMR spectrum of methyl-2-bromo-4,4,4-trichlorobutanoate, **3da**.

2021-11-05_PCH123_T5_P

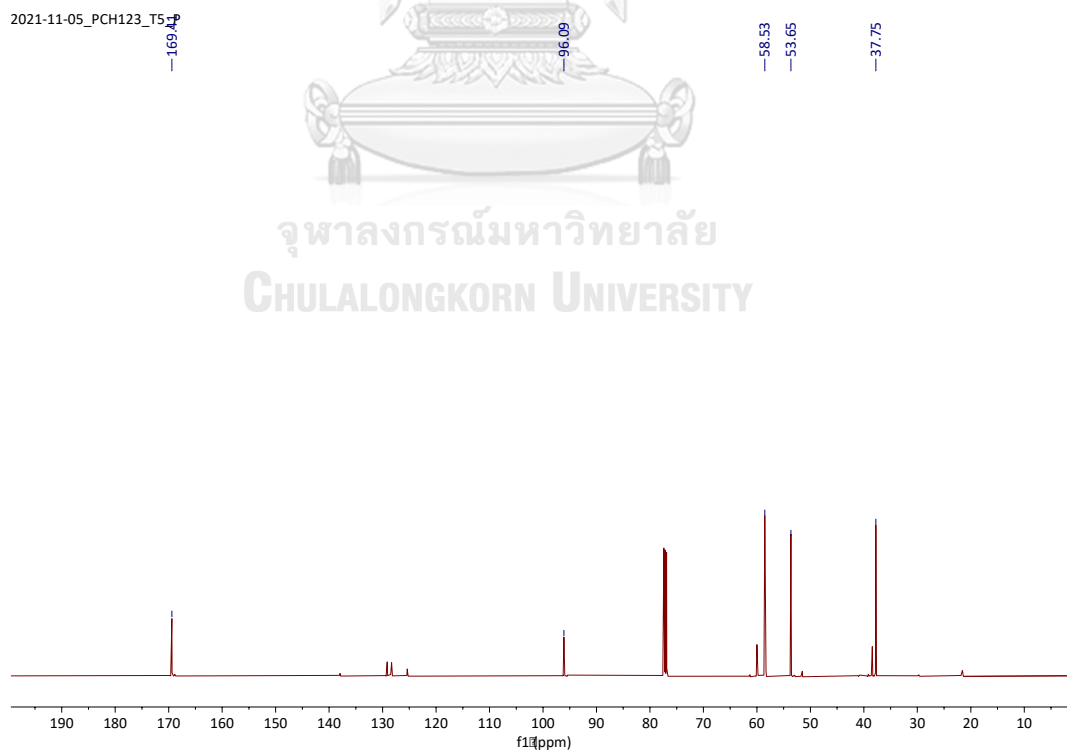
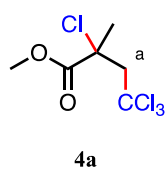


Figure A.70 ^{13}C NMR spectrum of methyl-2-bromo-4,4,4-trichlorobutanoate, **3da**.

2020-12-22-PCH001-MMA-CCl4



Name	Shift	H's	Class	J's
1	3.98	1	d	15.3
2	3.81	3	d	0.7
3	3.45	1	dd	0.6, 15.3
4	2.00	3	s	

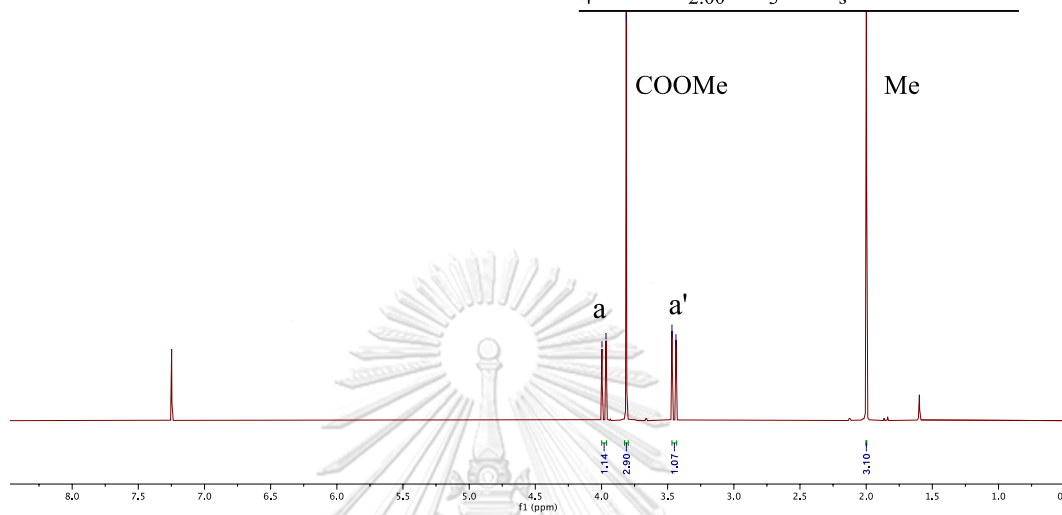


Figure A.71 ^1H NMR spectrum of methyl-2,4,4,4-tetrachloro-2-methylbutanoate, **4a**.

2020-12-22-PCH001-MMA-CCl4

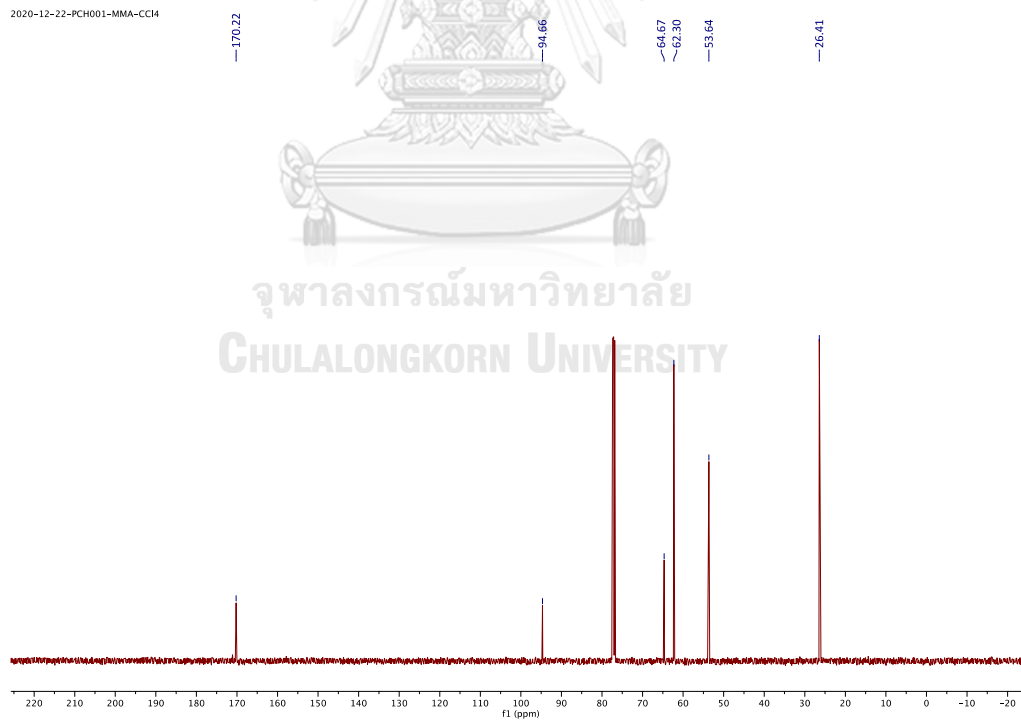


Figure A.72 ^{13}C NMR spectrum of methyl-2,4,4,4-tetrachloro-2-methylbutanoate, **4a**.

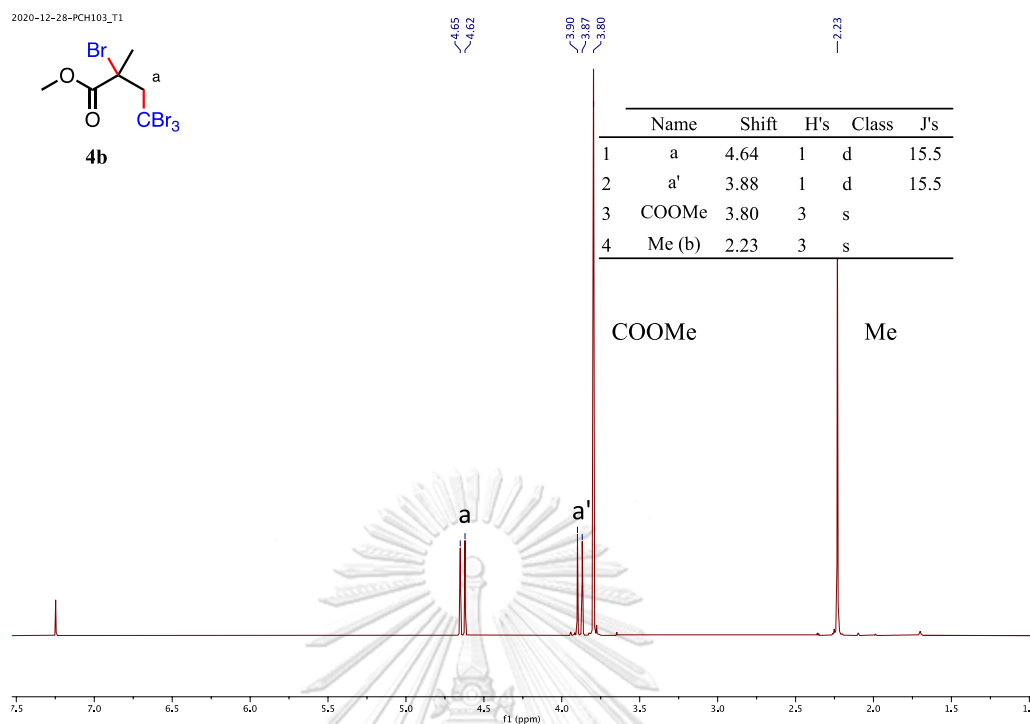


Figure A.73 ^1H NMR spectrum of methyl 2,4,4,4-tetrabromo-2-methylbutanoate, **4b**.

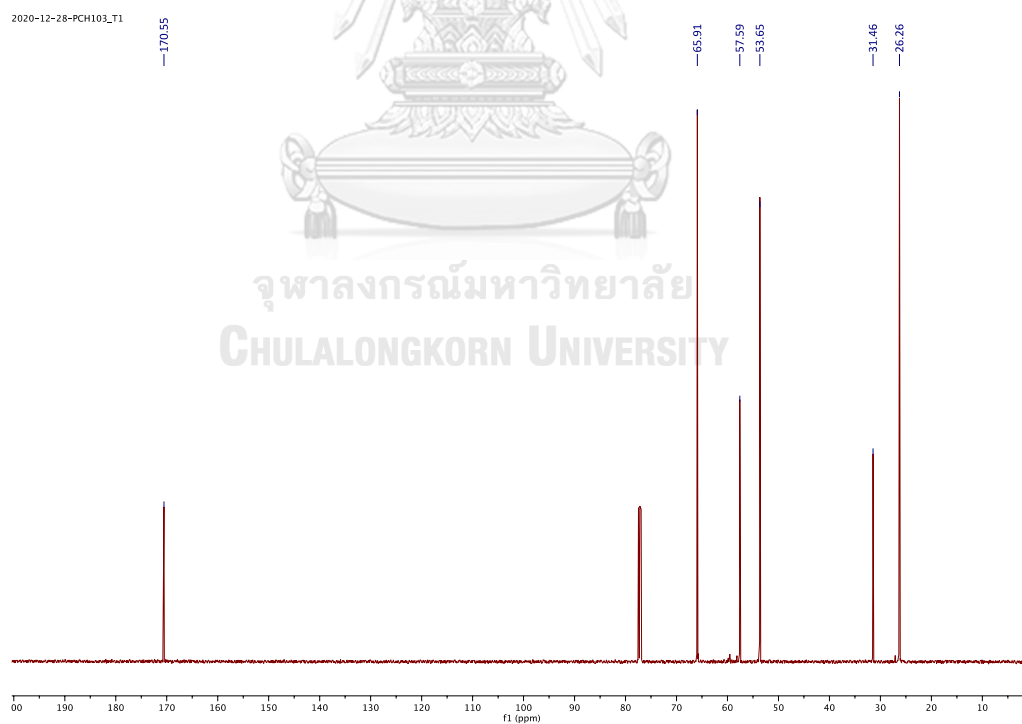


Figure A.74 ^{13}C NMR spectrum of methyl 2,4,4,4-tetrabromo-2-methylbutanoate, **4b**.

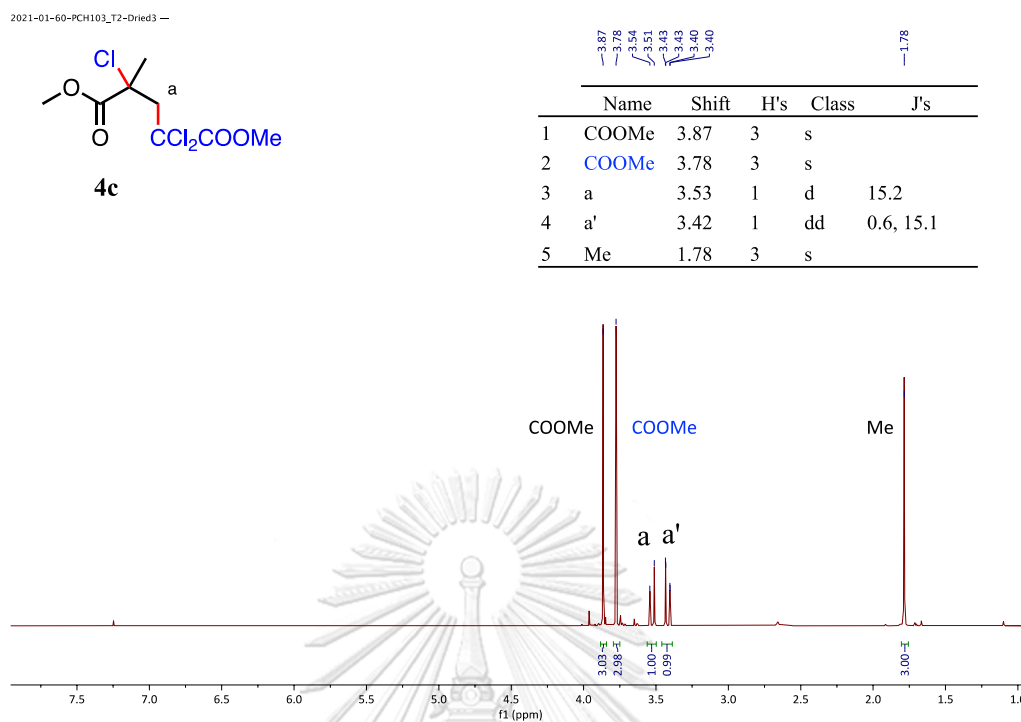


Figure A.75 ^1H NMR spectrum of dimethyl 2,2,4-trichloro-4-methylpentanedioate, **4c**.

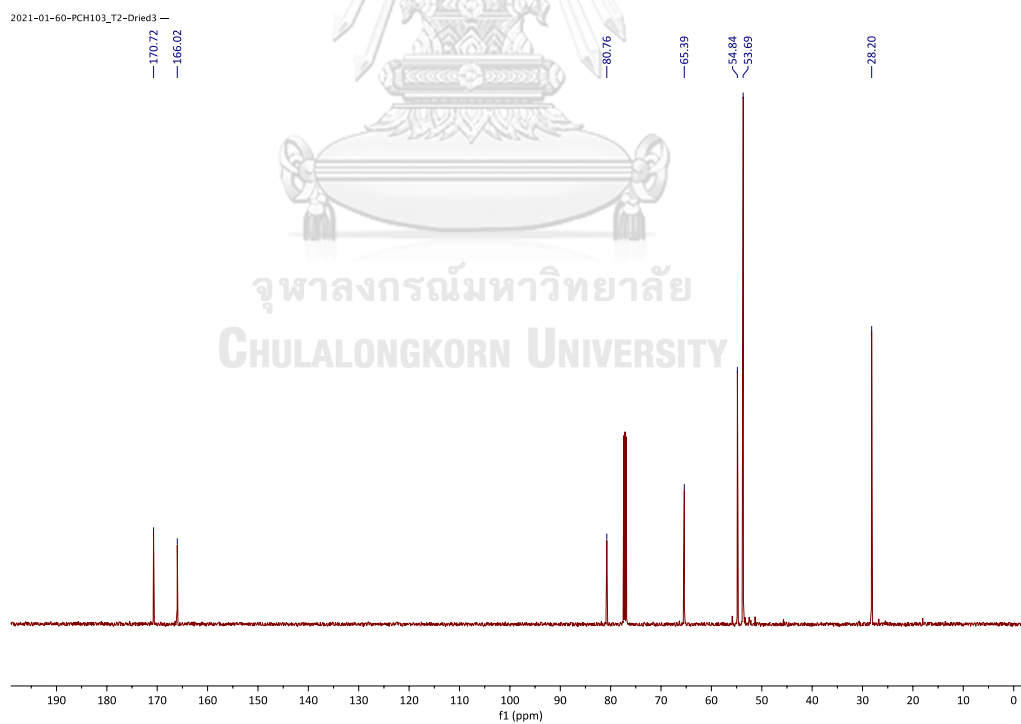
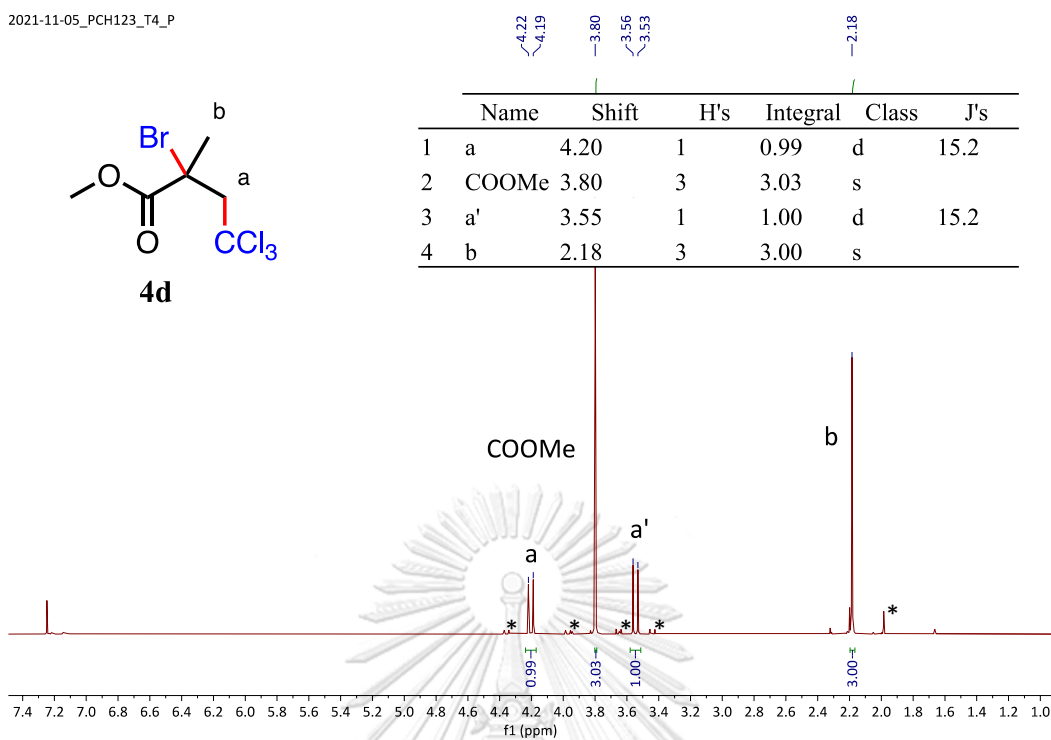


Figure A.76 ^{13}C NMR spectrum of dimethyl 2,2,4-trichloro-4-methylpentanedioate, **4c**.

2021-11-05_PCH123_T4_P



* by-product see Figure 3.12.

Figure A.77 ^1H NMR spectrum of methyl-2-bromo-4,4,4-trichloro-2-methylbutanoate, 4da.

2021-11-05_PCH123_T4_P

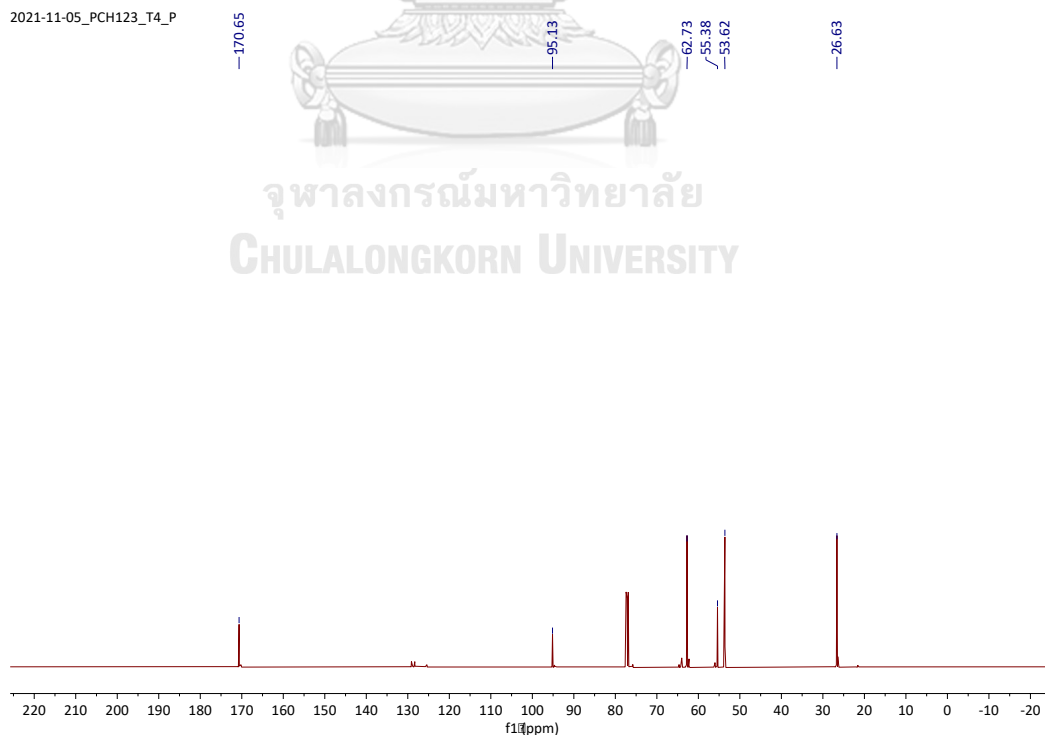


Figure A.78 ^{13}C NMR spectrum of methyl-2-bromo-4,4,4-trichloro-2-methylbutanoate, 4da.

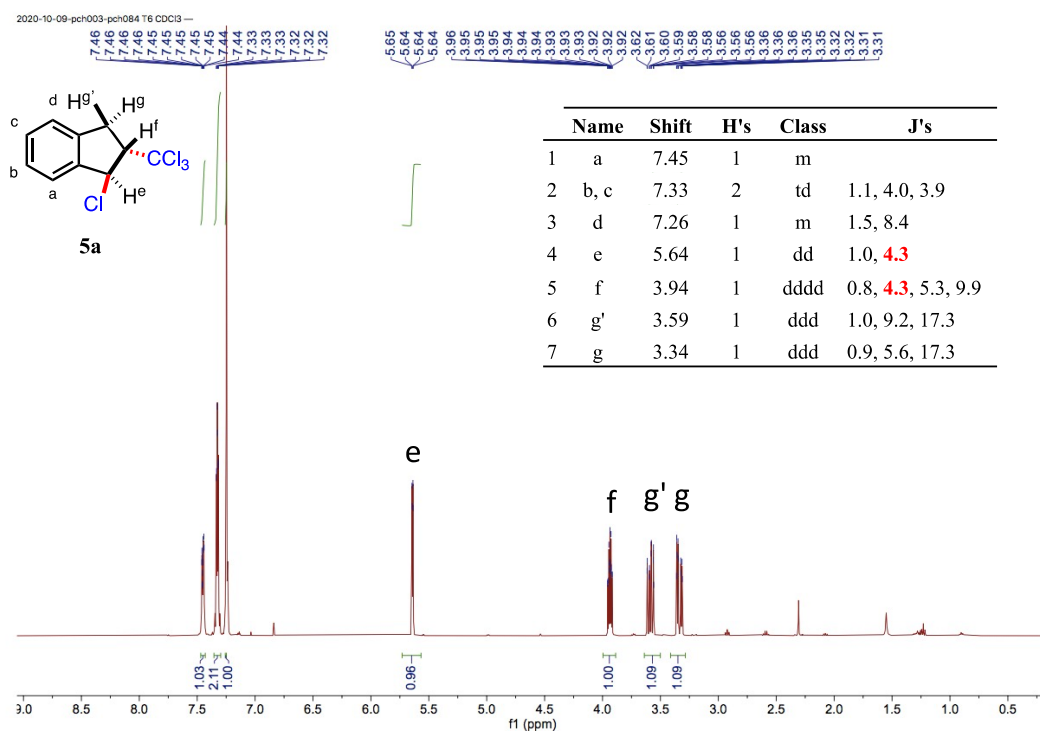


Figure A.79 ¹H NMR spectrum of anti-1-chloro-2-(trichloromethyl)-2,3-dihydro-1H-indene, **5a**.

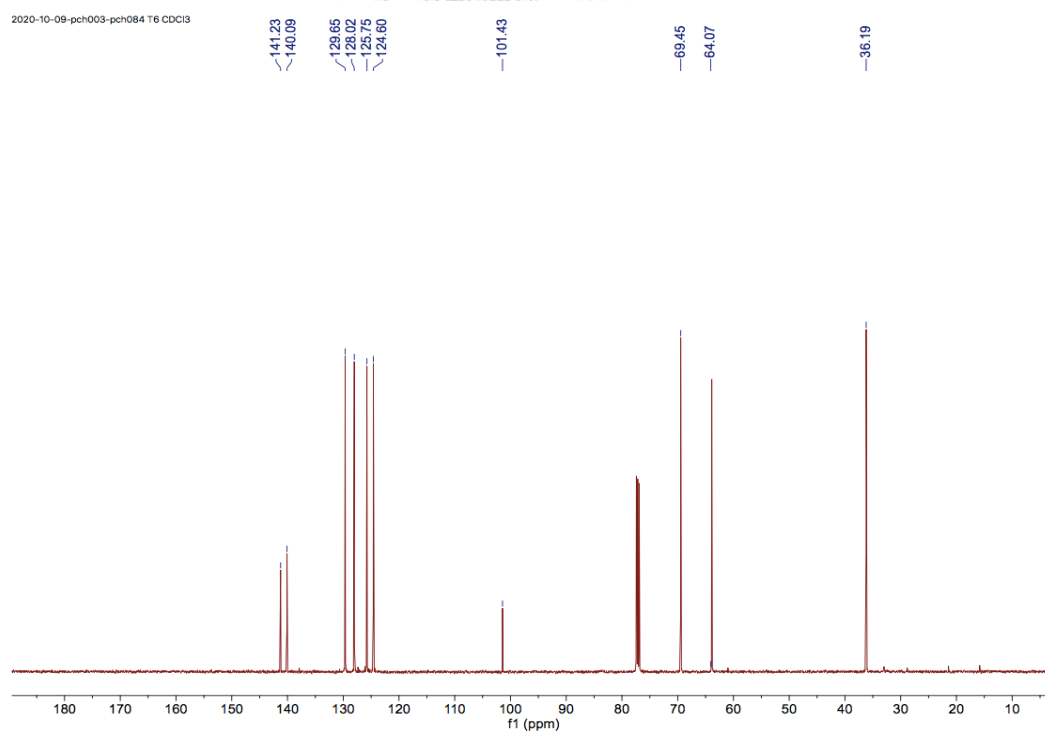


Figure A.80 ¹³C NMR spectrum of anti-1-chloro-2-(trichloromethyl)-2,3-dihydro-1H-indene, **5a**.

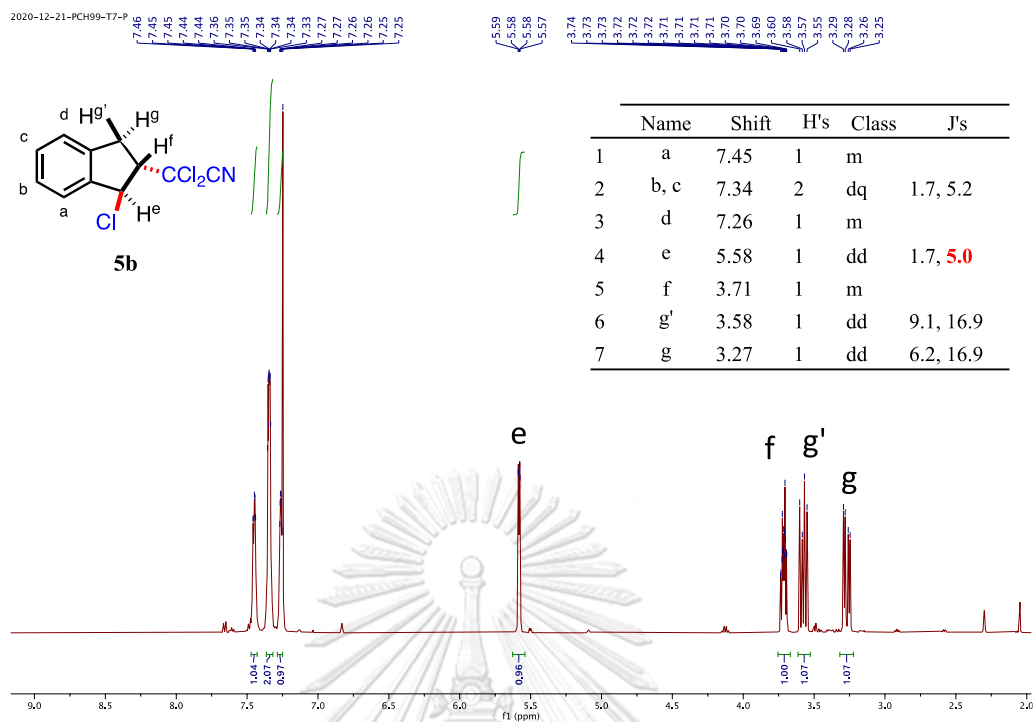


Figure A.81 ^1H NMR spectrum of anti-2,2-dichloro-2-(1-chloro-2,3-dihydro-1H-inden-2-yl) acetonitrile, **5b**.

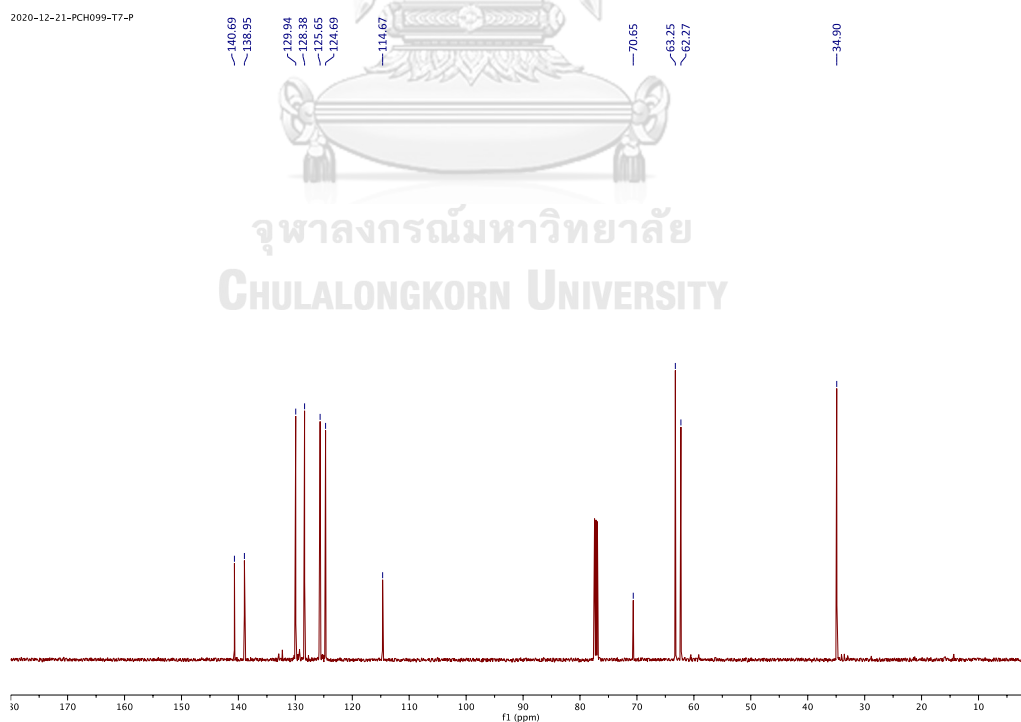


Figure A.82 ^{13}C NMR spectrum of anti-2,2-dichloro-2-(1-chloro-2,3-dihydro-1H-inden-2-yl) acetonitrile, **5b**.

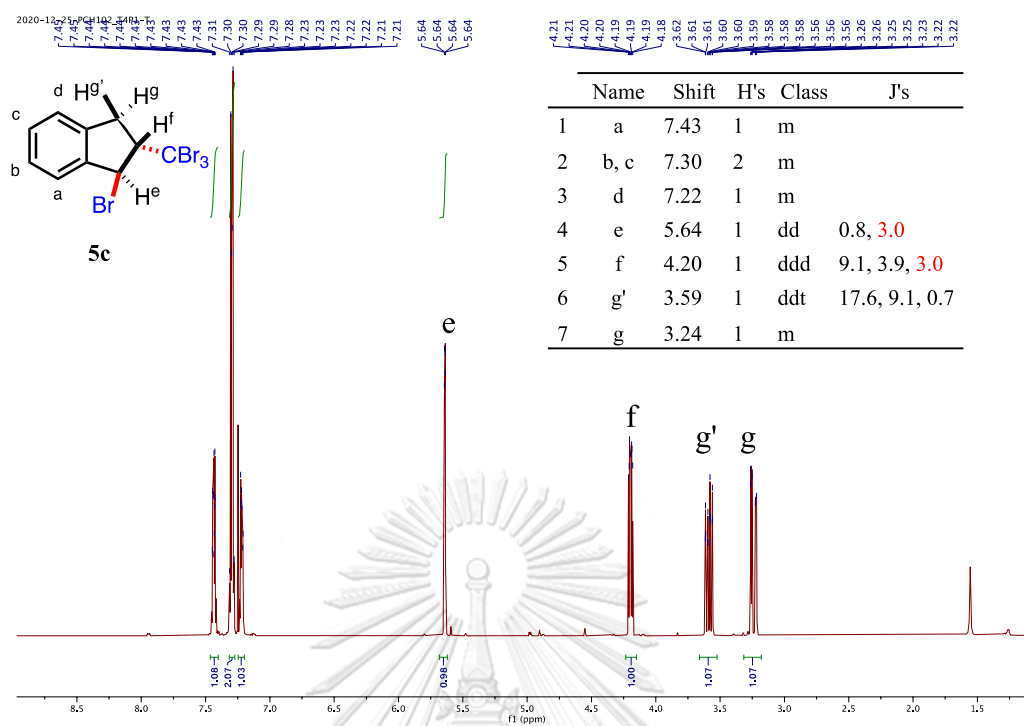


Figure A.83 ^1H NMR spectrum of anti-1-bromo-2-(tribromomethyl)-2,3-dihydro-1H-indene, **5c**.

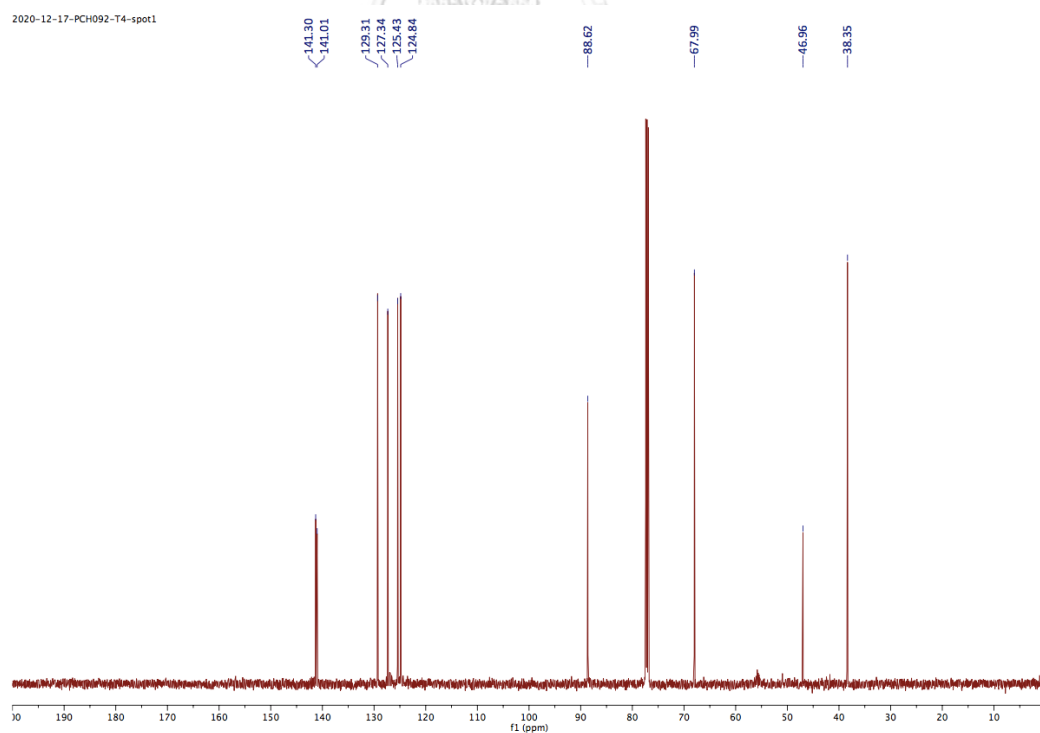


Figure A.84 ^{13}C NMR spectrum of anti-1-bromo-2-(tribromomethyl)-2,3-dihydro-1H-indene, **5c**.

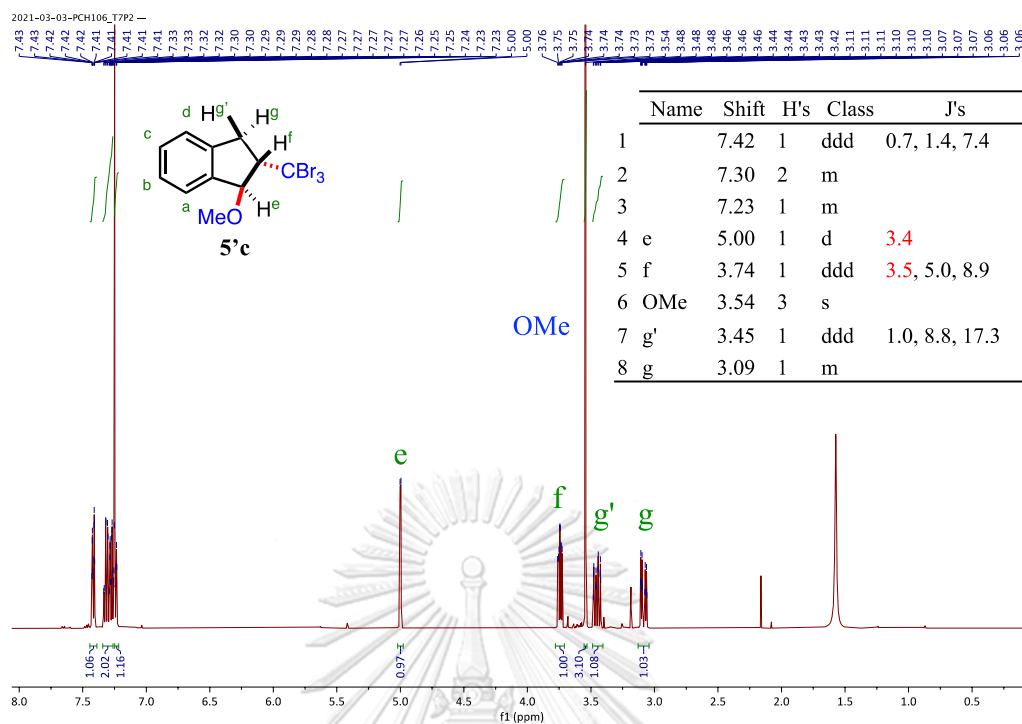


Figure A.85 ^1H NMR spectrum of anti-1-methoxy-2-(tribromomethyl)-2,3-dihydro-1H-indene, 5'c.

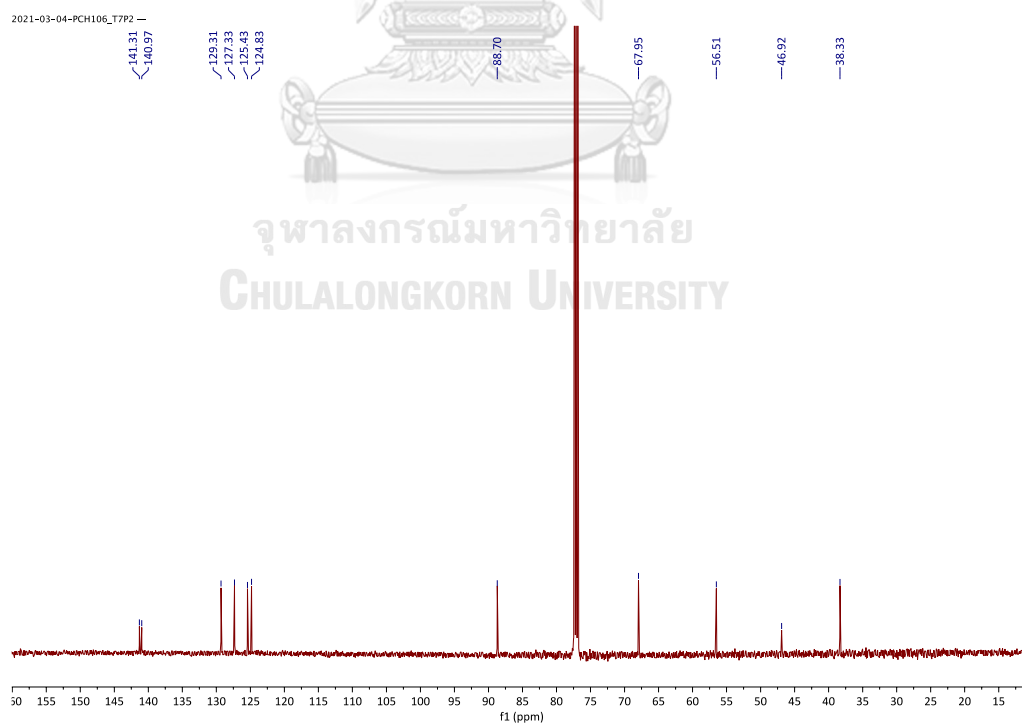
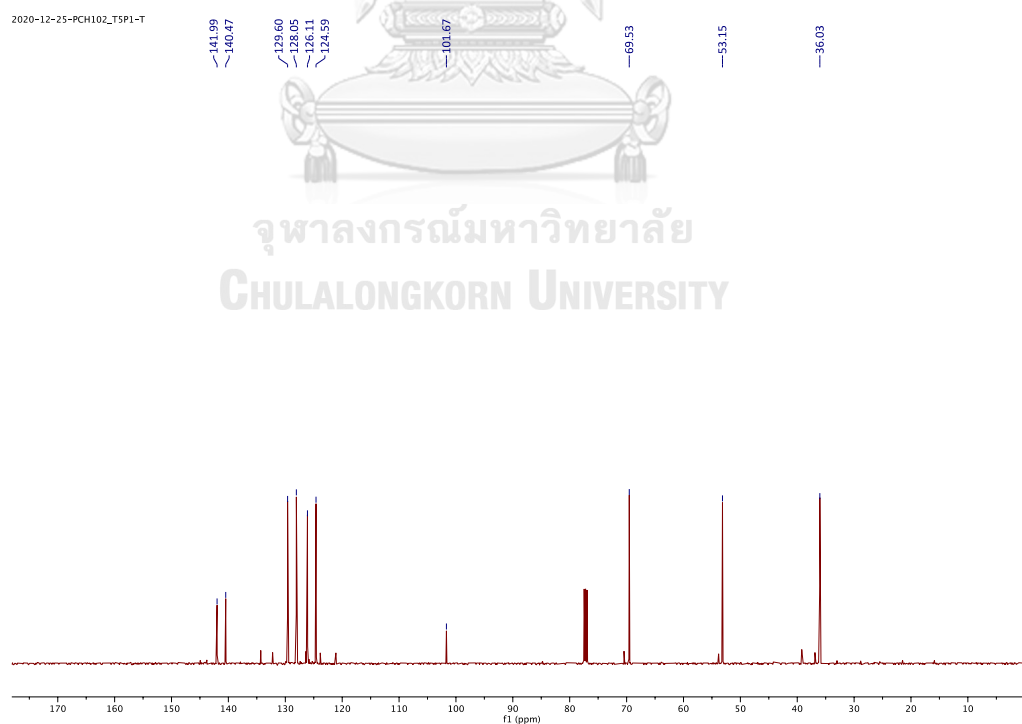
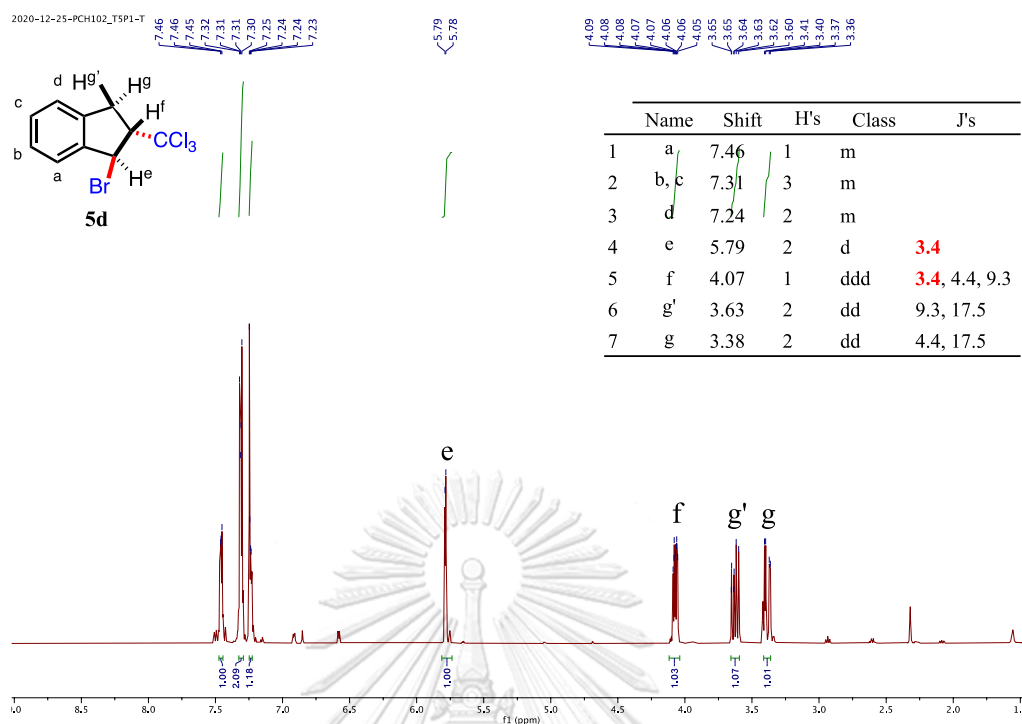


Figure A.86 ^{13}C NMR spectrum of anti-1-methoxy-2-(tribromomethyl)-2,3-dihydro-1H-indene, 5'c.



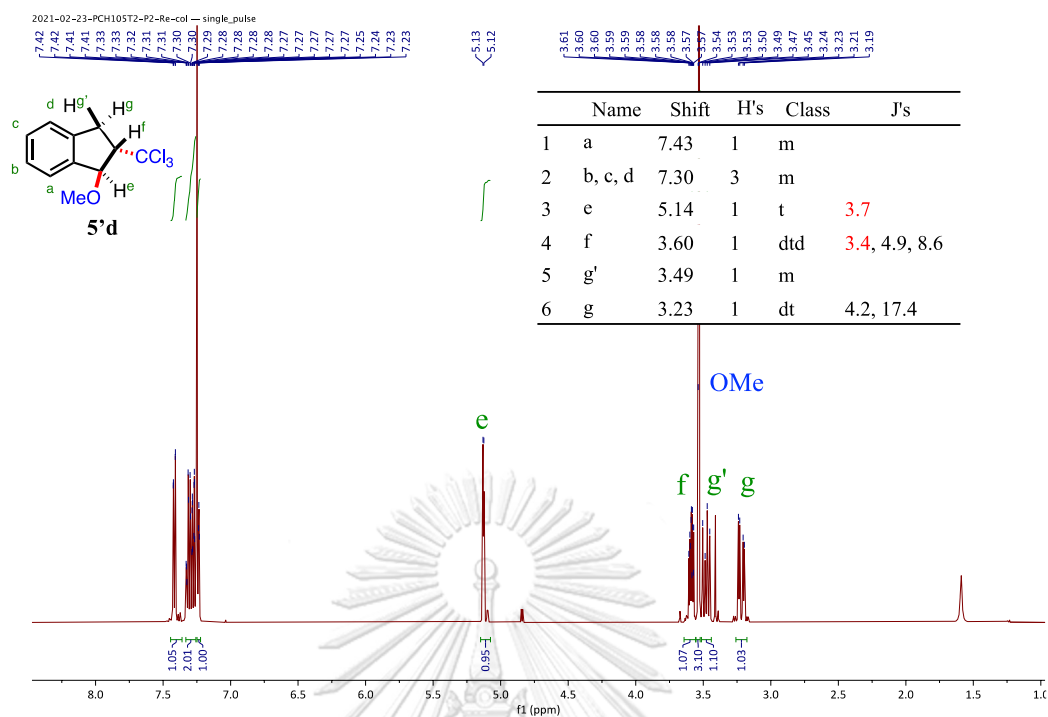


Figure A.89 ^1H NMR spectrum of anti-1-methoxy-2-(trichloromethyl)-2,3-dihydro-1H-indene, **5'd**.

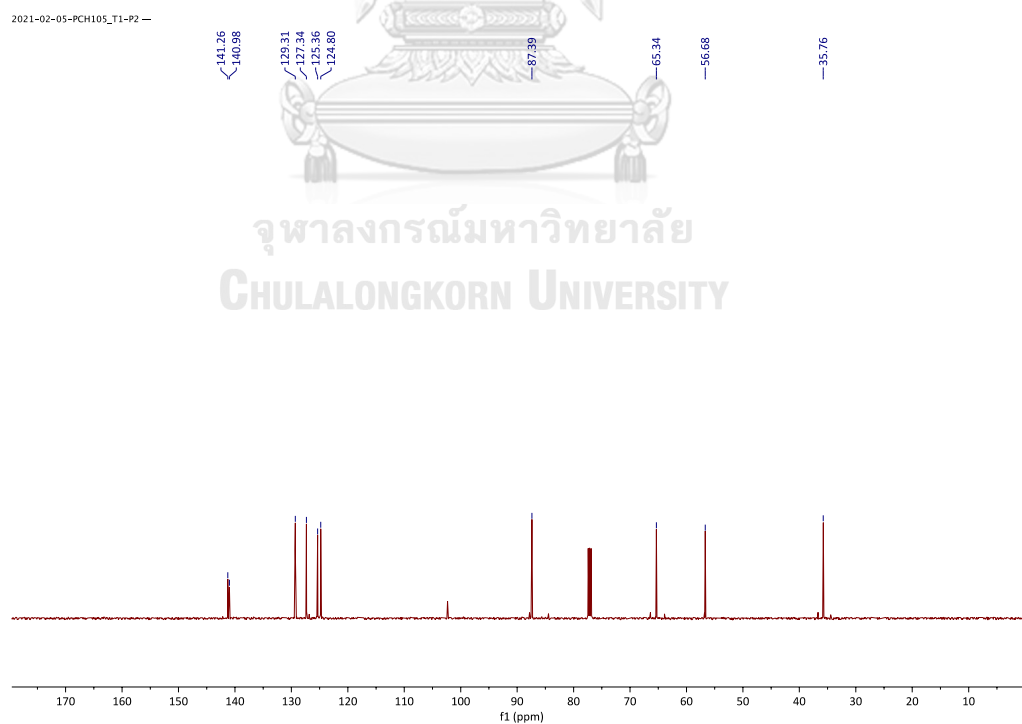
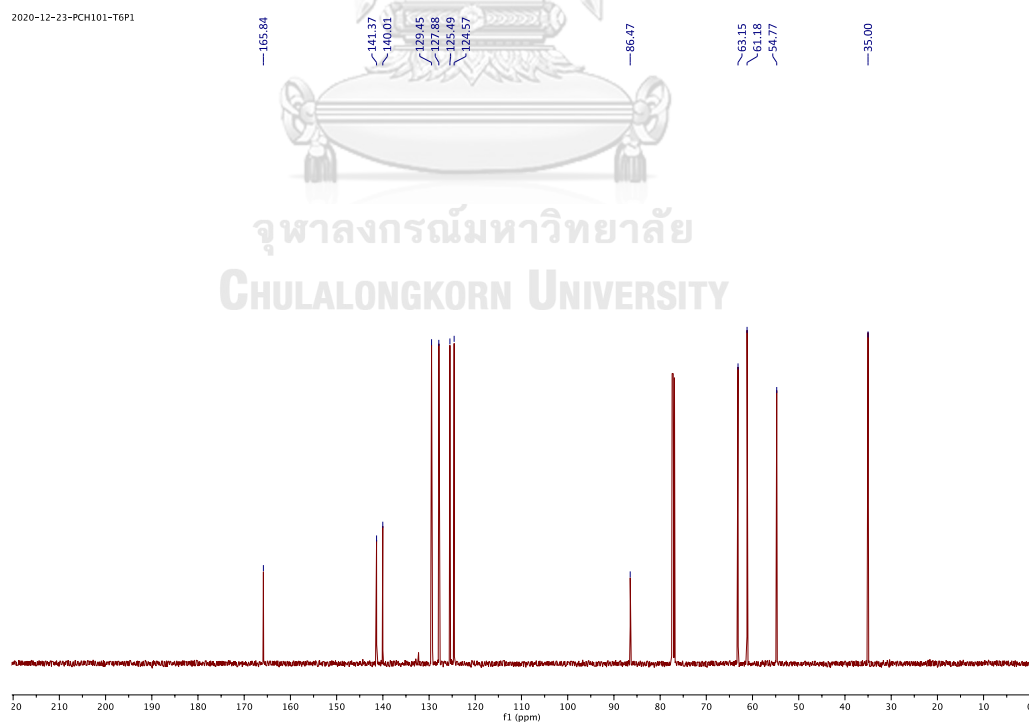
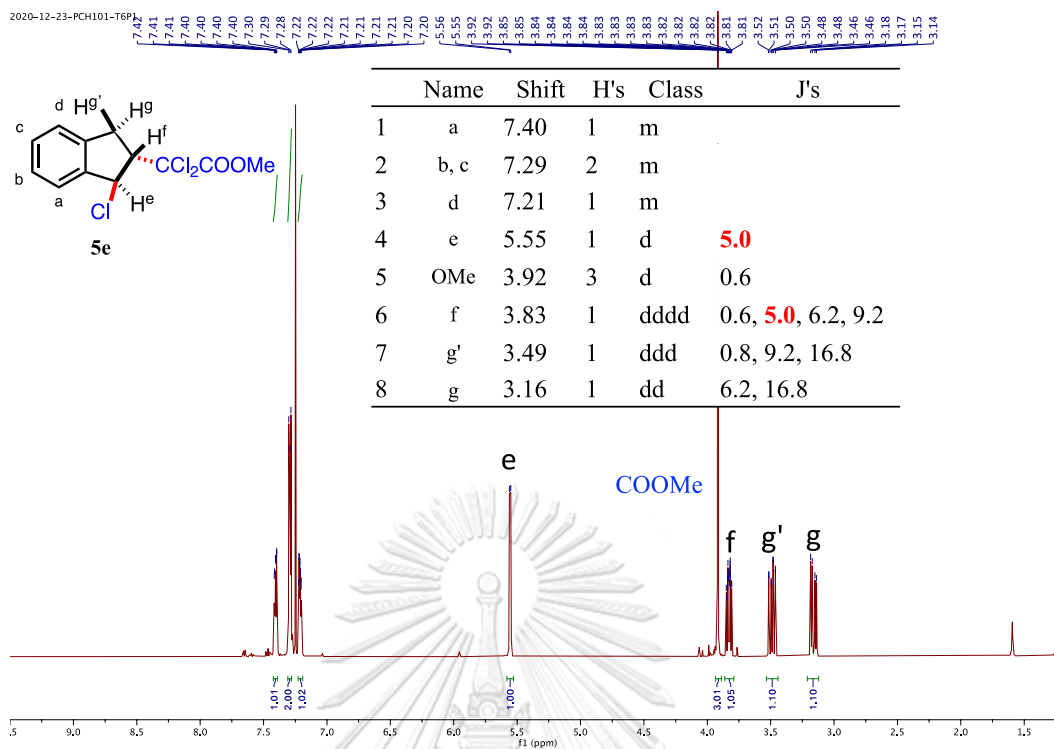
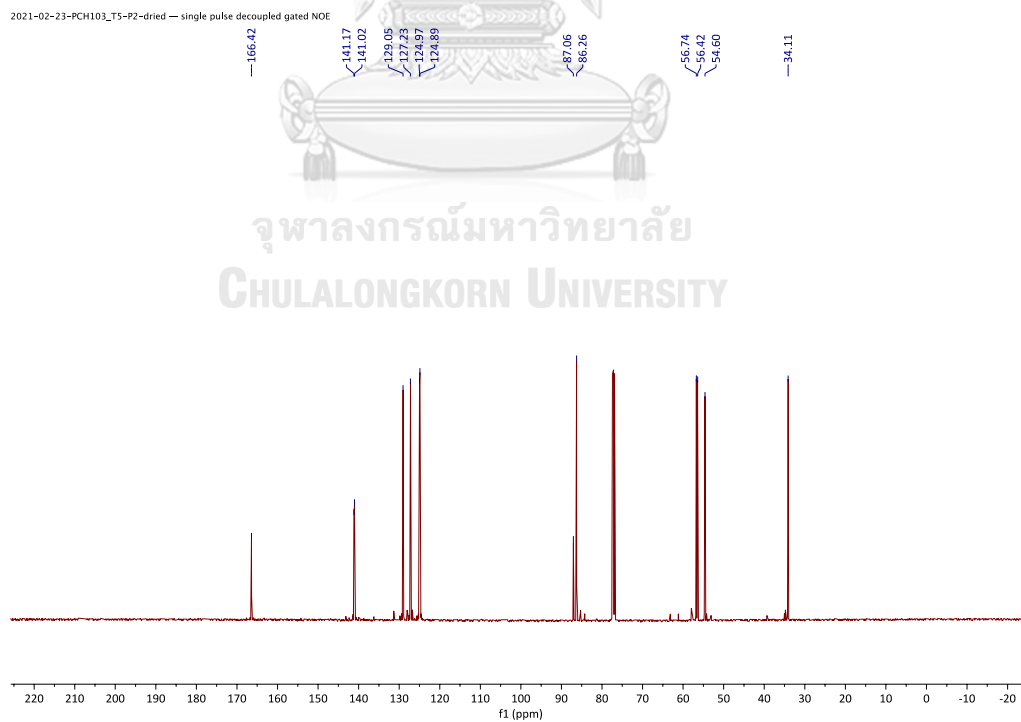
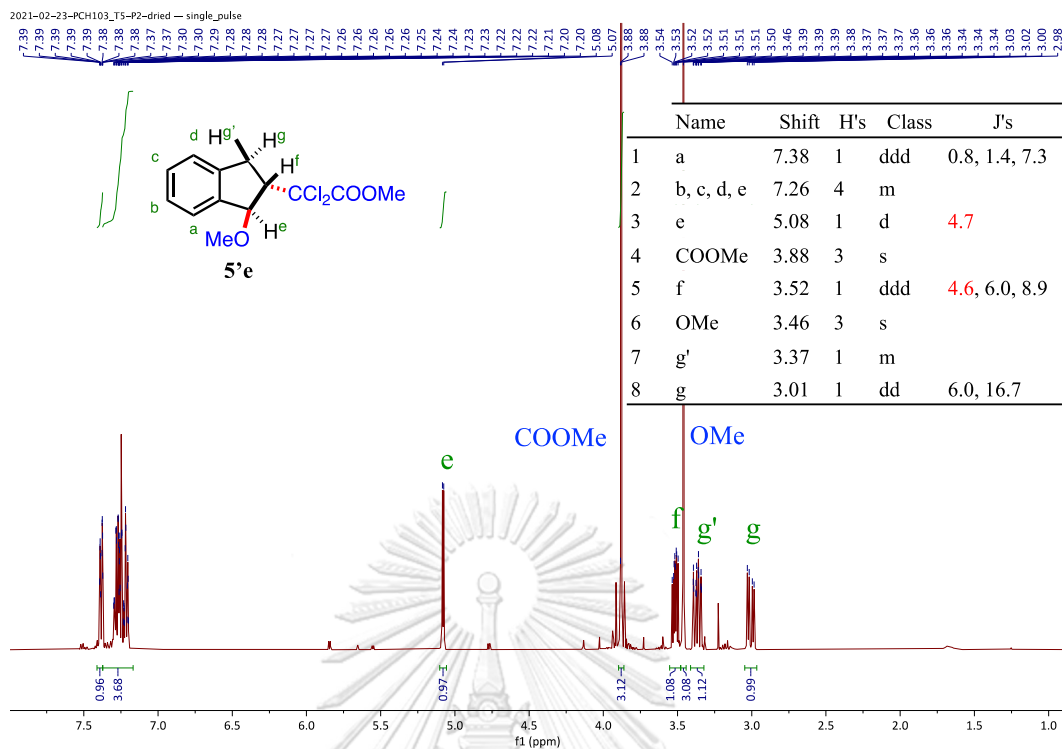


Figure A.90 ^{13}C NMR spectrum of anti-1-methoxy-2-(trichloromethyl)-2,3-dihydro-1H-indene, **5'd**.





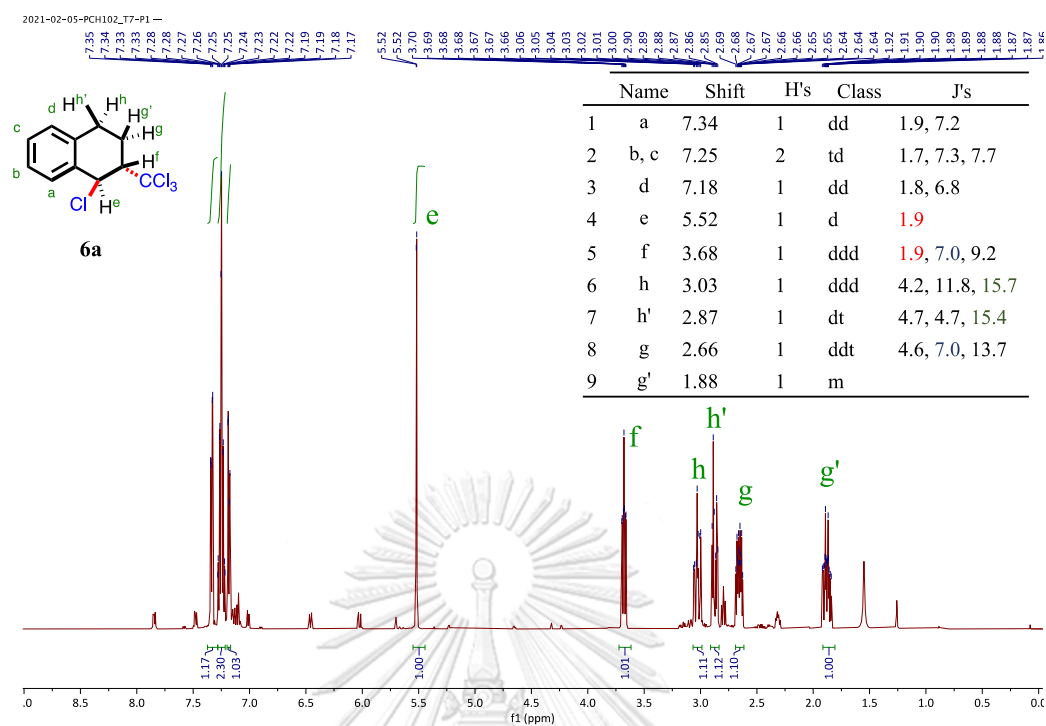


Figure A.95 ^1H NMR spectrum of anti-1-chloro-2-(trichloromethyl)-1,2,3,4-tetrahydronaphthalene, **6a**.

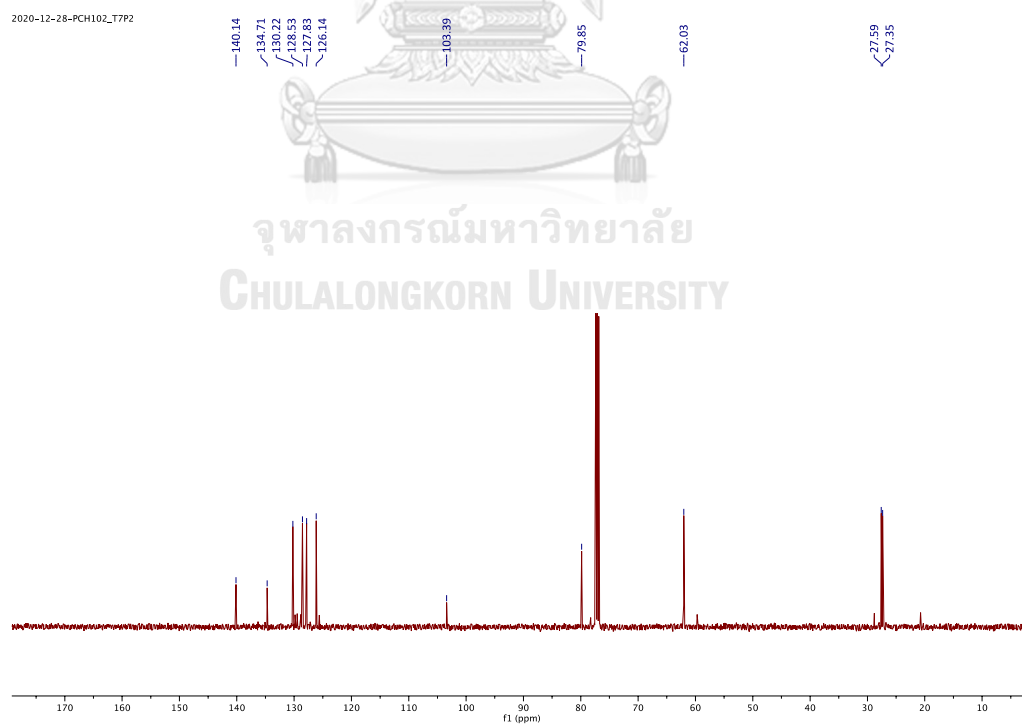


Figure A.96 ^{13}C NMR spectrum of anti-1-chloro-2-(trichloromethyl)-1,2,3,4-tetrahydronaphthalene, **6a**.

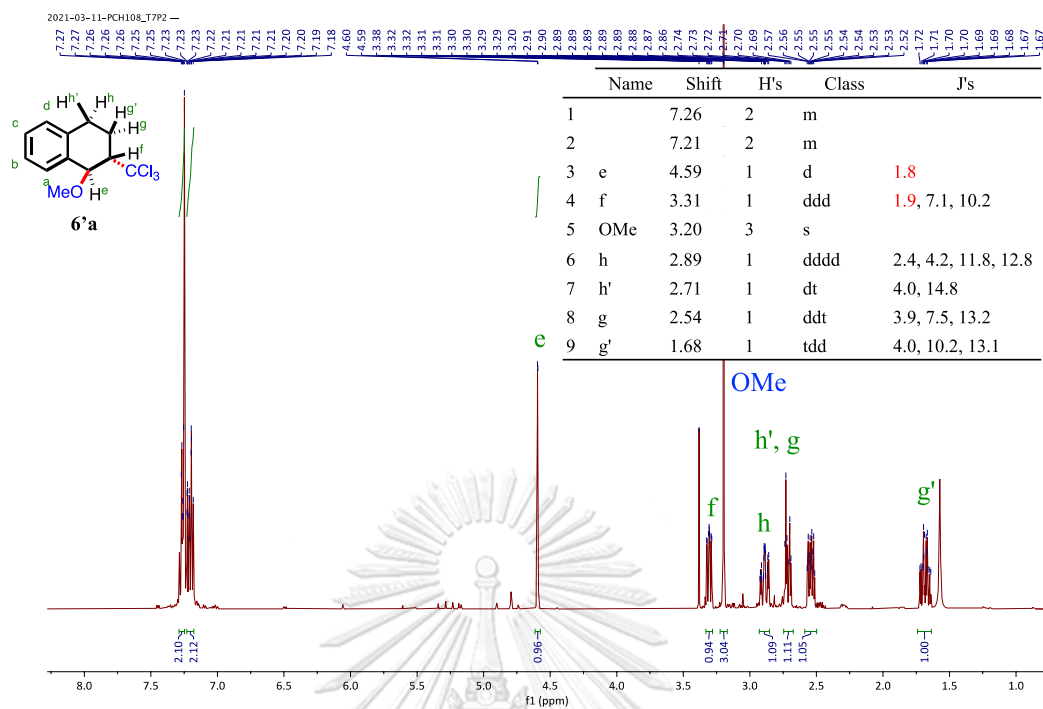


Figure A.97 ^1H NMR spectrum of anti-1-methoxy-2-(trichloromethyl)-1,2,3,4-tetrahydronaphthalene, **6'a**.

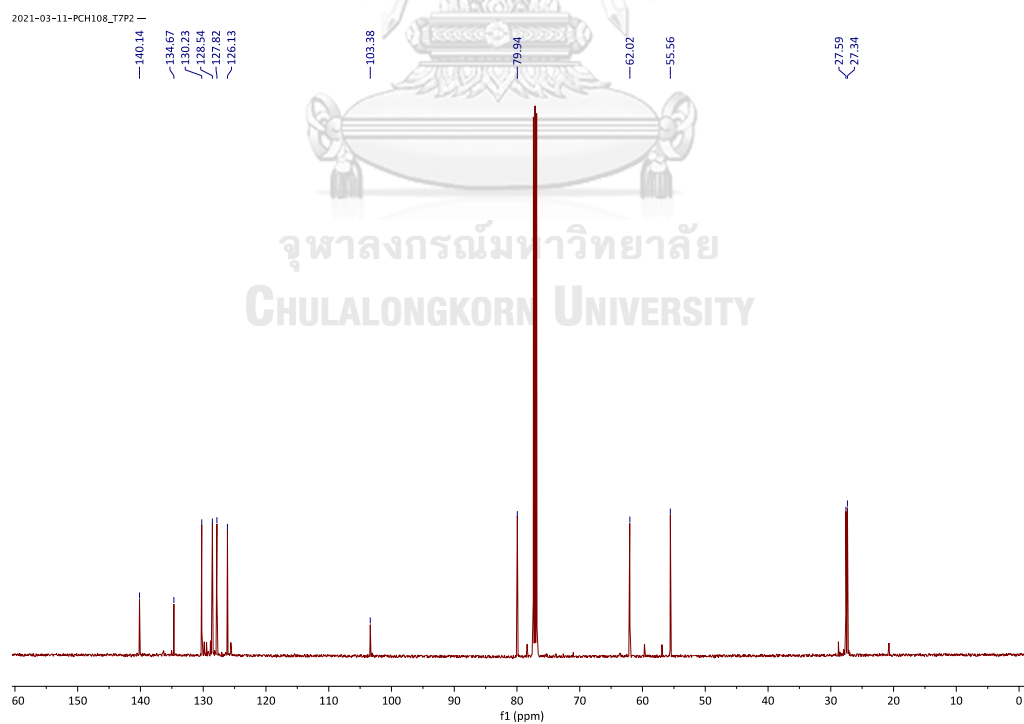


Figure A.98 ^{13}C NMR spectrum of anti-1-methoxy-2-(trichloromethyl)-1,2,3,4-tetrahydronaphthalene, **6'a**.

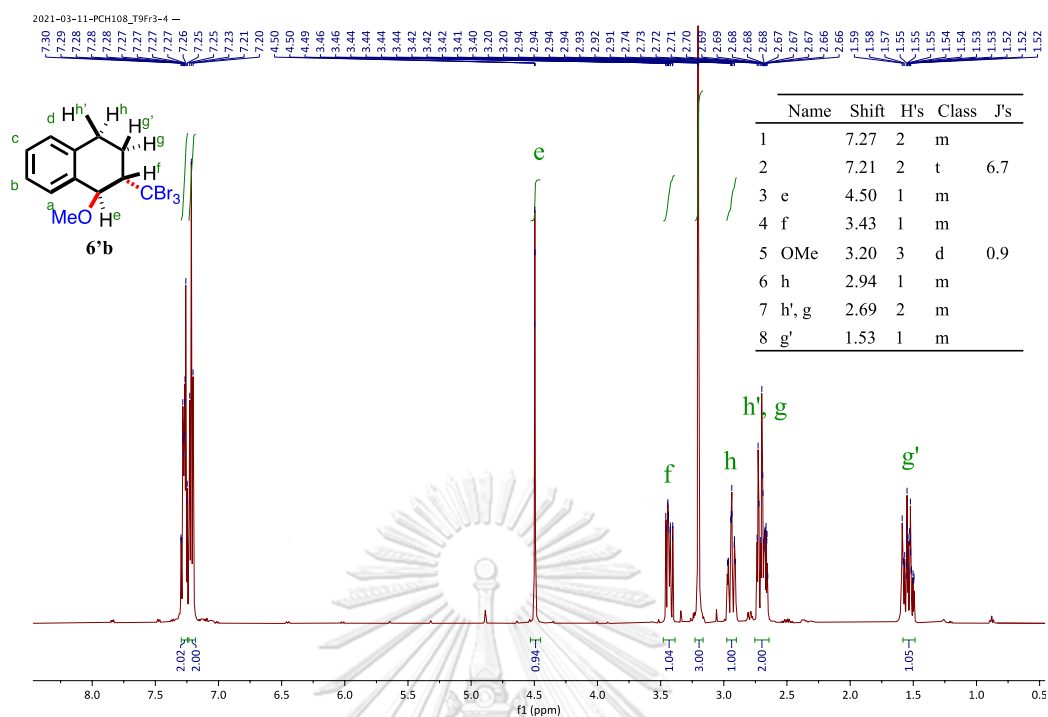


Figure A.99 ^1H NMR spectrum of anti-1-methoxy-2-(tribromomethyl)-1,2,3,4-tetrahydronaphthalene, **6'b**.

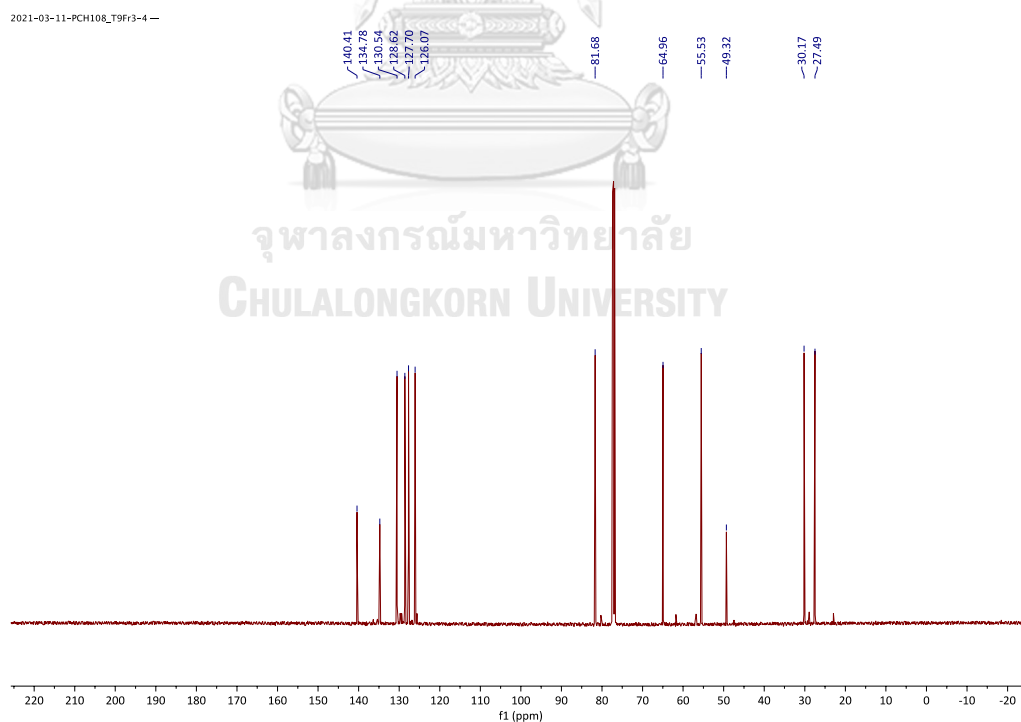
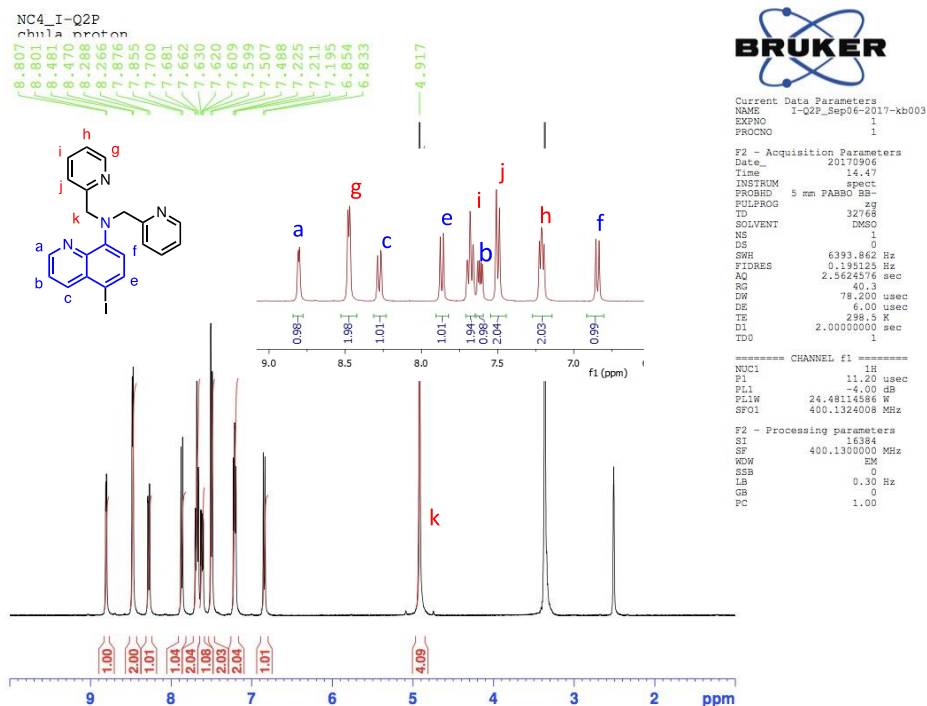
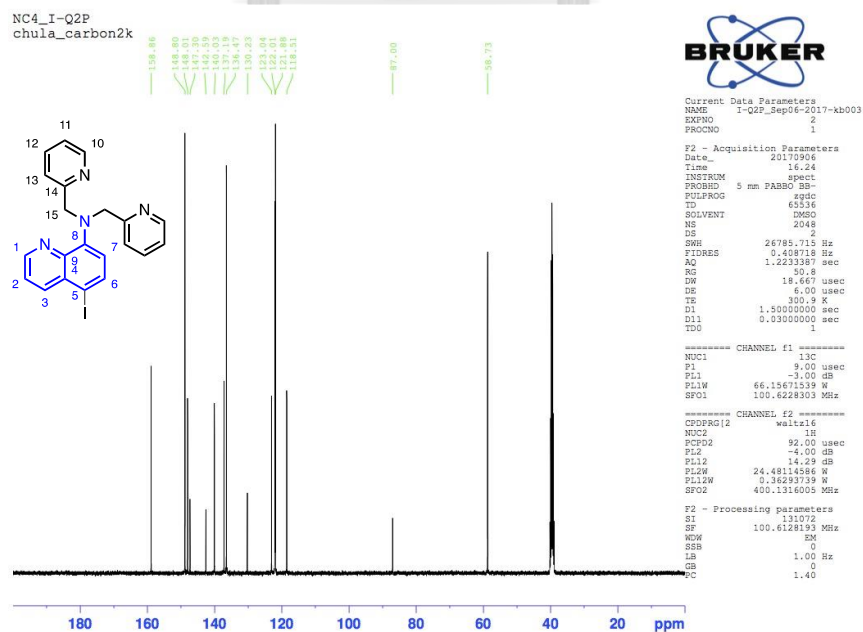


Figure A.100 ^{13}C NMR spectrum of anti-1-methoxy-2-(tribromomethyl)-1,2,3,4-tetrahydronaphthalene, **6'b**.

APPENDIX B

The atom transfer radical addition (ATRA) for halosulfonylation (C-S formation)

B.1 Ligands and Cu(II) complexes

B.1.1 ^1H NMR and ^{13}C spectraFigure B.1 ^1H NMR spectrum of ligand 1Q-I.Figure B.2 ^{13}C NMR spectrum of ligand 1Q-I.

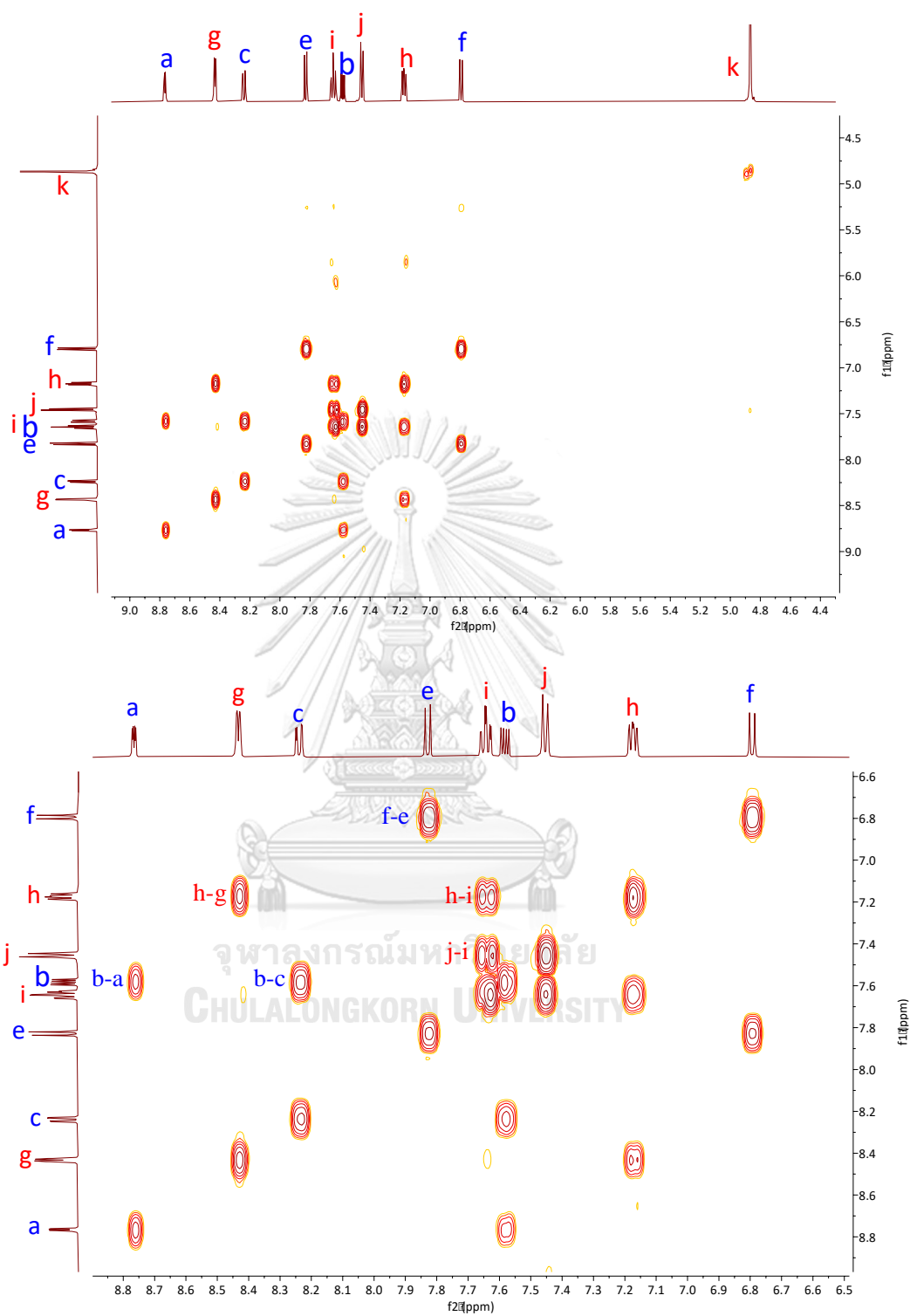


Figure B.3 COSY spectrum of ligand 1Q-I.

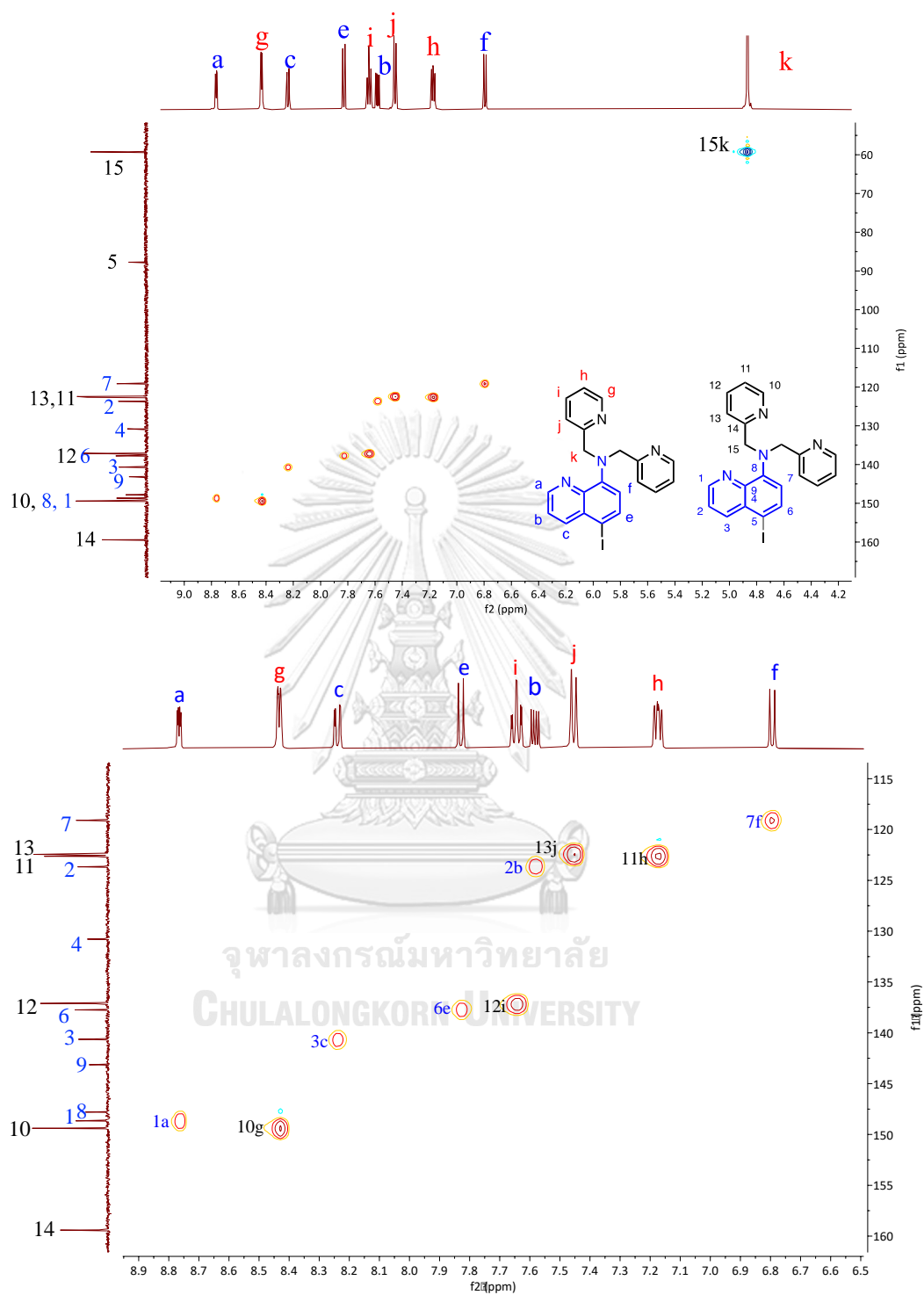


Figure B.4 HSQC spectrum of ligand 1Q-I.

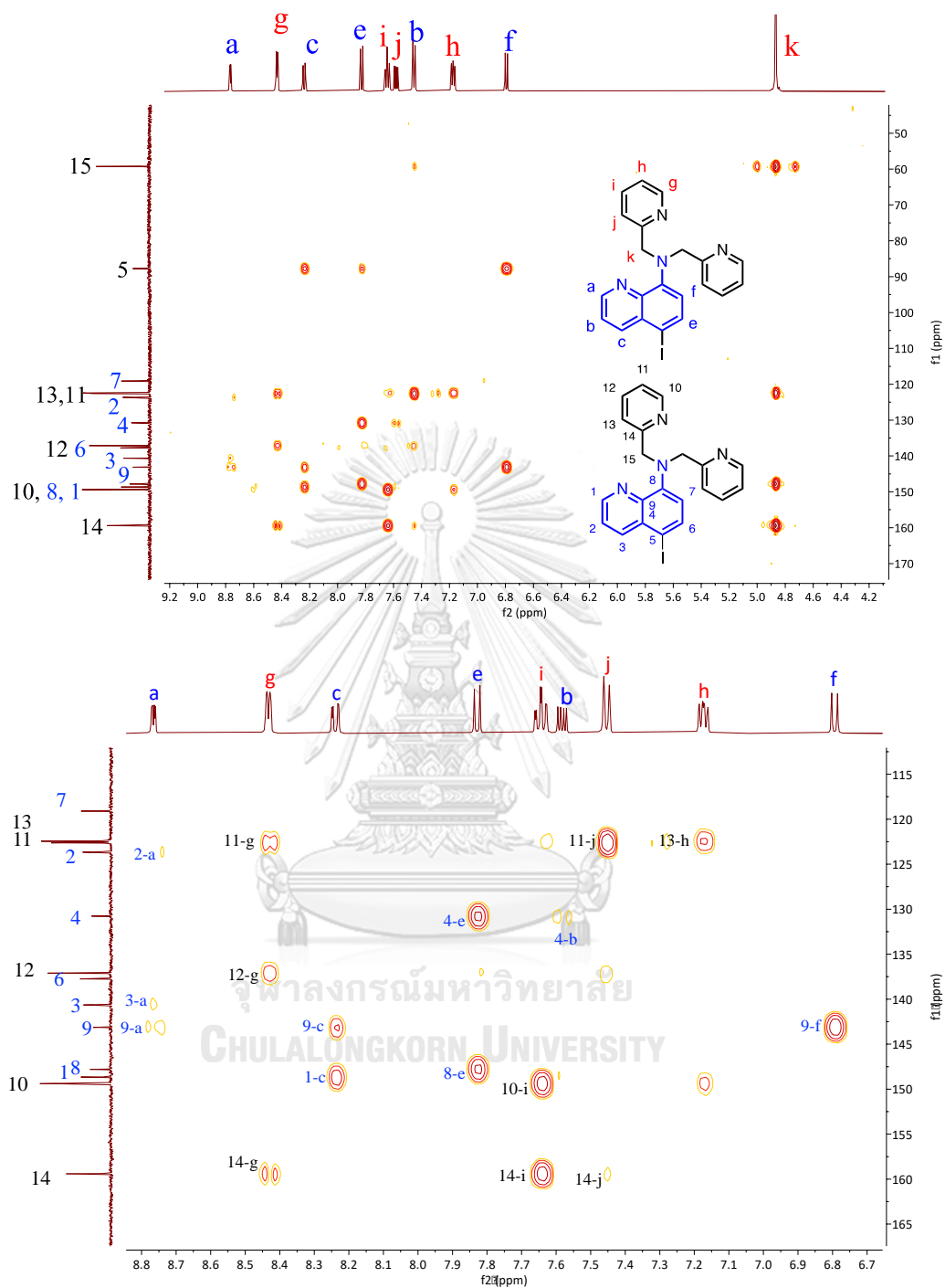
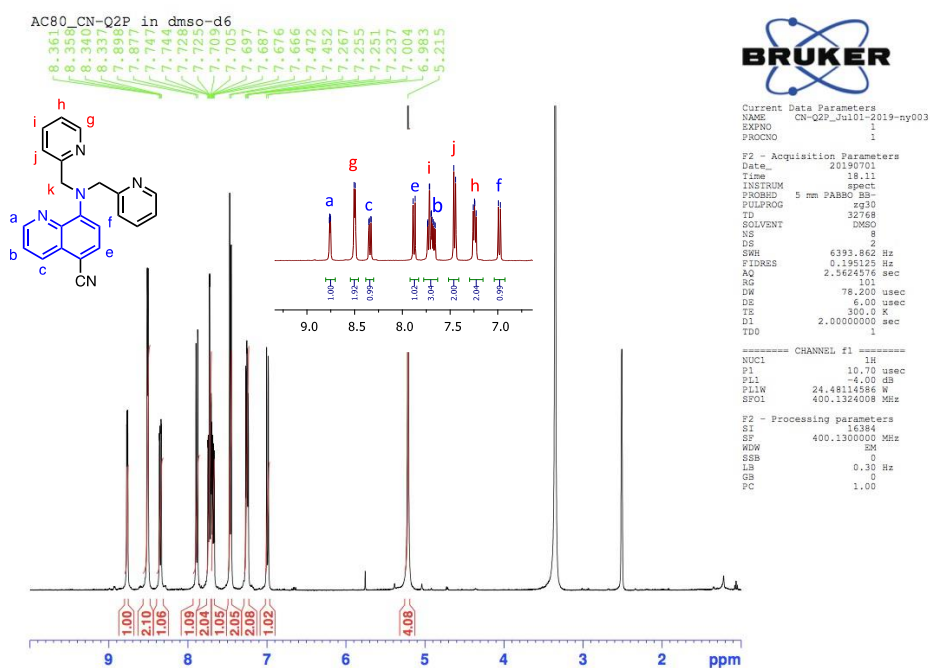
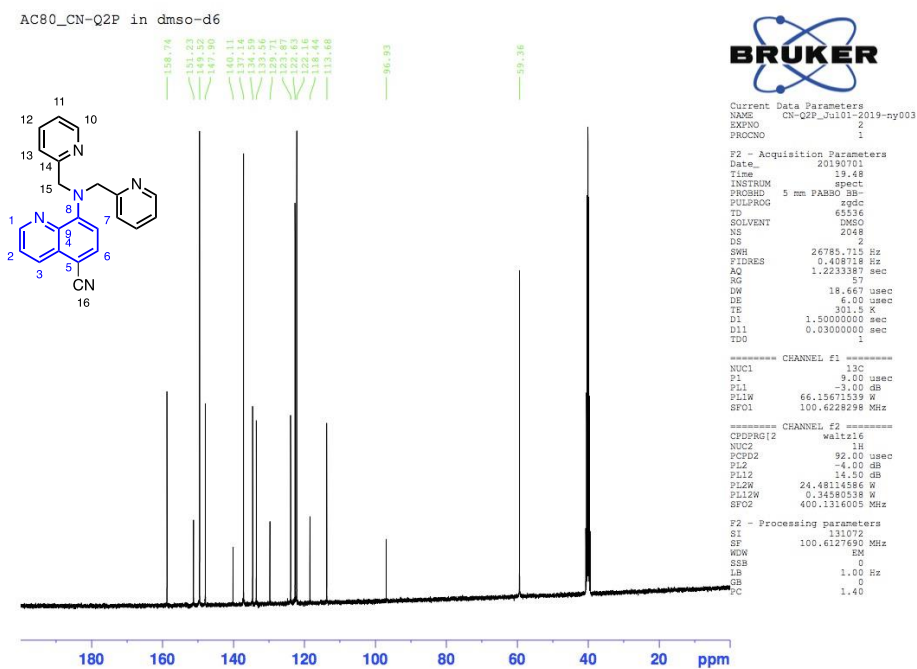


Figure B.5 HMBC spectrum of ligand 1Q-I.

Figure B.6 ^1H NMR spectrum of ligand 1Q-CN.Figure B.7 ^{13}C NMR spectrum of ligand 1Q-CN.

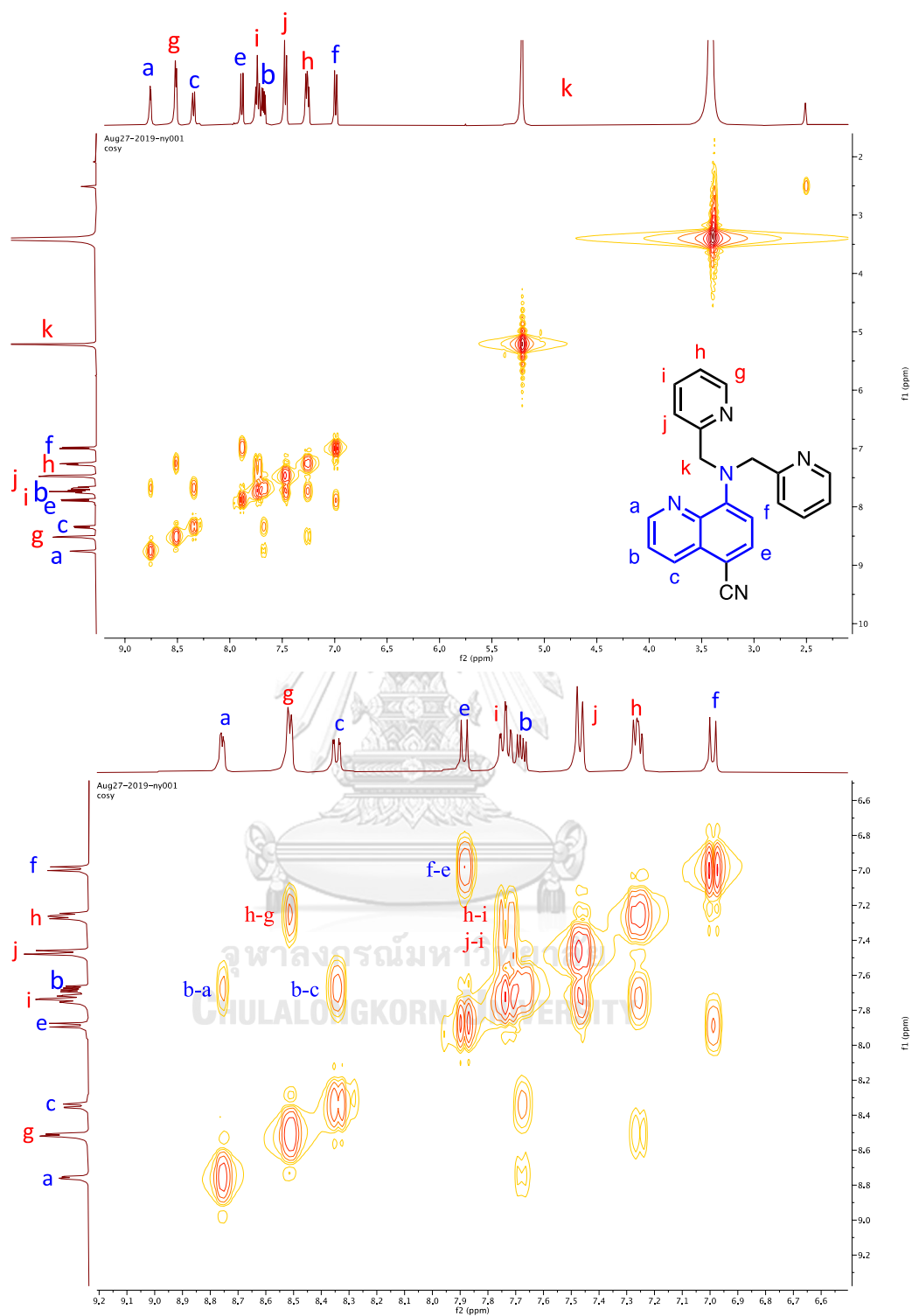


Figure B.8 COSY spectrum of ligand 1Q-CN.

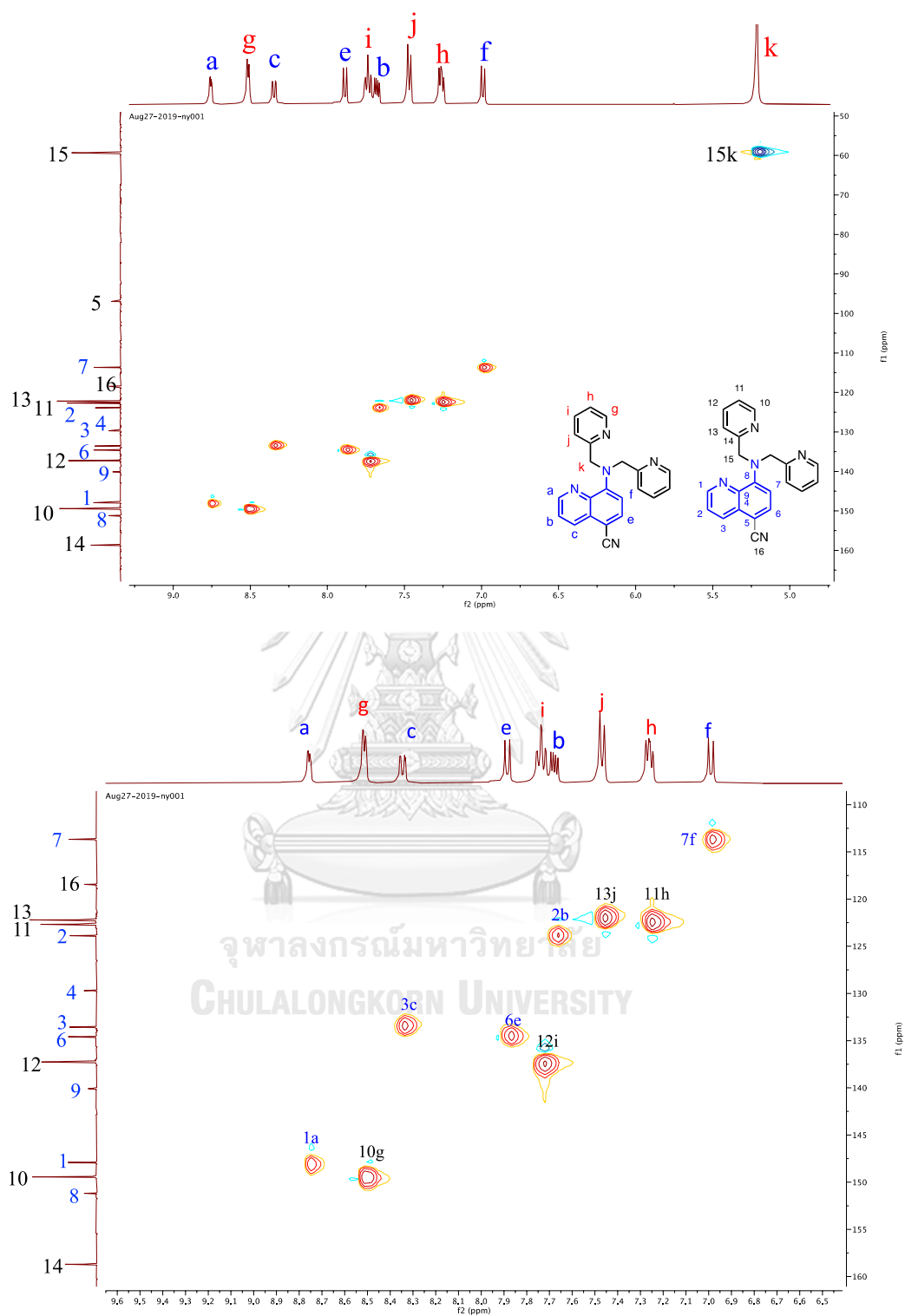


Figure B.9 HSQC spectrum of ligand 1Q-CN.

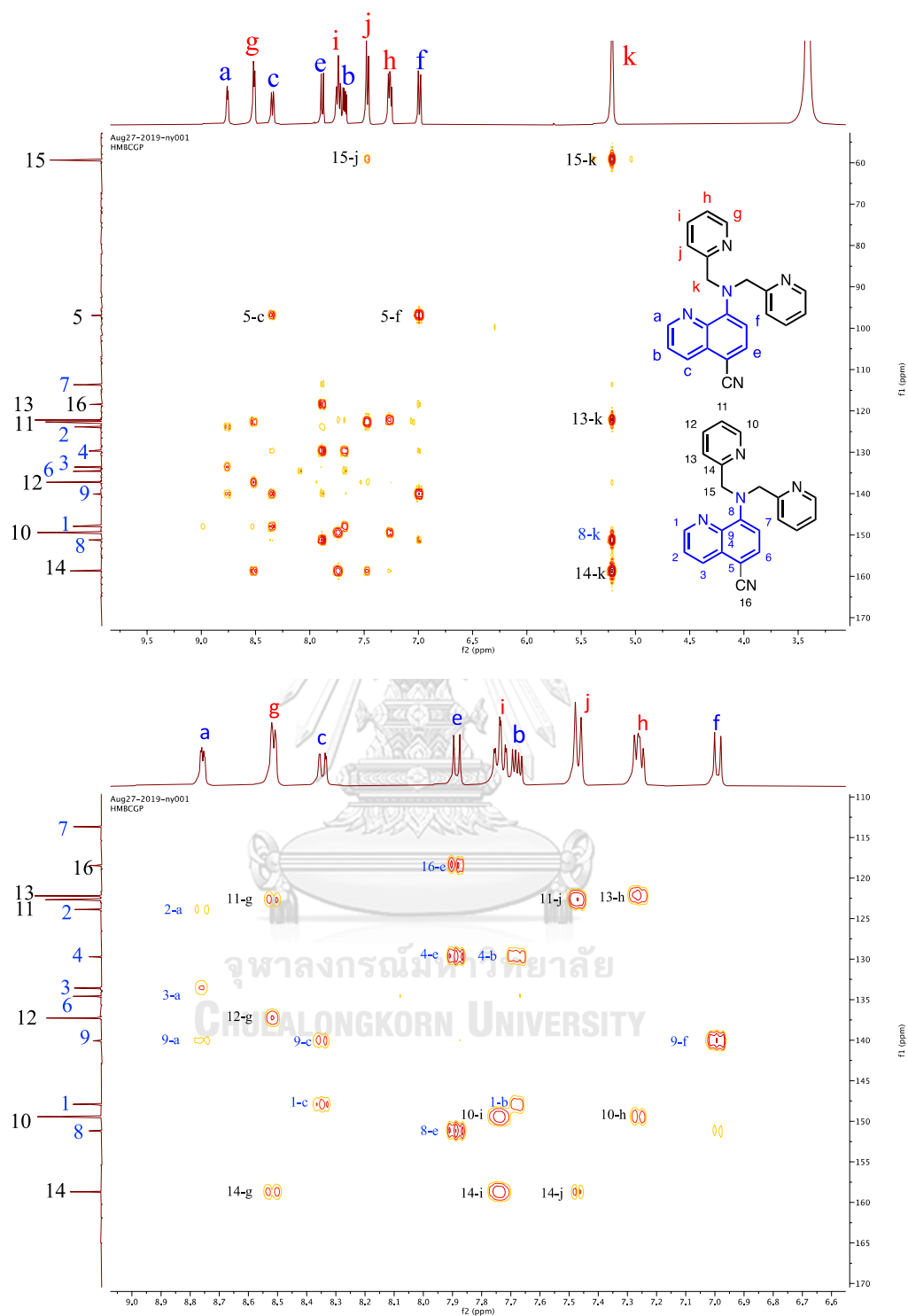
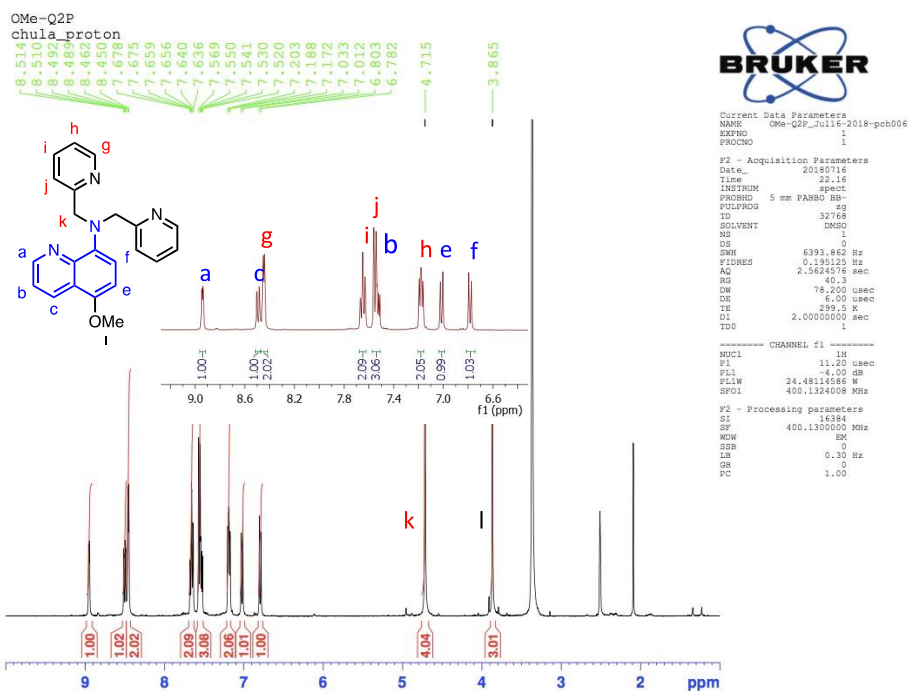
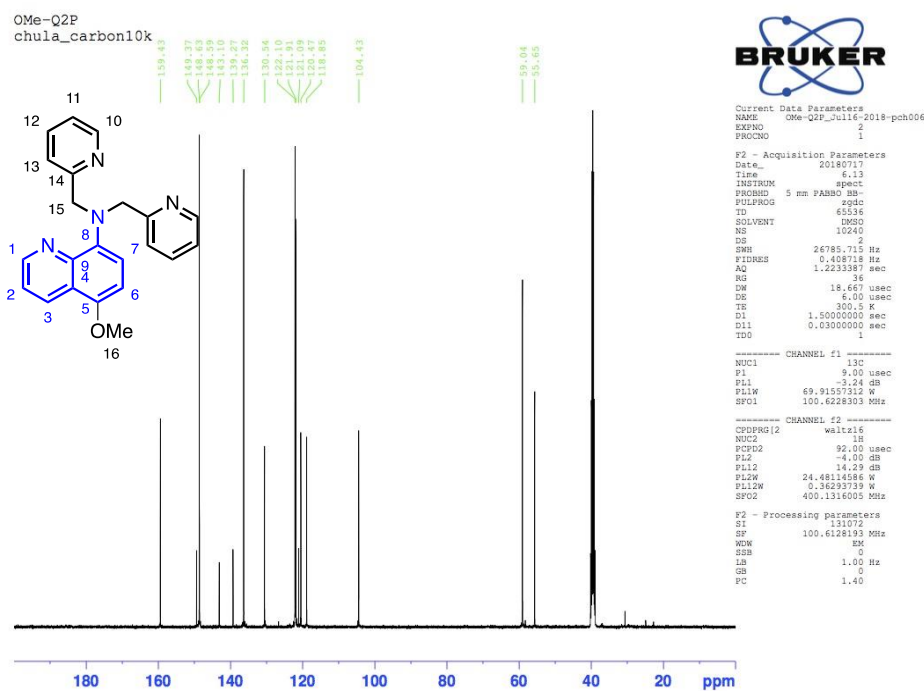


Figure B.10 HMBC spectrum of ligand 1Q-CN.

Figure B.11 ^1H NMR spectrum of ligand 1Q-OMe.Figure B.12 ^{13}C NMR spectrum of ligand 1Q-OMe.

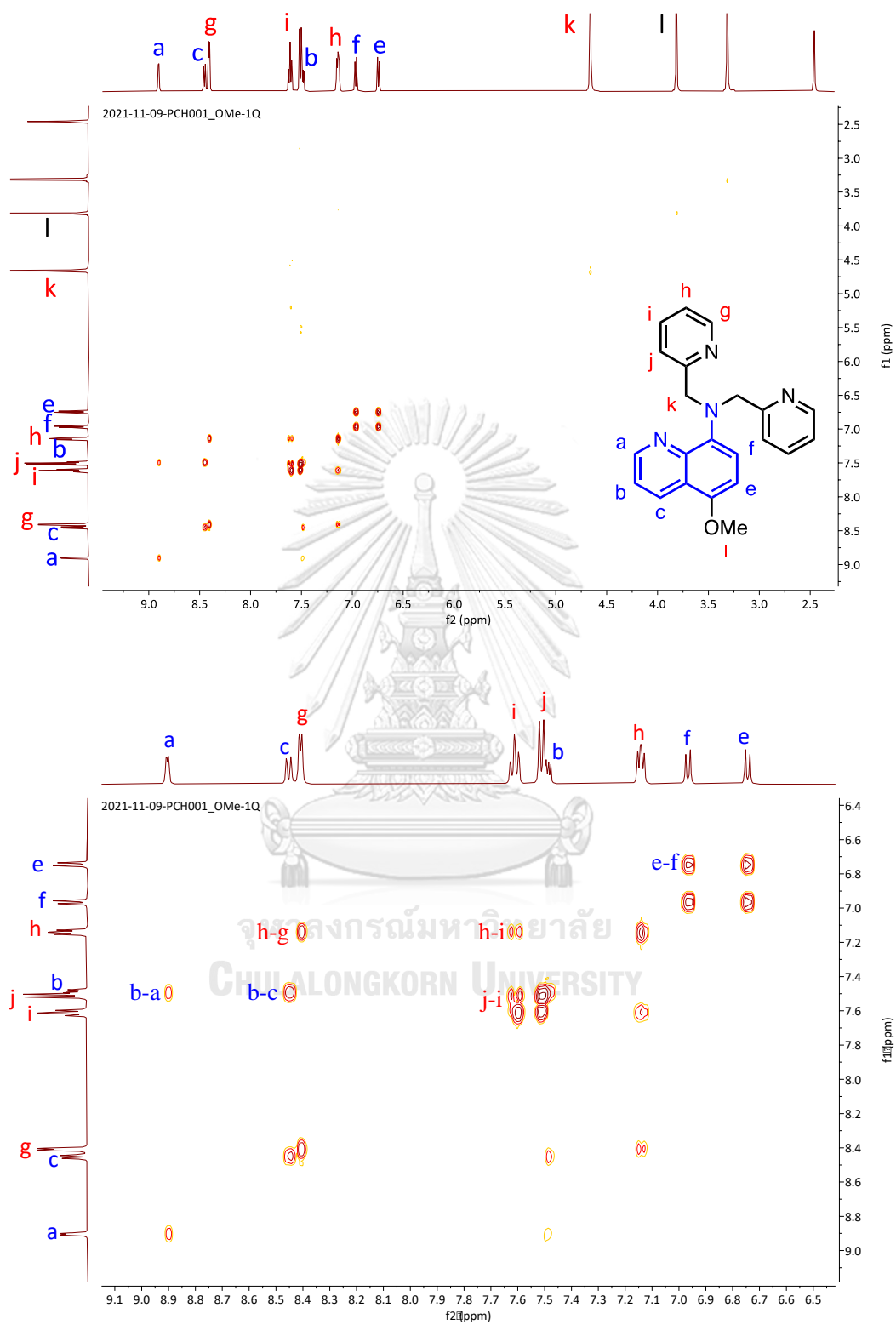


Figure B.13 COSY spectrum of ligand 1Q-OMe.

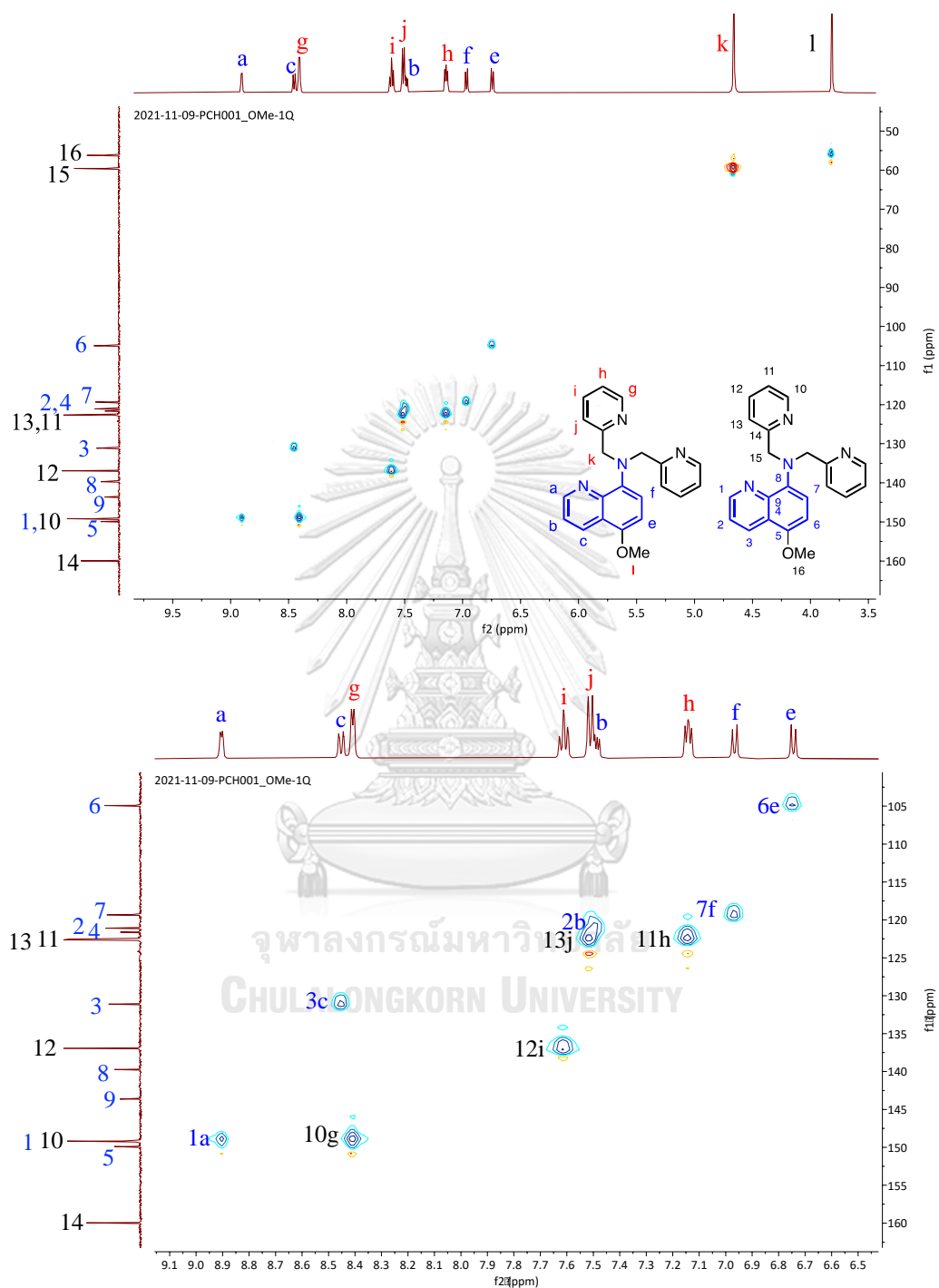


Figure B.14 HSQC spectrum of ligand 1Q-OMe.

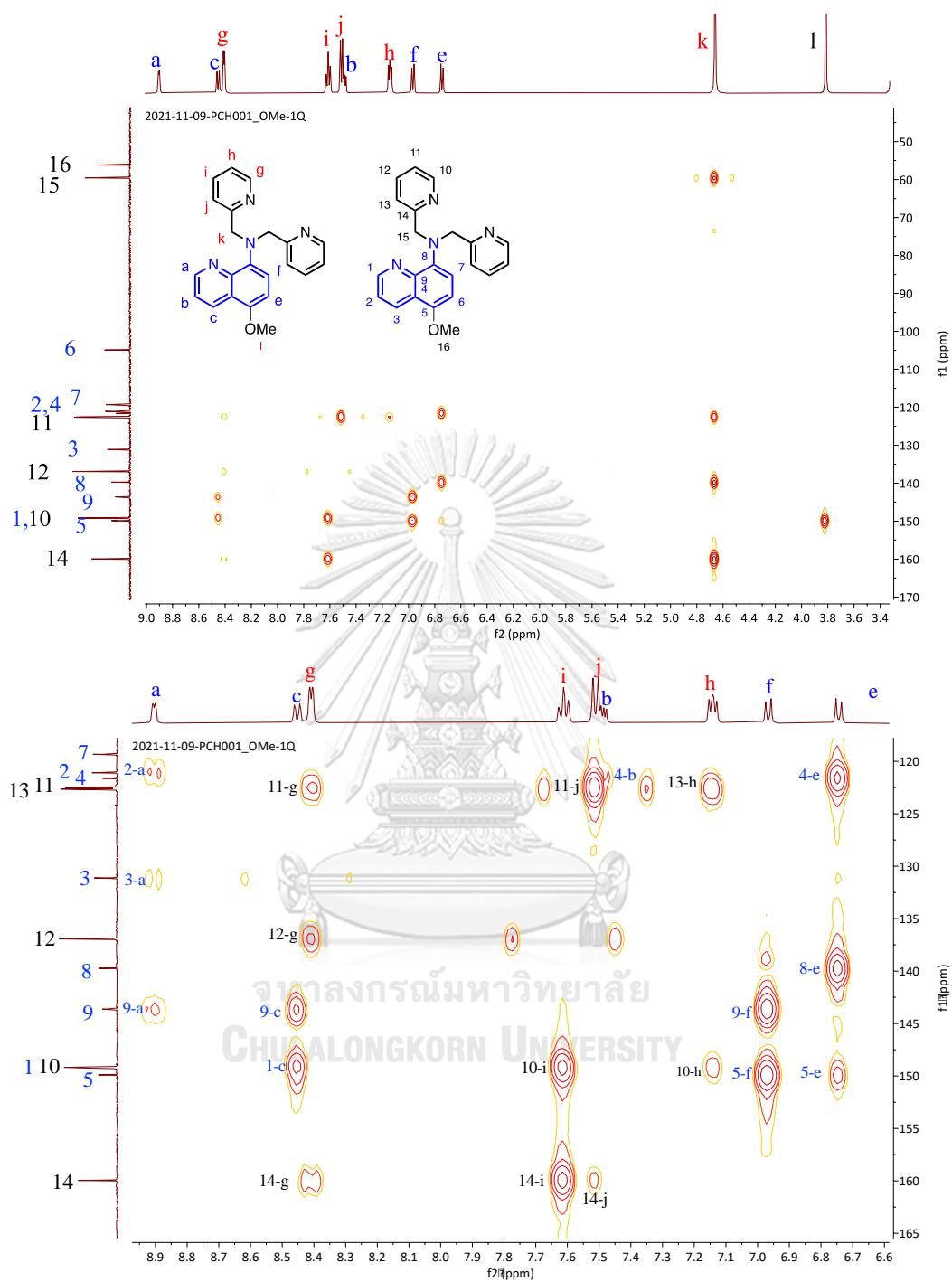


Figure B.15 HMBC spectrum of ligand 1Q-OMe.

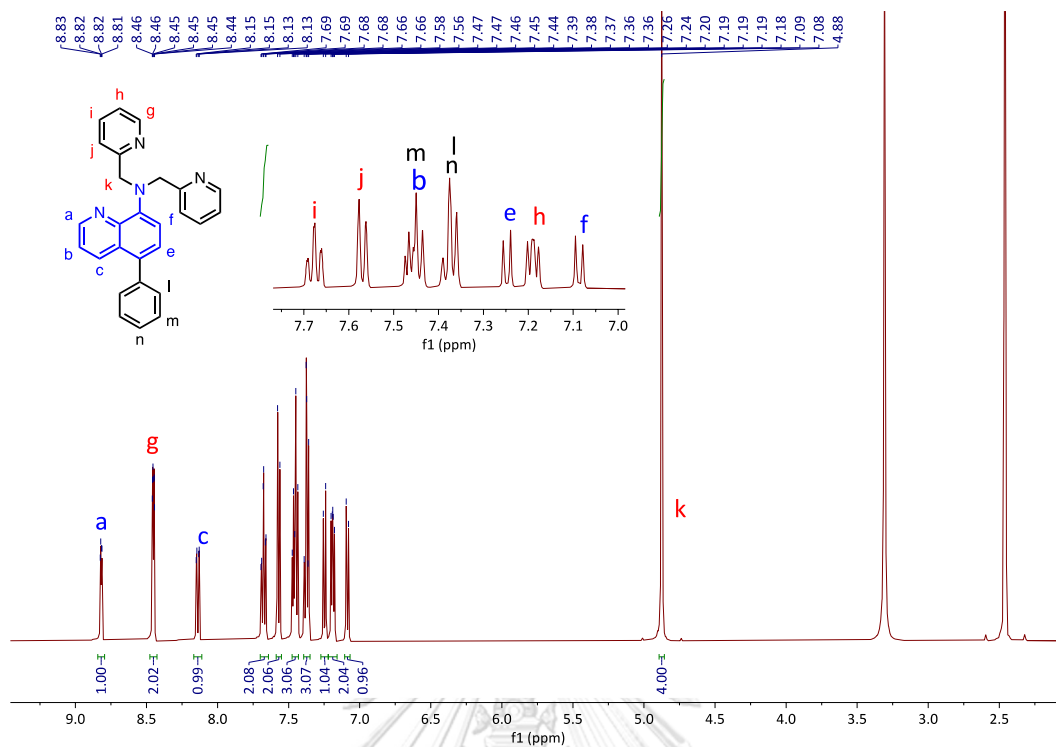


Figure B.16 ^1H NMR spectrum of ligand 1Q-Ph.

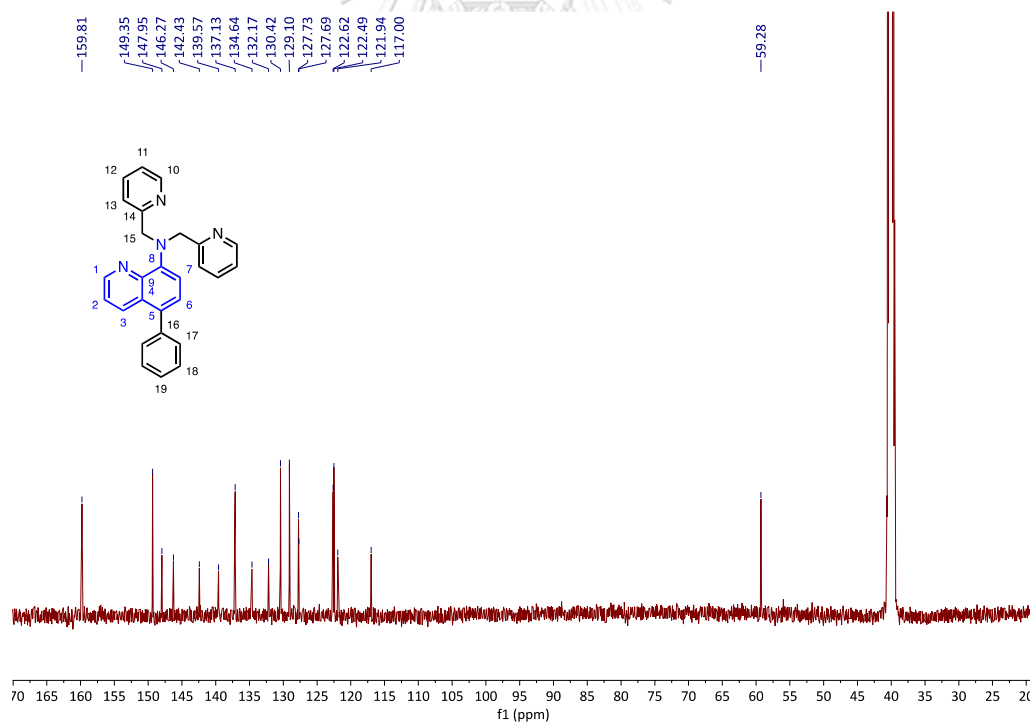


Figure B.17 ^{13}C NMR spectrum of ligand 1Q-Ph.

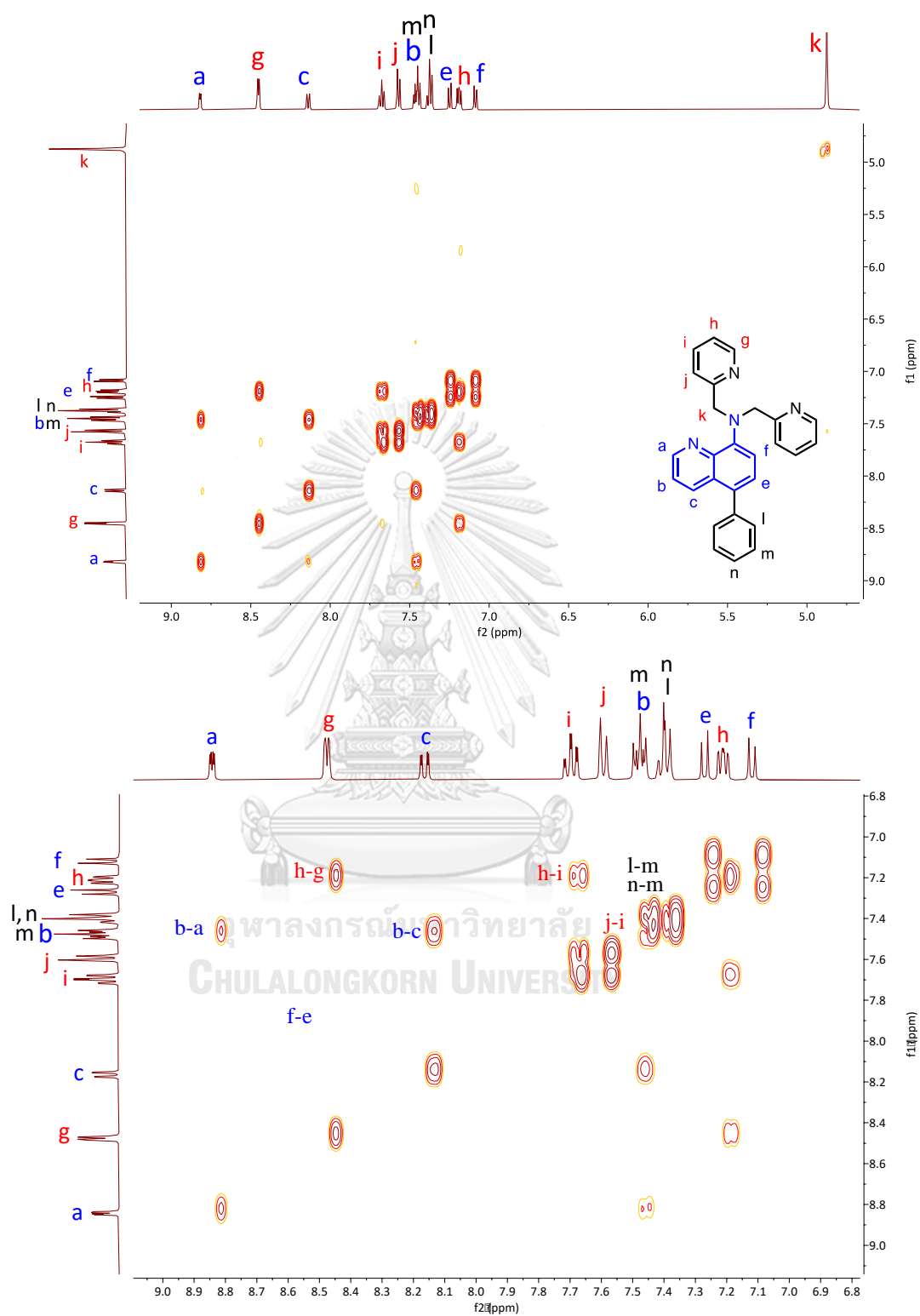


Figure B.18 COSY spectrum of ligand 1Q-Ph.

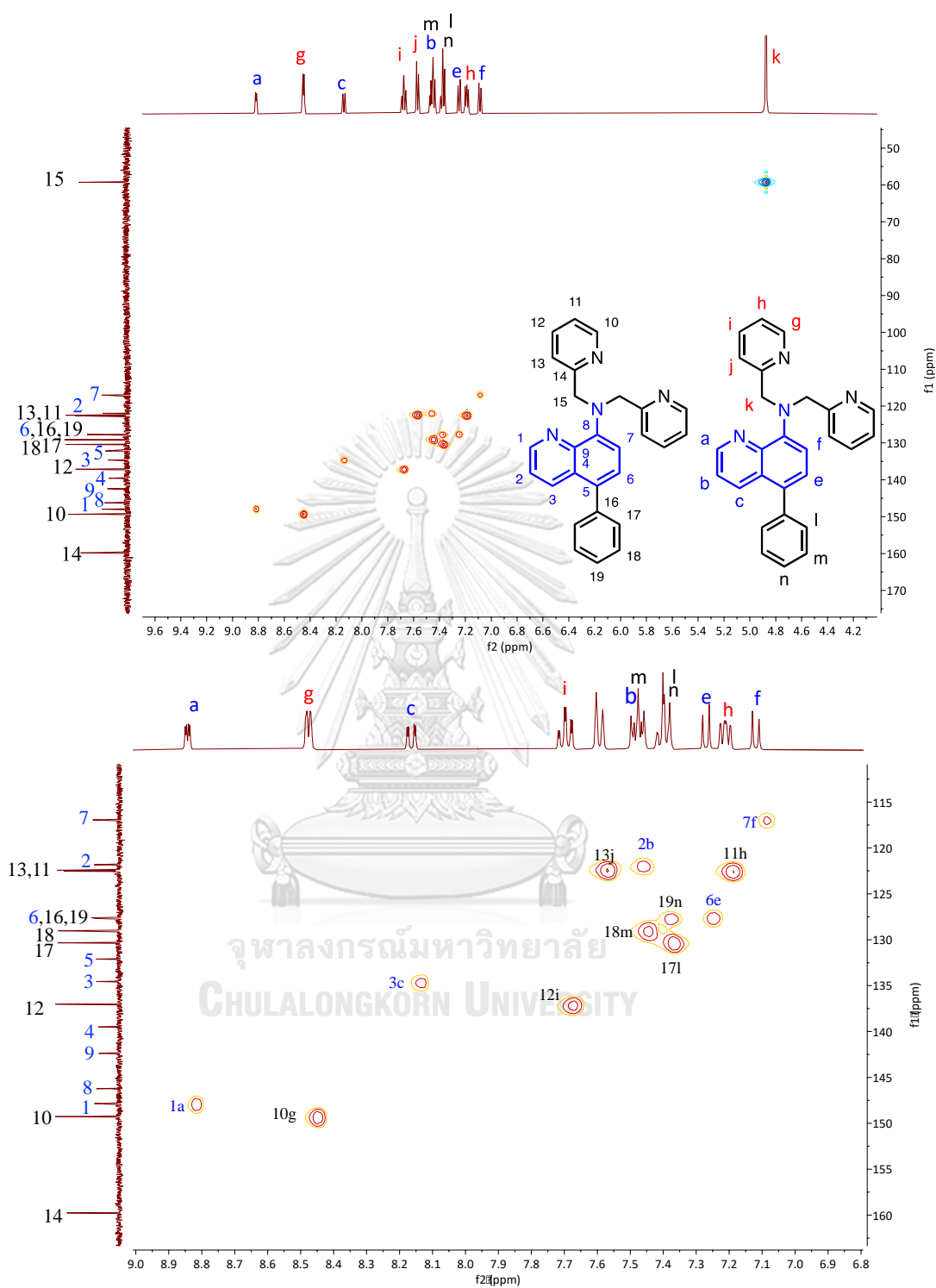


Figure B.19 HSQC spectrum of ligand 1Q-Ph.

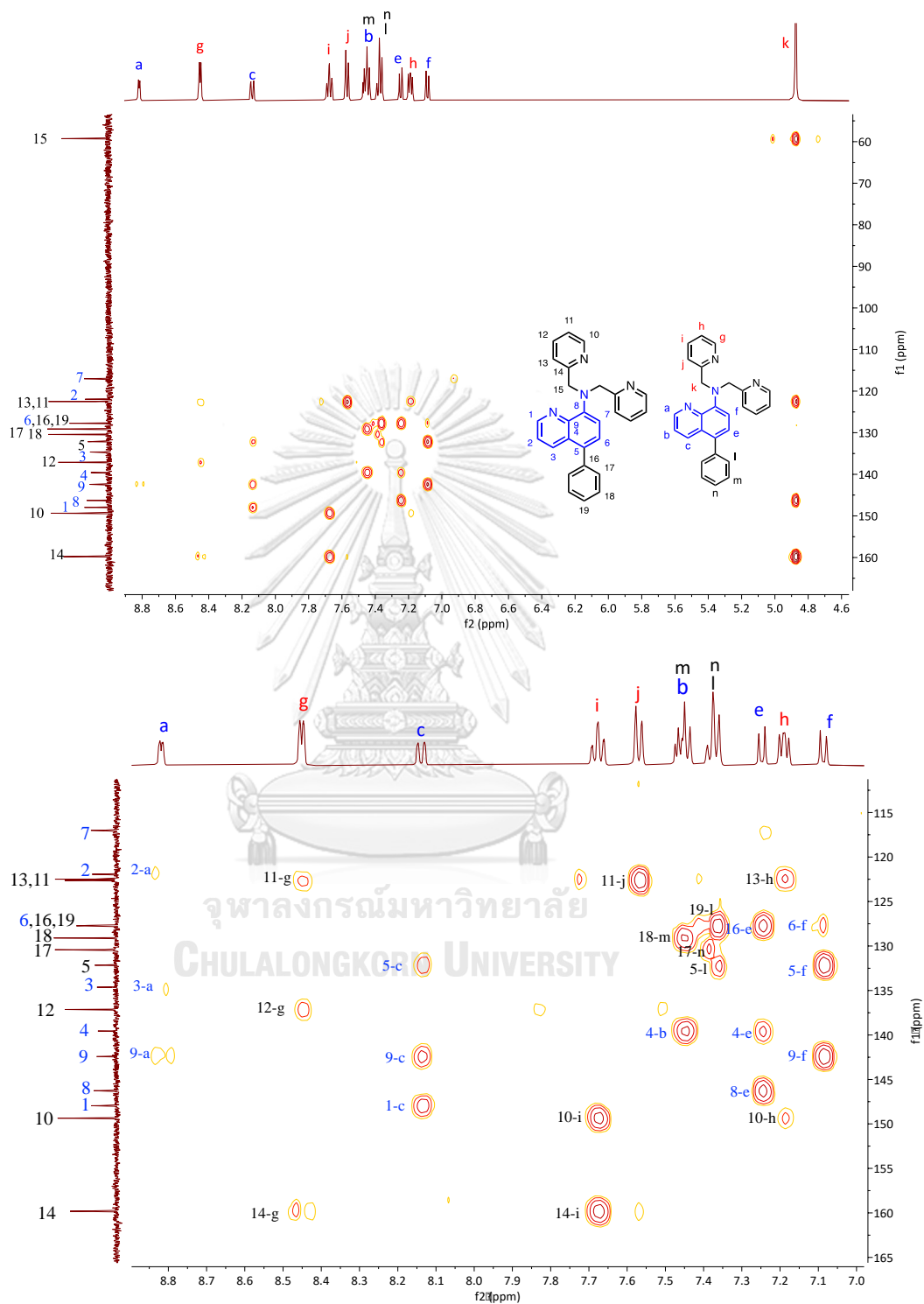
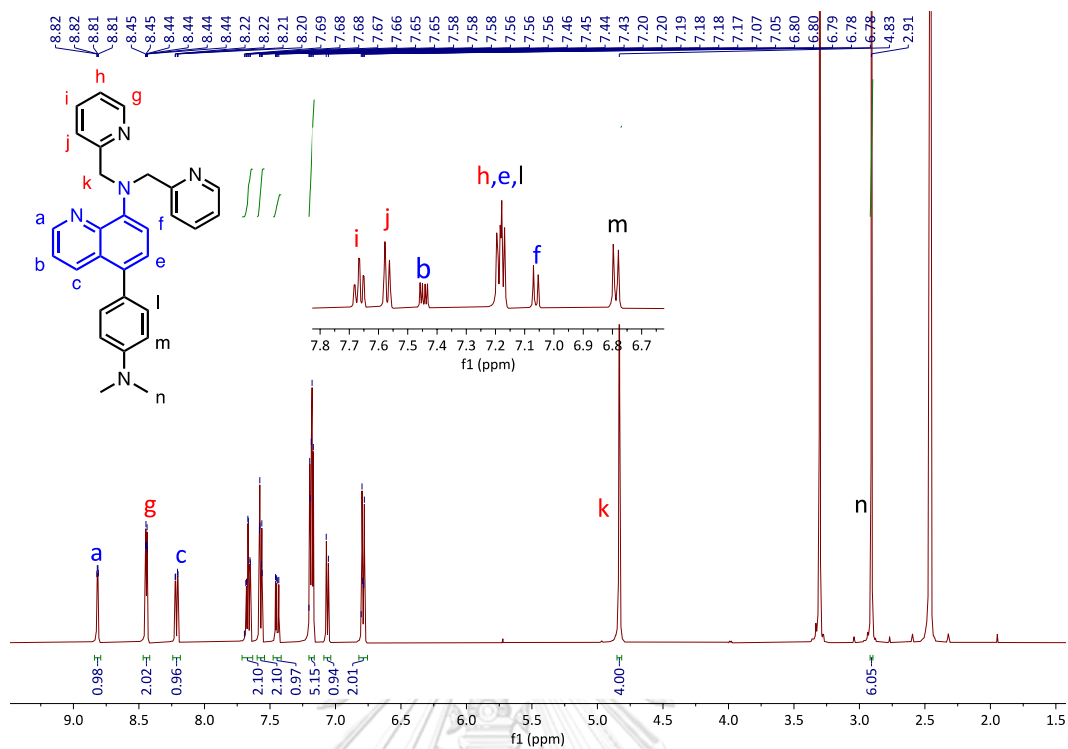
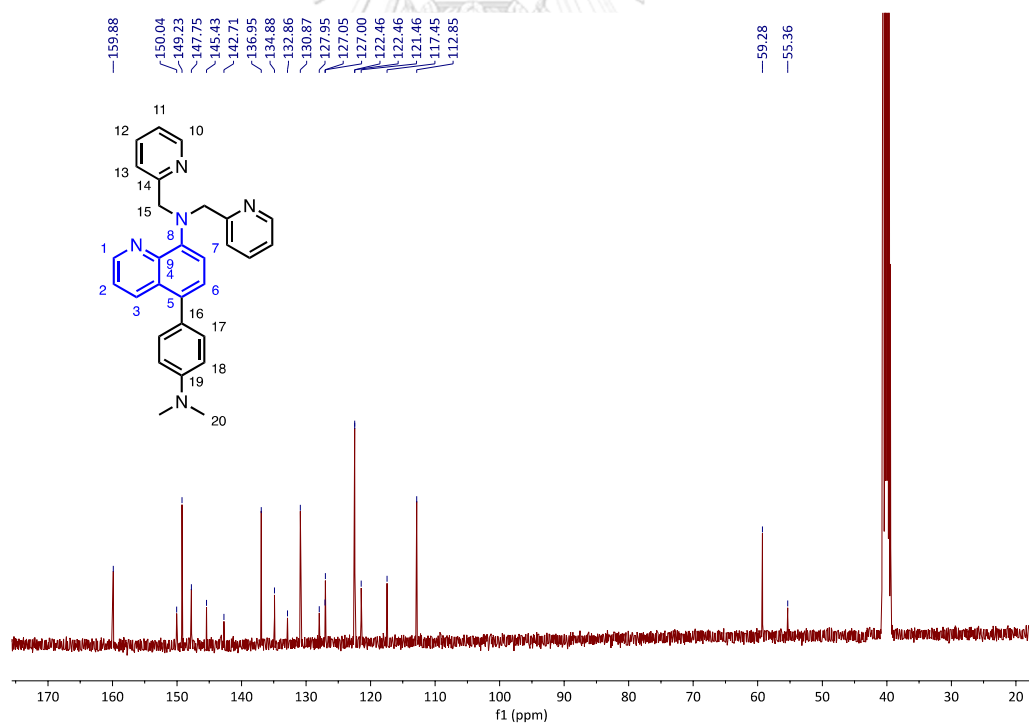


Figure B.20 HMBC spectrum of ligand 1Q-Ph.

Figure B.21 ^1H NMR spectrum of ligand 1Q-DMAP.Figure B.22 ^{13}C NMR spectrum of ligand 1Q-DMAP.

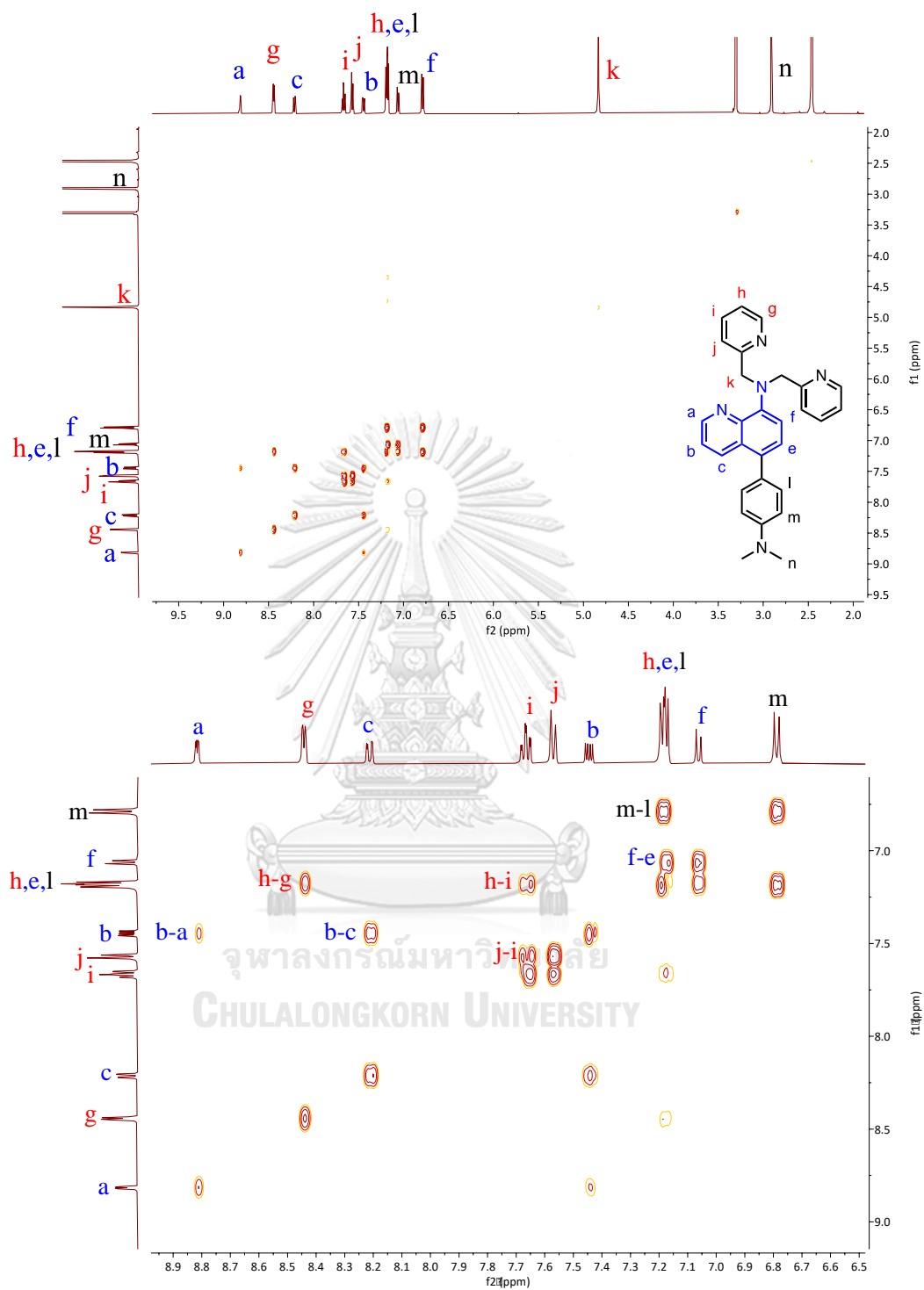


Figure B.23 COSY spectrum of ligand 1Q-DMAP.

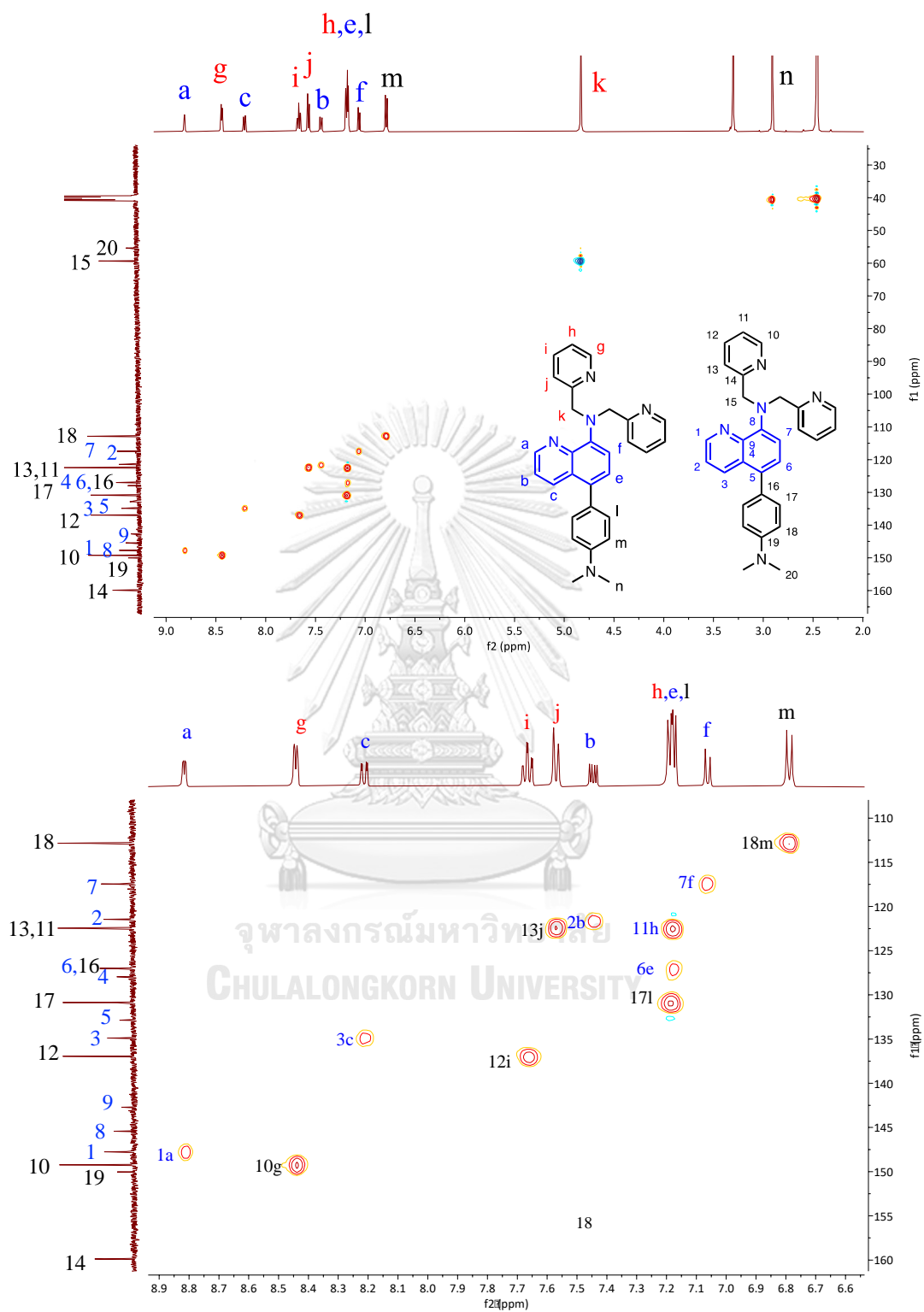


Figure B.24 HSQC spectrum of ligand 1Q-DMAP.

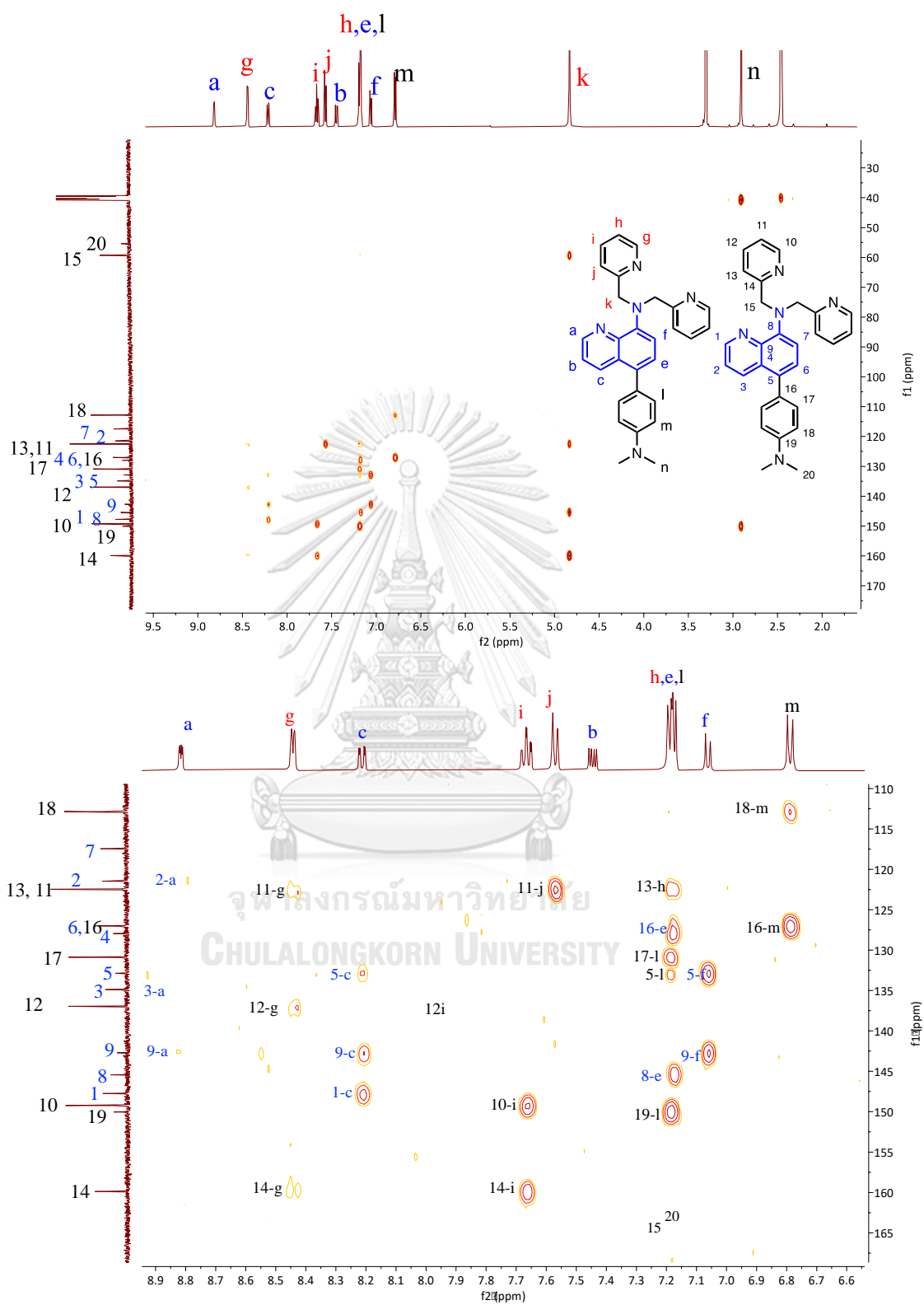


Figure B.25 HMBC spectrum of ligand 1Q-DMAP.

B.1.2 IR spectra

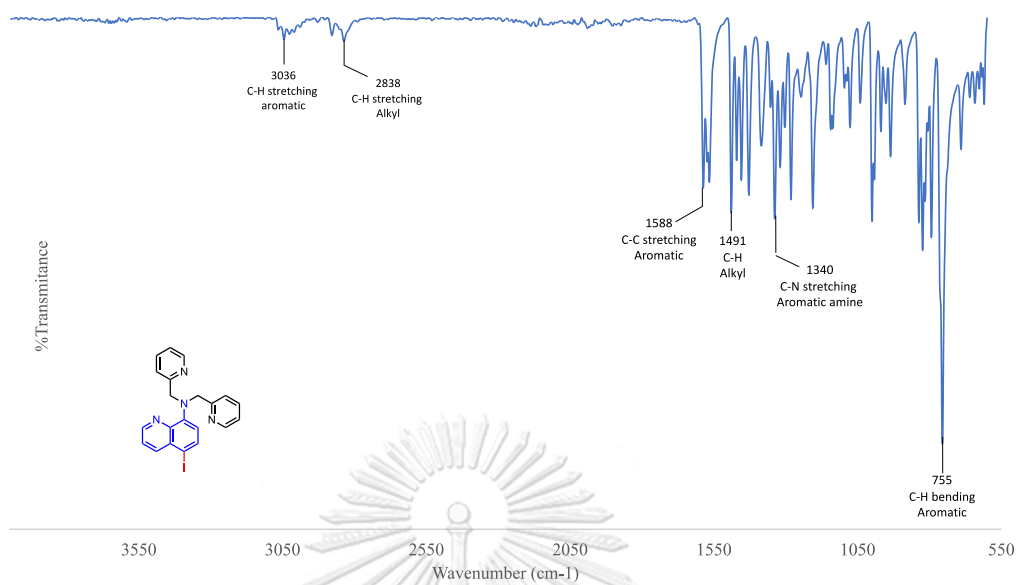


Figure B.26 IR spectrum of ligand 1Q-I.

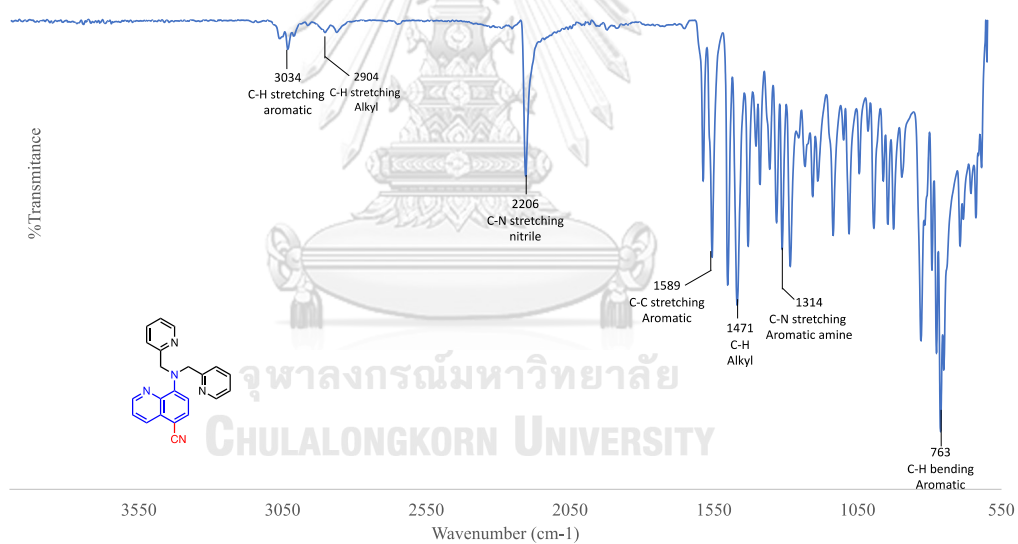


Figure B.27 IR spectrum of ligand 1Q-CN.

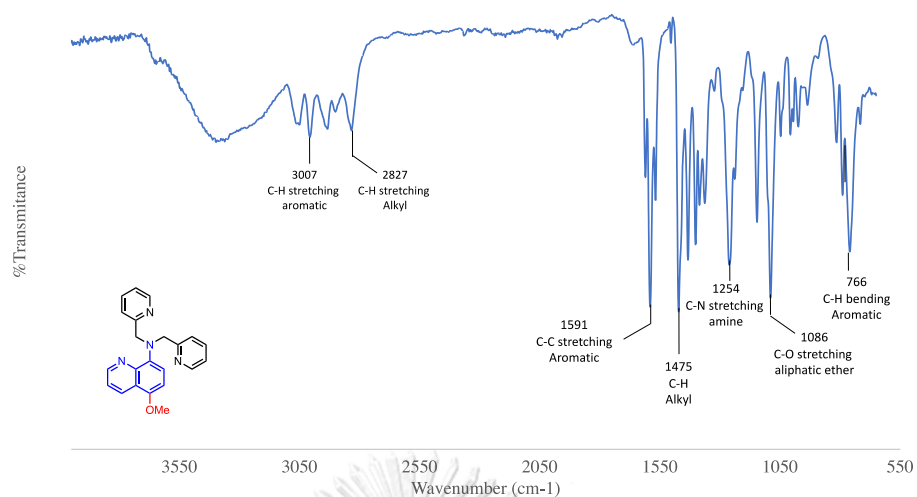


Figure B.28 IR spectrum of ligand 1Q-OMe.

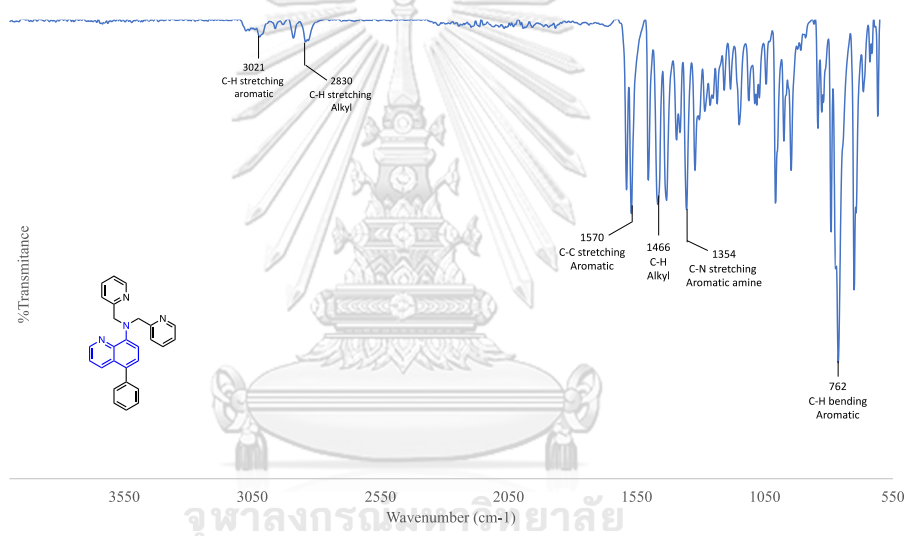


Figure B.29 IR spectrum of ligand 1Q-Ph.

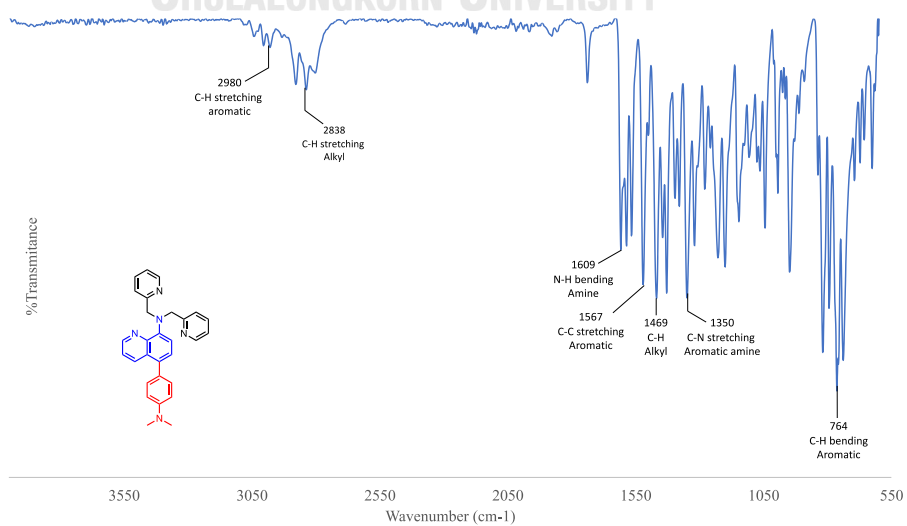


Figure B.30 IR spectrum of ligand 1Q-DMAP.

B.1.3 Mass spectrum

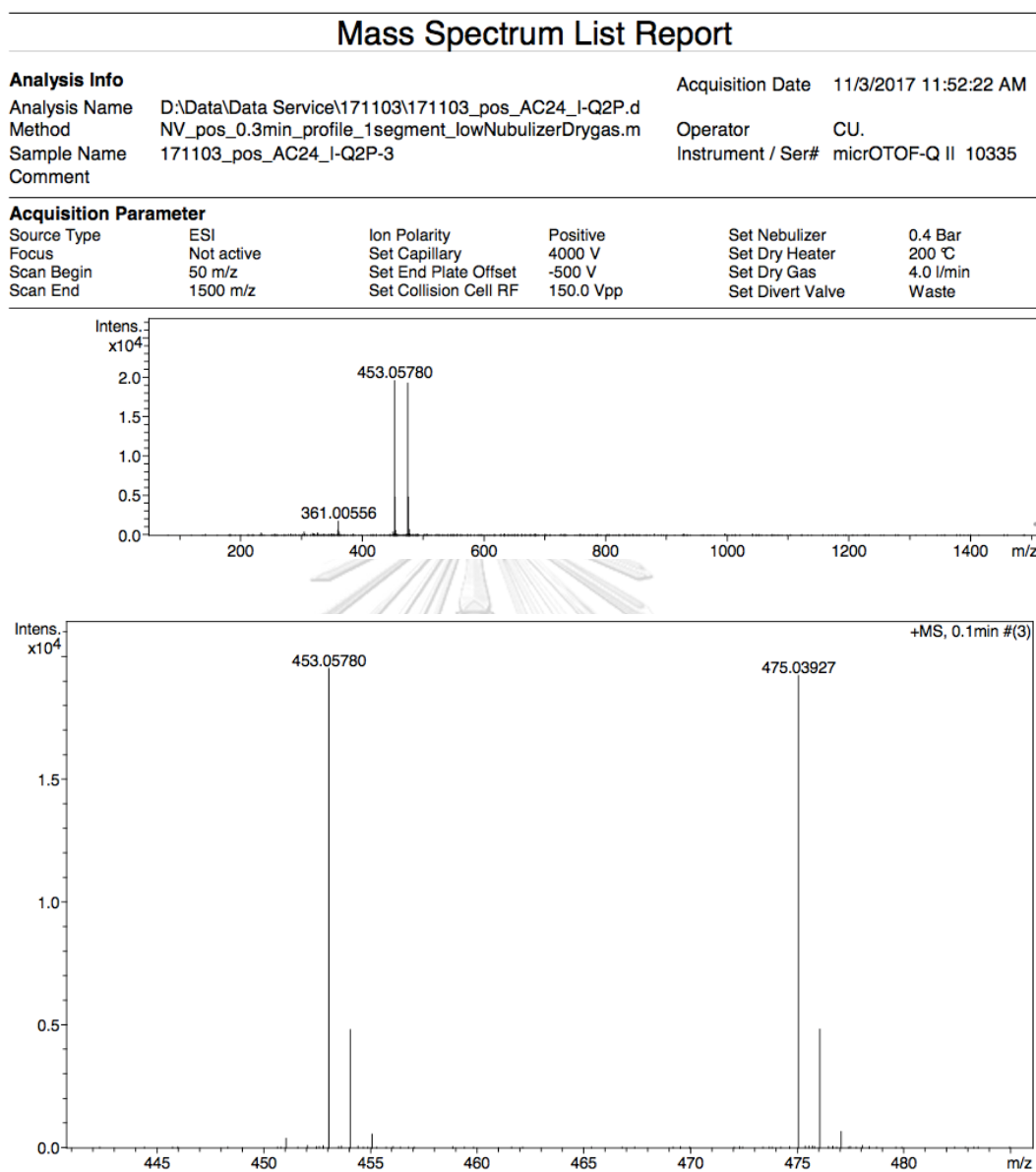


Figure B.31 Mass spectrum of ligand 1Q-I.

Mass Spectrum List Report

Analysis Info
Analysis Name D:\Data\Data Service\190813\CN-Q2P_RC4_01_2902.d
Method nv_pos_6min_profile_wguardcol_190624.m
Sample Name CN-Q2P
Comment
Acquisition Date 8/13/2019 8:49:36 PM
Operator CU.
Instrument / Ser# micrOTOF-Q II 10335

Acquisition Parameter

Source Type	ESI	Ion Polarity	Positive	Set Nebulizer	3.0 Bar
Focus	Not active	Set Capillary	4000 V	Set Dry Heater	200 °C
Scan Begin	100 m/z	Set End Plate Offset	-500 V	Set Dry Gas	8.0 l/min
Scan End	1500 m/z	Set Collision Cell RF	250.0 Vpp	Set Divert Valve	Waste

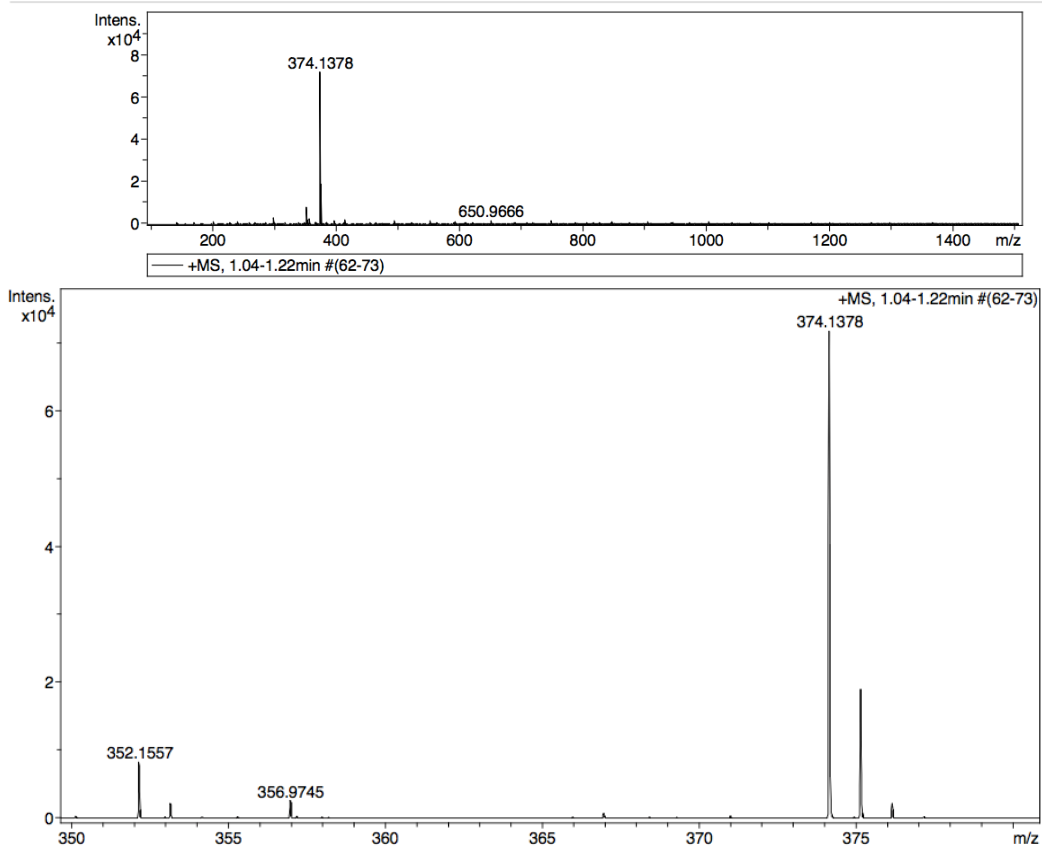


Figure B.32 Mass spectrum of ligand 1Q-CN.

Mass Spectrum List Report

Analysis Info
Analysis Name D:\Data\Data Service\190909\OMe-Q2P_RB4_01_3063.d Acquisition Date 9/9/2019 8:30:19 PM
Method nv_pos_6min_profile_wguardcol_190624.m Operator CU.
Sample Name OMe-Q2P Instrument / Ser# micrOTOF-Q II 10335
Comment

Acquisition Parameter

Source Type	ESI	Ion Polarity	Positive	Set Nebulizer	3.0 Bar
Focus	Not active	Set Capillary	4000 V	Set Dry Heater	200 °C
Scan Begin	100 m/z	Set End Plate Offset	-500 V	Set Dry Gas	8.0 l/min
Scan End	1500 m/z	Set Collision Cell RF	250.0 Vpp	Set Divert Valve	Waste

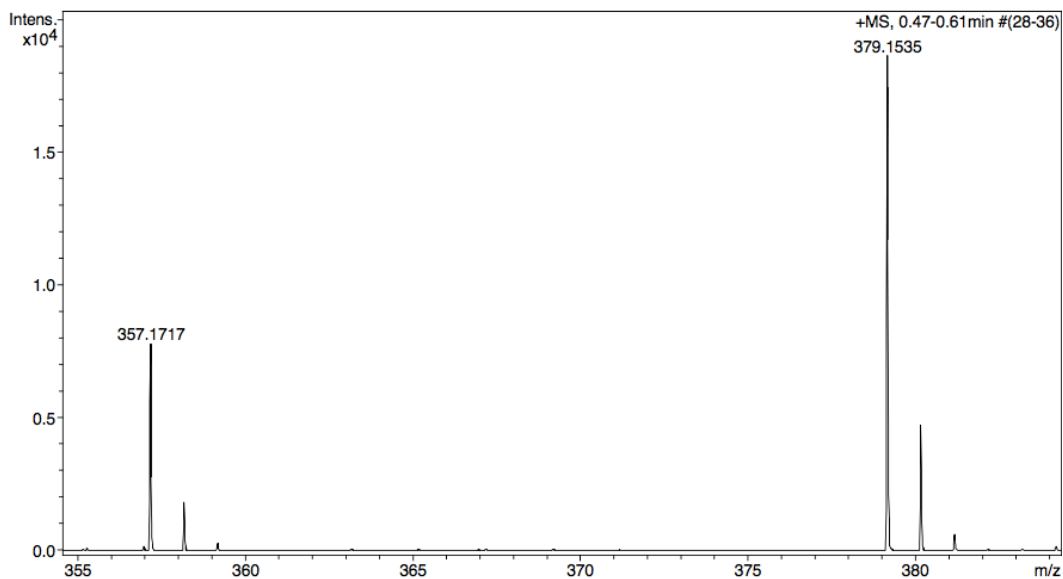
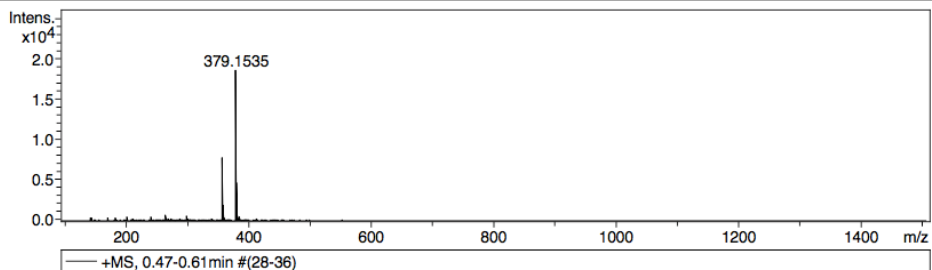


Figure B.33 Mass spectrum of ligand 1Q-OMe.

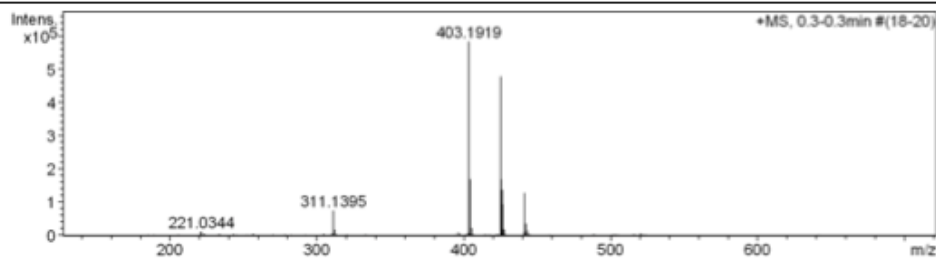
Mass Spectrum List Report

Analysis Info

Analysis Name	OSAP_Ph-Q2P.d	Acquisition Date	10/8/2021 1:42:44 PM
Method	Tune_Low_50-1000_NATTHAPAT2021.m	Operator	Administrator
Sample Name	Ph-Q2P	Instrument	micrOTOF 72
	OSAP		

Acquisition Parameter

Source Type	ESI	Ion Polarity	Positive	Set Corrector Fill	50 V
Scan Range	n/a	Capillary Exit	150.0 V	Set Pulsar Pull	337 V
Scan Begin	50 m/z	Hexapole RF	150.0 V	Set Pulsar Push	337 V
Scan End	3000 m/z	Skimmer 1	45.0 V	Set Reflector	1300 V
		Hexapole 1	24.3 V	Set Flight Tube	9000 V
				Set Detector TOF	2295 V



#	m/z	I	S/N	I %	Res.
1	221.0344	10982	618.1	1.9	4384
2	223.0317	3652	202.0	0.6	4399
3	233.1040	2487	127.8	0.4	4610
4	243.0139	2012	96.6	0.3	4736
5	256.1411	2622	116.3	0.4	4607
6	304.2588	3112	107.4	0.5	4479
7	310.1313	5105	172.2	0.9	4667
8	311.1395	73596	2486.2	12.6	4578
9	312.1426	15991	537.0	2.7	4584
10	313.1463	1908	62.9	0.3	4480
11	396.0777	8820	297.9	1.5	4878
12	397.0811	2442	81.8	0.4	5247
13	402.9272	2138	72.5	0.4	1783
14	403.1919	582904	20126.2	100.0	4574
15	403.7198	2470	84.1	0.4	1981
16	403.9243	1834	62.1	0.3	1600
17	404.1937	168234	5822.5	28.9	4904
18	405.1971	21138	732.3	3.6	5041
19	406.2021	1992	68.0	0.3	4164
20	425.1748	477737	17462.5	82.0	4556
21	425.7161	2111	75.9	0.4	1395
22	426.1771	135811	4976.6	23.3	4761
23	427.1793	17645	647.1	3.0	5043
24	441.1487	126396	4824.8	21.7	4769
25	442.1511	35030	1339.9	6.0	4772
26	443.1487	12880	493.1	2.2	4792
27	444.1482	3021	114.9	0.5	4811
28	488.1310	2499	108.3	0.4	4726
29	520.1570	5231	254.5	0.9	4897
30	521.1599	1767	85.1	0.3	4339

Figure B.34 Mass spectrum of ligand 1Q-Ph.

Mass Spectrum List Report

Analysis Info
Analysis Name D:\Data\Data Service\180316_pos_Dmap-Q2P.d
Method NV_pos_0.3min_profile_1segment_lowNubulizerDrygas.m
Sample Name 180316_pos_Dmap-Q2P
Comment
Acquisition Date 3/16/2018 2:54:03 PM
Operator CU.
Instrument / Ser# micrOTOF-Q II 10335

Acquisition Parameter

Source Type	ESI	Ion Polarity	Positive	Set Nebulizer	0.4 Bar
Focus	Not active	Set Capillary	4000 V	Set Dry Heater	200 °C
Scan Begin	50 m/z	Set End Plate Offset	-500 V	Set Dry Gas	4.0 l/min
Scan End	1500 m/z	Set Collision Cell RF	150.0 Vpp	Set Divert Valve	Waste

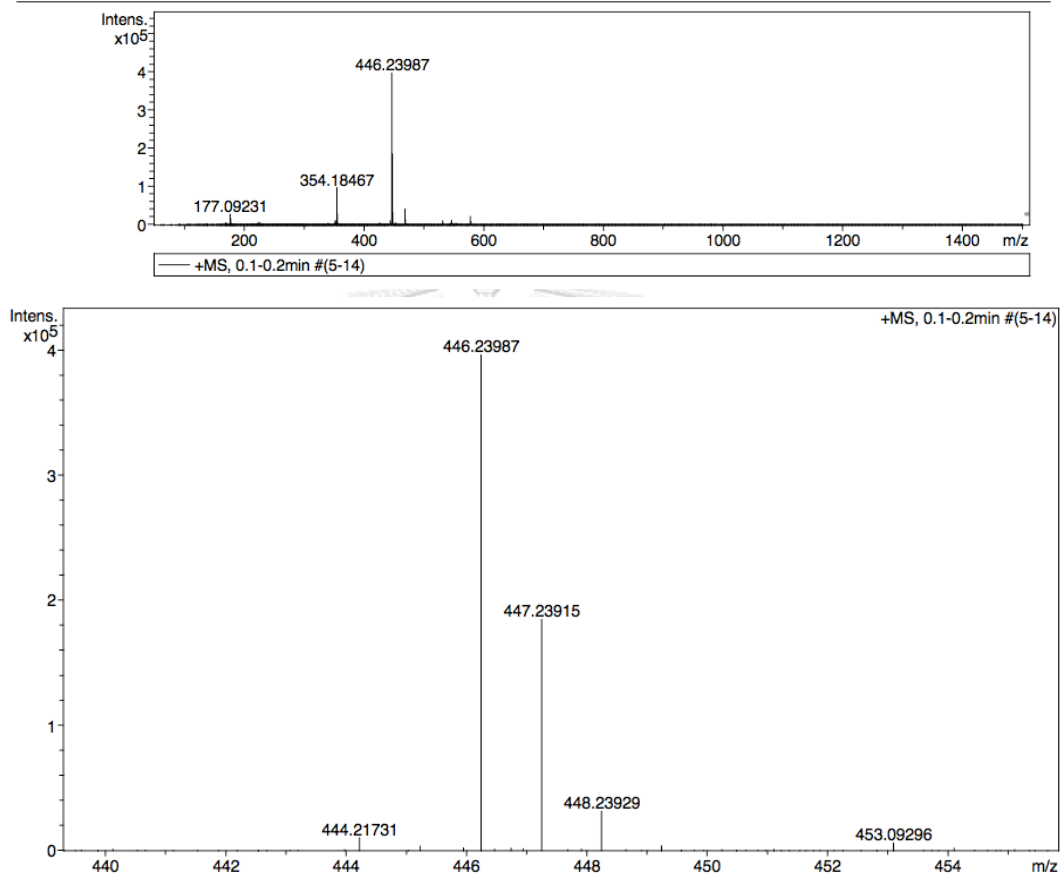


Figure B.35 Mass spectrum of ligand 1Q-DMAP.

B.1.4 UV-Visible spectroscopy

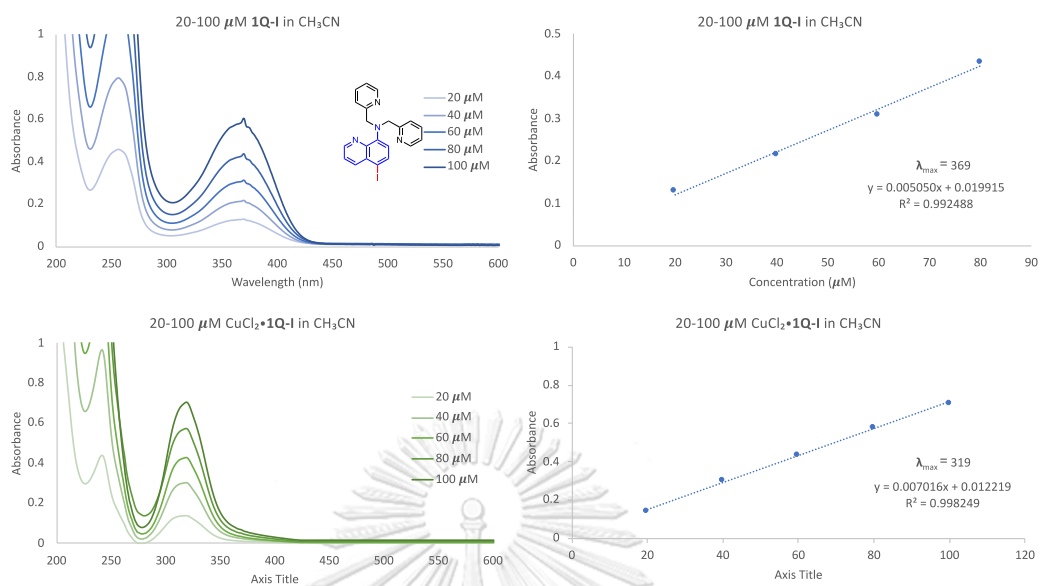


Figure B.36 Absorption spectrum of 1Q-I and $\text{CuCl}_2 \cdot 1\text{Q-I}$.

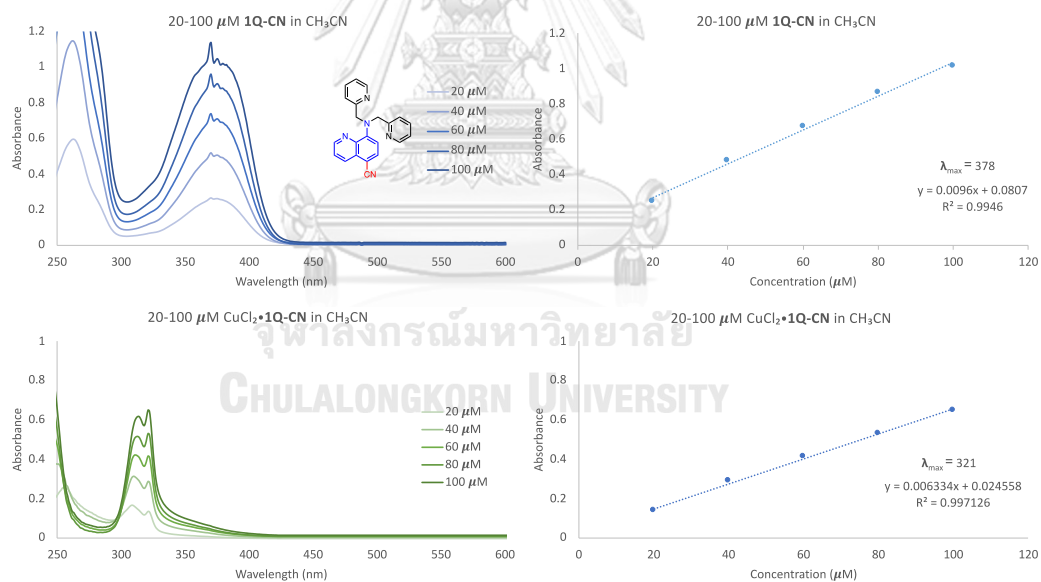


Figure B.37 Absorption spectrum of 1Q-CN and $\text{CuCl}_2 \cdot 1\text{Q-CN}$.

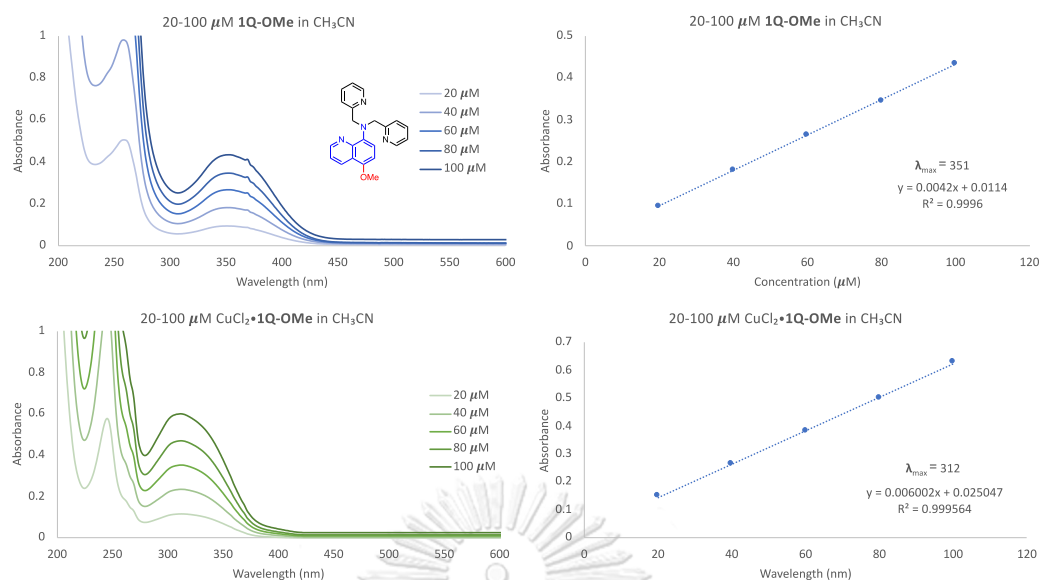


Figure B.38 Absorption spectrum of 1Q-OMe and $\text{CuCl}_2 \cdot 1\text{Q-OMe}$.

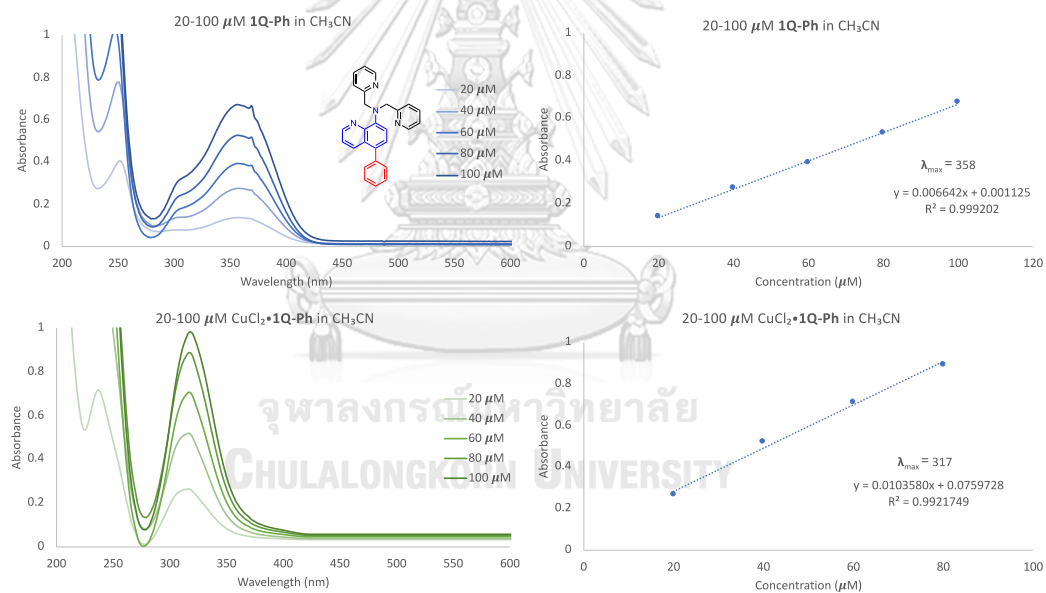


Figure B.39 Absorption spectrum of 1Q-Ph and $\text{CuCl}_2 \cdot 1\text{Q-Ph}$.

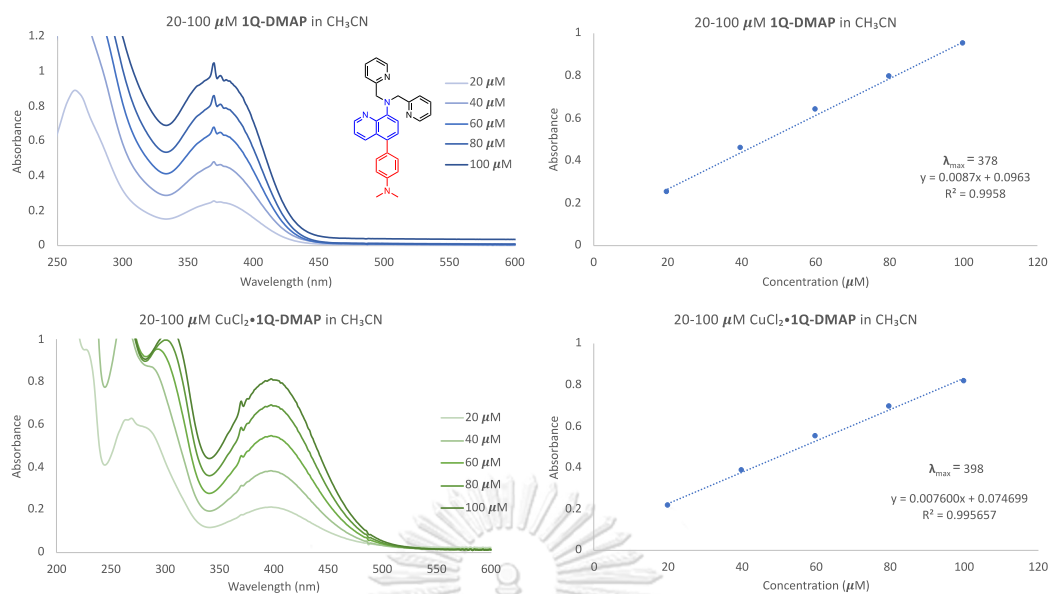


Figure B.40 Absorption spectrum of 1Q-DMAP and CuCl₂•1Q-DMAP.

B.2 Study of catalytic properties for chlorosulfonylation (C-S formation)

B.2.1 Reversibility study of complexation and decomplexation

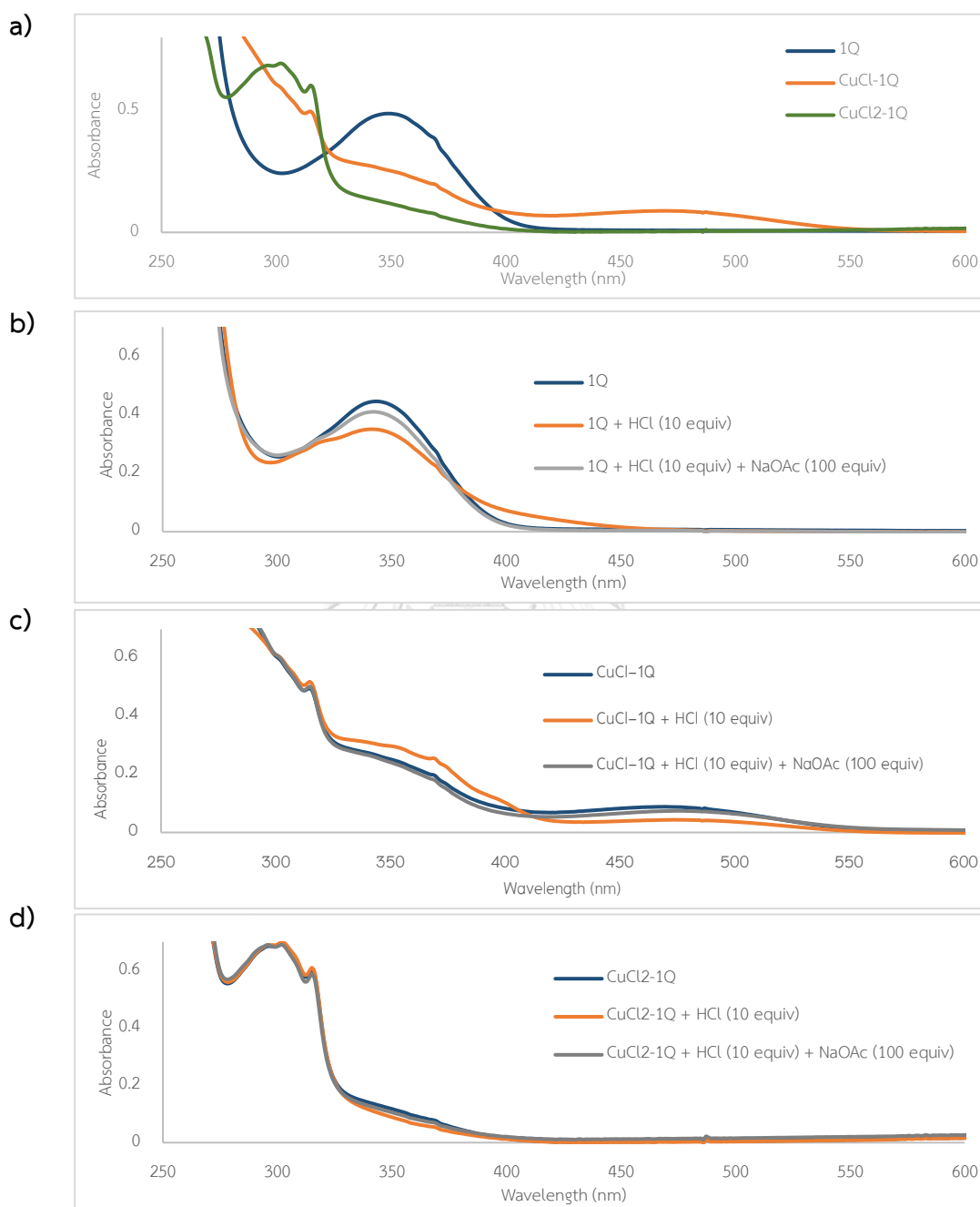


Figure B.41 Absorption spectra of a) 0.1 mM **1Q**, CuCl·**1Q** and CuCl₂·**1Q** complexes and absorption spectra of b) 0.1 mM **1Q**, c) CuCl·**1Q** and d) CuCl₂·**1Q** in CH₂Cl₂ in reversibility study of complexation and decomplexation under acidic and basic conditions.

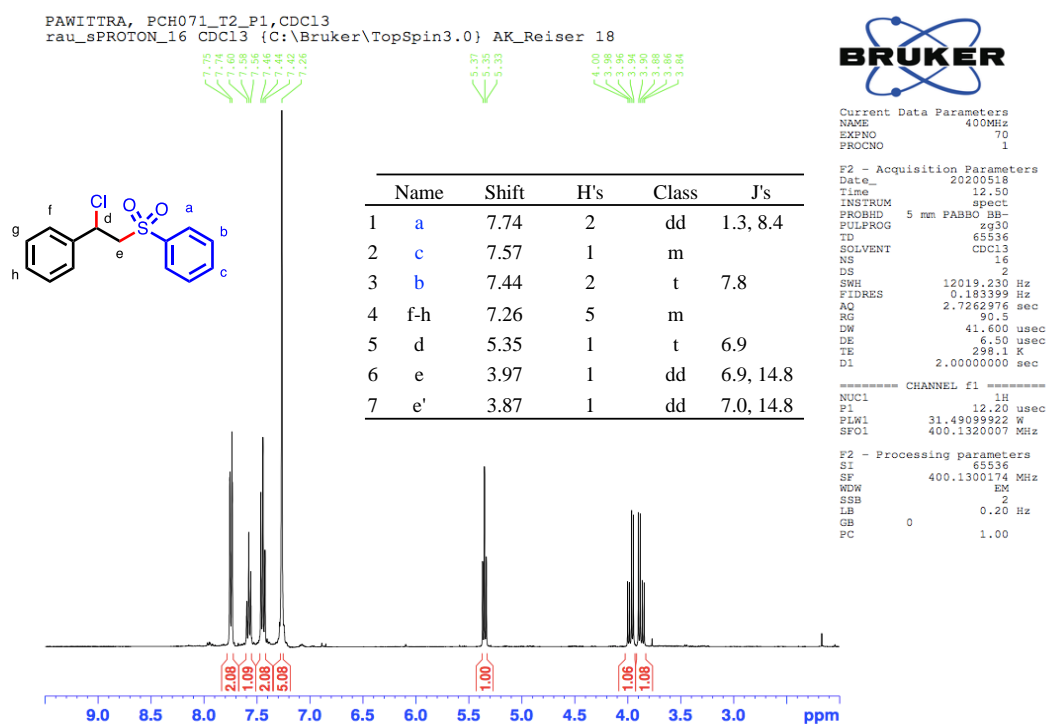
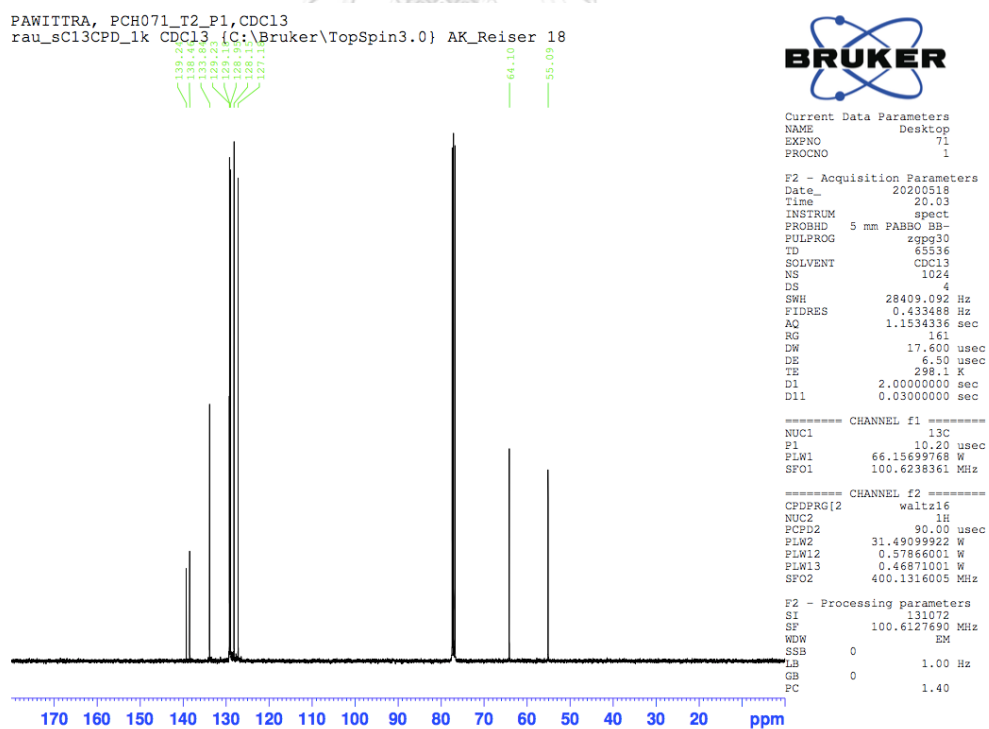
Table B.1 Catalyst comparison for chlorosulfonylation of activated and inactivated alkene in various conditions.^a

Alkene + $\xrightarrow[\text{solvent, rt, N}_2, \text{LED}]{\text{photocatalyst}}$ or

1 2a; R=H
2b; R=Me 3 4

			Activated alkene (Condition A)		Unactivated alkene (Condition B)		
Solvent	Photocatalyst (mol%)	LED					
ACN	[Cu ^{II} (dap)Cl ₂] (1)	530 nm	95%, 24 h ^[c]	Polymerized	64% (64:0), 16 h	86% ^[c] 83% ^[a] 48 h	N.R. ^[c]
	[Cu ^{II} (dmp) ₂ Cl]Cl (2)	455 nm	97%, 30 h ^[d]	-	-	15%, 48 h ^[d]	-
	Cu ^{II} Cl ₂ (2)/1Q (2)	455 nm	49%, 24 h, 83%, 48 h	52% (41:11), 24 h ^[b]	92% (54:38), 16 h	95%, 24 h ^[b]	35%, 48 h
DCM	[Cu ^{II} (dap)Cl ₂] (1)	530 nm	58%, 24 h	-	-	6%, 48 h	-
	[Cu ^{II} (dap)Cl ₂] (2)	455 nm	100%, 24 h	35%+polymerized, 24 h	60% (58:2), 16 h	27%, 24 h	11%, 48 h
	Cu ^{II} Cl ₂ (2)/1Q (2)	455 nm	60%, 24 h, 91%, 48 h	100% (85:15), 24 h	94% (51:43), 16 h	96%, 24 h ^[b]	68%, 48 h ^[b]

^aGeneral reaction conditions: **2a** or **2b** (500 μmol, 1.00 equiv.), photocatalyst (2.00 mol%), in CH₂Cl₂ (dry, degassed, 2.00 mL) irradiation under specified LED under N₂ atmosphere for giving reaction time. Condition A; 1.00 equivalent of Olefin (500 μmol) was used. Condition B; Olefin 2.00 equivalent of Olefin (1.00 mmol), and 1.00 equivalent of Na₂CO₃ (500 μmol) were used. Determined by ¹H NMR yield using 1,3,5-trimethoxybenzene or toluene as an internal standard. ^bIsolated yields are given. ^cref. *ACS Catal.* **2019**, 9, 1103–1109. ^dref. *Eur. J. Org. Chem.* **2020**, 1523–1533.

B.2.2 ^1H NMR and ^{13}C spectraFigure B.42 ^1H NMR spectrum of (1-chloro-2-(phenylsulfonyl)ethyl)benzene, **3aa**.Figure B.43 ^{13}C NMR spectrum of (1-chloro-2-(phenylsulfonyl)ethyl)benzene, **3aa**.

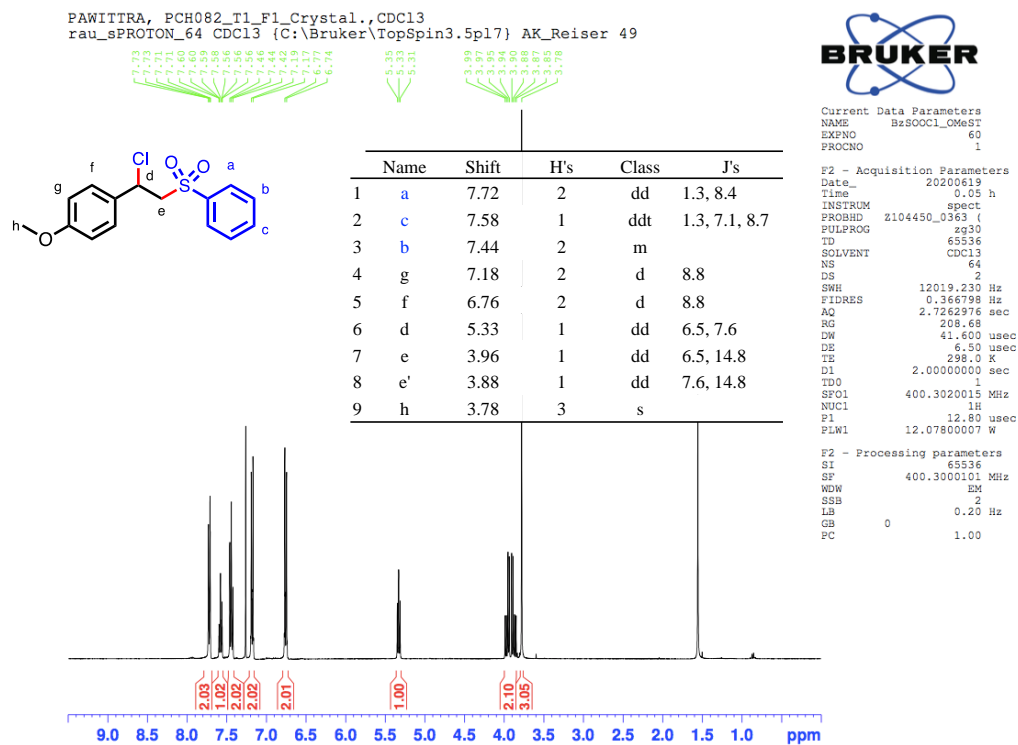


Figure B.44 ^1H NMR spectrum of 1-(1-chloro-2-(phenylsulfonyl)ethyl)-4-methoxybenzene, **3ba**.

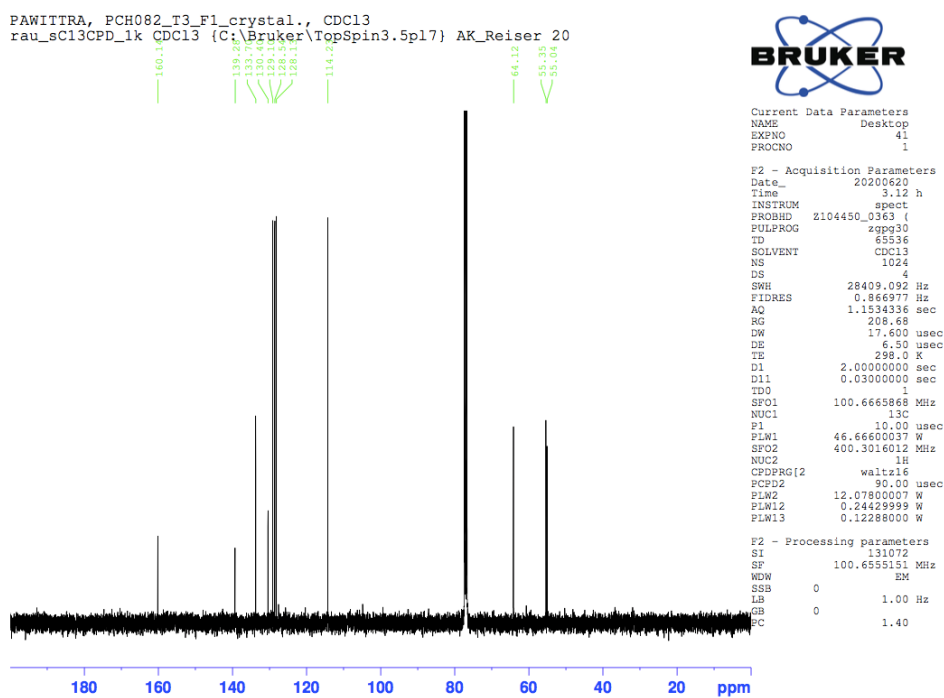


Figure B.45 ^{13}C NMR spectrum of 1-(1-chloro-2-(phenylsulfonyl)ethyl)-4-methoxybenzene, **3ba**.

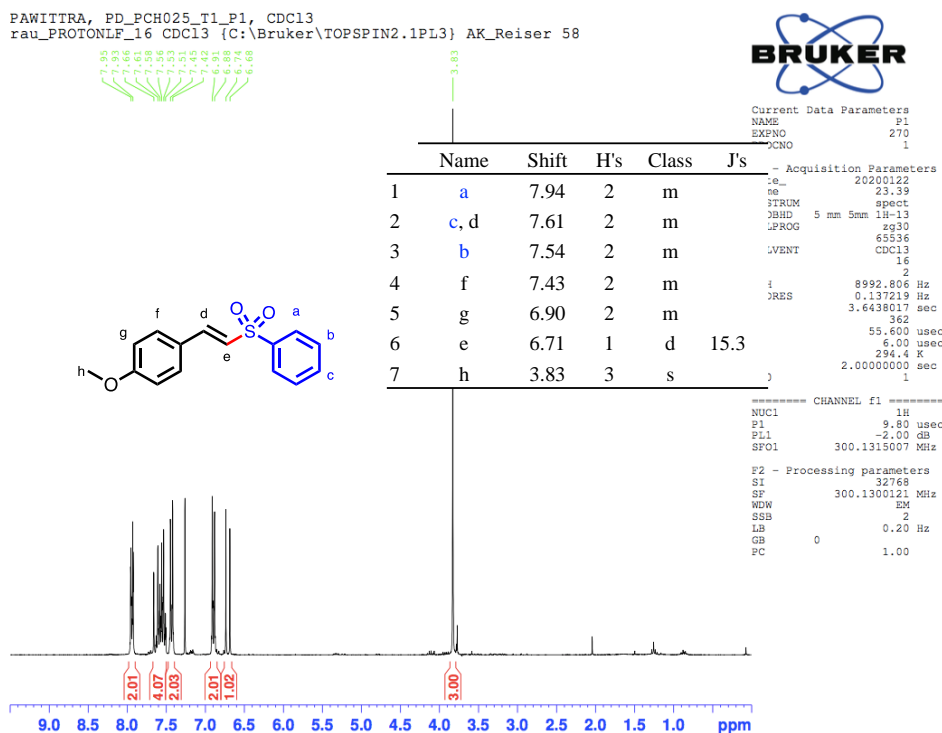


Figure B.46 ^1H NMR spectrum of (*E*)-1-methoxy-4-(2-(phenylsulfonyl)vinyl)benzene, (*E*)-4ba.

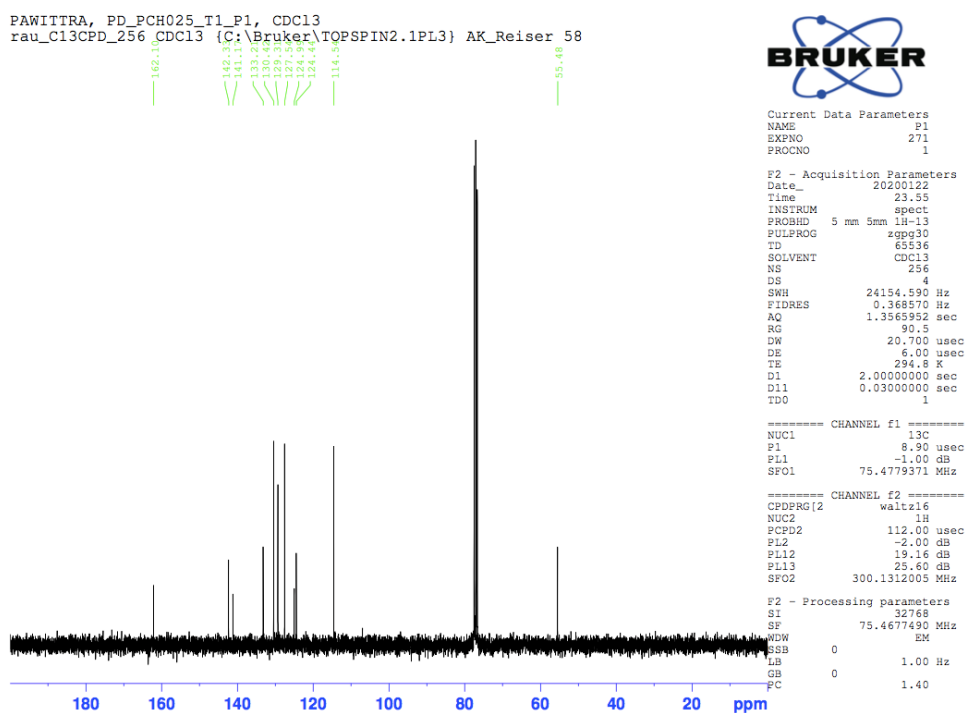


Figure B.47 ^{13}C NMR spectrum of (*E*)-1-methoxy-4-(2-(phenylsulfonyl)vinyl)benzene, (*E*)-4ba.

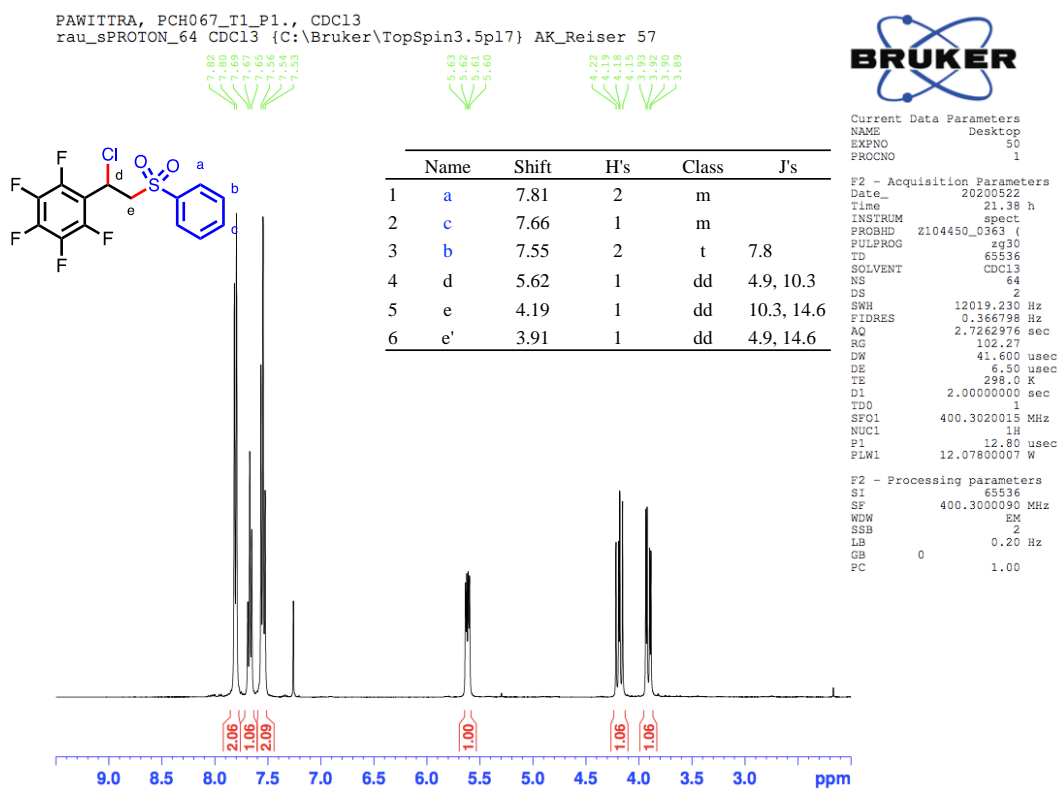


Figure B.48 ^1H NMR spectrum of 1-(1-chloro-2-(phenylsulfonyl)ethyl)-2,3,4,5,6-pentafluorobenzene, **3ca**.

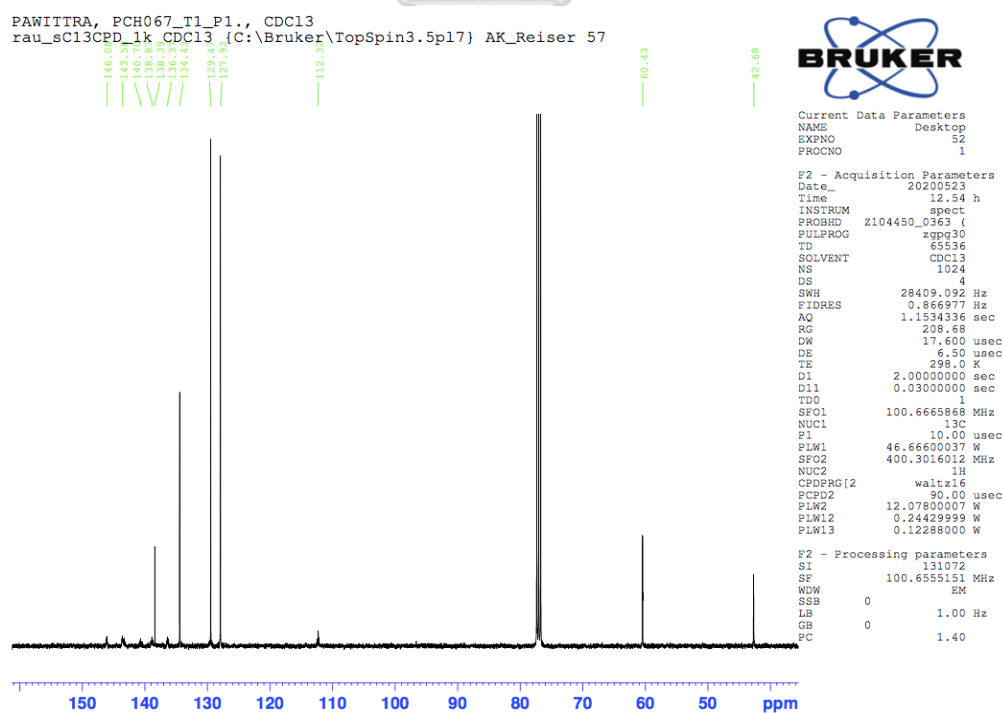


Figure B.49 ^{13}C NMR spectrum of 1-(1-chloro-2-(phenylsulfonyl)ethyl)-2,3,4,5,6-pentafluorobenzene, **3ca**.

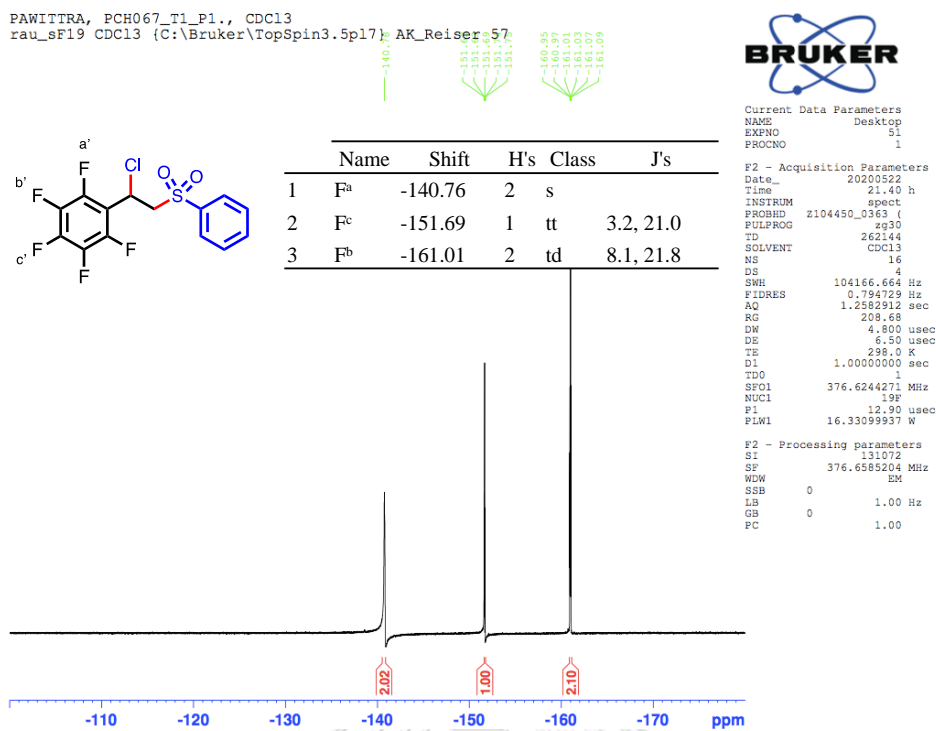


Figure B.50 ^{19}F NMR spectrum of 1-(1-chloro-2-(phenylsulfonyl)ethyl)-2,3,4,5,6-pentafluorobenzene, **3ca**.

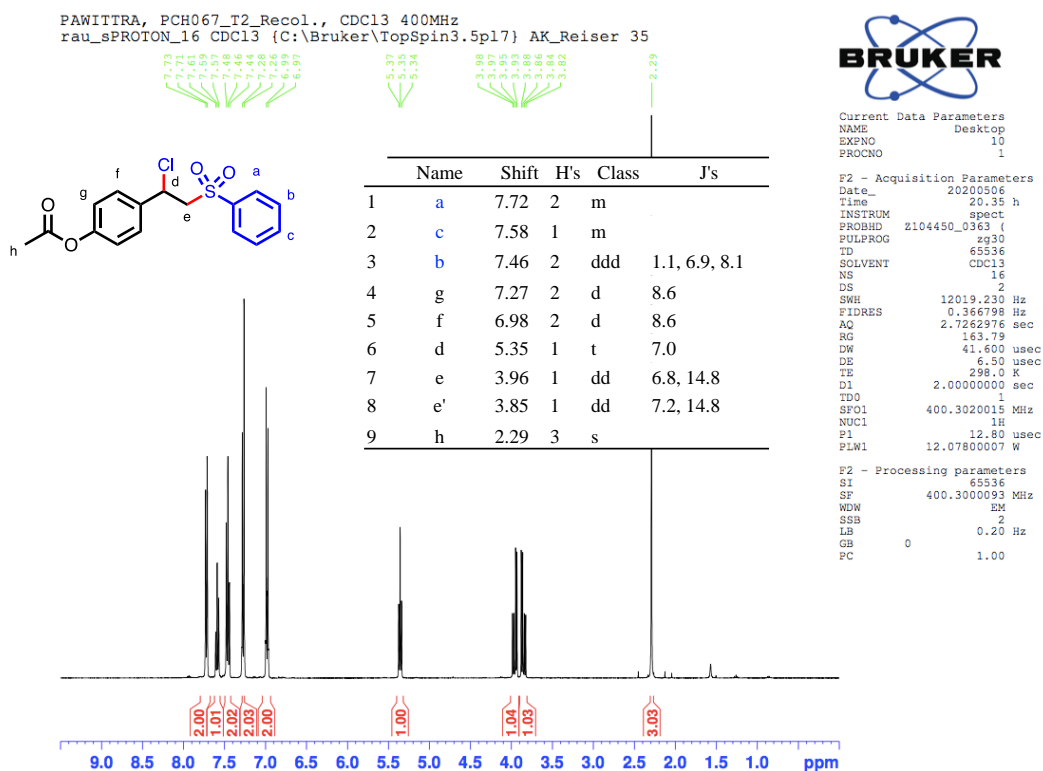


Figure B.51 ^1H NMR spectrum of 4-(1-chloro-2-(phenylsulfonyl)ethyl)phenyl acetate, 3da.

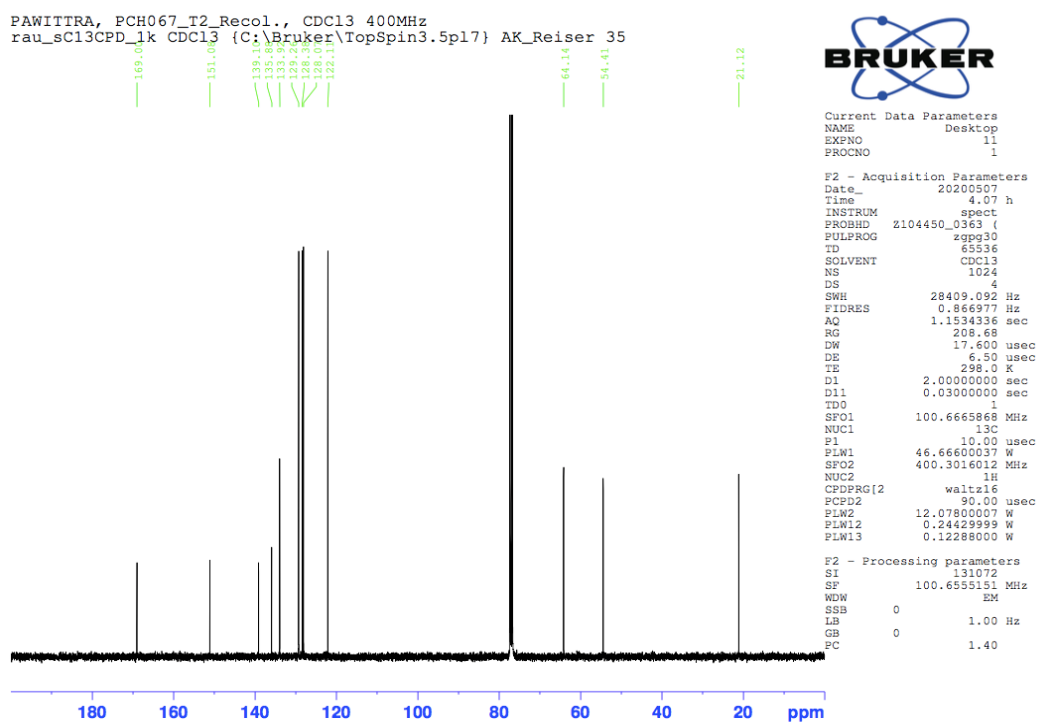


Figure B.52 ^{13}C NMR spectrum of 4-(1-chloro-2-(phenylsulfonyl)ethyl)phenyl acetate, 3da.

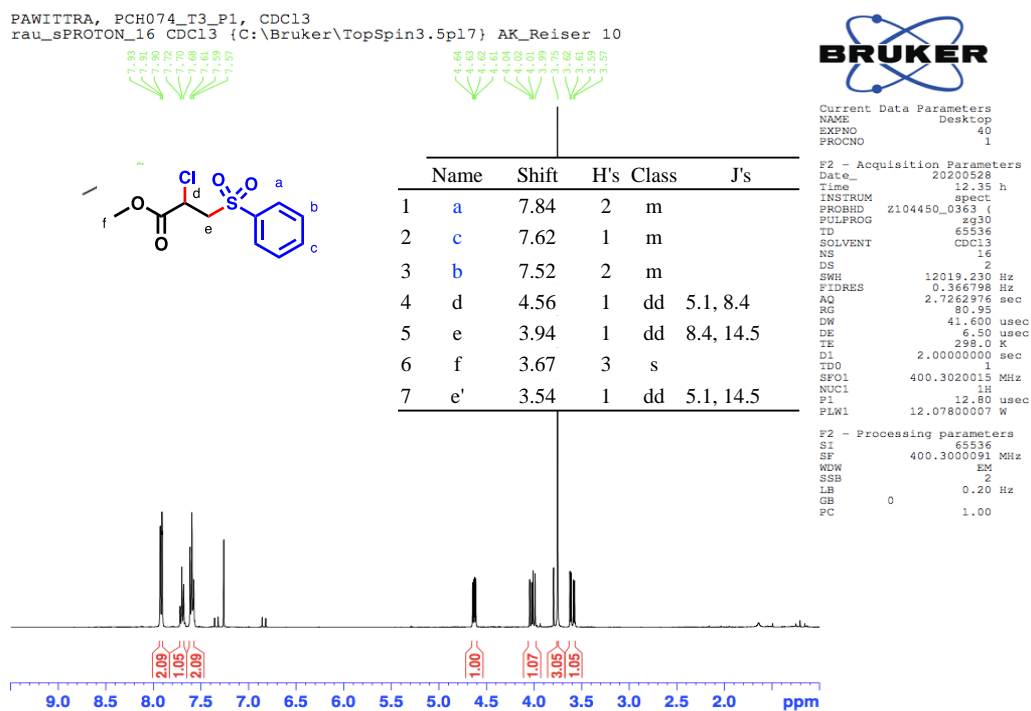


Figure B.53 ^1H NMR spectrum of methyl 2-chloro-3-(phenylsulfonyl)propanoate, **3ea**.

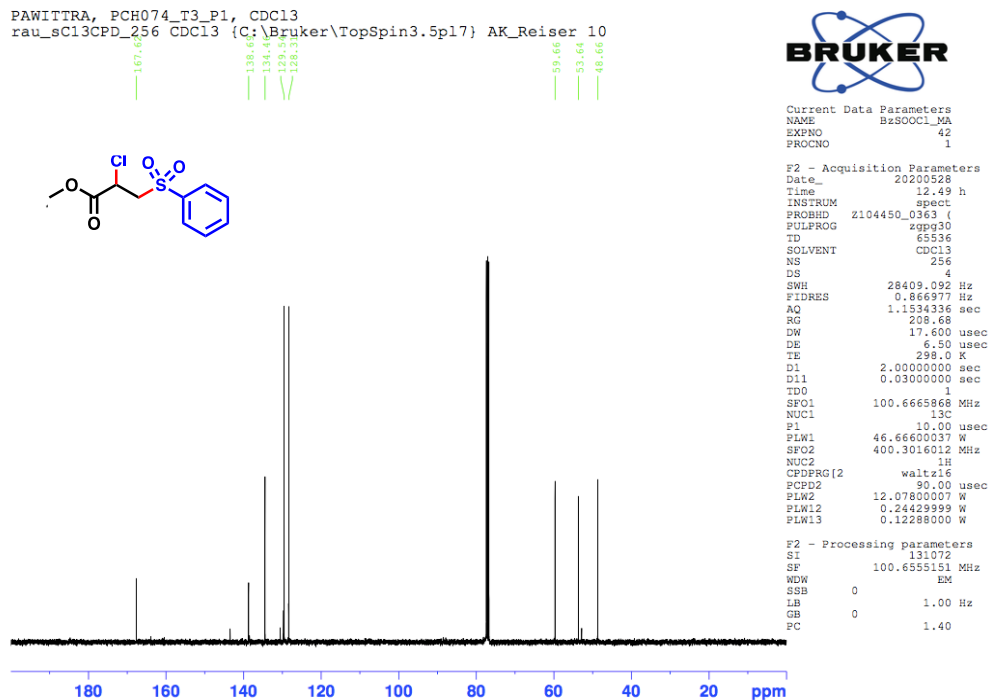


Figure B.54 ^{13}C NMR spectrum of methyl 2-chloro-3-(phenylsulfonyl)propanoate, **3ea**.

PAWIITRA, PCH069_T2_Recrys, CDCl3, 400MHz
 rau_sPROTON_64 CDCl3 (C:\Bruker\TopSpin3.5pl7) AK_Reiser 51

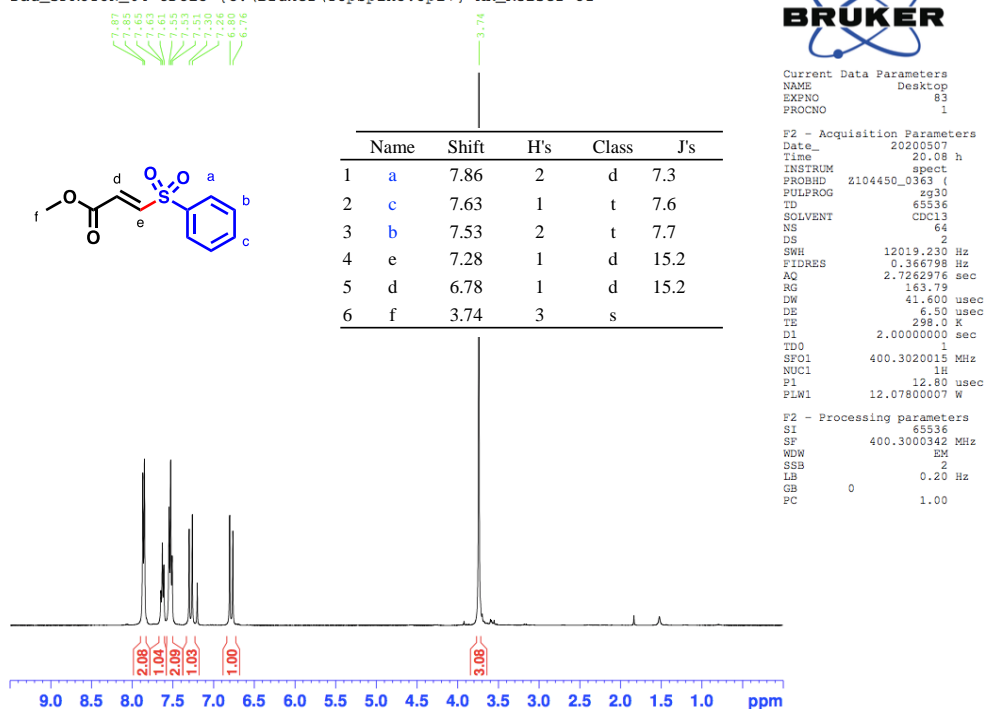


Figure B.55 ^1H NMR spectrum of methyl-(E)-3-(phenylsulfonyl)acrylate, (E)-4ea.

PAWIITRA, PCH069_T2_Recrys, CDCl3, 400MHz
 rau_sCl3CPD_1k_CDCl3 (C:\Bruker\TopSpin3.5pl7) AK_Reiser 51

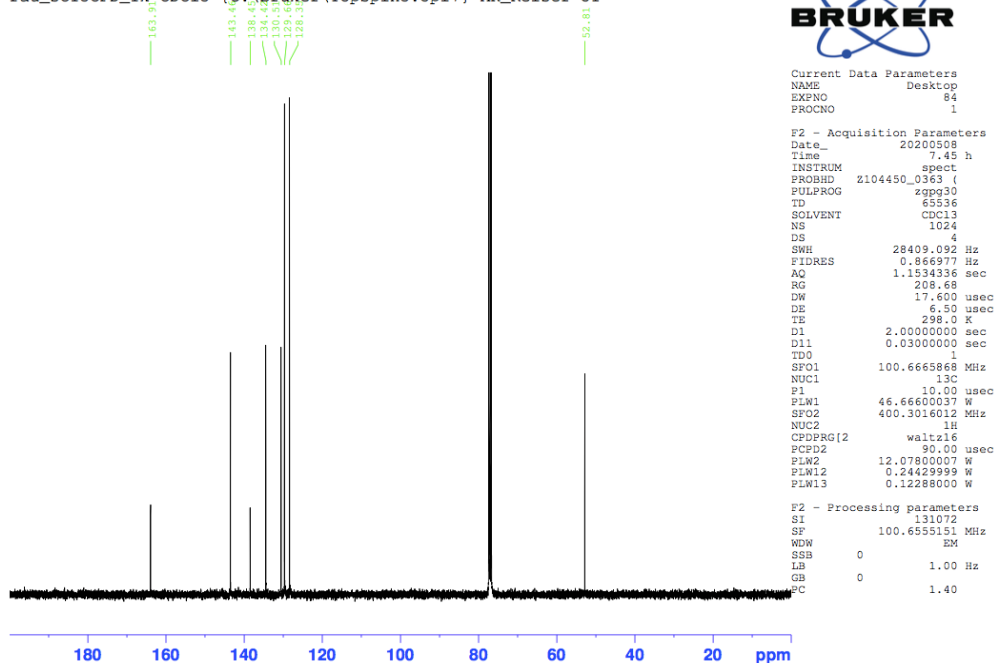
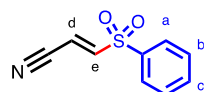


Figure B.56 ^{13}C NMR spectrum of methyl-(E)-3-(phenylsulfonyl)acrylate, (E)-4ea.

PAWITTRA, PCH067_T3_Recol., CDCl3 400MHz
 rau_sPROTON_16 CDCl3 (C:\Bruker\TopSpin3.5pl7) AK_Reiser 36



Name	Shift	H's	Integral	Class	J's
1	a	7.97	2	1.93	m
2	c	7.79	1	1.02	m
3	b	7.68	2	1.99	m
4	e	7.28	1	1.14	d 15.7
5	d	6.61	1	0.92	d 15.7



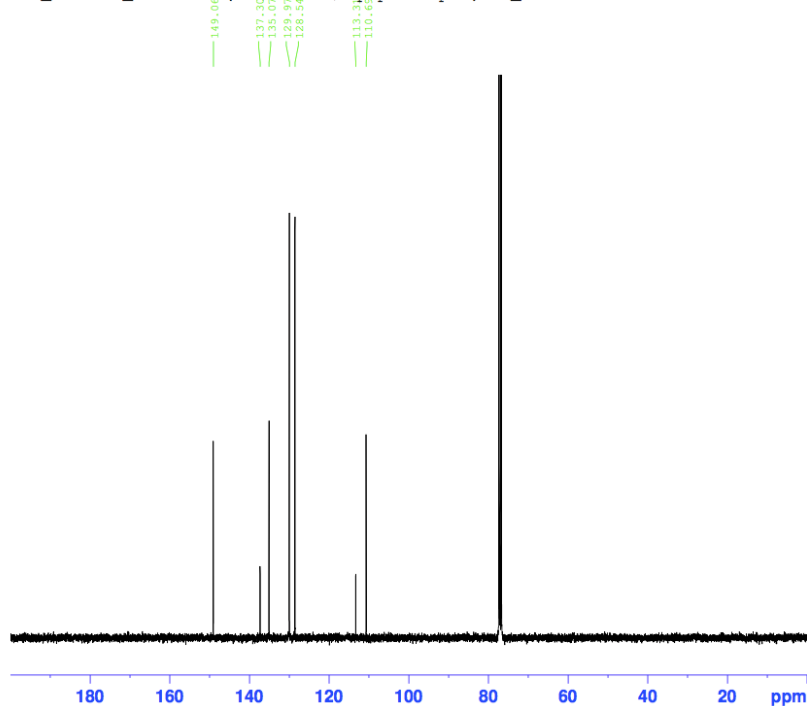
Current Data Parameters
 NAME Desktop
 EXPNO 15
 PROCNO 1

F2 - Acquisition Parameters
 Date_ 20200506
 Time 20:42 h
 INSTRUM spect
 PROBHD Z104450_0363 ()
 PULPROG zg30
 TD 65536
 SOLVENT CDCl3
 NS 16
 DS 2
 SWH 12019.230 Hz
 FIDRES 0.366798 Hz
 AQ 2.7262976 sec
 RG 208.68
 DW 41.600 usec
 DE 6.50 usec
 TE 298.0 K
 D1 2.0000000 sec
 TD0 1
 SFO1 400.3020015 MHz
 NUC1 1H
 P1 12.80 usec
 PLW1 12.07800007 W

F2 - Processing parameters
 SI 65536
 SF 400.2999871 MHz
 WDW EM
 SSB 2
 LB 0.20 Hz
 GB 0
 PC 1.00

Figure B.57 ^1H NMR spectrum of (E)-3-(phenylsulfonyl)acrylonitrile, (E)-4fa.

PAWITTRA, PCH067_T3_Recol., CDCl3 400MHz
 rau_sC13CPD_1k CDCl3 (C:\Bruker\TopSpin3.5pl7) AK_Reiser 36

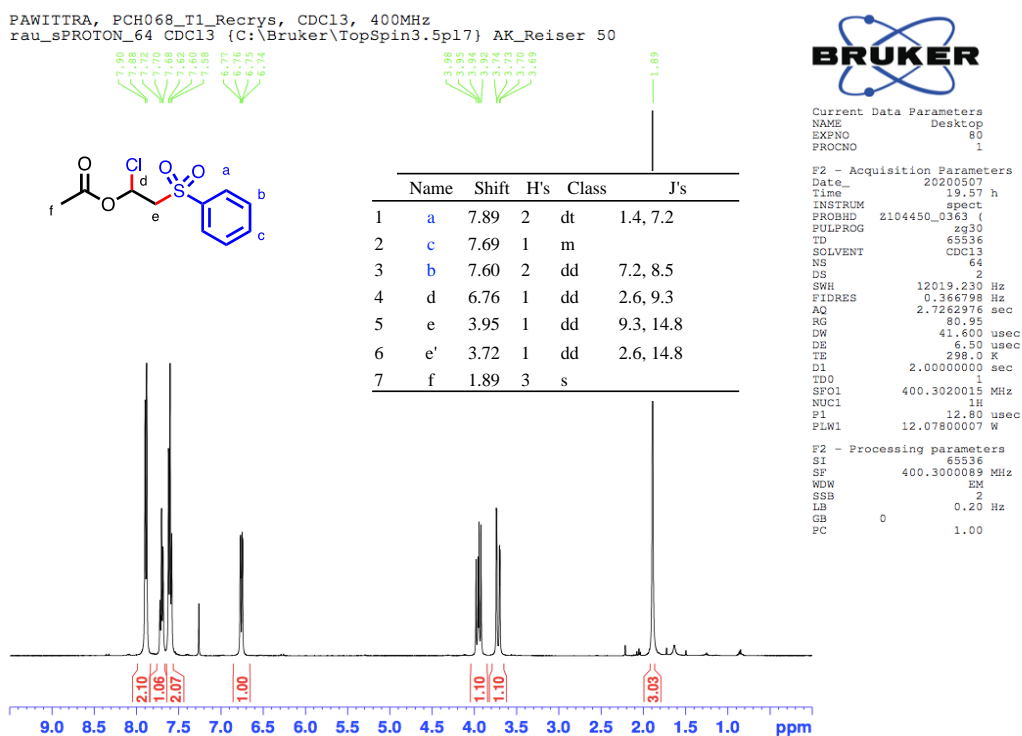
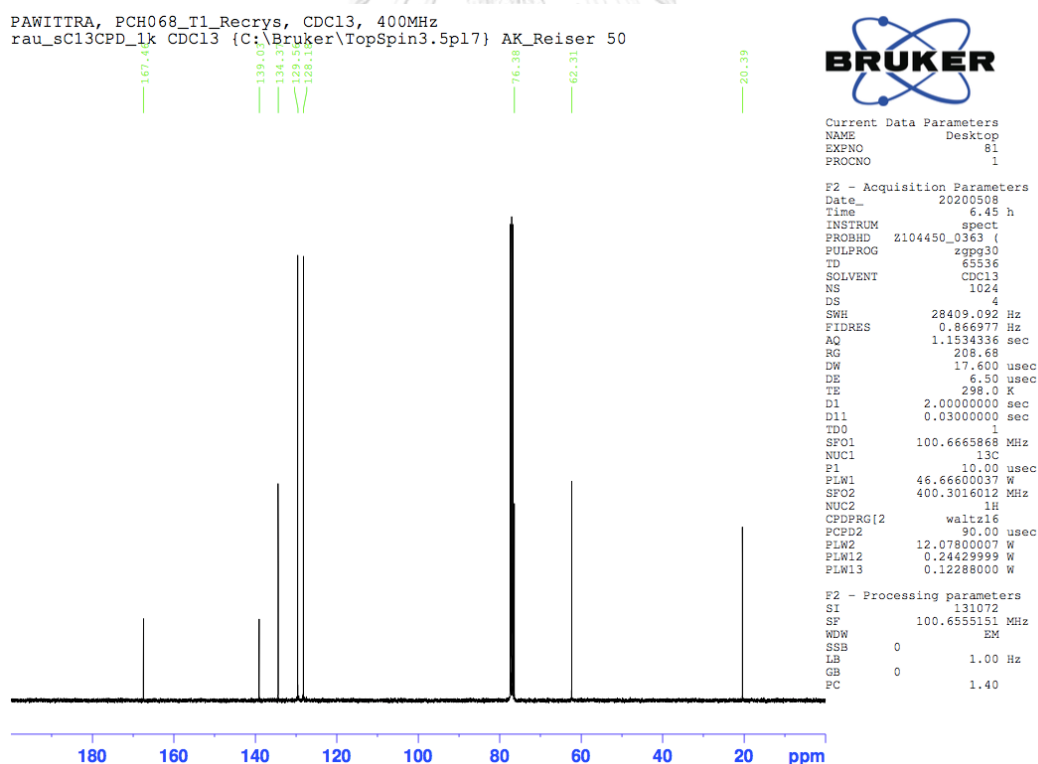


Current Data Parameters
 NAME Desktop
 EXPNO 19
 PROCNO 1

F2 - Acquisition Parameters
 Date_ 20200507
 Time 5:08 h
 INSTRUM spect
 PROBHD Z104450_0363 ()
 PULPROG zgpg30
 TD 65536
 SOLVENT CDCl3
 NS 1024
 DS 4
 SWH 28409.092 Hz
 FIDRES 0.866977 Hz
 AQ 1.1534336 sec
 RG 208.68
 DW 17.600 usec
 DE 6.50 usec
 TE 298.0 K
 D1 2.0000000 sec
 D11 0.0300000 sec
 TD0 1
 SFO1 100.6665868 MHz
 NUC1 13C
 P1 10.00 usec
 PLW1 46.66600037 W
 SFO2 400.3016012 MHz
 NUC2 1H
 CPDPRG2 waltz16
 PCPDZ 30.00 usec
 PLW2 12.07800007 W
 PLW12 0.24429999 W
 PLW13 0.12288000 W

F2 - Processing parameters
 SI 131072
 SF 100.6555151 MHz
 WDW EM
 SSB 0
 LB 1.00 Hz
 GB 0
 PC 1.40

Figure B.58 ^{13}C NMR spectrum of (E)-3-(phenylsulfonyl)acrylonitrile, (E)-4fa.

Figure B.59 ¹H NMR spectrum of 1-chloro-2-(phenylsulfonyl)ethyl acetate, **3ga**.Figure B.60 ¹³C NMR spectrum of 1-chloro-2-(phenylsulfonyl)ethyl acetate, **3ga**.

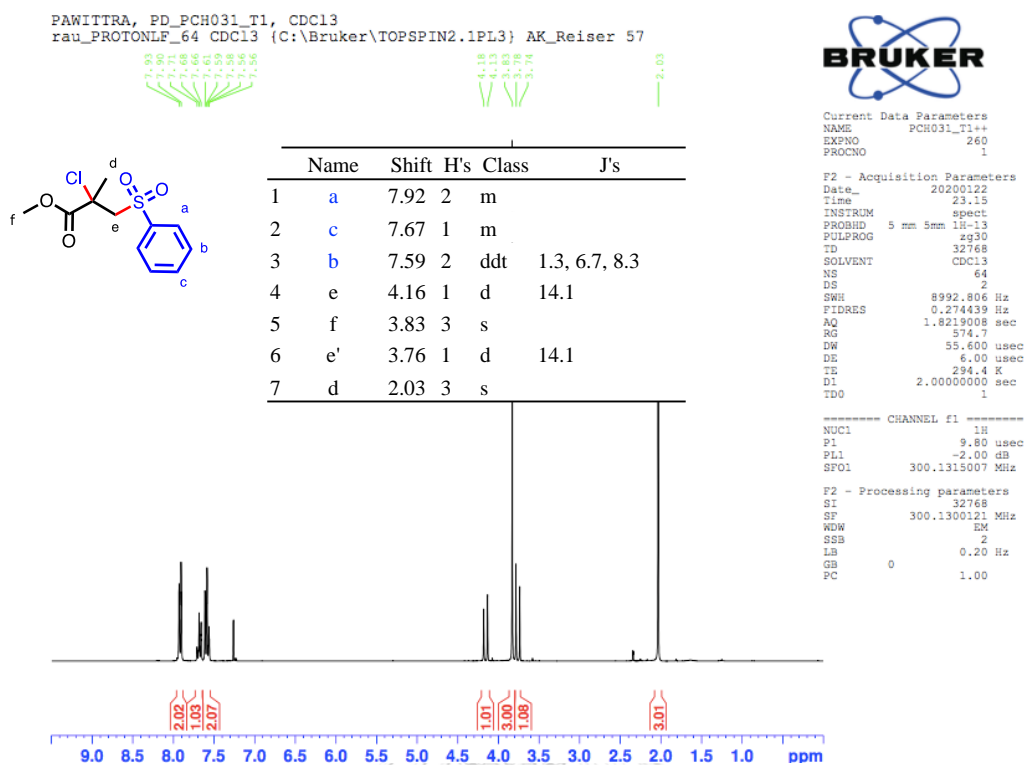


Figure B.61 ^1H NMR spectrum of methyl-2-chloro-2-methyl-3-(phenylsulfonyl)propanoate, **3ha**.

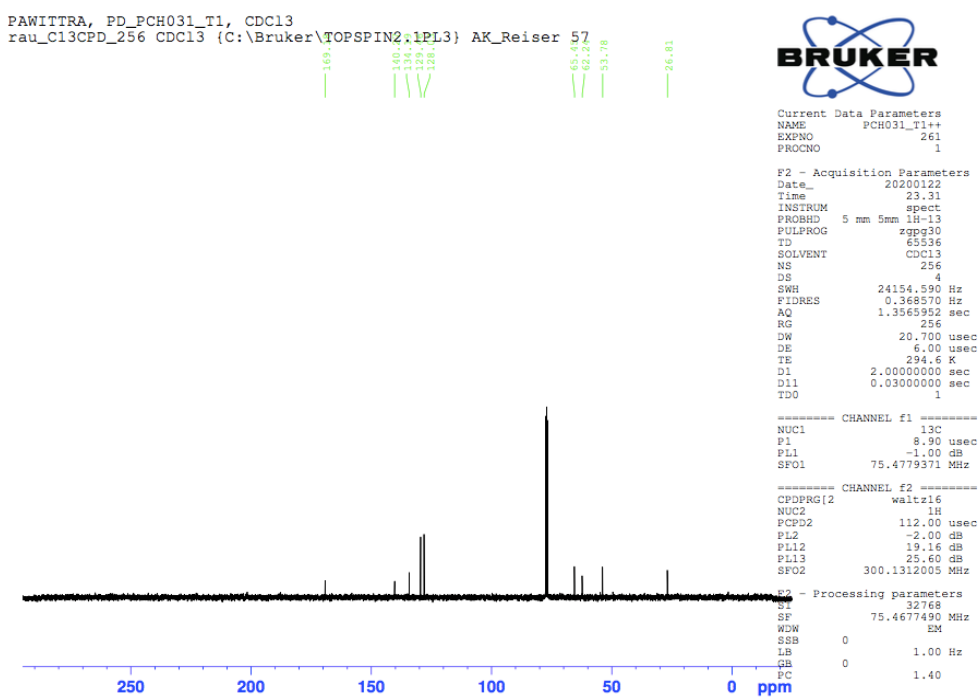


Figure B.62 ^{13}C NMR spectrum of methyl-2-chloro-2-methyl-3-(phenylsulfonyl)propanoate, **3ha**.

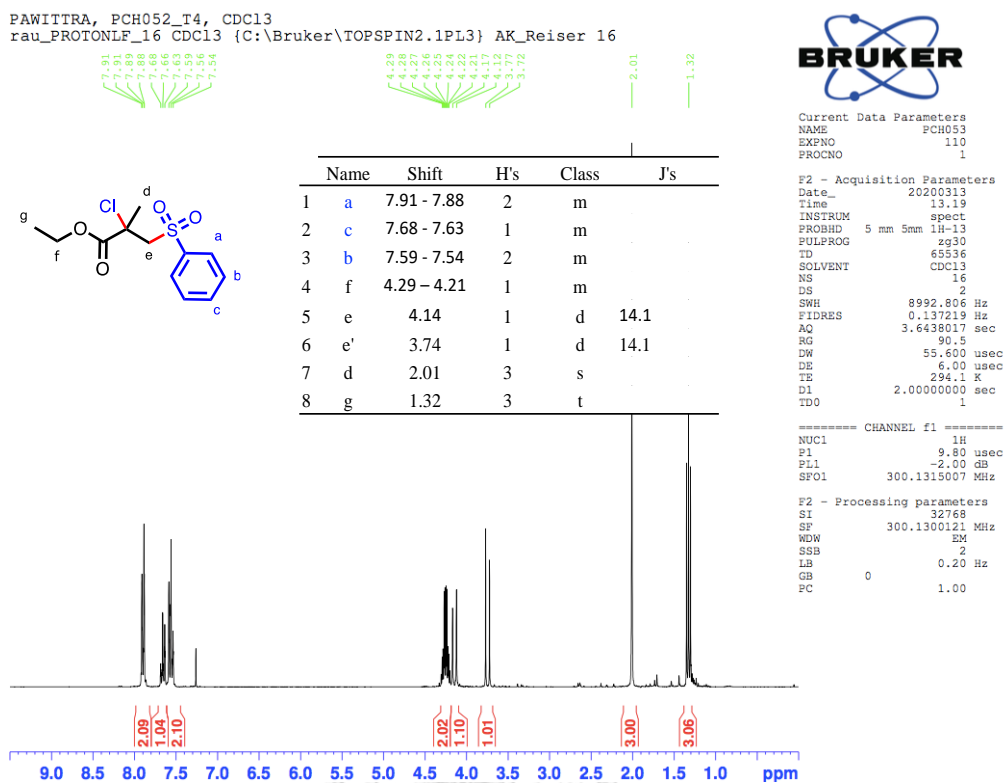


Figure B.63 ^1H NMR spectrum of ethyl-2-chloro-2-methyl-3-(phenylsulfonyl)propanoate, **3ia**.

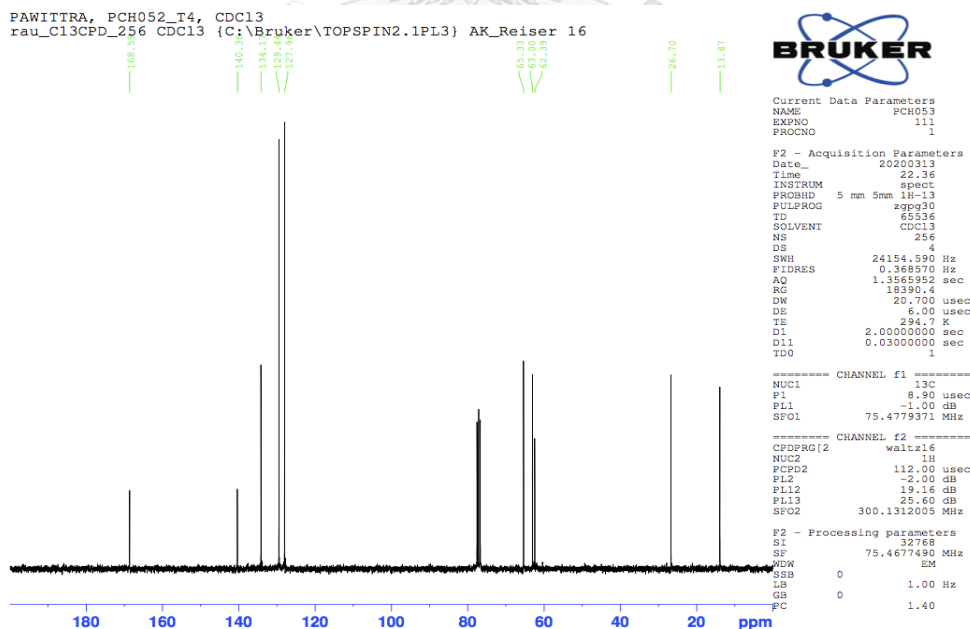
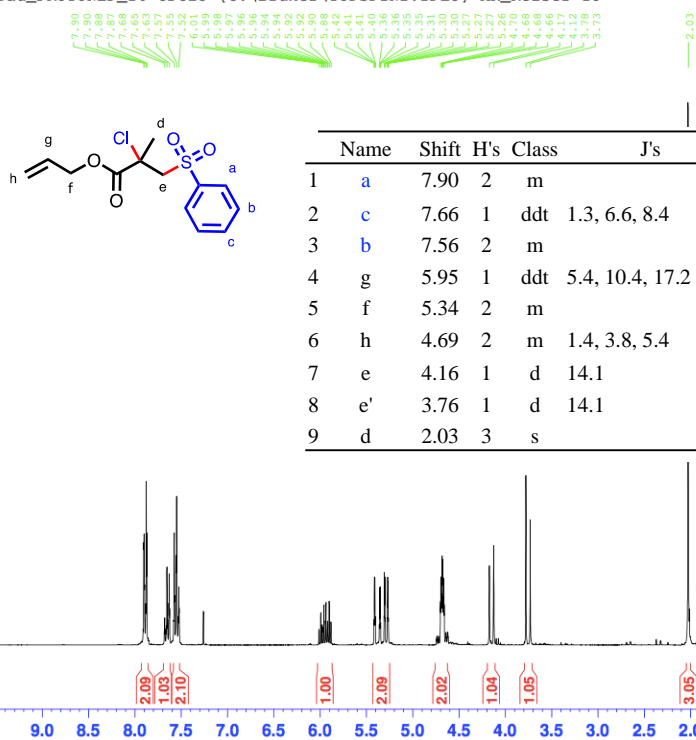


Figure B.64 ^{13}C NMR spectrum of ethyl-2-chloro-2-methyl-3-(phenylsulfonyl)propanoate, **3ia**.

PAWITTRA, PCH052_T3, CDCl3
 rau_PROTONLF_16 CDCl3 (C:\Bruker\TOPSPIN2.1PL3) AK_Reiser 15



Current Data Parameters
 NAME PCH053
 EXPNO 100
 PROCNO 1

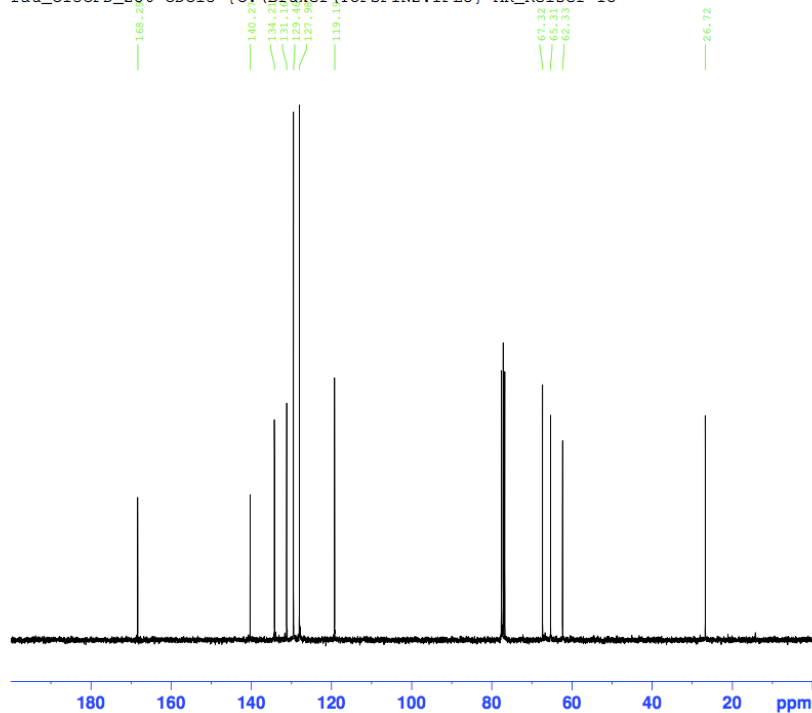
F2 - Acquisition Parameters
 Date_ 20200313
 Time 13.11
 INSTRUM spect
 PROBHD 5 mm 5mm 1H-13
 PULPROG zg30
 TD 65536
 SOLVENT CDCl3
 NS 16
 DS 2
 SWH 8992.806 Hz
 FIDRES 0.137219 Hz
 AQ 3.6438017 sec
 RG 71.8
 DW 55.600 usec
 DE 6.00 usec
 TE 294.2 K
 D1 2.0000000 sec
 TD0 1

===== CHANNEL f1 =====
 NUC1 1H
 P1 9.80 usec
 PL1 -2.00 dB
 SFO1 300.1315007 MHz

F2 - Processing parameters
 SI 32768
 SF 300.1300121 MHz
 WDW EM
 SSB 2
 LB 0.20 Hz
 GB 0
 PC 1.00

Figure B.65 ^1H NMR spectrum of allyl-2-chloro-2-methyl-3-(phenylsulfonyl)propanoate, **3ja**.

PAWITTRA, PCH052_T3, CDCl3
 rau_C13CPD_256 CDCl3 (C:\Bruker\TOPSPIN2.1PL3) AK_Reiser 15



Current Data Parameters
 NAME PCH053
 EXPNO 101
 PROCNO 1

F2 - Acquisition Parameters
 Date_ 20200313
 Time 22.05
 INSTRUM spect
 PROBHD 5 mm 5mm 1H-13
 PULPROG zgpg30
 TD 65536
 SOLVENT CDCl3
 NS 256
 DS 4
 SWH 24154.590 Hz
 FIDRES 0.368570 Hz
 AQ 1.3565952 sec
 RG 1149.4
 DW 20.700 usec
 DE 6.00 usec
 TE 294.7 K
 D1 2.0000000 sec
 D11 0.0300000 sec
 TD0 1

===== CHANNEL f1 =====
 NUC1 13C
 P1 8.90 usec
 PL1 -1.00 dB
 SFO1 75.4779371 MHz

===== CHANNEL f2 =====
 CPDPRG[2] waltz16
 NUC2 1H
 PCPD2 112.00 usec
 PL2 -2.00 dB
 PL12 19.16 dB
 PL13 25.60 dB
 SFO2 300.1312005 MHz

F2 - Processing parameters
 SI 32768
 SF 75.4677490 MHz
 WDW EM
 SSB 0
 LB 1.00 Hz
 GB 0
 PC 1.40

Figure B.66 ^{13}C NMR spectrum of allyl-2-chloro-2-methyl-3-(phenylsulfonyl)propanoate, **3ja**.

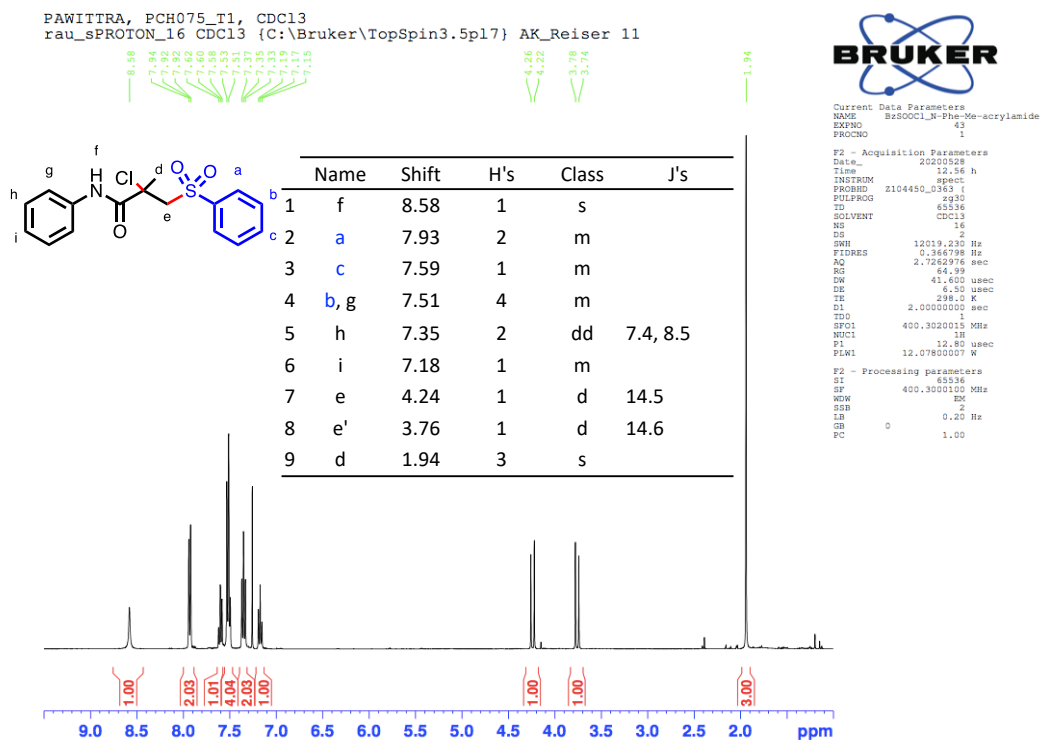


Figure B.67 ^1H NMR spectrum of 2-chloro-2-methyl-N-phenyl-3-(phenylsulfonyl)propanamide, **3ka**.

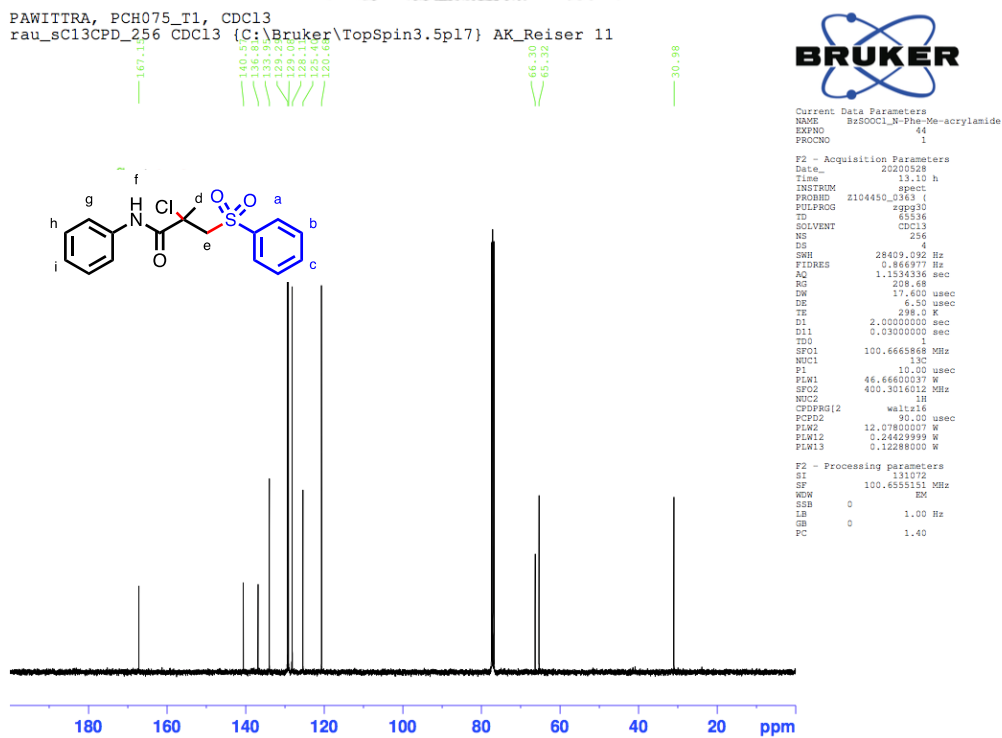


Figure B.68 ^{13}C NMR spectrum of 2-chloro-2-methyl-N-phenyl-3-(phenylsulfonyl)propanamide, **3ka**.

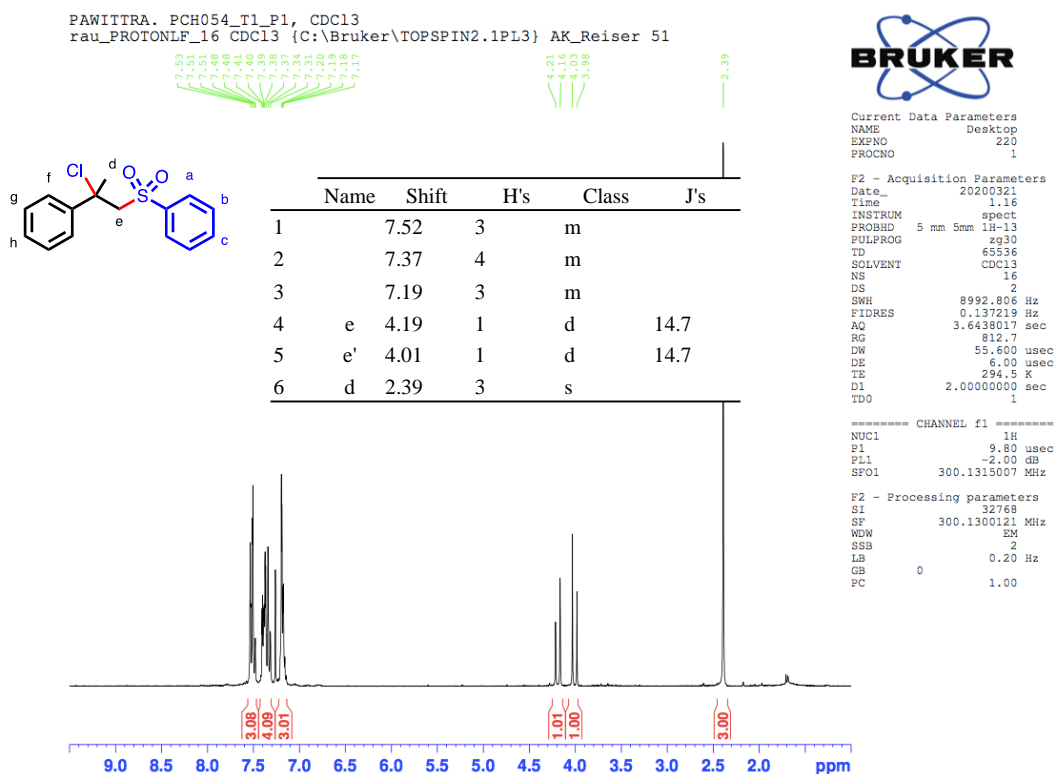


Figure B.69 ^1H NMR spectrum of (2-chloro-1-(phenylsulfonyl)propan-2-yl)benzene, 3a.

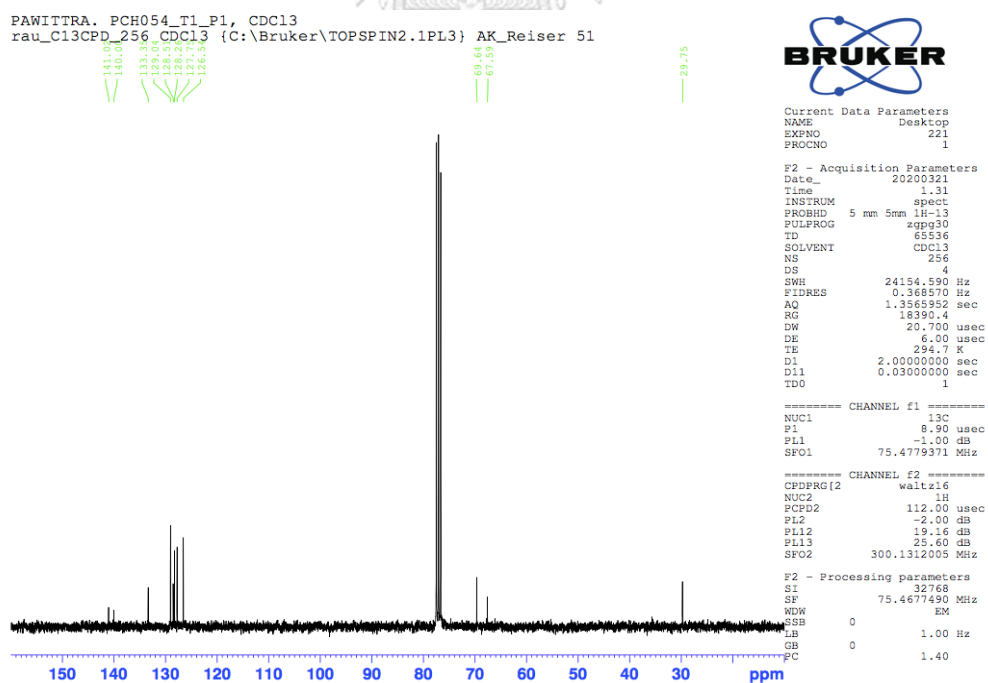
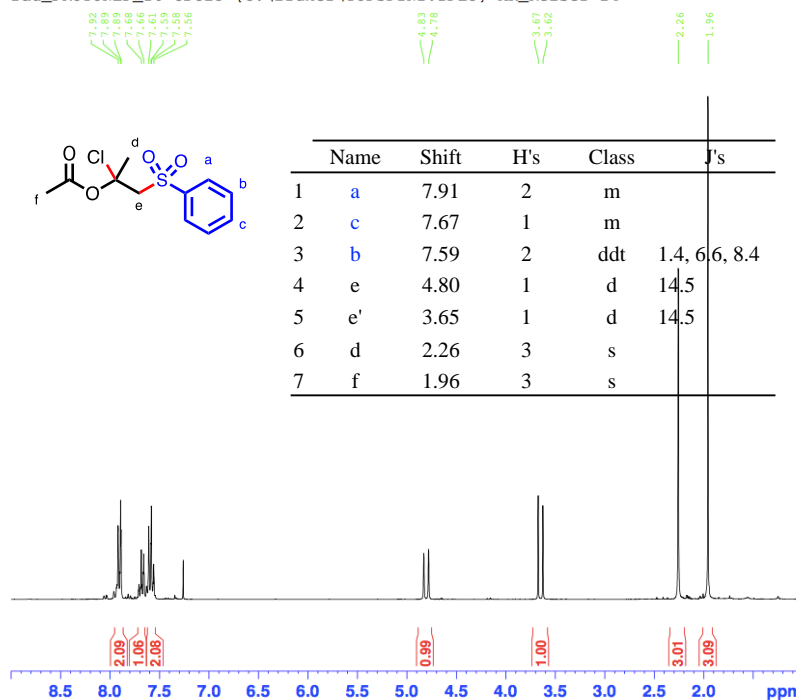


Figure B.70 ^{13}C NMR spectrum of (2-chloro-1-(phenylsulfonyl)propan-2-yl)benzene, 3a.

PAWITTRA, PCH065_T1, CDC13
 rau_PROTONLF_16 CDC13 {C:\Bruker\TOPSPIN2.1PL3} AK_Reiser 24



Current Data Parameters
 NAME +H2O2Cl_1so-propeneacetate
 EXPNO 80
 PROCNO 1

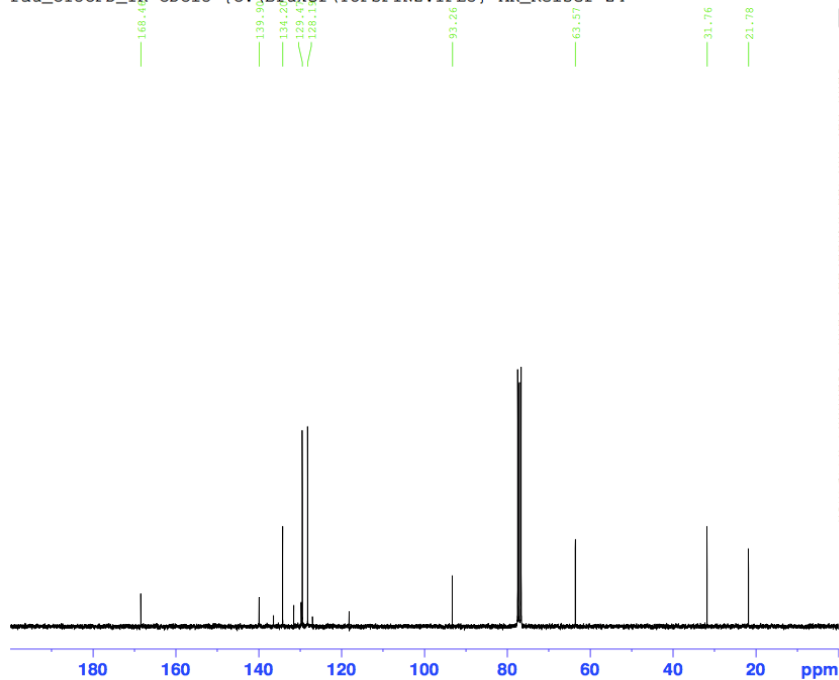
F2 - Acquisition Parameters
 Date_ 20200427
 Time 15.34
 INSTRUM spect
 PROBHD 5 mm QNP 1H/13
 PULPROG zg30
 TD 65536
 SOLVENT CDC13
 NS 16
 DS 2
 SWH 8992.806 Hz
 FIDRES 0.137219 Hz
 AQ 3.6438017 sec
 RG 962
 DR 55.600 usec
 DE 6.00 usec
 TE 294.1 K
 D1 2.0000000 sec
 DDD 1

CHANNEL f1
 NUC1 1H
 P1 7.80 usec
 PL1 1.00 dB
 SFO1 300.1313007 MHz

F2 - Processing parameters
 SI 32768
 SF 300.1300121 MHz
 WOK BK
 SSB 2
 LB 0.20 Hz
 GB 0
 PC 1.00

Figure B.71 ^1H NMR spectrum of 2-chloro-1-(phenylsulfonyl)propan-2-yl acetate, 3ma.

PAWITTRA, PCH065_T1, CDC13
 rau_C13CPD_1K CDC13 {C:\Bruker\TOPSPIN2.1PL3} AK_Reiser 24



Current Data Parameters
 NAME H2O2Cl_1so-propeneacetate
 EXPNO 81
 PROCNO 1

F2 - Acquisition Parameters
 Date_ 20200427
 Time 21.17
 INSTRUM spect
 PROBHD 5 mm QNP 1H/13
 PULPROG zgpg30
 TD 65536
 SOLVENT CDC13
 NS 1024
 DS 4
 SWH 24154.590 Hz
 FIDRES 0.368570 Hz
 AQ 1.3565992 sec
 RG 14596.5
 DR 20.700 usec
 DE 6.00 usec
 TE 294.8 K
 D1 2.0000000 sec
 D11 0.0300000 sec
 DDD 1

CHANNEL f1
 NUC1 13C
 P1 18.00 usec
 PL1 -9.00 dB
 SFO1 75.4779371 MHz

CHANNEL f2
 CPDPRG2 waltz16
 NUC2 1H
 PCPD2 112.00 usec
 PL2 1.00 dB
 PL12 23.71 dB
 PL13 27.00 dB
 SFO2 300.1313005 MHz

F2 - Processing parameters
 SI 32768
 SF 75.4677490 MHz
 WOK BK
 SSB 0
 LB 1.00 Hz
 GB 0
 PC 1.40

Figure B.72 ^{13}C NMR spectrum of 2-chloro-1-(phenylsulfonyl)propan-2-yl acetate, 3ma

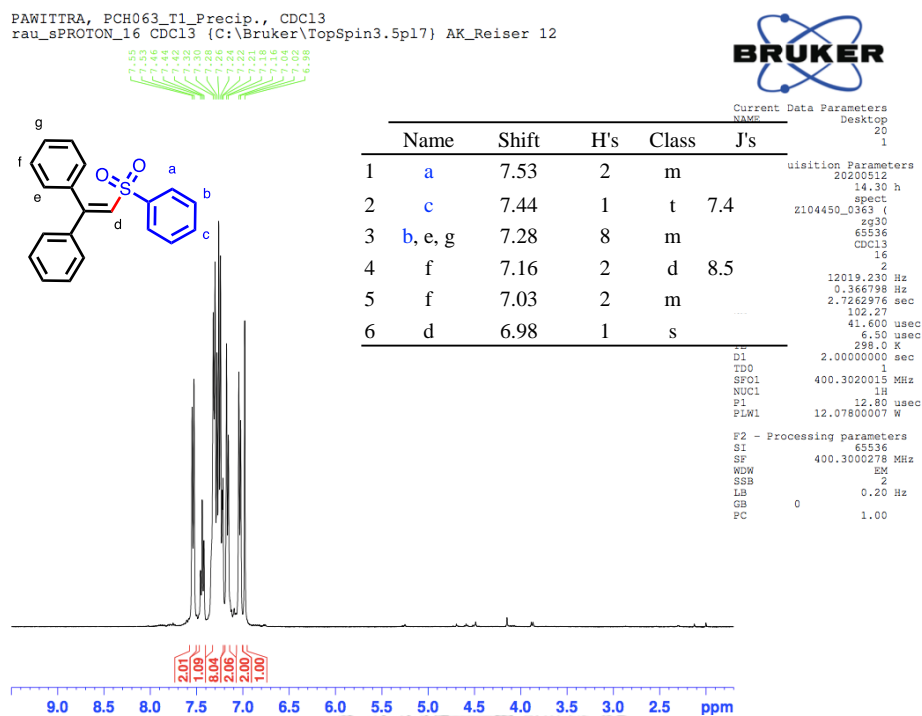


Figure B.73 ¹H NMR spectrum of (2-(phenylsulfonyl)ethene-1,1-diyl)dibenzene, **4na**.

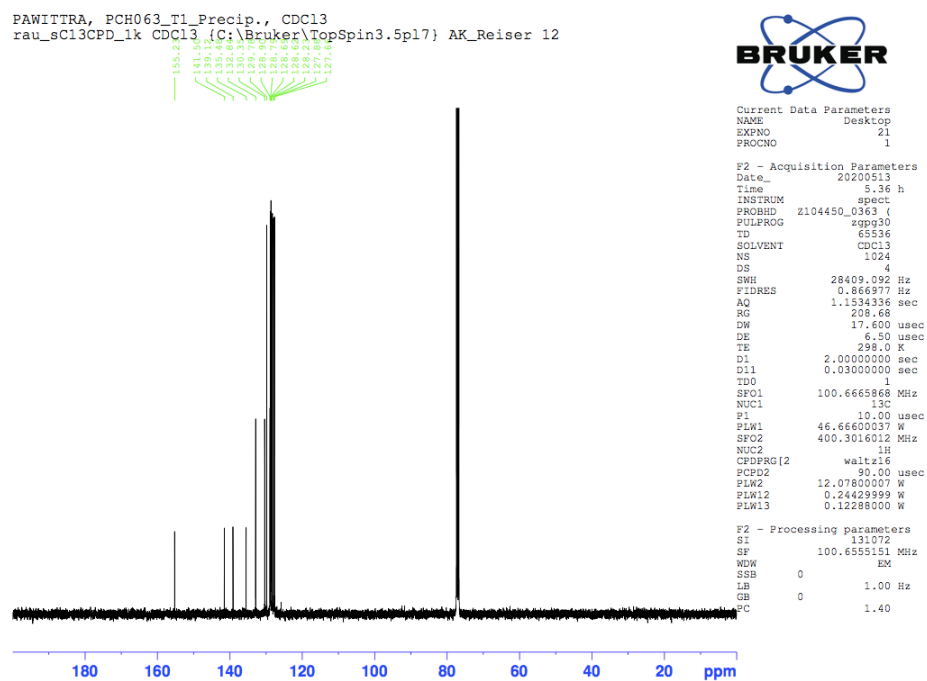
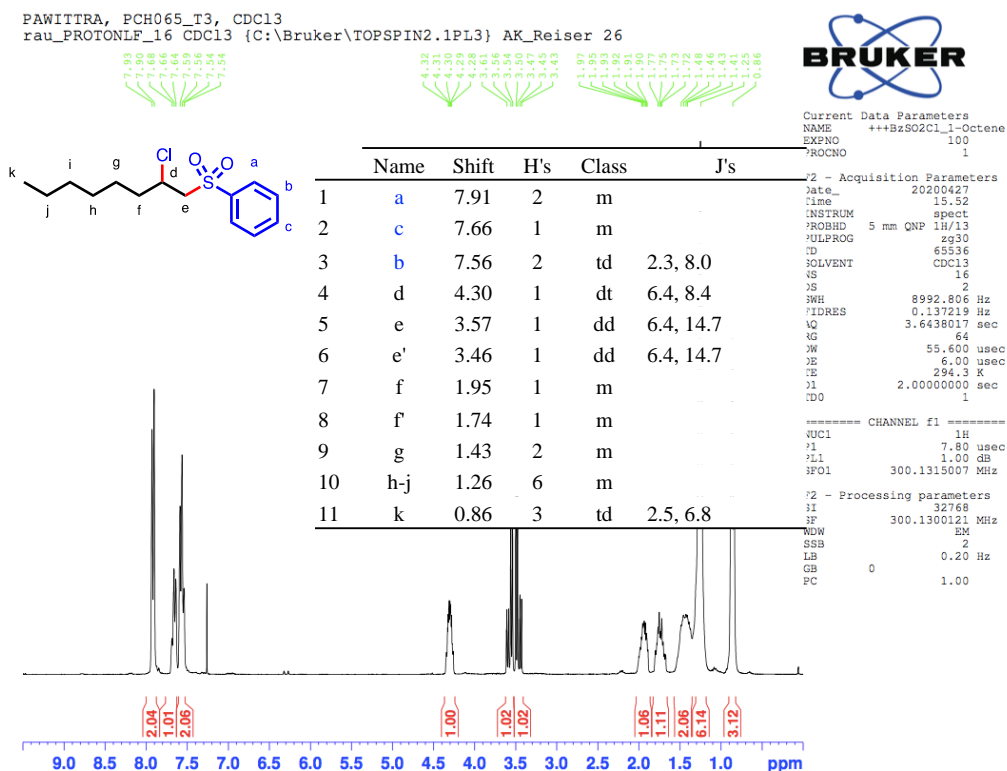
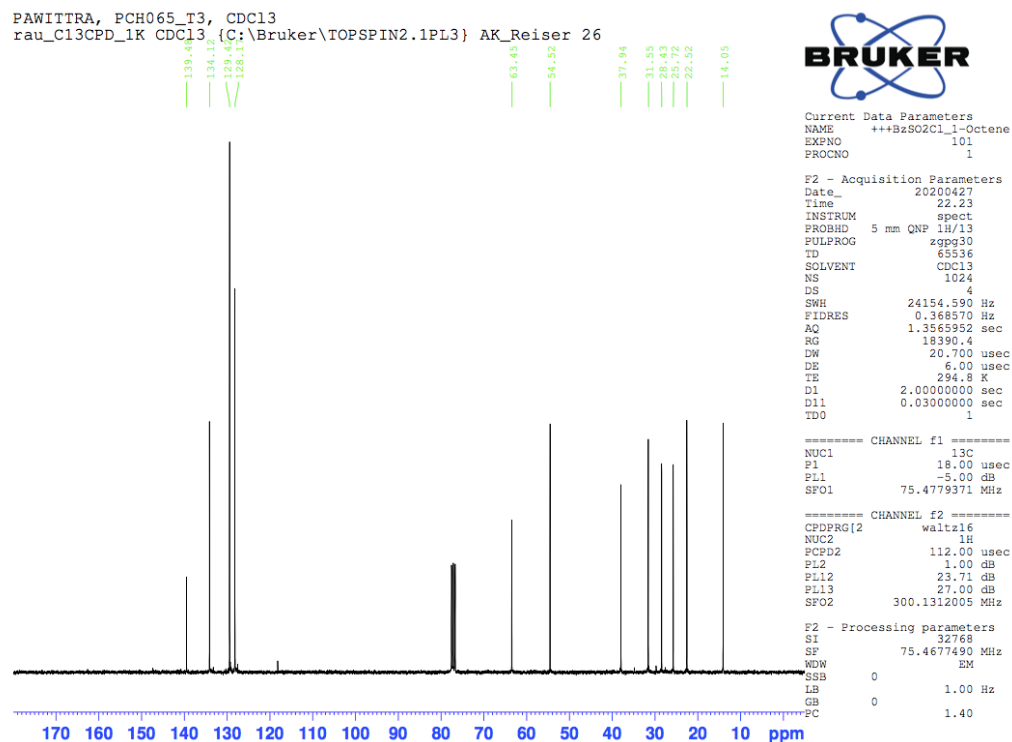
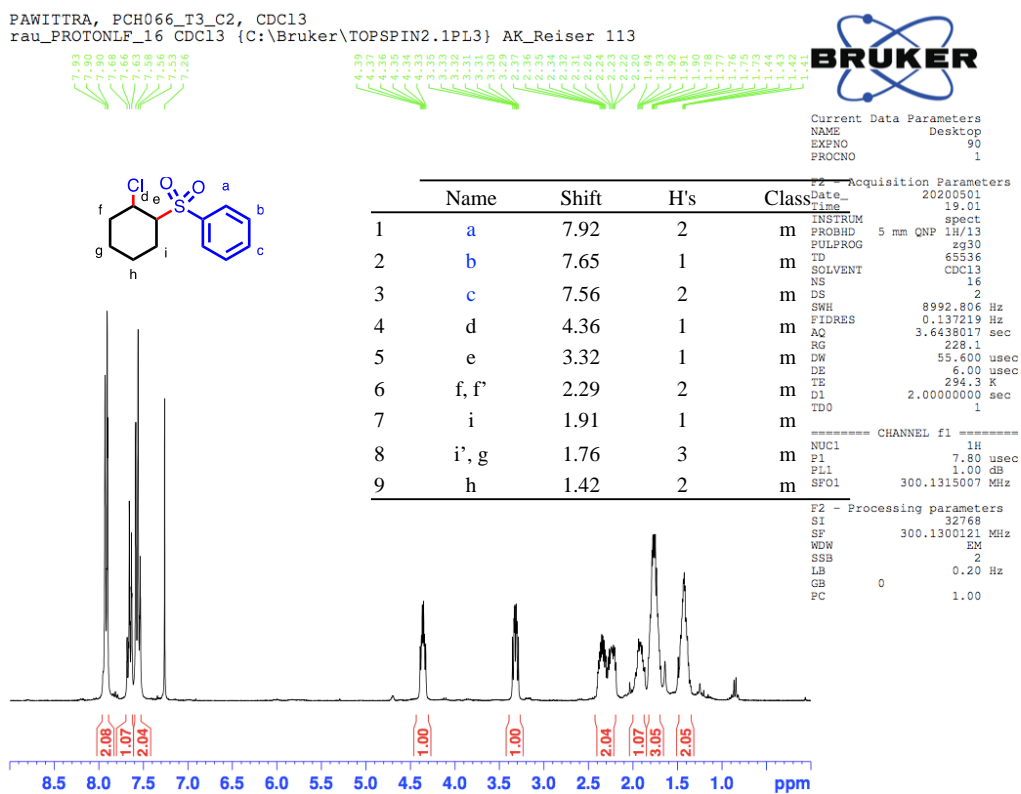
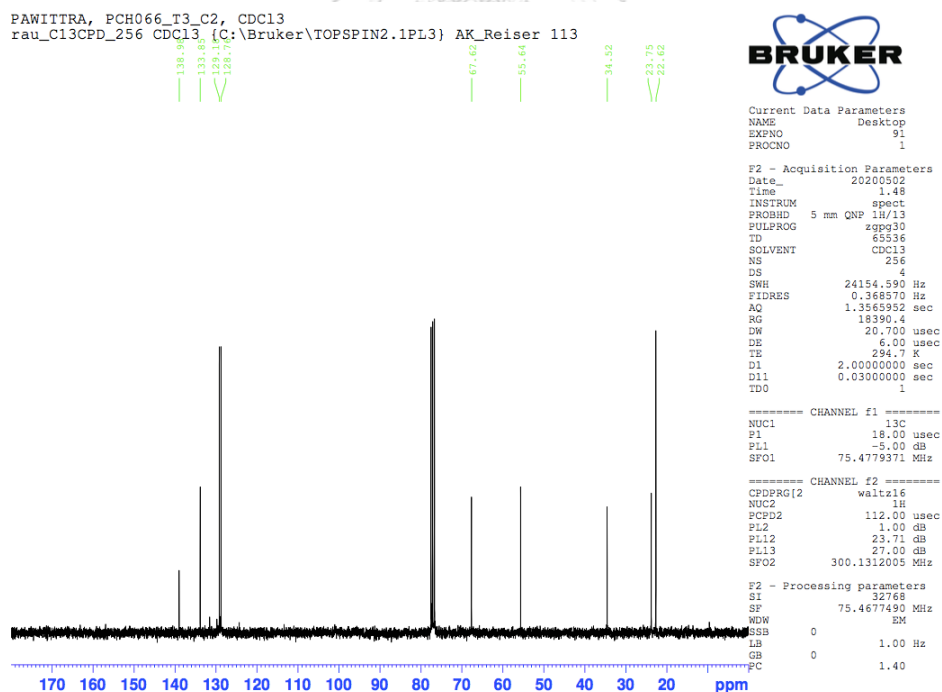
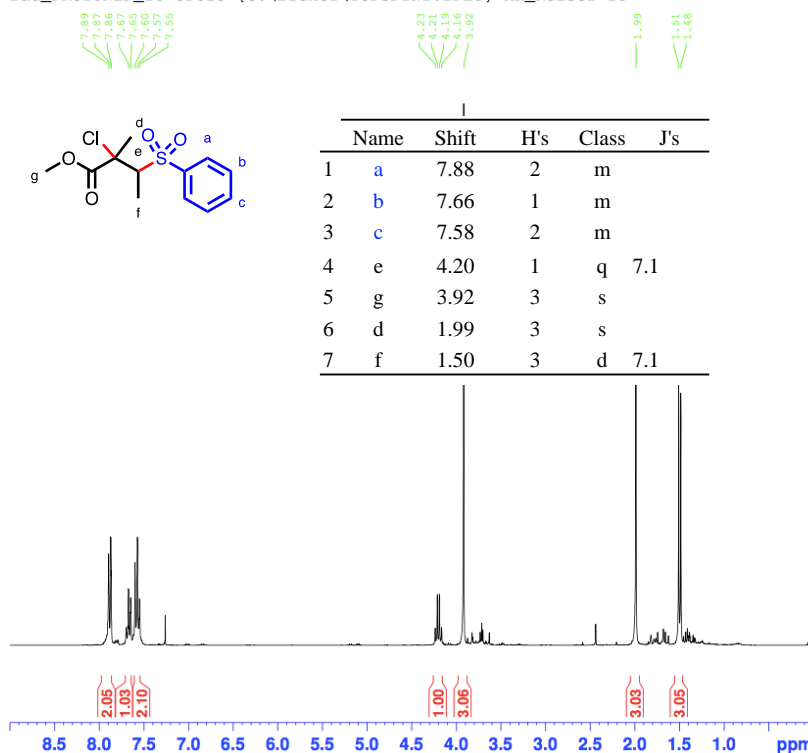


Figure B.74 ¹³C NMR spectrum of (2-(phenylsulfonyl)ethene-1,1-diyl)dibenzene, **4na**.

Figure B.75 ¹H NMR spectrum of ((2-chlorooctyl)sulfonyl)benzene, 30a.Figure B.76 ¹³C NMR spectrum of ((2-chlorooctyl)sulfonyl)benzene, 30a.

Figure B.77 ^1H NMR spectrum of ((2-chlorocyclohexyl)sulfonyl)benzene, *anti*-3pa.Figure B.78 ^{13}C NMR spectrum of ((2-chlorocyclohexyl)sulfonyl)benzene, *anti*-3pa.

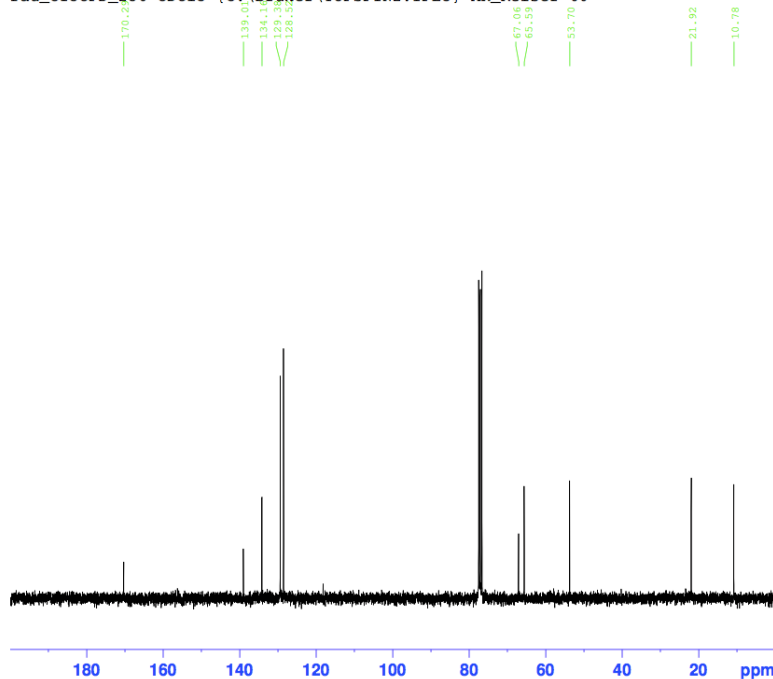
PAWITTRA, PCH065_T2, CDC13
 rau_PROTONLF_16 CDC13 {C:\Bruker\TOPSPIN2.1PL3} AK_Reiser 25



Current Data Parameters
 NAME BzS02Cl_MethylTiglate
 EXPNO 90
 PROCNO 1
 F2 - Acquisition Parameters
 Date_ 20200427
 Time 15.44
 INSTRUM spect
 PROBHD 5 mm QNP 1H/13
 PULPROG zgpg30
 TD 65536
 SOLVENT CDC13
 NS 16
 DS 2
 SWH 8992.806 Hz
 FIDRES 0.137219 Hz
 AQ 3.6438017 sec
 RG 114
 DW 55.600 usec
 DE 6.00 usec
 TE 294.2 K
 D1 2.0000000 sec
 TDO 1
 ===== CHANNEL f1 =====
 NUC1 1H
 P1 7.80 usec
 PL1 1.00 dB
 SFO1 300.1315007 MHz
 F2 - Processing parameters
 SI 32768
 SF 300.1300121 MHz
 WDW EM
 SSB 2
 LB 0.20 Hz
 GB 0
 PC 1.00

Figure B.79 ^1H NMR spectrum of methyl-2-chloro-2-methyl-3-(phenylsulfonyl)butanoate, **3qa**.

PAWITTRA, PCH065_T2_P1_C2, CDC13
 rau_C13CPD_256 CDC13 {C:\Bruker\TOPSPIN2.1PL3} AK_Reiser 60



Current Data Parameters
 NAME BzS02Cl_MethylTiglate
 EXPNO 301
 PROCNO 1
 F2 - Acquisition Parameters
 Date_ 20200501
 Time 13.14
 INSTRUM spect
 PROBHD 5 mm QNP 1H/13
 PULPROG zgpg30
 TD 65536
 SOLVENT CDC13
 NS 256
 DS 4
 SWH 24154.590 Hz
 FIDRES 0.368570 Hz
 AQ 1.3565952 sec
 RG 16384
 DW 20.700 usec
 DE 6.00 usec
 TE 294.7 K
 D1 2.0000000 sec
 D11 0.0300000 sec
 TDO 1
 ===== CHANNEL f1 =====
 NUC1 13C
 P1 18.00 usec
 PL1 -8.00 dB
 SFO1 75.4779371 MHz
 ===== CHANNEL f2 =====
 CPDPRG2 waitz16
 NUC2 1H
 PCPD2 112.00 usec
 PL2 1.00 dB
 PL12 23.71 dB
 PL13 27.00 dB
 SFO2 300.1312005 MHz
 F2 - Processing parameters
 SI 32768
 SF 75.4677490 MHz
 WDW EM
 SSB 0
 LB 1.00 Hz
 GB 0
 PC 1.40

Figure B.80 ^{13}C NMR spectrum of methyl-2-chloro-2-methyl-3-(phenylsulfonyl)butanoate, **3qa**.

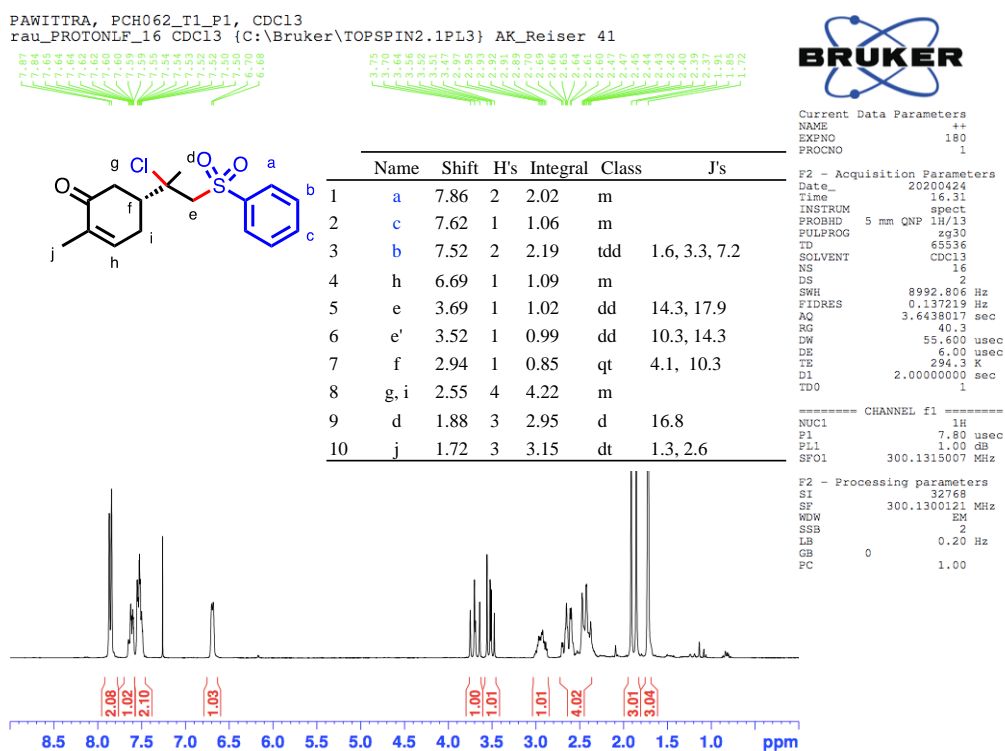


Figure B.81 ^1H NMR spectrum of (5R)-5-(2-chloro-1-(phenylsulfonyl)propan-2-yl)-2-methylcyclohex-2-en-1-one, **3ra**.

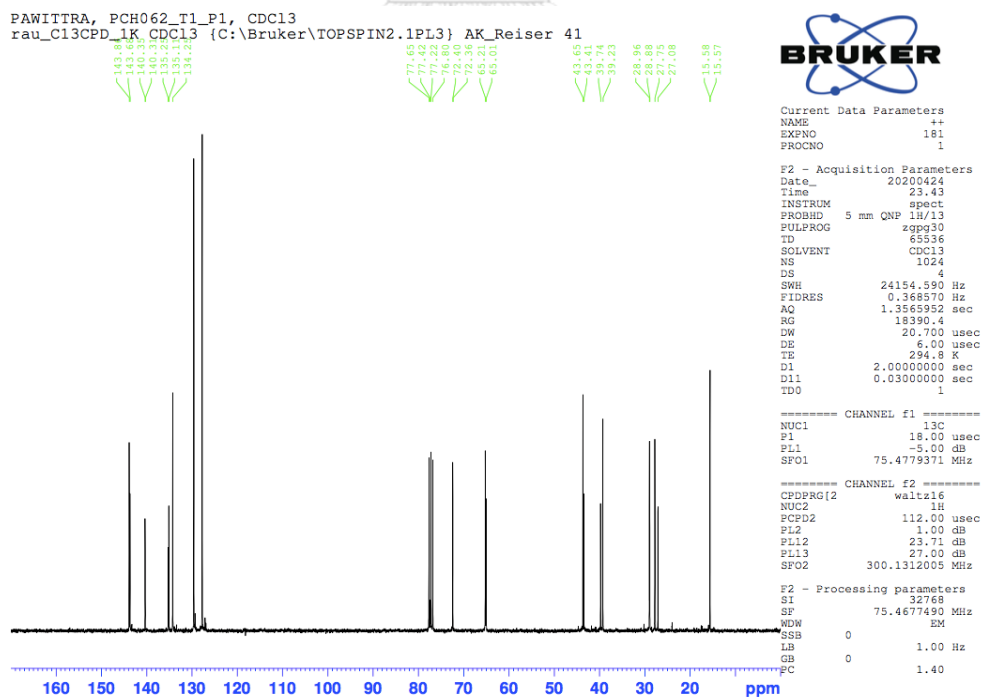


Figure B.82 ^{13}C NMR spectrum of (5R)-5-(2-chloro-1-(phenylsulfonyl)propan-2-yl)-2-methylcyclohex-2-en-1-one, **3ra**.

PAWITTRA, PCH074_T4_Precip., CDC13
 rau_PROTONLF_16 CDC13 (C:\Bruker\TOPSPIN2.1PL3) AK_Reiser 67

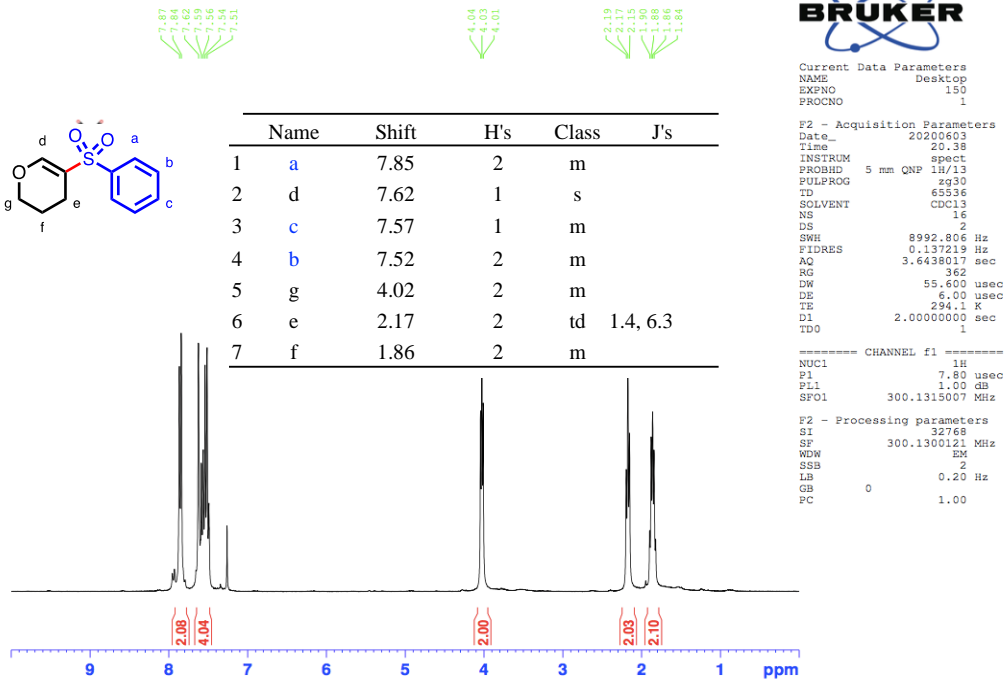


Figure B.83 ^1H NMR spectrum of 5-(phenylsulfonyl)-3,4-dihydro-2H-pyran, **4sa**

PAWITTRA, PCH074_T4_Precip., CDC13
 rau_C13CPD_256 CDC13 (C:\Bruker\TOPSPIN2.1PL3) AK_Reiser 67

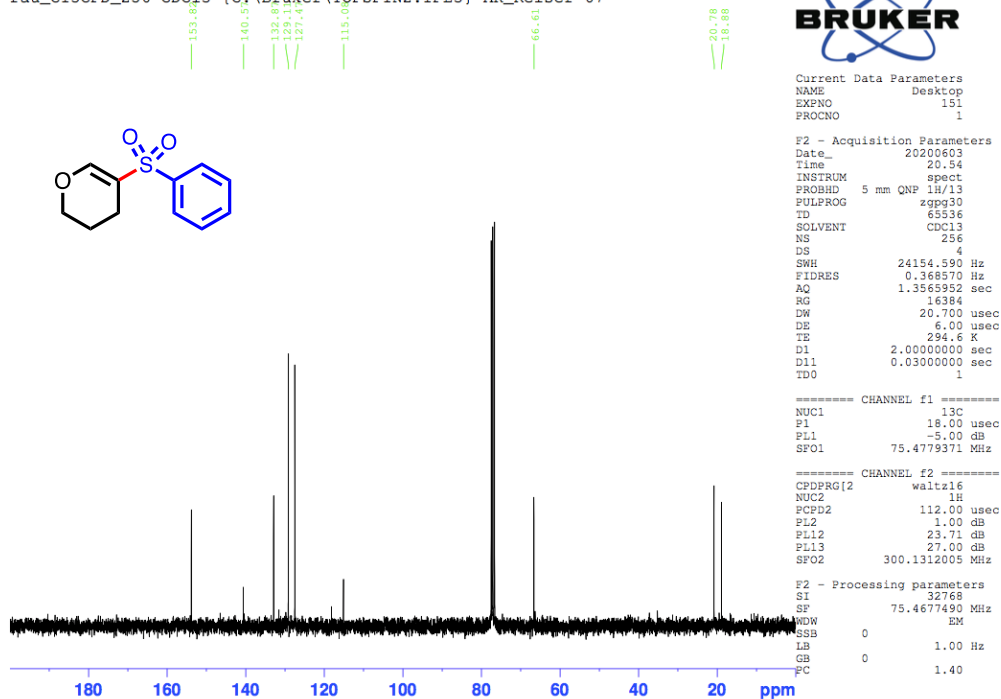


Figure B.84 ^{13}C NMR spectrum of 5-(phenylsulfonyl)-3,4-dihydro-2H-pyran, **4sa**

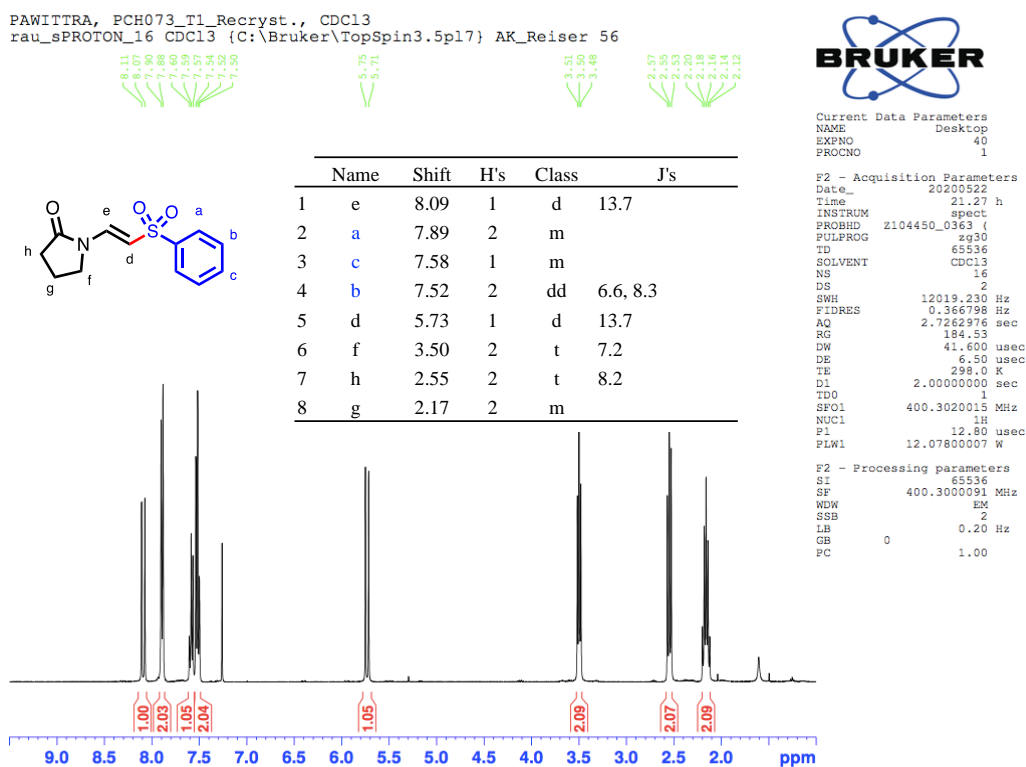


Figure B.85 ^1H NMR spectrum of (E)-1-(2-(phenylsulfonyl)vinyl)pyrrolidin-2-one, (E)-4ta

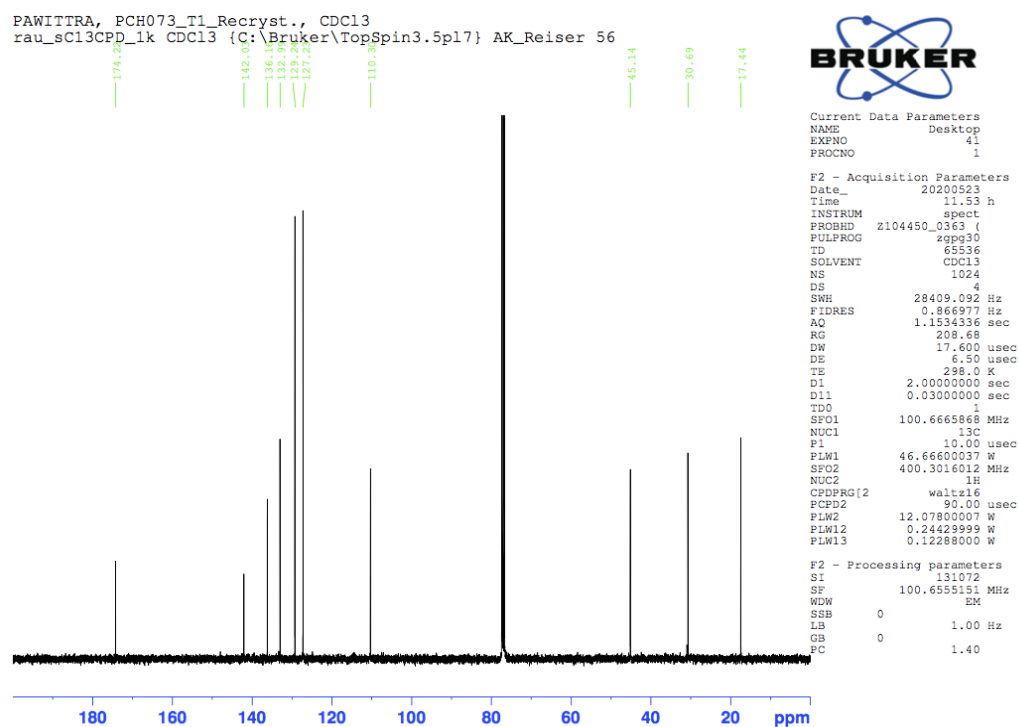


Figure B.86 ^{13}C NMR spectrum of (E)-1-(2-(phenylsulfonyl)vinyl)pyrrolidin-2-one, (E)-4ta

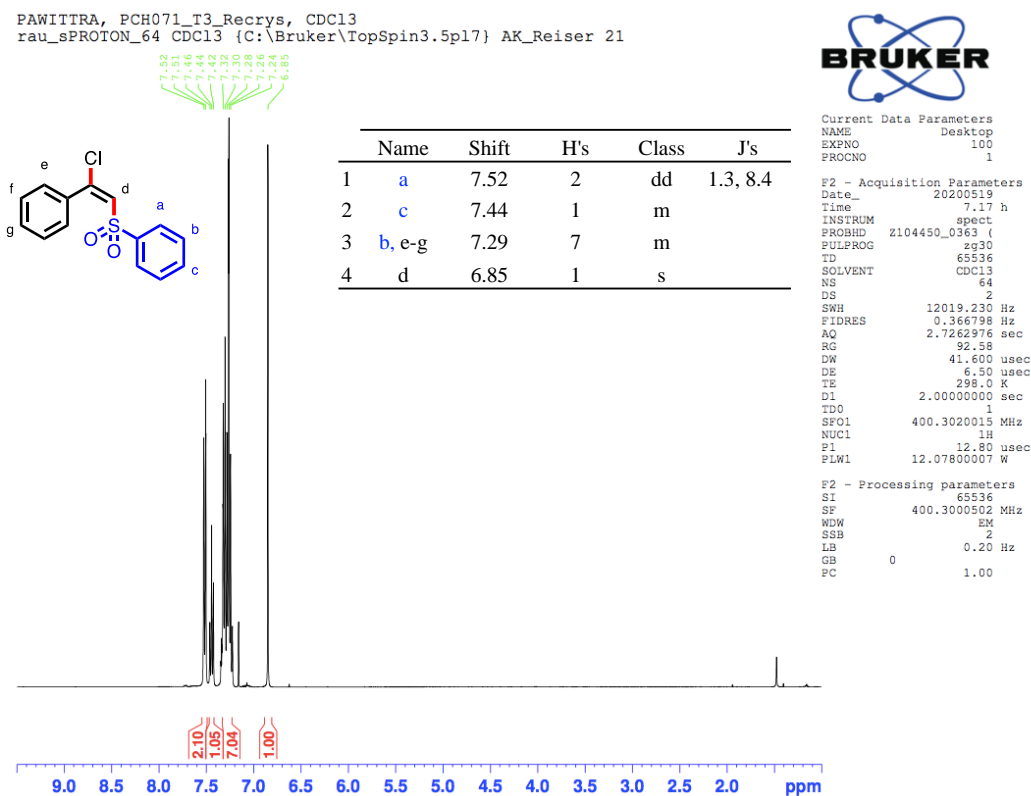


Figure B.87 ¹H NMR spectrum of (1-chloro-2-(phenylsulfonyl)vinyl)benzene, (*E*)-6aa

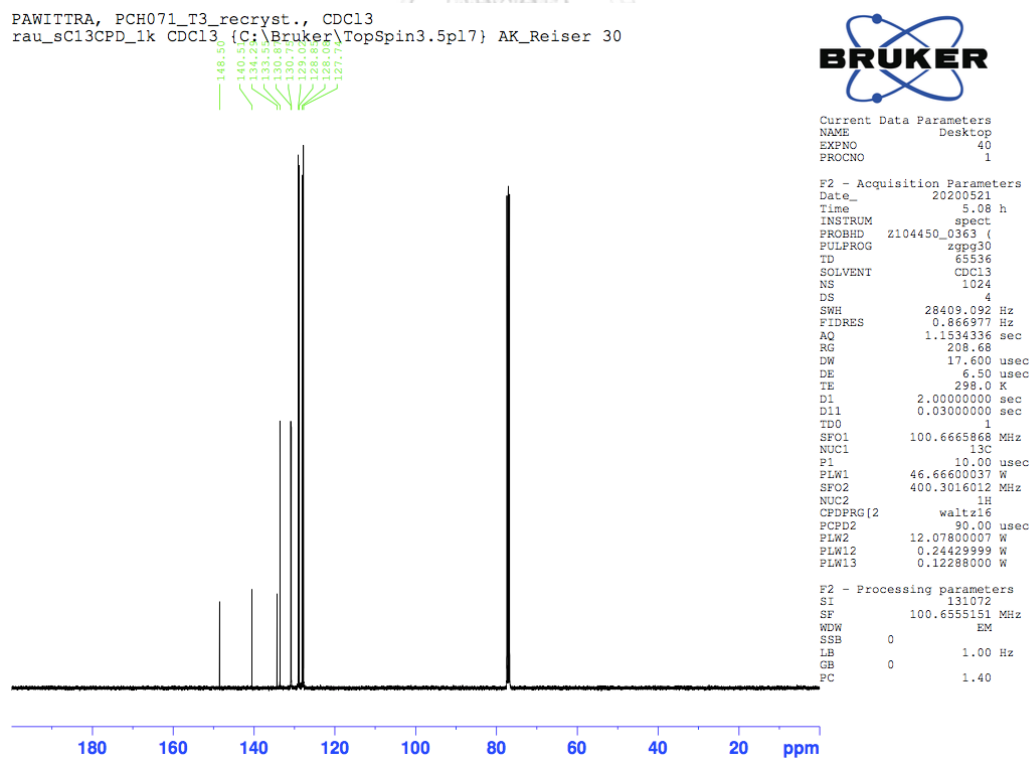


Figure B.88 ¹³C NMR spectrum of (1-chloro-2-(phenylsulfonyl)vinyl)benzene, (*E*)-6aa

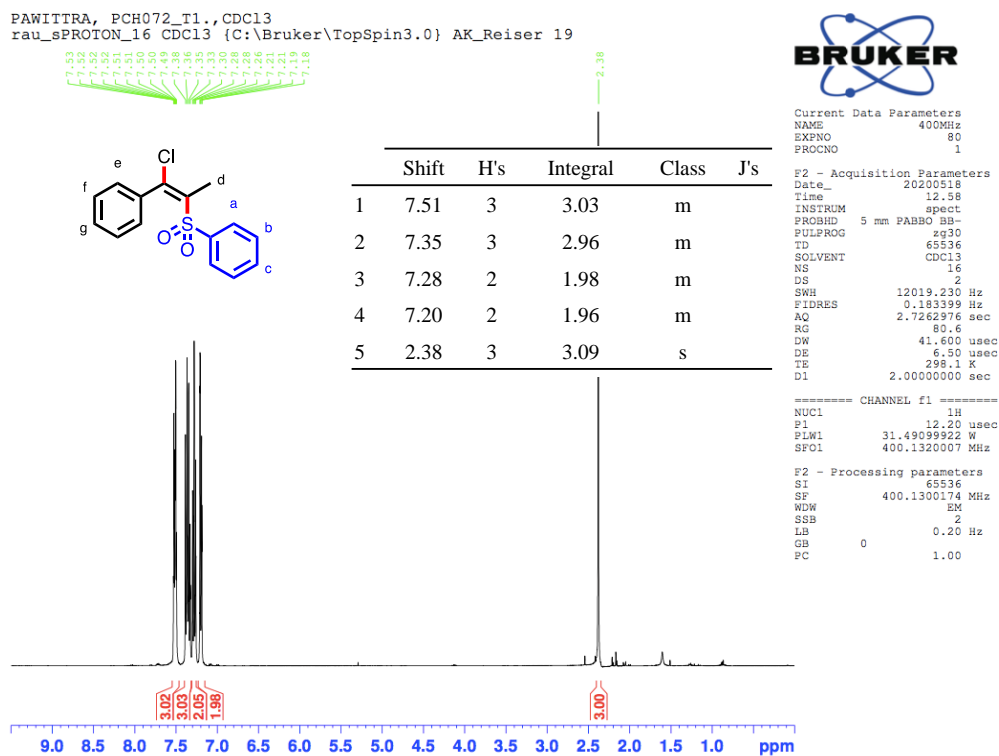


Figure B.89 ^1H NMR spectrum of ((1-chloro-1-phenylprop-1-en-2-yl)sulfonyl)benzene, (E)-6ba

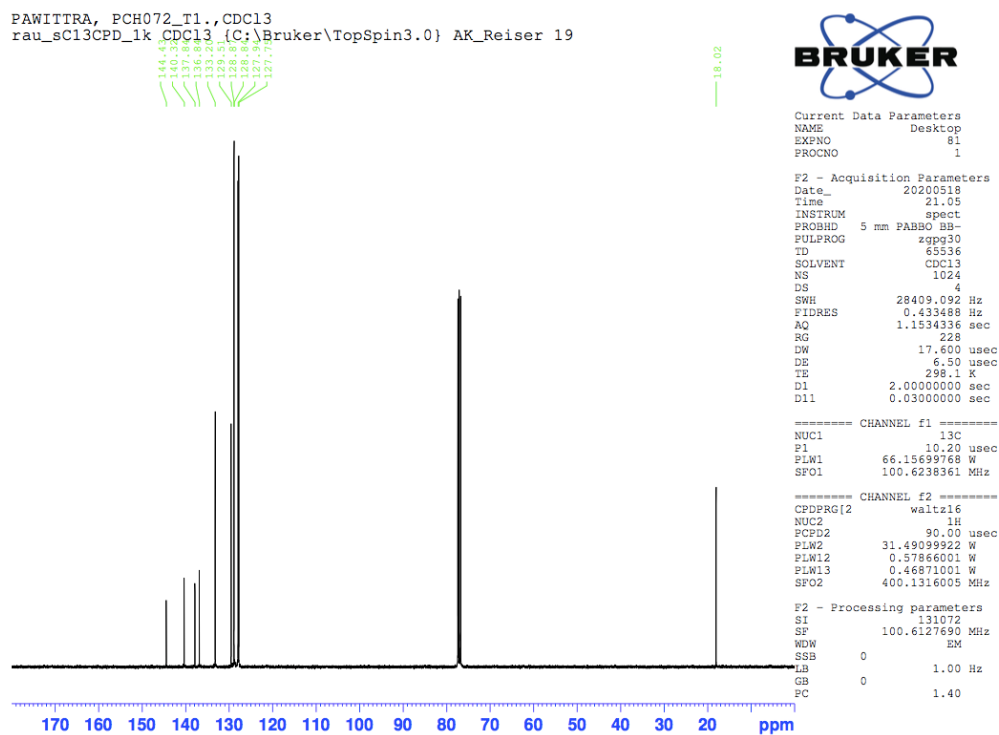
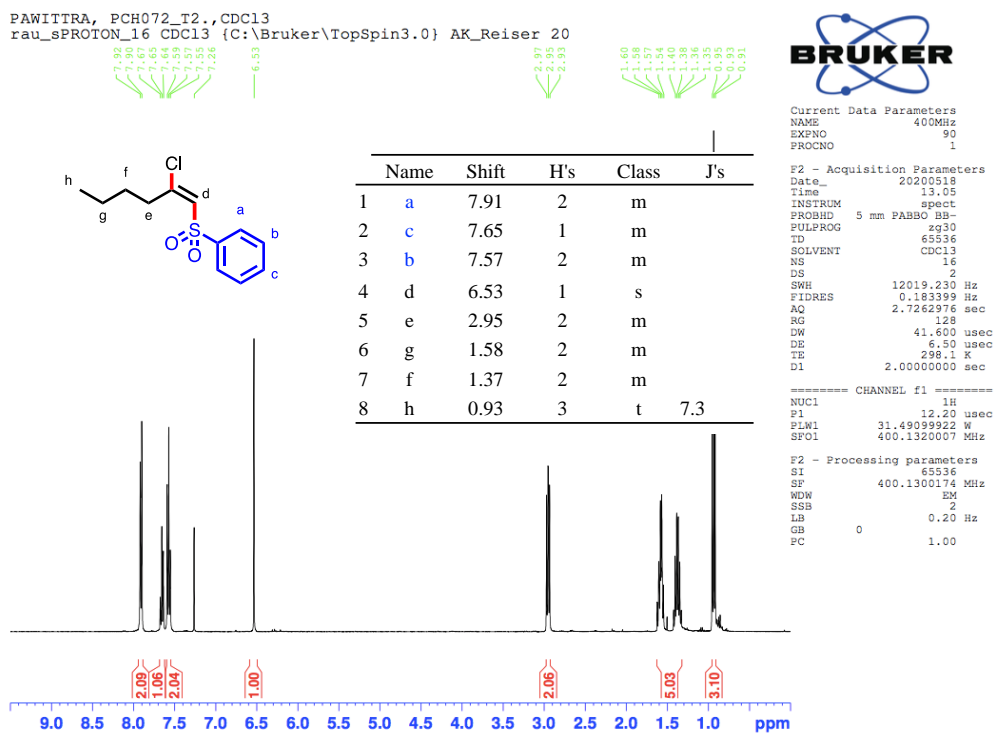
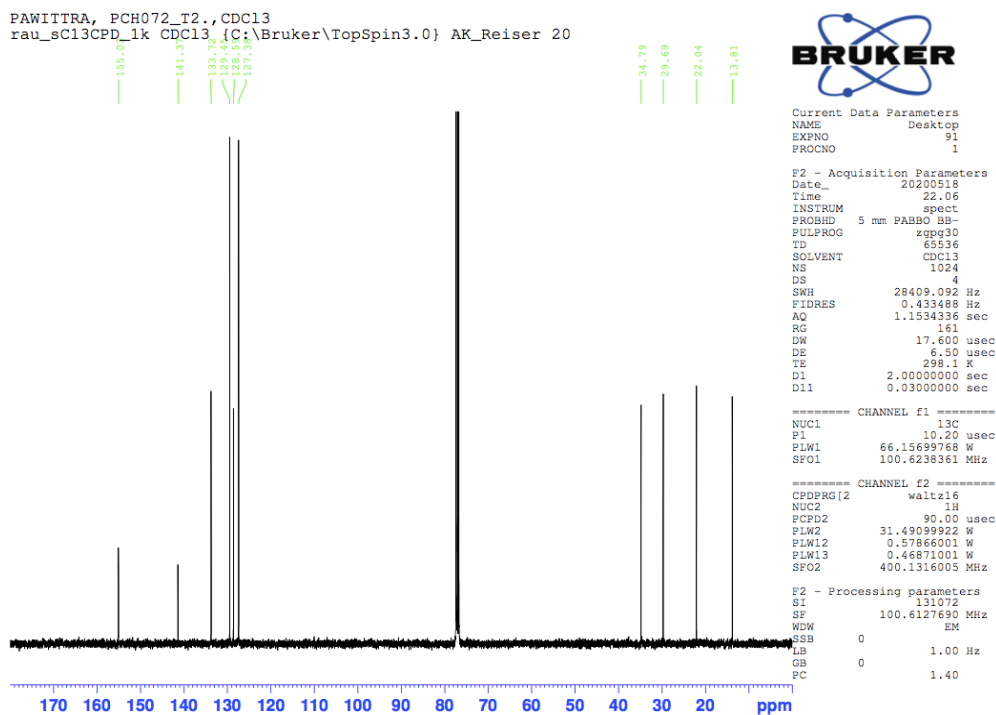
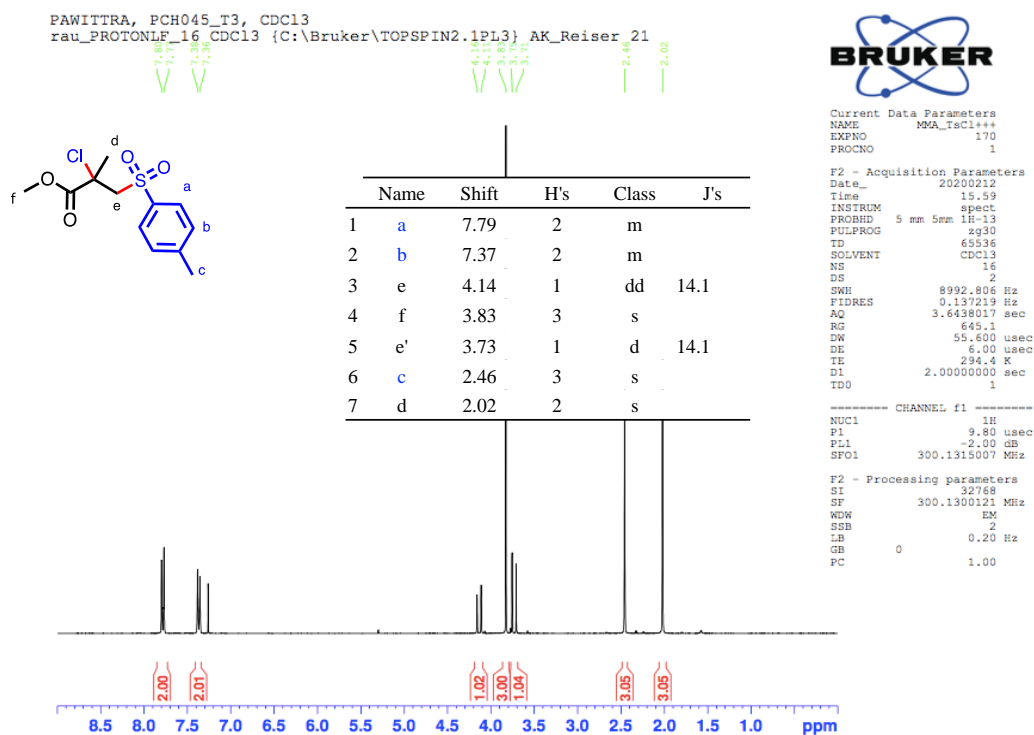
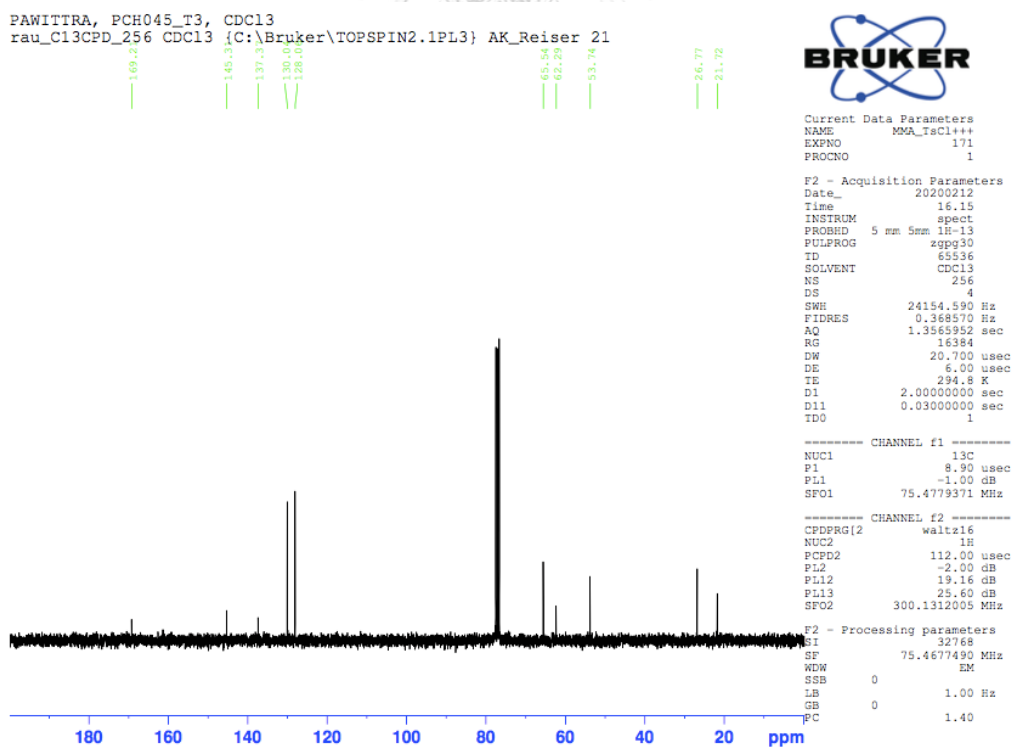


Figure B.90 ^{13}C NMR spectrum of ((1-chloro-1-phenylprop-1-en-2-yl)sulfonyl)benzene, (E)-6ba

Figure B.91 ¹H NMR spectrum of ((2-chlorohex-1-en-1-yl)sulfonyl)benzene, (*E*)-6caFigure B.92 ¹³C NMR spectrum of ((2-chlorohex-1-en-1-yl)sulfonyl)benzene, (*E*)-6ca

Figure B.93 ¹H NMR spectrum of methyl-2-chloro-2-methyl-3-tosylpropanoate, 3ibFigure B.94 ¹³C NMR spectrum of methyl-2-chloro-2-methyl-3-tosylpropanoate, 3ib

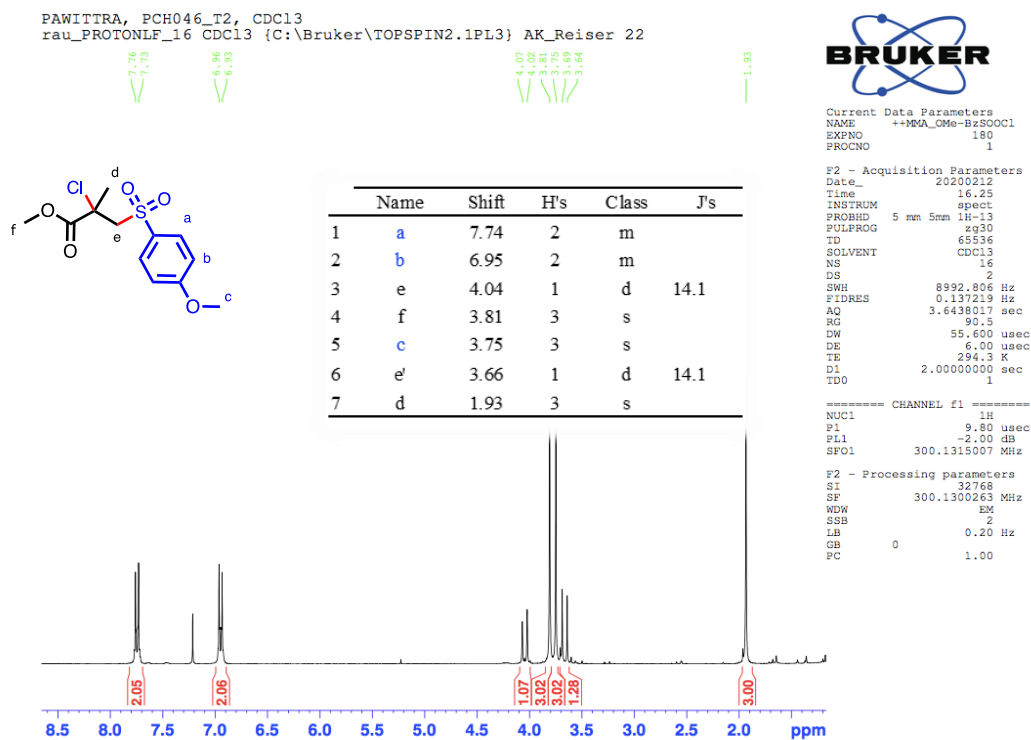


Figure B.95 ^1H NMR spectrum of methyl-2-chloro-3-((4-methoxyphenyl)sulfonyl)-2-methylpropanoate, **3ic**

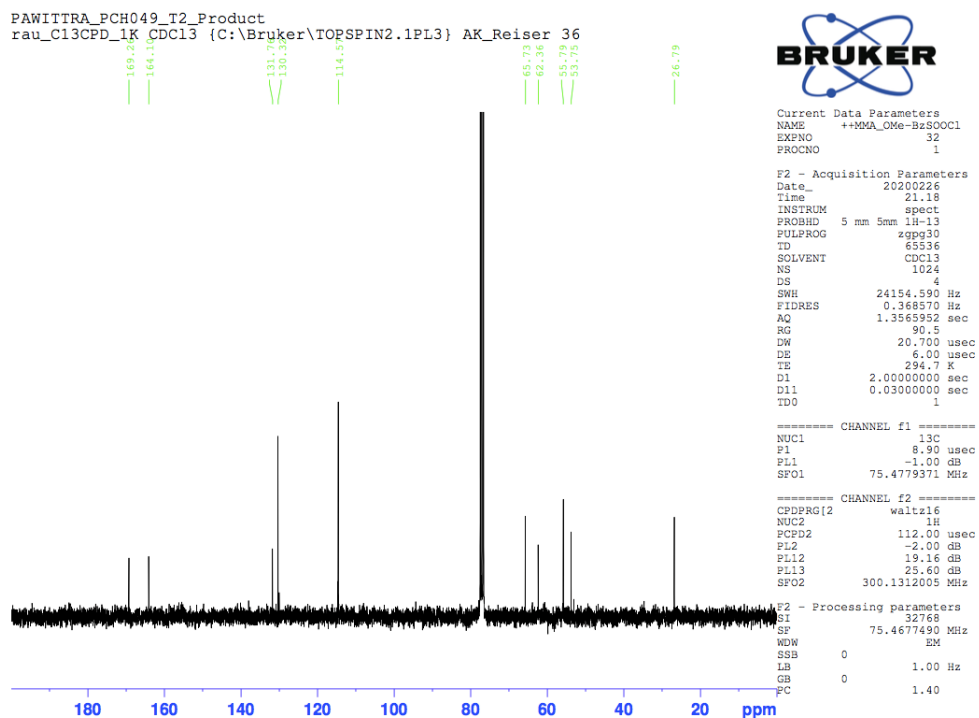


Figure B.96 ^{13}C NMR spectrum of methyl-2-chloro-3-((4-methoxyphenyl)sulfonyl)-2-methylpropanoate, **3ic**

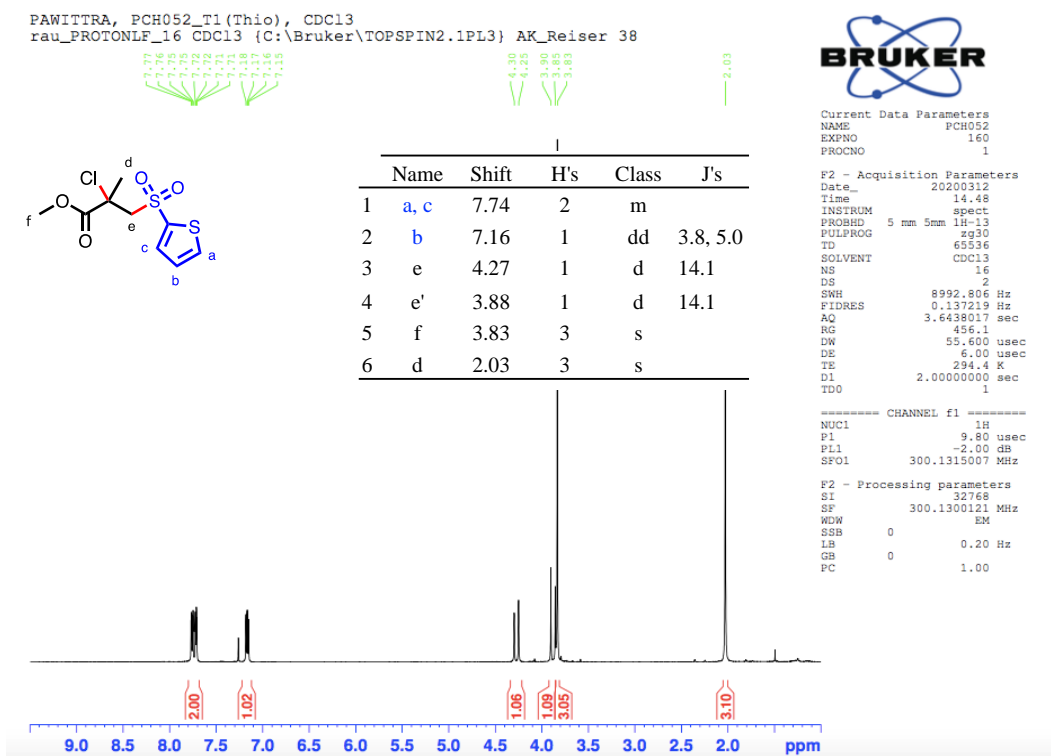


Figure B.97 ^1H NMR spectrum of methyl 2-chloro-2-methyl-3-(thiophen-2-ylsulfonyl)propanoate, **3id**

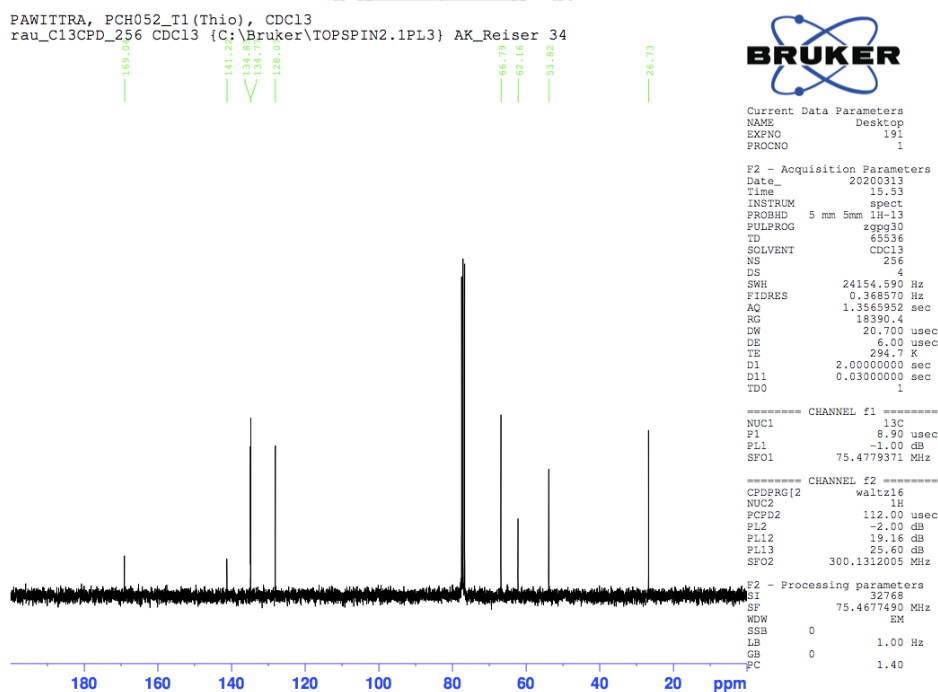


Figure B.98 ^{13}C NMR spectrum of methyl 2-chloro-2-methyl-3-(thiophen-2-ylsulfonyl)propanoate, **3id**

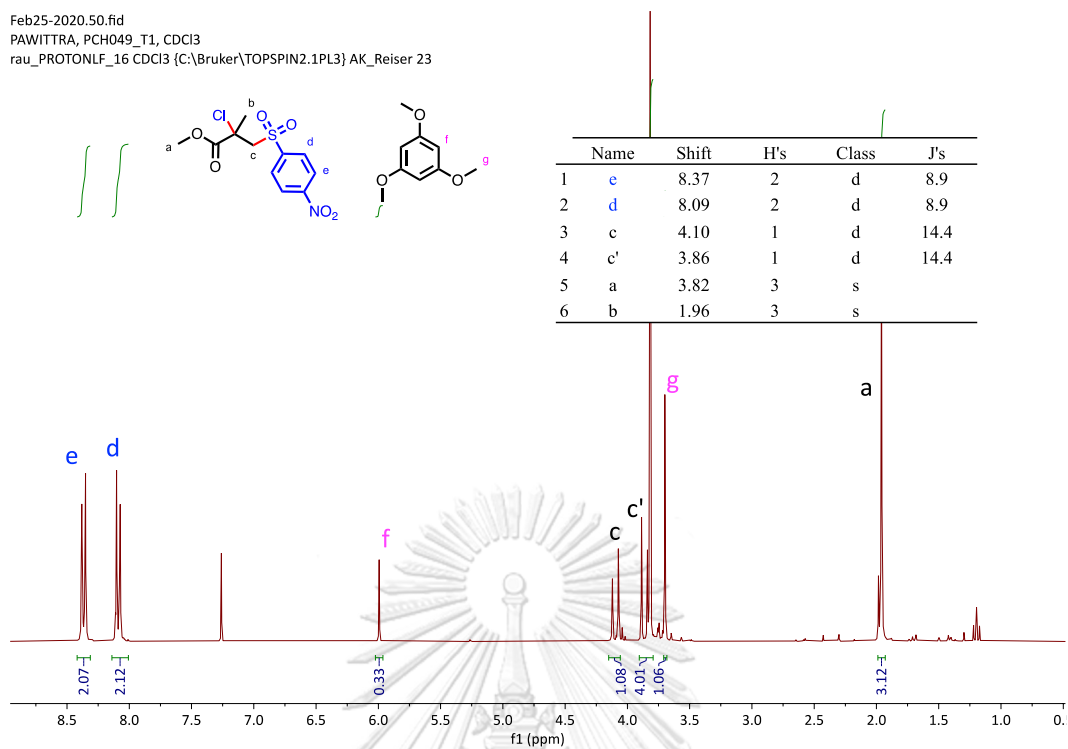


Figure B.99 ^1H NMR spectrum of crude product methyl-2-chloro-2-methyl-3-((4-nitrophenyl)sulfonyl)propanoate, **3ie**

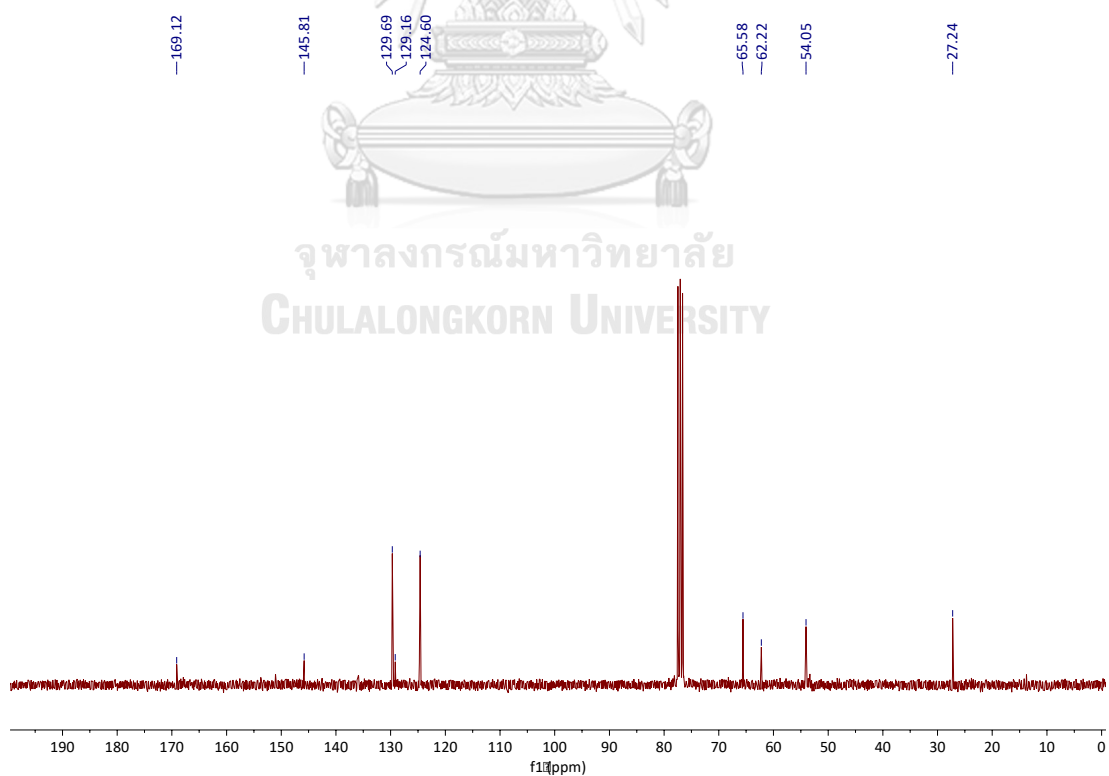


Figure B.100 ^{13}C NMR spectrum of methyl-2-chloro-2-methyl-3-((4-nitrophenyl)sulfonyl)propanoate, **3ie**

Mar16-2020.180.fid
 PAWITTRA, PCH053_T1_P2, CDCl3
 rau_PROTONLF_16 CDCl3 (C:\Bruker\TOPSPIN2.1PL3) AK_Reiser 50

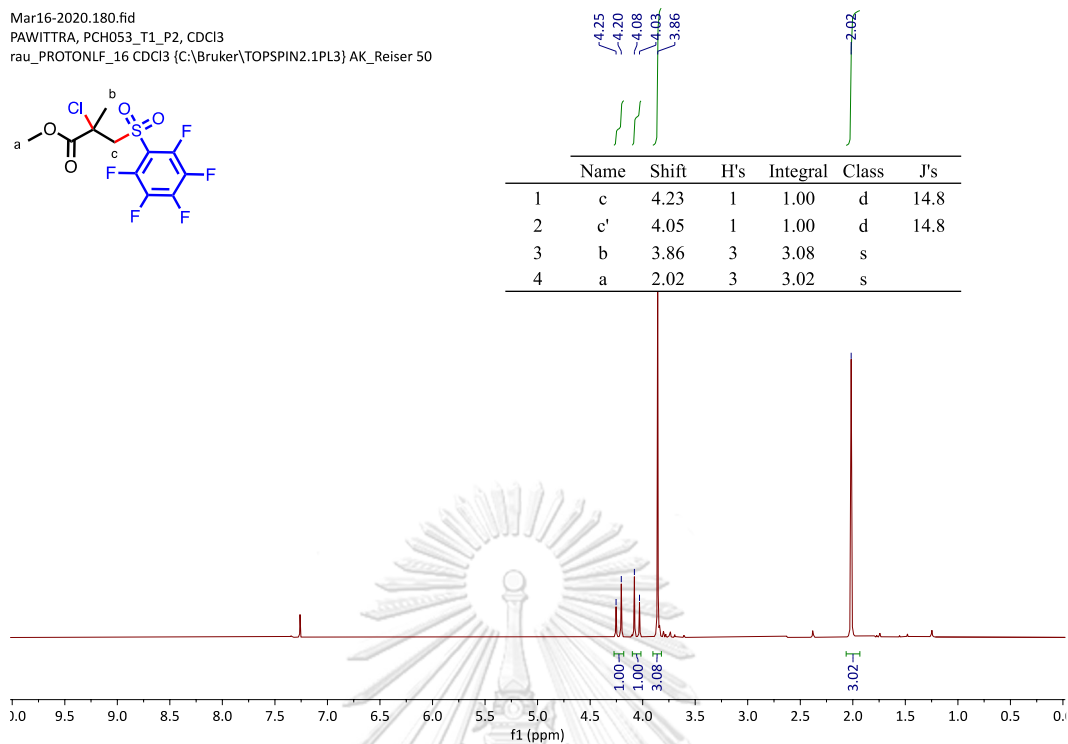
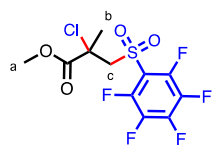


Figure B.101 ^1H NMR spectrum of methyl 2-chloro-2-methyl-3-((perfluorophenyl)sulfonyl)propanoate, **3if**

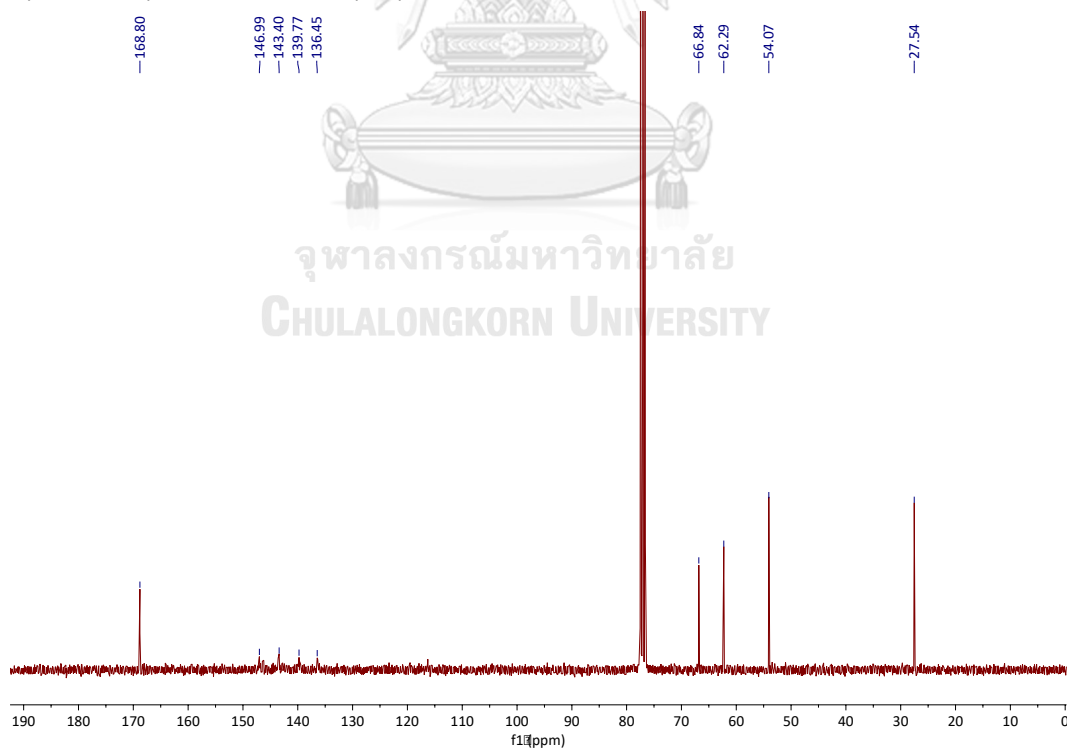


Figure B.102 ^{13}C NMR spectrum of methyl 2-chloro-2-methyl-3-((perfluorophenyl)sulfonyl)propanoate, **3if**

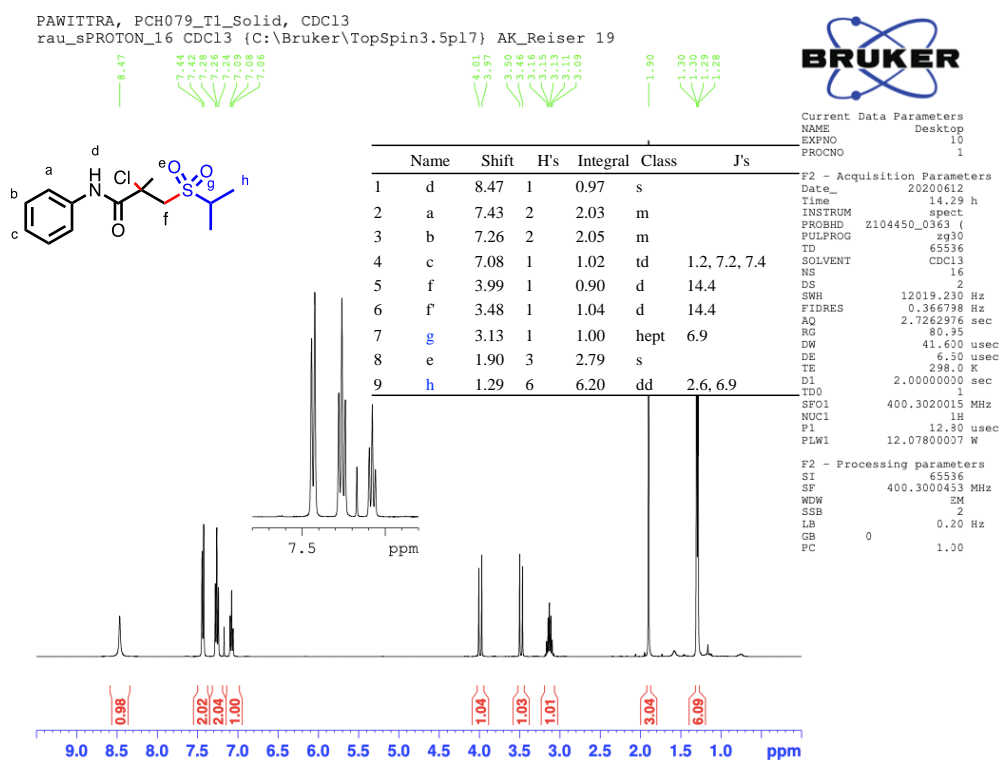


Figure B.103 ^1H NMR spectrum of 2-chloro-3-(isopropylsulfonyl)-2-methyl-N-phenylpropanamide, **3ug**

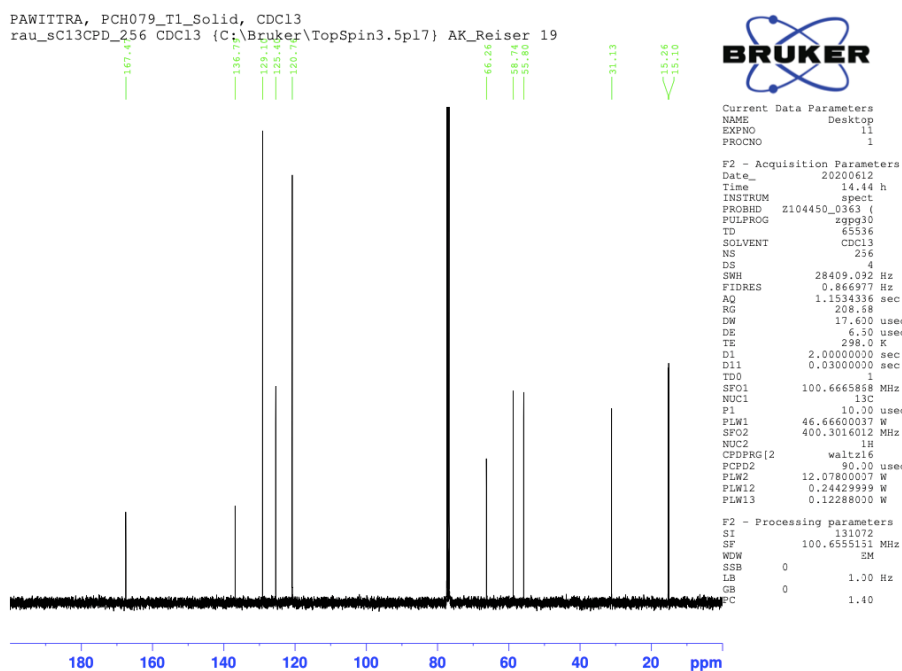


Figure B.104 ^{13}C NMR spectrum of 2-chloro-3-(isopropylsulfonyl)-2-methyl-N-phenylpropanamide, **3ug**

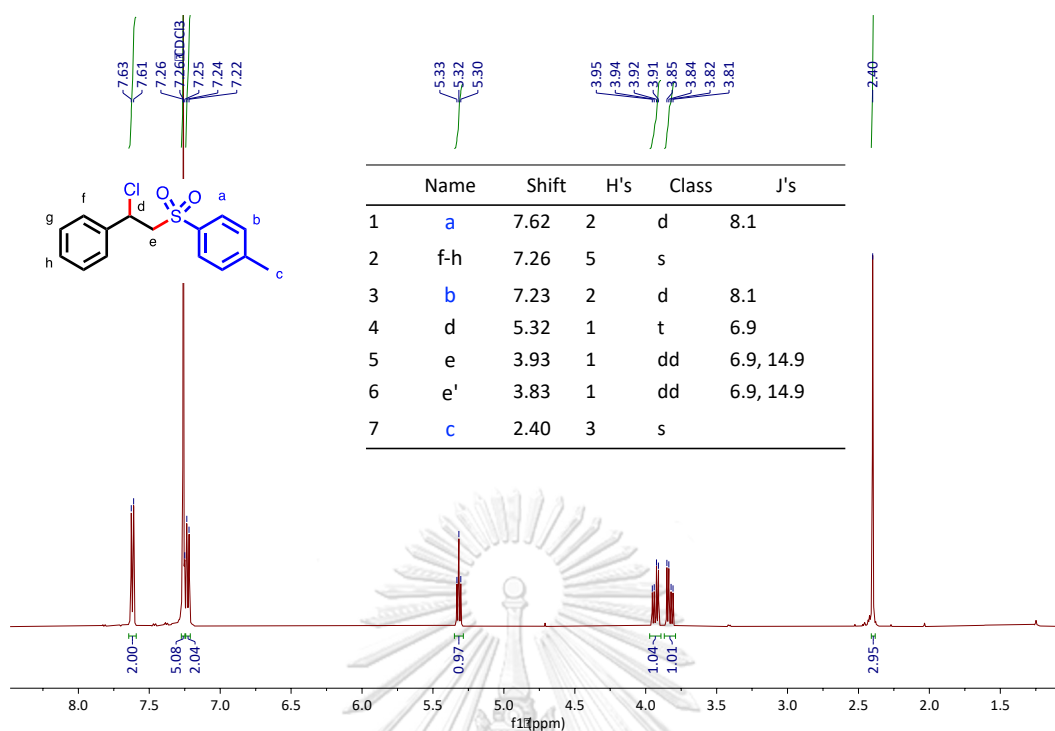


Figure B.105 ^1H NMR spectrum of 1-((2-chloro-2-phenylethyl)sulfonyl)-4-methylbenzene, **3ab**.

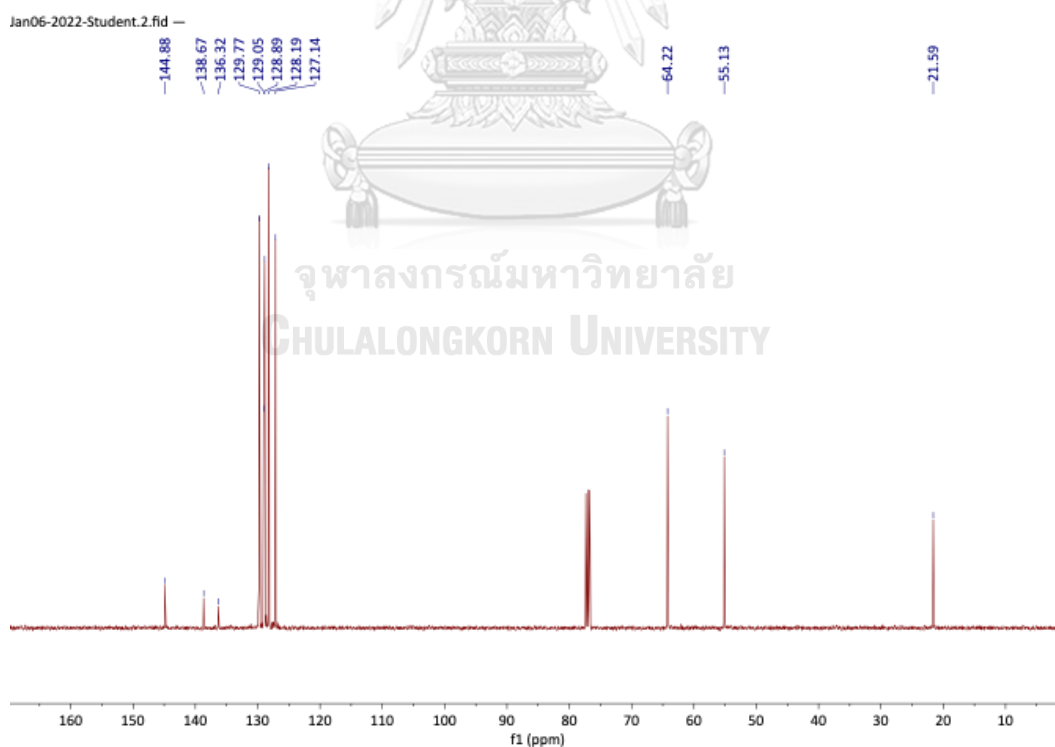


Figure B.106 ^{13}C NMR spectrum of 1-((2-chloro-2-phenylethyl)sulfonyl)-4-methylbenzene, **3ab**.

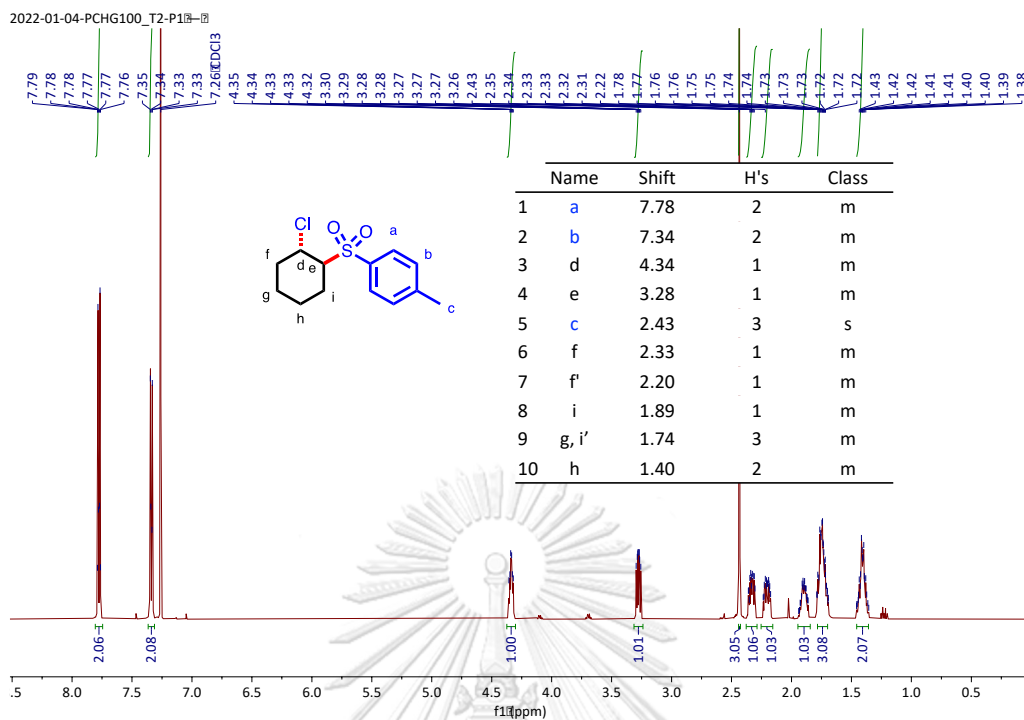


Figure B.107 ^1H NMR spectrum of 1-((2-chlorocyclohexyl)sulfonyl)-4-methylbenzene, *anti*-3pb

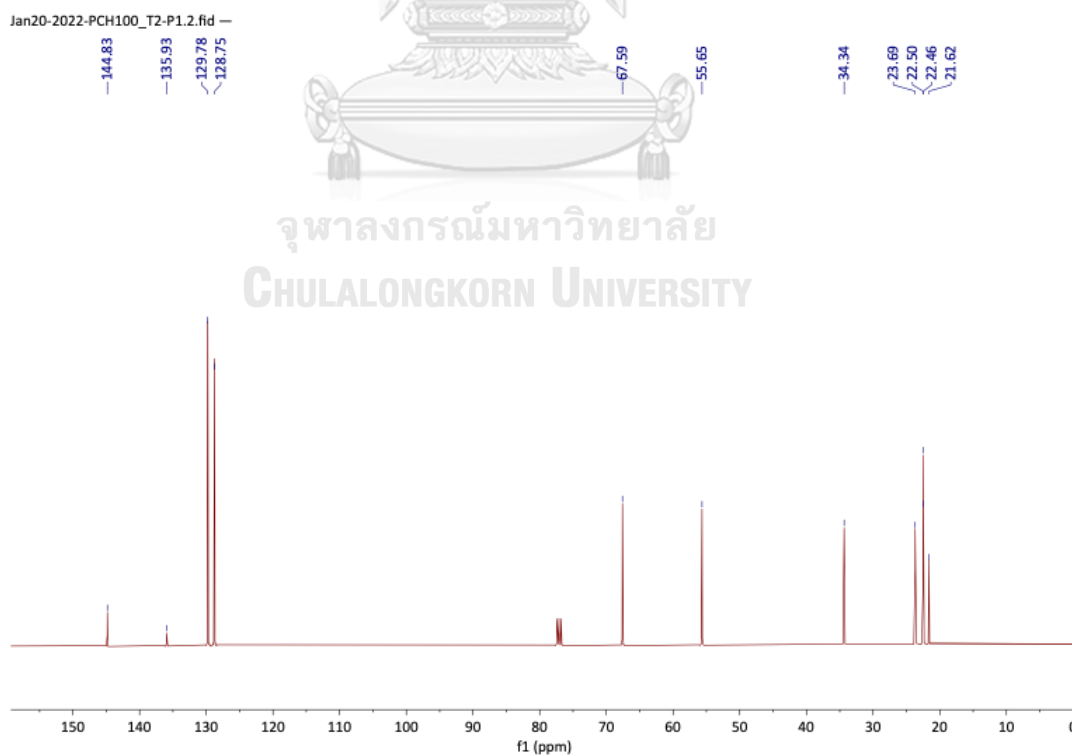


Figure B.108 ^{13}C NMR spectrum of 1-((2-chlorocyclohexyl)sulfonyl)-4-methylbenzene, *anti*-3pb.

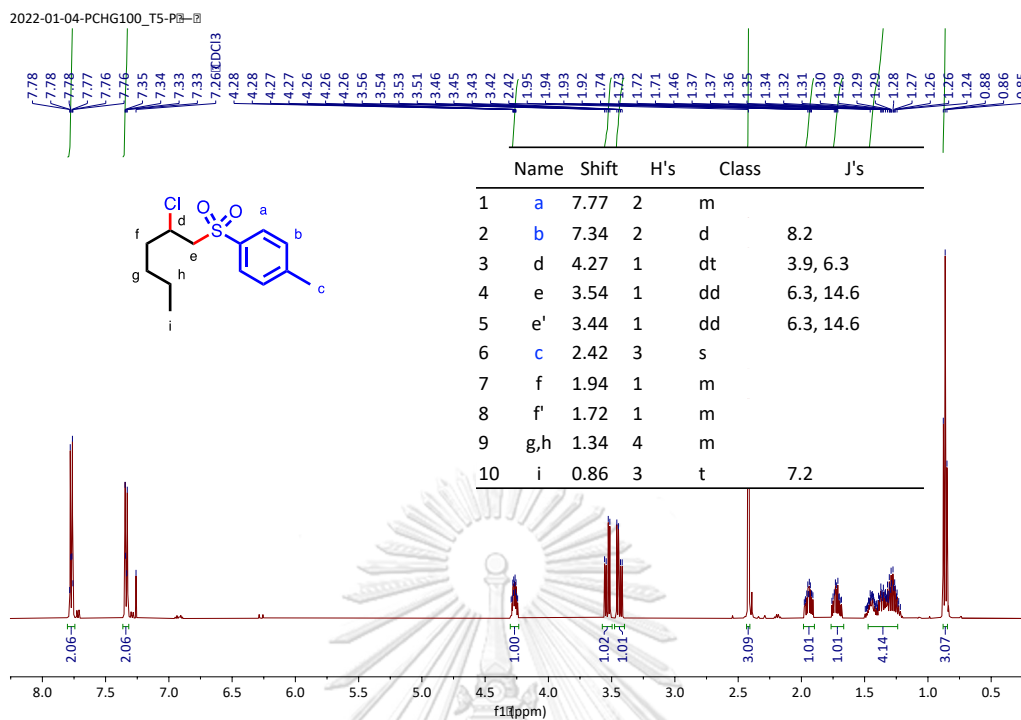


Figure B.109 ^1H NMR spectrum of 1-((2-chlorohexyl)sulfonyl)-4-methylbenzene, **3vb**

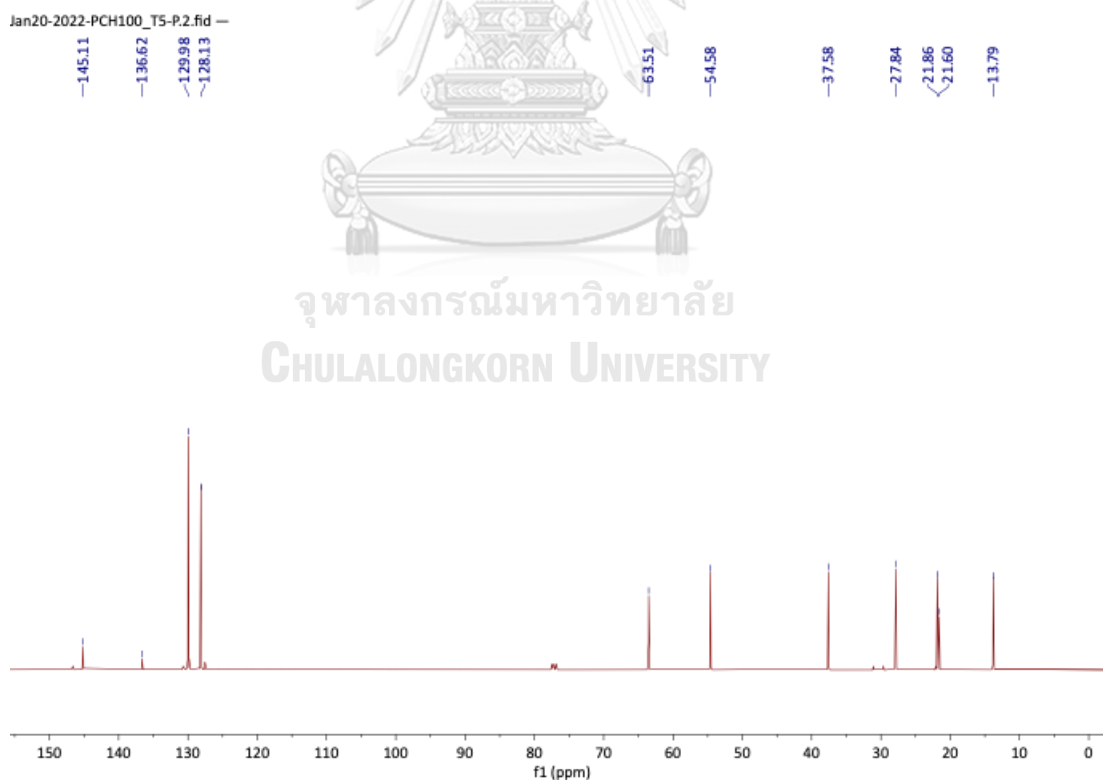


Figure B.110 ^{13}C NMR spectrum of 1-((2-chlorohexyl)sulfonyl)-4-methylbenzene, **3vb**

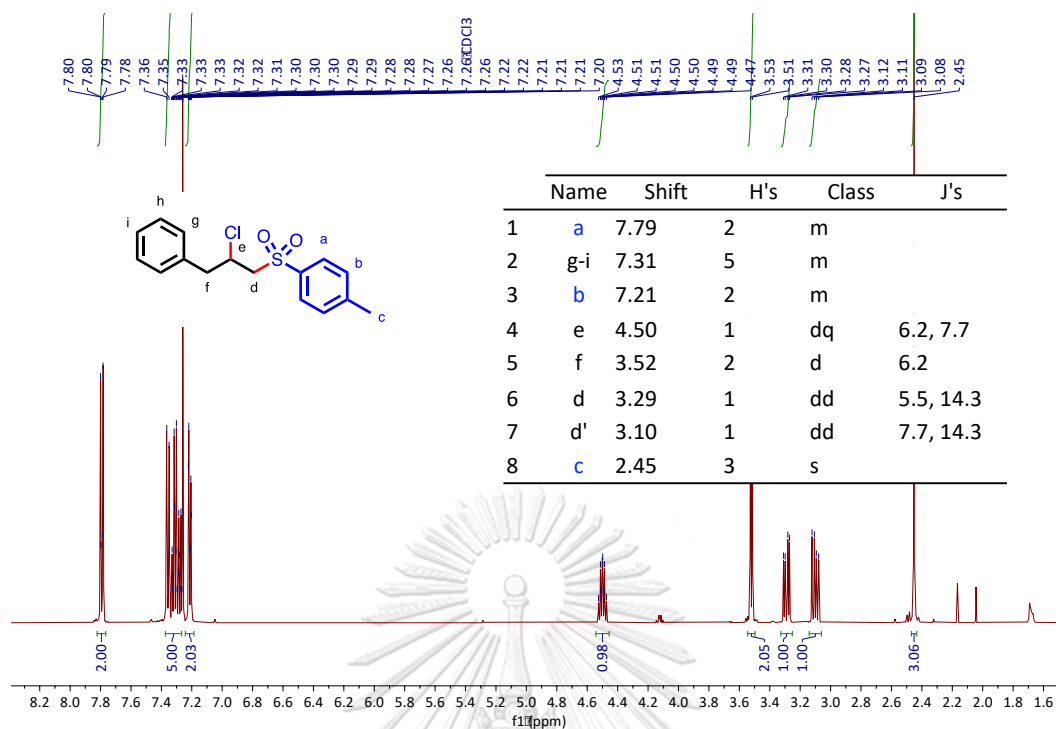


Figure B.111 ^1H NMR spectrum of 1-chloro-2-tosyl-2,3-dihydro-1*H*-indene, **3wb**.

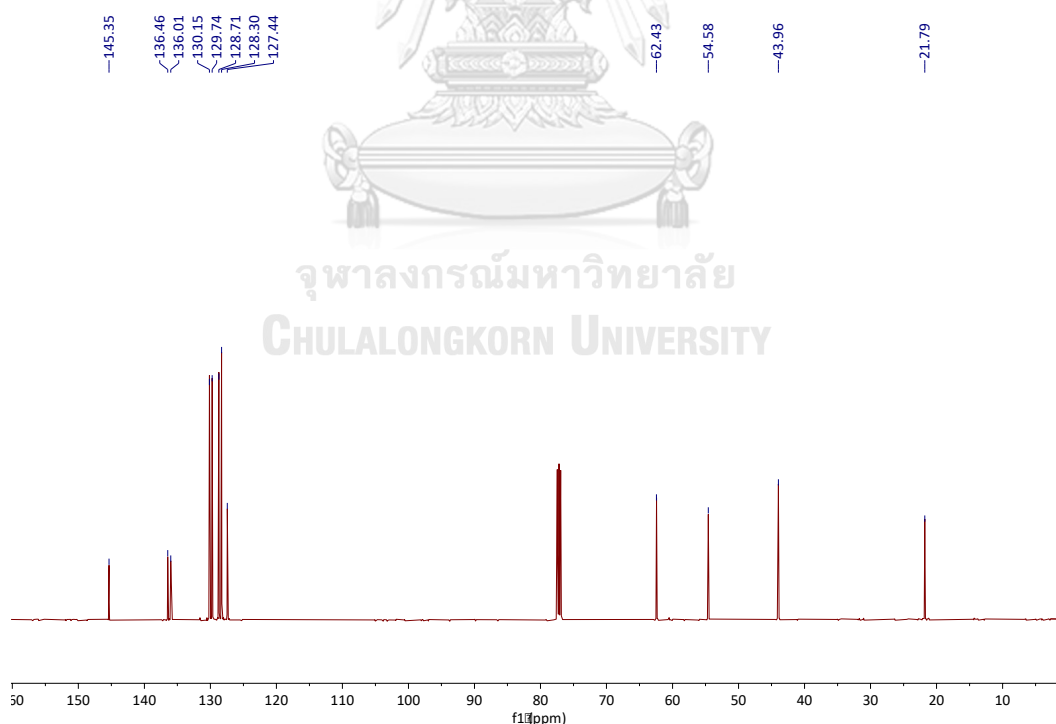


Figure B.112 ^{13}C NMR spectrum of 1-chloro-2-tosyl-2,3-dihydro-1*H*-indene, **3wb**

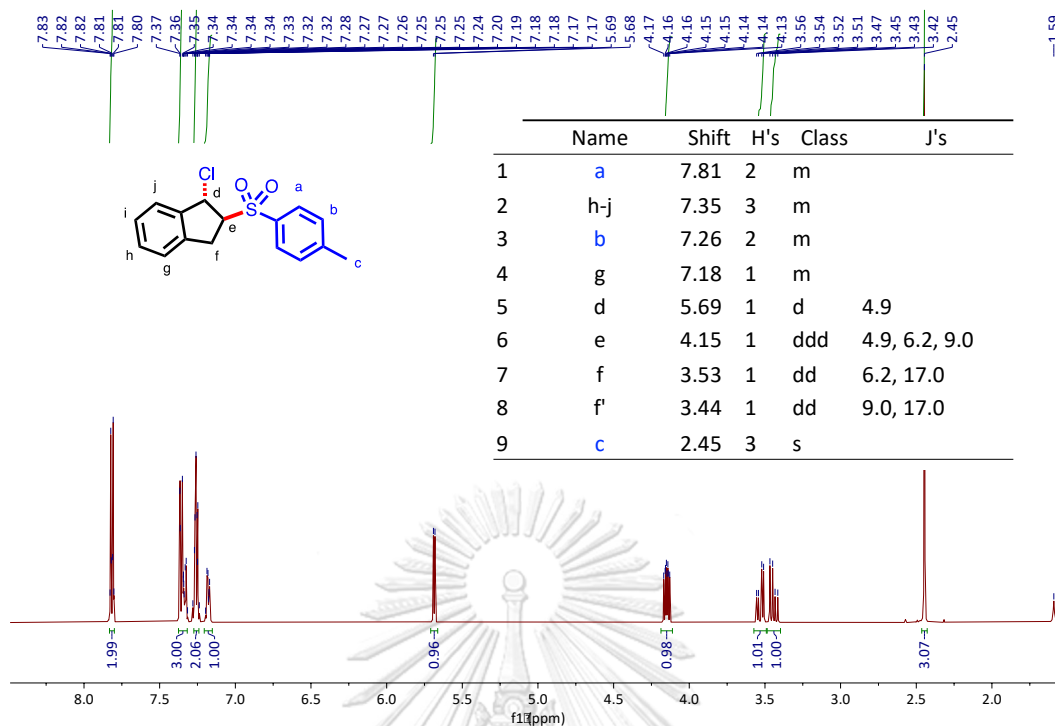


Figure B.113 ^1H NMR spectrum of 1-chloro-2-tosyl-2,3-dihydro-1*H*-indene, *anti*-3xb.

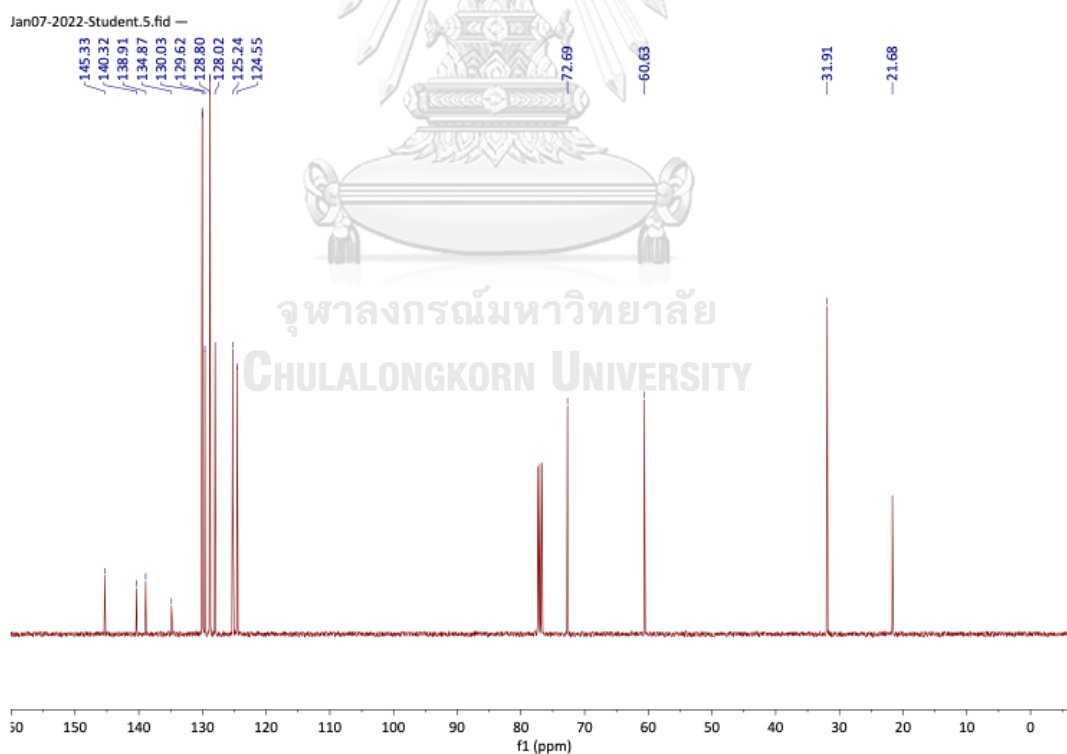


Figure B.114 ^{13}C NMR spectrum of 1-chloro-2-tosyl-2,3-dihydro-1*H*-indene, *anti*-3xb.

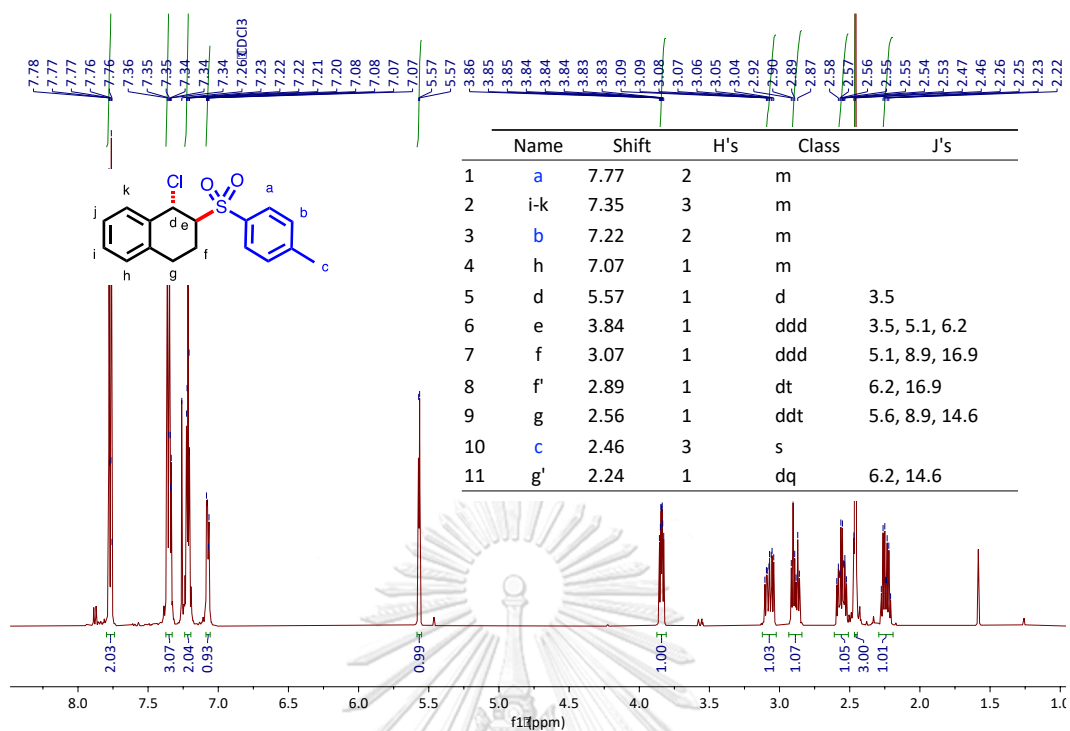


Figure B.115 ^1H NMR spectrum of 1-chloro-2-tosyl-2,3-dihydro-1H-indene, *anti-3yb*

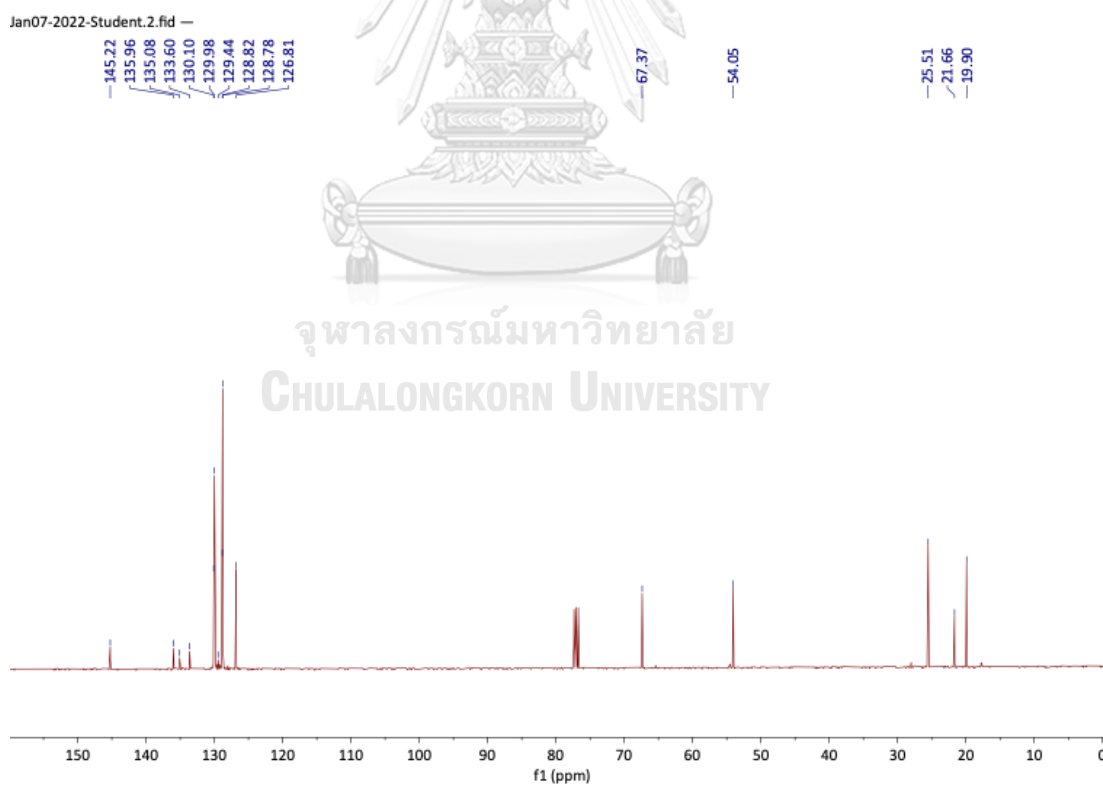


Figure B.116 ^{13}C NMR spectrum of 1-chloro-2-tosyl-2,3-dihydro-1H-indene, *anti-3yb*

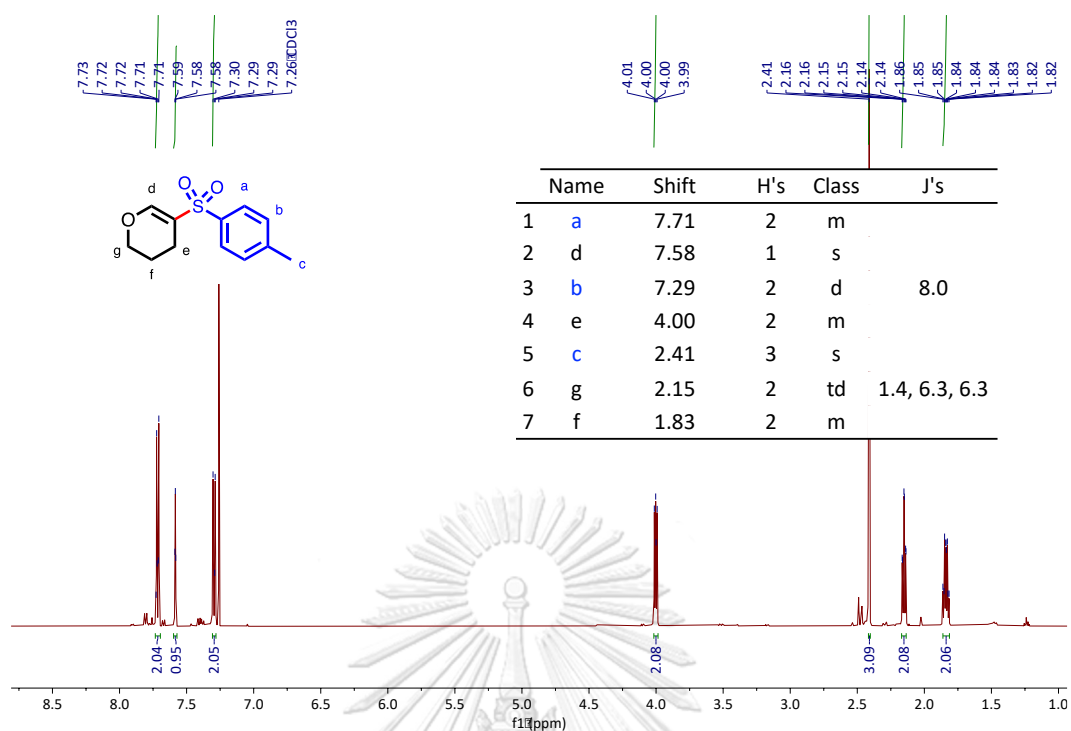


Figure B.117 ¹H NMR spectrum of 5-(4-methylbenzene)-3,4-dihydro-2H-pyran, **4sb**.

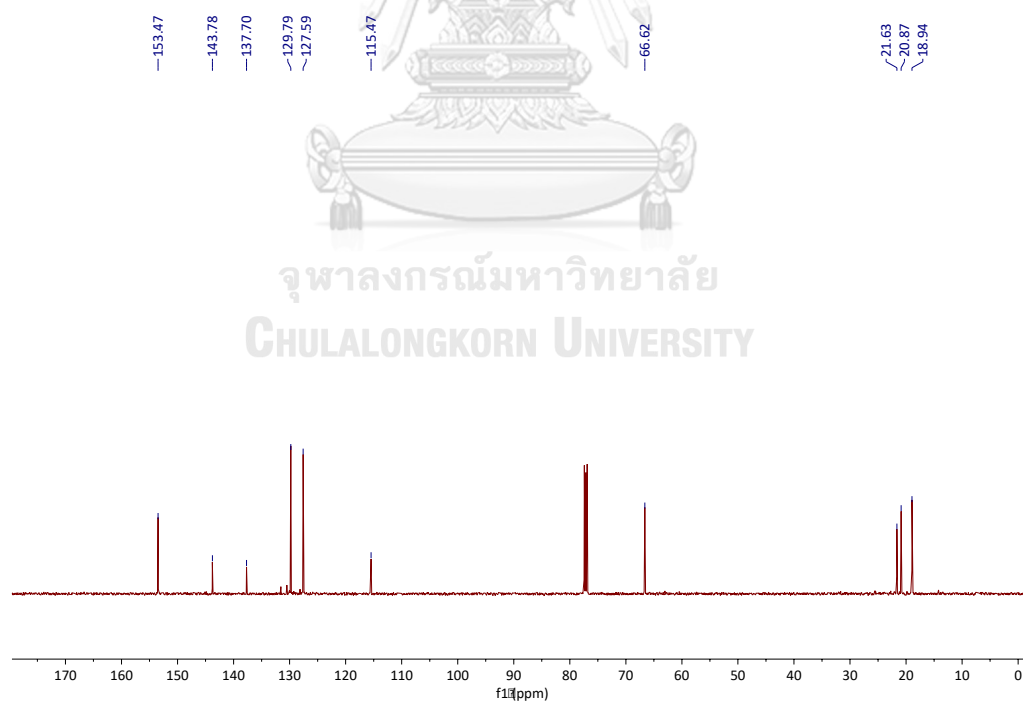


Figure B.118 ¹³C NMR spectrum of 5-(4-methylbenzene)-3,4-dihydro-2H-pyran, **4sb**.

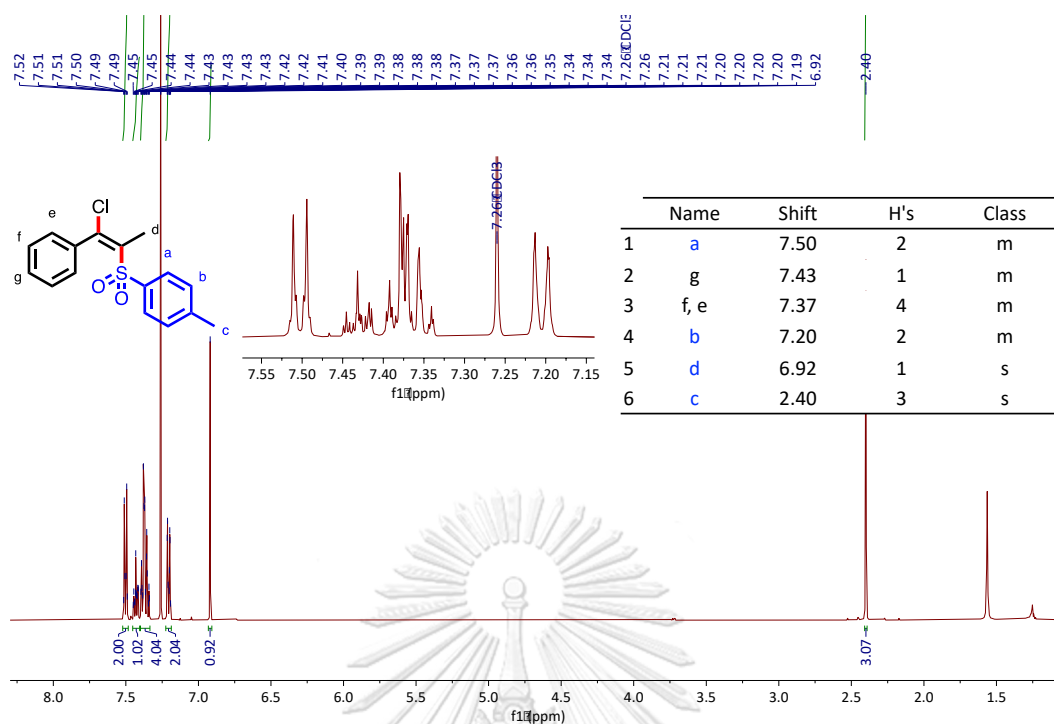


Figure B.119 ^1H NMR spectrum of 1-((2-chloro-2-phenylvinyl)sulfonyl)-4-methylbenzene, (**E**)-**6ab**.

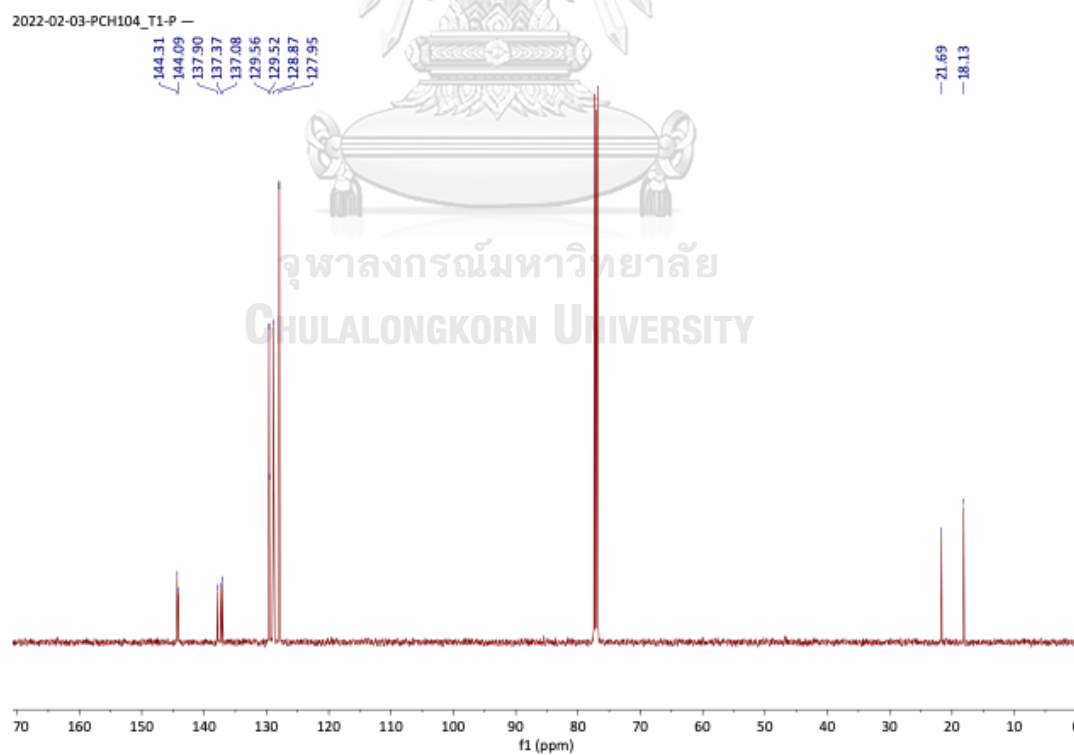


Figure B.120 ^{13}C NMR spectrum of 1-((2-chloro-2-phenylvinyl)sulfonyl)-4-methylbenzene, (**E**)-**6ab**.

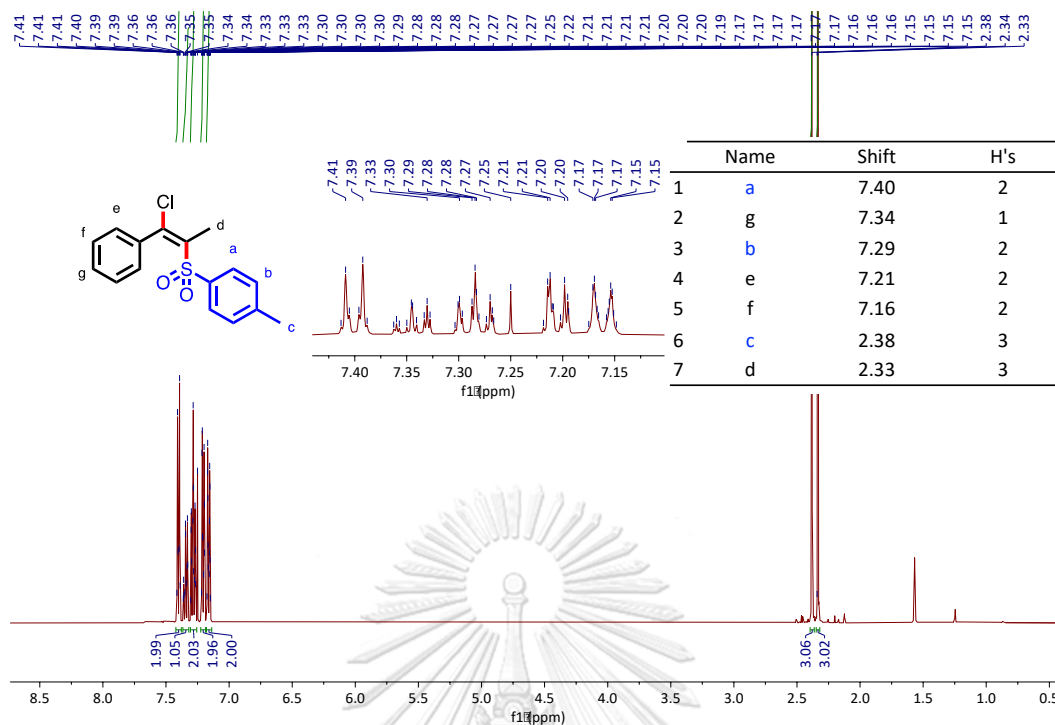


Figure B.121 ¹H NMR spectrum of 1-((1-chloro-1-phenylprop-1-en-2-yl)sulfonyl)-4-methylbenzene, (**(E)-6bb**)

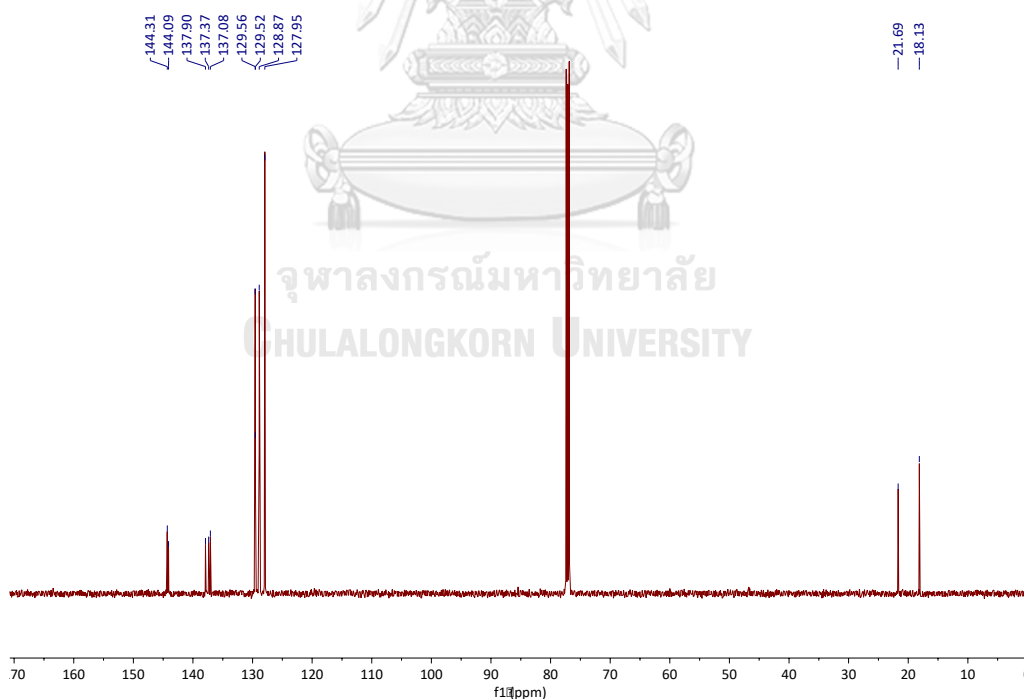


Figure B.122 ¹³C NMR spectrum of 1-((1-chloro-1-phenylprop-1-en-2-yl)sulfonyl)-4-methylbenzene, (**(E)-6bb**)

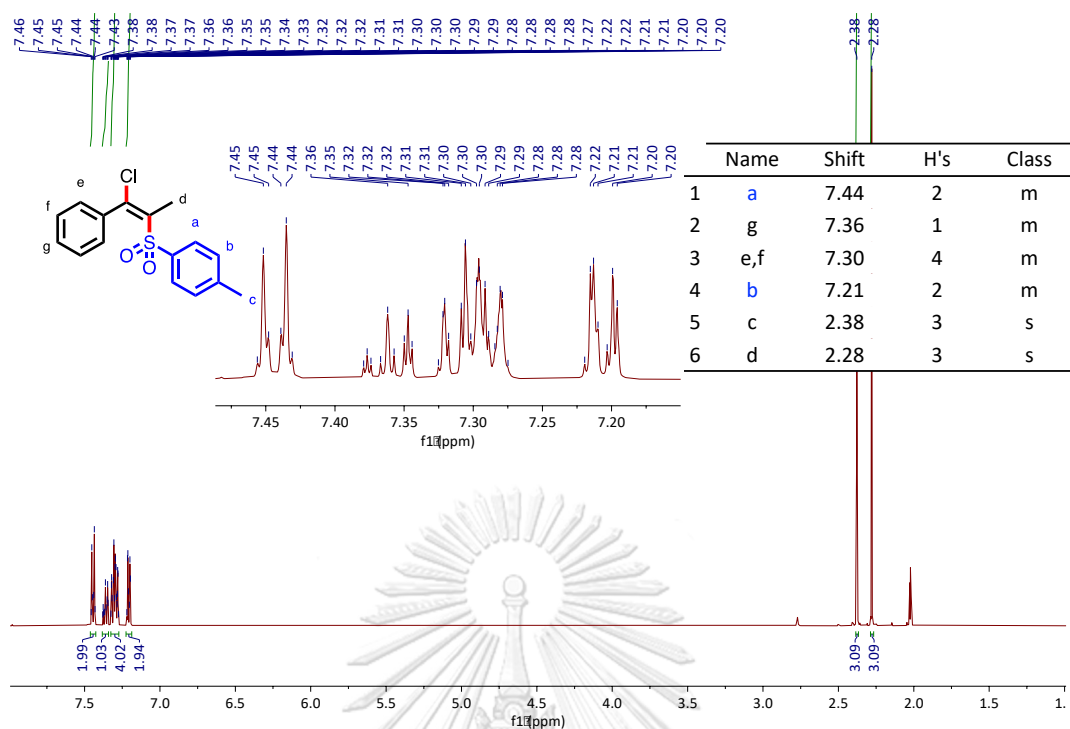


Figure B.123 ^1H NMR spectrum of 1-((1-chloro-1-phenylprop-1-en-2-yl)sulfonyl)-4-methylbenzene in acetone- d_6 , (*E*)-6bb

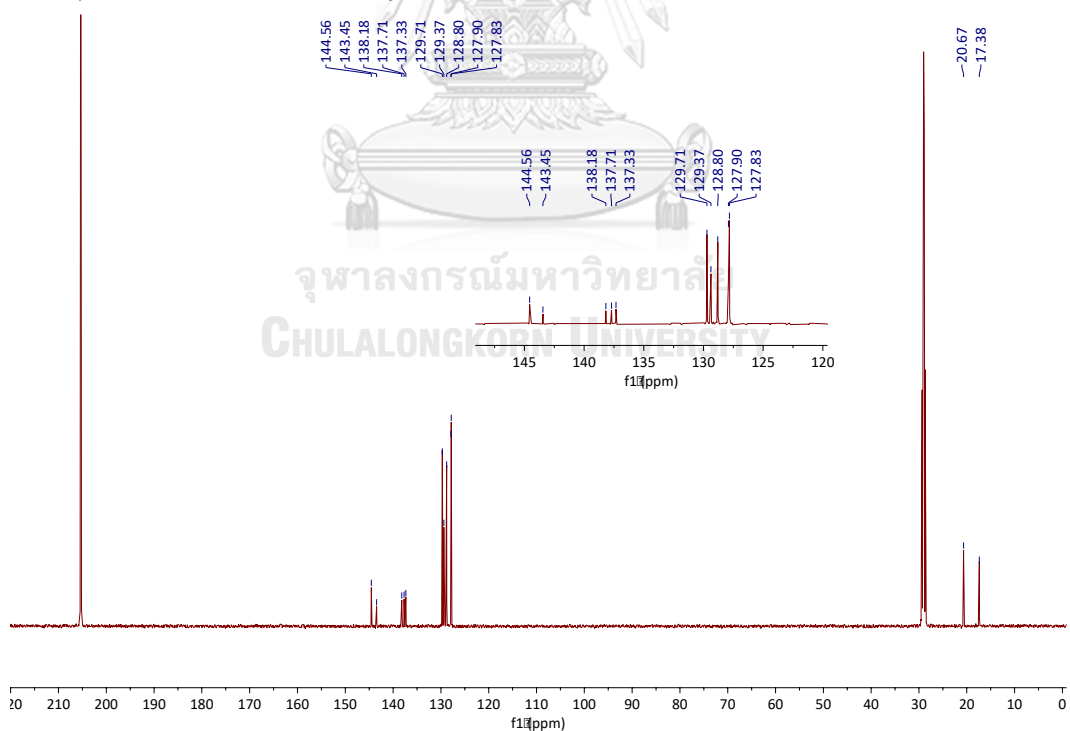


Figure B.124 ^{13}C NMR spectrum of 1-((1-chloro-1-phenylprop-1-en-2-yl)sulfonyl)-4-methylbenzene in acetone- d_6 , (*E*)-6bb

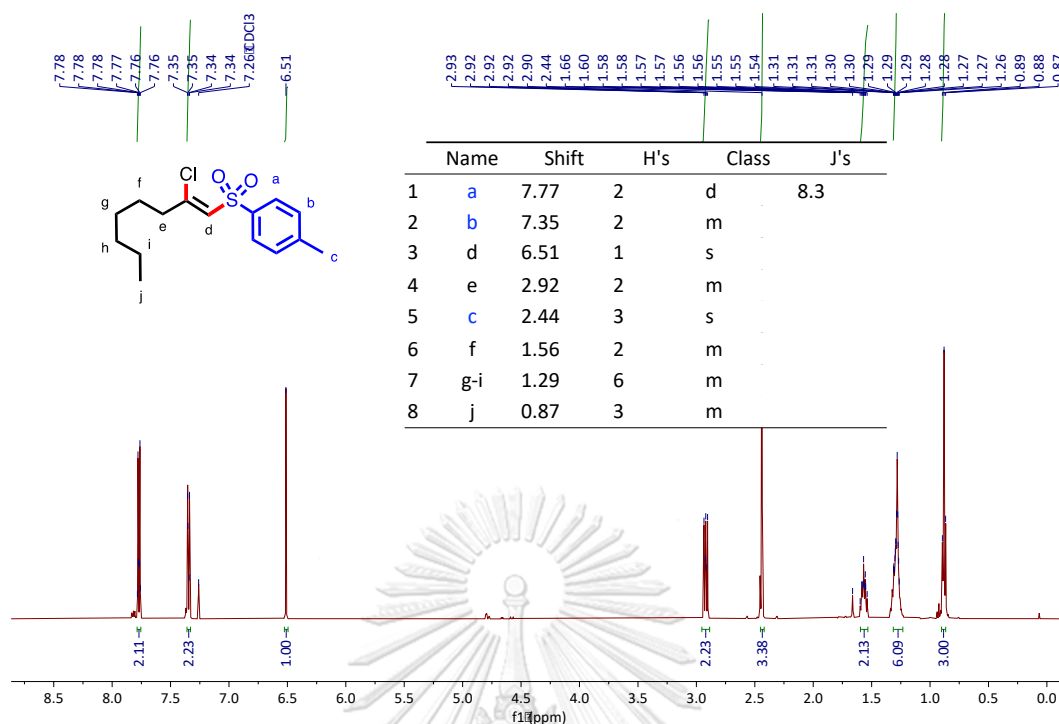


Figure B.125 ^1H NMR spectrum of 1-((2-chloro-1-octenyl)sulfonyl)-4-methylbenzene, (*E*)-6db.

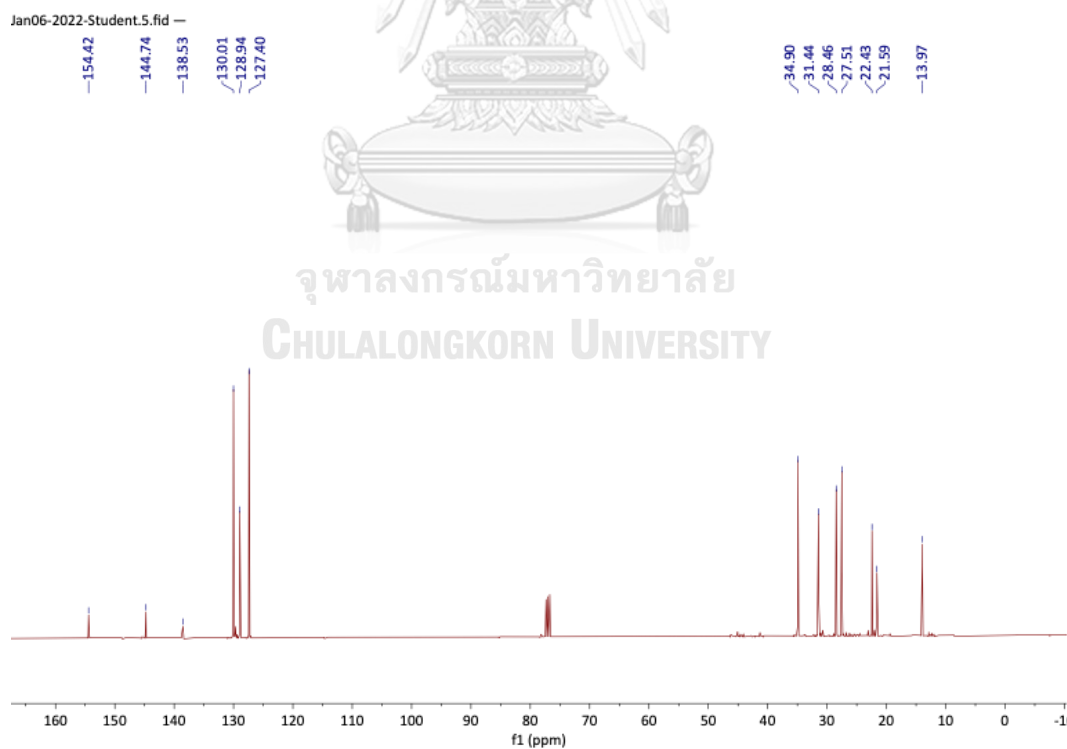
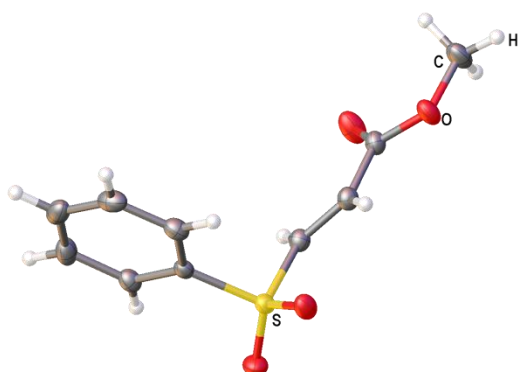


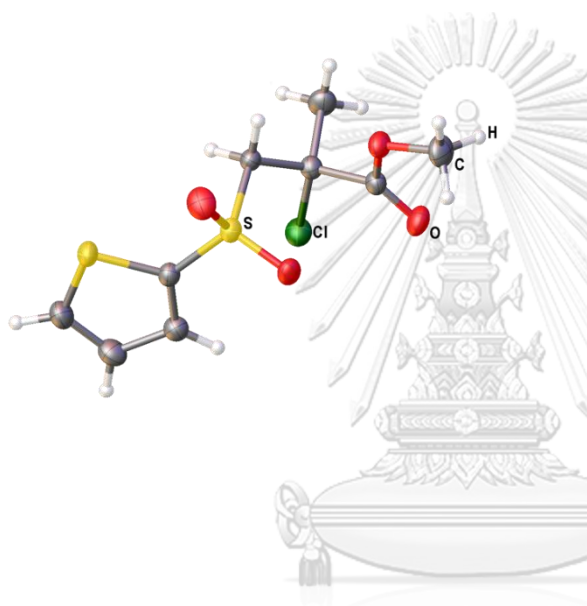
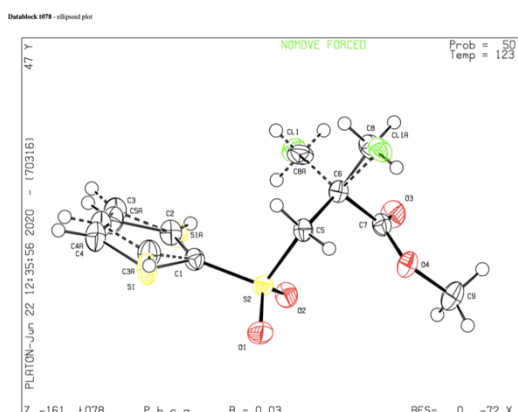
Figure B.126 ^{13}C NMR spectrum of 1-((2-chloro-1-octenyl)sulfonyl)-4-methylbenzene, (*E*)-6db

B.2.3 X-ray Crystallography of Products



Formula	C ₁₀ H ₁₀ O ₄ S
$D_{calc.}/g\text{ cm}^{-3}$	1.447
μ/mm^{-1}	2.732
Formula Weight	226.24
Colour	clear colourless
Shape	prism
Size/mm ³	0.35×0.10×0.07
T/K	123.00(10)
Crystal System	triclinic
Space Group	<i>P</i> -1
$a/\text{Å}$	5.6396(3)
$b/\text{Å}$	7.7098(3)
$c/\text{Å}$	12.5575(5)
$\alpha/^\circ$	86.092(3)
$\beta/^\circ$	86.490(3)
$\gamma/^\circ$	72.547(4)
$V/\text{Å}^3$	519.18(4)
Z	2
Z'	1
Wavelength/Å	1.54184
Radiation type	Cu K_α
$\theta_{min}/^\circ$	3.531
$\theta_{max}/^\circ$	72.895
Measured Refl's.	10867
Indep't Refl's	2047
Refl's $I \geq 2\sigma(I)$	1876
R_{int}	0.0330
Parameters	138
Restraints	0
Largest Peak	0.400
Deepest Hole	-0.373
GooF	1.056
wR_2 (all data)	0.0696
wR_2	0.0678
R_1 (all data)	0.0302
R_1	0.0272

Figure B.127 X-ray crystallography of product (*E*)-4ea.



Formula	C ₉ H ₁₁ ClO ₄ S ₂
<i>D</i> _{calc.} / g cm ⁻³	1.558
μ /mm ⁻¹	4.431
Formula Weight	282.75
Colour	clear colourless
Shape	block
Size/mm ³	0.33×0.17×0.14
<i>T</i> /K	122.99(10)
Crystal System	orthorhombic
Space Group	<i>Pbca</i>
<i>a</i> /Å	13.0211(2)
<i>b</i> /Å	12.0754(2)
<i>c</i> /Å	15.3306(3)
α /°	90
β /°	90
γ /°	90
<i>V</i> /Å ³	2410.51(7)
<i>Z</i>	8
<i>Z</i> '	1
Wavelength/Å	1.39222
Radiation type	Cu K
θ _{min} /°	5.209
θ _{max} /°	74.706
Measured Refl's.	15488
Indep't Refl's	3328
Refl's I \geq 2 σ (I)	3134
<i>R</i> _{int}	0.0352
Parameters	202
Restraints	203
Largest Peak	0.414
Deepest Hole	-0.364
Goof	1.113
<i>wR</i> ₂ (all data)	0.0884
<i>wR</i> ₂	0.0868
<i>R</i> ₁ (all data)	0.0359
<i>R</i> ₁	0.0339

Figure B.128 X-ray crystallography of product 3id.

Bond precision: C-C = 0.0030 Å Wavelength=0.71073

Cell: a=13.3111 (4) b=16.8142 (5) c=6.5598 (2)
 alpha=90 beta=92.490 (1) gamma=90

Temperature: 296 K

	Calculated	Reported
Volume	1466.80 (8)	1466.80 (8)
Space group	P 21/c	P 1 21/c 1
Hall group	-P 2ybc	-P 2ybc
Moiety formula	C16 H15 Cl O2 S	C16 H15 Cl O2 S
Sum formula	C16 H15 Cl O2 S	C16 H15 Cl O2 S
Mr	306.79	306.79
Dx, g cm ⁻³	1.389	1.389
Z	4	4
Mu (mm ⁻¹)	0.400	0.400
F000	640.0	640.0
F000'	641.33	
h, k, lmax	18, 22, 8	17, 22, 8
Nref	3809	3797
Tmin, Tmax	0.908, 0.923	0.721, 0.746
Tmin'	0.908	

Correction method= # Reported T Limits: Tmin=0.721 Tmax=0.746
 AbsCorr = MULTI-SCAN

Data completeness= 0.997 Theta (max)= 28.757

R(reflections)= 0.0381 (2897) wR2 (reflections)=
 S = 1.061 Npar= 182 0.1020 (3797)

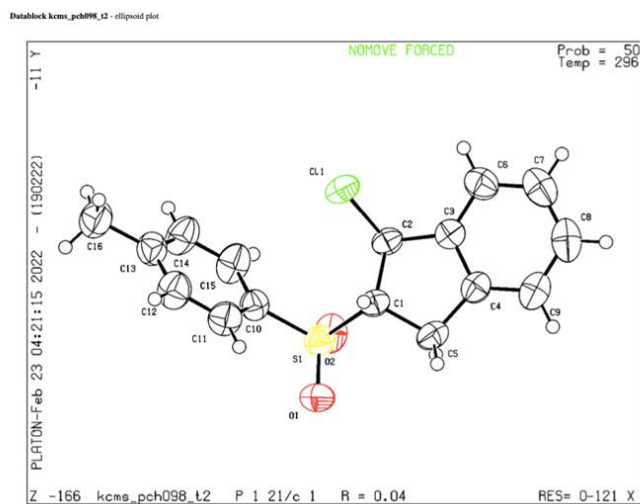


Figure B.129 X-ray crystallography of product *anti-3xb*.

Bond precision: C-C = 0.0024 Å Wavelength=0.71073
 Cell: a=13.9572 (3) b=7.7698 (2) c=14.3457 (3)
 alpha=90 beta=95.603 (1) gamma=90
 Temperature: 296 K

	Calculated	Reported
Volume	1548.28 (6)	1548.28 (6)
Space group	P 21/n	P 1 21/n 1
Hall group	-P 2yn	-P 2yn
Moiety formula	C17 H17 Cl O2 S	C17 H17 Cl O2 S
Sum formula	C17 H17 Cl O2 S	C17 H17 Cl O2 S
Mr	320.82	320.81
Dx, g cm ⁻³	1.376	1.376
Z	4	4
Mu (mm ⁻¹)	0.383	0.383
F000	672.0	672.0
F000'	673.34	
h, k, lmax	18, 10, 19	18, 10, 19
Nref	3894	3876
Tmin, Tmax	0.875, 0.902	0.695, 0.746
Tmin'	0.875	

Correction method= # Reported T Limits: Tmin=0.695 Tmax=0.746
 AbsCorr = MULTI-SCAN

Data completeness= 0.995 Theta (max)= 28.417

R(reflections)= 0.0371 (3300) wR2 (reflections)=
 0.1016 (3876)
 S = 1.067 Npar= 191

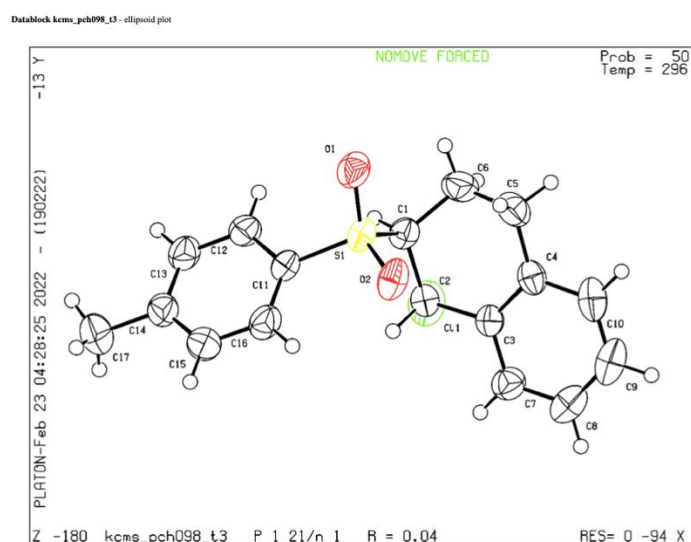


Figure B.130 X-ray crystallography of product *anti-3yb*.

REFERENCES

- [1] C.-J. Wallentin, J.D. Nguyen, P. Finkbeiner, C.R.J. Stephenson, Visible Light-Mediated Atom Transfer Radical Addition via Oxidative and Reductive Quenching of Photocatalysts, *J. Am. Chem. Soc.*, 134 (2012) 8875-8884.
- [2] C.-J. Wallentin, J.D. Nguyen, C.R.J. Stephenson, Radical Carbon–Carbon Bond Formations Enabled by Visible Light Active Photocatalysts, *CHIMIA*, 66 (2012) 394-398.
- [3] T. Koike, M. Akita, Visible-Light-Induced Redox Reactions by Ruthenium Photoredox Catalyst, in: P.H. Dixneuf, C. Bruneau (Eds.) *Ruthenium in Catalysis*, Springer International Publishing, Cham, 2014, pp. 371-395.
- [4] E. Yoshioka, S. Kohtani, E. Tanaka, Y. Hata, H. Miyabe, Carbon radical addition–cyclization reaction induced by ruthenium-photocatalyst under visible light irradiation, *Tetrahedron*, 71 (2015) 773-781.
- [5] C.K. Prier, D.A. Rankic, D.W.C. MacMillan, Visible Light Photoredox Catalysis with Transition Metal Complexes: Applications in Organic Synthesis, *Chem. Rev.*, 113 (2013) 5322-5363.
- [6] M. Pirtsch, S. Paria, T. Matsuno, H. Isobe, O. Reiser, [Cu(dap)₂Cl] As an Efficient Visible-Light-Driven Photoredox Catalyst in Carbon–Carbon Bond-Forming Reactions, *Chem. Eur. J.*, 18 (2012) 7336-7340.
- [7] J.-M. Kern, J.-P. Sauvage, Photoassisted C–C coupling via electron transfer to benzylic halides by a bis(di-imine) copper(I) complex, *J. Chem. Soc., Chem. Commun.*, (1987) 546-548.
- [8] A. Hossain, A. Bhattacharyya, O. Reiser, Copper's rapid ascent in visible-light photoredox catalysis, *Science*, 364 (2019) eaav9713.
- [9] C. Sandoval-Pauker, G. Molina-Aguirre, B. Pinter, Status report on copper (I) complexes in photoredox catalysis; photophysical and electrochemical properties and future prospects, *Polyhedron*, 199 (2021) 115105.
- [10] M. Zhong, X. Pannecoucke, P. Jubault, T. Poisson, Recent advances in photocatalyzed reactions using well-defined copper(I) complexes, *Beilstein J. Org. Chem.*, 16 (2020) 451-481.

- [11] T.P. Nicholls, A.C. Bissember, Developments in visible-light-mediated copper photocatalysis, *Tetrahedron Lett.*, 60 (2019) 150883.
- [12] J.M. Muñoz-Molina, T.R. Belderrain, P.J. Pérez, Atom Transfer Radical Reactions as a Tool for Olefin Functionalization – On the Way to Practical Applications, *Eur. J. Inorg. Chem.*, (2011) 3155-3164.
- [13] A.J. Clark, Copper Catalyzed Atom Transfer Radical Cyclization Reactions, *Eur. J. Org. Chem.*, (2016) 2231-2243.
- [14] S. Engl, O. Reiser, Copper Makes the Difference: Visible Light-Mediated Atom Transfer Radical Addition Reactions of Iodoform with Olefins, *ACS Catal.*, 10 (2020) 9899-9906.
- [15] R.N. Ram, S. Sadanandan, D. Kumar Gupta, β,β,β -Trichloroethyl-NH-Enamine as Viable System for 5-Endo-trig Radical Cyclization via Multifaceted CuI–CuII Redox Catalysis: Single Step Synthesis of Multi-Functionalized NH-Pyrroles, *Adv. Synth. Catal.*, 361 (2019) 5661-5676.
- [16] A.J. Clark, A. Cornia, F. Felluga, A. Gennaro, F. Ghelfi, A.A. Isse, M.C. Menziani, F. Muniz-Miranda, F. Roncaglia, D. Spinelli, Arylsulfonyl Groups: The Best Cyclization Auxiliaries for the Preparation of ATRC γ -Lactams can be Acidolytically Removed, *Eur. J. Org. Chem.*, (2014) 6734-6745.
- [17] J.V. Geden, A.J. Clark, S.R. Coles, C.S. Guy, F. Ghelfi, S. Thom, Copper mediated cyclization of 1-substituted enamides, dienamides and trienamides: regiochemistry, indigoid formation and methyl migration-aromatization, *Tetrahedron Lett.*, 57 (2016) 3109-3112.
- [18] M.S. Kharasch, E.V. Jensen, W.H. Urry, ADDITION OF CARBON TETRABROMIDE AND BROMOFORM TO OLEFINS, *J. Am. Chem. Soc.*, 68 (1946) 154-155.
- [19] M.S. Kharasch, E.V. Jensen, W.H. Urry, Reactions of Atoms and Free Radicals in Solution. X. The Addition of Polyhalomethanes to Olefins, *J. Am. Chem. Soc.*, 69 (1947) 1100-1105.
- [20] J.K. Kochi, HOMOLYTIC ADDITION TO OLEFINS: CHAIN TERMINATION BY METAL HALIDES, *J. Am. Chem. Soc.*, 78 (1956) 4815-4815.
- [21] F. Minisci, R. Galli, Influence of the electrophilic character on the reactivity of free

radicals in solution reactivity of alkoxy, hydroxy, alkyl and azido radicals in presence of olefins, *Tetrahedron Lett.*, 3 (1962) 533-538.

[22] M. Asscher, D. Vofsi, 744. Chlorine-activation by redox-transfer. Part III. The "abnormal" addition of chloroform to olefins, *J. Am. Chem. Soc.*, (1963) 3921-3927.

[23] L. Forti, F. Ghelfi, U.M. Pagnoni, Ferrocene promoted addition of methyl 2,2-dichloro-carboxylates to 1-alkenes, *Tetrahedron*, 53 (1997) 4419-4426.

[24] L. Forti, F. Ghelfi, E. Libertini, U.M. Pagnoni, E. Soragni, Halogen atom transfer radical addition of α -polychloroesters to olefins promoted by Fe⁰ filings, *Tetrahedron*, 53 (1997) 17761-17768.

[25] K. Thommes, B. Içli, R. Scopelliti, K. Severin, Atom-Transfer Radical Addition (ATRA) and Cyclization (ATRC) Reactions Catalyzed by a Mixture of [RuCl₂Cp*(PPh₃)] and Magnesium, *Chemistry – A European Journal*, 13 (2007) 6899-6907.

[26] L. Quebatte, K. Thommes, K. Severin, Highly Efficient Atom Transfer Radical Addition Reactions with a Ru(II) Complex as a Catalyst Precursor, *J. Am. Chem. Soc.*, 128 (2006) 7440-7441.

[27] F. Simal, L. Wlodarczak, A. Demonceau, Alfred F. Noels, New, Highly Efficient Catalyst Precursors for Kharasch Additions – [RuCl(Cp*)(PPh₃)₂] and [RuCl(Ind)(PPh₃)₂], *Eur. J. Org. Chem.*, 2001 (2001) 2689-2695.

[28] J.D. Nguyen, J.W. Tucker, M.D. Konieczynska, C.R.J. Stephenson, Intermolecular Atom Transfer Radical Addition to Olefins Mediated by Oxidative Quenching of Photoredox Catalysts, *J. Am. Chem. Soc.*, 133 (2011) 4160-4163.

[29] M. Mitani, I. Kato, K. Koyama, Photoaddition of alkyl halides to olefins catalyzed by copper(I) complexes, *J. Am. Chem. Soc.*, 105 (1983) 6719-6721.

[30] O. Reiser, Shining Light on Copper: Unique Opportunities for Visible-Light-Catalyzed Atom Transfer Radical Addition Reactions and Related Processes, *Acc. Chem. Res.*, 49 (2016) 1990-1996.

[31] H. Nishiyama, H. Ikeda, T. Saito, B. Kriegel, H. Tsurugi, J. Arnold, K. Mashima, Structural and Electronic Noninnocence of α -Diimine Ligands on Niobium for Reductive C–Cl Bond Activation and Catalytic Radical Addition Reactions, *J. Am. Chem. Soc.*, 139 (2017) 6494-6505.

- [32] L.A. van de Kuil, D.M. Grove, R.A. Gossage, J.W. Zwikker, L.W. Jenneskens, W. Drenth, G. van Koten, Mechanistic Aspects of the Kharasch Addition Reaction Catalyzed by Organonickel(II) Complexes Containing the Monoanionic Terdentate Aryldiamine Ligand System [C₆H₂(CH₂NMe₂)₂-2,6-R-4], *Organometallics*, 16 (1997) 4985-4994.
- [33] A.C. G. M. Sheldrick, *Sect. A: Found. Adv.*, 2015, 71, 3–8.
- [34] F. Minisci, Free-radical additions to olefins in the presence of redox systems, *Acc. Chem. Res.*, 8 (1975) 165-171.
- [35] T. Pintauer, K. Matyjaszewski, Atom transfer radical addition and polymerization reactions catalyzed by ppm amounts of copper complexes, *Chem. Soc. Rev.*, 37 (2008) 1087-1097.
- [36] H. Nagashima, K.-i. Ara, H. Wakamatsu, K. Itoh, Stereoselective preparation of bicyclic lactams by copper- or ruthenium-catalysed cyclization of N-allyltrichloroacetamides: a novel entry to pyrrolidine alkaloid skeletons, *J. Chem. Soc., Chem. Commun.*, (1985) 518-519.
- [37] H. Nagashima, K. Seki, N. Ozaki, H. Wakamatsu, K. Itoh, Y. Tomo, J. Tsuji, Transition-metal-catalyzed radical cyclization: copper-catalyzed cyclization of allyl trichloroacetates to trichlorinated γ -lactones, *J. Org. Chem.*, 55 (1990) 985-990.
- [38] M. Knorn, T. Rawnier, R. Czerwiec, O. Reiser, [Copper(phenanthroline)(bisisonitrile)]⁺-Complexes for the Visible-Light-Mediated Atom Transfer Radical Addition and Allylation Reactions, *ACS Catal.*, 5 (2015) 5186-5193.
- [39] D. Yang, Y.-L. Yan, B.-F. Zheng, Q. Gao, N.-Y. Zhu, Copper(I)-Catalyzed Chlorine Atom Transfer Radical Cyclization Reactions of Unsaturated α -Chloro β -Keto Esters, *Org. Lett.*, 8 (2006) 5757-5760.
- [40] A.A. Rexit, X. Hu, Intermolecular atom transfer radical addition of α,α,α -trichloromethyl ketones and alkenes mediated by a CuCl/bpy system, *Tetrahedron*, 71 (2015) 2313-2316.
- [41] W.T. Eckenhoff, T. Pintauer, Atom Transfer Radical Addition in the Presence of Catalytic Amounts of Copper(I/II) Complexes with Tris(2-pyridylmethyl)amine, *Inorg. Chem.*, 46 (2007) 5844-5846.
- [42] W.T. Eckenhoff, S.T. Garrity, T. Pintauer, Highly Efficient Copper-Mediated Atom-

Transfer Radical Addition (ATRA) in the Presence of Reducing Agent, *Eur. J. Inorg. Chem.*, 2008 (2008) 563-571.

[43] T. Pintauer, W.T. Eckenhoff, C. Ricardo, M.N.C. Balili, A.B. Biernesser, S.J. Noonan, M.J.W. Taylor, Highly Efficient Ambient-Temperature Copper-Catalyzed Atom-Transfer Radical Addition (ATRA) in the Presence of Free-Radical Initiator (V-70) as a Reducing Agent, *Chem. Eur. J.*, 15 (2009) 38-41.

[44] W.T. Eckenhoff, T. Pintauer, Structural Comparison of Copper(I) and Copper(II) Complexes with Tris(2-pyridylmethyl)amine Ligand, *Inorg. Chem.*, 49 (2010) 10617-10626.

[45] B. Zhao, J.-Y. Lu, Y. Li, D.-H. Tu, Z.-T. Liu, Z.-W. Liu, J. Lu, Regioisomerized atom transfer radical addition (ATRA) of olefins with dichlorofluorocarbons, *RSC Adv.*, 5 (2015) 101412-101415.

[46] M.N.C. Balili, T. Pintauer, Photoinitiated ambient temperature copper-catalyzed atom transfer radical addition (ATRA) and cyclization (ATRC) reactions in the presence of free-radical diazo initiator (AIBN), *Dalton Trans.*, 40 (2011) 3060-3066.

[47] J.M. Muñoz-Molina, A. Caballero, M.M. Díaz-Requejo, S. Trofimenko, T.R. Belderrain, P.J. Pérez, Copper-Homoscorpionate Complexes as Active Catalysts for Atom Transfer Radical Addition to Olefins, *Inorg. Chem.*, 46 (2007) 7725-7730.

[48] J.M. Muñoz-Molina, T.R. Belderrain, P.J. Pérez, An Efficient, Selective, and Reducing Agent-Free Copper Catalyst for the Atom-Transfer Radical Addition of Halo Compounds to Activated Olefins, *Inorg. Chem.*, 49 (2010) 642-645.

[49] J.M. Muñoz-Molina, W.M.C. Sameera, E. Álvarez, F. Maseras, T.R. Belderrain, P.J. Pérez, Mechanistic and Computational Studies of the Atom Transfer Radical Addition of CCl₄ to Styrene Catalyzed by Copper Homoscorpionate Complexes, *Inorg. Chem.*, 50 (2011) 2458-2467.

[50] J.M. Muñoz-Molina, T.R. Belderrain, P.J. Pérez, Copper-Catalyzed Synthesis of 1,2-Disubstituted Cyclopentanes from 1,6-Dienes by Ring-Closing Kharasch Addition of Carbon Tetrachloride, *Adv. Synth. Catal.*, 350 (2008) 2365-2372.

[51] W.T. Eckenhoff, T. Pintauer, Atom transfer radical addition (ATRA) catalyzed by copper complexes with tris[2-(dimethylamino)ethyl]amine (Me₆TREN) ligand in the

presence of free-radical diazo initiator AIBN, Dalton Trans., 40 (2011) 4909-4917.

[52] A. Kaur, E.E. Gorse, T.G. Ribelli, C.C. Jerman, T. Pintauer, Atom transfer radical addition (ATRA) catalyzed by copper complexes with N,N,N',N'-tetrakis(2-pyridylmethyl)ethylenediamine (TPEN) ligand, Polymer, 72 (2015) 246-252.

[53] M.J.W. Taylor, W.T. Eckenhoff, T. Pintauer, Copper-catalyzed atom transfer radical addition (ATRA) and cyclization (ATRC) reactions in the presence of environmentally benign ascorbic acid as a reducing agent, Dalton Trans., 39 (2010) 11475-11482.

[54] J.-P. Wan, D. Hu, F. Bai, L. Wei, Y. Liu, Stereoselective Z-halosulfonylation of terminal alkynes using sulfonylhydrazides and CuX (X = Cl, Br, I), RSC Advances, 6 (2016) 73132-73135.

[55] R. Chaudhary, P. Natarajan, Visible Light Photoredox Activation of Sulfonyl Chlorides: Applications in Organic Synthesis, ChemistrySelect, 2 (2017) 6458-6479.

[56] L. Liu, C. Wang, Copper-catalyzed redox-neutral regioselective chlorosulfonylation of vinylarenes, React. Chem. Eng., 6 (2021) 1376-1380.

[57] X. Li, X. Shi, M. Fang, X. Xu, Iron Halide-Mediated Regio- and Stereoselective Halosulfonylation of Terminal Alkynes with Sulfonylhydrazides: Synthesis of (E)- β -Chloro and Bromo Vinylsulfones, J. Org. Chem., 78 (2013) 9499-9504.

[58] S.K. Pagire, S. Paria, O. Reiser, Synthesis of β -Hydroxysulfones from Sulfonyl Chlorides and Alkenes Utilizing Visible Light Photocatalytic Sequences, Org. Lett., 18 (2016) 2106-2109.

[59] K. Zeng, L. Chen, Y. Chen, Y. Liu, Y. Zhou, C.-T. Au, S.-F. Yin, Iron(III) Chloride-Mediated Regio- and Stereoselective Chlorosulfonylation of Alkynes and Alkenes with Sodium Sulfinates, Adv. Synth. Catal., 359 (2017) 841-847.

[60] T.-f. Niu, J. Cheng, C.-l. Zhuo, D.-y. Jiang, X.-g. Shu, B.-q. Ni, Visible-light-promoted oxidative difunctionalization of alkenes with sulfonyl chlorides to access β -keto sulfones under aerobic conditions, Tetrahedron Lett., 58 (2017) 3667-3671.

[61] S.K. Pagire, A. Hossain, O. Reiser, Temperature Controlled Selective C-S or C-C Bond Formation: Photocatalytic Sulfonylation versus Arylation of Unactivated Heterocycles Utilizing Aryl Sulfonyl Chlorides, Org. Lett., 20 (2018) 648-651.

[62] P. Chakrasali, K. Kim, Y.-S. Jung, H. Kim, S.B. Han, Visible-Light-Mediated Photoredox-

Catalyzed Regio- and Stereoselective Chlorosulfonylation of Alkynes, *Org. Lett.*, 20 (2018) 7509-7513.

[63] L.M. Kammer, B. Lipp, T. Opatz, Photoredox Alkenylation of Carboxylic Acids and Peptides: Synthesis of Covalent Enzyme Inhibitors, *J. Org. Chem.*, 84 (2019) 2379-2392.

[64] X. Wang, B. Hu, P. Yang, Q. Zhang, D. Li, Synthesis of vinyl sulfones through sulfonylation of styrenes with sulfonyl chlorides under metal-free conditions, *Tetrahedron*, 76 (2020) 131082.

[65] L. Liu, P. Xue, Q. Chen, C. Wang, Copper-Catalyzed Heck-Type Couplings of Sulfonyl Chlorides with Olefins: Efficient and Rapid Access to Vinyl Sulfones, *Tetrahedron Lett.*, 80 (2021) 153319.

[66] L. Liu, C. Wang, Allyl sulfones construction via copper catalysis from α -methylstyrene derivatives and sulfonyl chlorides, *Tetrahedron Lett.*, 88 (2022) 153553.

[67] P.-J. Xia, F. Liu, S.-H. Li, J.-A. Xiao, Tunable photocatalytic oxysulfonylation and chlorosulfonylation of α -CF₃ alkenes with sulfonyl chlorides, *Org. Chem. Front.*, 9 (2022) 709-714.

[68] S.H. Suzol, A.H. Howlader, Z. Wen, Y. Ren, E.E. Laverde, C. Garcia, Y. Liu, S.F. Wnuk, Pyrimidine Nucleosides with a Reactive (β -Chlorovinyl)sulfone or (β -Keto)sulfone Group at the C5 Position, Their Reactions with Nucleophiles and Electrophiles, and Their Polymerase-Catalyzed Incorporation into DNA, *ACS Omega*, 3 (2018) 4276-4288.

[69] K.A. Scott, J.T. Njardarson, Analysis of US FDA-Approved Drugs Containing Sulfur Atoms, *Top. Curr. Chem.*, 376 (2018) 5.

[70] J.W. Choi, S. Kim, J.-H. Park, H.J. Kim, S.J. Shin, J.W. Kim, S.Y. Woo, C. Lee, S.M. Han, J. Lee, A.N. Pae, G. Han, K.D. Park, Optimization of Vinyl Sulfone Derivatives as Potent Nuclear Factor Erythroid 2-Related Factor 2 (Nrf2) Activators for Parkinson's Disease Therapy, *J. Med. Chem.*, 62 (2019) 811-830.

[71] M. Gallhof, L. Kell, M. Brasholz, Ligand Substitution of Ru(II)-Alkylidenes to Ru(bpy)₃²⁺: Sequential Olefin Metathesis/Photoredox Catalysis, *Chem. Eur. J.*, 26 (2020) 1772-1775.

[72] S.M. Hell, C.F. Meyer, A. Misale, J.B.I. Sap, K.E. Christensen, M.C. Willis, A.A. Trabanco, V. Gouverneur, Hydrosulfonylation of Alkenes with Sulfonyl Chlorides under

Visible Light Activation, *Angew. Chem. Int. Ed.*, 59 (2020) 11620-11626.

[73] A. Jílková, P. Rubešová, J. Fanfrlík, P. Fajtová, P. Řezáčová, J. Brynda, M. Lepšík, H. Mertlíková-Kaiserová, C.D. Emal, A.R. Renslo, W.R. Roush, M. Horn, C.R. Caffrey, M. Mareš, Druggable Hot Spots in the Schistosomiasis Cathepsin B1 Target Identified by Functional and Binding Mode Analysis of Potent Vinyl Sulfone Inhibitors, *ACS Infect. Dis.*, 7 (2021) 1077-1088.

[74] S.Y. Woo, J.H. Kim, M.K. Moon, S.-H. Han, S.K. Yeon, J.W. Choi, B.K. Jang, H.J. Song, Y.G. Kang, J.W. Kim, J. Lee, D.J. Kim, O. Hwang, K.D. Park, Discovery of Vinyl Sulfones as a Novel Class of Neuroprotective Agents toward Parkinson's Disease Therapy, *J. Med. Chem.*, 57 (2014) 1473-1487.

[75] A.S. Falcão, L.A.R. Carvalho, G. Lidónio, A.R. Vaz, S.D. Lucas, R. Moreira, D. Brites, Dipeptidyl Vinyl Sulfone as a Novel Chemical Tool to Inhibit HMGB1/NLRP3-Inflammasome and Inflammation-miRs in A β -Mediated Microglial Inflammation, *ACS Chem. Neurosci.*, 8 (2017) 89-99.

[76] X.-J. Tang, W.R. Dolbier Jr., Efficient Cu-catalyzed Atom Transfer Radical Addition Reactions of Fluoroalkylsulfonyl Chlorides with Electron-deficient Alkenes Induced by Visible Light, *Angew. Chem. Int. Ed.*, 54 (2015) 4246-4249.

[77] D.B. Bagal, G. Kachkovskiy, M. Knorn, T. Rawner, B.M. Bhanage, O. Reiser, Trifluoromethylchlorosulfonylation of Alkenes: Evidence for an Inner-Sphere Mechanism by a Copper Phenanthroline Photoredox Catalyst, *Angew. Chem. Int. Ed.*, 54 (2015) 6999-7002.

[78] A. Hossain, S. Engl, E. Lutsker, O. Reiser, Visible-Light-Mediated Regioselective Chlorosulfonylation of Alkenes and Alkynes: Introducing the Cu(II) Complex [Cu(dap)Cl₂] to Photochemical ATRA Reactions, *ACS Catal.*, 9 (2019) 1103-1109.

[79] S. Engl, O. Reiser, Making Copper Photocatalysis Even More Robust and Economic: Photoredox Catalysis with [CuI(dmp)₂Cl]Cl, *Eur. J. Org. Chem.*, (2020) 1523-1533.

[80] M. Alkan-Zambada, X. Hu, Cu-Catalyzed Photoredox Chlorosulfonation of Alkenes and Alkynes, *J. Org. Chem.*, 84 (2019) 4525-4533.

[81] C.L. Ricardo, T. Pintauer, One-Pot Sequential Azide-Alkyne [3+2] Cycloaddition and Atom Transfer Radical Addition (ATRA): Expanding the Scope of In Situ Copper(I)

Regeneration in the Presence of Environmentally Benign Reducing Agent, *Eur. J. Inorg. Chem.*, (2011) 1292-1301.

[82] W.T. Eckenhoff, S.T. Garrity, T. Pintauer, Highly Efficient Copper-Mediated Atom-Transfer Radical Addition (ATRA) in the Presence of Reducing Agent, *Eur. J. Inorg. Chem.*, (2008) 563-571.

[83] J. Hojitsiriyant, P. Chaibuth, K. Boonkitpatarakul, V. Ruangpornvisuti, T. Palaga, K. Chainok, M. Sukwattanasinitt, Effects of amino proton and denticity of quinoline-pyridine based dyes on Cd²⁺ and Zn²⁺ fluorescence sensing properties, *J. Photochem. Photobiol. A: Chem.*, 415 (2021) 113307.

[84] D. Ma, Q. Cai, H. Zhang, Mild Method for Ullmann Coupling Reaction of Amines and Aryl Halides, *Org. Lett.*, 5 (2003) 2453-2455.

[85] Bruker AXS Inc., APEX3, SADABS and SAINT, Madison, Wisconsin, USA, 2016.

[86] G. Sheldrick, SHELXT - Integrated space-group and crystal-structure determination, *Acta Cryst. A*, 71 (2015) 3-8.

[87] G. Sheldrick, Crystal structure refinement with SHELXL, *Acta Cryst. C*, 71 (2015) 3-8.

[88] K.A. Bussey, A.R. Cavalier, M.E. Mraz, K.D. Oshin, A. Sarjeant, T. Pintauer, Synthesis, characterization, X-ray crystallography analysis, and catalytic activity of bis(2-pyridylmethyl)amine copper complexes containing coupled pendent olefinic arms in atom transfer radical addition (ATRA) reactions, *Polyhedron*, 114 (2016) 256-267.

[89] Z. Liu, J. Xu, W. Ruan, C. Fu, H.-J. Zhang, T.-B. Wen, A half-sandwich 1,2-azaborolyt ruthenium complex: synthesis, characterization, and evaluation of its catalytic activities, *Dalton Trans.*, 42 (2013) 11976-11980.

[90] A. Hossain, S. Engl, E. Lutsker, O. Reiser, Visible-Light-Mediated Regioselective Chlorosulfonylation of Alkenes and Alkynes: Introducing the Cu(II) Complex [Cu(dap)Cl₂] to Photochemical ATRA Reactions, *ACS Catalysis*, 9 (2019) 1103-1109.

[91] A.A. Isse, C.Y. Lin, M.L. Coote, A. Gennaro, Estimation of Standard Reduction Potentials of Halogen Atoms and Alkyl Halides, *J. Phys. Chem. B*, 115 (2011) 678-684.

[92] Y. Abderrazak, A. Bhattacharyya, O. Reiser, Visible-Light-Induced Homolysis of Earth-Abundant Metal-Substrate Complexes: A Complementary Activation Strategy in Photoredox Catalysis, *Angew Chem Int Ed Engl*, 60 (2021) 21100-21115.

- [93] R. Fayad, S. Engl, E.O. Danilov, C.E. Hauke, O. Reiser, F.N. Castellano, Direct Evidence of Visible Light-Induced Homolysis in Chlorobis(2,9-dimethyl-1,10-phenanthroline)copper(II), *J. Phys. Chem. Lett.*, 11 (2020) 5345-5349.
- [94] M. Mitani, M. Nakayama, K. Koyama, The cuprous chloride catalyzed addition of halogen compounds to olefins under photo-irradiation, *Tetrahedron Lett.*, 21 (1980) 4457-4460.
- [95] J.F. Franz, W.B. Kraus, K. Zeitler, No photocatalyst required – versatile, visible light mediated transformations with polyhalomethanes, *Chem. Commun.*, 51 (2015) 8280-8283.
- [96] J.K. Bower, A.D. Cypcar, B. Henriquez, S.C.E. Stieber, S. Zhang, C(sp³)-H Fluorination with a Copper(II)/(III) Redox Couple, *Journal of the American Chemical Society*, 142 (2020) 8514-8521.
- [97] P. Chaibuth, N. Chuaytanee, J. Hojitsiryanont, K. Chainok, S. Wacharasindhu, O. Reiser, M. Sukwattanasinitt, Copper(II) Complexes of Quinoline-based Ligands for Efficient Photoredox Catalysis of Atom Transfer Radical Addition (ATRA) Reaction, *New Journal of Chemistry*, (2022).
- [98] C.M.M. da Silva Corrêa, M.D.C.M. Fleming, M.A.B.C.S. Oliveira, E.M.J. Garrido, The importance of polar, resonance, steric and solvent effects in the addition of sulfonyl radicals to alkenes, *J. Chem. Soc., Perkin Trans. 2*, (1994) 1993-2000.
- [99] W. Truce, C. Goralski, The Copper-Catalyzed Addition of Arenesulfonyl Chlorides to 1,1-Diphenylthylene and Cyclic Aryl-Substituted Olefins, *J. Org. Chem.*, 35 (1970) 4220-4222.

VITA

NAME Pawittra Chaibuth

DATE OF BIRTH 26 July 1992

PLACE OF BIRTH Chiang Mai

HOME ADDRESS 36/220 Chaengwattana Road, Thung Song Hong, Lak Si, Bangkok, Thailand 10210.

PUBLICATION

1. Hojitsiriyant, J.; Chaibuth, P.; Boonkitpatarakul K.; Ruangpornvisuti, V.; Palaga, T.; Chainok K. and Sukwattanasinitt, M. Effects of amino proton and denticity of quinoline-pyridine based dyes on Cd²⁺ and Zn²⁺ fluorescence sensing properties. J. Photochem. Photobiol. A: Chem. 2021, 415, 113307.
2. Chaibuth, P.; Chuaytanee, N.; Hojitsiriyant, J.; Chainok, K.; Wacharasindhu, S.; Reiser, O. and Sukwattanasinitt M. Copper (II) complexes of quinoline-based ligands for efficient photoredox catalysis of atom transfer radical addition (ATRA) reaction. New J. Chem., (2022), DOI: 10.1039/d2nj01218a.